A Transient Heat Transfer and Thermodynamic Analysis of the Apollo Service Module Propulsion System

CONTRACT NO. NAS 9-3349

Submitted to:

NASA MANNED SPACECRAFT CENTER
PRIMARY PROPULSION BRANCH
Houston, Texas

FOREWORD

This is the final report of a Transient Heat Transfer and Thermodynamic Analysis of the Apollo Service Module Propulsion System conducted for the NASA Manned Spacecraft Center, Houston, Texas. The study was conducted under NASA Contract NAS 9-3349 from 28 July, 1964, to 28 July, 1965, by the Lockheed - California Company. Mr. J. B. Werner was Program Manager; Mr. B. A. Nevelli was the Phase I Project Engineer and Mr. P. S. Starrett was the Phase II Project Engineer. The NASA Technical Monitor was Mr. L. Rhodes.

This report is contained in two volumes: Volume I, Phase I Transient Thermal Analysis, and Volume II, Phase II Thermal Test Program. Appendix D of Volume I, which is classified "Confidential", is bound separately. The remainder of Volume I and all of Volume II are unclassified.

Other reports prepared under this contract are:

LR 18900	A Transient Heat Transfer and Thermodynamic Analysis of the Apollo Service Module Propulsion System - Summary Report
LR 18901	An Introduction to Spacecraft Thermal Control
LR 18902	Thermal Analyzer Computer Program for the Solution of General Heat Transfer Problems
LR 18903	Thermal Analyzer Computer Program for the Solution of Fluid Storage and Pressurization Problems
LR 18904	Computer Program for the Calculation of Incident Orbital Radiant Heat Flux
LR 18905	Computer Program for the Calculation of Three-Dimensional Configuration Factors

This report was prepared by Lockheed's Thermodynamics Department and Rye Canyon Research Laboratory. The principal contributers to Volume I, in addition to Mr. Nevelli, were Messrs. H. R. Holmes, M. A. Kazarian, H. D. Schultz and I. Shuldiner. The discussion of low-gravity fluid mechanics and heat transfer was prepared by Messrs. R. W. Deible and H. M. Satterlee of the Lockheed Missiles and Space Company. The principal

FOREWORD (Cont.)

contributors to Volume II, in addition to Mr. Starrett, were Messrs. K. J. Kahn, M. A. Kazarian, and H. H. Ogimachi. Grateful acknowledgement is made to Mr. R. E. Butler , who was responsible for the test instrumentation, and Mr. R. B. David, who was responsible for computer programming and data processing.

TABLE OF CONTENTS

TABLE OF CONTENTS (cont.)

TABLE OF CONTENTS (cont.)

TABLE OF CONTENTS (cont.)

LIST OF FIGURES

LIST OF FIGURES (Cont.)

LIST OF FIGURES (Cont.)

LIST OF FIGURES (Cont.)

LIST OF FIGURES (Cont.)

LIST OF FIGURES (Cont.)

LIST OF FIGURES (Cont.)

LIST OF FIGURES (Cont.)

LIST OF FIGURES (Cont.)

LIST OF TABLES

LIST OF TABLES (Cont.)

SUMMARY

This volume presents the results of a transient heat transfer and thermodynamic analysis of the Apollo Service Module Propulsion System performed for the NASA Manned Spacecraft Center. The accompanying thermal test program is described in Volume II of this report.

The primary objective of this study was to determine the three-dimensional transient heat transfer and thermodynamic behavior of the Service Propulsion System for three entire Missions:

1. Earth Suborbital
2. Earth Orbital
3. Lunar Orbital Rendezvous

The secondary objective was to develop and improve techniques for performing such an analysis, including the development and modification of several digital computer programs.

All mission profiles start at the time of launch, and ascent heating is included in the analysis. The analyses take into account external heating due to the relative position and orientation of the Apollo spacecraft with respect to the Earth, moon, and sun. The analysis of the Lunar Orbital Rendezvous Mission includes the normal roll orientation during the translunar and transearth phases and orientations providing maximum and minimum heating to the Service Propulsion System from external sources. The mission profiles and configurations analyzed were supplied by the Manned Spacecraft Center.

The analytical study provides temperature-time histories of all Service Module components important to the Service Propulsion System. In addition, the analysis provides pressurization requirements, pressure-time histories, and mass transfer rates for the propellant tanks through the use of a new Fluid Storage and Pressurization Program.

The Service Module is represented in the study by three separate thermal networks. The network generated for the basic analysis, consisting of approximately 850 nodes, 1500 conduction resistors, and 700 radiation resistors, includes all Service Module Components with the exception of the cryogenic tankage and Reaction Control System. The propellant tankage, service propulsion engine, and helium bottles are represented in a simplified fashion. The second thermal network, consisting of approximately 300 nodes, 275 conduction

resistor, and 450 radiation resistors was generated to represent the service propulsion engine and plumbing for a detailed analysis of these components. The third network, consisting of approximately 150 nodes, 275 conduction resistors, and 90 radiation resistors, represents each of the propellant tanks and the helium pressurization system. These networks put together for the first time nearly all of the interacting thermal aspects of the Apollo Service Module. A total of 300 computer hours were used.

The results of the study indicate that the thermal design philosophy of the Service Module (SM) is basically sound. The liberal use of light weight super-insulation, the large thermal mass of the propellant tanks and the selected surfaces effectively control the general Service Module temperature level. However, temperatures of several Service Propulsion System (SPS) components exceed their prescribed temperature limits during the Lunar Orbit Rendezvous and Earth Orbital Missions. These components are in the region of the fuel cells, the thrust chamber, and the disconnect panels. The fuel cells are a very significant heat source for the SM and are either partially or totally responsible for each thermal problem discovered, with the exception of the disconnect panels. It cannot be overemphasized that the assumption of the Block I fuel cell location for the Lunar Mission has a major effect on the analytical results for that mission. The Earth Orbital Mission is expected to be a problem as the fuel cells remain in their aft location. The expected relocation of the fuel cells in Block II will reduce the thermal problem of the Lunar Orbit Rendezvous Mission. Since for the Lunar Orbital Rendezvous Mission the Bay 4 shell and beams are well insulated with aluminized Mylar, most of the heat dissipated by the fuel cells to the SM interior must be rejected by conduction through the aft bulkhead, and subsequently radiated to space from those portions of the bulkhead which are not covered by the aft heat shield. The assumption of a total heat rejection of 750 Btu/hr and a surface emissivity of 0.3 resulted in an equilibrium fuel cell temperature of about 300°F, and a peak temperature of 335°F following transearth injection. As a result, the Bay 4 aft bulkhead and engine web mount achieve maximum temperatures of 255°F and 500°F, respectively. For the Earth Orbital Mission, Bay 4 is uninsulated except for the shell, thus allowing additional heat rejection through the radial beams. The maximum fuel cell temperature is 235°F, and the maximum temperatures on the Bay 4 aft

bulkhead and engine web mount are 210° F and 200° F, respectively.

The aft bulkhead radiates to the propellant and pressurant plumbing lines directly below it, causing peak line temperatures of 240° F for the Lunar Mission and 150° F for the Earth Orbital Mission. Propellant feed lines which extend from the bipropellant valve assembly to the aft bulkheads are heated by radiation from both the thrust chamber and the engine web mounts. Because there is practically no available means of heat rejection for these lines, maximum temperature of 380° F for the Lunar Mission and 210° F for the Earth Orbital Mission are predicted. The maximum allowable temperature of these lines for normal engine operation is 135° F.

Since the thrust chamber must dissipate heat by radiation to the surroundings, the effect of the fuel cell heating to the engine web mounts has a large effect on the chamber temperature history. A maximum chamber backwall temperature of 680° F is predicted although the calculations provided by NASA predicted a maximum temperature of only 327° F. This discrepancy results primarily from the assumption of an 80° F radiation sink in the NASA analysis, and a computed radiation sink (consisting of the engine web mounts, propellant tanks and lines, gimbal ring, etc.) in the Lockheed analysis. With the fuel cells mounted to the aft bulkhead, a more appropriate radiation sink temperature for those portions of the chamber which view Bay 4 is on the order of 300-400° F.

The pitch actuator upper temperature limit is exceeded due to its proximity to the thrust chamber and the Bay 4 engine web mount. The maximum predicted temperatures are 233° F and 170° F for the Lunar and Earth Orbital Missions, respectively. The allowable temperature limit is 140° F.

The only region of the vehicle which experiences unacceptably low temperatures are the propellant disconnect couplings adjacent to the disconnect panels. These panels are situated such that they view deep space for much of the missions. Minimum temperatures on these panels are -44° F during the Lunar Mission, and -73° F during the Earth Orbital Mission. The corresponding coupling temperature are 35° F and 15° F due to conduction heat exchange with the panels. The minimum acceptable coupling temperature is 40° F.

No SPS thermal problems were discovered for the Earth Suborbital Mission. This is a result of the short mission duration (1700 sec) and the absence

of fuel cell operation, the electrical power being supplied by batteries. Although one 240 sec SPS engine burn is scheduled, the SM is jettisoned shortly thereafter, allowing insufficient time for a sizeable quantity of heat to be conducted through the chamber walls and radiated to the surroundings.

No thermal problems were found for the propellant storage and pressurization systems for any of the missions analyzed. The propellant temperatures decrease monotonically from their initial assumed value of 70° F. The minimum bulk propellant temperature for the Lunar Orbit Rendezvous Mission is 64° F and occurs at the Bay 2 oxidizer tank. The minimum temperature of the helium pressurant gas is -79° F and occurs during lunar orbit insertion. Even in the event of an abort during lunar orbit where transearth injection might be required almost immediately following lunar orbit insertion, the pressurant gas would remain above its minimum allowable temperature of -150°F. At the end of the Lunar Mission 21 lb of helium remain in each bottle.

I - INTRODUCTION

A complete heat transfer and thermodynamic analysis of the Apollo Service Module Propulsion System is vital to the Apollo Program because of the importance of the propulsion system to mission success and crew safety. The wide range of thermal enviroments encountered during the missions adds to the complexity of the problem. The spacecraft will be subjected to direct insolation, Earth reflection and emission, moon reflection and emission, and the extreme cold of deep space. The lunar emission at the subsolar point, for example, is almost as intense as the direct solar insolation, while the heat flux received over the dark side of the moon is essentially zero.

Many components are characterized by narrow temperature tolerances. Service Module storable propellants, for example, must be kept above 40° F to prevent freezing and separation, and below 80° F to limit the ullage pressure. Similar 40° F to 80° F limits apply to the helium drain coupling, propellant disconnect coupling, flexible connectors, quantity indicator and mixture ratio control, and the propellant side of the heat exchangers. The propellant feed lines and injector valves have an upper limit of 135° F, which is the maximum temperature for normal engine operating conditions. Similarly, other Service Propulsion System components must remain within prescribed temperature limits to insure the successful completion of the Apollo missions.

Thus, a highly accurate and detailed thermal analysis of the Service Propulsion System is required. This report describes the detailed thermal analysis performed by the Lockheed-California Company. Although these analyses put together for the first time nearly all of the interacting thermal aspects of the Apollo Service Module, they were carried out to examine the thermal behavior of the Service Propulsion System. Other Service Module components are included only insofar as they affect the propulsion system.

The primary objective of this study is to determine the three-dimensional transient heat transfer and thermodynamic behavior of the Apollo Service Propulsion System for three prescribed missions:

1. Earth Suborbital

2. Earth Orbital

3. Lunar Orbit Rendezvous

The secondary objective is to develop and improve techniques for performing such an analysis, including the development and modification of several digital computer programs.

The principal requirement of the study is to provide temperature-time histories of all Service Module components important to the Service Propulsion System. In addition, pressurization requirements, pressure-time histories, and mass transfer histories of the propellant tanks are obtained through the use of a new Fluid Storage and Pressurization Program.

Generally in the course of designing a complex spacecraft, individual thermal analyses are made of the various components. However, to gain an understanding of how the components will function collectively, there is a need for a comprehensive and complete analysis which considers the spacecraft as a whole, rather than an independent collection of parts. The anlaysis presented in this report examines the Service Module as an entity.

The fundamental philosophy of carrying out the complete transient thermodynamic analysis of the Apollo Service Propulsion System is to "fly" the vehicle on the computer. The use of high-speed digital computers and sophisticated computer programs allows an essentially complete simulation of the Apollo Service Module, its components, and its missions. The analysis was carried out in the following steps:

1. Data Acquisition and Program Network Conception

The initial part of the study was devoted to establishing the mission requirements, and obtaining data on the Service Module configuration and design, propulsion system, mission profiles, and other data required for the analysis. During this initial period, the analytical methods and techniques utilized in the analysis were established and work was initiated in setting up the thermal networks for the heat transfer analyses. It took five months to complete the data acquisition.

2. Computer Program Development and Modification

The second step was the development, modification, and application of computer programs to meet the specific requirements of the study. Computer programs were used to calculate orbital heat inputs, some radiation

configuration factors, transient heat transfer, and the thermodynamic performance of the fluid storage and pressurization system. The major part of this task was the development of the Fluid Storage and Pressurization Program as a set of subroutines for the Thermal Analyzer Program. Other modifications included the extension of the Orbital Radiation Program to include lunar orbits, the addition of output plotting routines for the Orbital Radiation and Thermal Analyzer Programs, and the addition of a data search routine for use with a thermal properties library and optional geometrical resistor and capacitor input routines for the Thermal Analyzer Program.

3. Preparation of Computer Program Inputs

The third step was the generation of data inputs and boundary conditions for the analyses, including ascent heating, orbital radiation, propulsion system heat inputs, and radiation configuration factors. Data inputs were prepared for the three prescribed missions. In addition to the normal roll made for the translunar and transearth portions of the mission, orientations for minimum and maximum heating to the Service Propulsion System were analyzed. The thermal network representation of the Service Module includes all major components, with the exception of the cryogenic tankage and the Reaction Control System packages. Separate thermal networks were constructed to analyze in detail the combination of engine and plumbing and to analyze the propellant tankage and pressurization system.

4. Generation of Program Results and Data Evolution

The final analytical step was the computer thermal analysis of the Service Module, employing the networks, heat inputs, and other boundary conditions and data generated during the three previous steps for the prescribed mission. The basic network consists of approximately 850 nodes, 1500 conduction resistors, and 800 radiation resistors. This analysis puts together for the first time nearly all of the interacting thermal aspects of the Apollo Service Module.

Completion of the four major analytical tasks provides sufficient data to assess the thermal design and performance of the Service Propulsion System. The following sections document the results of the analytical work and

include recommendations based on the results obtained during the course of the study. Volume II of this Final Report describes and documents the results of the accompanying Thermal Test Program.

II - STUDY GROUND RULES

Ground rules for the Apollo Serviee Module (SM) heat transfer study consist of the assumed configuration, missions, and other parameters necessary to perform the required analyses. Some aspects of the assumed configuration and missions differ from the anticipated actual parameters due to the lack of information in some areas. In all cases, the assumed parameters and deviations were jointly agreed to by the Lockheed-California Company and the NASA Manned Spacecraft Center.

CONFIGURATION

The Block I configuration (Spacecraft 012, Reference 1) was assumed for all missions analyzed, even though the manned Lunar Orbit Rendezvous mission utilizes the Block II configuration. The decision to use the Block I configuration for all missions was based primarily on the following factors:

1. At the time the study was initiated, the design details on the Block II configuration were insufficient to perform an analysis in the required detail.
2. The analysis can be updated at a future time to reflect the latest Block II configuration.

It was also felt that differences between the Block I and Block II configurations would have relatively little effect on the overall analytic results, although this has been disproved in certain areas. The primary difference between the two configurations is the relocation of the fuel cells to the upper portion of Bay 4 in the Block II spacecraft. In addition, the cryogenic bottles are situated in Bay 4 instead of Bay 1, and Bay 1 contains additional equipment for Block II. Another difference is the relocation of the Environmental Control System (ECS) and Electrical Power System (EPS) radiator panels. The exact location, size, and performance of the four radiator panels are still not finalized for Block II.

Since the primary purpose of this study was to perform a thermal analysis of the Service Propulsion System (SPS), components which do not affect the thermal performance of the SPS were neglected in the analysis. Thus, the cryogenic storage system in Bay I and the Reaction Control System (RCS) were not analyzed, with the exceptions that the effect of protuberance heating due to the RCS was accounted for in ascent heating calculations and RCS flame impingement was considered. These are the only major components located in the Service Module which were neglected in the analysis.

STRUCTURE

The Service Module (SM) structure is a cylinder 154 in. in diameter and 155 in. long formed by six panels constructed of one inch aluminum honeycomb. The interior area between the forward and aft bulkheads, also made from aluminum honeycomb, is divided unsymmetrically into three pairs of diametrically opposite sectors by six radial beams. Figure 2-1 shows a view of the SM structure with the shell panels removed and a cut-away view showing many of the SM components. The vehicle coordinate system, formed by three mutually perpendicular axes, is shown in Figure 2-2. The X axis coincides with the longitudinal axis of the vehicle, with the positive direction forward. The +Y axis is 27° 15' clockwise (when looking forward) from radial beam 1. The + Z axis (direction of the Comand Module crew's feet) is 12° 45 clockwise from radial beam 3.

Sector One contains the tanks for the cryogenic storage subsystem which supplies oxygen and hydrogen to the ECS and to the EPS. As noted these bottles do not affect the SPS and were therefore not included in the analysis.

Sectors Two and Five contain the oxidizer (nitrogen tetroxide) tanks for the main SPS engine. Each tank is fabricated of 6 AL 4 V titanium, and has a volume of approximately 175 cubic feet. Installation is accomplished by the use of aluminum skirts riveted to the tank and bolted to the aft bulkhead. The forward end of the tank is allowed to slide through a cutout in the forward bulkhead. This "slip joint" arrangement allows for expansion and contraction, and thereby precludes the possibility of SM and tank structural deflections.

Sectors Three and Six contain the fuel (50:50 mixture of UDMH and hydrazine) tanks for the main engine. Each tank has an internal volume of approximately 135 cubic feet. The tank fabrication and installation is similar to that of the oxidizer tanks. The basic dimensions for both the fuel and oxidizer tanks are shown in Figure 2-3.

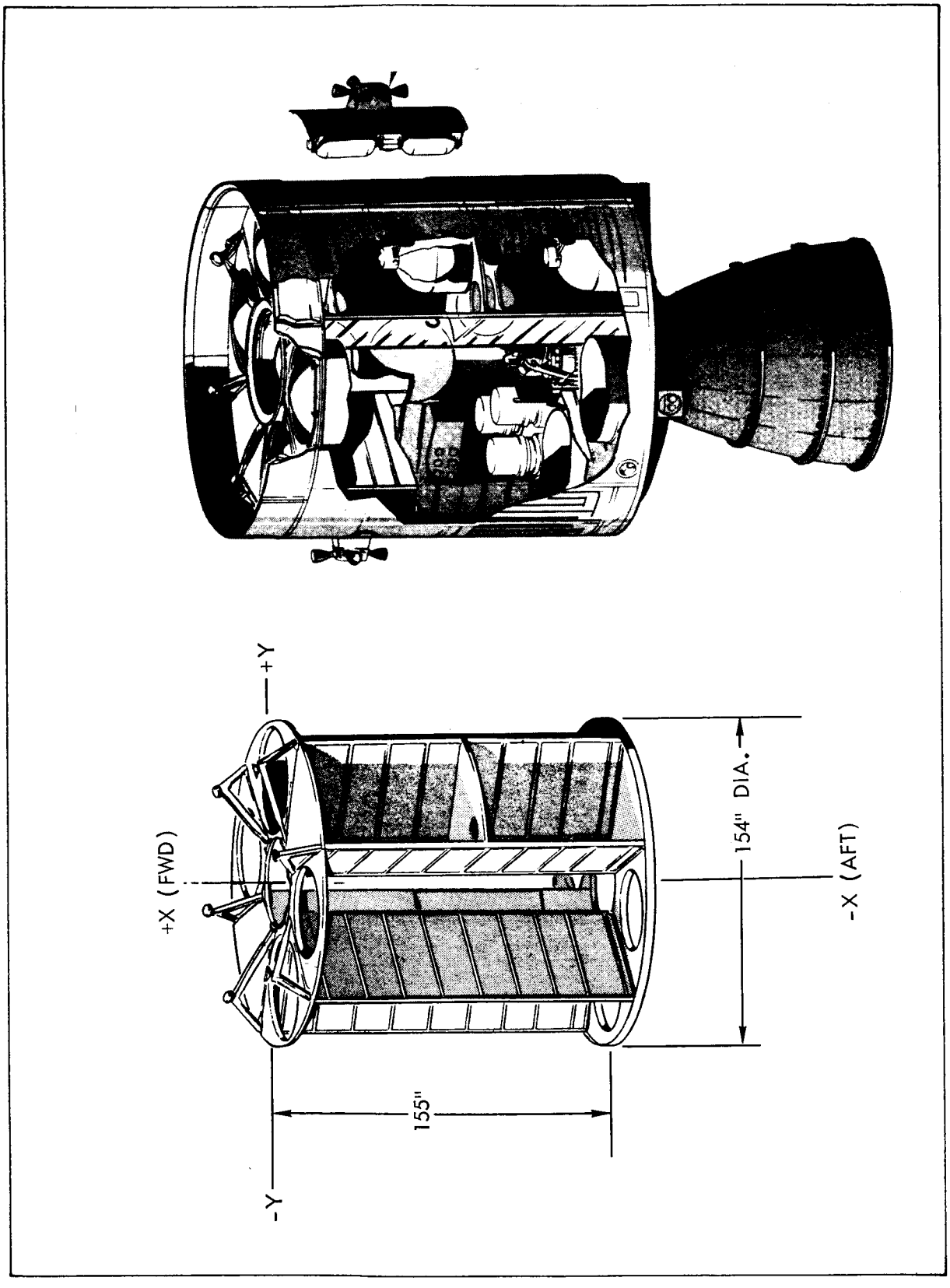

Figure 2-1. Service Module Configuration

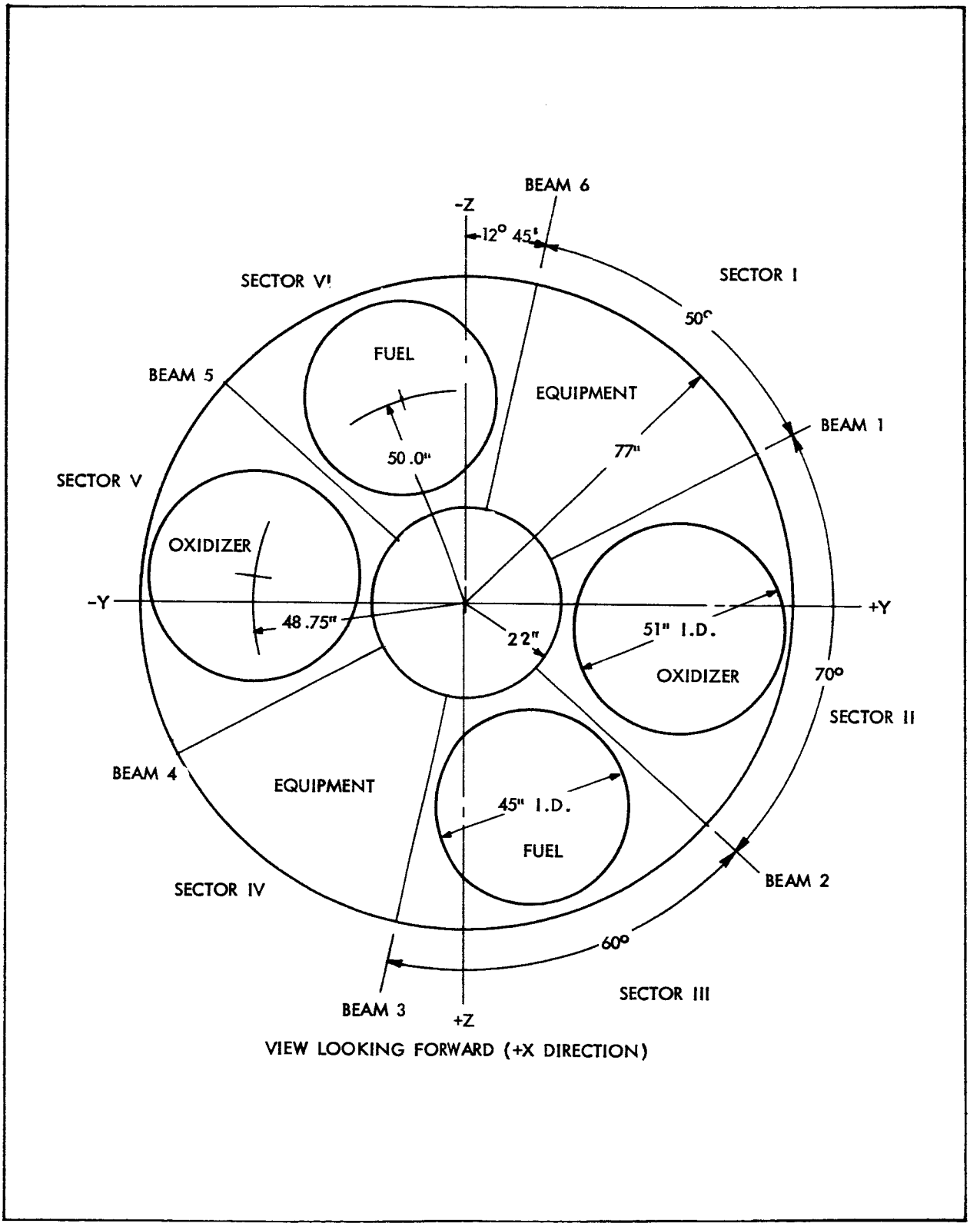

Figure 2-2. Service Module Coordinate System

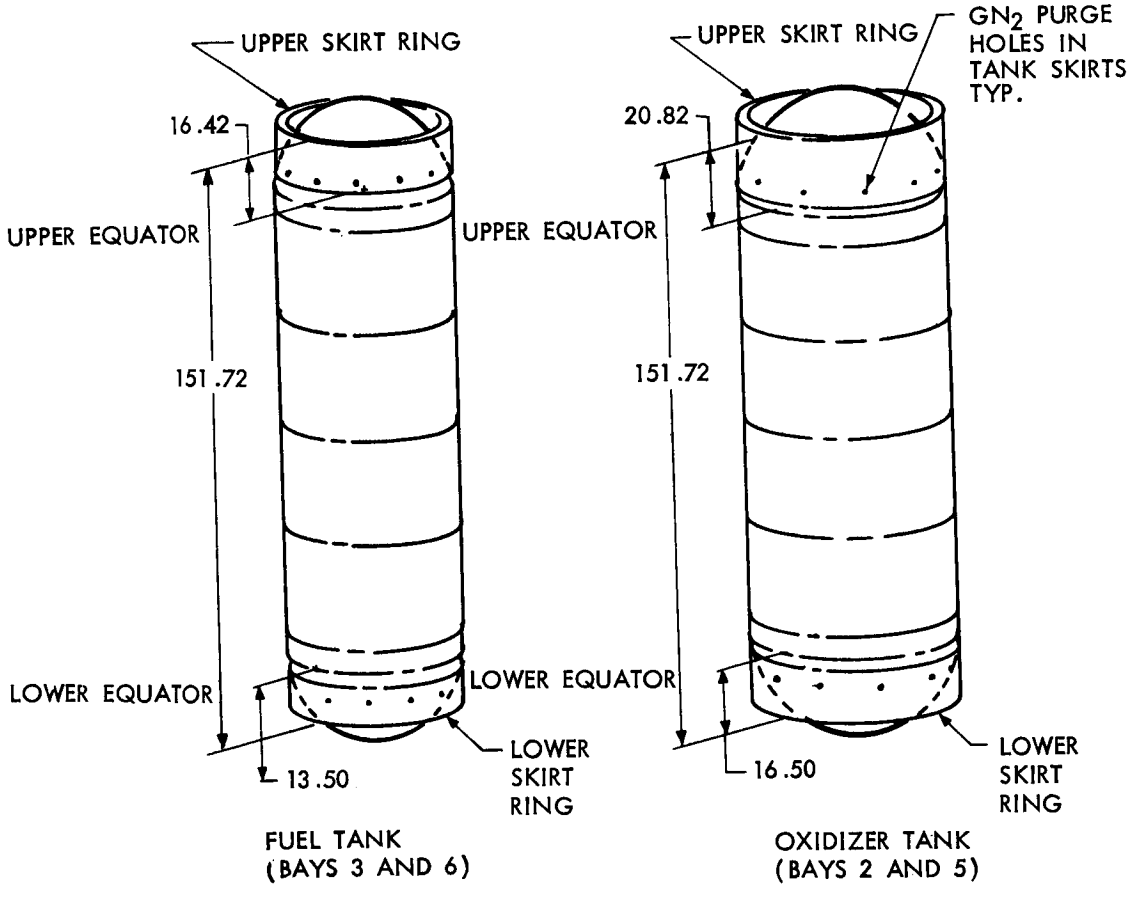

Figure 2-3. Service Module Propellant Tanks

Sector Four (Fig. 2-4) houses the fuel cells for the EPS which generates and distributes the power required of the spacecraft for the mission modes. Each cell is cylindrical, about 44 inches in height, 20 inches in diameter, and weighs 250 pounds without its base. The three fuel cells are mounted within individual bases which are about 24 inches in diameter and 22 inches in height. The cells are bolted to shock mounts attached to bases bolted to the aft bulkhead. Auxiliary EPS equipment includes electrical wiring, hard lines, and the connections needed for the cells' operations and output. The inner cap side of radial beam 4 supports the power control panel and the RCS control unit. Beam 4 holds the helium distribution and test panel.

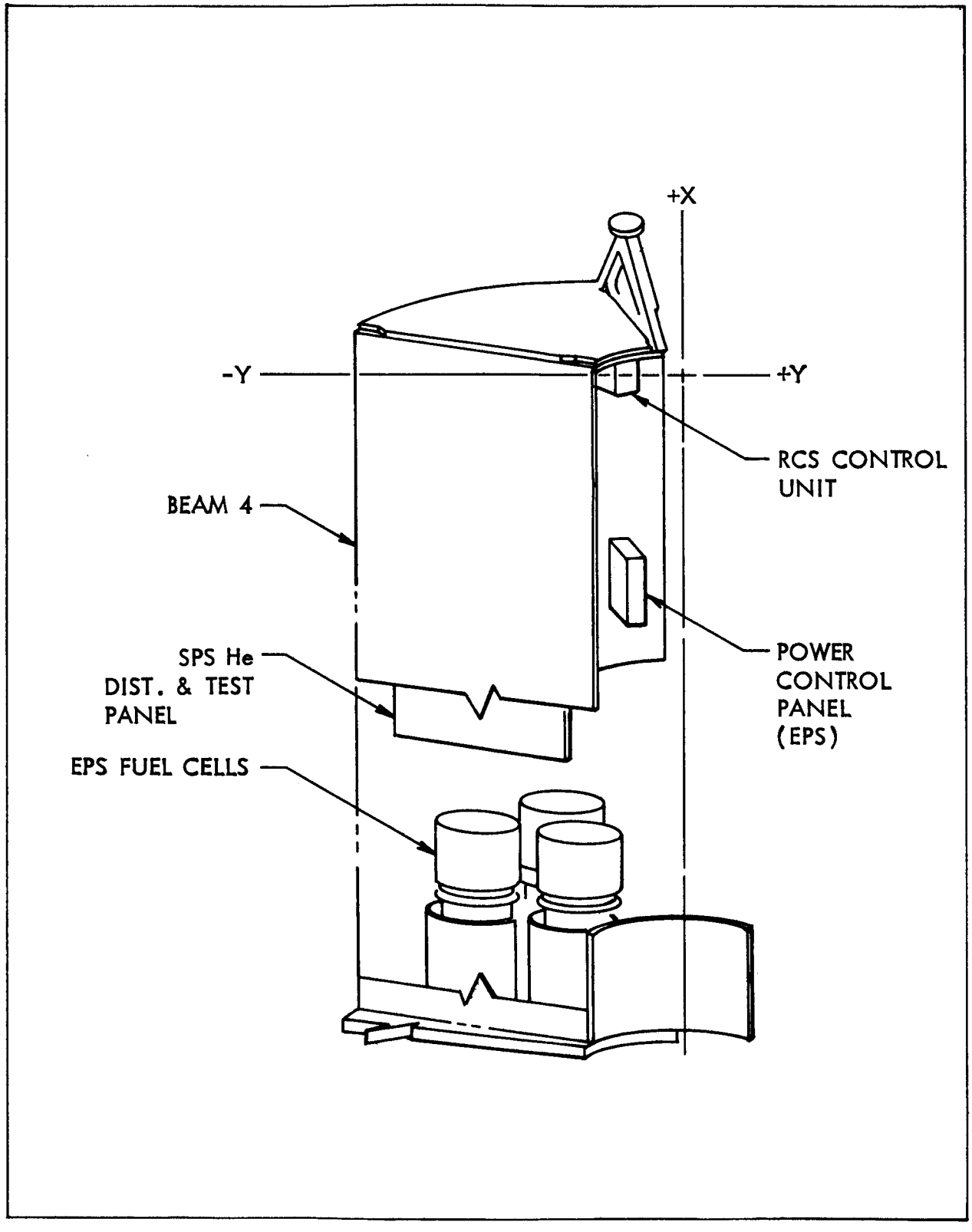

Figure 2-4. Sector Four - Equipment

The center section of the SM houses the SPS engine and two helium pressurization tanks. As shown in Figure 2-5, the center section is 44 inches in diameter and extends the entire length of the SM. The engine and helium tanks are exposed to the six bays except where they are shielded by the engine web mounts and center webs shown in Figure 2-5. Engine web mounts are located in Sectors One, Three, Four and Six and extend from the aft bulkhead (station X_s 200) to station X_s 227. The center webs are located in Sectors One and Four only. The Sector One web extends from the forward bulkhead (station X_s 355) to station X_s 255.5. The Sector Four web extends from the forward bulkhead to station X_s 289.

The main service propulsion engine is attached to the SM at the aft bulkhead, the center line plane of the engine gimbal being approximately 5 in. below the aft bulkhead. Above the engine gimbal, the combustion chamber, hardware, and other equipment extend into the center section. Below the gimbal the engine nozzle extends into the adapter area.

The two large spherical helium tanks, fabricated from 6 AL 4V titanium, pressurize the main propellant tanks. Each helium tank has an outside diameter of 41 inches, a weight of about 390 lb. and a volume capacity of about 19 cubic feet. The helium tanks are suspended by two bosses welded to each tank and resting in housings attached to radial beams 1 and 4. Extensions anchored to radial beams 1 to 6 and 4 to 3 strengthen the housings. These tanks are lowered into place prior to mating the command module to the service module.

The aft heat shield for the service module is located below the aft bulkhead. Its lowest point is approximately 13 in. below the bulkhead. The function of the heat shield is to protect the propellant plumbing lines from the heat of the main engine nozzle. The shield is constructed of fiberglass laminates approximately 0.01 in. thick. In those regions where excessive radiation from the nozzle extension reaches the heat shield,

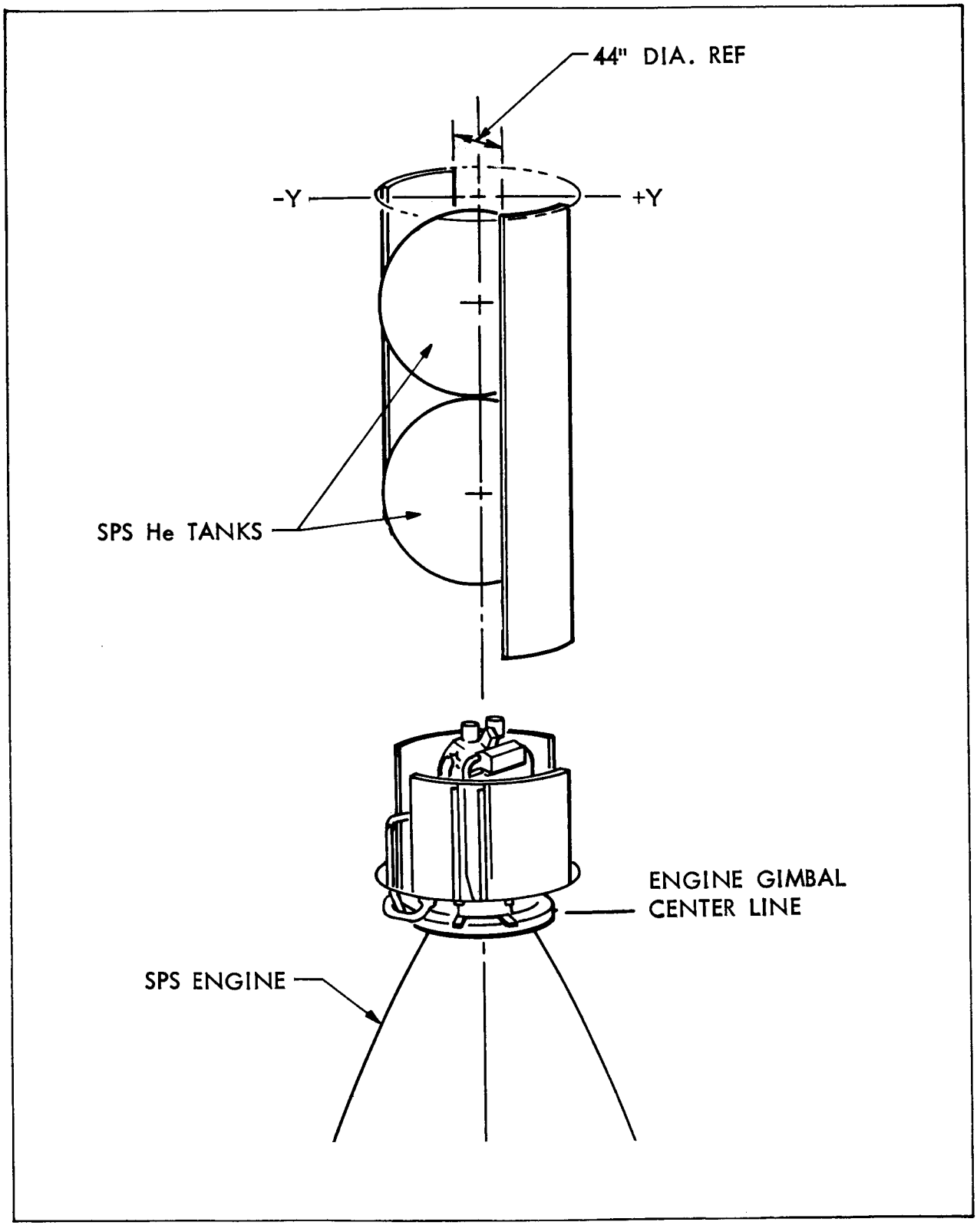

Figure 2-5. Center Section

it is further protected by 0.005 in. thick stainless steel separated from the fiberglass by 0.5 in. of quartz fiber insulation.

SERVICE PROPULSION SYSTEM

The SPS is comprised of an ablative cooled thrust chamber fed by liquid nitrogen titroxide ($N_2 O_4$) oxidizer and a 50:50 mixture of hydrazine and UDMH fuel. Both fuel and oxidizer are forced out of their respective tanks by helium pressurant. The helium tanks empty in parallel, forcing propellant out of one pair of fuel-oxidizer tanks, the storage tanks, into the other pair, the sump tanks. Propellant in the sump tanks then flows to the engine valve assembly and is released as needed for engine firing. A schematic of the SPS is shown in Figure 2-6.

The SPS engine is shown in Figure 2-7. Gimballing of the engine is achieved by the pitch and yaw actuators and the gimbal ring assembly. The gimbal ring is physically attached to the aft bulkhead by structural mounting brackets and to the engine web mounts by cylindrical support arms. These attachments appear on both sides of the engine, along the Z axis. The yaw actuator connects the gimbal ring and a support arm attached to the structural mounting bracket on the -Z axis. The pitch actuator connects the gimbal ring and the injector. The gimbal ring is also connected to the injector by two support arms along the Y axis. The injector and bipropellant valve assembly are located on top of the ablative thrust chamber.

The nozzle extension is constructed of three axial segments. The design used for this analysis consisted of a 0.03 in. columbium segment between area ratios 6 and 20, a 0.02 in. columbium segment between area ratios 20 and 40, and a 0.025 in. titanium segment between area ratios 40 and 62.5

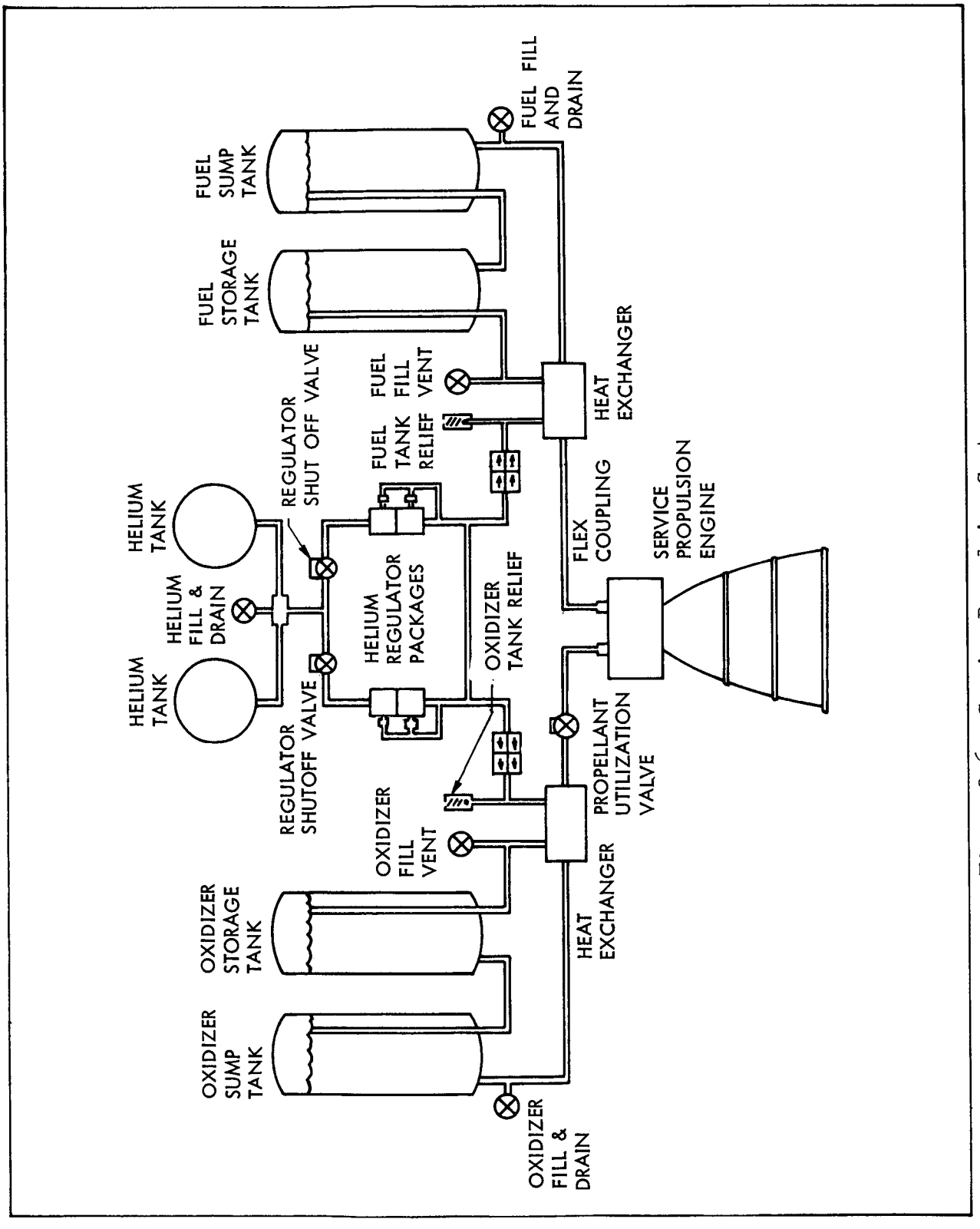

Figure 2-6. Service Propulsion System

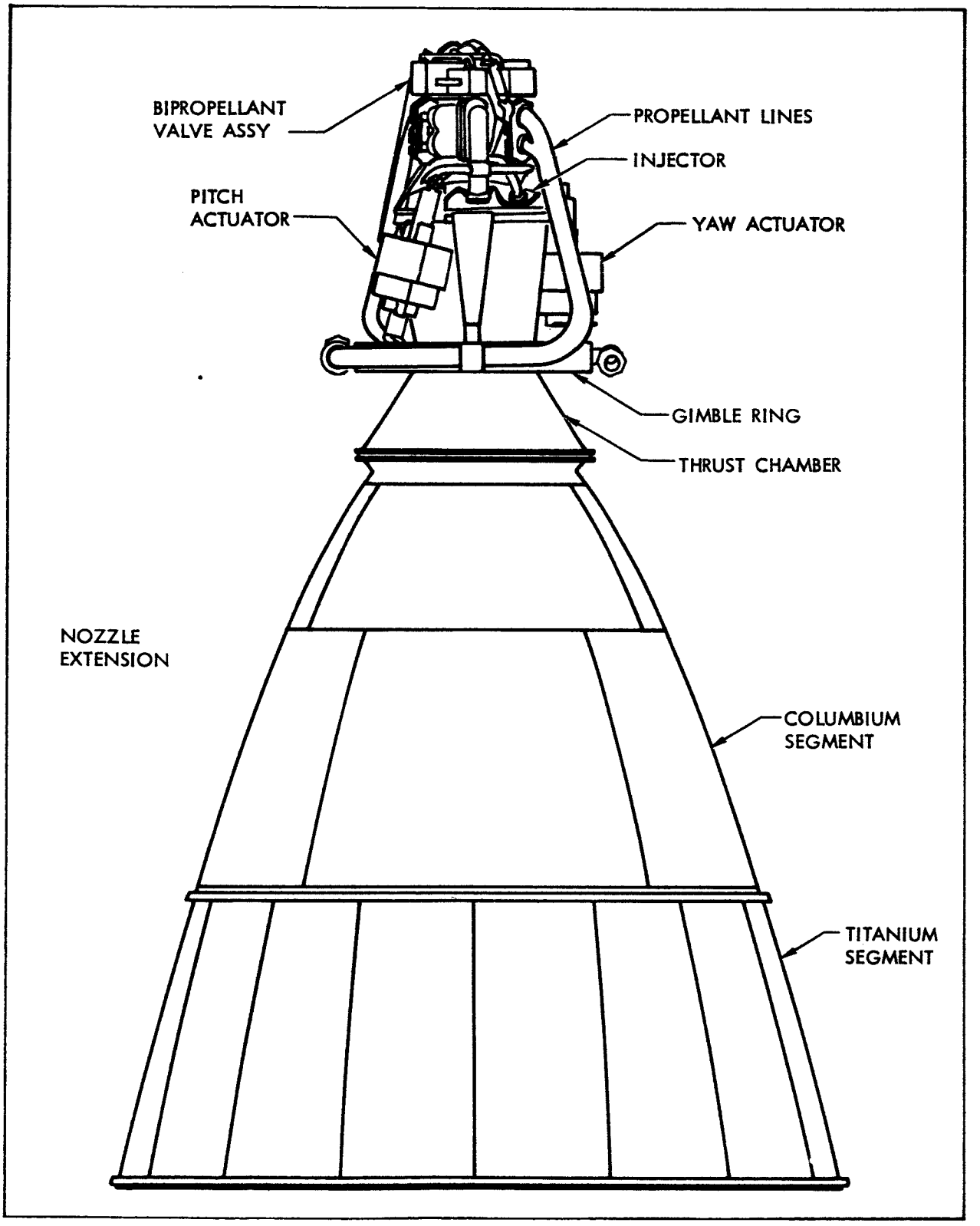

Figure 2-7. Service Propulsion Engine Configuration

INSULATION AND OTHER COMPONENTS

Insulation composed of crinkled, aluminized mylar is used in all sectors of the SM and between the SM and the Command Module (CM). The insulation is designed to maintain the temperature of the on-board propellants within operating limits. Material used for insulation is only 0.0005 in. thick per sheet. The design thickness is 40 layers. Rectangular blankets of 50-in. width are cut to the desired length, sewn together with nylon thread, and then cut to pattern sizes by means of templates. Installation is accomplished by using hollow aluminum support rods, nylon buttons and cords, spring clamps, and also reflecting, pressure-sensitive tape.

Figure 2-8 shows the arrangement of the forward bulkhead insulation and its enclosure by the fairing. The "fireman's net" curtain is made large enough to overlap the hollow aluminum rod which holds it to the top edge of the fairing. The overlap allows length for sewing the ends to the underside of the curtain.

The insulation for each tank may be likened to a shower curtain except for one thing: the insulation curtain is extended to form a collar at each end. The extensions have their ends overlapped at the circular edge, are sewn together, and taped to the tank skirt. The curtain itself is formed from several pieces of aluminized Mylar. The curtain is suspended at the forward and aft edges of the radial beams, the inner face of the outer shell, and the inner web by hollow aluminum rods. The latter rest in spring clamps attached to the structure at inner edge lines. Figure 2-9 illustrates this arrangement.

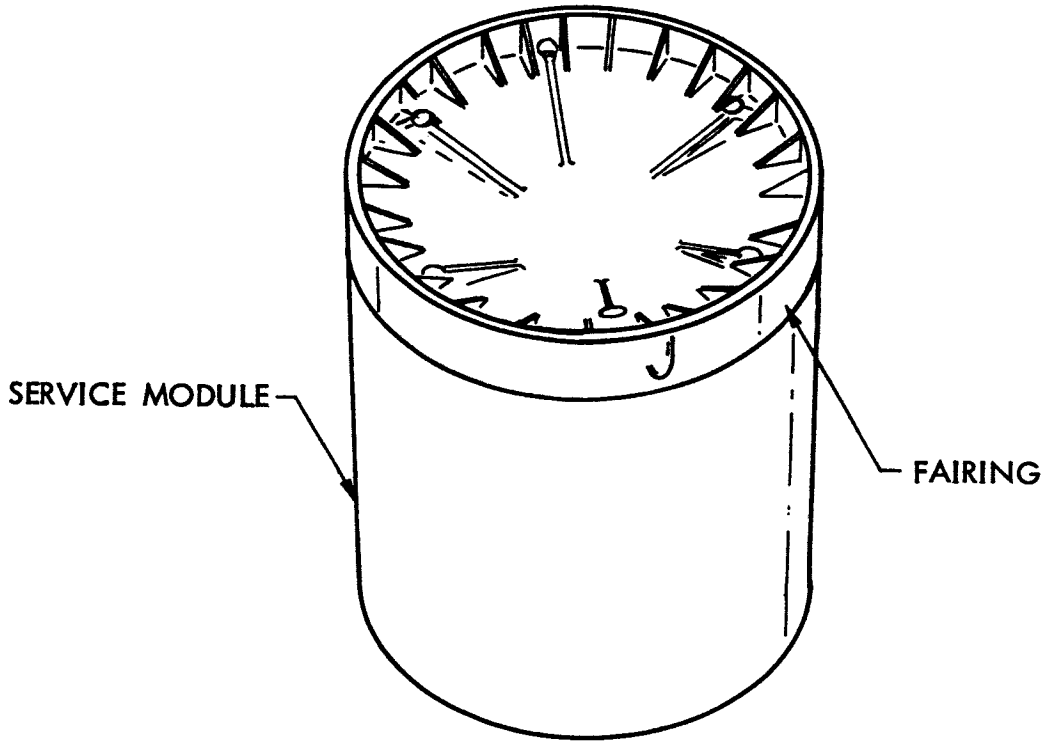

Figure 2-8. Forward Bulkhead Insulation

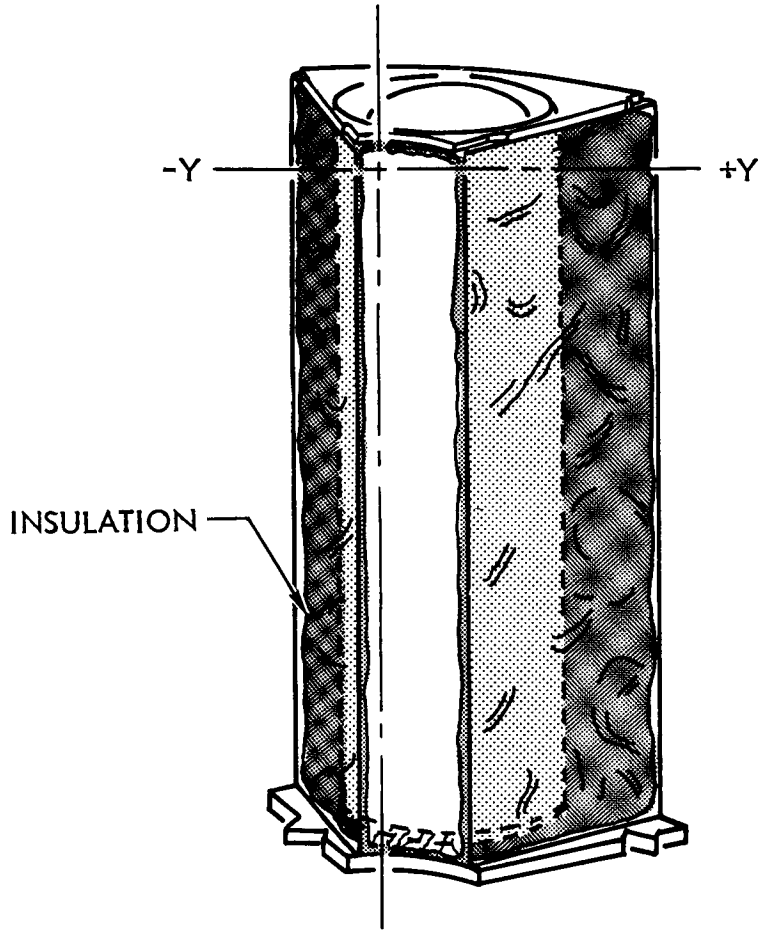

Figure 2-9. Propellant Tank Insulation

Aluminized Mylar insulation of Sector one is accomplished by means of two three-sided "shower-curtain" arrangements. The upper curtain insulates the space occupied by the oxygen and hydrogen cryogenic tanks, while the lower curtain insulates the space occupied by the lower cryogenic tanks. The inner web is not insulated since it has an engine access. Neither the aft surface of the forward bulkhead nor the forward surface of the aft shelf is insulated. Insulation of Sector Four is also accomplished by a three-sided curtain of aluminized Mylar.

The RCS provides three-axis control of the SM during mission flight modes. It consists of four interchangeable and replaceable modular packages which are installed at four different places, as shown in Figure 2-9. Although the RCS modules were not analyzed in this study, their effect on the SM and SPS was included.

Heat shields placed on the outer shell around the engine assembly protect the outer shell from RCS engine flame impingement. These are made of quartz fiber insulation covered by 321 CRES sheets. The insulation thickness varies from 0.18 in. to 0.50 in. depending on the magnitude of the anticipated heat flux.

In four sectors of the outer skin, the panel is partially formed by two radiator systems using water glycol as coolant. The radiator panels of the electrical power system are located aft in Sector One and forward in Sector Four. The radiator panels for the environment control system are located aft in Sectors Two and Five. Along with the SM, fairing, and adaptor, two of the radiator panels are shown in Figure 2-10.

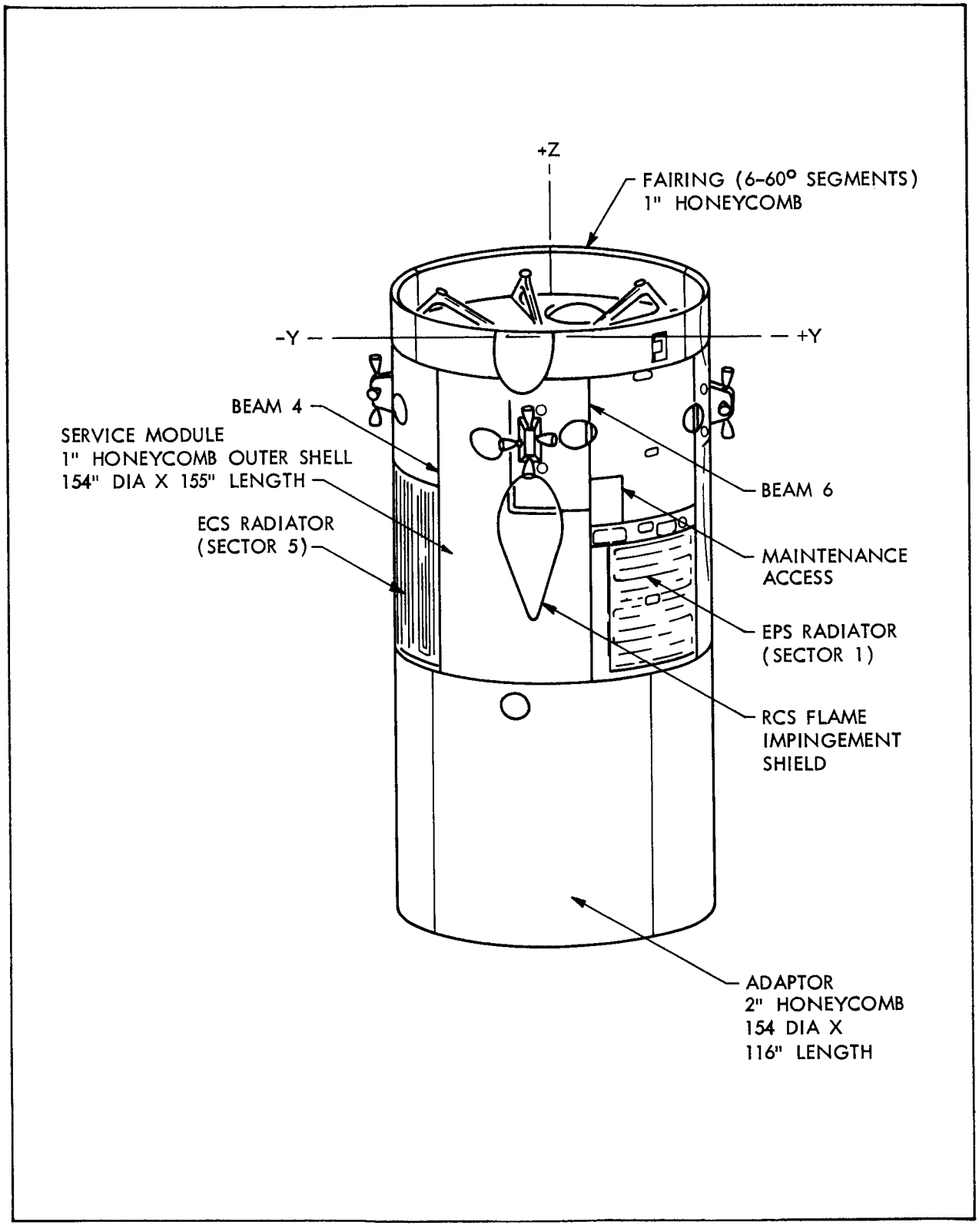

Figure 2-10. Service Module, Fairing, and Adaptor

MISSIONS

Transient heat transfer and thermodynamic analyses of the Service Module were performed for the following missions:

1. The Manned Lunar Orbit Rendezvous Mission
2. The unmanned ballistic Earth Suborbital Mission designated as Mission 201
3. The 14-day manned Earth Orbital Mission

Details of these missions are presented in References 2,3, and 4. Mission parameters important to the analyses performed are summarized in Appendix D. This appendix, classified Confidential, is bound separately.

MATERIAL PROPERTIES AND BOUNDARY CONDITIONS

Besides the basic selection of a configuration and mission for the analysis, several other ground rules had to be established before analysis could be performed. The first of these is the selection of material properties. A list of those properties which were supplied by MSC is given in Table 2-1. Appendix A contains a complete listing of the thermal properties used in the analysis, with the exception of fluid properties which are a part of the material properties library presented in Reference 8.

Boundary conditions provide another group of ground rules. These include temperatures and heating rates which were impressed on the thermal network. Several of these differ with each mission. For all missions the following ground rules hold:

Table 2-1 Material Properties Data Provided by MSC

Component	Properties				
	α_s	ϵ	K $\left(\frac{\text{Btu}}{\text{hr ft}^{\circ}\text{F}}\right)$	C_p $\left(\frac{\text{Btu}}{\text{lb}^{\circ}\text{R}}\right)$	ρ $\left(\frac{\text{lb}}{\text{in}^3}\right)$
Honeycomb Shell External Surface	0.548	0.548	---	---	---
All Internal Surfaces	---	0.25	---	---	---
Coated Columbium Nozzle	---	0.85	---	---	---
Coated Titanium Nozzle	---	0.90	---	---	---
Uncoated Titanium Nozzle	---	0.30	---	---	---
Thrust Chamber-Virgin Material	---	---	0.086	0.30	0.052
Thrust Chamber-Charred Material	---	0.7	0.260	0.30	0.035
Fuel Cells	---	0.3	---	---	---

1) The command module is a 70°F constant temperature heat sink
2) All structure and propellant temperatures are 70°F at lift-off

Fuel cell operation depends on the particular mission. For the Earth Sub-orbital Mission the fuel cells are not in operation. For the Earth Orbital and Lunar Orbital Rendezvous Missions the fuel cells start operating at lift-off, and collectively dissipate by radiation to the surroundings a constant heat rate of 750 Btu/hr for the entire mission.

The temperature distributions over the four radiator panels were not computed but rather were assumed to be known boundary conditions, using preliminary data provided by MSC. The EPS radiator data consisted of steady state temperature distributions over the radiator at the Earth subsolar point, and at a point in the Earth's shadow. In lieu of additional data, a sinusoidal temperature variation between these extremes was assumed, using a period of 88.3 min for Earth orbit, 122 min for Lunar orbit, and 30 min for the translunar and transearth roll. The temperature extremes for the EPS radiator nodes are shown in Figure 2-11.

The ECS data included cyclic temperature distributions at each of three longitudinal stations during Earth and lunar orbits, and constant average temperature values at the same locations during the translunar and transearth roll. These data are shown in Figures 2-12 through 2-14. The location of the radiator nodes referred to on the figures is shown in Figure 4-1 of section IV.

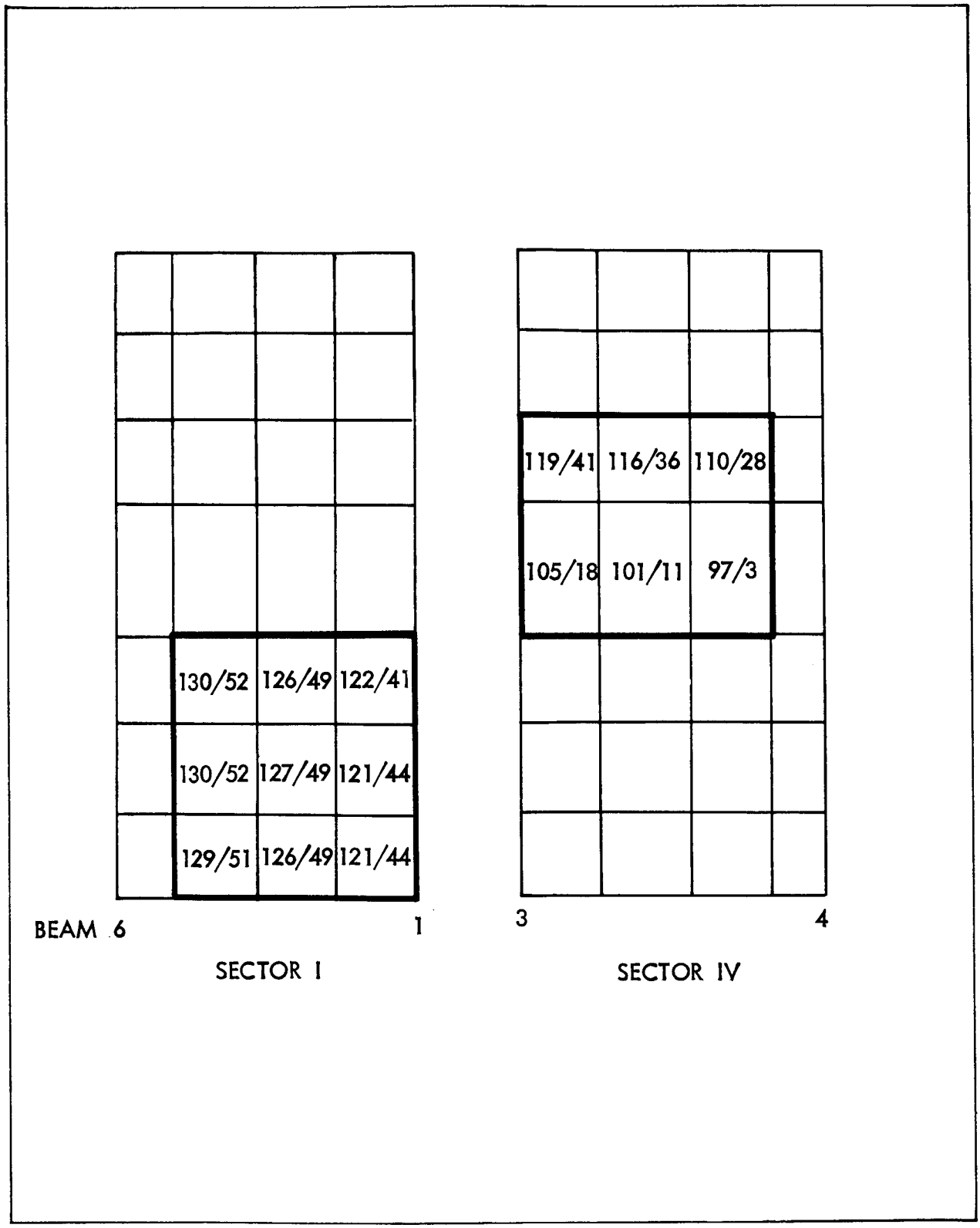

Figure 2-11. Temperature Extremes for EPS Radiator Nodes During Earth Orbit

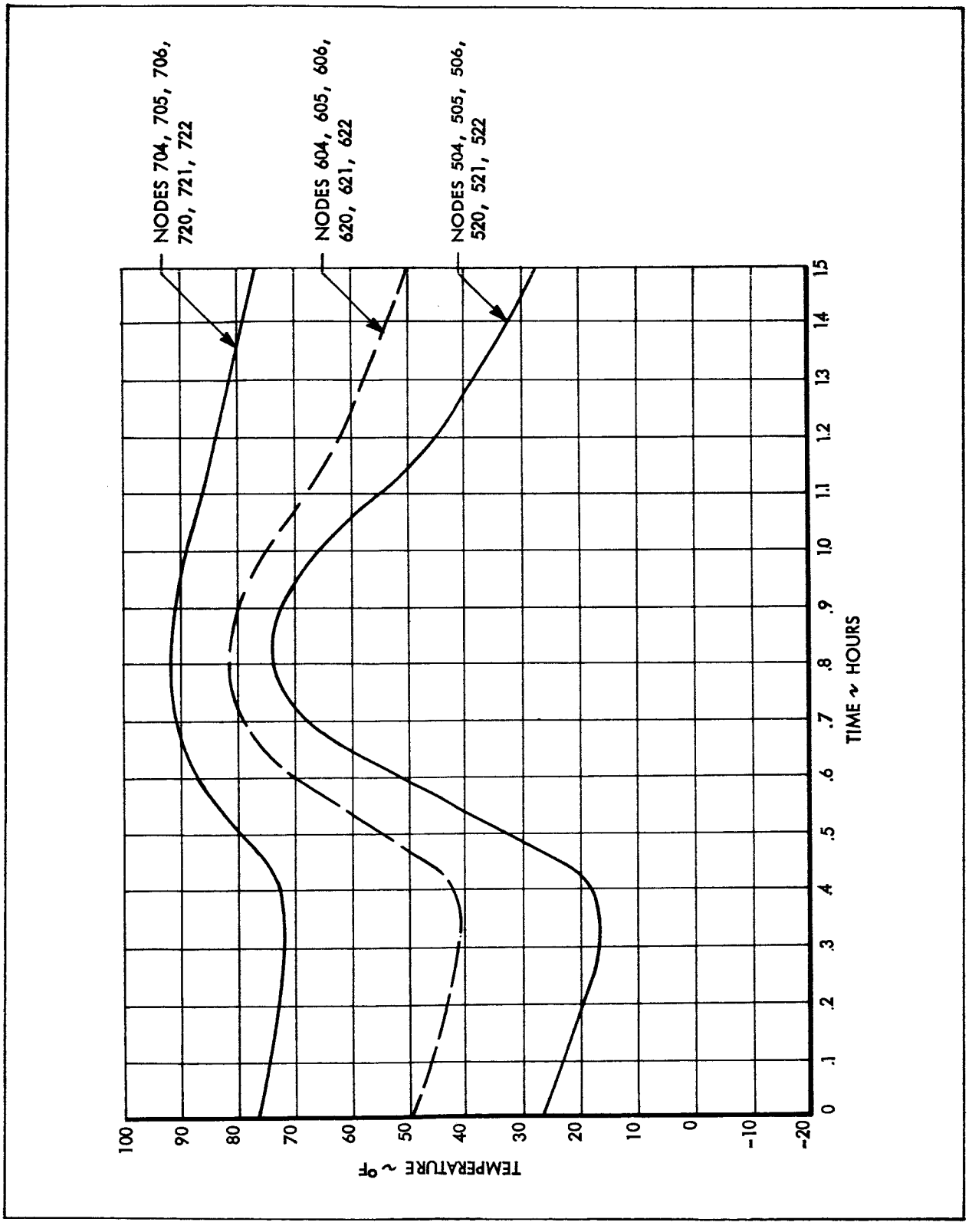

Figure 2-12. Temperature Histories for ECS Radiator Nodes During Earth Orbit

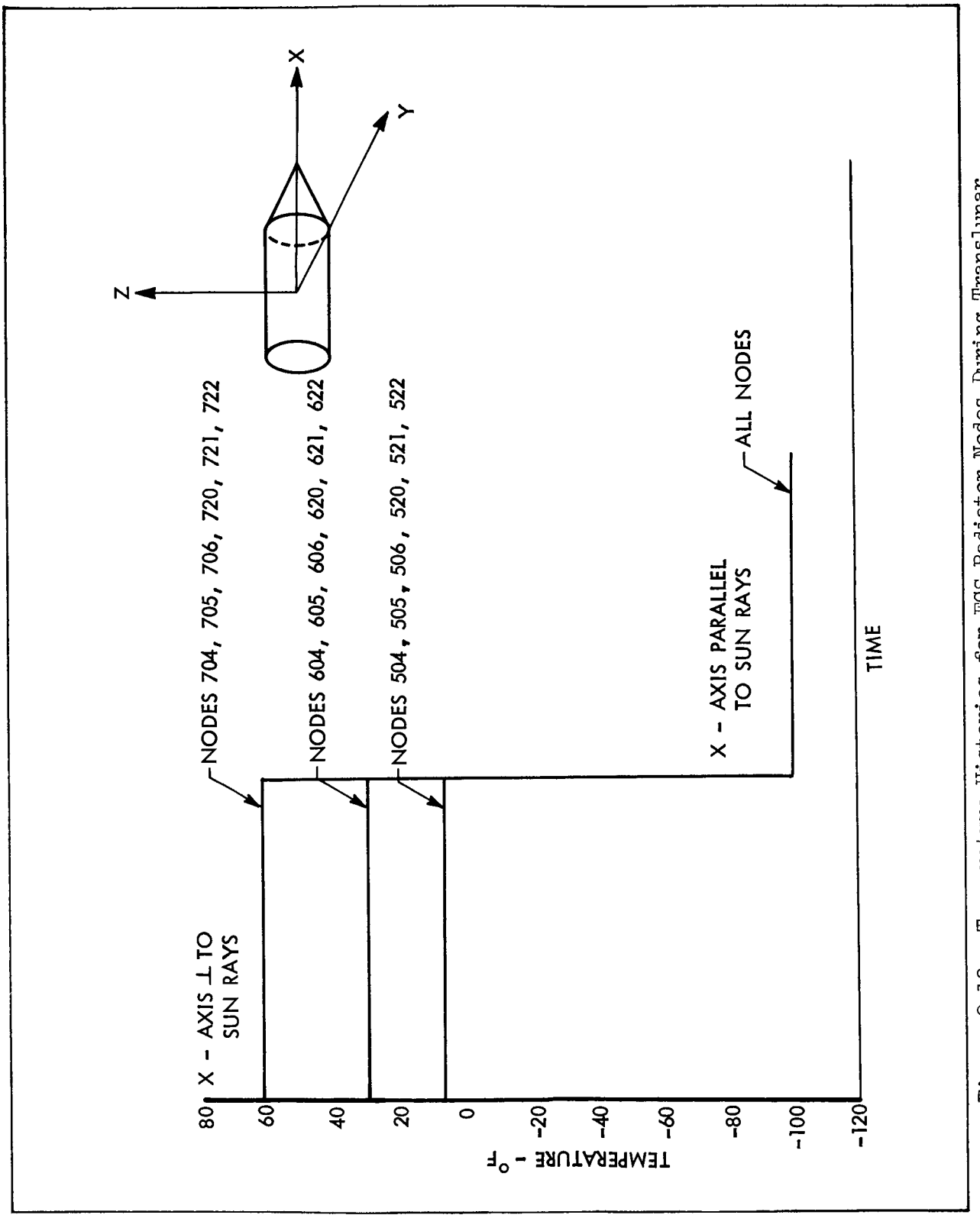

Figure 2-13. Temperature Histories for ECS Radiator Nodes During Translunar and Transearth Phases

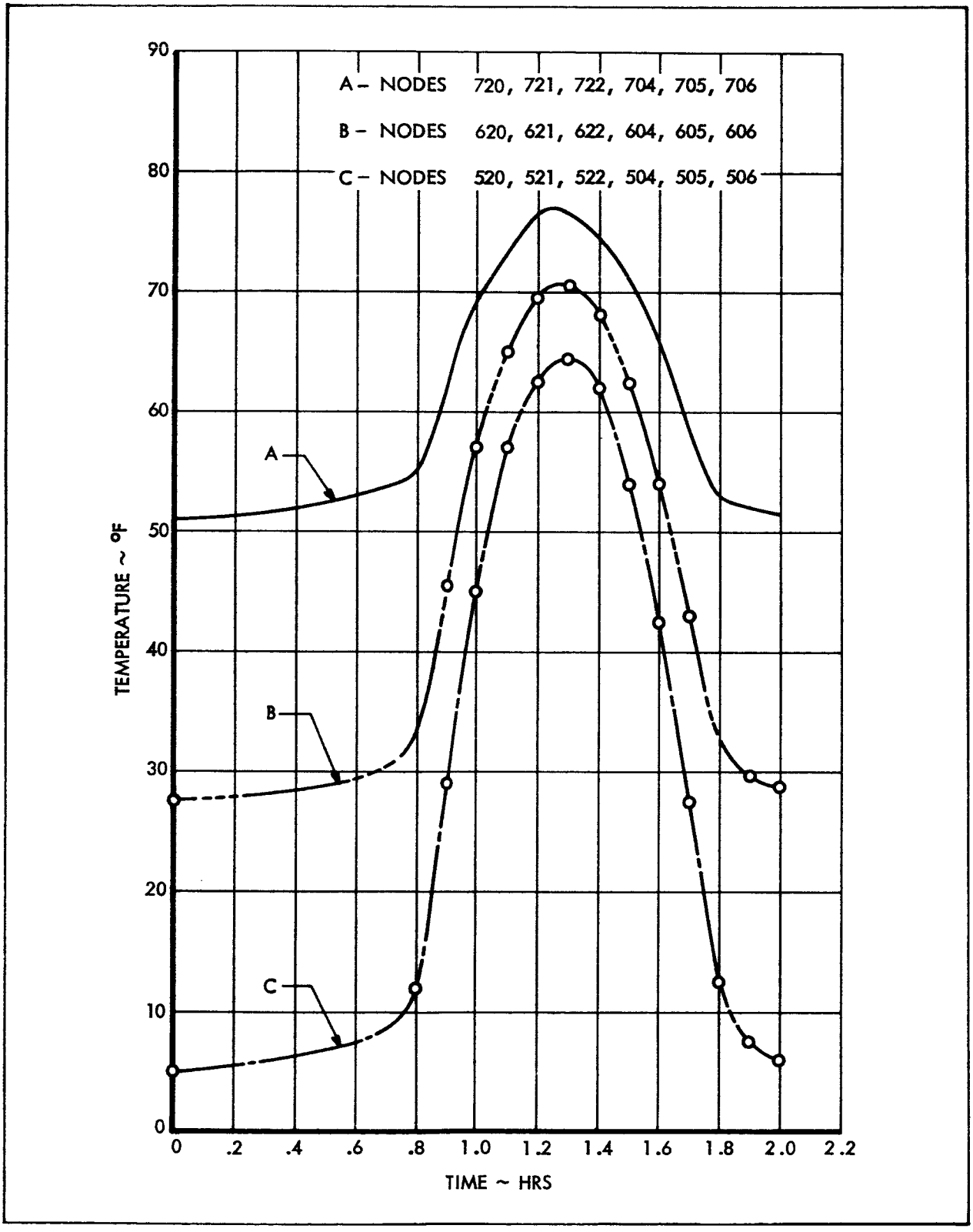

Figure 2-14. Temperature Histories for ECS Radiator Nodes During Lunar Orbit

Propellant loading also varies for each mission. Earth Suborbital propellant loading is 14,000 lb of oxidizer and 7000 lb of fuel, which provided 20% excess burn capacity. Helium loading for this mission amounts to 52 lb. Only 5700 lb of oxidizer, 2850 lb of fuel, and 30 lb of helium are required for the Earth Orbital Mission because of the relatively short total SPS burn time. The Lunar Orbit Rendezvous Mission requires a total of 45,000 lb of propellant, with a two-to-one oxidizer to fuel weight ratio. This includes a 25% reserve in propellant, and requires 95.4 lb of helium for pressurization.

SPS COMPONENT TEMPERATURE LIMITS

A major objective of this study was to verify the adequacy of the SPS thermal design. In order to do this, it is first necessary to obtain the temperature limits of the various SPS components and, if possible, the bases for them. Table 2-2 presents temperature limits for the major SPS components along with their respective criteria. The temperature limits of smaller components such as couplings, connectors, valves, etc, are listed in Table 2-3. All of these data were provided by MSC.

Table 2-2 Temperature Limits of Major SPS Components

SPS COMPONENT	MIN TEMP	CRITERION	MAX TEMP	CRITERION
Injector Valve	40°F	Propellant freezing and Fuel Separation	135°F	Upper propellant temperature for normal engine operating conditions
Gimbal Actuator	-10°F	Bearing lubricant and friction drag	140°F	Actuator electric motor overheating if started above 140°F
Gimbal Bearings	-10°F	Bearing lubricant	200°F	Differential thermal expansion and associated loads
Ablative Chamber		No established lower limit	140°F	Backwall limit prior to adverse firing sequence when backwall temperature rise is 350°F
Propellant Feed Lines	40°F	Propellant freezing and fuel separation	135°F	Upper propellant temperature for normal engine operating conditions
Disconnect	40°F	Propellant freezing	140°F	Prevent fuel vaporization in actuator dump line which would affect valve response and repeatability.

Table 2-2 (Continued)

SPS COMPONENT	MIN TEMP	CRITERION	MAX TEMP	CRITERION
S/M SPS Check Valves on Pressurization Components Panel	40°F	Prevent propellant freezing during non-flowing conditions.	100°F	Seal material limit in check valve; Propellant vapor leakage is critical at this point.
S/M SPS Propellant Tank Contents (Propellant ullage gas)	40°F Prior to 80% propellant depletion	Propellant freezing	80°F	Limit based on fully loaded propellant tank conditions, max full tank ullage pressure is 175 psia due to propellant volume growth and ullage pressure increase; Burst disk rupture pressure is 220 ± 7 psi. Ullage pressure can go to 205 psi.
	50°F at 80% propellant depletion	Maintain ullage pressure with available helium supply.	80°F	Temperature can be increased during propellant utilization. A weight of 2 1/2 lb/°F due to residual vaporized propellants in the tanks.
Helium Tanks (Non-flowing periods)	50°F	Limit based on deliverable helium capacity. Initially required for possible abort, and near depletion for normal utilization. Temperatures after blow down starting below 50°F would exceed materials and seals lower limit. Helium gas in bottle may reach -120°F starting from 50°F.	80°F	During utilization, limit based on solenoid, regulator and check valve upper temperature limit considering Joule-Thompson heating effects. Initial throttling from 80°F brings gas in vicinity of components to 110°F.

Table 2-2 (Continued)

SPS COMPONENT	MIN TEMP	CRITERION	MAX TEMP	CRITERION
Helium Tanks (Non-flowing periods)	40°F	This limit applies after abort possibility is passed and up to 80% propellant depletion. After 80% depletion 50°F is required again.		

Table 2-3 Temperature Limits of Miscellaneous SPS Components

SPEC	ITEM	MIN TEMP °F	MAX TEMP °F
MC273-0009	Coupling, Helium Tank, Fill Drain	-150 40	80 80
MC144-0023	Coupling, System Test Point Disconnect	30	150
MC273-0012B	Coupling, Propellant-SPS-Disconnect	40	140
MC273-0018	Coupling, N_2O_4 Tank, Fill & Drain	-65	160
MC273-0020	Coupling, Hyd/UDMH Tank, Fill Vent Disconnect	-65	160
MC273-0022	Coupling, N_2O_4 Tank, Fill Vent Disconnect	-65	160
MC273-0039	Connector, Flexible, Prop. Sys., Fuel Helium	40 -150	80 80
MC273-0040	Connector, Flexible, Prop. Sys., N_2O_4 Helium	40 -150	80 80
MC284-0018	Valve, Solenoid, Helium, 5/8 inch Fluid	30 -90	150 80
MC284-0020	Regulator Unit-Pressure, Helium SPS Fluid	30 -90	150 80
MC284-0027	Valve-Relief, Pressure, Helium SPS	40	120
MC362-0007	Heat Exchanger N_2O_4 - Helium AMB N_2O_4 Helium	30 40 -140	150 80 80

Table 2-3 (Continued)

SPEC	ITEM		MIN TEMP °F	MAX TEMP °F
MC362-0008	Heat Exchanger, Fuel-Helium	AMB	30	150
		N_2O_4	40	80
		Helium	-140	80
MC901-0008A	Prop Qnty Ind & Mixture Ratio Control		40	80
		N_2	50	140

III - METHOD OF APPROACH

The Phase I study of the Apollo Service Module was a thermal design audit of a vehicle whose design was assumed to be completely defined. This type of analysis requires detailed knowledge of the vehicle mission; equipment location and mountings; and gauges, thermal properties, surface finishes, and dimensions of all of the vehicle structure. The analysis which was performed was the most accurate thermal appraisal possible within the limitations of computer technology, computer storage, and the design details known.

The study was primarily concerned with transient temperature histories of the Service Module Propulsion System. System temperatures result from the thermal balance existing between the Service Module and its surroundings. The thermal balance is influenced by vehicle configuration, structure thermal properties and surface finishes, radiation configuration factors between components and their surroundings, and all internal and external heat inputs to the system.

The detailed steps through which the analysis progressed are listed below:

1. The external heat inputs, ascent heating, and orbital radiation were computed.
2. The physical system was converted into a form amenable to computer solution.
3. Transient temperature analyses of the SM were performed for the Lunar Orbital Rendezvous Mission, and the Earth Suborbital and Orbital Missions, accounting for conduction and radiation between all components which exchange significant thermal energy. It was assumed that the SPS temperatures would not significantly effect these analyses, so that the SPS environment was reasonably well established.
4. Detailed analyses of the SPS engine, propellant lines, and pressurant lines were performed separately from the basic analysis, utilizing the basic analysis results as boundary conditions. The analyses were made for the Lunar Orbit Rendezvous and Earth Orbital Missions.

5. A separate detailed analysis of the propellant and pressurant systems was performed for the Lunar Orbit Rendezvous Mission.

The analyses of the engine, plumbing, and propellant/pressurant systems were conducted separately due to computer storage capacity restrictions. The thermal network for the basic analysis was so large that the storage capacity (16000 locations) of the Thermal Analyzer Program was exceeded, and re-programming was required to perform the analysis. Another reason for separating the analyses was the complexity involved in attempting to describe in one program the thermal networks, vehicle orientations, engine firings, propellant flow rates, impressed temperatures, and all of the other details that affect the thermal behaviour of the Service Module.

BASIC SERVICE MODULE ANALYSIS

Ascent heating analyses were performed for both a Saturn I and a Saturn V launch. Orbital heating analyses were performed for the Earth and lunar orbits, the near Earth and near moon mission phases, and the translunar and transearth mission phases.

The next step in the analysis was the generation of a thermal network to represent the entire Service Module, with the exception of the cryogenic storage system and the RCS, which were not analyzed. The purpose of this network was to perform a transient temperature analysis of the vehicle during the Lunar Orbit Rendezvous Mission and the Earth Suborbital and Orbital Missions. These analyses were performed using the Thermal Analyzer Program (Reference 5). This program was developed by the Lockheed-California Company in order to obtain detailed transient temperature distributions in complex three-dimensional structures. The program makes use of the electrical resistance-capacitance analogy. Solution is effected by converting the physical system into one consisting of lumped thermal capacities connected by thermal resistors, and using the finite-difference approach to solve for the temperatures.

The program permits direct solution of complex transient problems involving conduction, convection, radiation and heat storage. Furthermore, since it is possible to specify any quantity as an arbitrary function of any other,

such problems as change of state, variable thermodynamic properties, arbitrary variable boundary conditions, and other nonlinear effects can be solved.

The Thermal Analyzer has the ability to accept various subroutines, or functions, as required by the particular problem. The program also accepts standard FORTRAN statements, allowing the user to add his own subroutines as required.

The finite difference, lumped-parameter system utilizes standard network analysis equations. The heat flow q across resistor R connecting two points at temperatures T_j and T_k is given by the following equation (analogous to Ohm's electrical law):

$$q = \frac{T_j - T_k}{R}$$

At a given node point k connected to several other nodes j by resistors R_j, the solution is effected by applying Kirchoff's law at a point, or

$$\sum_j{}' \frac{T_{j,\theta} - T_{k,\theta}}{R_j} + Q_k = C_k \frac{dT_k}{d\theta} \qquad (3\text{-}1)$$

where

$T_{j,\theta}$ = Temperature at time θ of any arbitrary node j connected to node k by a resistor R_j

R_j = Resistor connecting nodes j and k

$T_{k,\theta}$ = Temperature of node k at time θ

$T_{k,\theta+\Delta\theta}$ = Temperature of node k after time increment $\Delta\theta$

C_k = Capacity of node k

Q_k = Arbitrary heat input into node k (can be positive or negative)

If it is assumed that the surrounding temperatures T_j remain constant over a time interval $\Delta\theta$, Equation 3-1 can be integrated directly. However, when the same problem was run with different energy balance equations, it was found that a linearized form of Equation 3-1 produced results which were less sensitive to $\Delta\theta$ and therefore more stable than those obtained with the inte-

grated equation. The linearized equation is obtained by making the following assumption:

$$\frac{dT_k}{d\theta} = \frac{T_{k,\theta+\Delta\theta} - T_{k,\theta}}{\Delta\theta} \tag{3-2}$$

and by solving Equation 3-1 directly to obtain the following expression:

$$T_{k,\theta+\Delta\theta} = \frac{\Delta\theta}{C_k}\left[\sum_j \frac{T_{j,\theta} - T_{k,\theta}}{R_j} + Q_k\right] + T_{k,\theta} \tag{3-3}$$

If $C_k = 0$, e.g., in a steady-state case, $T_{k,\theta}$ in Equation 3-1 is replaced with $T_{k,\theta+\Delta\theta}$ to give

$$T_{k,\theta+\Delta\theta} = \frac{\sum_j \frac{T_{j,\theta}}{R_j} + Q_k}{\sum_j 1/R_j} \tag{3-4}$$

If no capacitor is specified for node k, no heat balance is taken, and T_k remains unchanged. Two blocks of temperature values are maintained, one for time θ and one for time $\theta + \Delta\theta$. At the end of each time cycle, the temperatures at time $\theta + \Delta\theta$ are moved into the block for temperature at θ.

Using the Thermal Analyzer Program, it was possible to obtain the temperature distributions throughout the SM during the missions, and thereby determine the thermal environment for the SPS engine and plumbing lines, and the fluid storage and pressurization system analyses. The engine, propellant tanks, and pressurization system were represented in a rather coarse fashion in the basic network. An attempt was made to account for all modes of significant heat transfer in the basic network although the highly reflective internal surfaces and the unknowns regarding the heat transfer through the aluminized Mylar insulation necessitated considerable simplification. In general, the radiation network considered only direct radiation between components, and did not consider interreflections. The aluminized Mylar insulation was treated as a radiation barrier, with the effective emissivity given by a correlation of the manufacturers test data. Until the distance between layers is sufficient that conduction is negligible, the effective emissivity

is very sensitive to the spacing. For most practical applications the heat transfer is approximately proportional to $D^{0.84}$, where D is the number of layers per inch. A density of 160 layers per inch was assumed, as specified by MSC. The predicted heat transfer through the insulation is therefore probably conservative, since a less dense spacing will probably result under zero gravity operation.

Besides the ascent and orbital heat inputs, other boundary conditions for the basic analysis were as follows:

- The CM heat shield temperature was specified as $70^{\circ}F$.
- The temperature histories of all radiator nodes were specified, using MSC supplied data.
- The temperature history of the thrust chamber surface was specified, using MSC supplied data.
- During engine firings, the temperature of the nozzle extension was specified, using MSC supplied data.
- The total fuel cell heat rejection to the interior of the SM was 750 Btu/hr. (The fuel cells were inoperative during the Sub-orbital Mission)

Once the network had been generated and boundary inputs specified, the transient temperature analyses of the basic SM were performed for the three missions.

SPS PLUMBING AND ENGINE ANALYSES

The SPS plumbing and engine analyses were performed only for the Lunar and Earth Orbital Missions. No problems should arise during the brief Sub-orbital Mission if the thermal performance is satisfactory during the other two, since a heavily insulated system was being analyzed. A thermal network was generated to represent the SPS engine and all propellant and pressurant lines which are part of the SPS. The network included both disconnect panels on the aft bulkhead. The temperature histories of the aft bulkhead, radial beam 4, fuel cells, etc., were obtained from the basic analysis and used as boundary conditions to the plumbing/engine analysis. The entire SPS thermal environment was specified by the temperature histories of approximately 45 nodes from the basic analysis. The plumbing/engine thermal analyses were then performed again using the Thermal Analyzer Program. At the end of each SPS engine firing, the temperatures of all helium and propellant

lines through which fluid flowed were set equal to the temperature of the fluid remaining in the appropriate reservoir. Also during engine firing and for a short period thereafter, the temperature histories of the thrust chamber nodes were specified, using MSC supplied data.

FLUID STORAGE AND PRESSURIZATION SYSTEM ANALYSIS

A detailed analysis of the fluid storage and pressurization system was performed for the Lunar Orbit Rendezvous Mission, using the Fluid Storage and Pressurization Program (Reference 6). The thermal environment was specified by the temperatures of the surrounding beams, shell, bulkheads, etc., obtained from the basic analysis. Pressurant requirements were determined mainly by the propellant usage requirements, although the thermal conditions within the tank, the volatility of the liquids, and the conditions within the pressurant bottle are influencing factors, and were all accounted for.

The Fluid Storage and Pressurization Program is built around the Thermal Analyzer Program, and handles such problems as interphase heat and mass transfer, expulsion and replenishment of fluids, effects of low gravity forces, radiation interchange between the tank wall and the liquid surface, and conditions within the pressurant bottle. A thermal resistance-capacitance analog network is generated for each propellant tank by the program, but the user must specify the network describing the tank external thermal environment.

Initial conditions of the system are used to compute the initial resistor and capacitor values. Updating of the network elements is done whenever either of the following occur from the previous element update:

1) The average liquid or gas temperature changes more than two degrees
2) The total tank pressure changes more than two psi.
3) The magnitude of the gravity vector changes (gravity to a non-gravity condition).

This is done as a computer timesaving device to prevent excessive calling of subroutine RECALC. Items 1) and 2) are tolerances on thermal properties, smaller changes than these are assumed to have a negligible effect.

During engine firing, liquid is drained from the tanks and the tank pressure falls due to the expanded gas volume. Helium enters the ullage

space to raise the pressure up to the minimum set by the pressure regulator. Interphase mass transfer takes place mainly during liquid expulsion when liquid evaporates in order to maintain its partial pressure in the ullage space. Condensation can occur when the average gas space temperature falls below the average liquid temperature. On Apollo, this is a minor effect.

The program computes the effects of the various thermodynamic processes by mass and energy balances. These effects are then combined with heat transfer through the thermal network, and then the entire system is balanced by the Thermal Analyzer. The frequency of computations is determined by the minimum R-C product except during the firing periods when a much smaller time step (2 seconds) is used.

EXTERNAL HEAT SOURCES

Ascent Heating

The shell ascent heating rates were computed by the Eckert Aerodynamic Heating Subroutine of the Thermal Analyzer Program (Reference 5). This routine employs the reference temperature technique to compute the wall heat transfer when given trajectory, flow field, and atmospheric data in a prescribed format. Trajectory data were based on the Saturn I for the Earth Suborbital and Orbital Missions and the Saturn V for the Lunar Oribt Rendezvous Mission. Actually, the Saturn IB is to be used rather than the Saturn I analyzed, however this is not expected to significantly affect the results obtained. Flow field parameters (the ratios of local to freestream Mach number, static temperature, and Reynolds number) were based on wind tunnel measurements provided by the MSC Aerodynamics Branch. These data were obtained in the Langley Unitary Plan Wind Tunnel at Mach numbers of 2.98, 3.71, and 4.44, and freestream Reynolds numbers per foot of 2×10^6, 4×10^6, and 6×10^6, on a 0.045 scale (6.95 in. diameter) model of the Apollo spacecraft. Flow field data received were in the form of local static pressure as a function of axial station for each of the above test conditions. Heat transfer data were in the form of measured heating rates over the SM shell with and without the RCS present.

The flow field parameters required as input to the computer program are shown in Figure 3-1. The broken lines represent wind tunnel data for the

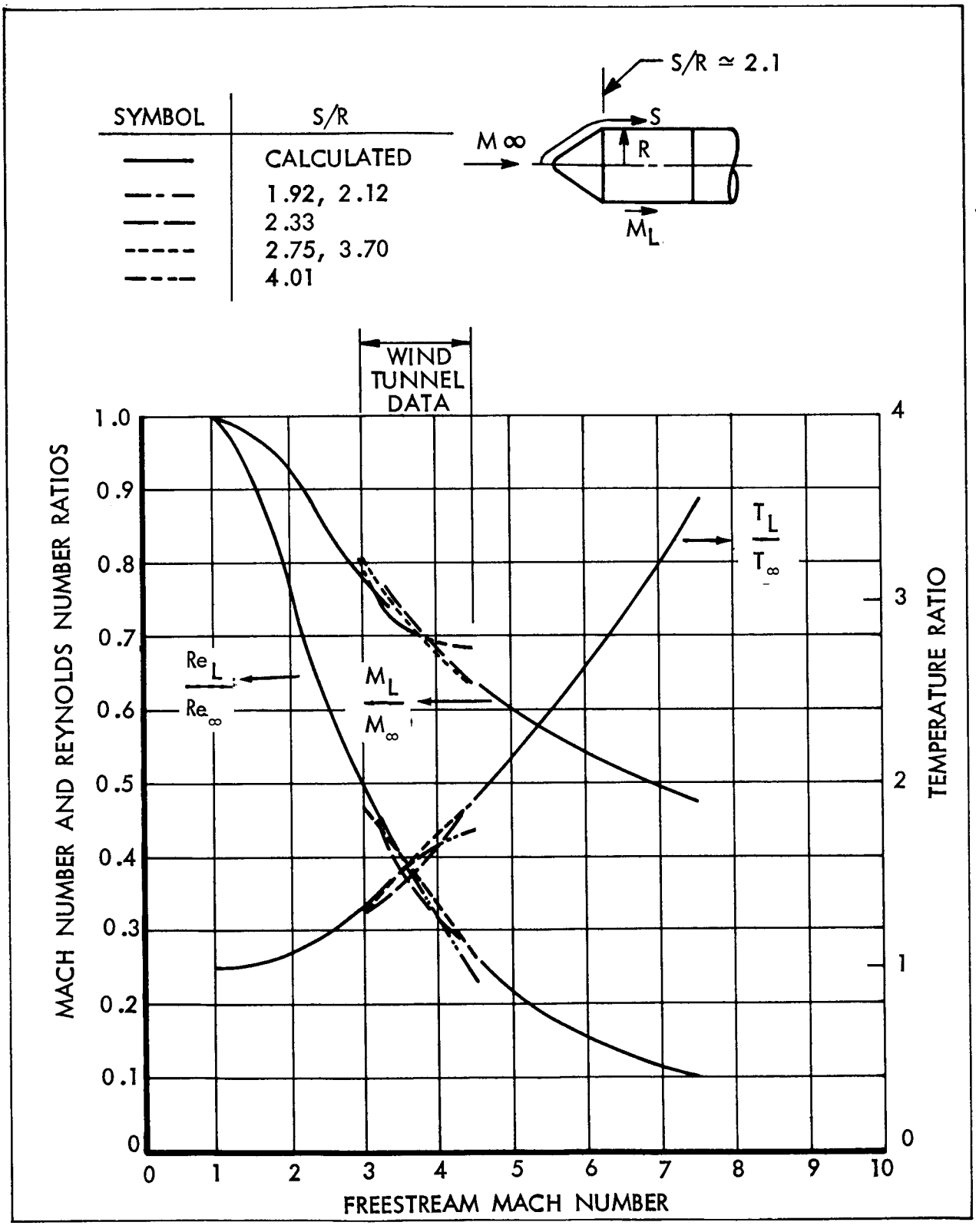

Figure 3-1. Summary of CM Ascent Flow Field Calculations

vehicle stations noted; the solid lines represent theory based on the assumption that the boundary layer edge fluid passed through a normal bow shock and then expanded isentropically to a local-to-freestream pressure ratio of 0.9, as suggested by the wind tunnel data. With the exception of one measurement at S/R = 4.01 during the Mach 4.44 tests, the data from the various axial stations plot as relatively narrow bands.

Protuberance heating factors for the shell nodes were based on the Langley wind tunnel data. Since measurements were available only for the range of Mach numbers from 2.98 to 4.44, the calculations were based on data for Mach 4.44, which most nearly coincides with the flight conditions during peak ascent heating. Maps showing the ratios of measured heating rates with and without the RCS present were plotted on a scale drawing of the shell nodal layout. The average protuberance heating factor for each affected node was estimated from these plots, and subsequently used in the ascent heating analysis as a multiplying factor to the Eckert heating rates to a smooth skin. The map constructed from the Mach 4.44 test data is shown in Figure 3-2. The asymmetry about the RCS package is due to the upstream umbilical fairing, scimitar antenna fairing housing, and CM vent.

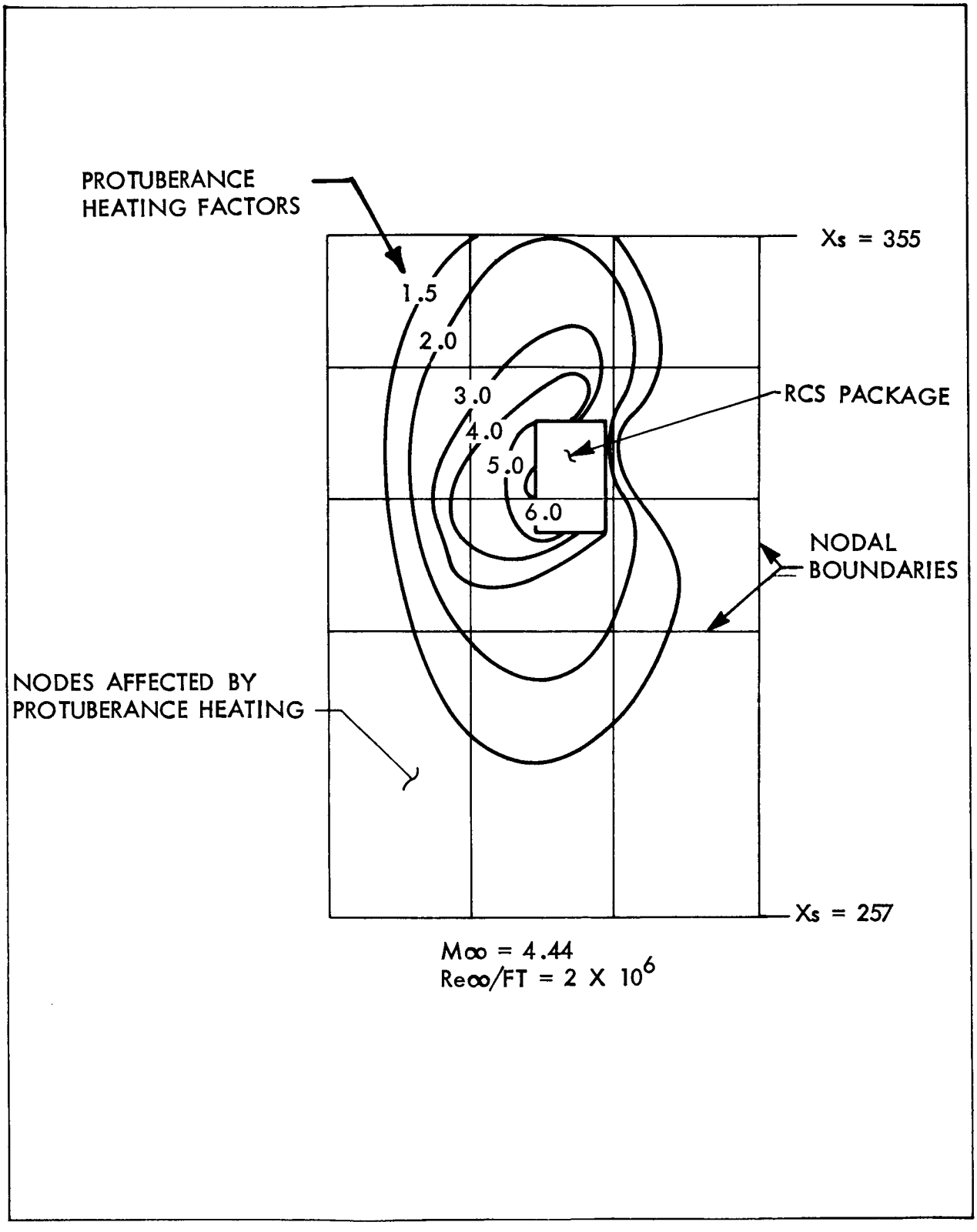

Figure 3-2. Protuberance Heating Factors Resulting From RCS Package Downstream of CM Umbilical Fairing

Another problem was the selection of a characteristic dimension. The proper dimension is not readily apparent because of complications arising from the Launch Escape System (LES) and its truss structure attachment to the CM. The Langley heat transfer data for the forward half of the SM were well correlated using the wetted distance from the nose of the LES as the characteristic dimension. However, this method underpredicted the heat transfer over the rear half of the SM by 15 to 30 percent. This is illustrated by Figure 3-3, which shows the measured heating rate distribution over the SM for one of the Mach 3 tests. The increased heating over the aft portion is typical of the Langley wind tunnel data for the three test Mach numbers. In the ascent heating analysis, the characteristic dimension was taken as the wetted distance from the LES tower nose with appropriate correction factors, derived from the Langley tests, used to account for the increased heating over the aft portion of the SM and the S-IV adapter.

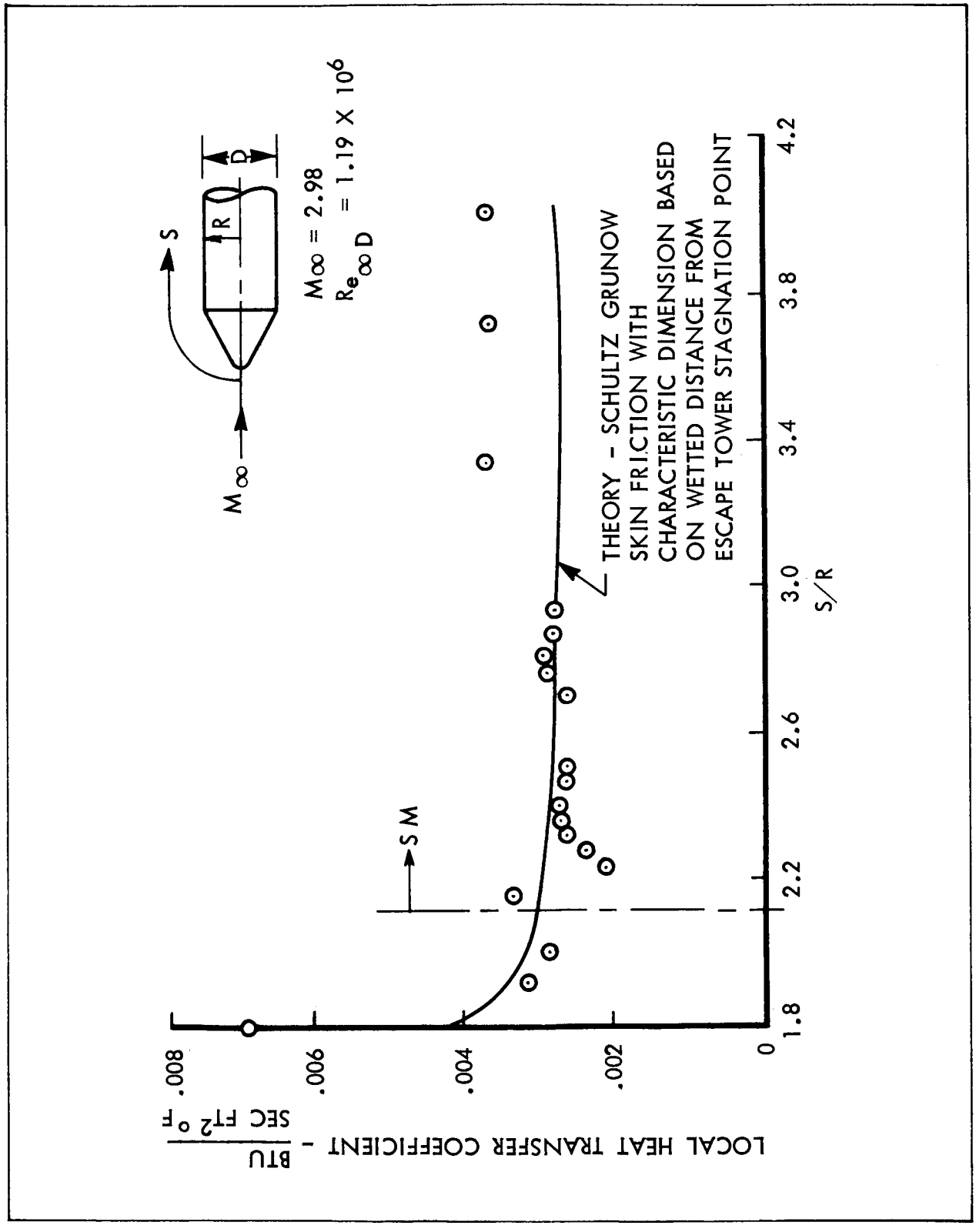

Figure 3-3. Measured Heat Transfer Coefficients of Apollo Service Module Model - Langley Unitary Plan Wind Tunnel Tests

Orbital Radiation

Orbital heating calculations were performed for five separate mission phases: Earth orbit, near planet, translunar and transearth, midcourse correction, and lunar orbit. The Earth and lunar orbit heating rate histories were obtained using the Lockheed Orbital Radiation Program (Reference 7) in the form of punched IBM cards suitable for direct input into the Thermal Analyzer Program. For the near planet phases, i.e., those portions of the translunar and transearth trajectories where the Apollo spacecraft is within three body radii of the Earth or the moon, the instantaneous heating rates were computed at several points along the trajectory, again using the Orbital Radiation Program. Continuous heating rate curves were then generated from the data. During the two rev/hr roll, all solar heating rates were interpolated from a single periodic curve, which was sinusoidal between 0-900 sec., and had a value of zero between 900-1800 sec. The solar inputs during the midcourse corrections were hand computed. Since the -Z axis was assumed to face the sun, the magnitude of the incident solar flux is 443 Btu/hr ft^2 times the cosine of the circumferential body angle measured from the -Z axis.

The calculation of radiant inputs to the nozzle extension, aft bulkhead, and the aft heat shield was complicated by the vehicle shading effects which had to be considered. During lunar orbit, the nose down orientation required that the shading of the aft bulkhead and heat shield by the nozzle extension be determined in order to compute solar inputs, and that shading of the nozzle extension and heat shield by the aft bulkhead be determined in order to compute lunar emission and albedo. Earth orbit shading factors were not required for the Lunar Orbit Rendezvous Mission because the SIVB adaptor encloses the aft end of the SM. Shading factors were required, however, for the Earth Orbit and Earth Suborbital Missions.

Shading factors for direct insolation were computed by illuminating an appropriately oriented scale model of the aft end of the SM by a distant projection lamp representing the sun. The nodal layout was drawn on the model, and the shading factors for several simulated orbit positions determined by the shadow line. The orientation relative to the light rays was accurately determined by attaching the model to the swivel head of a camera

tripod. A protractor was attached to a non-rotating base of the tripod, thus permitting angular measurements within one degree.

Planetary emission and albedo to the aft end were computed as the incident flux without shading decreased by the ratio of the view factors from the surface to the planet with and without consideration of the interfering surface. This approximation does not take into account non-uniform radiosity of the Earth or the moon. However, during the Earth orbital phase of the Lunar Mission, the aft end of SM does not receive external heat inputs because of the presence of the S-IVB adaptor, while during lunar orbit, the solar irradiation is far more significant than lunar emission or albedo because of the nose-down orientation. Thus, the error involved in neglecting non-uniform radiosity has a negligible effect on the Lunar Orbital Rendezvous Mission analysis. For the Earth Orbital and Suborbital Missions, Earth emission and albedo heating to the aft end is significant, but less than the solar heating. Therefore, the error in predicted surface temperature due to the approximation of uniform radiosity of the Earth should be insignificant.

The heating rates were input as curves or tables into the Thermal Analyzer Program. The appropriate heating rates were called for depending on the time of the mission.

IV-NETWORK GENERATION

The SM was represented in the three analyses by separate thermal networks. The network generated for the basic analysis included all SM components with the exception of the cryogenic tankage and the RCS. The propellant tankage, SPS engine, and helium bottles were represented in a rather coarse fashion. A second thermal network was generated to represent the SPS engine and plumbing for the detailed analysis of these components. The third network represented the propellant tanks and helium pressurization bottles. Portions of the network generated for the basic analysis were included with the second and third networks. The temperatures of these components obtained from the basic analysis served as boundary conditions in the detailed analysis.

In all thermal networks generated, the placement of nodes depended on the anticipated size of the gradients in each area, and the importance of the region to the overall results. Thus, on radial beams, where gradients were small and where temperatures were primarily sought as boundary conditions, the network was relatively coarse, whereas networks for the SPS plumbing were extremely fine.

Network parameters, i.e. capacitors and resistors, were computed from basic conductive and radiative equations. All thermal capacitors were computed through the basic formula

$$C = A\delta\int_{T_1}^{T_2} \frac{\rho C_v}{T}\, dT + \int_o^{\delta} \rho\, C_v\, A dx$$

where C = Thermal capacity ~ Btu/°F

ρ = Density ~ lbs/ft^3

C_v = Specific heat at constant volume ~ $\frac{\text{Btu}}{\text{lb-°F}}$

$\int_0^{\delta} A\, dx$ = Volume of lump ~ ft^3

Since in nearly all computations ρ and C_v were assumed constant over the temperature range involved, the equation generally used was

$$C = \rho V C_v$$

Conduction resistors were computed by the equation

$$R = 3600 \int_0^{\delta} \frac{dx}{kA_k(x)}$$

where R = Thermal resistance $\sim \frac{\text{sec-°F}}{\text{Btu}}$

A_k = Cross-sectional conductive heat transfer area $\sim$ ft^2

x = Distance along conductive path $\sim$ ft

k = Thermal conductivity $\sim$ Btu/hr-ft-°F

For rectangular nodes the equation reduces to

$$R = \frac{3600\,\delta}{kA_k}$$

Radiation resistors are computed by the Thermal Analyzer Program at each time step in the analysis. All that is required in the hand computations is a factor which contains the constants necessary for the specific radiation resistor. These are computed as

$$K_{rad} = \frac{\epsilon_{12}\, A_1\, F_{12}}{3600}$$

where E_{12} = Emissivity factor

A_1 = Area of radiating surface $\sim$ ft^2

F_{12} = Shape factor from radiating to absorbing surface

K_{rad} = Radiation resistor constant factor $\sim \frac{\text{ft}^2\text{-hr}}{\text{sec}}$

The computer then calculates the radiation resistors according to the formula

$$R = \frac{1}{\sigma K_{rad}\left[(T_1+460)^2+(T_2+460)^2\right]\left[(T_1+460)+(T_2+460)\right]}$$

where σ = Stefan-Boltzmann Constant

Most of the radiation shape factors were computed by an optical configuration factor device developed by Lockheed. The method is used to determine the shape factor from a differential element to any surface. A scale model illuminated by a projection lamp (representing the differential element) casts a shadow onto the surfaces of a marked wall. The shape factor is obtained directly from the number of sectors of the wall pattern which are shaded by the model. This method is extremely useful for obtaining rapid data and for analyzing complex shapes which are tedious to solve by analytical methods. Since the measured shape factor is from a differential element to the viewed object, it is necessary to integrate over the viewing surface to obtain the area to area shape factor. However, the work involved can generally be minimized by selecting the more complex shape as the viewed object and integrating over the less complex surface. The optical shape factor device is discribed in detail in Reference 8.

Shape factors between the propellant tanks and their surroundings were computed by the Lockheed Radiation Configuration Factor Program (Ref. 9). This program computes shape factors between any two bodies whose surfaces and boundary surfaces defined by equations of the form

$$Ax^2 + By^2 + Cz^2 + Dxy + Exz + Fyz + Gx + Hy + Iz + J = 0$$

The program has the capability of accounting for the shading effects of interfering surfaces.

BASIC SERVICE MODULE ANALYSIS

The thermal network generated for the basic analysis of the Service Module consisted of approximately 850 nodes, 1500 conduction resistors, and 700 radiation resistors. This extremely large network exceeded the storage capacity of the Thermal Analyzer computer program, but was finally accomodated after some re-programming (Reference 5). Each propellant tank was represented in the basic network as a single lump, with a time dependent thermal capacitance to account for fluid withdrawal. Each helium pressurization bottle and the gas within it were represented as individual nodes connected by a convection resistor.

The nodal layouts for the various SM components are described below. Figures are presented showing the location of nodes and conduction resistors only. The radiation resistor locations are described in the text. A complete listing of the network, including capacitor and the nodes which each resistor connects, and resistor values is given in Appendix B.

External Shell

The nodal network for the external shell, excluding the CM/SM fairing and the S-IVB adaptor, is shown in Figure 4-1. The selection of nodal locations on the shell is strongly influenced by the natural constraints of beam and radiator locations. As a result, 224 nodes were required. All of these nodes absorb and emit external radiation except the nodes covered by the RCS heat shields and the nodes representing radiator panels. The radiator temperatures were input values, using data supplied by MSC.

The skins and aluminum core were lumped together in computing the network capacitors and resistors. The neglect of temperature gradients through the panel was justified by a separate analysis, described in Section IX, which predicted a maximum temperature gradient of only $6^{\circ}F$ during the translunar roll.

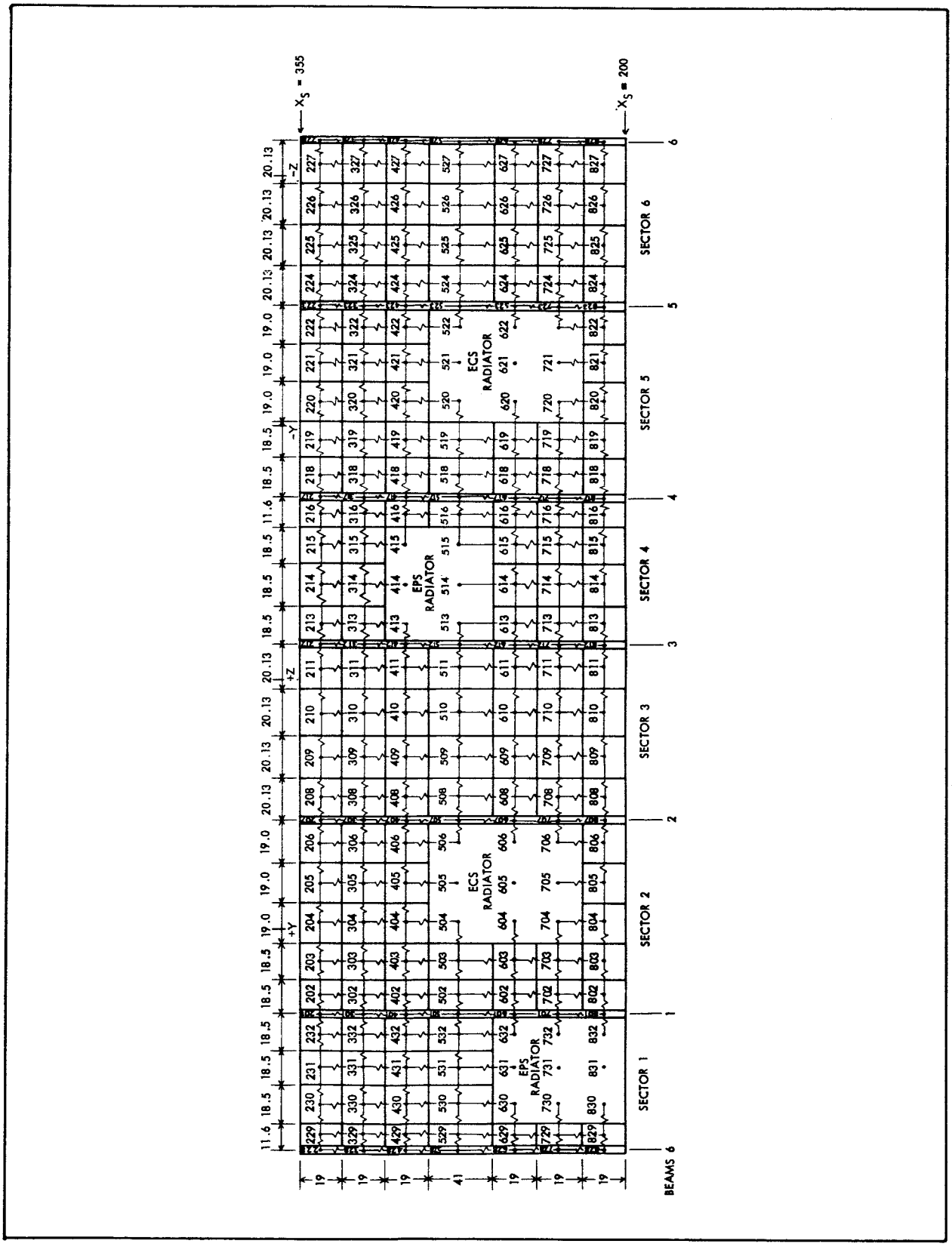

Figure 4-1. External Shell Nodal Layout

LOCKHEED CALIFORNIA COMPANY

Internally, radiation resistors were placed between each shell node and the adjacent propellant tank in bays 2, 3, 5, and 6, and between most bay 4 shell nodes and the fuel cells. The shell nodes which radiate to the fuel cell are listed in Appendix B.

Forward and Aft Bulkheads

The forward bulkhead network, shown in Figure 4-2, consists of 32 nodal areas bounded by a series of radial lines and concentric circles drawn from the origin. In the computation of resistor and capacitor values the aluminum core and skins were again lumped together, thus neglecting the temperature gradient normal to the skins. This is completely justified by the high conductivity of the core and the fact that aluminized Mylar insulation is applied to both sides of the bulkhead. The forward bulkhead was connected by conduction resistors to the shell, radial beams, center webs, and propellant tank skirts. Bulkhead node 16 was connected to the fuel cells by a radiation resistor.

The network layout for the aft bulkhead (Fig. 4-2) is identical to the one generated for the forward bulkhead. The corresponding network parameters, however, are different since the aft bulkhead is thicker. As before, the skins and core were lumped to compute network parameters. Again, the justification for this is the high conductivity of the aluminum core, and the presence insulation covering both facing plates. Conduction resistors connect the bulkhead to the shell, beams, engine web mount, and engine gimbal ring attachments. Radiation resistors connect the aft bulkhead nodes around the periphery to space to the nozzle extension, and to the aft heat shield. The interior bulkhead nodes radiate to the plumbing lines, and in addition, all bay 4 bulkhead nodes radiate to the fuel cell.

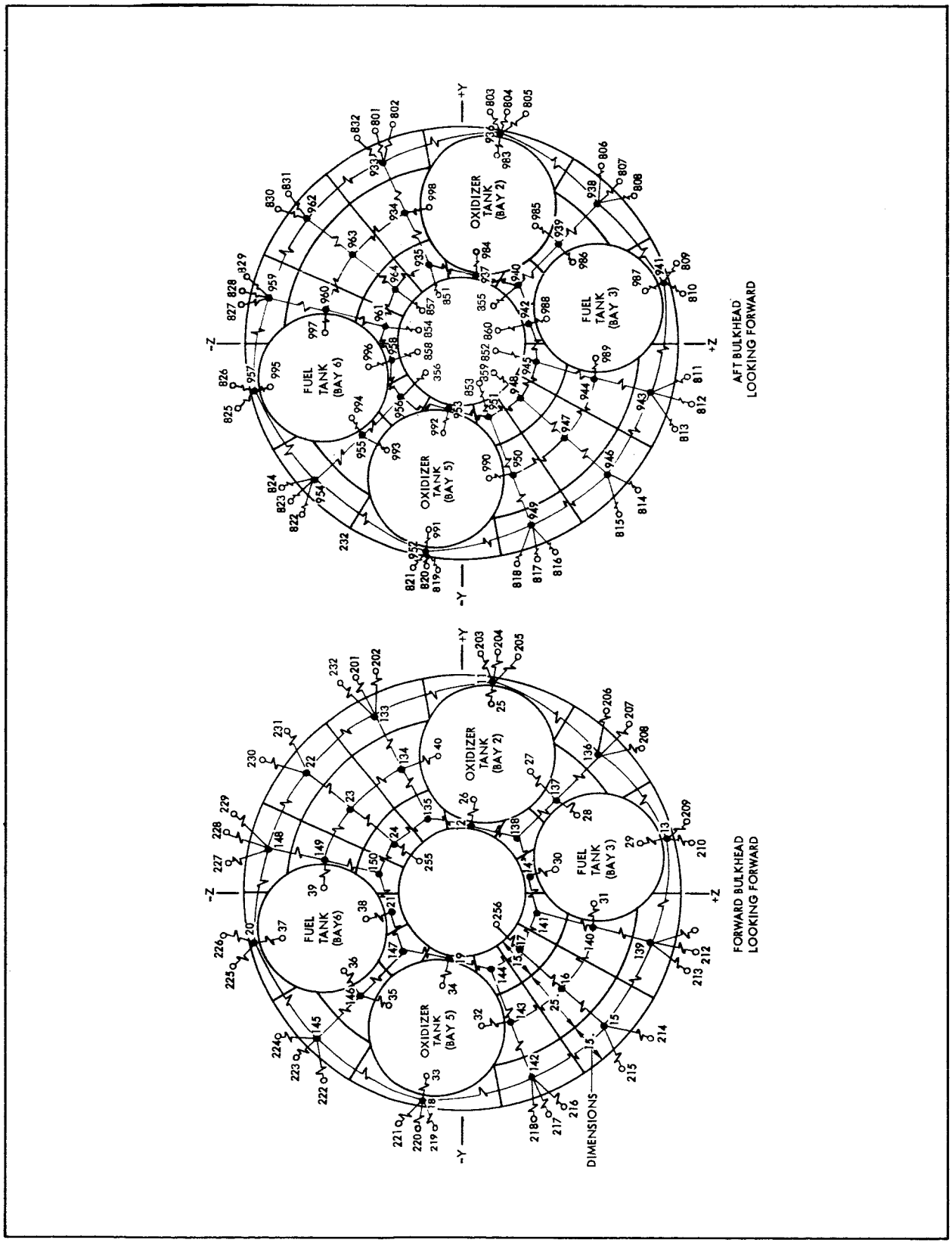

Figure 4-2. Forward and Aft Bulkheads Nodal Layout

LOCKHEED CALIFORNIA COMPANY

Radial Beams

Figure 4-3 shows the nodal layouts for the six radial beams. Each beam was divided into 21 rectangular areas. The node boundaries in the longitudinal and radial directions correspond to those on the shell and bulkheads, respectively, to simplify the integration of the three networks. The shell and bulkhead nodes to which the beam nodes were attached are also shown on Figure 4-3. Although the node boundaries are identical for all six beams, the conduction networks were slightly different along the inner edge of beams 1, 3, 4, and 6 to facilitate the connection with the center webs. The capacitor and resistor values for corresponding nodes on the various beams also differ because of construction differences and attached equipment. The CM support arms were assumed to conduct to a 70°F sink, representing the CM heat shield.

Radiation resistors connect each beam node with the adjacent propellant tank in bays 2, 3, 5, and 6. Also, some nodes on beams 3 and 4 (see Appendix B for a complete listing) were connected by radiation resistors to the fuel cells.

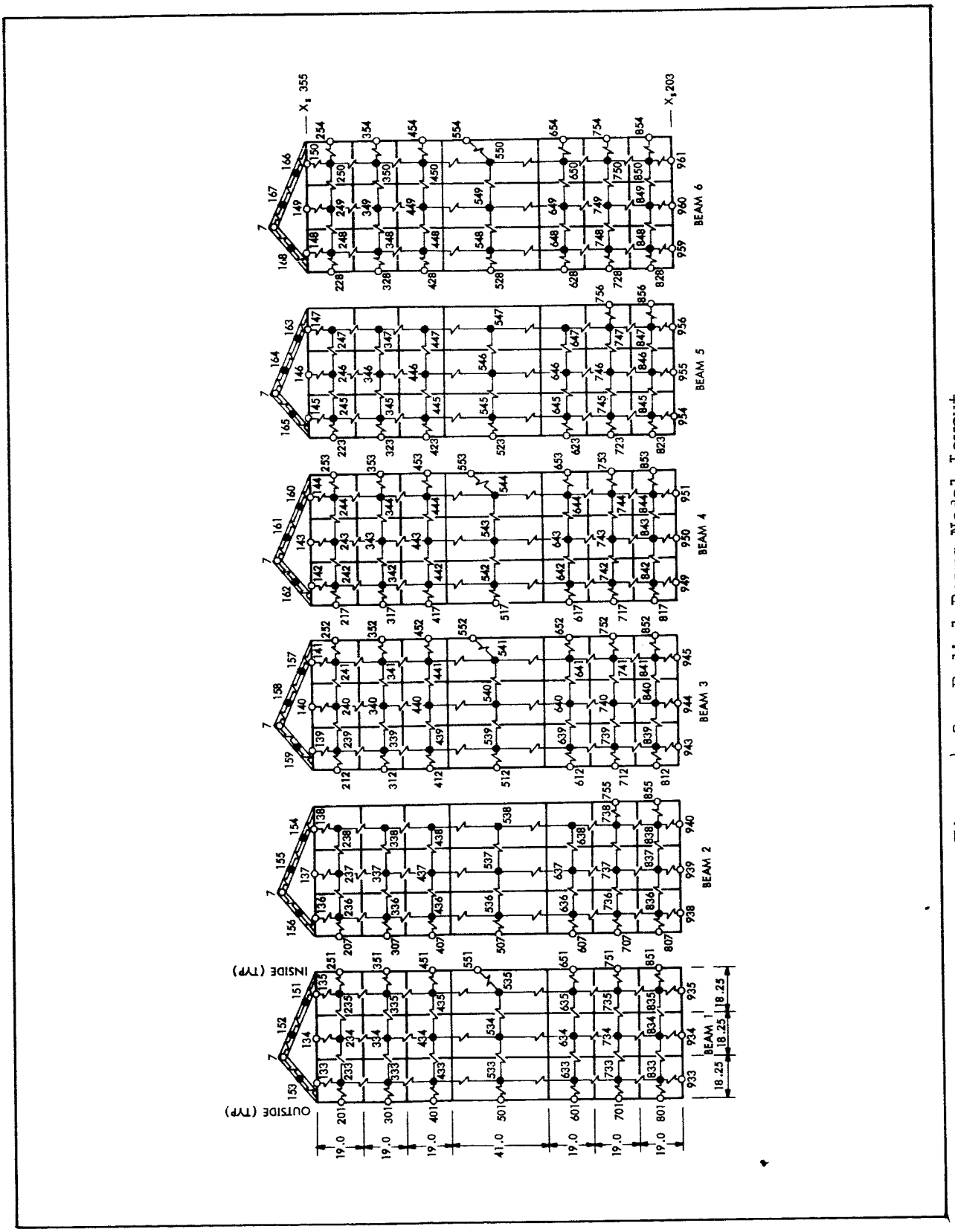

Figure 4-3. Radial Beams Nodal Layout

LOCKHEED
CALIFORNIA COMPANY

Engine Web Mounts

The nodal layouts for the two engine web mounts are shown in Figure 4-4. Both are divided into ten rectangular nodes, interconnected by conduction resistors. In addition, radiation resistors were placed between the web mount and the thrust chamber, and between the web mount and the components within the particular bay (fuel tanks or fuel cells). The web mounts were connected to the aft bulkhead and radial beams by conduction resistors.

Center Webs

The networks for the center webs in bays 1 and 4 are shown in Figure 4-5. Each node was connected to the adjacent nodes on the beam edges by conduction resistors. The helium bottles were connected to the center webs by both conduction and radiation resistors. The bay 4 side of the sector 4 web was also connected to the fuel cell by radiation resistors.

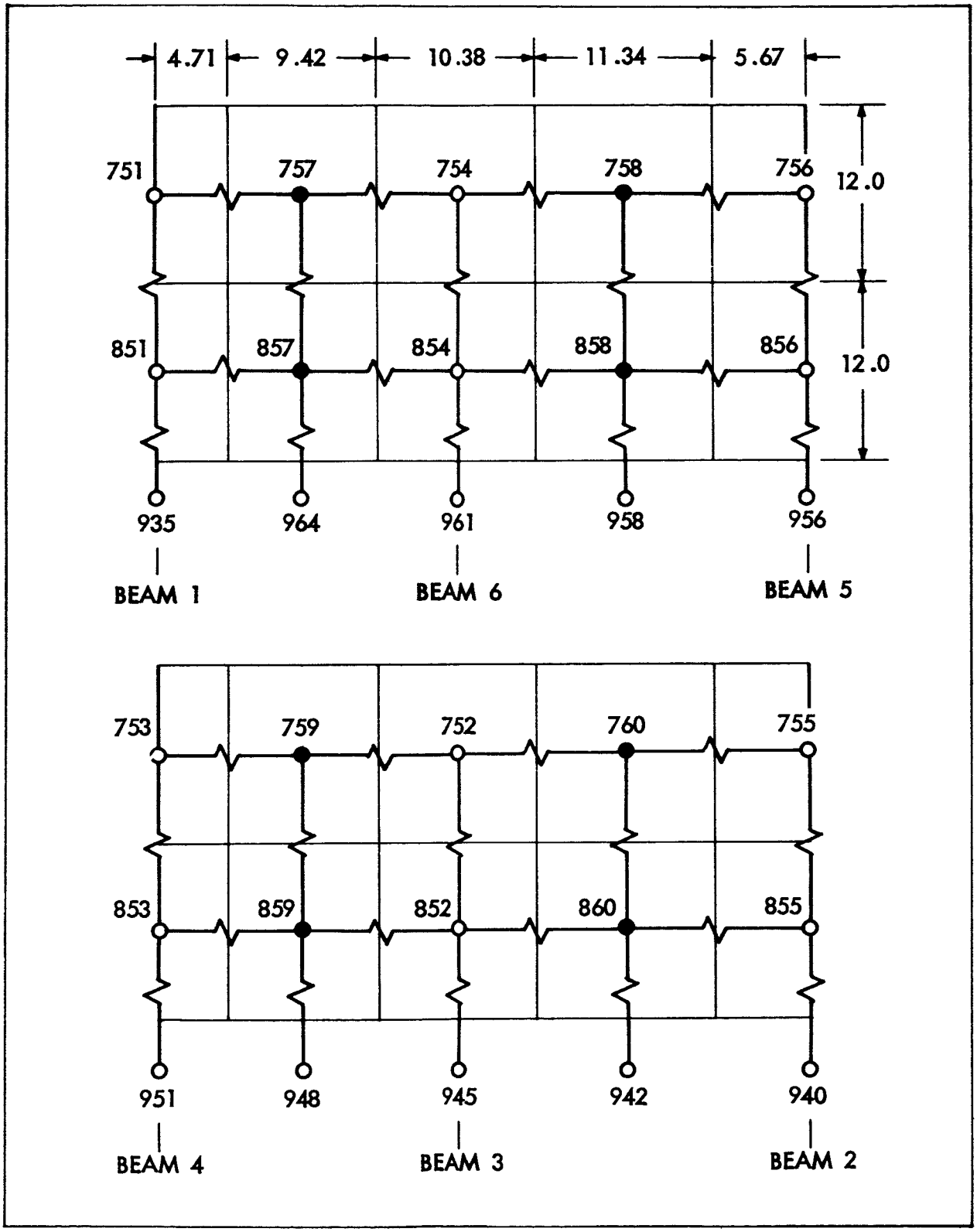

Figure 4-4. Engine Web Mounts Nodal Layout

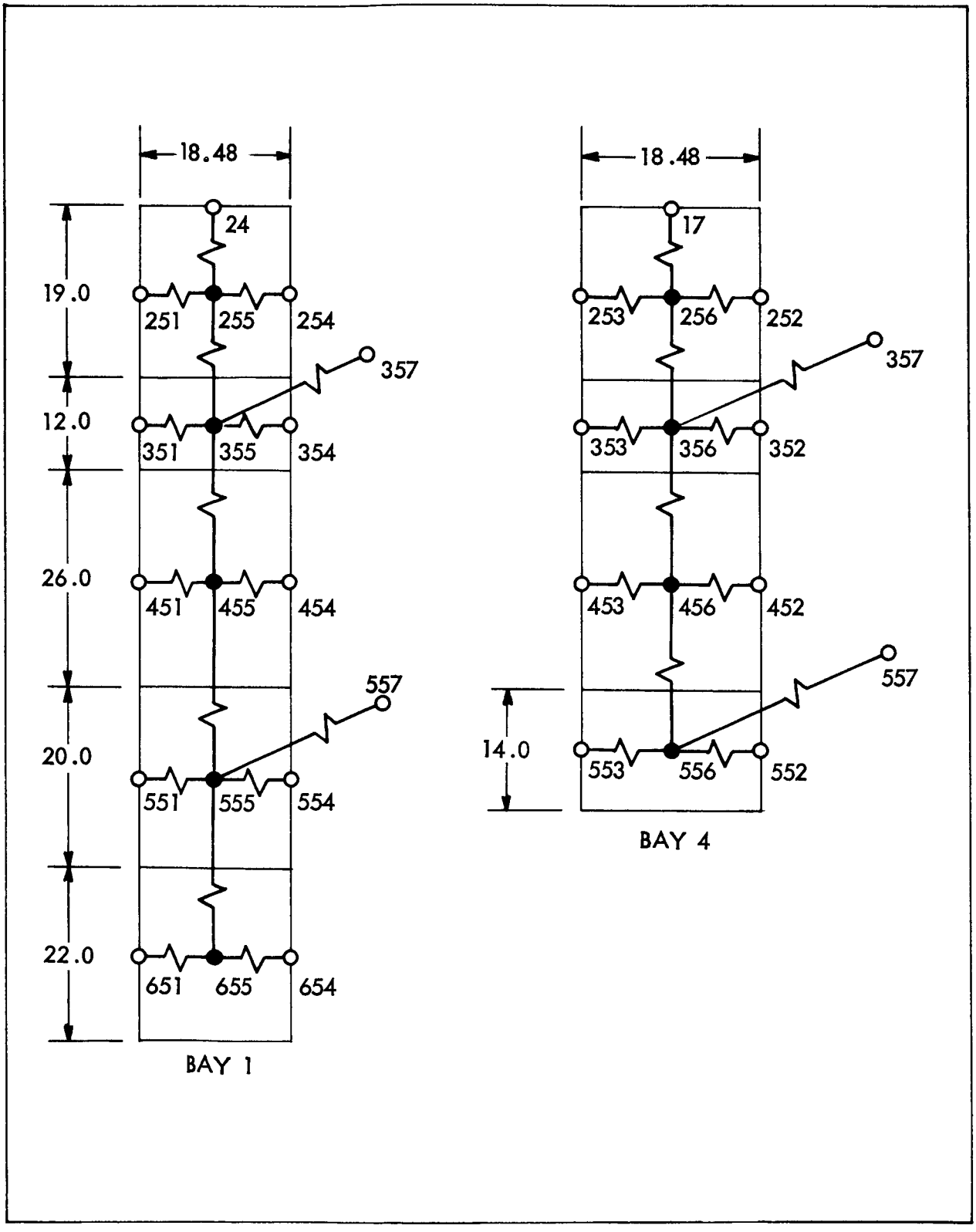

Figure 4-5. Center Webs Nodal Layout

Aft Heat Shield

The nodal layout for the aft bulkhead heat shield is shown in Figure 4-6. Nodes were placed on the inner and outer skins, where applicable, and were connected by conduction resistors through the quartz fiber insulation. The outer skin nodes radiated to space and to the nozzle extension. Interior nodes radiated to the adjacent bulkhead node. The quartz fiber insulation does not cover the fiberglass inner skin around the periphery of the heat shield. The nodes in this region (1033 through 1040) were connected by radiation resistors to the aft bulkhead and to space. Nodes 1041 through 1049 and 1081-1083 were connected to the thrust chamber and to the aft bulkhead by radiation resistors.

Conduction in the plane of the heat shield is negligible compared to the heat transfer in the normal direction, and therefore was neglected. Also, the temperature of the interior surface of the flexible boot connecting the heat shield and nozzle was assumed equal to the thrust chamber surface temperature since radiation exchange with the thrust chamber is by far it's primary mode of heat transfer. After the analysis had been performed Lockheed was informed that the thichness of the boot was to be considerably reduced. In that event, consideration should be given to modifying the network to account for heat transfer through the boot and radiation exchange between the external surface of the boot, the nozzle extension, and space.

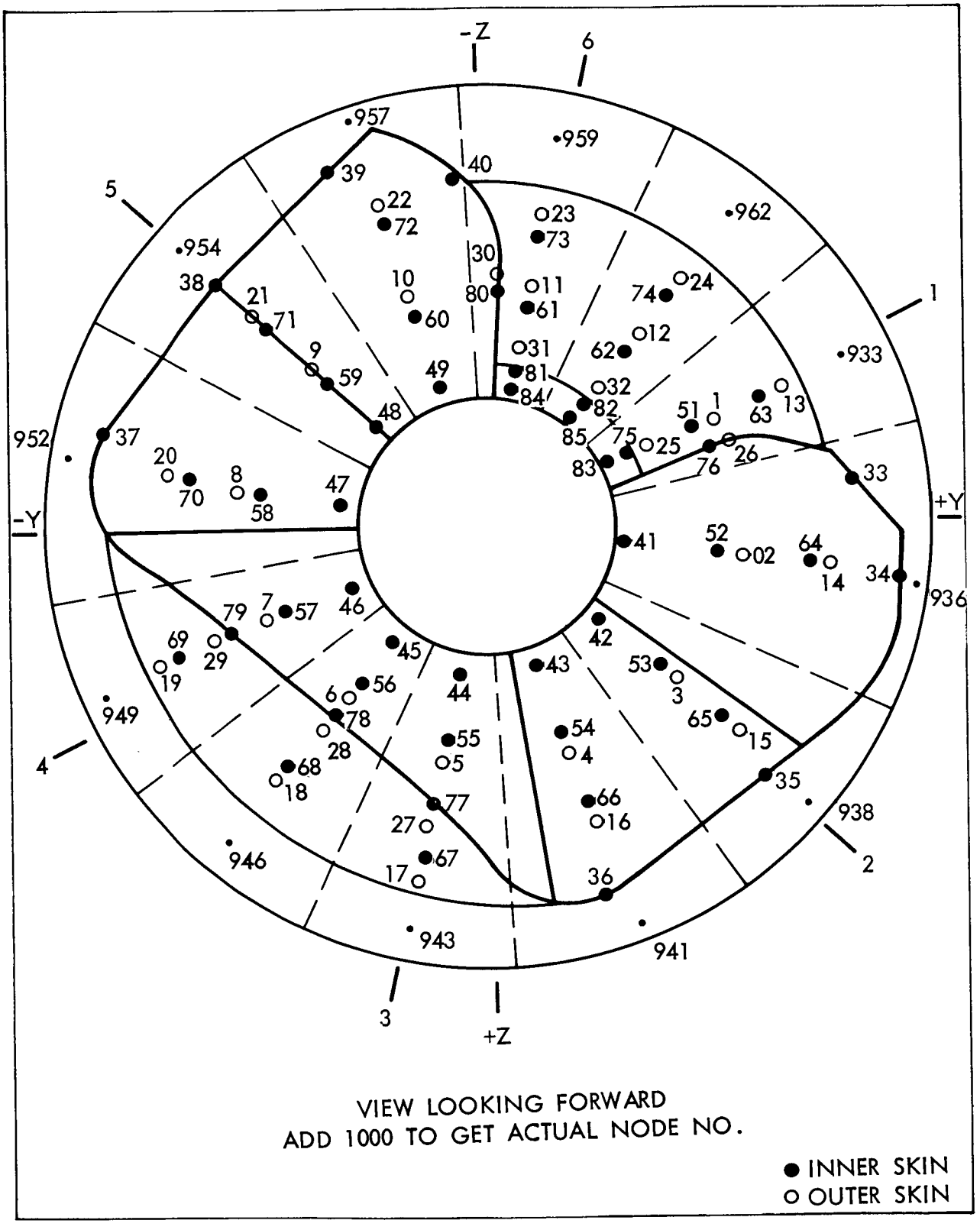

Figure 4-6. Aft Heat Shield Nodal Layout

RCS Heat Shields

The RCS heat shield networks consisted of nodes on the outer surfaces connected to space by radiation resistors, and to the SM shell by conduction resistors. These networks are shown in figure 4-7.

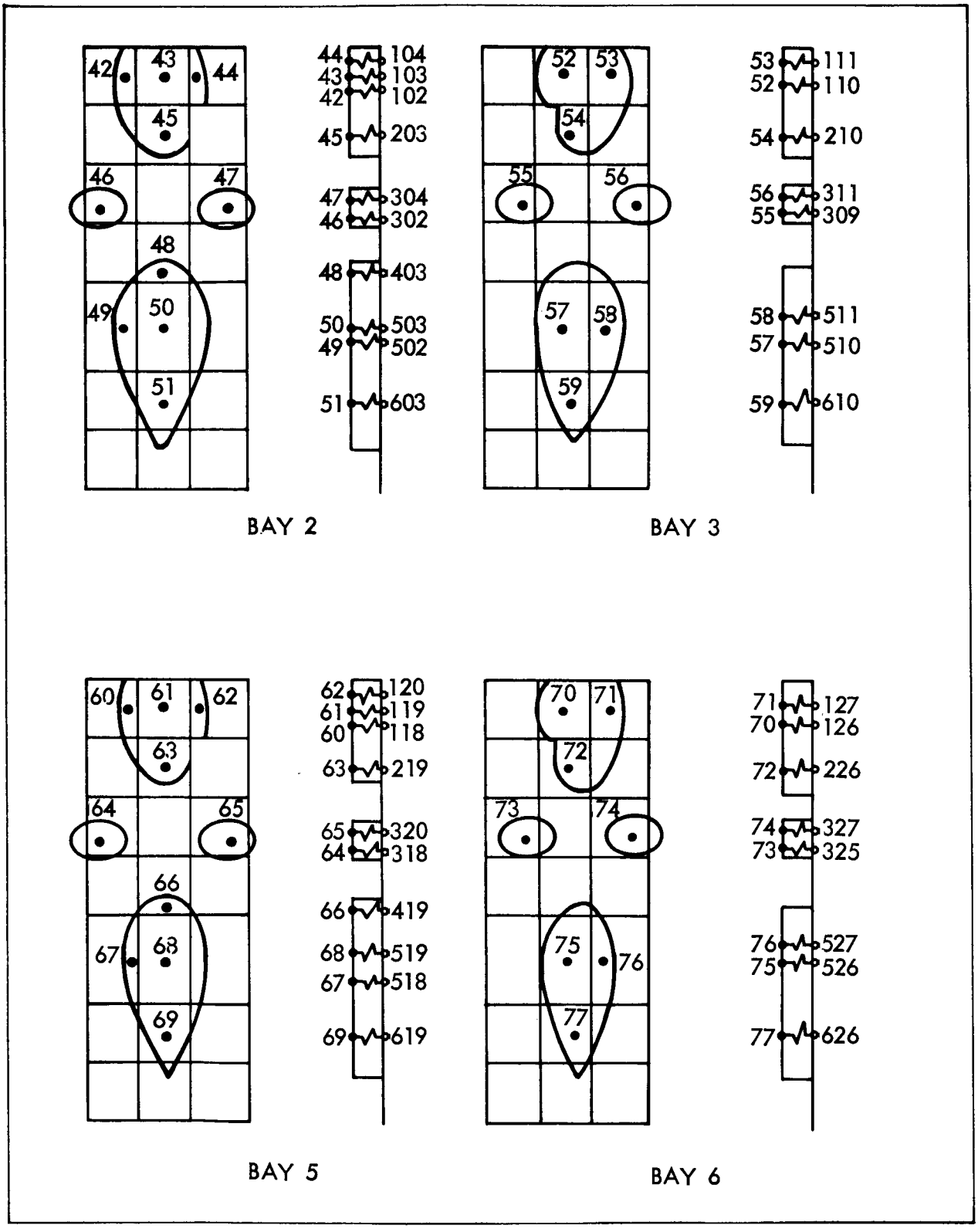

Figure 4-7. RCS Heat Shields Nodal Layout

LOCKHEED
CALIFORNIA COMPANY

SPS Engine and Nozzle Extension

The SPS engine was treated in a simplified fashion in the main network with a detailed analysis performed separately. The engine representation in the main network consisted of three nodes at three longitudinal stations of the thrust chamber, with radiation resistors between these nodes and the surroundings (engine web mounts in bays 1, 3, 4 and 6 and oxidizer tanks in bays 2 and 5). The temperatures of these nodes were impressed on the network, using data provided by MSC. The temperature-time history at the throat is shown in Figure 9-4. This plot is representative of the temperature history of the entire chamber exterior surface since the axial temperature gradient is very small.

The nodal boundaries for the nozzle extension were generated by six equally spaced radial planes through the X-axis, and planes normal to the axis at area ratios 20 and 40. The 36 nodes thus generated received external heat inputs where appropriate, and radiated to space, the aft bulkhead, and the aft heat shield. The nozzle extension temperatures were impressed during engine firings, but normally were computed by a heat balance. The impressed temperatures at the three axial stations are listed in Table 4-1 as a function of the engine firing duration.

Because all 36 nodes on the nozzle view one another, the internal radiation network had to be greatly simplified. It was assumed that each nozzle node exchanged radiation with the diametrically opposite node, with a view factor equal to its total view factor to all other nozzle nodes. The network for the nozzle extension and thrust chamber is shown in Figure 4-8.

TABLE 4-1 Impressed Nozzle Extension Temperatures During SPS Engine Firings

FIRING DURATION	AREA RATIO		
	6-20	20-40	40-62.5
3 sec.	800° F	500° F	300° F
12 sec.	1580° F	1225° F	770° F
20 sec. or longer	1900° F	1510° F	1250° F

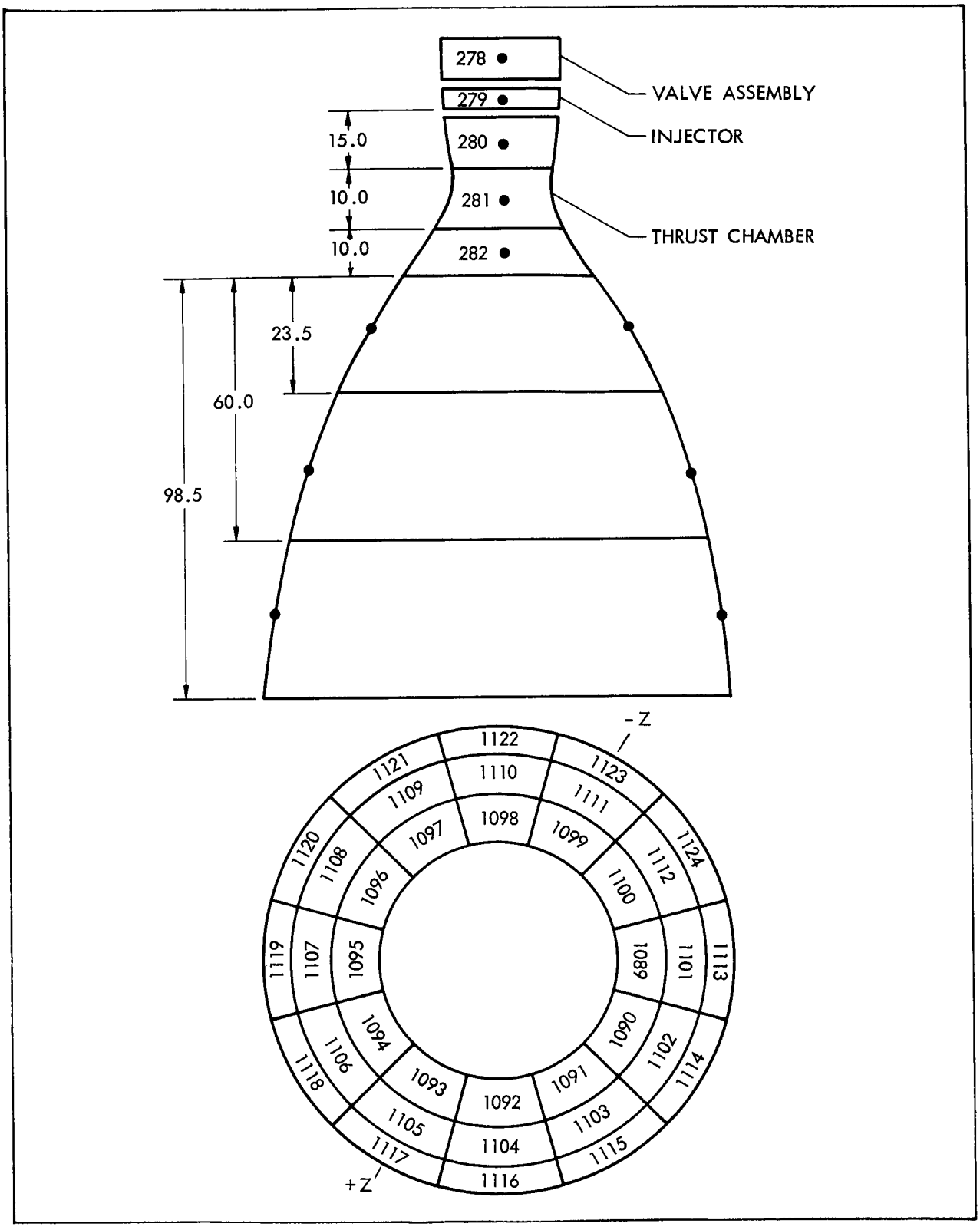

Figure 4-8. SPS Engine and Nozzle Extension Nodal Layout for Basic Analysis

LOCKHEED
CALIFORNIA COMPANY

Propellant Tanks and Helium Pressurization Bottles

As noted above, each propellant tank was represented in the basic analysis as a single node with time dependent thermal capacitance to account for propellant usage. Each tank was connected to each surrounding beam and shell node and to the helium bottles by radiation resistors. Also, both oxidizer tanks were connected to the thrust chamber by radiation resistors. Each tank skirt was divided into four nodes, as shown in Figure 4-9, to complete the conduction network to the forward and aft bulkhead.

The helium bottles and the gas within it were represented as individual lumps, connected by a convection resistor. The bottles were connected to the center webs by conduction and radiation resistor. Also, radiation was accounted for between the lower bottle and the fuel cells, and between the upper bottle and the CM heat shield.

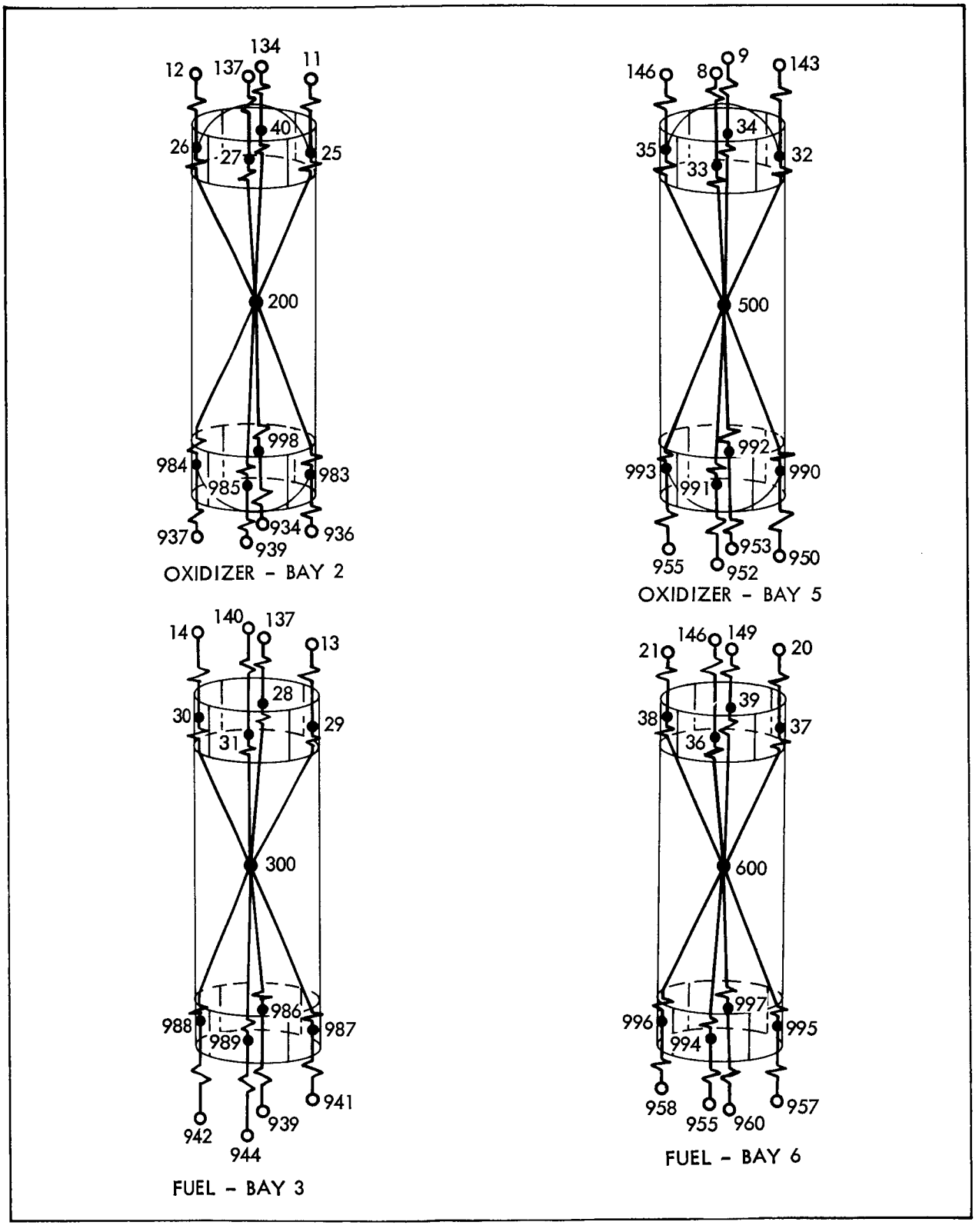

Figure 4-9. Propellant Tank Skirts Nodal Layout

LOCKHEED
CALIFORNIA COMPANY

DETAILED SPS PLUMBING AND ENGINE ANALYSIS

The thermal network for the detailed plumbing and engine analysis consisted of approximately 300 nodes, 275 conduction resistors, and 450 radiation resistors. The temperature histories of 45 of these nodes (representing basic structure) were obtained from the basic SM analysis and served as boundary conditions to this analysis. Transient thermal analysis were performed on all propellant lines and helium pressurization lines. An analysis of the thrust chamber, injector, bipropellant valves, gimbal ring and actuators, support arms, and engine attachments was also performed, although a lack of details necessitated a rather coarse network. The network generated for the plumbing-engine analysis is described below.

Structure

With the exception of the engine web mounts, the temperature histories of structural components were input quantities and thus served merely as boundary conditions to the detailed plumbing and engine analysis. A separate transient temperature analysis was performed of the web mounts because of the dependence of the thrust chamber cool down on the web mount temperatures. The thrust chamber temperature distributions provided by MSC were generated on the assumption of a surrounding radiation sink temperature of 80°F, which is a poor assumption for the web mount if the fuel cells are mounted to the aft bulkhead in bay 4. Because of their interdependence, a simultaneous thermal analysis of the thrust chamber and engine web mounts was required. As shown in Section V, much higher temperatures are predicted for both the thrust chamber and web mounts when their interactions are accounted for.

The structure temperatures input to the plumbing and engine analysis included nodes on the aft bulkhead, radial beam 4, the inner edge of the beams to which the web mounts attach, and the inner webs. In addition, the temperatures of the propellant tanks, helium bottles, and the fuel cells were input quantities, using data from the basic analysis. The node locations for these components are identical to those shown for the basic analysis, and are shown in Figures 4-10 and 4-11 with their new node designation numbers.

That structure not shown did not have its node numbers changed. Since most of these temperatures were specified, the only structural conduction network required is that for the engine web mount. Each structure node, however, is connected by either a radiation or conduction resistor to plumbing or engine components as described below.

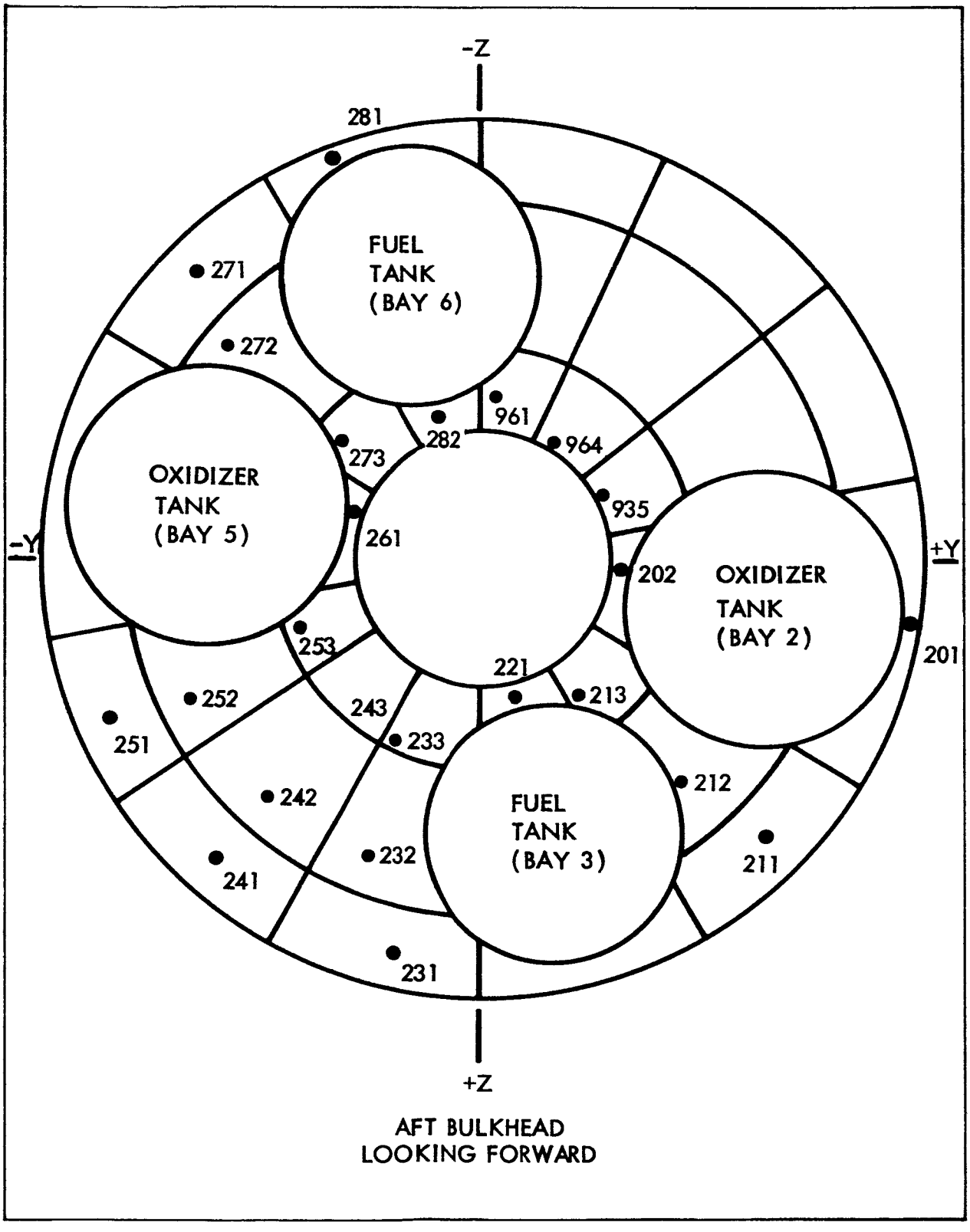

Figure 4-10. Aft Bulkhead Nodal Layout for Plumbing Analysis

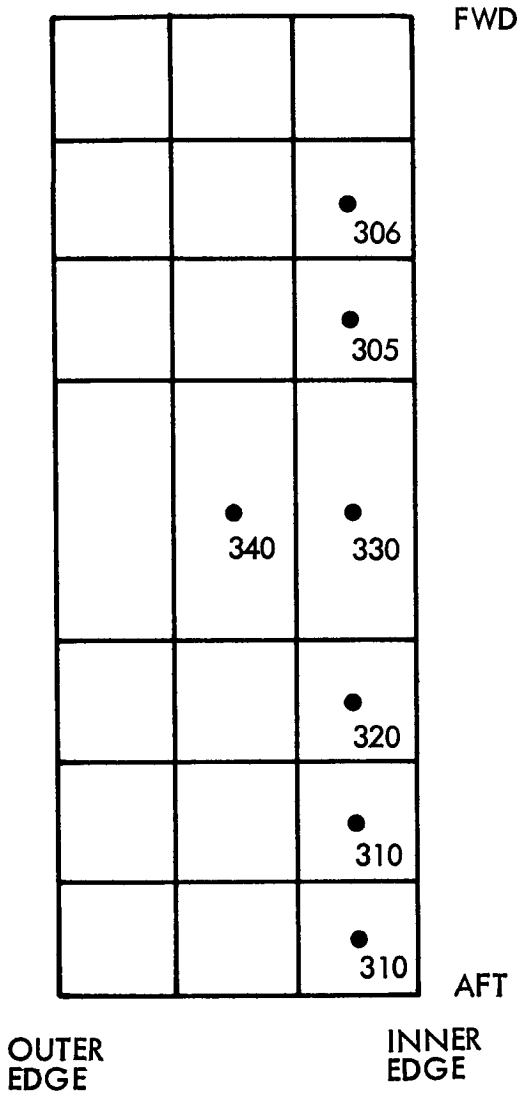

Figure 4-11. Beam 4 Nodal Layout for Plumbing Analysis

Plumbing Lines

The nodal layouts for the propellant and pressurant plumbing lines and associated equipment are shown in figures 4-12 through 4-18. Each node was connected to adjacent line nodes by conduction resistors, and to the surroundings by radiation resistors. Where two lines were extremely close, they were connected by radiation resistors. In most cases, details of valves, couplings, regulators, etc., were unavailable. As a result, the temperatures of these items, presented in Section V, are actually the adjacent line temperatures. The positions at which these components were assumed to be located are shown in each figure.

The lines enclosed by the aft bulkhead and aft heat shield are sketched in Figure 4-12, and the corresponding nodal representation is shown in Figure 4-13. The node boundaries correspond to those on the bulkhead. In addition to the conduction network, all nodes radiate to the adjacent bulkhead node and/or propellant tank. The inner layer of the aluminized Mylar insulation, which is located on the inside of the heat shield, was assumed to be at the same temperature as the nearest bulkhead node. As a result, the radiation resistors between line and bulkhead were computed on the assumption of unity view factor based on the total surface area of the line.

Figure 4-14 shows the arrangement of the helium lines leading from the bottles to the aft bulkhead area, and Figure 4-15 is the corresponding nodal layout. The node boundaries for the lines correspond to those on beam 4, to which they are physically attached. The lines entering the bulkhead area are designated A, B, C, and D on Figures 4-13 and 4-15 for identification. In addition to the conduction network, each plumbing node which was covered by insulation radiated to the adjacent beam node with a view factor of unity based on the total surface area of the tube, i.e., the assumption was again made that the temperature of the inner layer of insulation was the same as the local beam temperature. In the vicinity of the helium valves and regulators, the insulation is cut out to allow these components to protrude. Nodes in this region, therefore, radiated to the adjacent beam node with a view factor of only 0.5. Since most of bay 4 is insulated, it was assumed

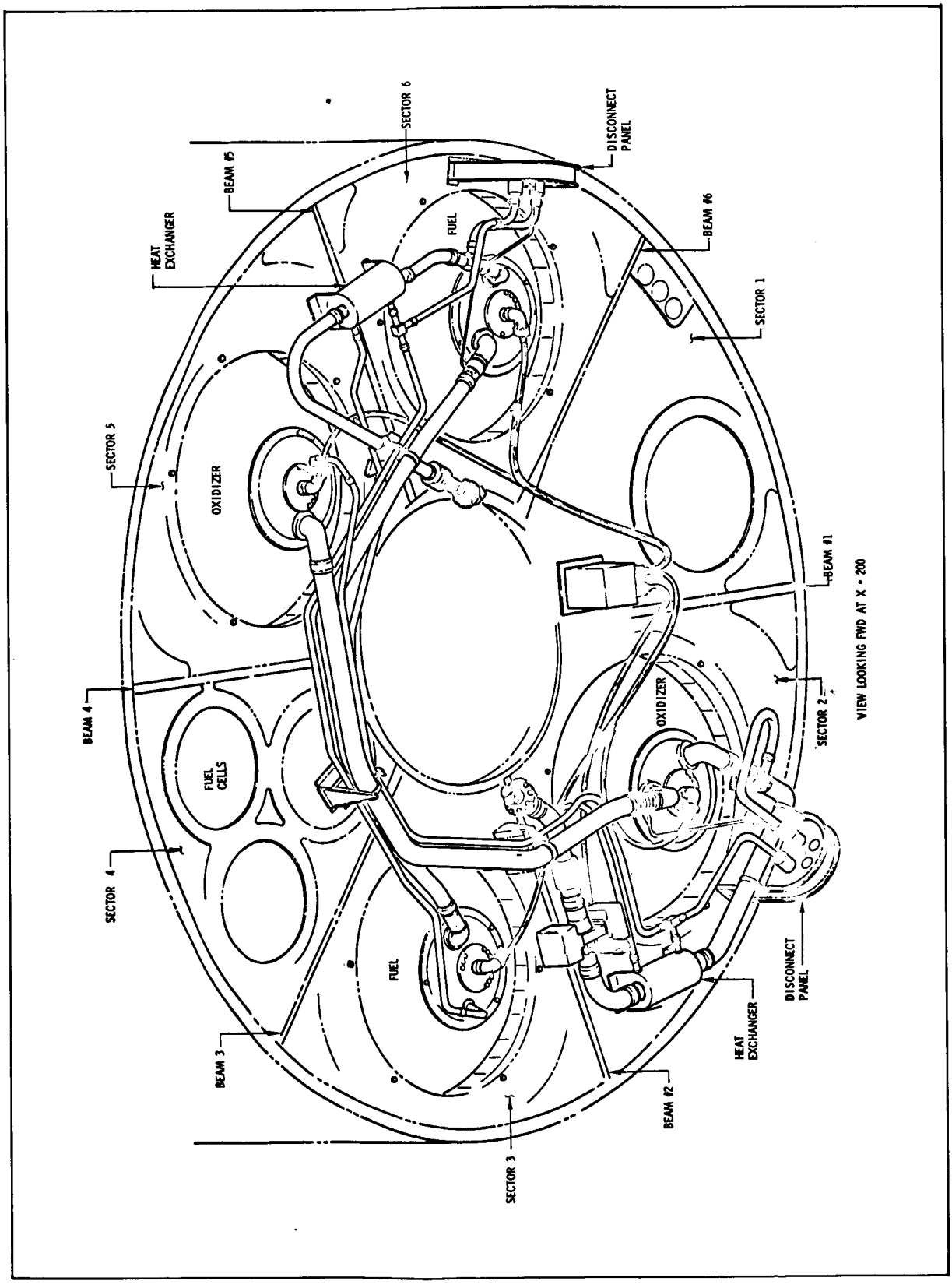

Figure 4-12. SPS Plumbing in Aft Bulkhead Region

LOCKHEED
CALIFORNIA COMPANY

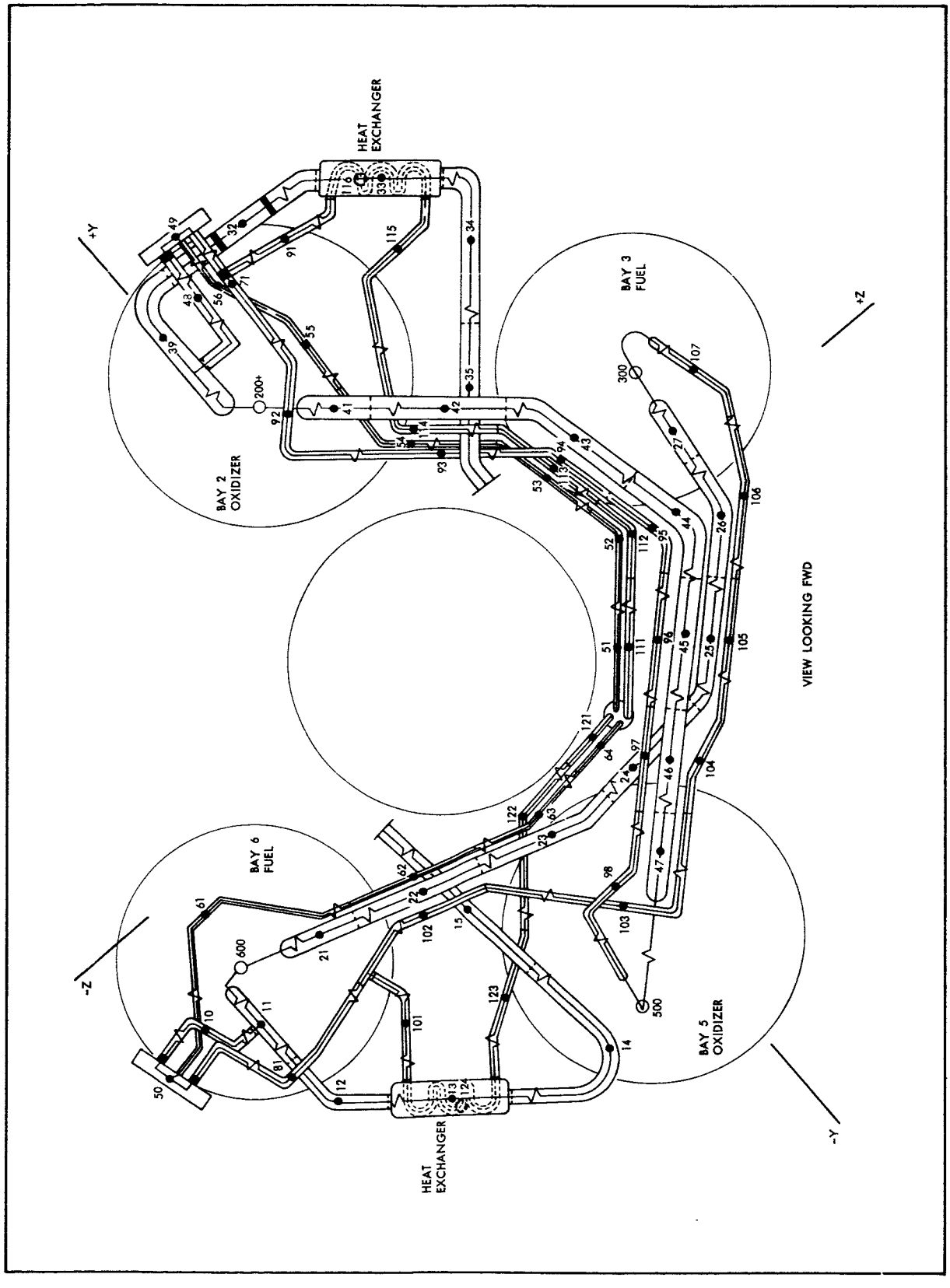

Figure 4-13. SPS Plumbing Nodal Layout in Aft Bulkhead Region

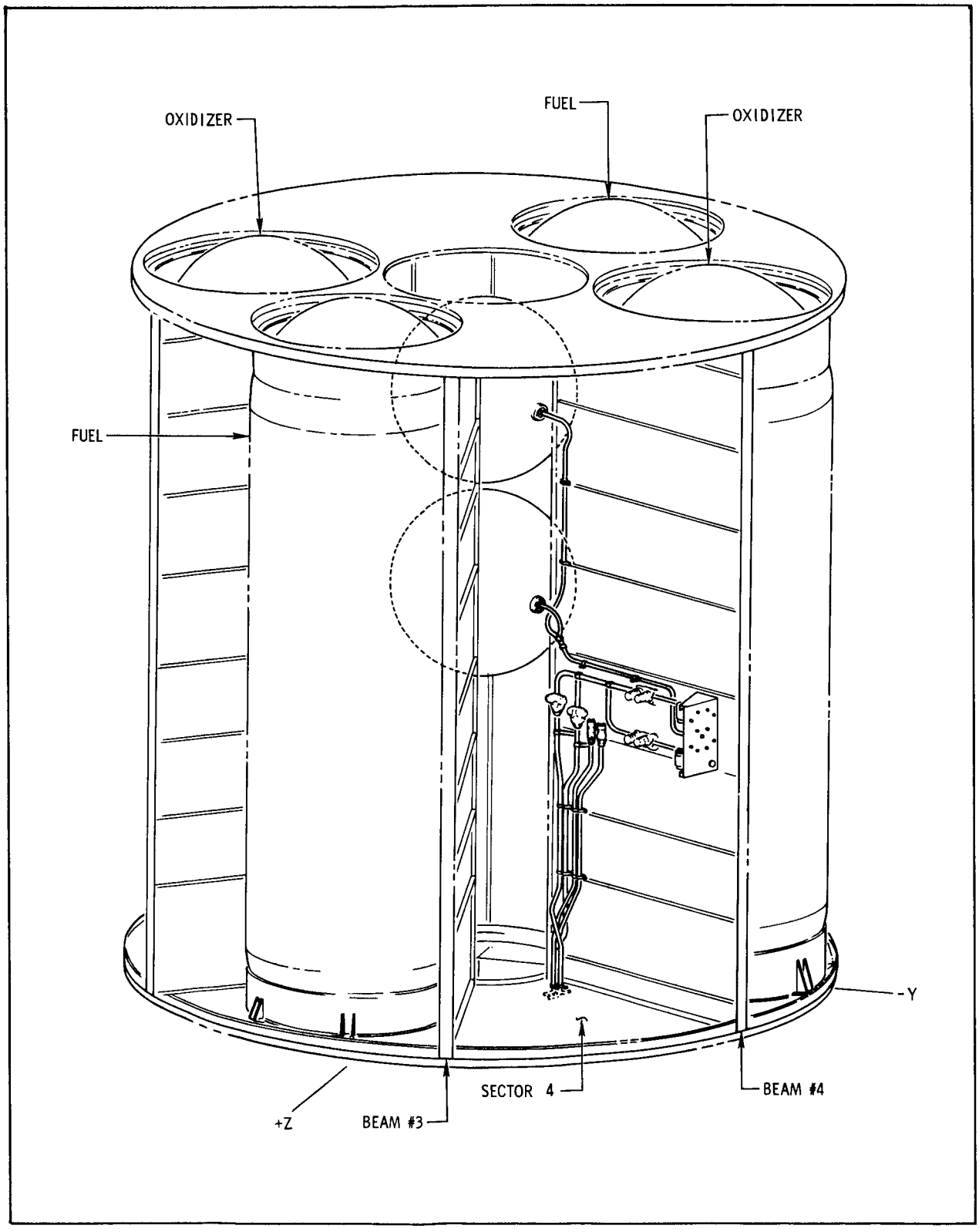

Figure 4-14. Bay 4 Helium Lines

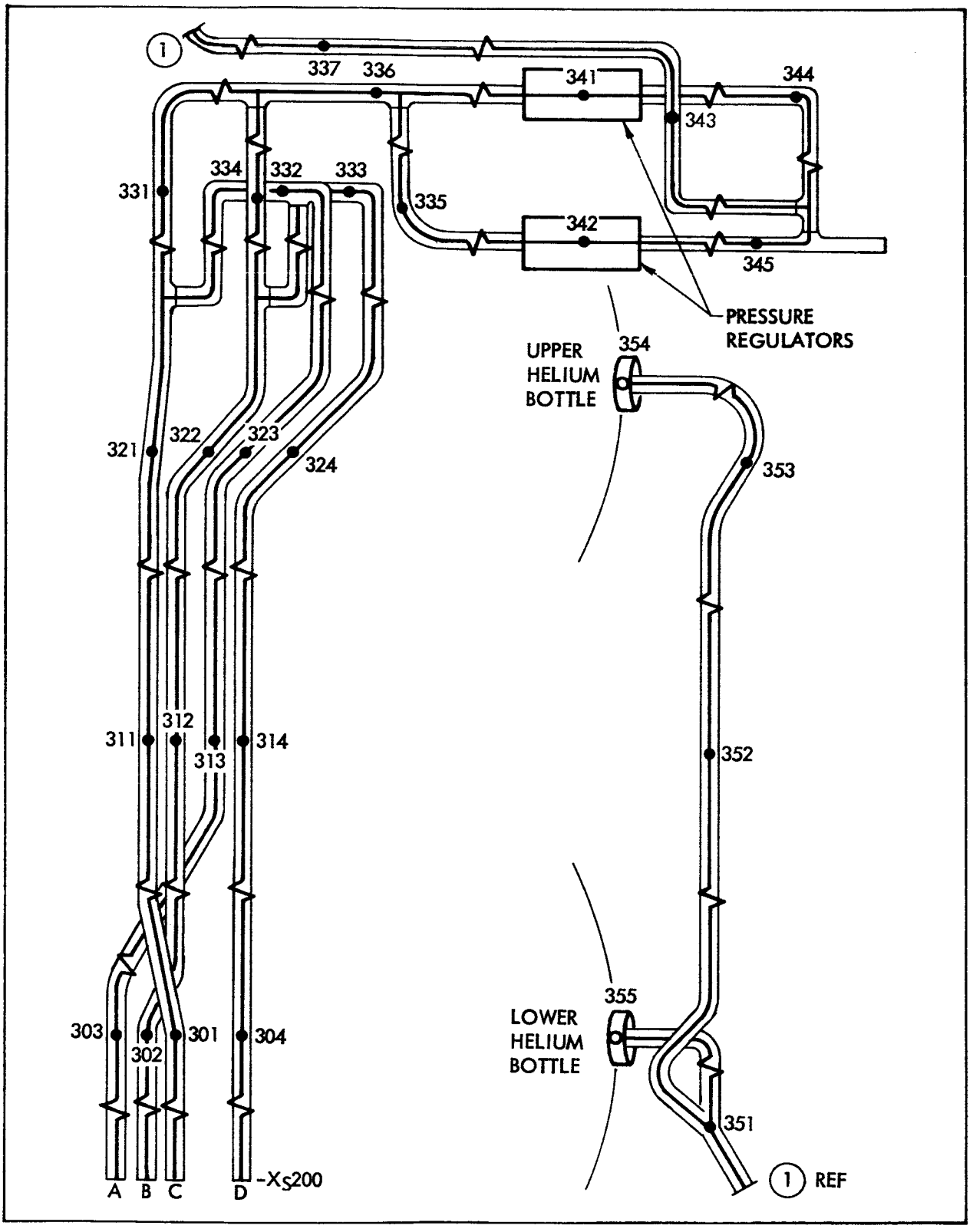

Figure 4-15. Bay 4 Helium Lines Nodal Layout

LOCKHEED
CALIFORNIA COMPANY

that the inner layer of insulation throughout the bay would be nearly at the fuel cell temperature. Therefore, the remainder of the radiation resistors to these lines were connected to the fuel cells.

Propellant feed lines, bipropellant valve drain lines, and other lines extending from the bipropellant valves to the aft bulkhead region are illustrated in Figure 4-16. Table 4-2 assists in identifying the node locations for the smaller lines. The resistors connecting these lines to the engine structure, to propellant tanks and to surrounding structure are similar to those shown. Radiation was also accounted for between these lines whenever it appeared significant compared to line-structure radiation. Figure 4-17 shows the nodal layout of these same lines in the aft bulkhead region. They are connected to surrounding components in the same manner as are the aft bulkhead lines previously mentioned.

Disconnect Panels

The network used to calculate disconnect panel temperatures is not easily illustrated. Each panel was considered as a single node which radiated to space and to the bulkhead. The panels were assumed insulated from the bulkhead, hence no conduction resistors were placed between the panels and bulkhead. The lines which extended through the panels are capped on the ends; thus, additional radiation resistors were run from these caps to space. Both the panels and caps were also connected to the adjacent line nodes by conduction resistors. Figure 4-18 shows the nodal layout for the panels.

Engine Network

The detailed SPS engine network, including that for the thrust chamber, gimbaling structure, supports, injector, and valve assembly is shown in Figures 4-19 through 4-21. Figure 4-19 shows the gimbal and support structure. The thrust chamber exterior radiates to the engine web mounts, the propellant tanks in Bays 2 and 5, the aft heat shield, plumbing lines, and all components shown in Figure 4-19 with the exception of the engine mount brackets. In general, radiation between these components and the surroundings (web mounts, propellant tanks, etc.) was not included because the temperature difference is small and the emissivities of the components were unknown. The additional effort involved in computing radiation shape factors, etc., was therefore not justified. For radiation exchange with the thrust chamber, the emissivity of

Table 4-2

NODE NUMBERS FOR ADDITIONAL FILL, DRAIN, AND BLEED LINES

Bipropellant Valve Actuator Dump Line	Fuel Fill and bleed line	Biprop. Valve Actuator Seal Drain	Biprop. Valve Seal Drain-Fuel
28	125*	135*	145*
29	126	136	146
30	127	137	147
65	128		
66	129	139	149
67	130	140	150
68	131	141	151
69	132	142	152
70	133	143	153

Bipropellant Valve Seal Drain-Oxidizer	Oxidizer Fill and Bleed Line
155	165*
156	166
157	167
159	169
160	170
161	171
162	172
163	173

*Nodes are located parallel with line node designated at left

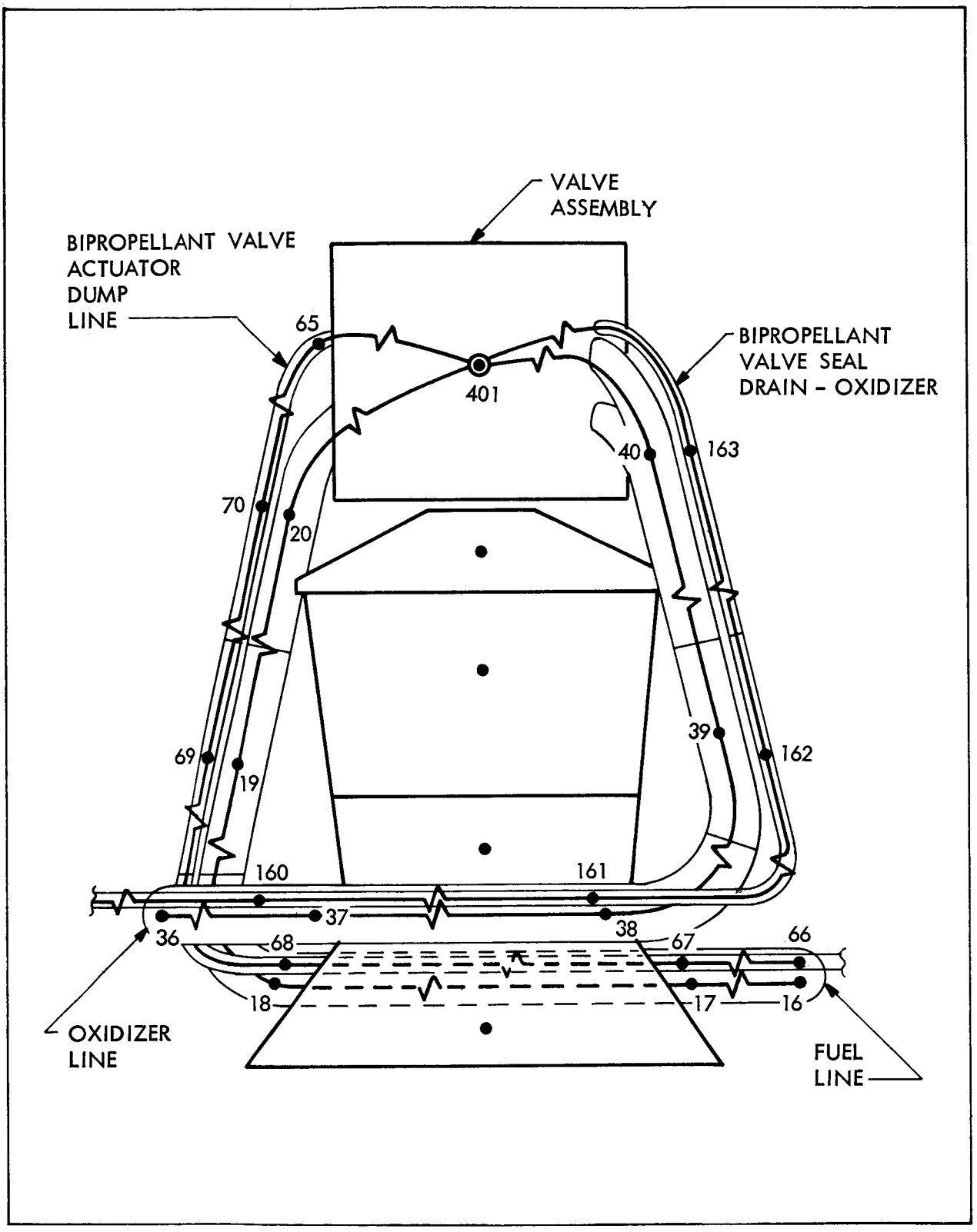

Figure 4-16. Fill, Drain, and Bleed Lines Nodal Layout in Thrust Chamber Region

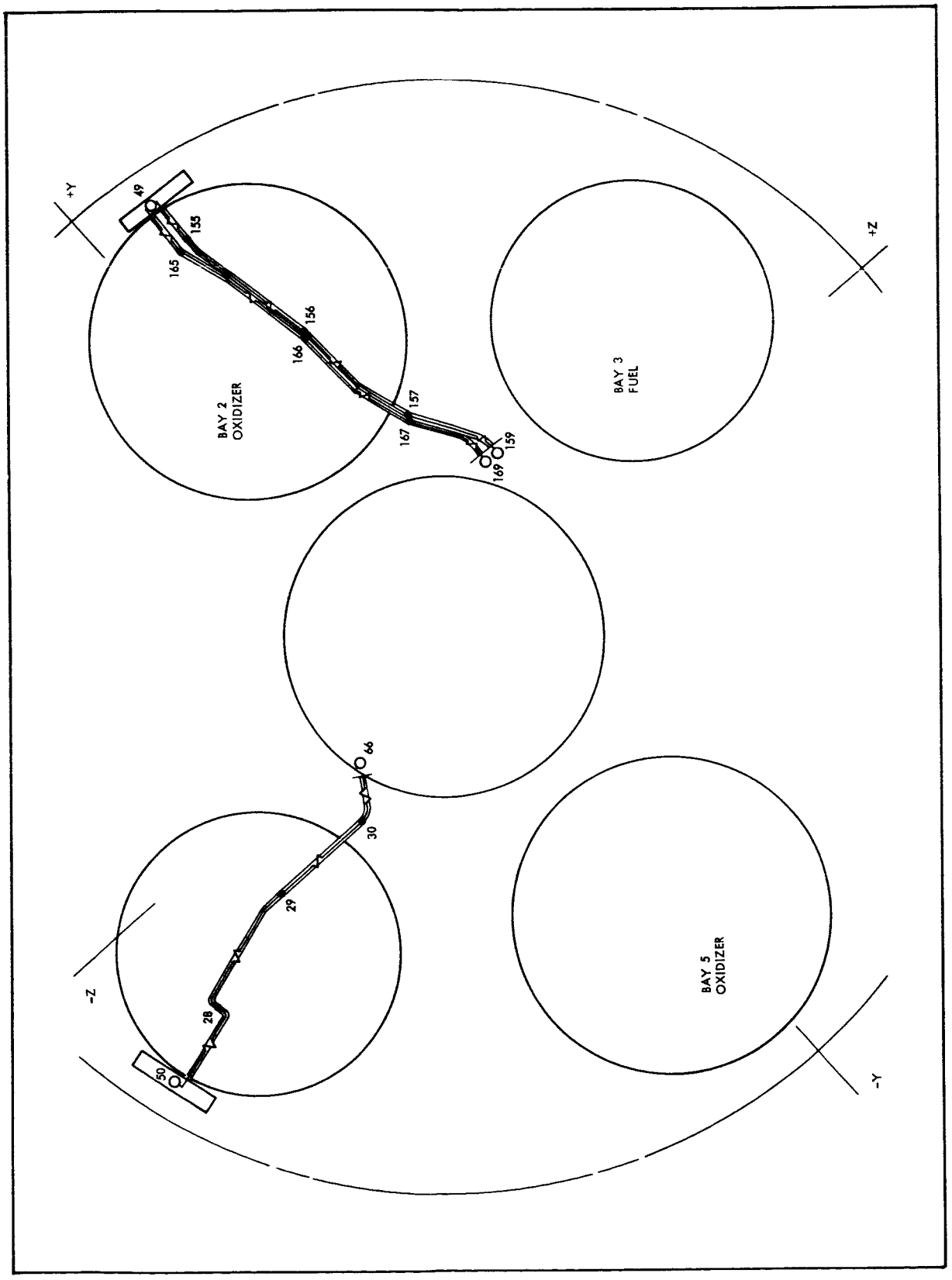

Figure 4-17. Fill, Drain, and Bleed Lines Nodal Layout in Aft Bulkhead Region

LOCKHEED
CALIFORNIA COMPANY

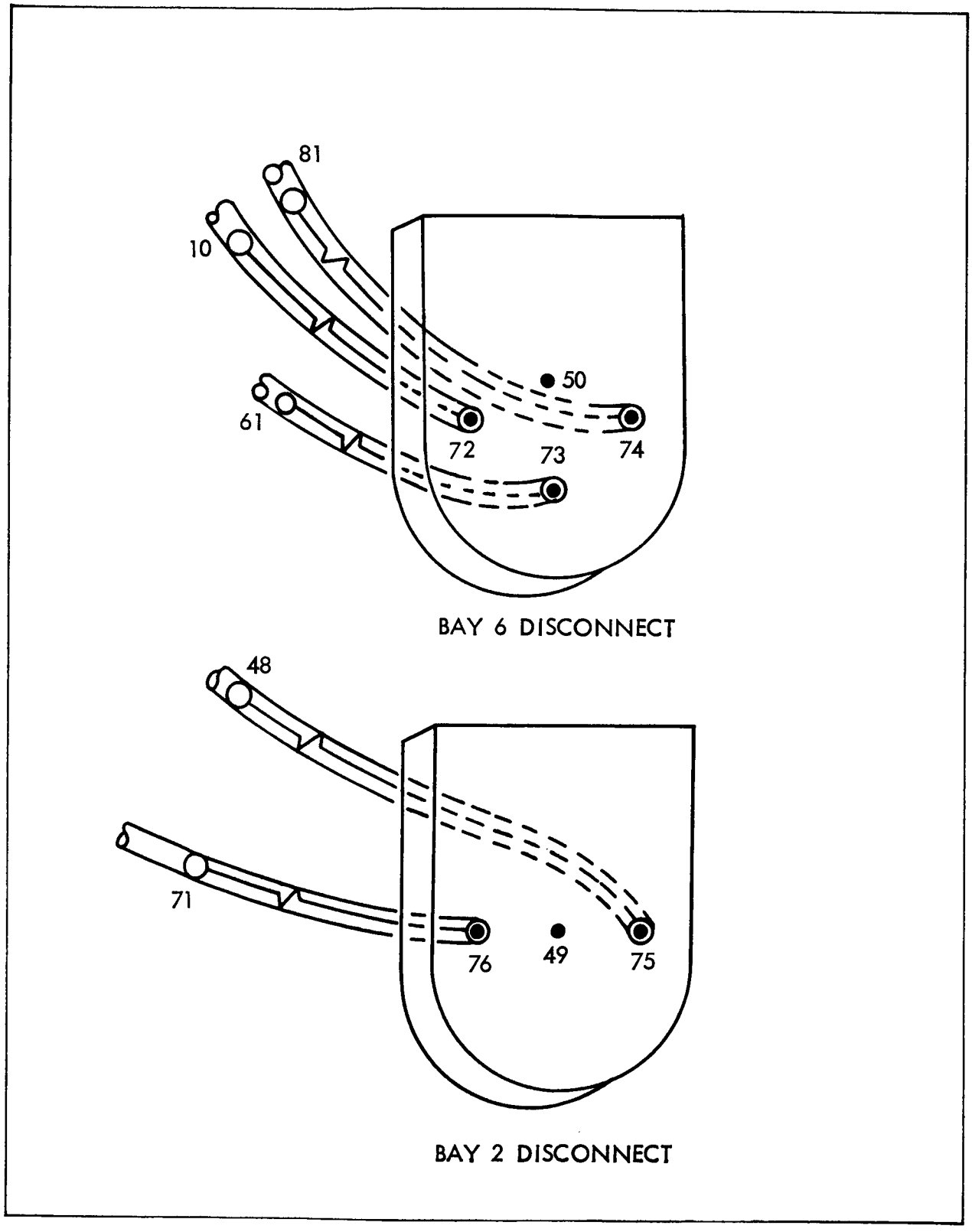

Figure 4-18. Disconnect Panels Nodal Layout

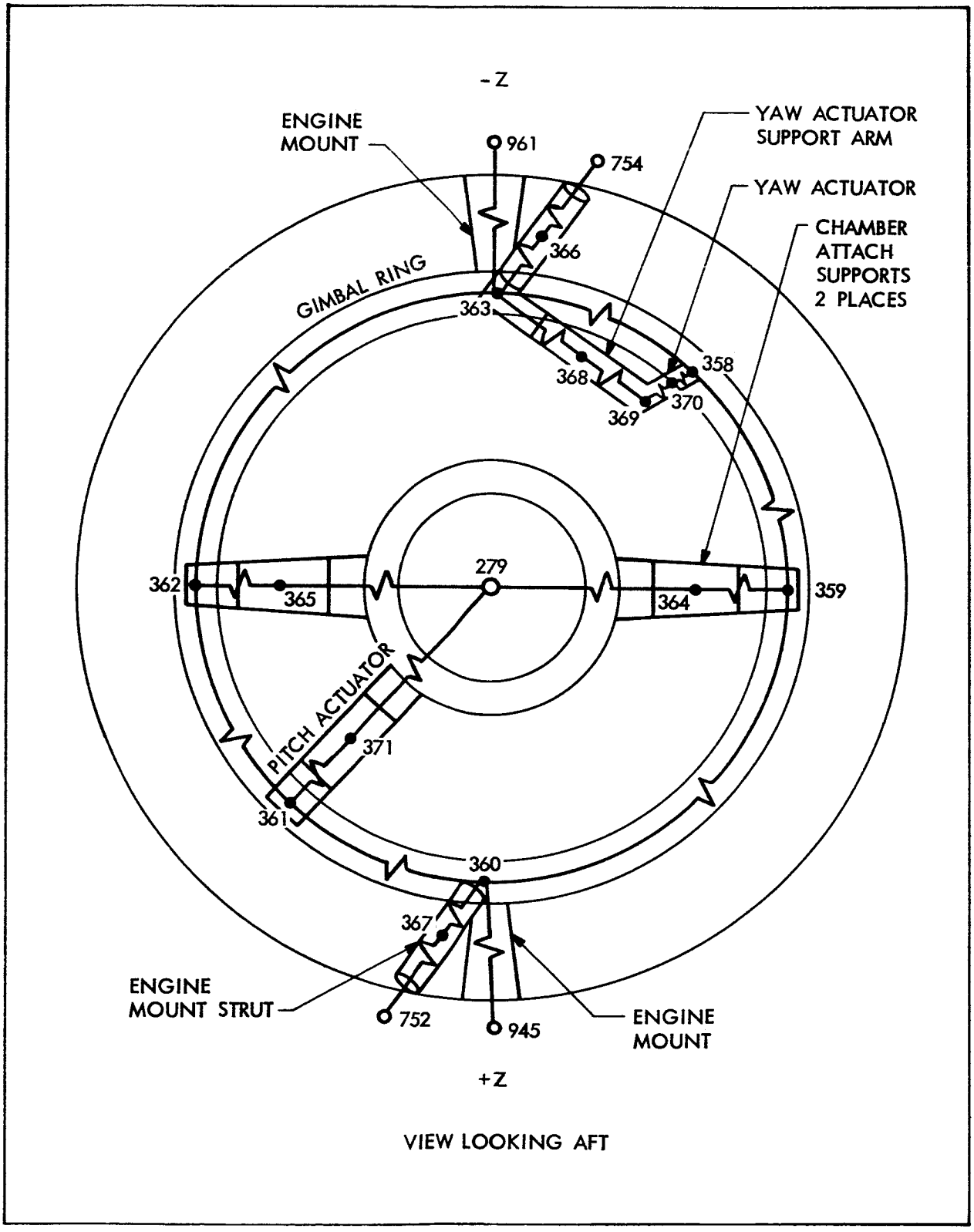

Figure 4-19. Gimbal Ring and Engine Supports Nodal Layout

the bare (uncoated) metal was generally assumed. Since the thrust chamber is considerably warmer than any other surface viewed by the components shown in Figure 4-19, their predicted temperatures are probably conservative, i.e., warmer than would be predicted if radiation to the surroundings were included.

Figure 4-20 presents an external view of the SPS engine thrust chamber, injector, and valves, showing sections into which the thrust chamber is axially divided. The injector and valve assembly were each represented by single nodes. The two are connected by radiation and conduction resistors. Although no details were available on the structural attachment between injector and valves, estimates were made on the size of pipe which would actually connect them. The thrust chamber, valves and injector were each connected by radiation resistors to the web mounts, the center sections, the propellant tanks and to various smaller components which surround them.

Cross-sections of the thrust chamber at the center of each axial section are also shown in Figure 4-20. The chamber was divided into four nodes radially and four circumferentially. Combined with the axial divisions, this resulted in a 48-node thrust chamber network. The radial nodes were distributed such that the interior two nodes were twice as thick as the two surface nodes. Thus the surface node centers were actually located on the chamber surface, as illustrated. These nodes are connected by conduction resistors in the radial direction only, since the resistance circumferentially and axially is so much greater than it is radially. Both the capacitors and resistors which make up this network were input as functions of time to account for the ablation and charring which takes place during engine firings.

Figure 4-21 shows two views of the thrust chamber interior radiation network. The nodes shown adjacent to the surfaces (413-416) are dummy nodes which provide for reflections off the walls. The network accounts for radiation from every interior node to every node it views. This includes radiation to space, to the injector, and to the nozzle extension, as well as to all chamber nodes. The radiation network which was used in this area is based on the Oppenheim method of solution. It can be used with the Thermal Analyzer Program providing the following modifications are made to the network parameters:

1) A zero capacitance dummy node is connected directly and singularly to each structure node.

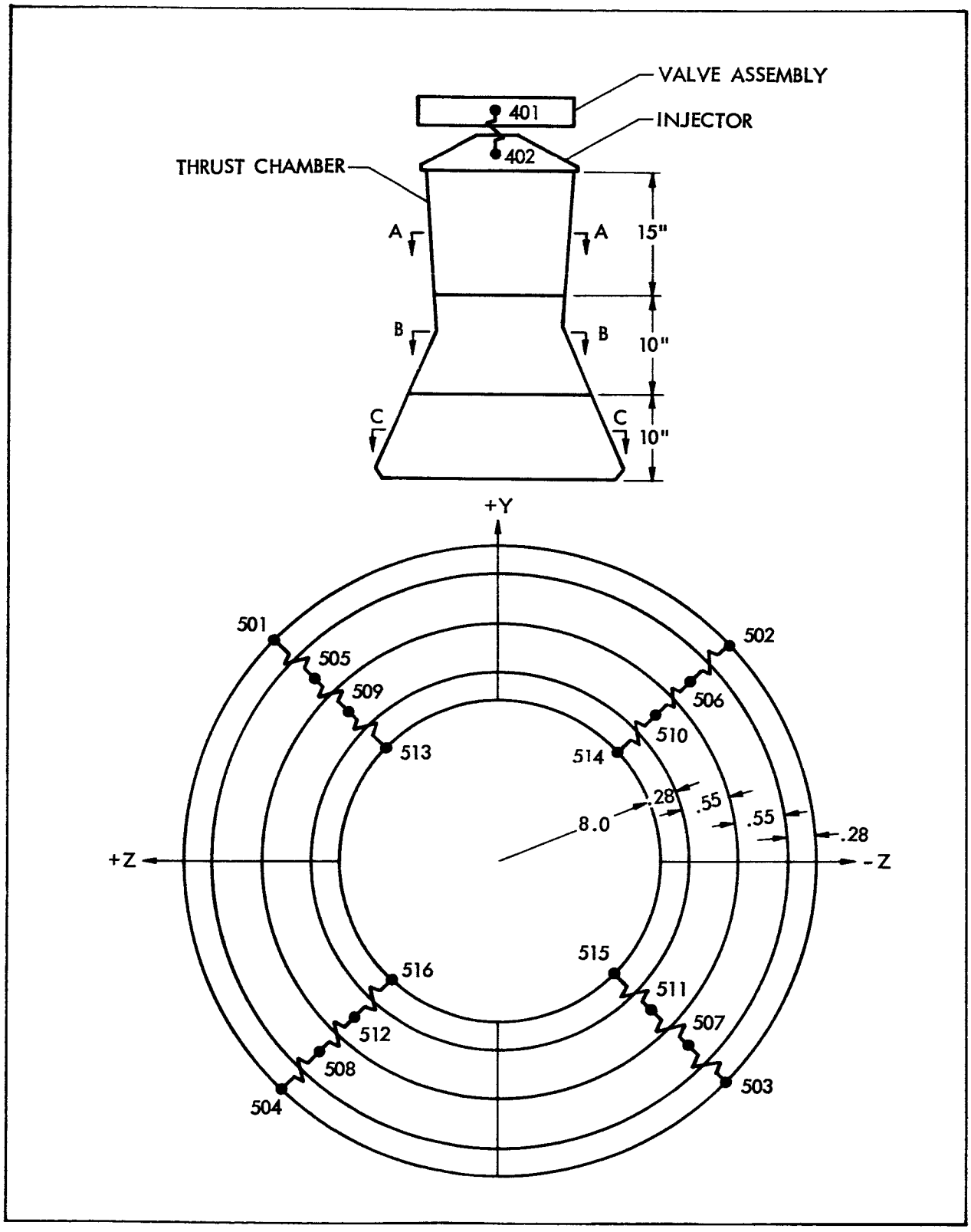

Figure 4-20. SPS Engine Nodal Layout

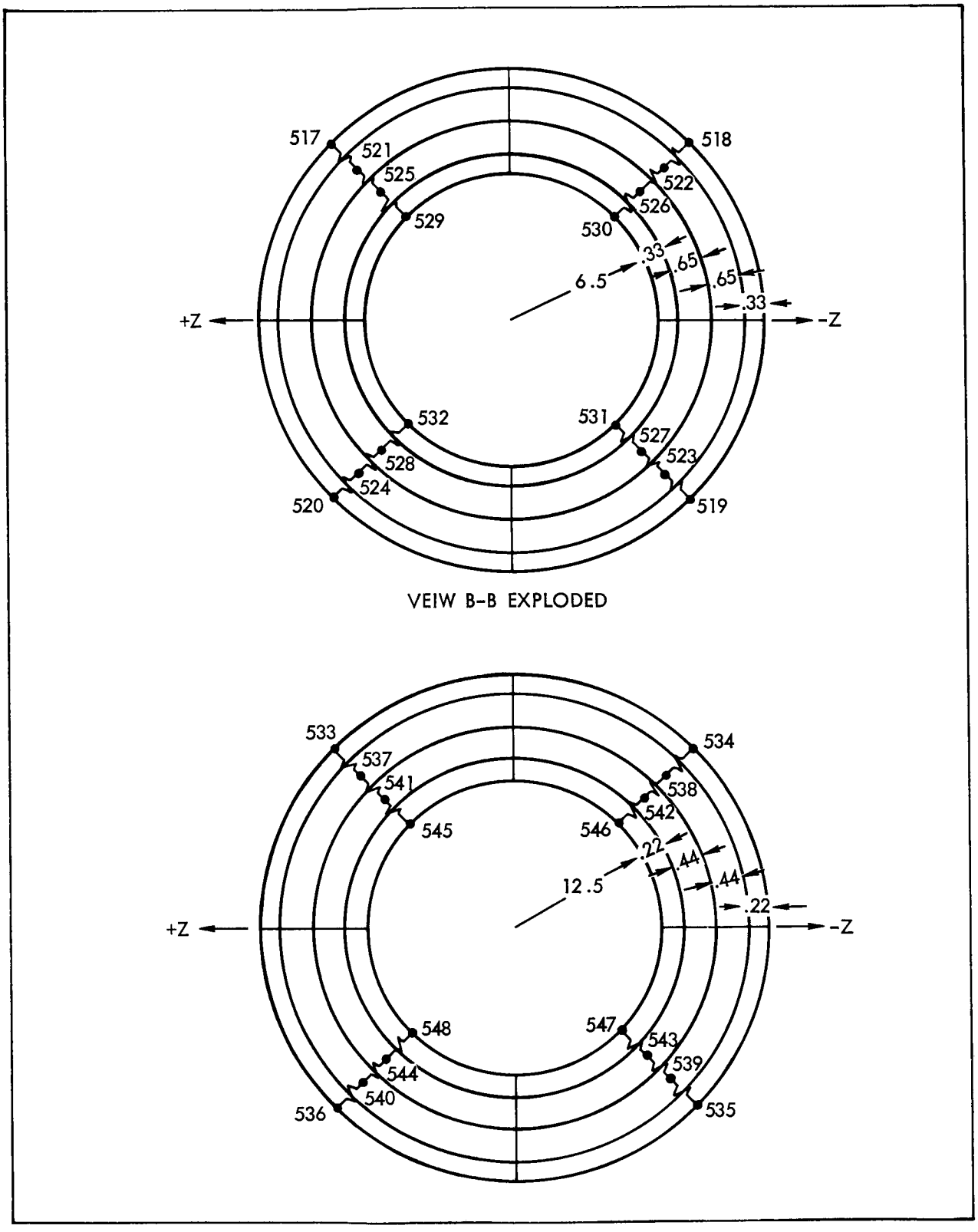

Figure 4-20. SPS Engine Nodal Layout (Continued)

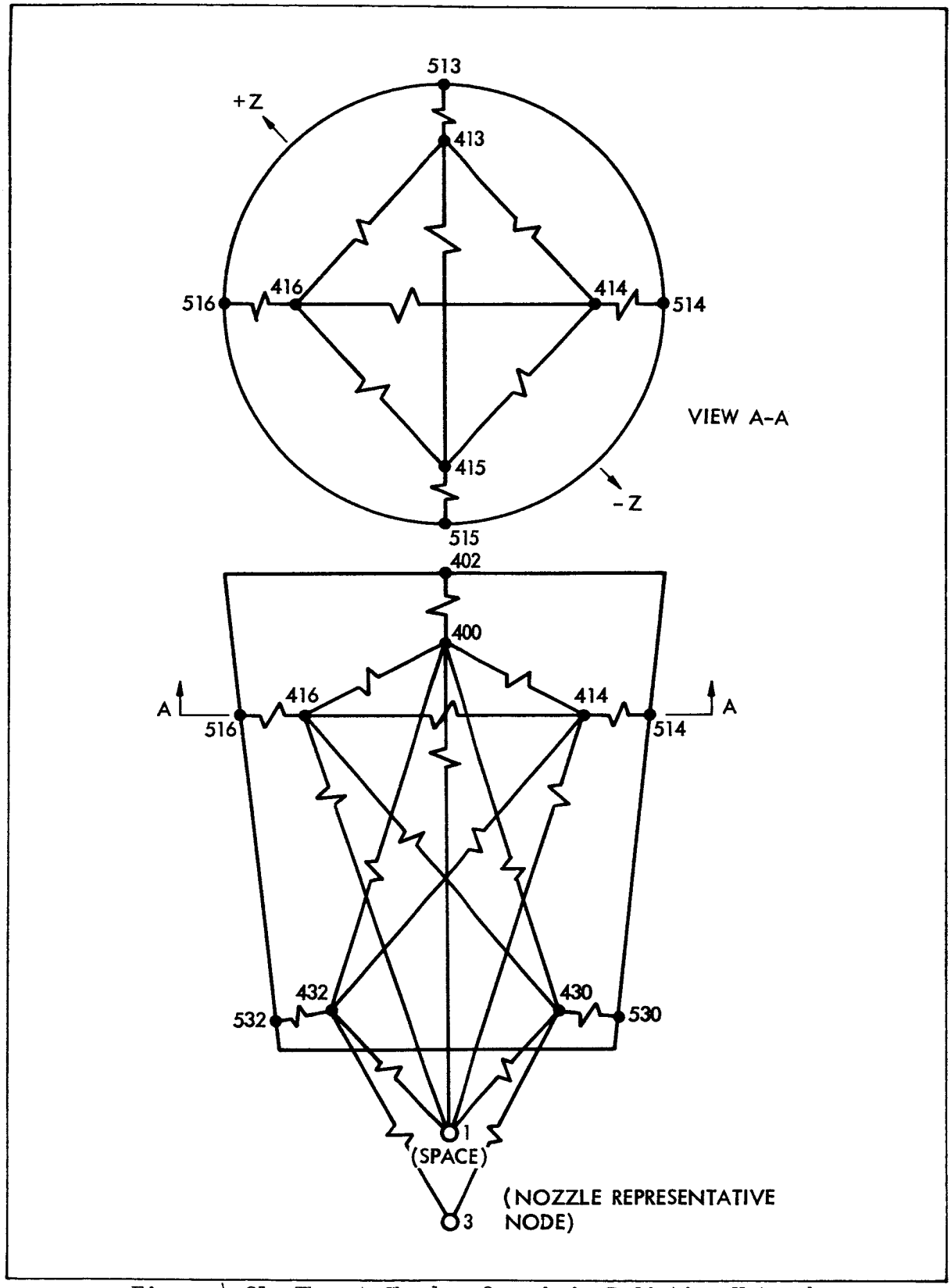

Figure 4-21 Thrust Chamber Oppenheim Radiation Network

2) A radiation resistor is inserted between this dummy node and its corresponding structure node whose radiation K-factor is computed by

$$K = \frac{A_1 \epsilon_1}{(1-\epsilon_1)\ 3600}$$

3) Radiation resistors interconnect all dummy nodes, and are computed by

$$K = \frac{A_1 F_{12}}{3600}$$

DETAILED FLUID STORAGE AND PRESSURIZATION SYSTEM ANALYSIS

The thermal network generated for the detailed fluid storage and pressurization analysis represented the propellant tanks and contained fluid, the helium bottles and pressurization gas, and the surrounding SM structure (beams, shell, bulkheads, and center webs).

The internal network for the propellant tanks is shown in Figure 4-22. The cylindrical sections are divided into 64 equal volume nodes, whose boundaries are formed by five equally spaced planes normal to the axis, two orthogonal planes through the axis, and three concentric cylinders parallel to the axis. The 16 nodes in each hemispherical dome are bounded by the orthogonal planes and by three concentric hemispheres whose radii coincide with the radii of the concentric cylinders. The outermost nodes represent the tank walls. All nodes are interconnected by conduction resistors. The network parameters are computed and updated by the program as the solution progresses as was discussed in Section III.

The external network for the propellant tanks consisted of conduction resistors along the tank skirts to the bulkheads, and radiation resistors between the tank nodes and the SM outer shell, beams, helium bottles, thrust chamber, and engine web mounts, where applicable. The temperatures of approximately 50 nodes from the basic analysis were used to represent the external environment for each propellant tank. These were connected to various tank nodes by approximately 70 resistors. A complete listing of the network, including radiation resistors, is given in Appendix B. Temperatures on the tank skirts were computed, rather than impressed, on the assumption that the bulkhead temperatures from the basic analysis were relatively independent of the propellant tank temperature, whereas the tank skirt temperatures were not.

The internal network for the helium bottle consisted of two nodes, representing the container and the gas, respectively, and connected by a convection resistor. The same external network, shown in Figure 4-23, was used for analyses of each of the four propellant tanks. The conduction network for the center webs was taken from the basic analysis and is presented in Figure 4-24. A transient temperature analysis was performed on the web mount nodes to which the helium bottle is attached, on the assumption that the

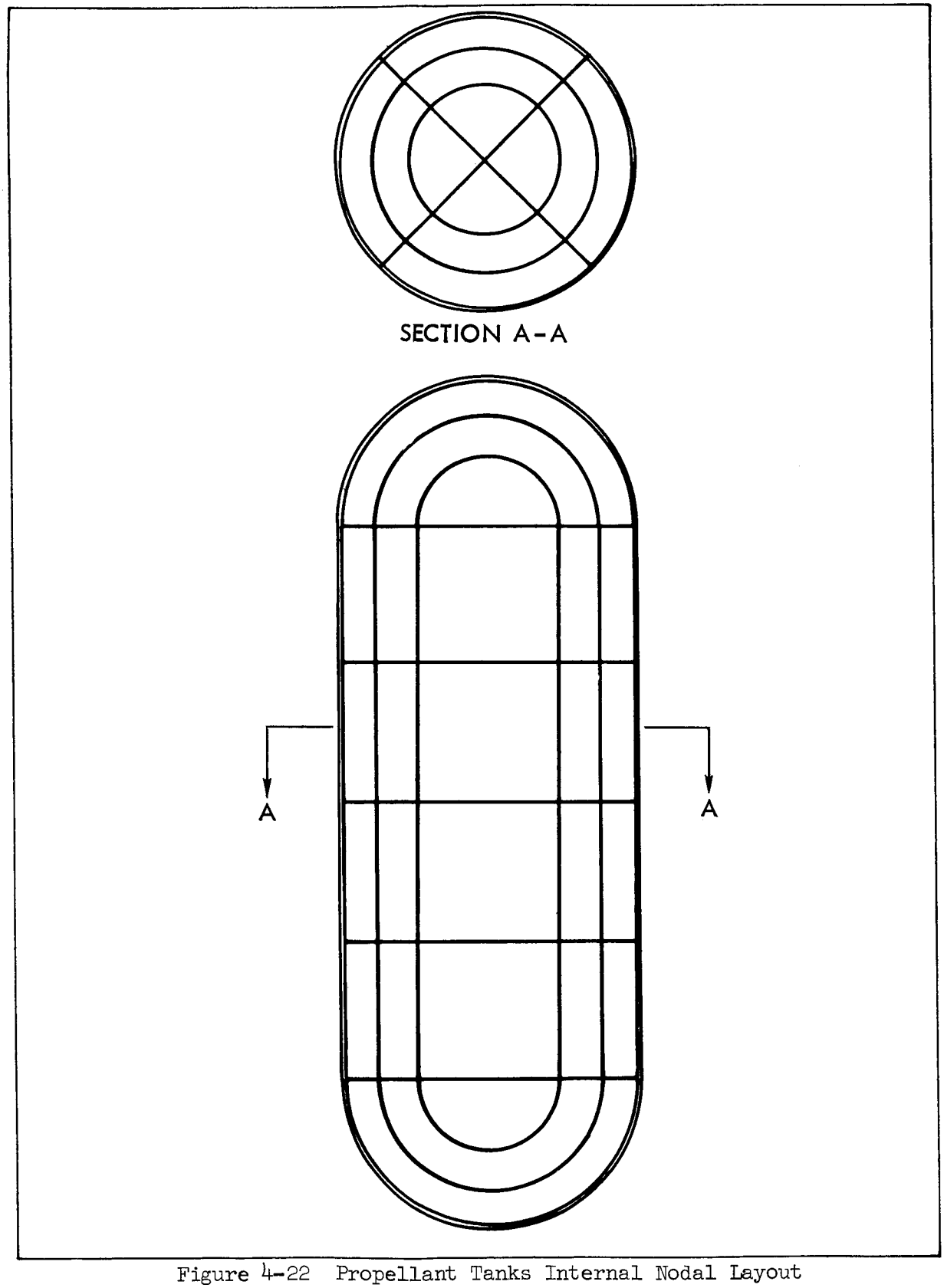

Figure 4-22 Propellant Tanks Internal Nodal Layout

LOCKHEED
CALIFORNIA COMPANY

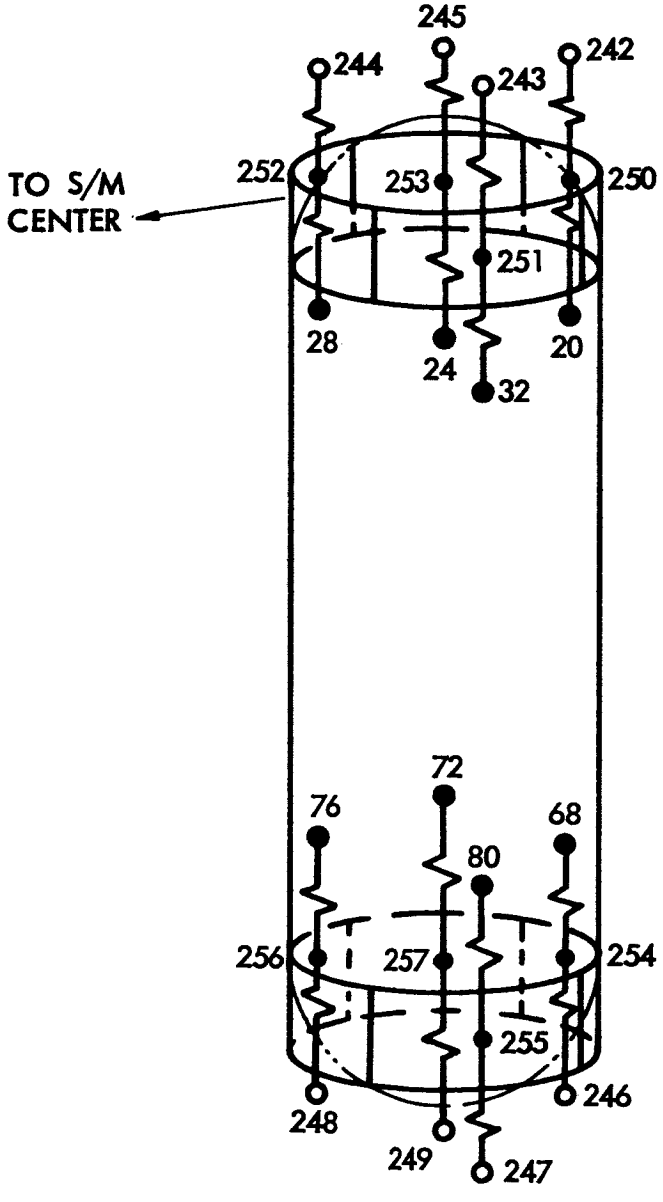

Figure 4-23 Propellant Tank Skirt Nodal Layout

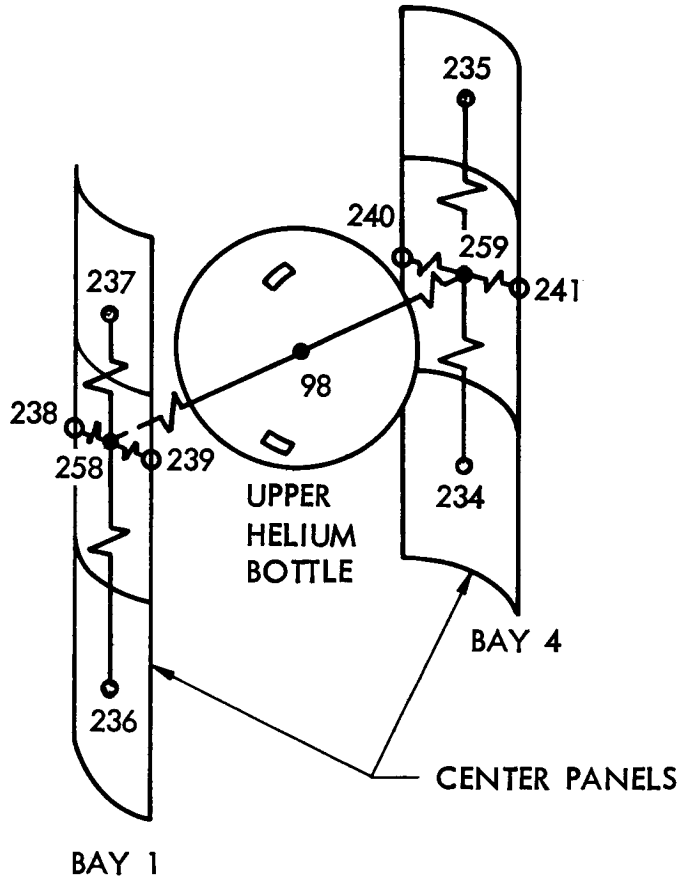

Figure 4-24 Helium Bottle Nodal Layout

LOCKHEED
CALIFORNIA COMPANY

temperatures computed from the basic analysis were highly dependent on the helium bottle temperature. Thus, the impressed temperatures were those along the edge of the web mounts, where the temperatures are more influenced by other factors.

V - ANALYSIS OF ASCENT HEATING AND ORBITAL RADIATION

The first step in the analytical process is the determination of the spacecraft thermal environment for each mission profile. The Service Module experiences its most severe heating during boost, and hence peak shell temperature will occur during this period. Following injection into earth orbit, the spacecraft is subjected to thermal radiation from the following sources:

- Insolation (direct solar)
- Albedo (reflected solar)
- Planetary (Earth and moon) emission

The SM external environment as computed using the methods discussed in Section III is presented in the pages to follow. These data were then used to compute the temperature data presented in Sections VI through VIII.

ASCENT HEATING

Ascent heating analyses for the Service Module basic shell were conducted for both a Saturn I and a Saturn V boost trajectory (Fig. 5-1). For both analyses it was found that aerodynamic heating rates were negligible compared to orbital radiative heating at about 150 sec. after lift-off. Also, the temperatures at this time correlated well with those calculated using orbital radiation data. Therefore, the ascent phase of the mission was assumed to end at 150 sec. although boost continues past this time. Orbital heat inputs were impressed on the vehicle subsequent to this time.

The maximum shell temperatures during boost are shown in Figures 5-2 and 5-3 for the Saturn I and Saturn V trajectories respectively. Both figures show regions of large temperature discontinuity or gradients. The most noticeable of these occur in Sectors 2, 3, 5, and 6 where the RCS packages are located. The high temperatures ($\approx 400^{\circ}$ F) are a result of localized increased heating near RCS protuberances. Likewise, the exceptionally low temperatures ($< 150^{\circ}$ F) are for those shell nodes located beneath the RCS heat shield insulation. Temperatures of nodes bordering the bulkheads or any of the beams are generally lower than their surroundings due to heat conduction to the adjacent heavy structure. The figures show that generally peak temperatures for the Saturn I mission are from 20° F to 25° F higher than those for the Saturn V mission.

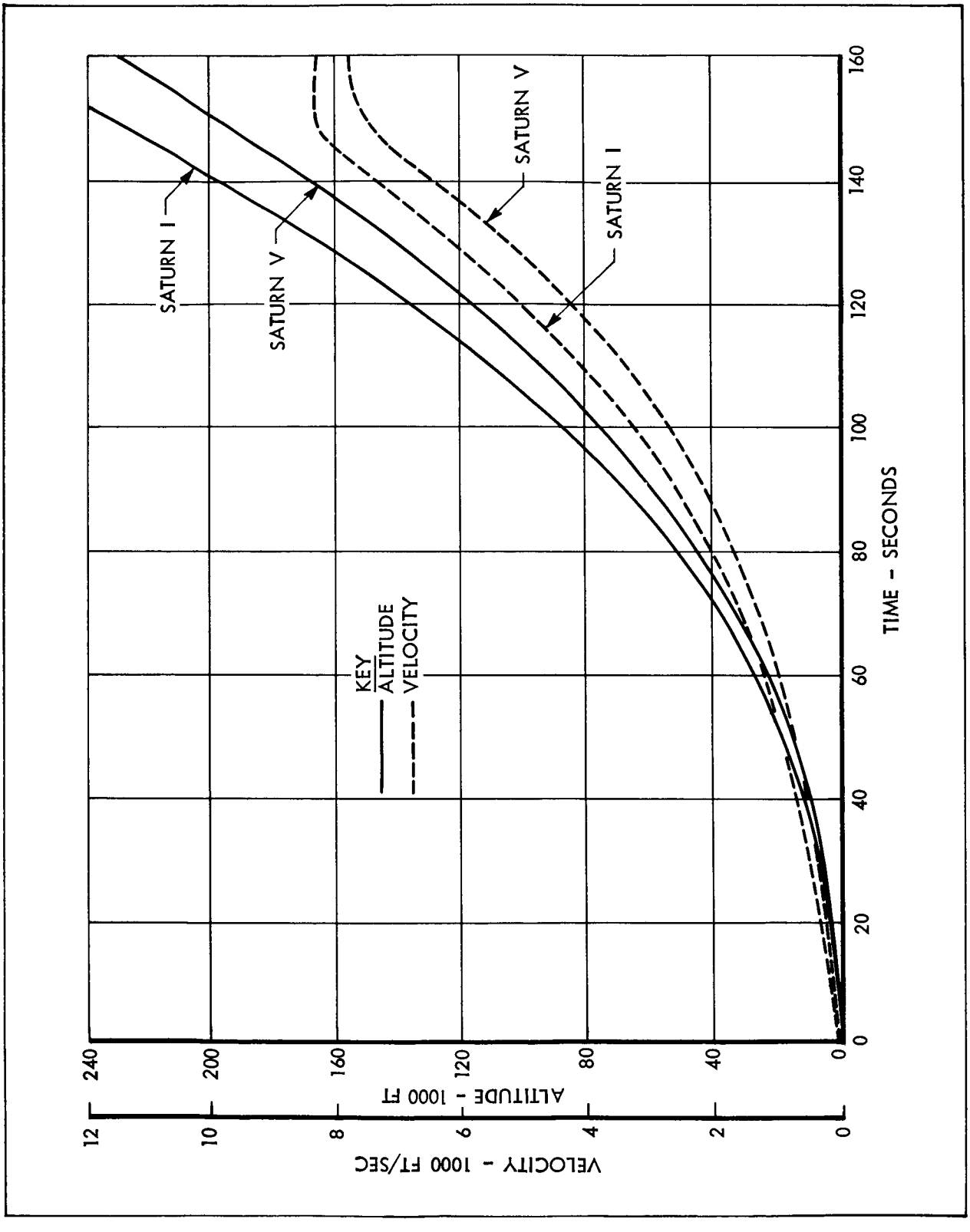

Figure 5-1 Apollo Ascent Trajectories

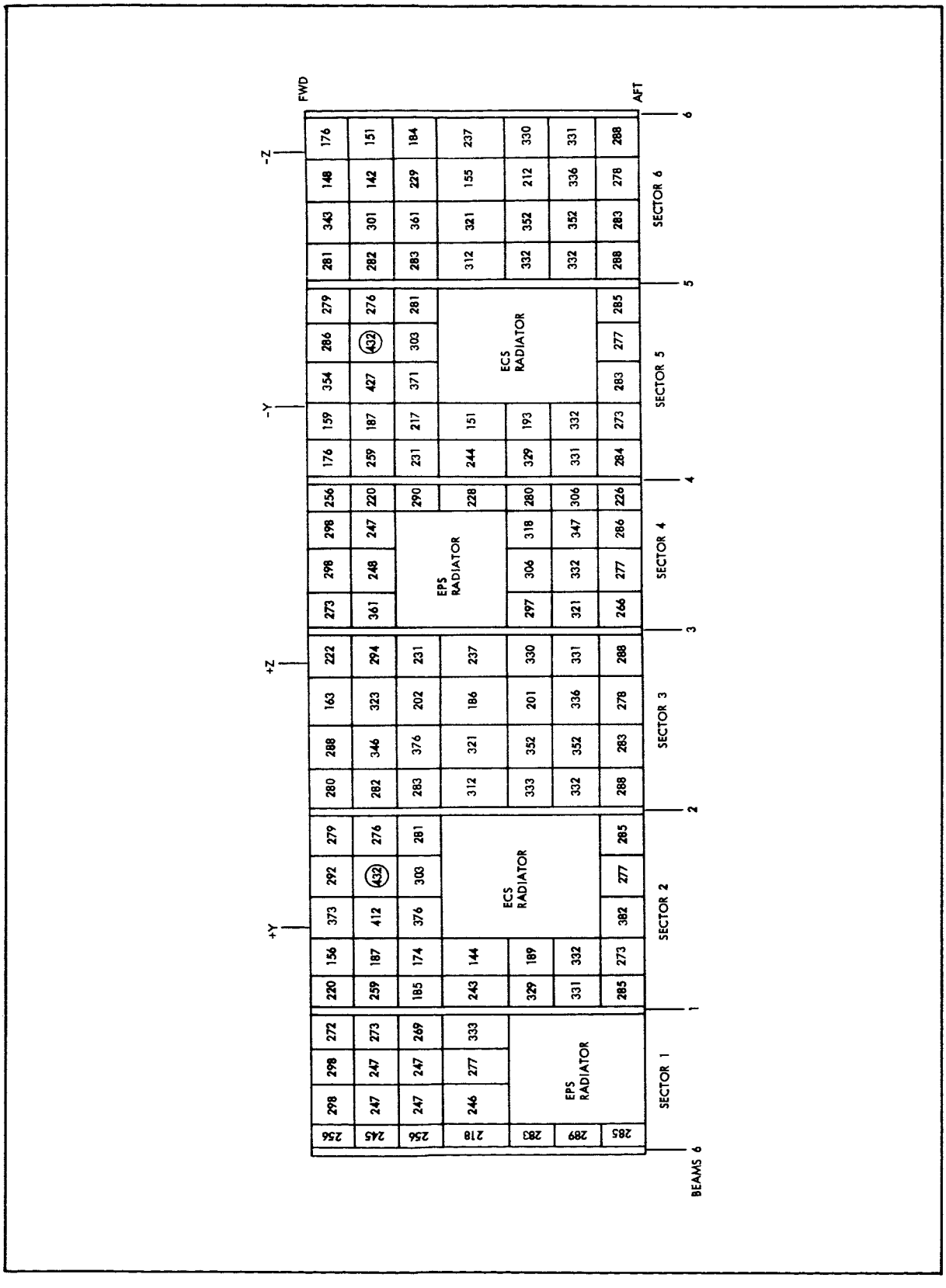

Figure 5-2 Maximum Ascent Temperatures for Shell Nodes, Saturn I Launch Vehicle

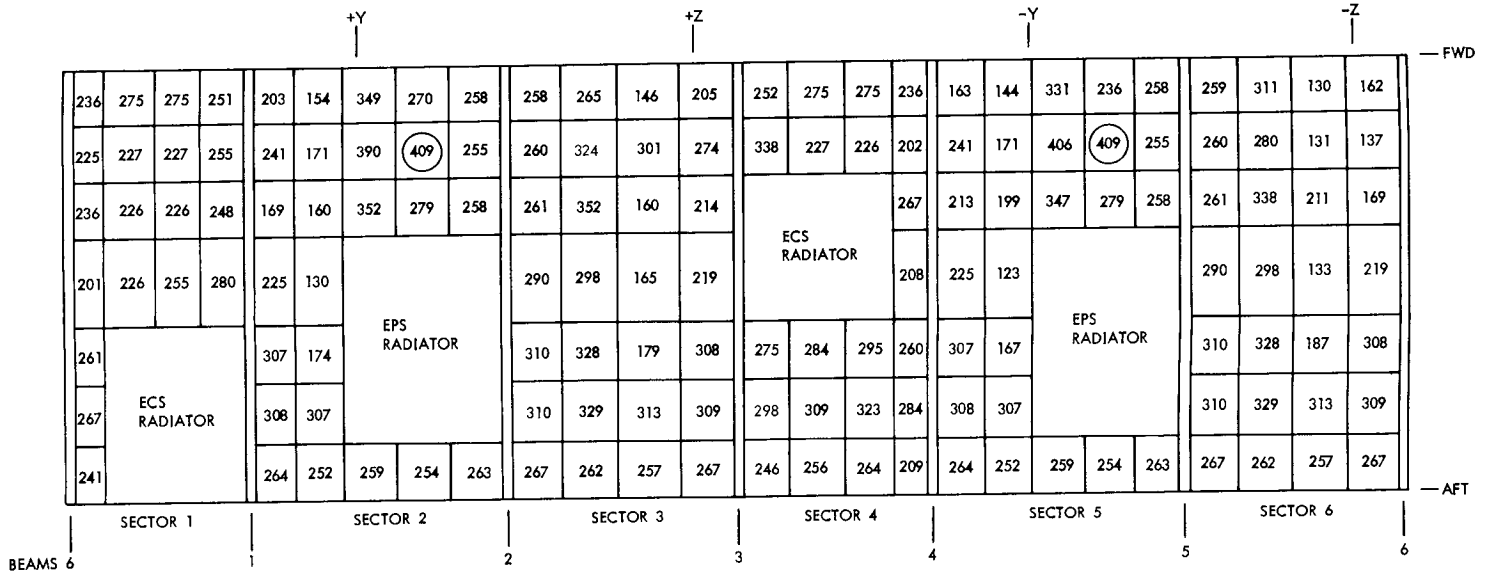

Figure 5-3 Maximum Ascent Temperatures for Shell Nodes, Saturn V Launch Vehicle

Figure 5-4 presents the peak temperatures attained by the RSC heat shields for the Saturn V mission. The values shown are merely average tempeatures over the surface designated. Heat shield temperatures for the Saturn I mission would run slightly higher than these.

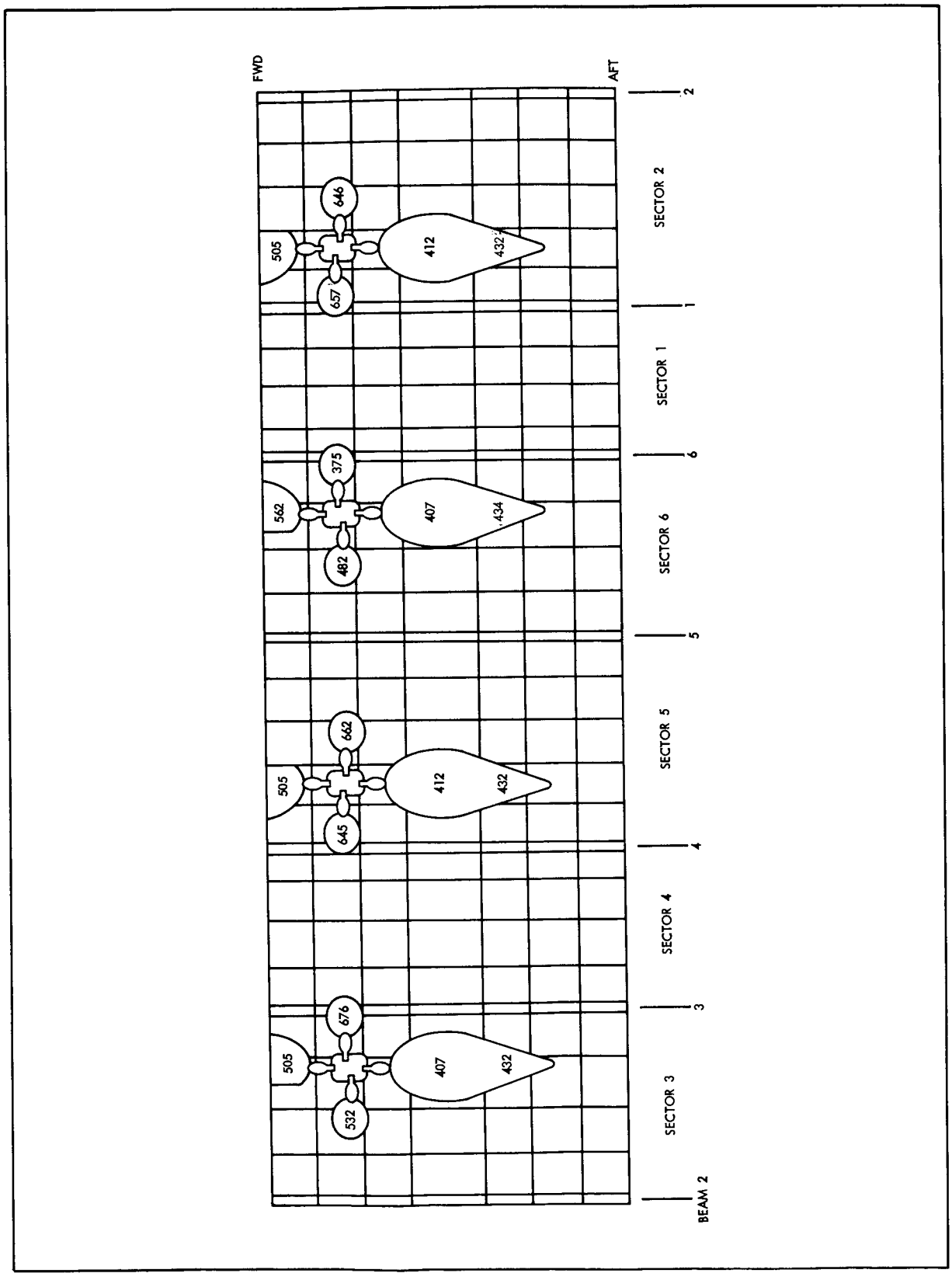

Figure 5-4 Maximum Ascent Phase RCS Heat Shield Temperatures
Saturn V Launch Vehicle

Before the ascent heating computations were performed, several test cases were run to determine temperature gradients through the honeycomb shell. The analyses were performed for a shell node which experienced no protuberance heating effects and which could be considered insulated from its surroundings. Both the inner and outer faces of the honeycomb, plus an equivalent skin which combined the two face sheets, were analyzed. Figure 5-5 shows the results of these analyses. A 40° F temperature gradient exists between the maximum inner and outer skin temperatures. The lumped skin, however, predicts temperatures to within 20° F of either actual skin temperature. Considering the additional storage and computations necessary to analyze both skins for the mission, it was decided that the lumped skin temperatures were accurate enough for the usage intended.

The foregoing ascent heating temperature data indicate that there may be thermal problems during this period. Even for the "lumped" case, aluminum structure temperatures over 430° F were predicted in the area of protuberances. As indicated in Figure 5-5, the actual temperature could be 20 - 40° F higher when gradients across the core are accounted for.

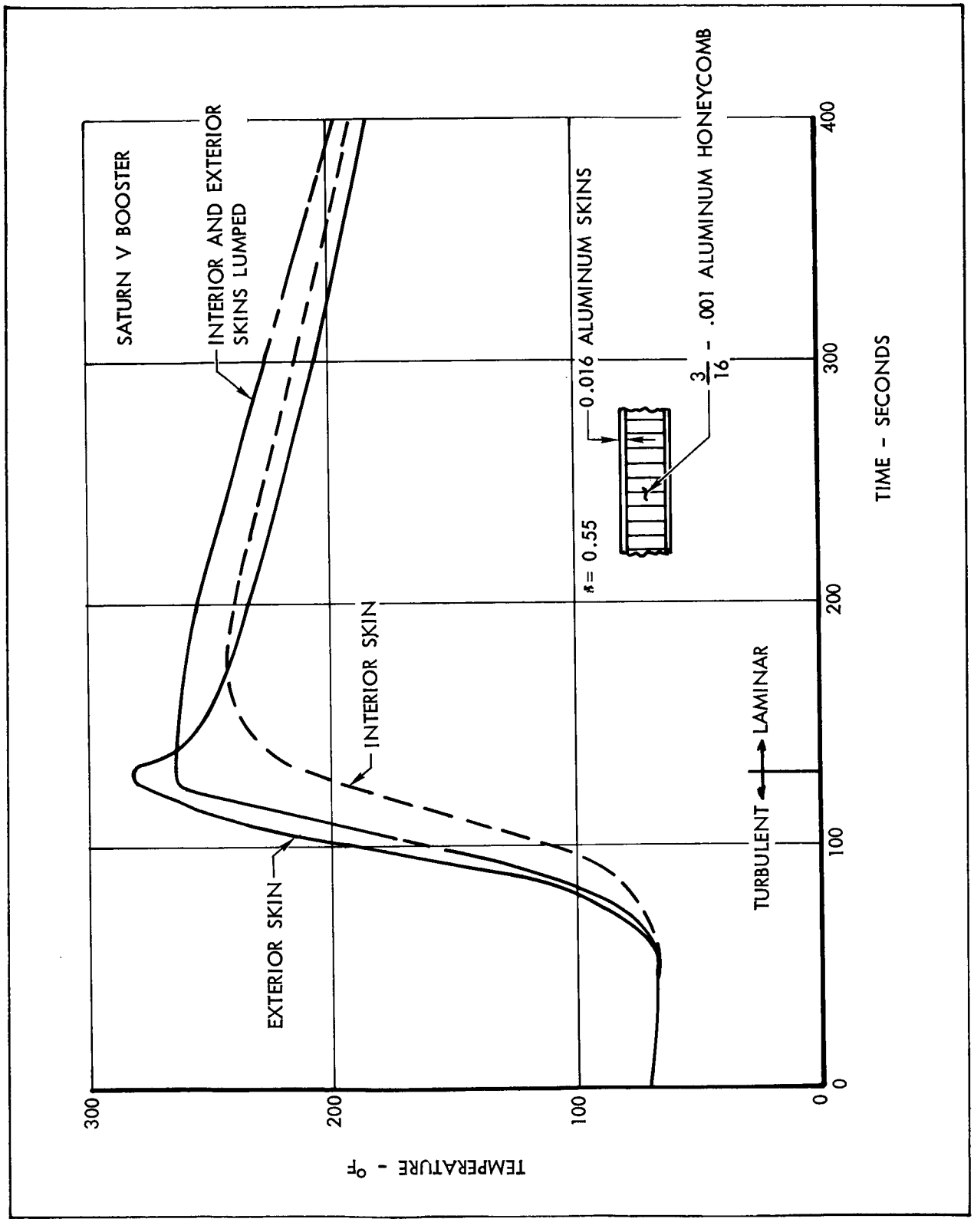

Figure 5-5 Ascent Skin Temperatures for Apollo Service Module, Station X_s 300

ORBITAL RADIATION

Orbital radiation calculations were performed for the Earth Suborbital and Orbital Missions and the Earth and lunar orbit phases of the Lunar Orbit Rendezvous Mission. The calculations for two nodes, described below, are typical of the results obtained. A large number of similar calculations were made for all external nodes for all orbital mission phases.

Figures 5-6 and 5-7 show the Earth orbital radiant heat flux incident to shell nodes 104 and 127. Node 104 is 21.6 degrees clockwise (when looking forward) from the + Y axis. Node 127 is 5.6 degrees clockwise from the -Z axis. The vehicle is planet oriented with the +X axis aligned with the flight path and the +Z axis parallel to the zenith. The heating calculations were performed with the Orbital Radiation Program, and machine plotted using a Calcomp Plotter.

The orbital heating to node 104 consists primarily of direct solar irradiation because of the small view factor for Earth emission and albedo. The incident Earth emission is comparatively uniform throughout the orbit with an average value of 14.2 Btu/hr ft^2. The integrated albedo heat pulse is approximately half that of Earth emission, and reaches a maximum value of 20.7 Btu/hr ft^2 at the subsolar point.

The heating to shell node 127 consists primarily of Earth emission, which is comparatively uniform throughout the orbit with an average value of 72 Btu/hr ft^2. Albedo is less significant but achieves a higher maximum intensity (115 Btu/hr ft^2) at the subsolar point. The solar input to node 127 consists of two "spikes" as the SM enters and leaves the Earth's shadow.

Figures 5-8 and 5-9 show the lunar orbit irradiation for the same two shell nodes. Here the +X axis is pointing toward the center of the moon and the +Z axis is aligned with the flight path. Thus, node 127 is located near the trailing edge of the vertical cylinder, and node 104 is around on the side of the vehicle, facing South. Because of the nose down orientation and the equatorial orbit, the lunar emission is nearly identical for nodes 104 and 127 and reaches a maximum intensity of 105 Btu/hr ft^2 at the subsolar point. Likewise, the albedo inputs are nearly identical and reach a maximum intensity of 8 Btu/hr ft^2 at the subsolar point. The solar inputs, however, are considerably different. Node 104 receives a large solar input as the vehicle

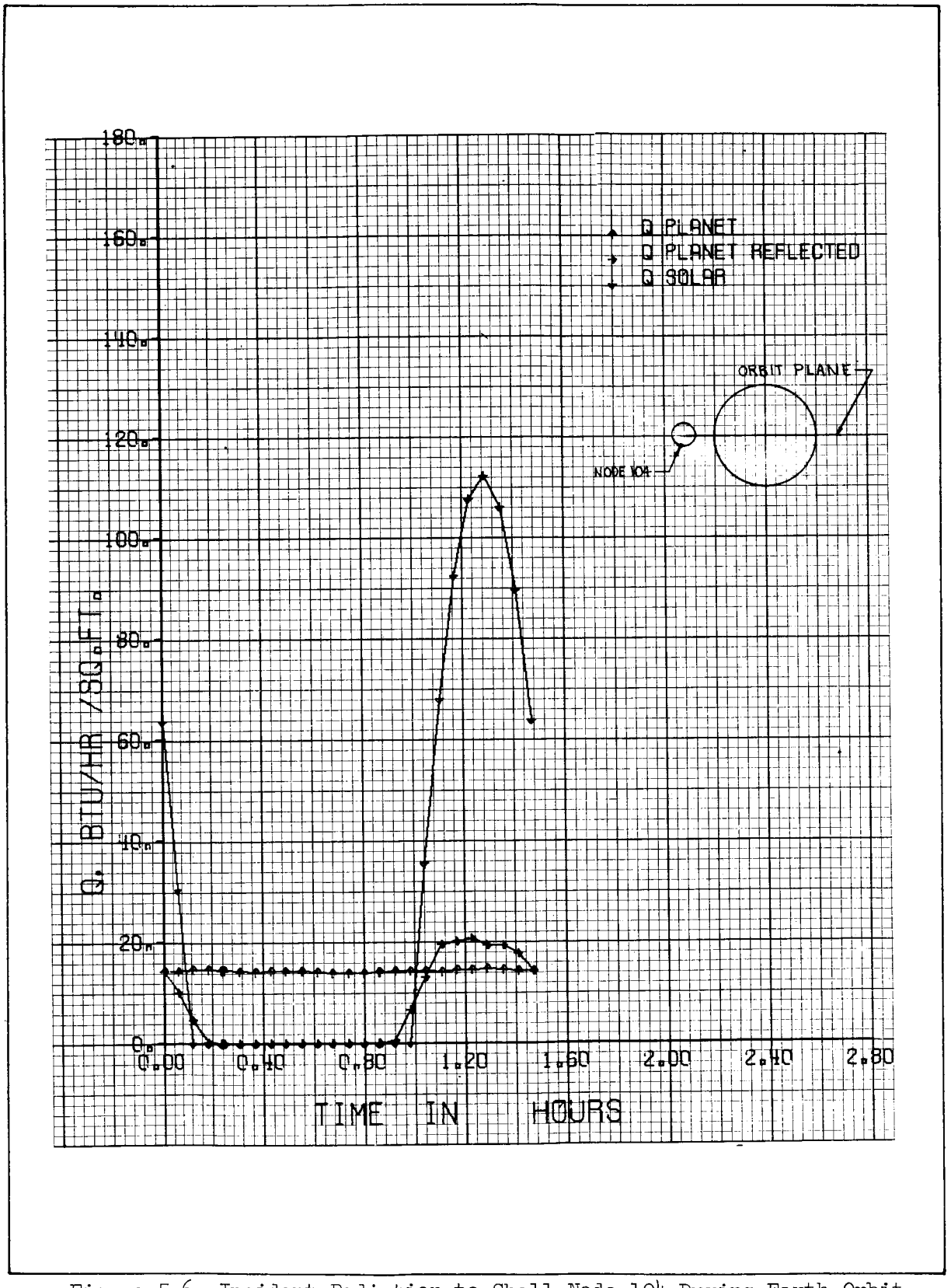

Figure 5-6 Incident Radiation to Shell Node 104 During Earth Orbit

LOCKHEED
CALIFORNIA COMPANY

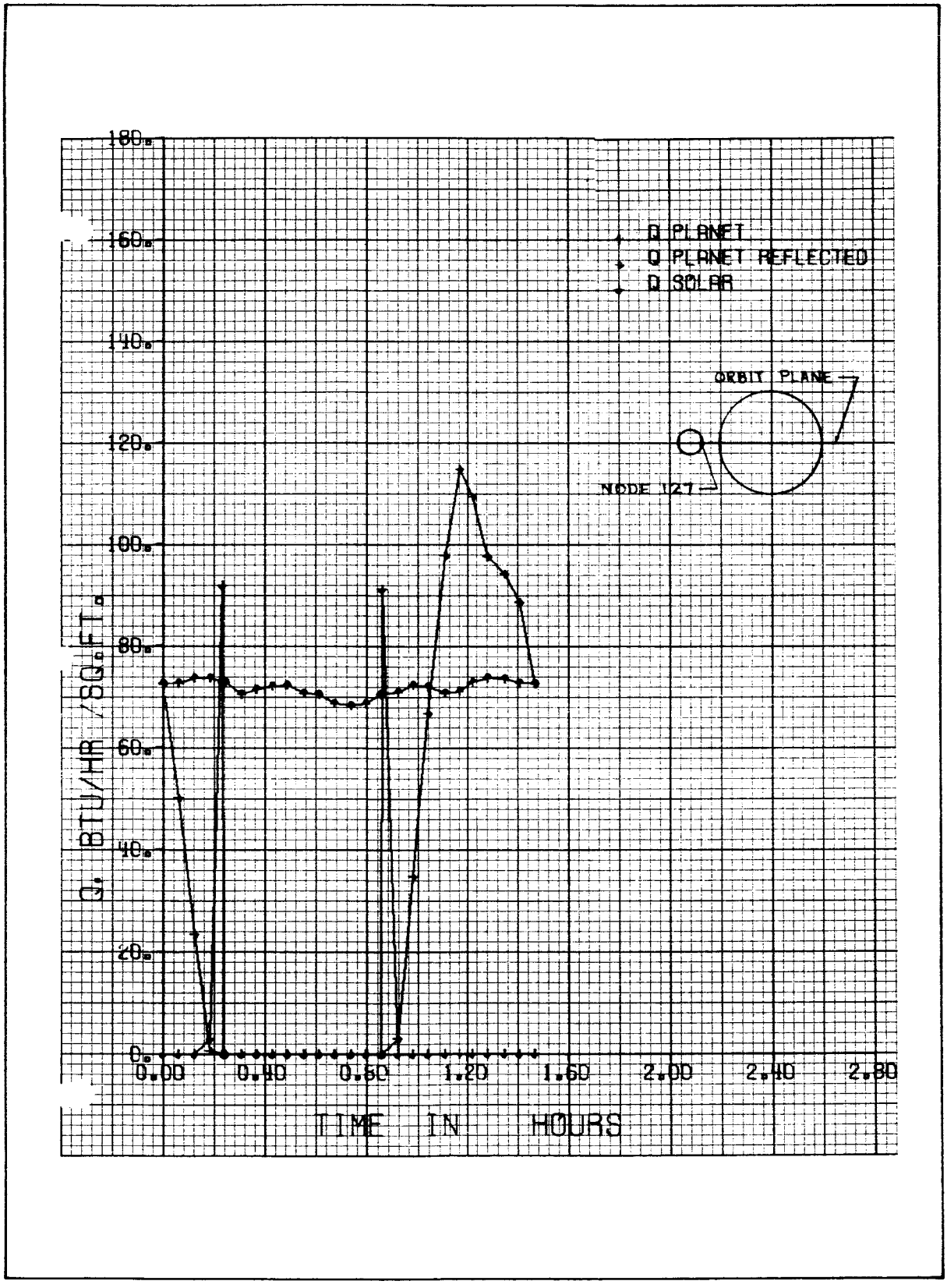

Figure 5-7 Incident Radiation to Shell Node 127 During Earth Orbit

LOCKHEED CALIFORNIA COMPANY

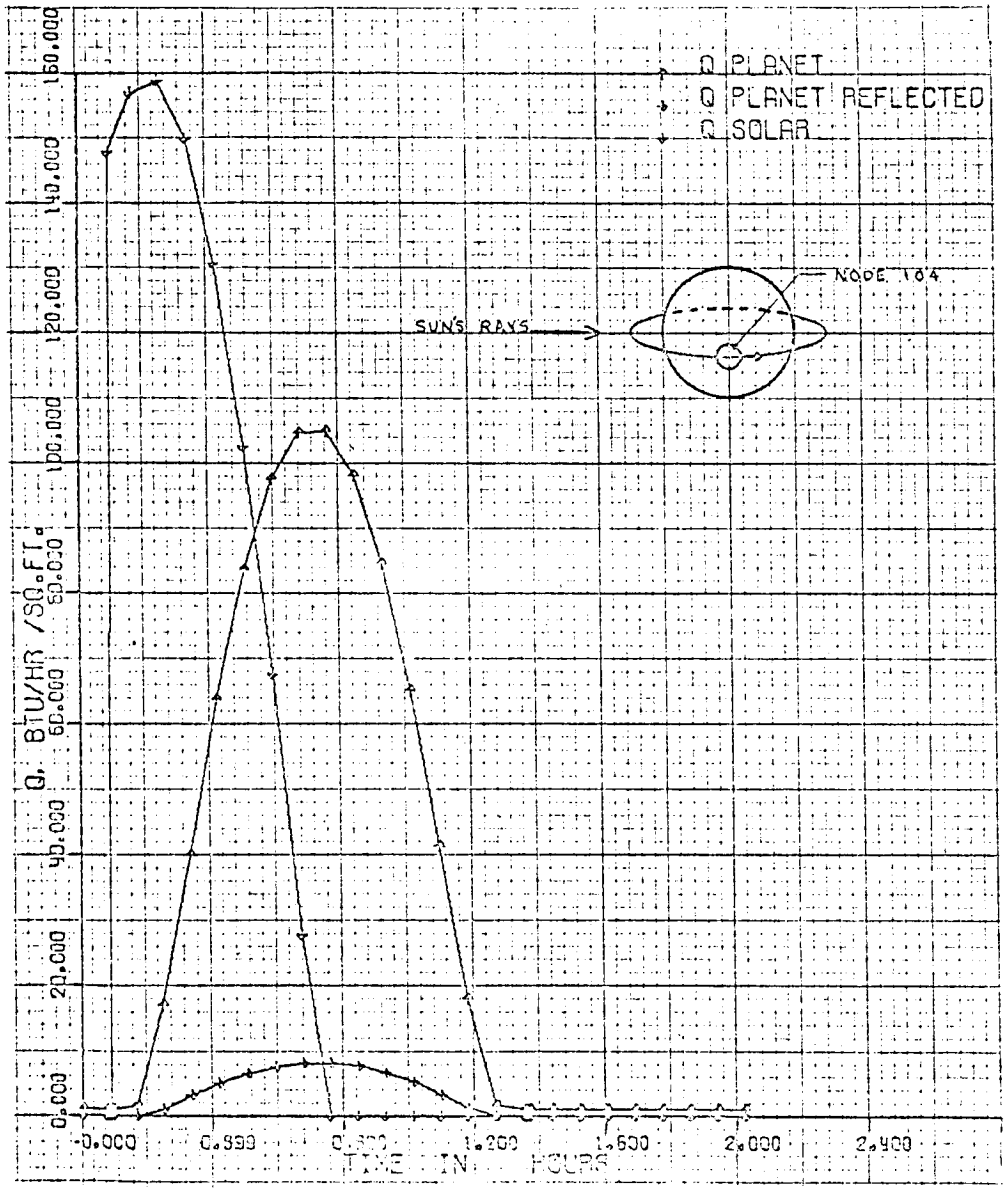

Figure 5-8 Incident Radiation to Shell Node 104 During Lunar Orbit

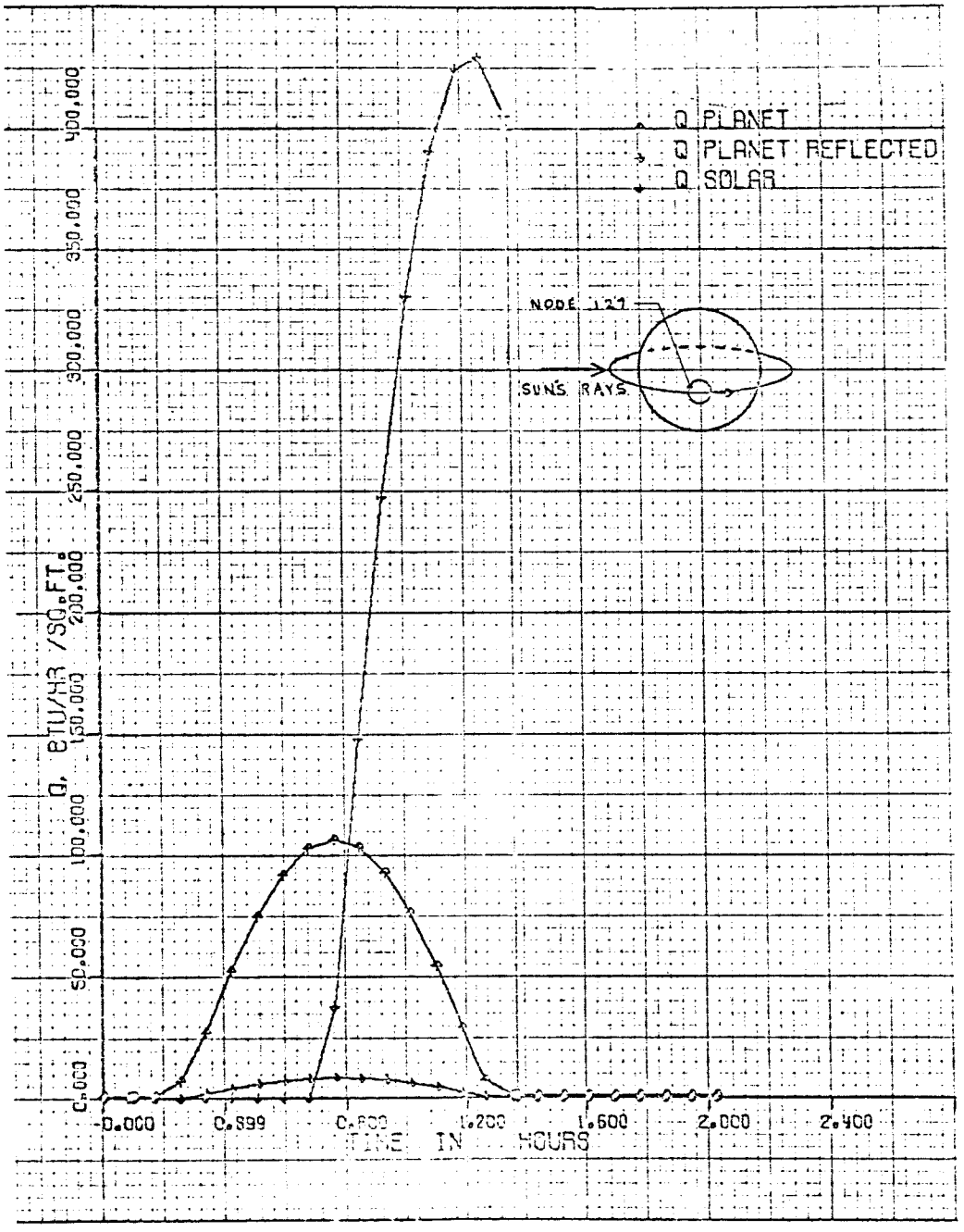

Figure 5-9 Incident Radiation to Shell Node 127 During Lunar Orbit

leaves the Moon's shadow. The intensity increases to a maximum of 159 Btu/hr ft^2 at the terminator and then decreases sinusoidally to zero at the sub-solar point. At this point, node 127 is exposed to solar irradiation. The intensity increases sinusoidally to a maximum value of 430 Btu/hr ft^2 at the terminator. By the time the vehicle reaches the shadow point, the solar flux decreases to 400 Btu/hr ft^2. On the dark side of the moon the incident flux to shell nodes is less than 2 Btu/hr ft^2 and is due entirely to lunar emission.

Orbital heating calculations were performed for each of the 26 sets of circumferential shell nodes around the SM, and for all nodes on the aft bulkhead, aft heat shield, and nozzle extension. A second set of lunar orbit heating calculations were performed for an orientation consisting of the +X axis aligned with the flight path and the +Z axis parallel to the zenith. All of these calculations were provided to NASA in the form of punched IBM cards suitable for direct input to the Thermal Analyzer Program.

VI - ANALYSIS OF SERVICE MODULE BASIC STRUCTURE, LUNAR ORBIT RENDEZVOUS MISSION

The anlaysis of the Service Module (SM) basic structure includes the investigation of all SM temperatures for the entire Lunar Orbit Rendezvous Mission, with the exception of the cryogenic tankage and Reaction Control System (RCS) packages, which were neglected (see Section II), and the Service Propulsion System (SPS) plumbing, engine, and pressurization components, which were analyzed separately. The temperature histories obtained in this analysis were used as boundary conditions for the separate plumbing, engine, and pressurization analyses, which are described in Section VII. A summary of these data is shown in Table 6-1.

TABLE 6 - 1

Summary of SM Structure Temperatures during Lunar Orbit Rendezvous Mission

Module Component	Temperature (^{o}F) *Maximum	*Minimum
Shell	247	-123
Radial Beams	121	-10
Forward Bulkhead	194	-56
Aft Bulkhead	200	-38

* Maximum and minimum temperatures over entire mission for normal orientation (except for boost phase).

This section presents temperature data for the shell, radial beams, bulkheads, heat shield, and the nozzle extension during the Lunar Rendezvous Mission. In the discussions to follow, unless otherwise noted, the translunar and transearth data are for the normal, two-revolution per hour, roll orientation. In addition, two other orientations were investigated, namely:

- Maximum SM heating, with the engine nozzle pointing towards the sun.
- Minimum SM heating, with the engine nozzle pointing away from the sun.

Only that portion of the mission during which these orientations are employed is discussed. This is because orbital and midcourse correction temperatures quickly reach the values obtained during normal orientation. Therefore, it was not necessary to analyze the transients following an attitude change from

a maximum or minimum SM heating orientation to the normal translunar or transearth orientation.

To avoid classifying the transient temperature histories contained in this and the following sections, time references of specific events (e.g. transearth injection, etc.) are omitted. Mission profiles containing the sequence of events important to the analyses are included in the separate, classified appendix D.

OUTER SHELL

Complete temperature histories for five representative shell nodes are shown in Figure 6-1. By noting similarities in location, data for all other shell nodes may be approximated from the figure. These plots were obtained from the Calcomp plotter used in conjunction with the Thermal Analyzer Program. The initial scale routines were not satisfactory. Improved scale routines were eventually obtained.

The temperature history of node 710 is typical of those shell nodes which are not significantly influenced by adjacent nodes. Shell node 611 is adjacent to radial beam 3, and due to conduction heat exchange with the beam, has a slightly smaller cyclic temperature variation. The temperature of shell node 810 is influenced by conduction to an adjacent aft bulkhead node. Node 801 is a portion of the "T" section at the outer edge of radial beam 1, and due to its large mass compared to its surface area exposed to space, cycles over a relatively small temperature range. The temperature of shell node 703 is influenced by the input temperature history of the adjacent ECS radiator node, which has a much smaller cyclic temperature variation than the basic shell. Computing intervals were reduced during periods in the vicinity of SPS engine firings.

Shell maximum and minimum temperatures for typical mission segments are shown in Figure 6-2. These data include earth orbit, translunar and transearth roll, midcourse corrections, and lunar orbit. The overall maximum and minimum temperatures on the shell are encircled for each mission phase. The same method of presenting maximum and minimum structure temperatures is used throughout this report.

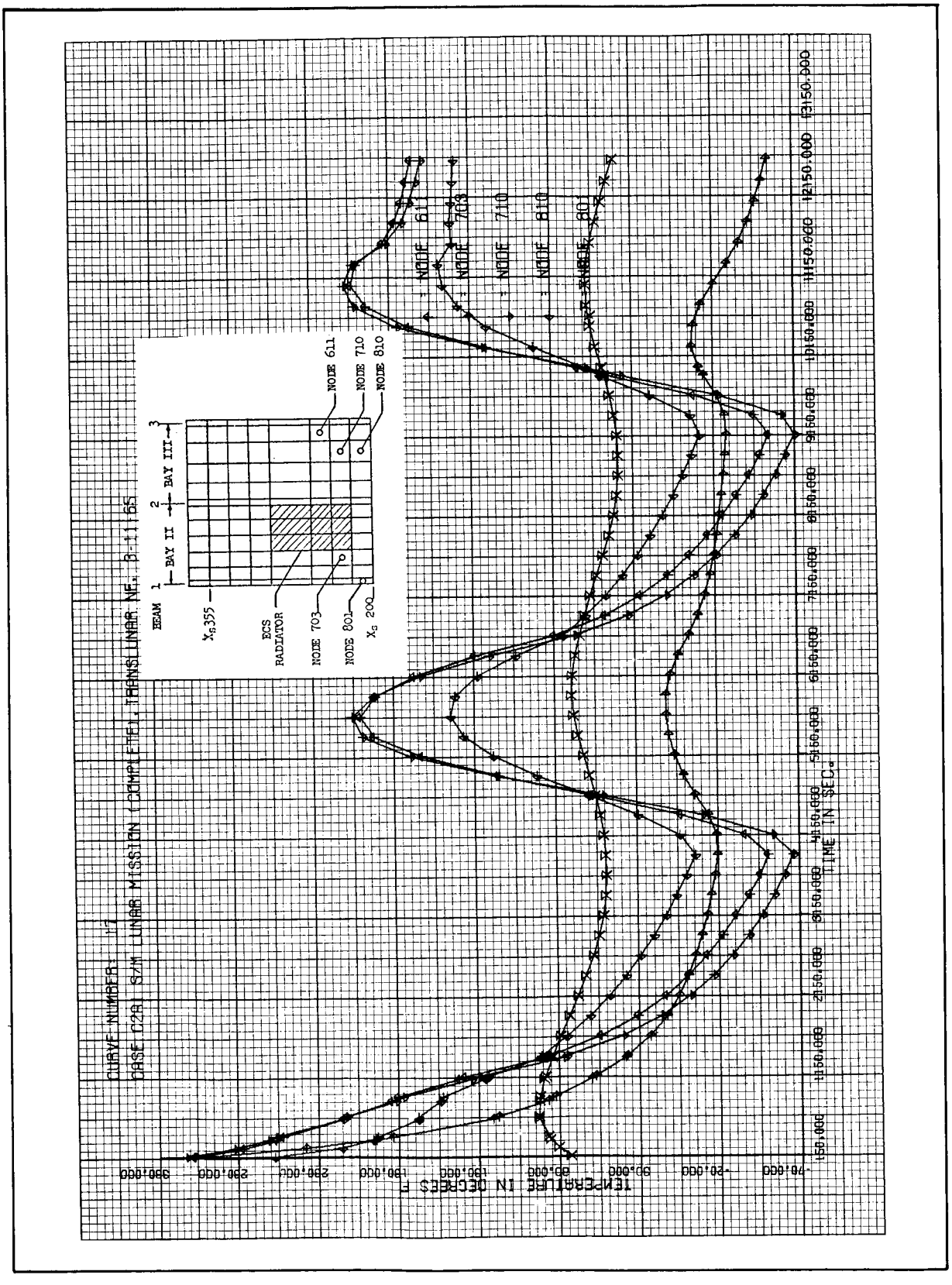

Figure 6-1a Shell Temperature Histories for Lunar Orbit Rendezvous Mission

LOCKHEED CALIFORNIA COMPANY

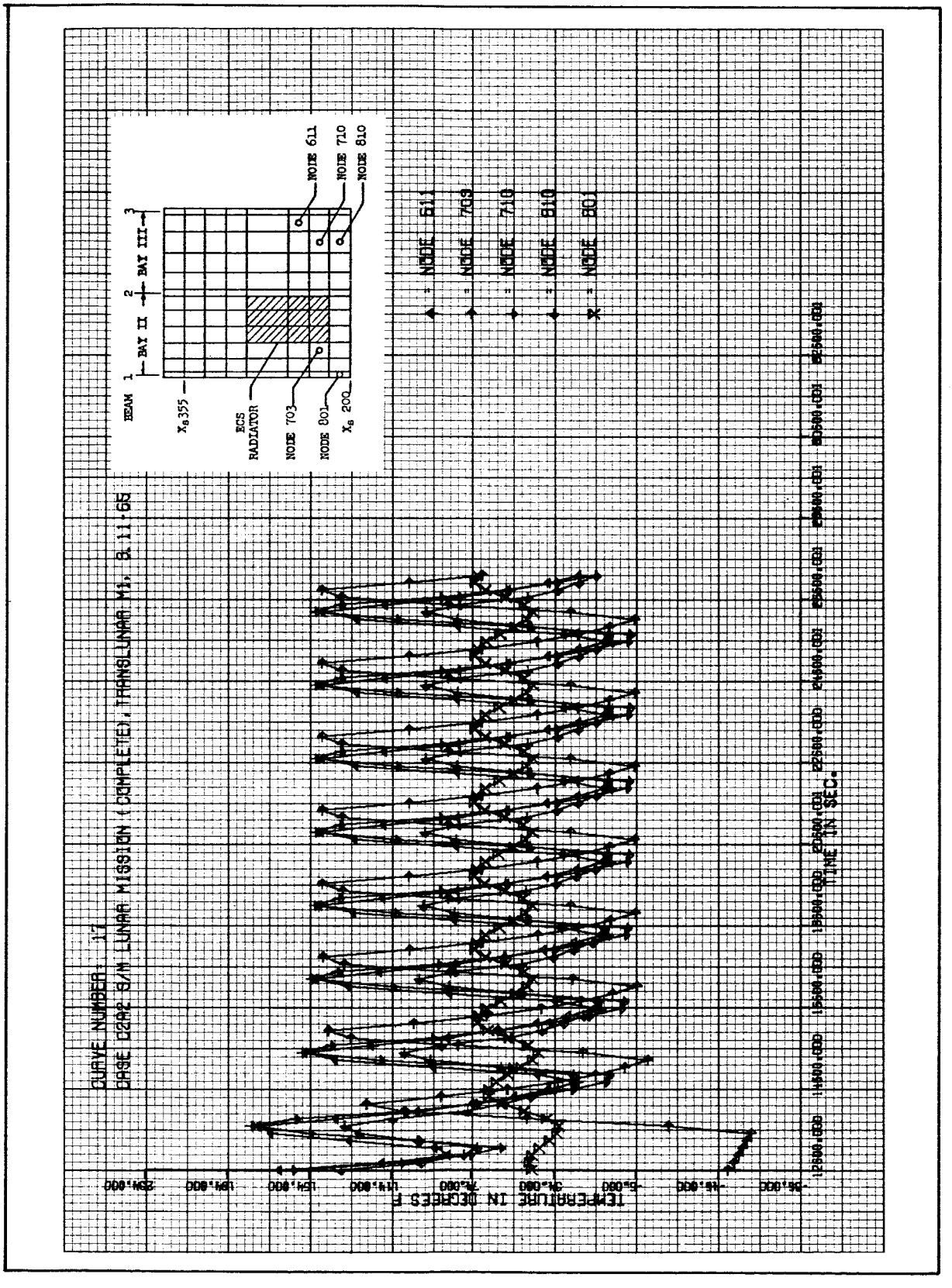

Figure 6-1b Shell Temperature Histories for Lunar Orbit Rendezvous Mission (Continued)

LOCKHEED CALIFORNIA COMPANY

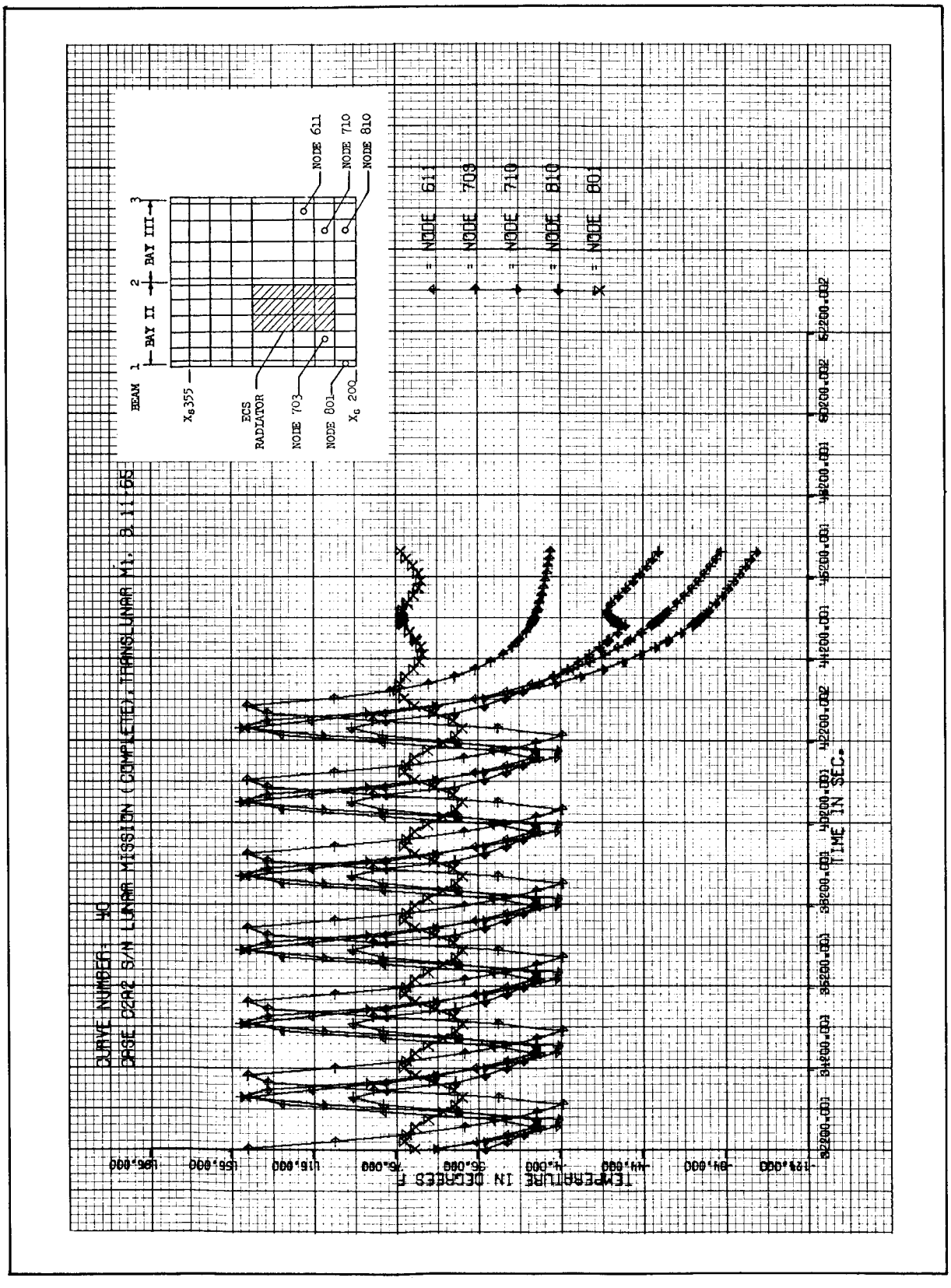

Figure 6-1c Shell Temperature Histories for Lunar Orbit Rendezvous Mission (Continued)

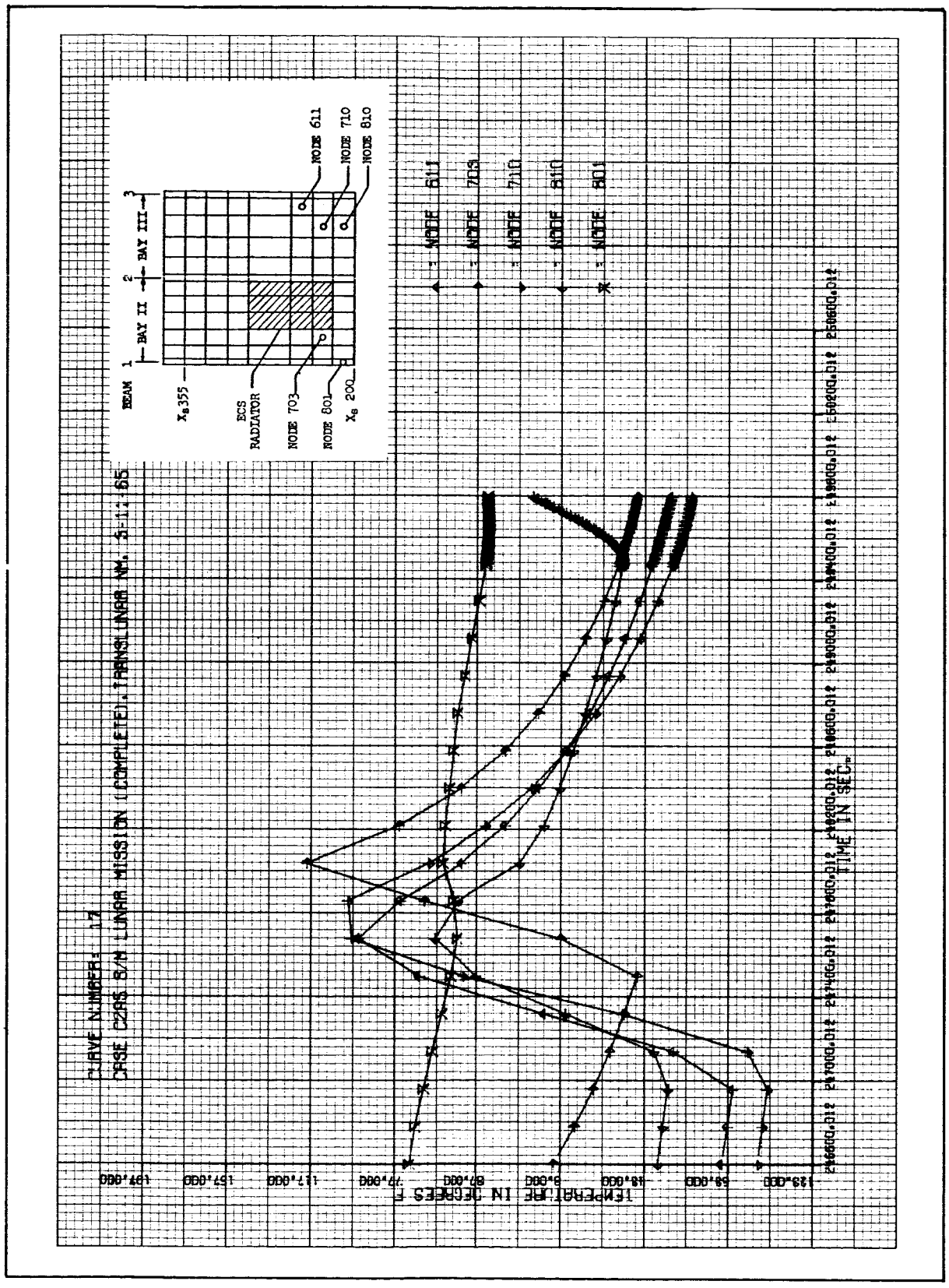

Figure 6-1d Shell Temperature Histories for Lunar Orbit Rendezvous Mission (Continued)

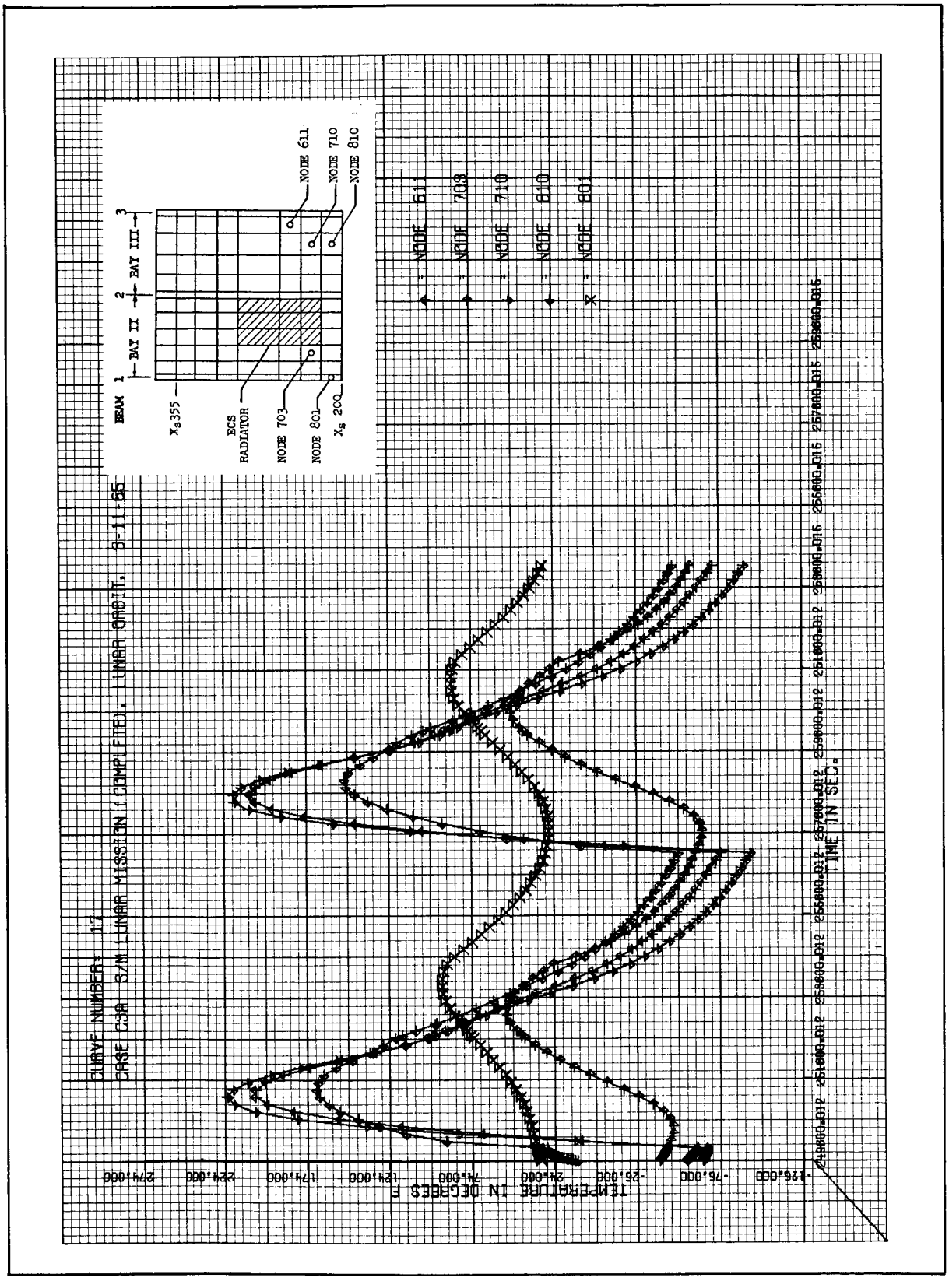

Figure 6-1e Shell Temperature Histories for Lunar Orbit Rendezvous Mission (Continued)

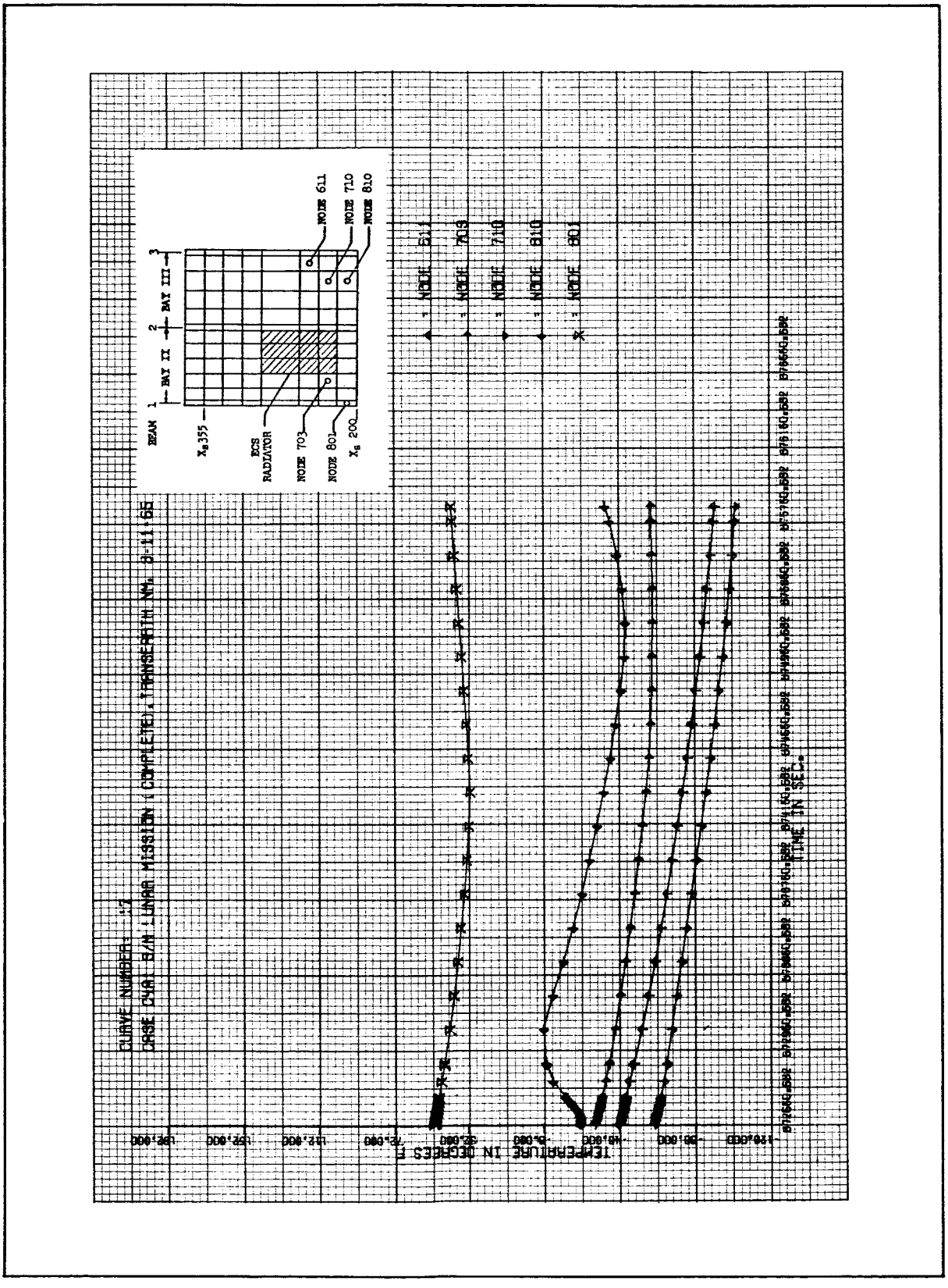

Figure 6-1f Shell Temperature Histories for Lunar Orbit Rendezvous Mission (Continued)

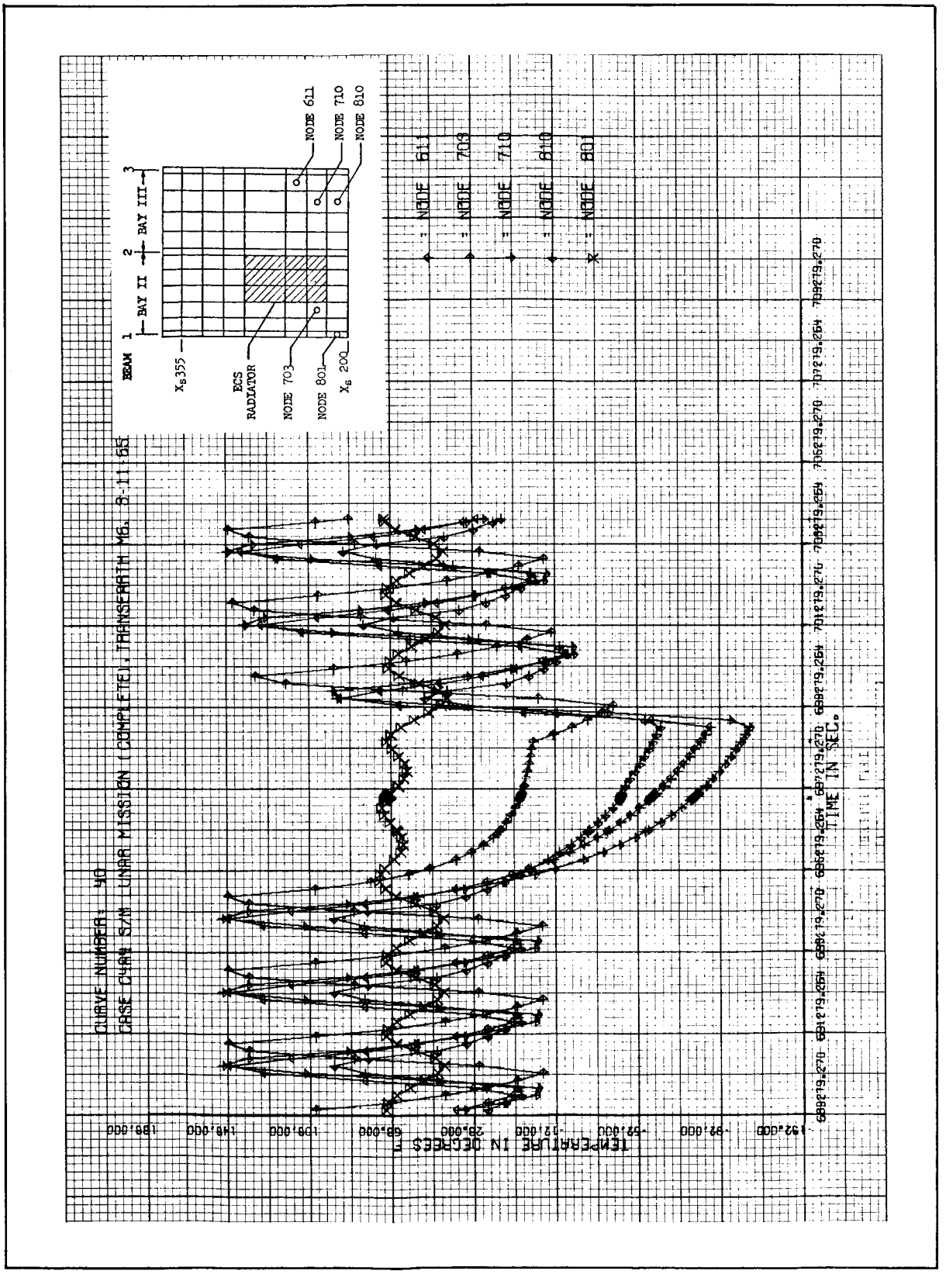

Figure 6-1g Shell Temperature Histories for Lunar Orbit Rendezvous Mission (Continued)

LOCKHEED CALIFORNIA COMPANY

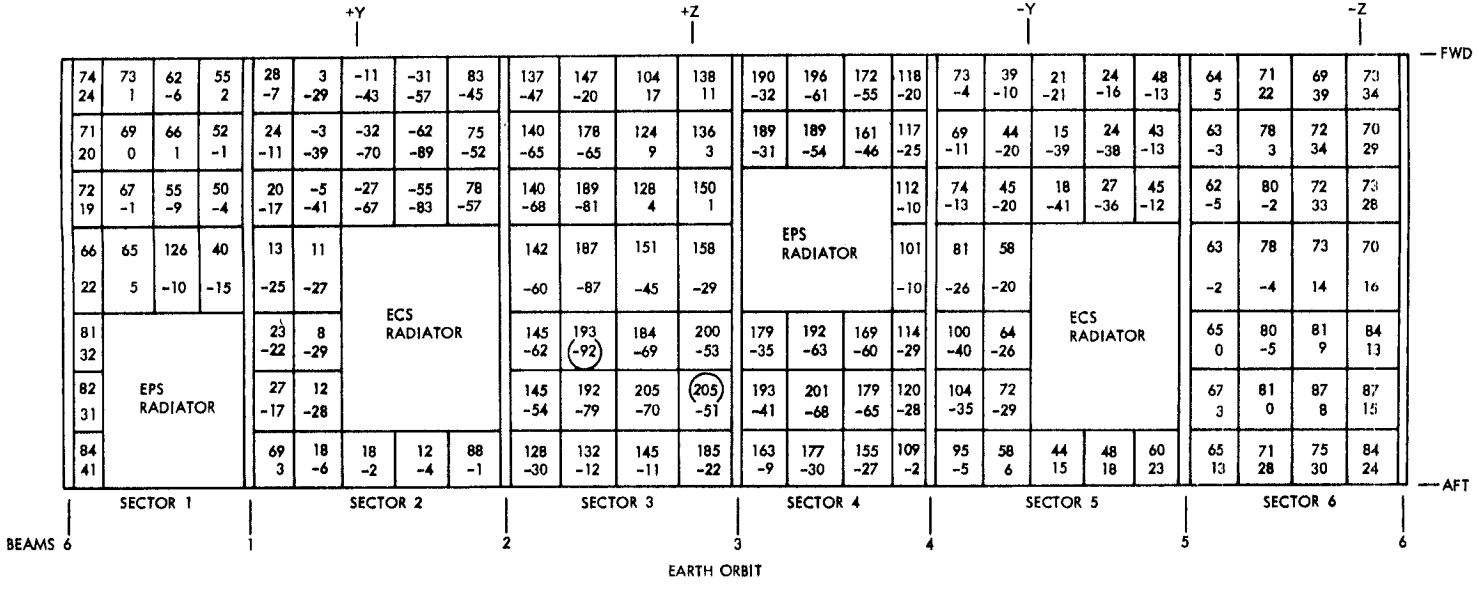

Figure 6-2a Maximum/Minimum Temperatures for Shell Nodes, Lunar Orbit Rendezvous Mission

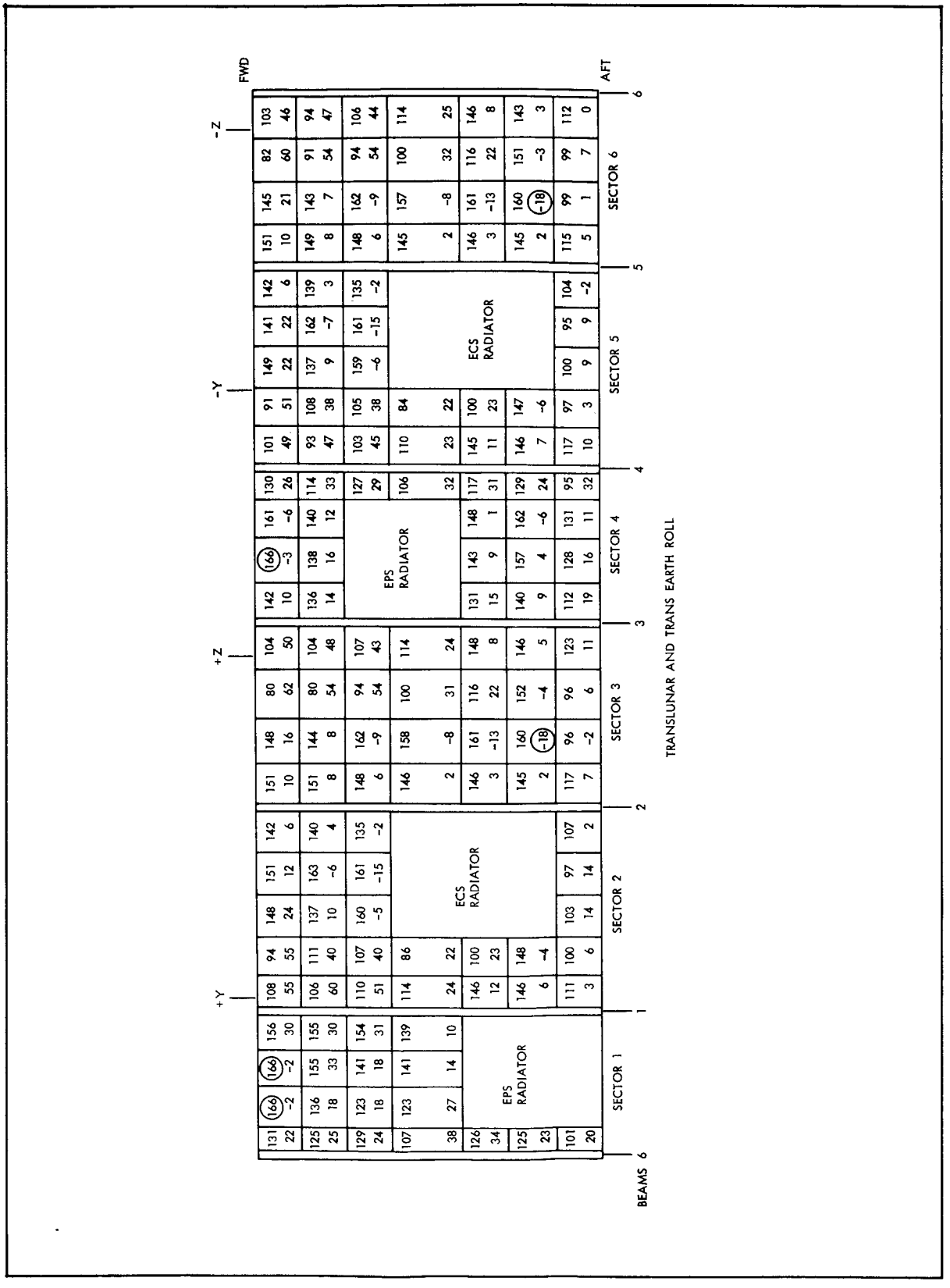

Figure 6-2b Maximum/Minimum Temperatures for Shell Nodes, Lunar Orbit Rendezvous Mission (Continued)

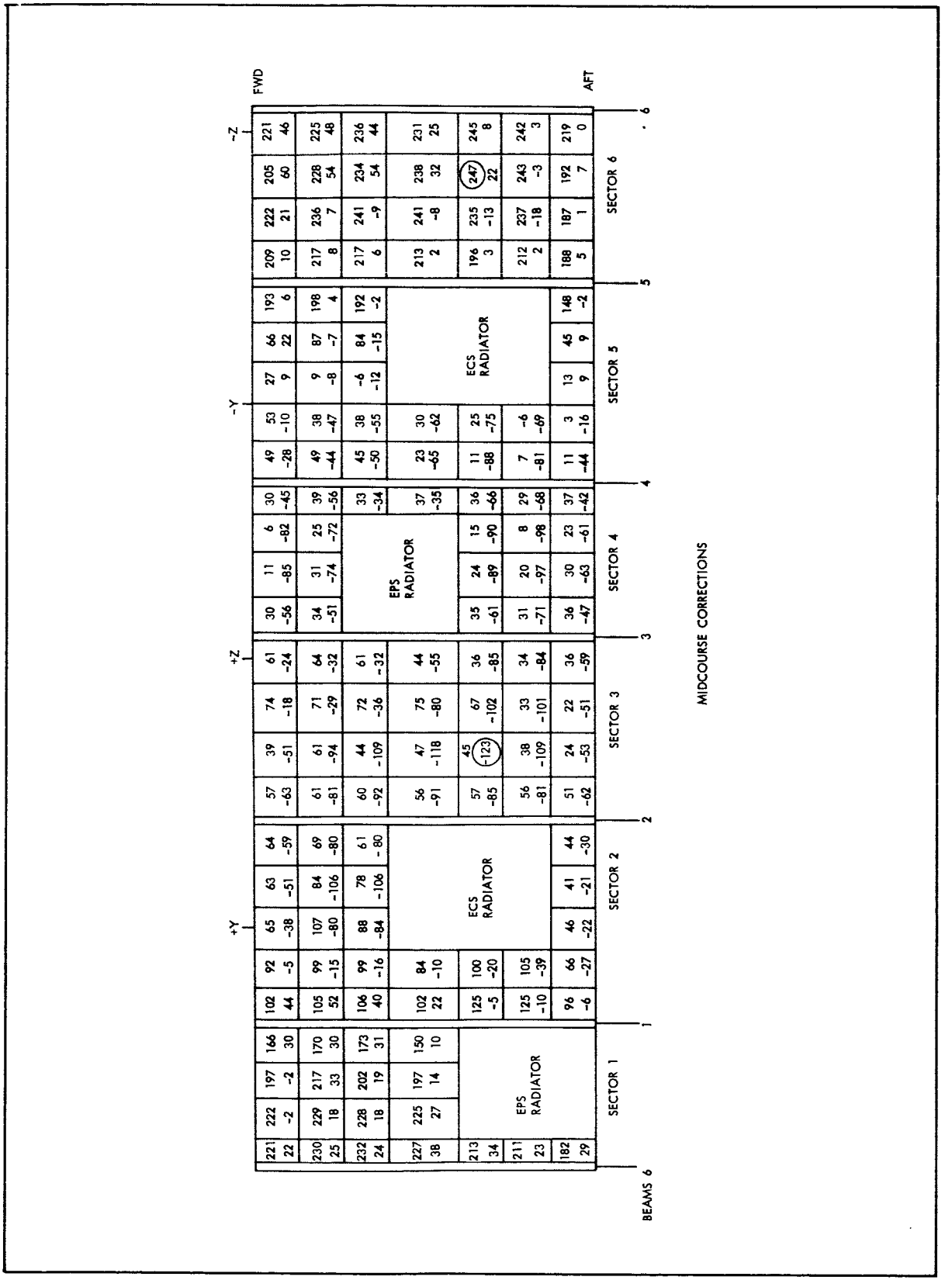

Figure 6-2c Maximum/Minimum Temperatures for Shell Nodes, Lunar Orbit Rendezvous Mission (Continued)

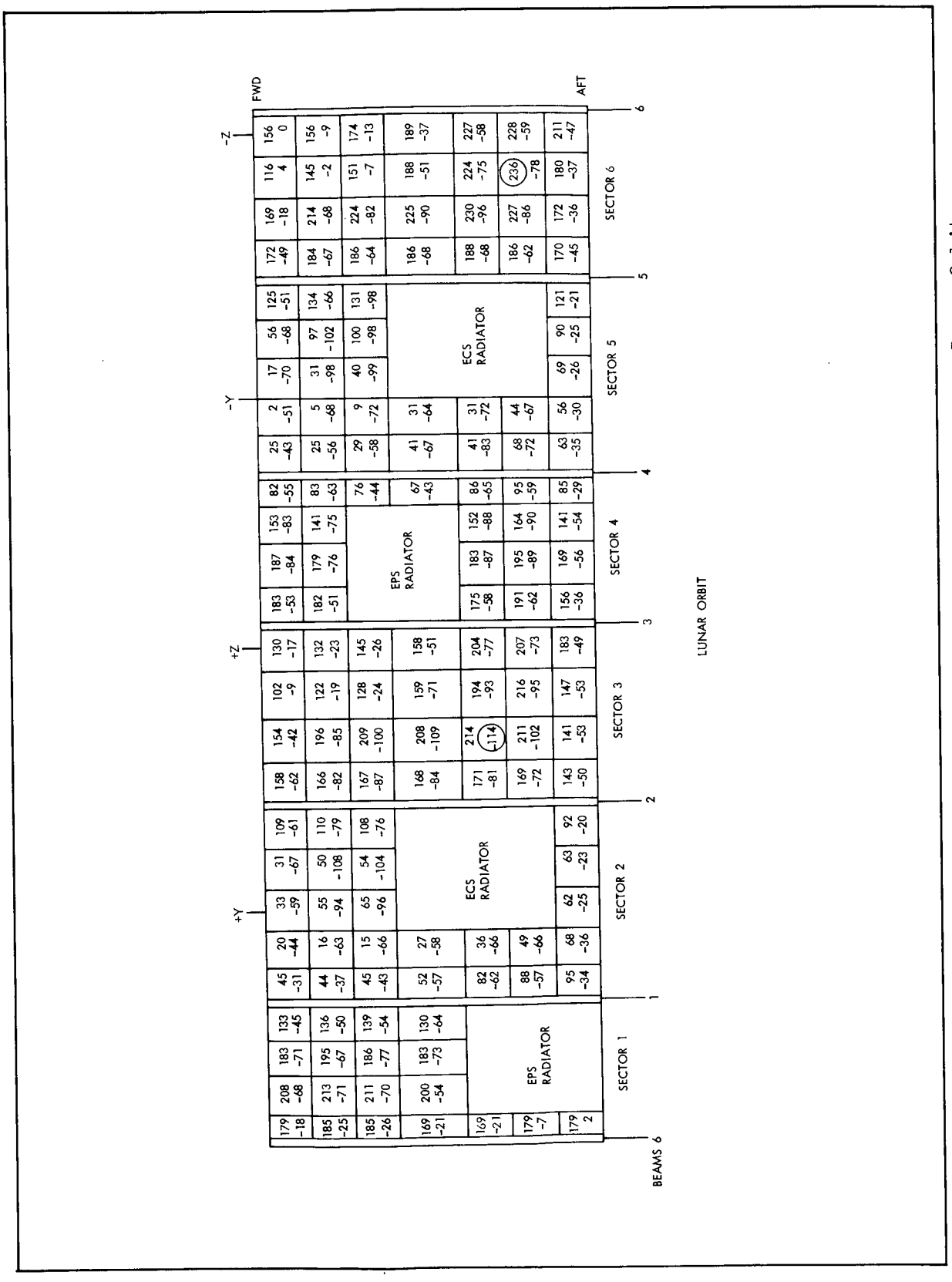

Figure 6-2d Maximum/Minimum Temperatures for Shell Nodes, Lunar Orbit Rendezvous Mission (Continued)

Maximum SM heating (SPS engine pointing towards the sun) and minimum SM heating (CM pointing towards the sun) results for these same five shell nodes are presented in Figures 6-3 and 6-4 respectively. The maximum heating curves (Figure 6-3) show that shell positions located closest to the heated aft bulkhead (800 series) are the warmest, and those further away become successively cooler. The minimum heating temperatures (Figure 6-4) are not appreciably affected by solar heating since neither bulkhead of the SM is subjected to insolation. Instead, these curves merely illustrate the influence of the vehicle interior. Thus, 800 series shell nodes are the warmest since they are most influenced by the fuel cells, and 700 series next most influenced, etc. Node 611 is slightly warmer than its surrounding nodes due to conduction from the nearby beam.

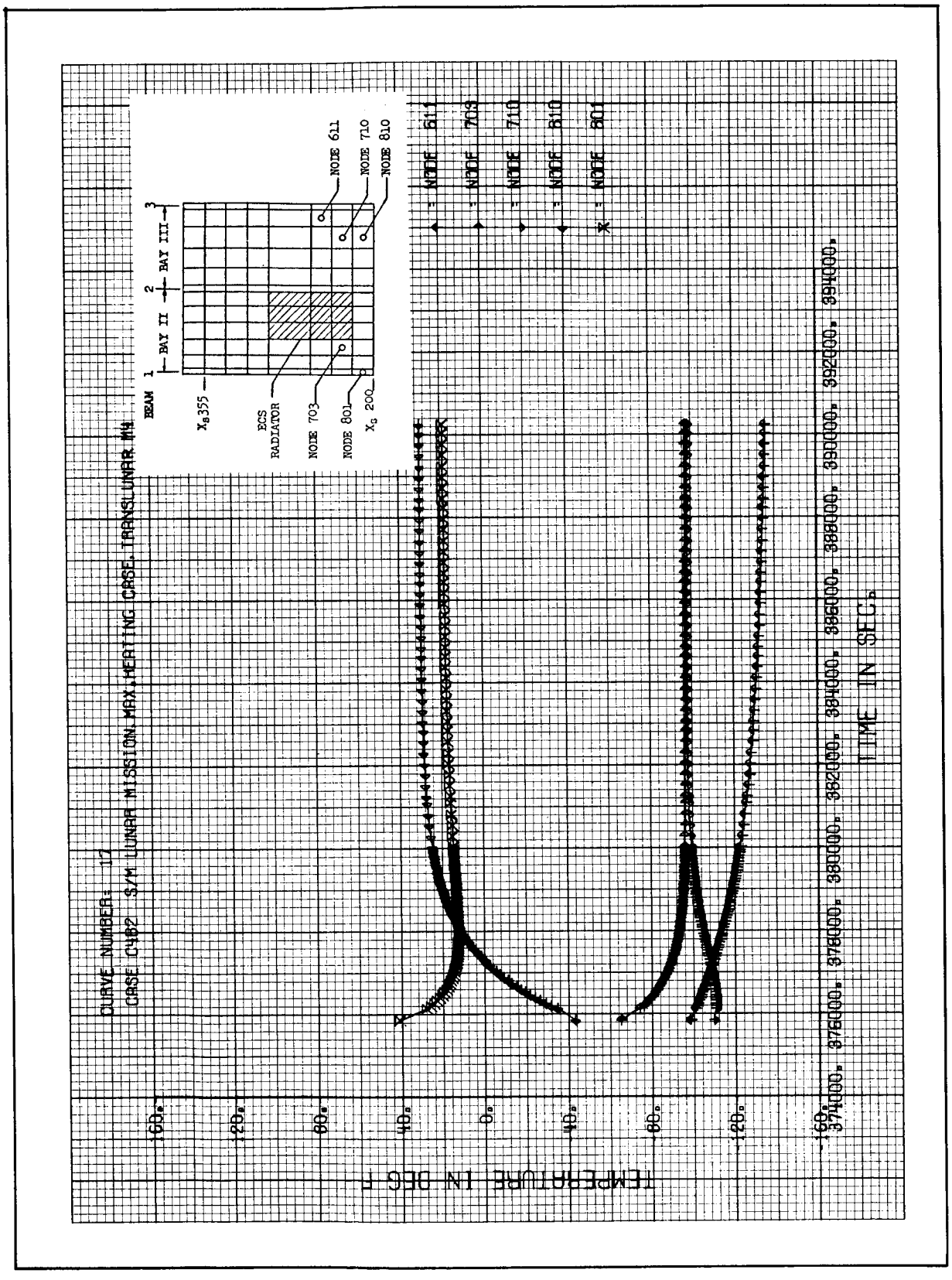

Figure 6-3 Shell Temperature Histories for Maximum Heating Orientation

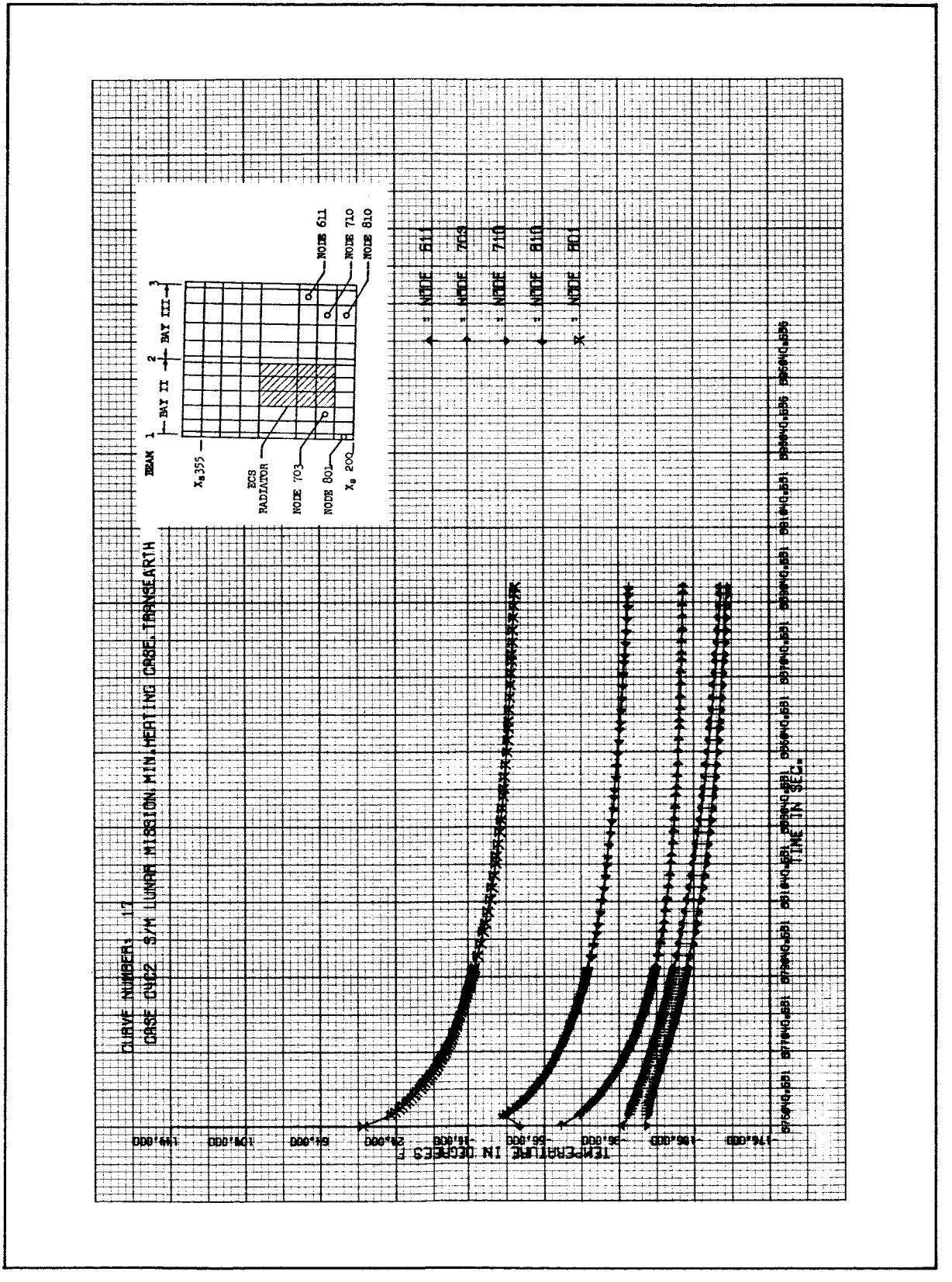

Figure 6-4a Shell Temperature Histories for Minimum Heating Orientation

LOCKHEED CALIFORNIA COMPANY

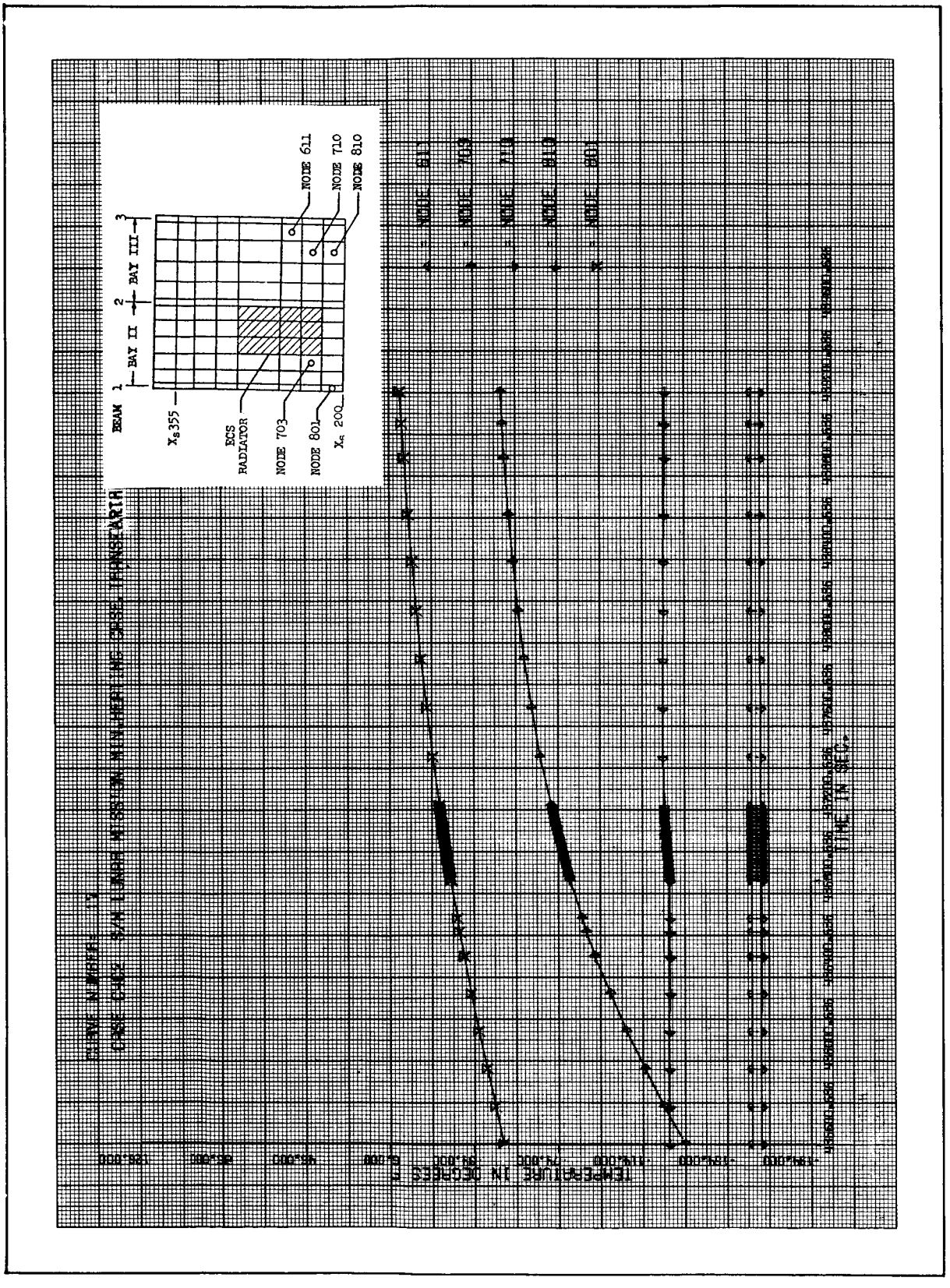

Figure 6-4b Shell Temperature Histories for Minimum Heating Orientation (Continued)

LOCKHEED CALIFORNIA COMPANY

RADIAL BEAMS

Figure 6-5 shows the orbital temperature history of five representative radial beam nodes. Following an initial temperature rise due to conduction from the shell during ascent, all of these nodes except 644 cool below their initial value of 70°F. This is a result of the relatively cool shell temperatures during earth orbit. The temperature of beam node 644 steadily increases due to its proximity to the fuel cells. During the translunar roll, the nodes on beams 5 and 6 remain cool, while node 644 reaches 100°F.

Maximum and minimum beam temperatures are shown in Figure 6-6. Approximations for temperatures between those shown may be obtained by interpolation of the data. It can be seen that, in general, all beams have approximately the same maximum and minimum temperatures during a given mission phase, and hence the transient temperature history for all beams is reasonably well established.

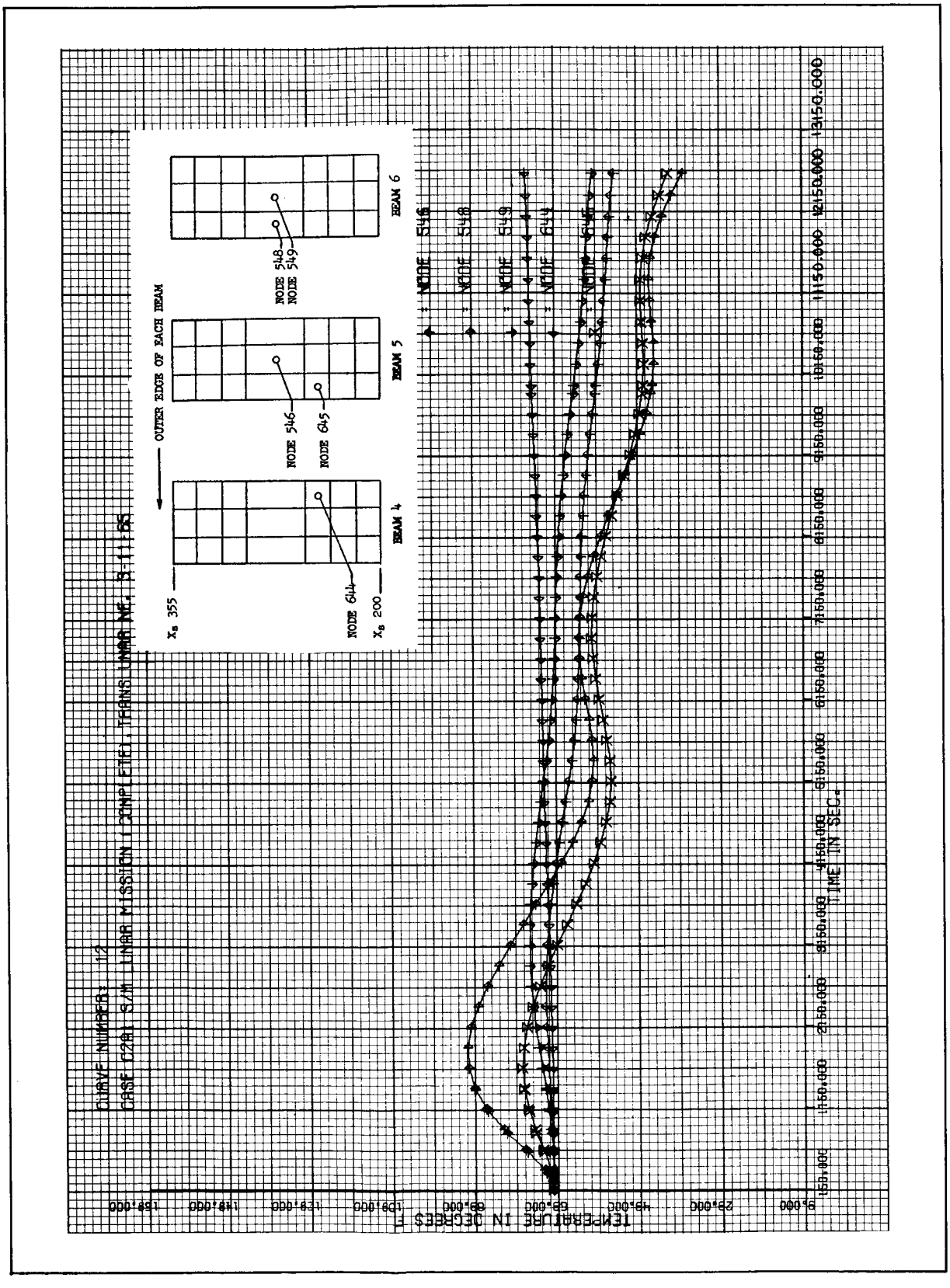

Figure 6-5a Radial Beam Temperature Histories for Lunar Orbit Rendezvous Mission

LOCKHEED
CALIFORNIA COMPANY

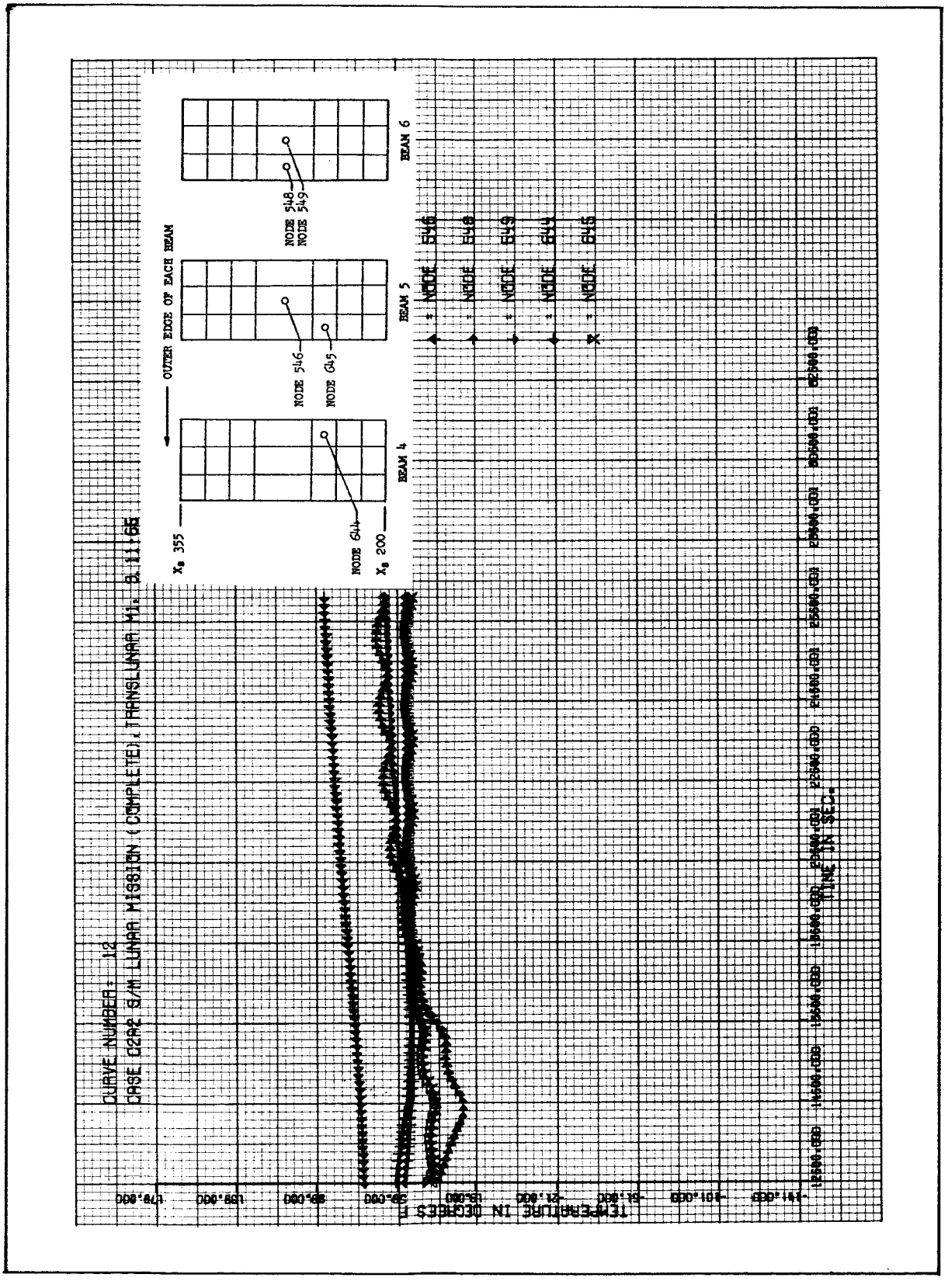

Figure 6-5b Radial Beam Temperature Histories for Lunar Orbit Rendezvous Mission (Continued)

LOCKHEED
CALIFORNIA COMPANY

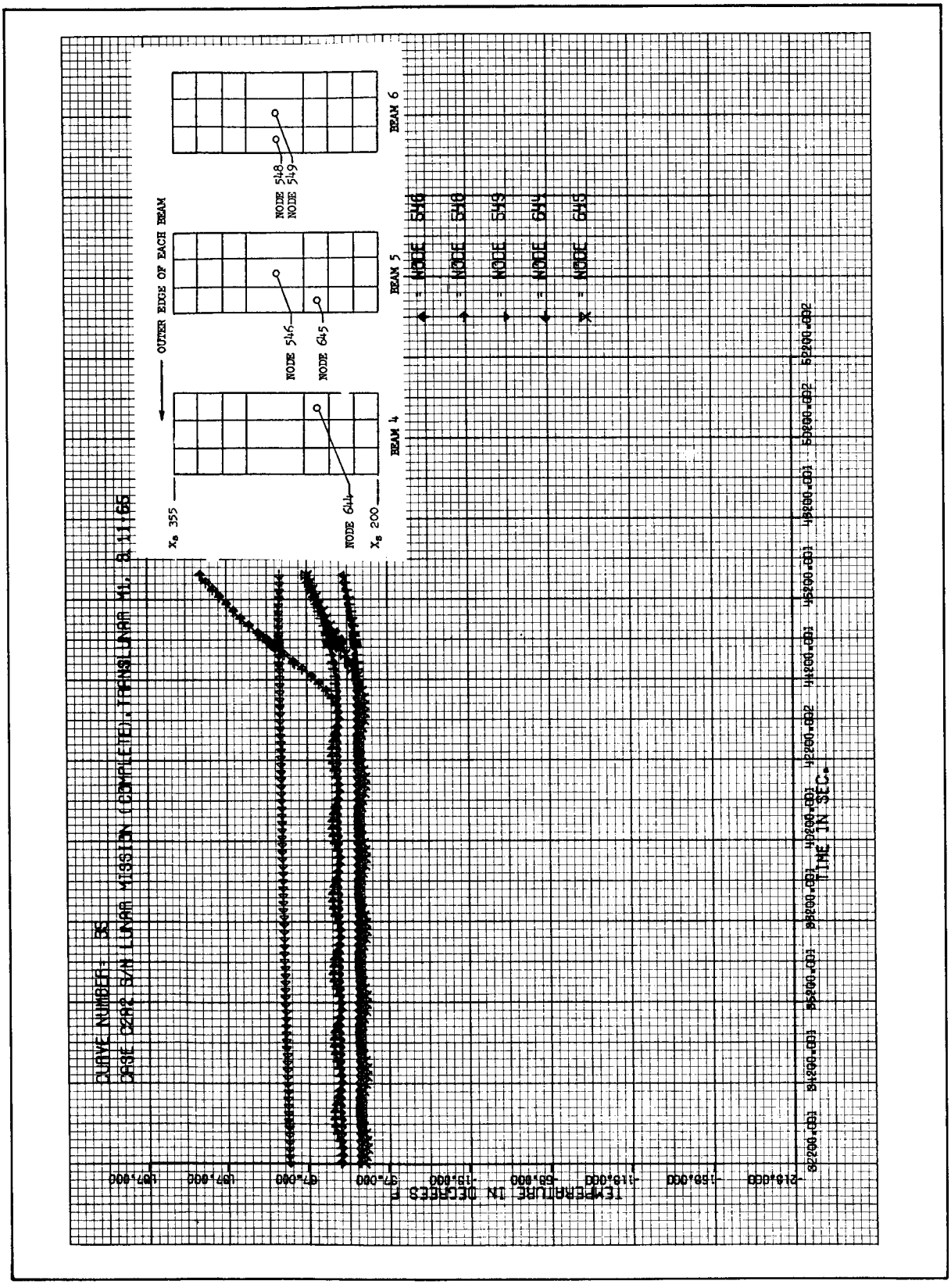

Figure 6-5c Radial Beam Temperature Histories for Lunar Orbit Rendezvous Mission (Continued)

LOCKHEED
CALIFORNIA COMPANY

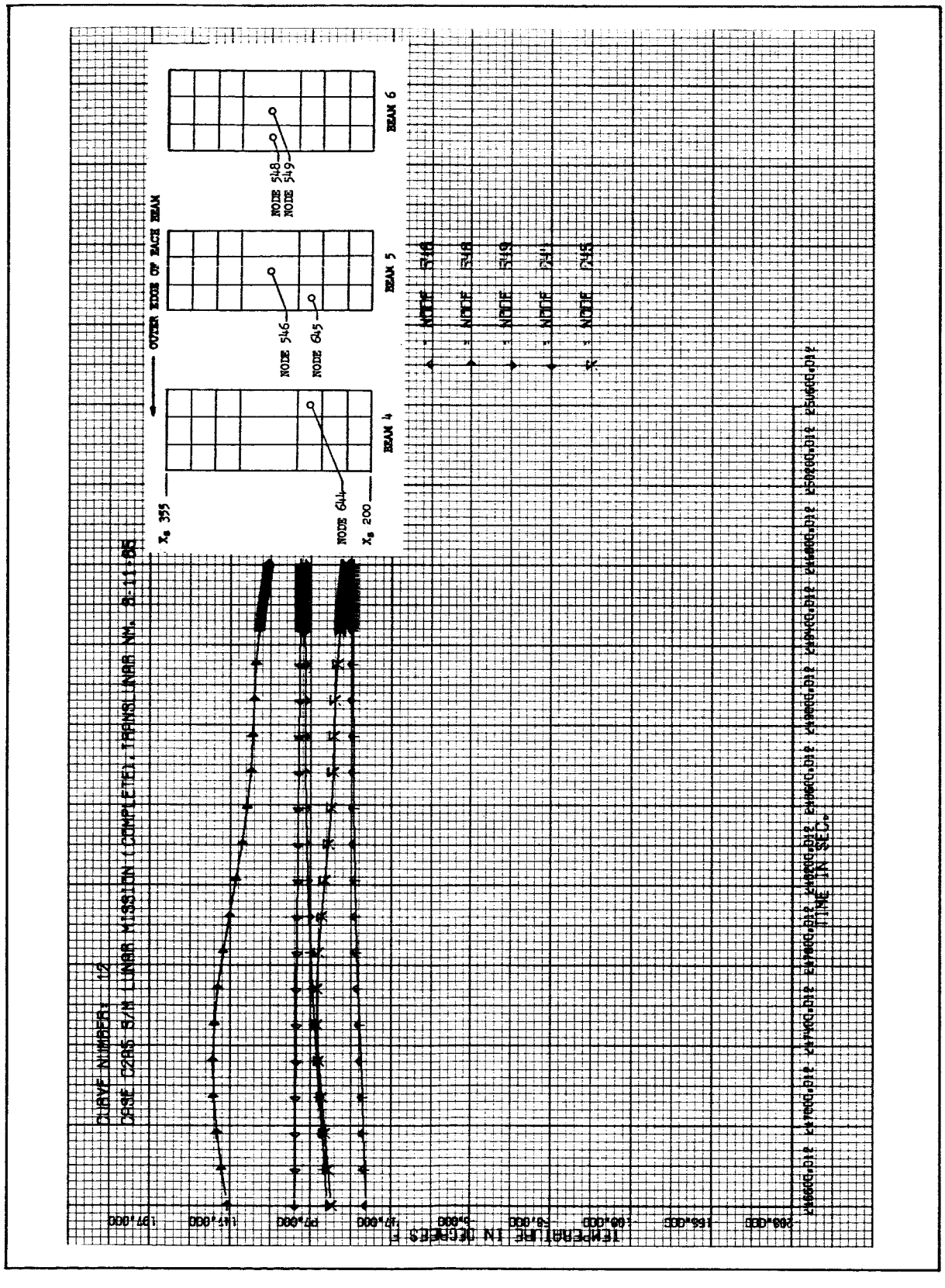

Figure 6-5d Radial Beam Temperature Histories for Lunar Orbit Rendezvous Mission (Continued)

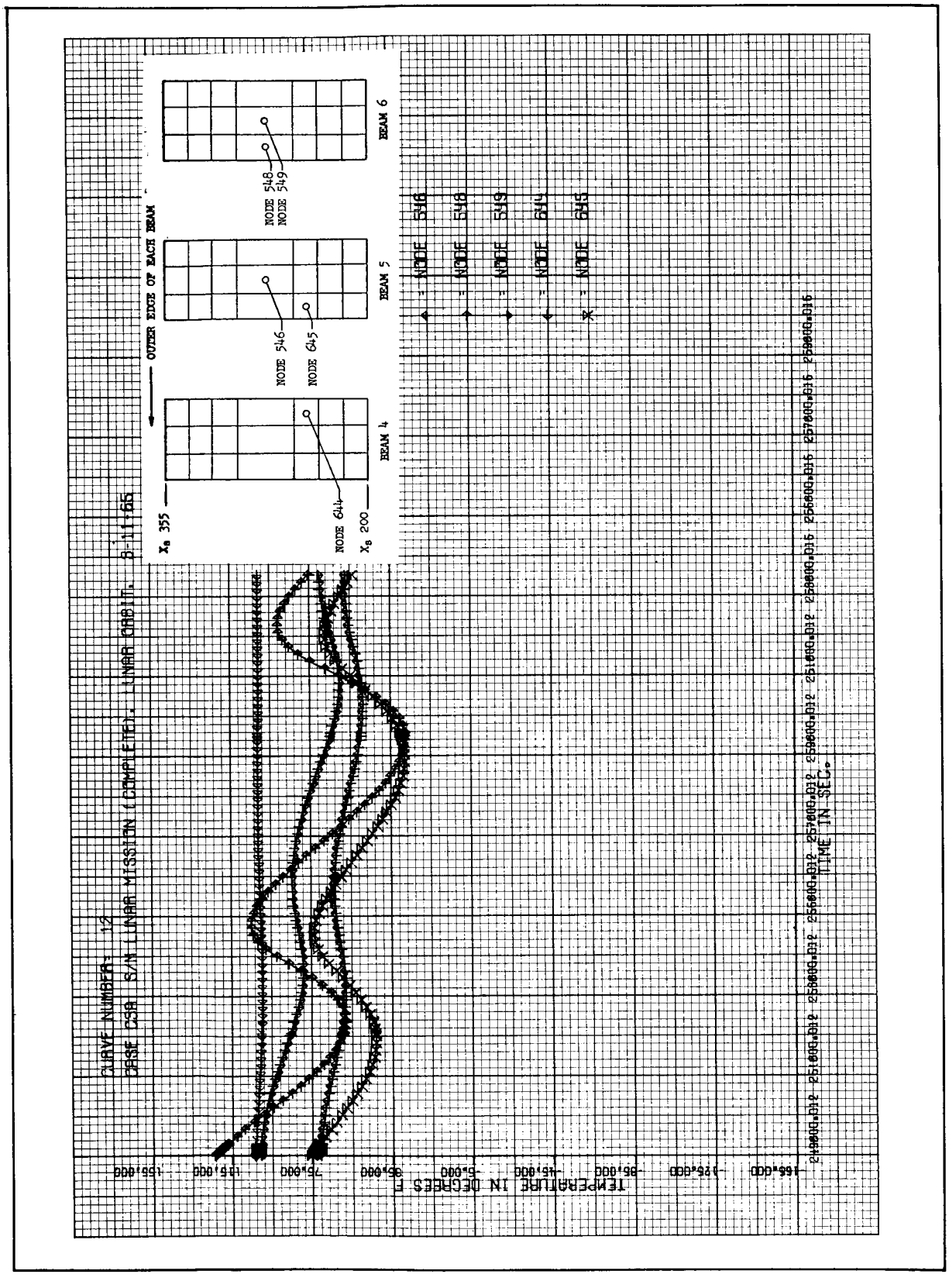

Figure 6-5e Radial Beam Temperature Histories for Lunar Orbit Rendezvous Mission (Continued)

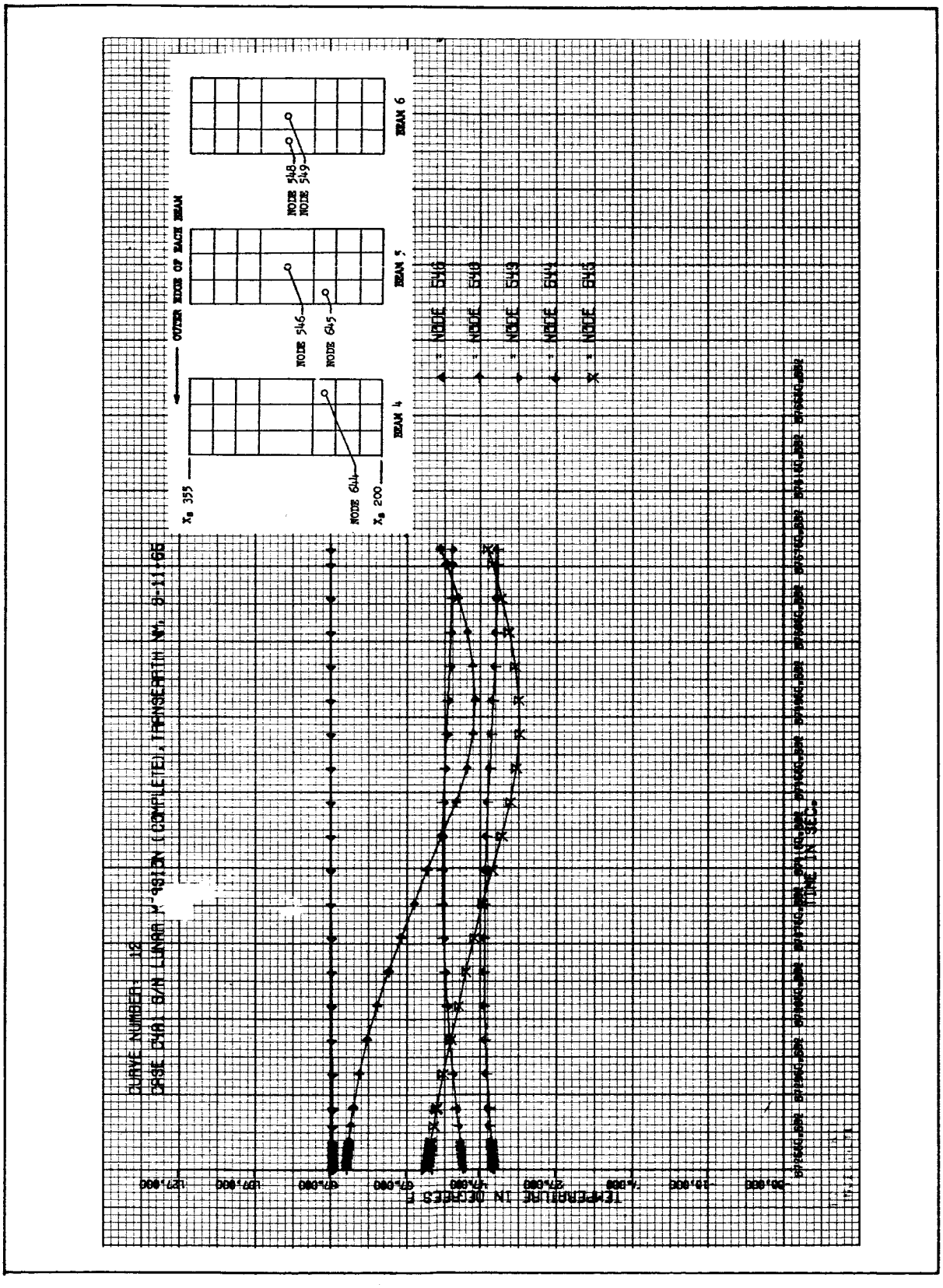

Figure 6-5f Radial Beam Temperature Histories for Lunar Orbit Rendezvous Mission (Continued)

LOCKHEED CALIFORNIA COMPANY

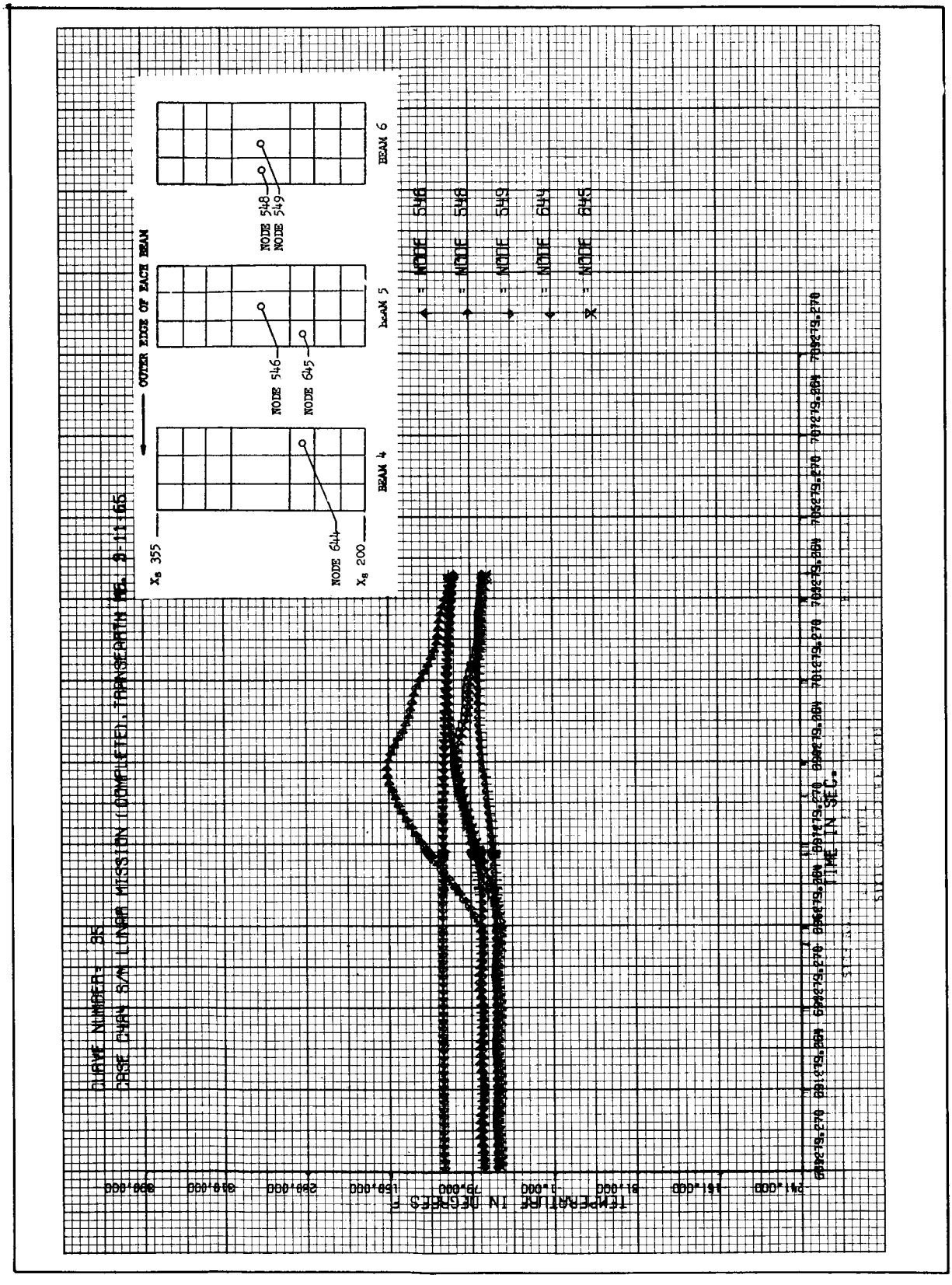

Figure 6-5g Radial Beam Temperature Histories for Lunar Orbit Rendezvous Mission (Continued)

LOCKHEED
CALIFORNIA COMPANY

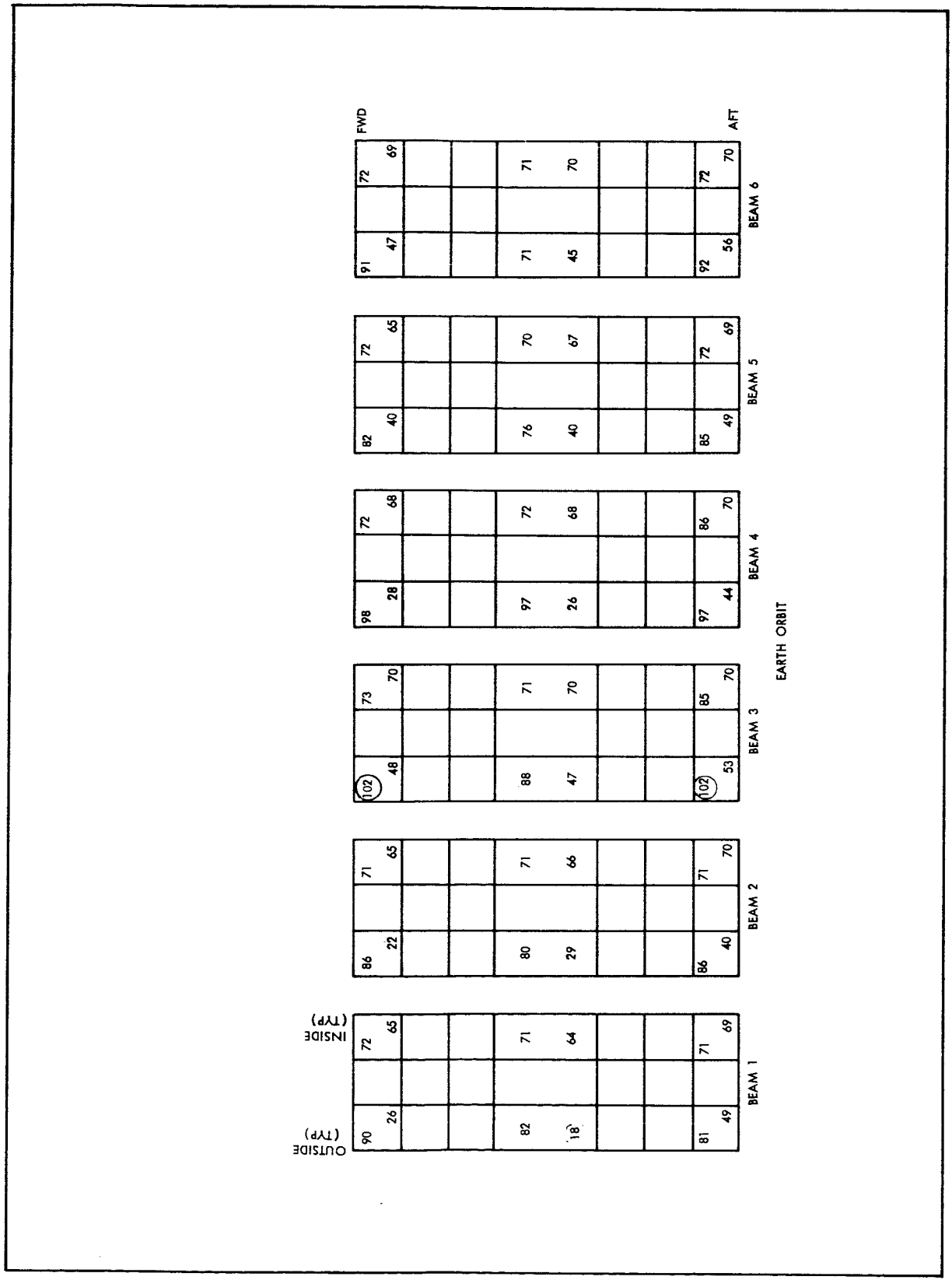

Figure 6-6a Maximum/Minimum Temperatures for Radial Beam Nodes, Lunar Orbit Rendezvous Mission

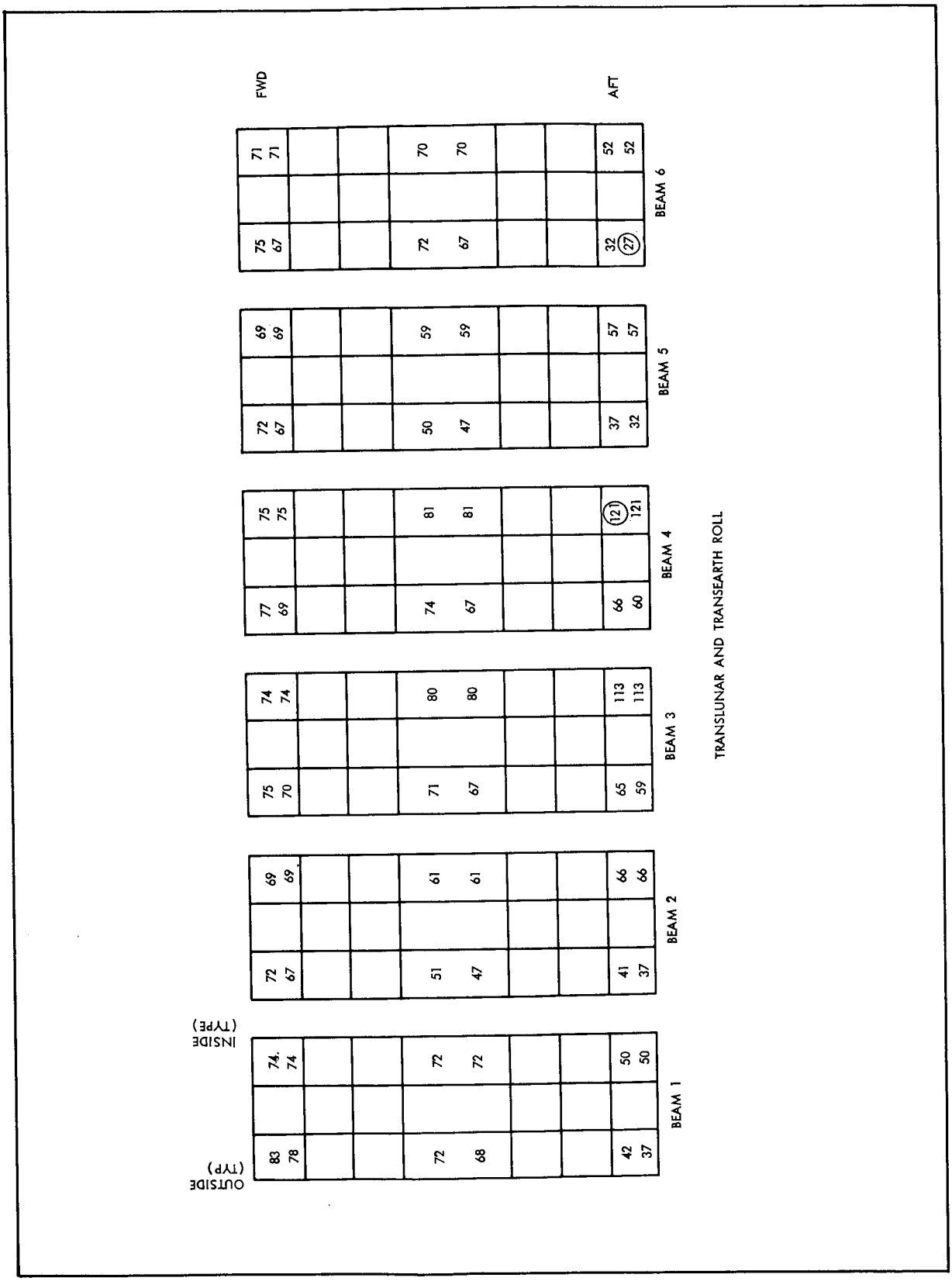

Figure 6-6b Maximum/Minimum Temperatures for Radial Beam Nodes, Lunar Orbit Rendezvous Mission (Continued)

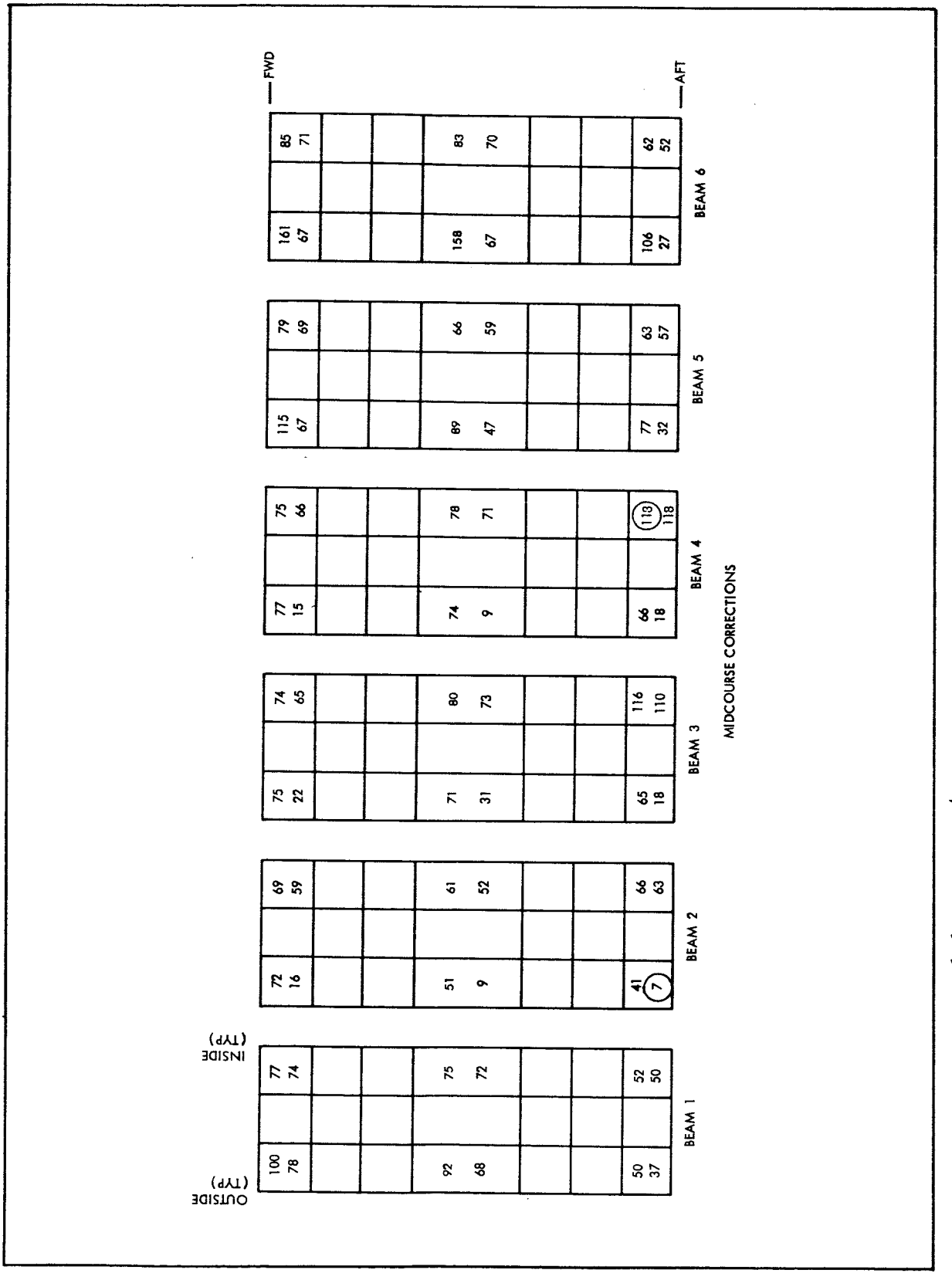

Figure 6-6c Maximum/Minimum Temperatures for Radial Beam Nodes, Lunar Orbit Rendezvous Mission (Continued)

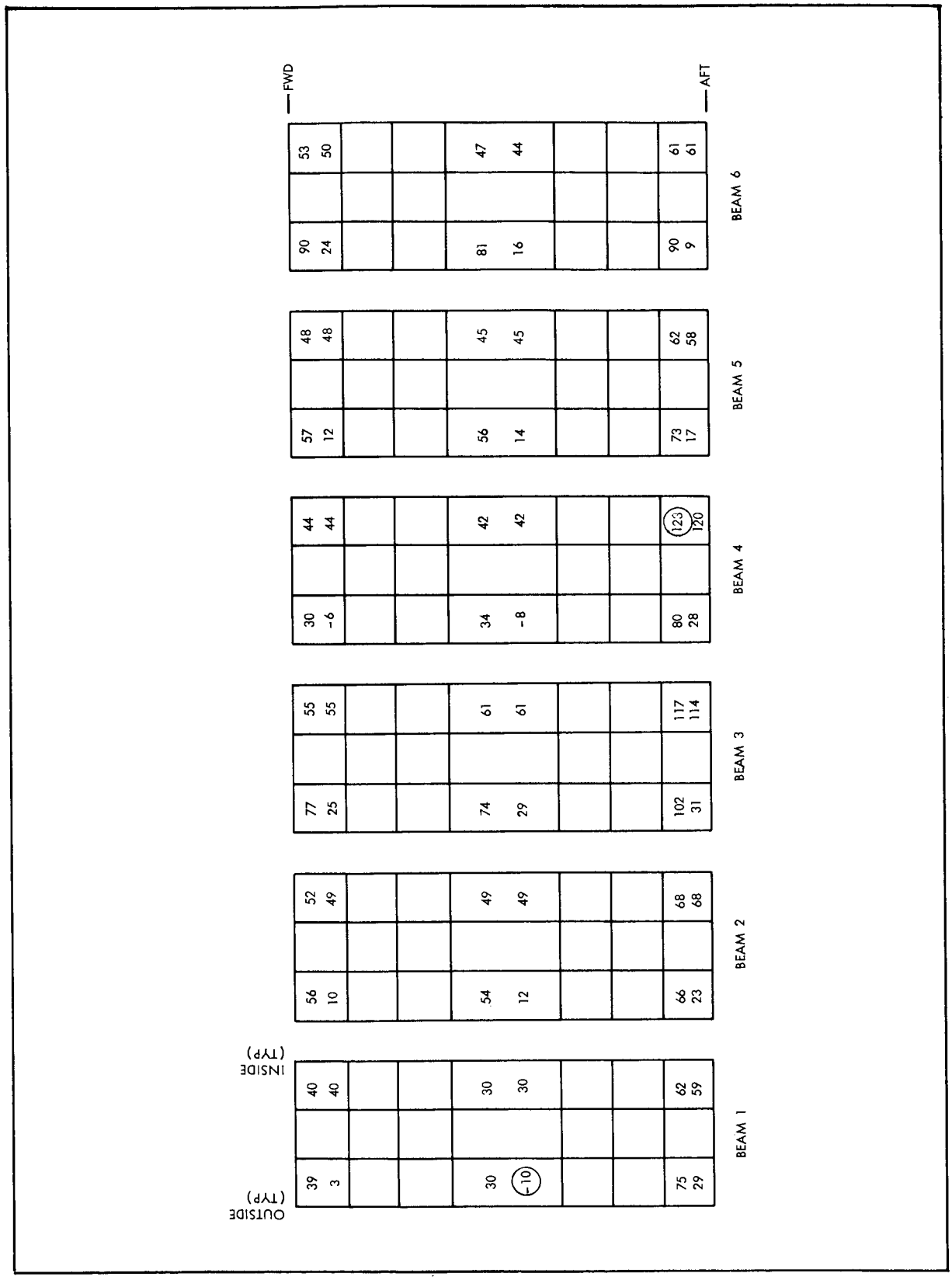

Figure 6-6d Maximum/Minimum Temperatures for Radial Beam Nodes, Lunar Orbit Rendezvous Mission (Continued)

LOCKHEED CALIFORNIA COMPANY

Temperature histories for the same five beam nodes are shown in Figures 6-7 and 6-8 for the maximum and minimum SM heating orientations respectively. The relative positions of the curves for each of these orientations do not change; however the maximum heating orientation results in higher temperatures of all nodes due to the additional heat input to the module. The rate at which these nodes cool is determined by their position relative to the shell and the fuel cell bay. Thus, beam node 644, which borders Bay 4 and is as far from the shell as any node of those shown, remains the warmest. Likewise, beam node 548, which does not border Bay 4 and is adjacent to the shell, is cooler than the others.

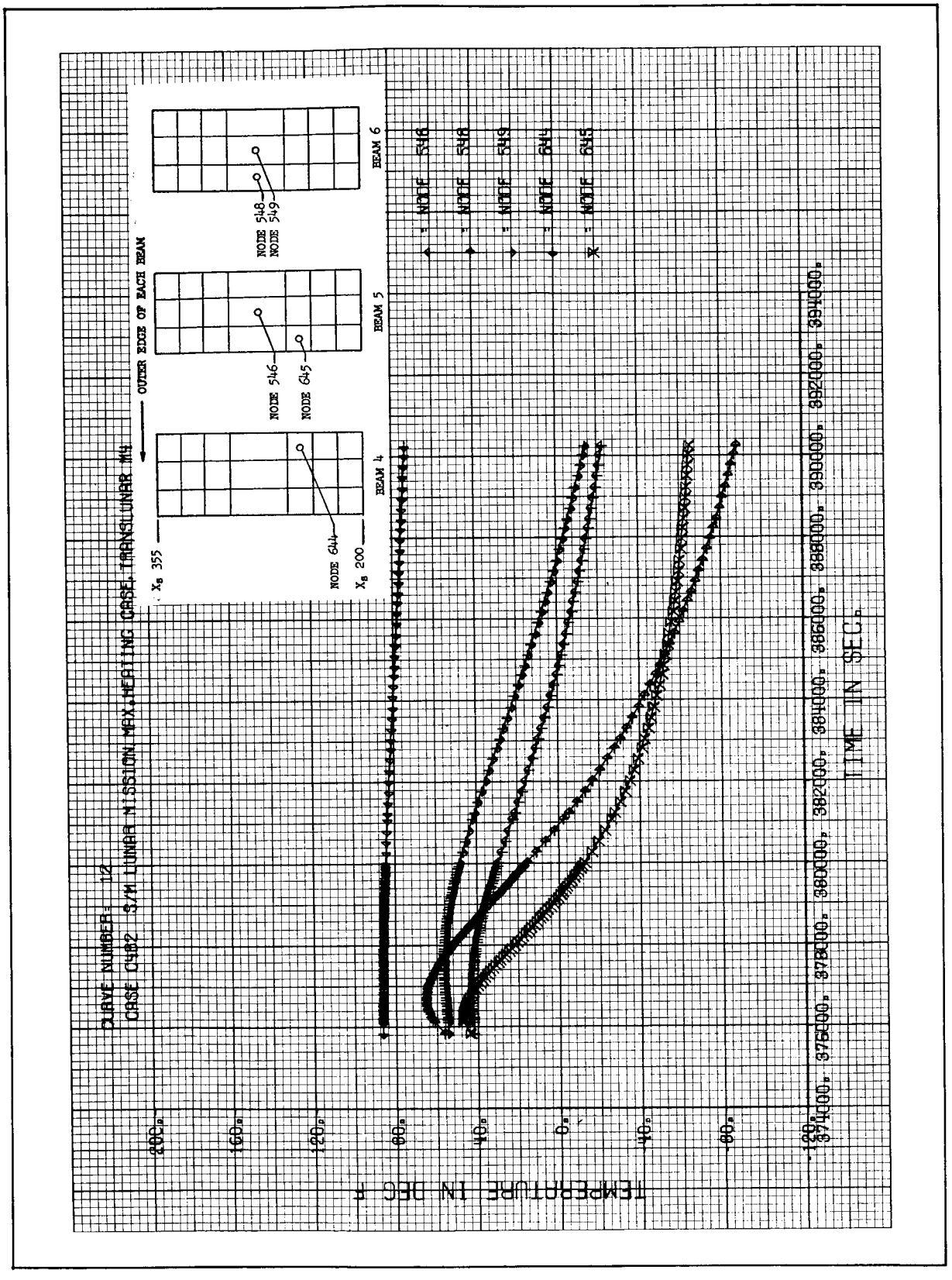

Figure 6-7a Radial Beam Temperature Histories for Maximum Heating Orientation

LOCKHEED
CALIFORNIA COMPANY

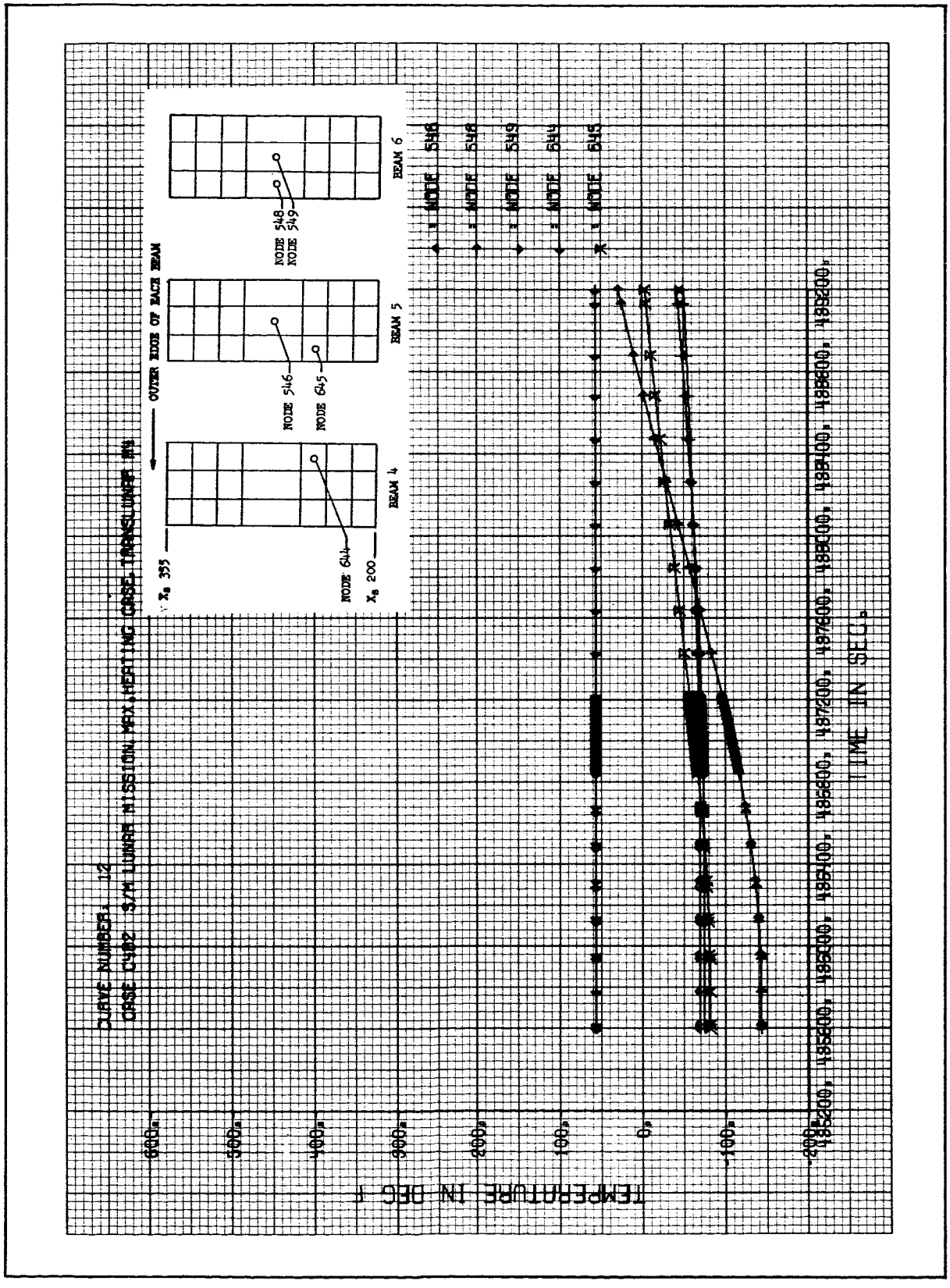

Figure 6-7b Radial Beam Temperature Histories for Maximum Heating Orientation (Continued)

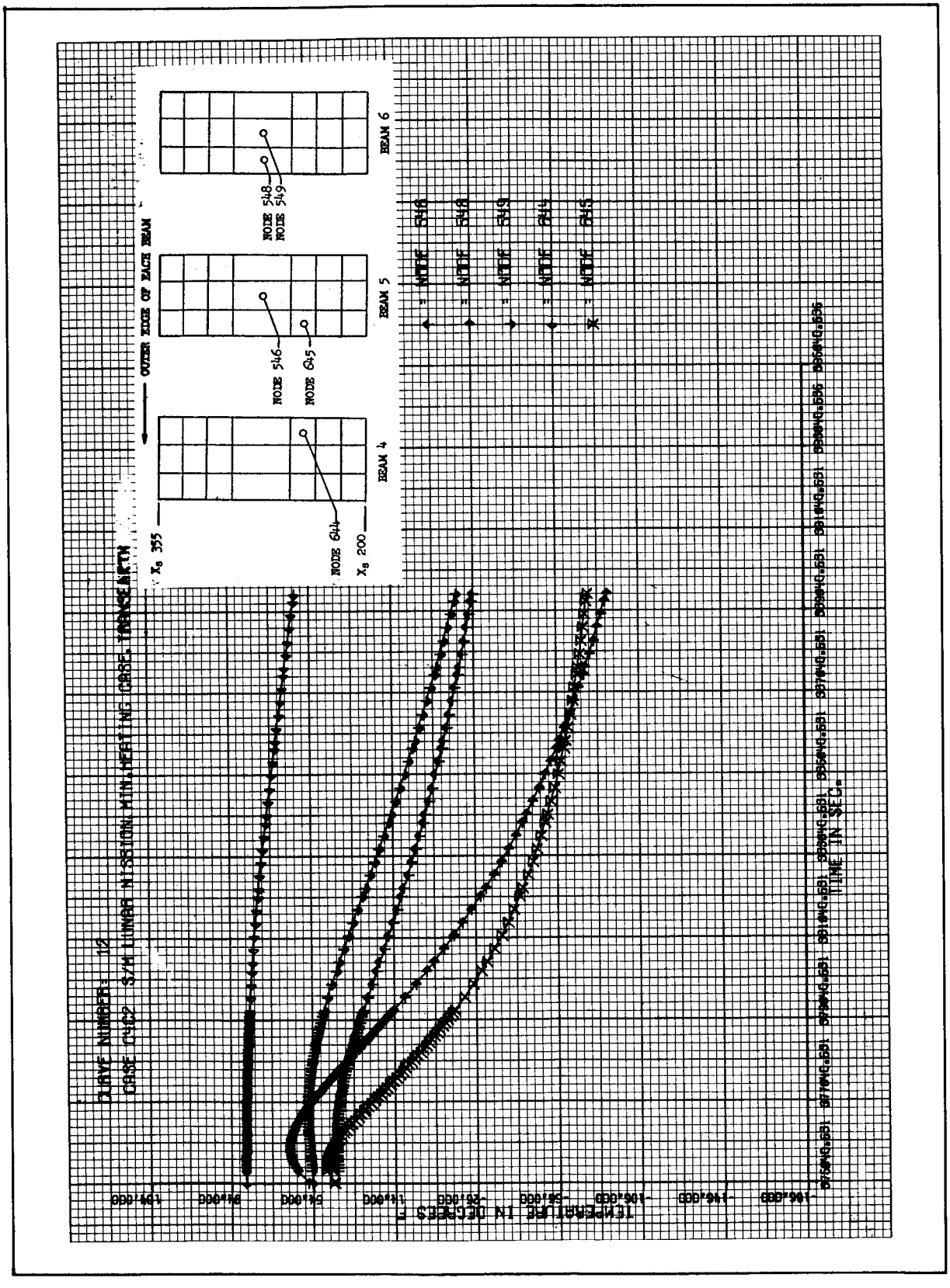

Figure 6-8a Radial Beam Temperature Histories for Minimum Heating Orientation

LOCKHEED CALIFORNIA COMPANY

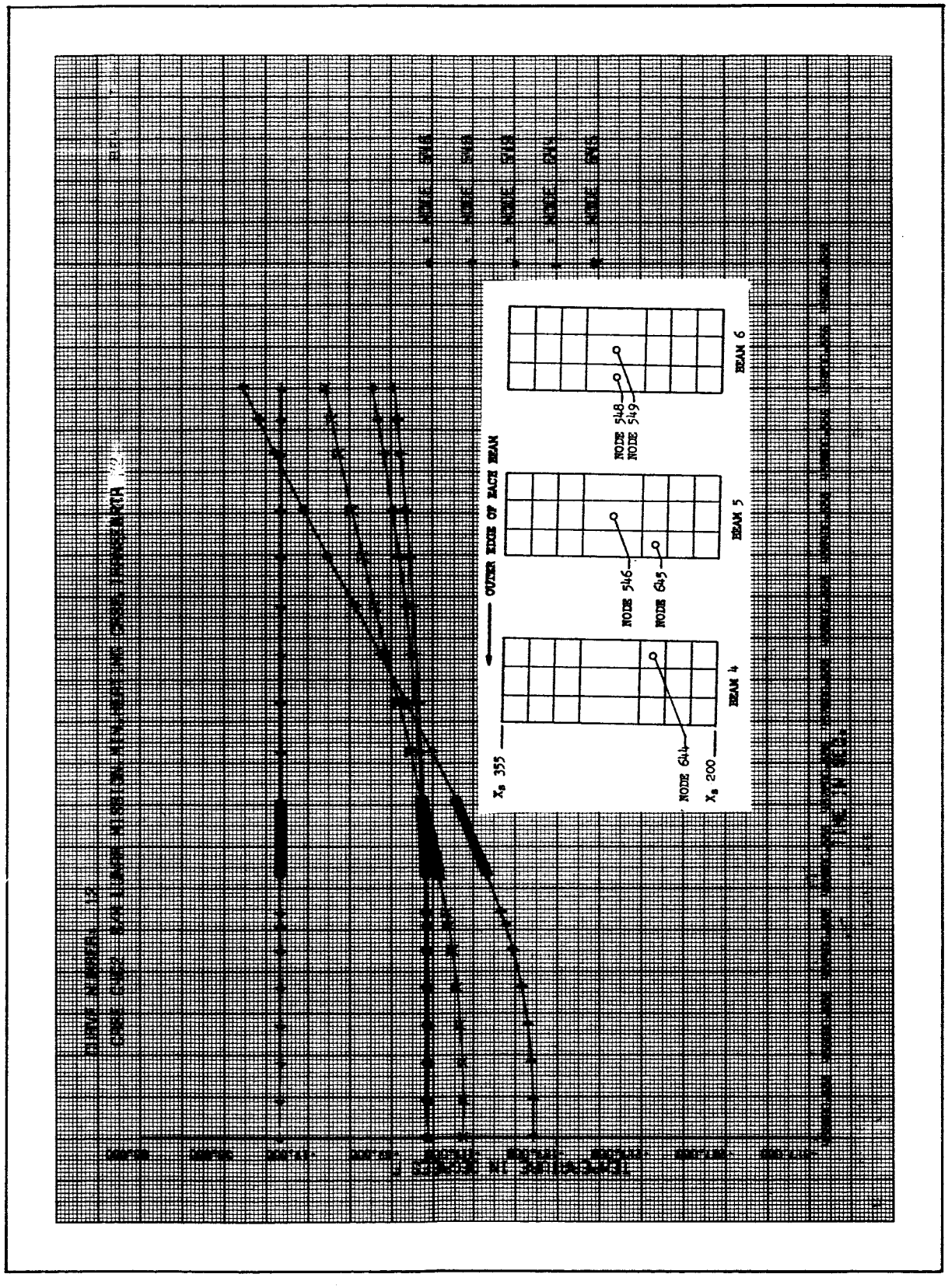

Figure 6-8b Radial Beam Temperature Histories for Minimum Heating Orientation (Continued)

FORWARD AND AFT BULKHEADS

The temperature histories of five nodes located on the aft bulkhead are shown in Figure 6-9. The aft bulkhead nodes are important since their temperatures serve as boundary conditions to the plumbing analysis. There is little temperature change on the bulkhead until the adaptor is jettisoned, with the exception of node 944 which is located in bay 4, aft bulkhead, and is heated by the fuel cell. During the translunar phase, none of these bulkhead temperatures cycle significantly. Once in lunar orbit the average temperature of each of the aft bulkhead nodes is increased. This is a consequence of the nose down orientation which permits solar heating to the aft bulkhead area which is not covered by the heat shield. The aft bulkhead is not exposed to solar radiation for the assumed orientation during the translunar phase.

Figure 6-10 shows maximum and minimum bulkhead temperatures for the entire mission. While little temperature variation is experienced by those nodes located away from the shell, temperatures of those nodes bordering the shell vary considerably - following the adjacent shell nodes.

Figure 6-11 shows temperature histories for the same five aft bulkhead nodes but for the maximum heating orientation. Very little change is noted between the normal orientation and maximum heating orientation temperature profiles. The reason is that the heat input to the shell-bordering nodes (none of which are plotted) is nearly the same whether received directly from solar radiation or by conduction from the adjacent shell. This heat input is also only part of that received by these bulkhead nodes, for they are heated additionally by the fuel cells and the propellant tanks. Thus node 944, situated partly in Bay 4, is heated more than the other nodes shown. Figure 6-12 shows temperature histories during minimum SM heating conditions. For this orientation, all temperatures are seen to decrease uniformly, since no external heat inputs are present.

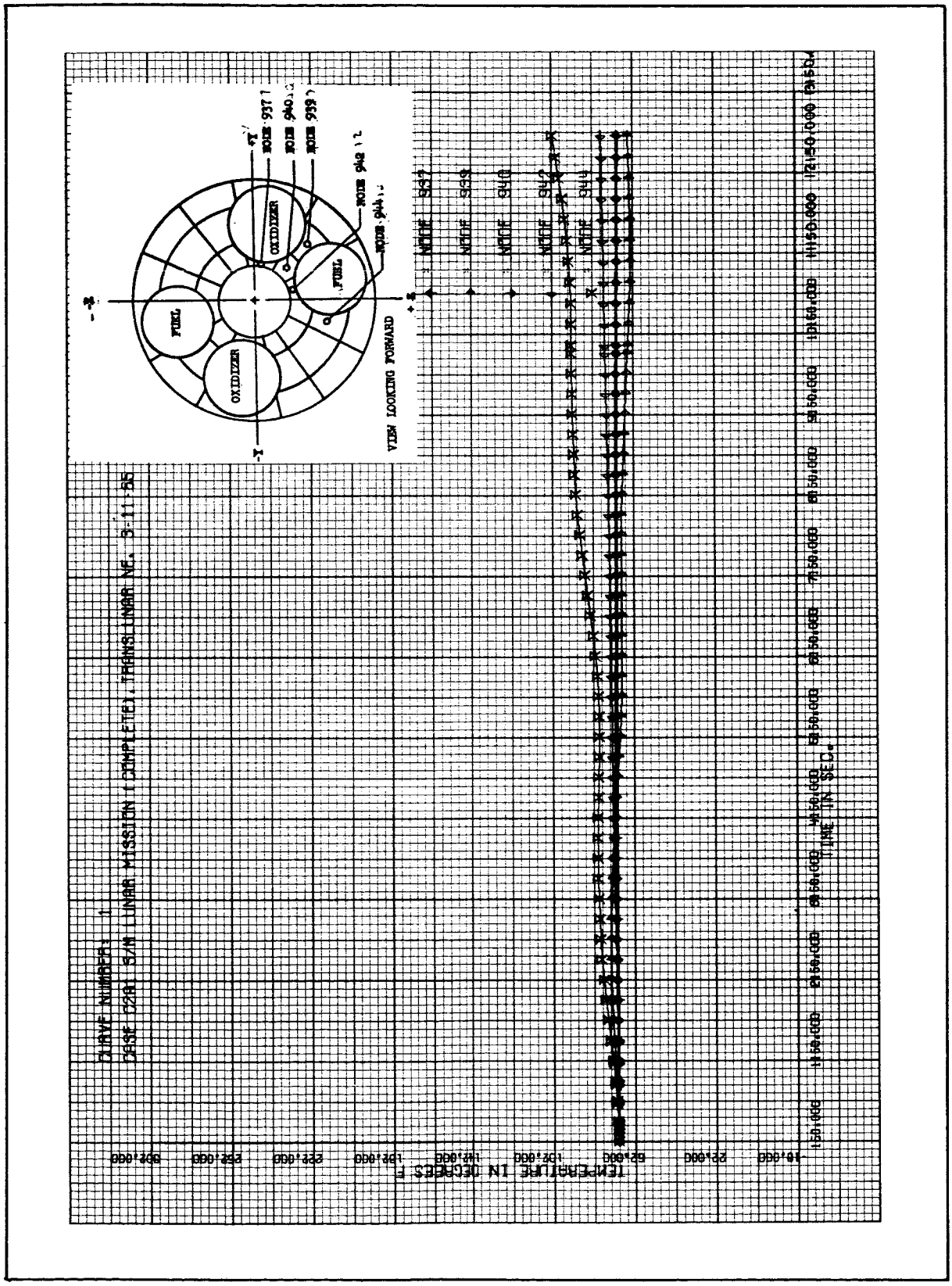

Figure 6-9a Aft Bulkhead Temperature Histories for Lunar Orbit Rendezvous Mission

LOCKHEED
CALIFORNIA COMPANY

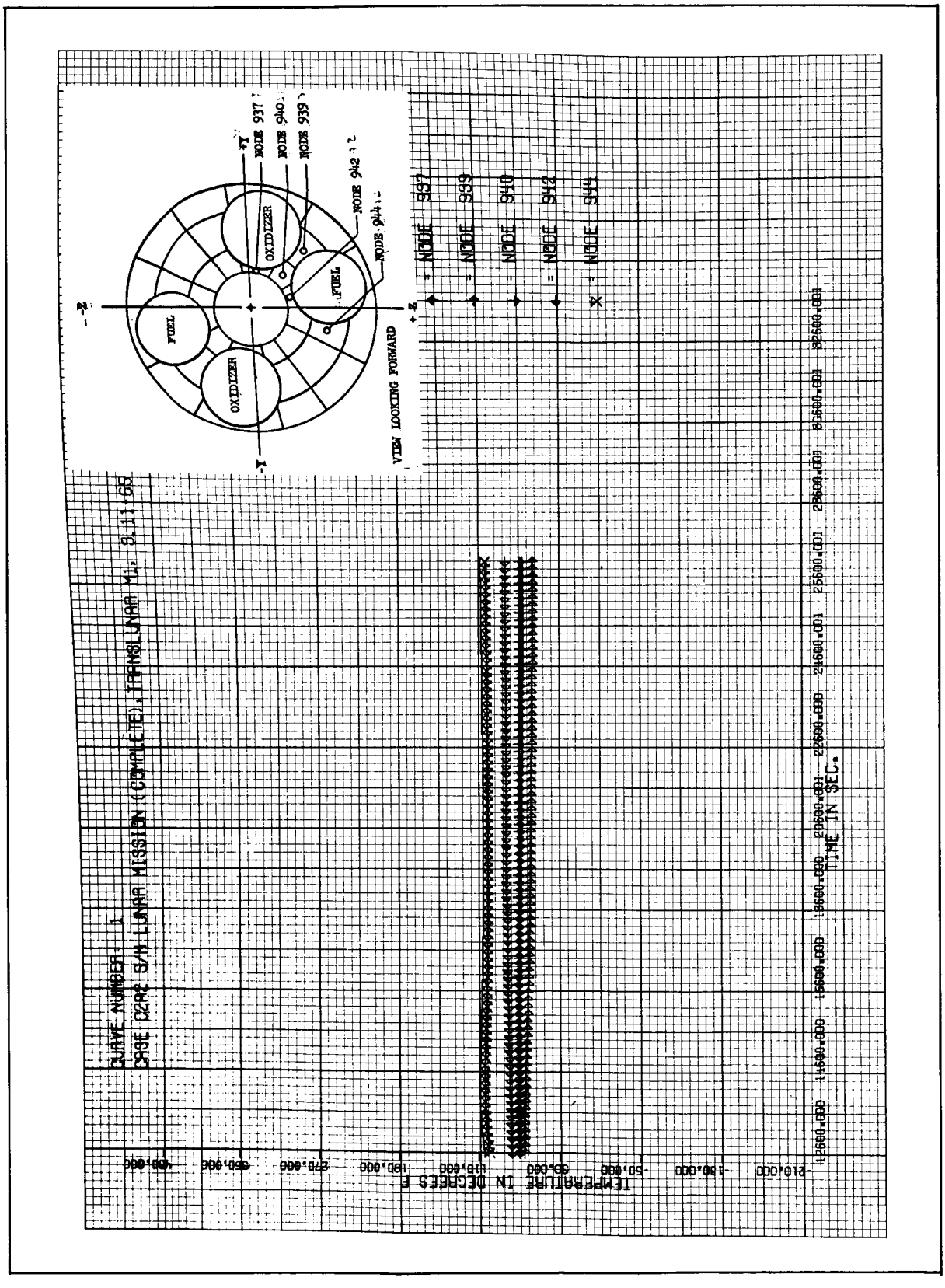

Figure 6-9b Aft Bulkhead Temperature Histories for Lunar Orbit Rendezvous Mission (Continued)

LOCKHEED
CALIFORNIA COMPANY

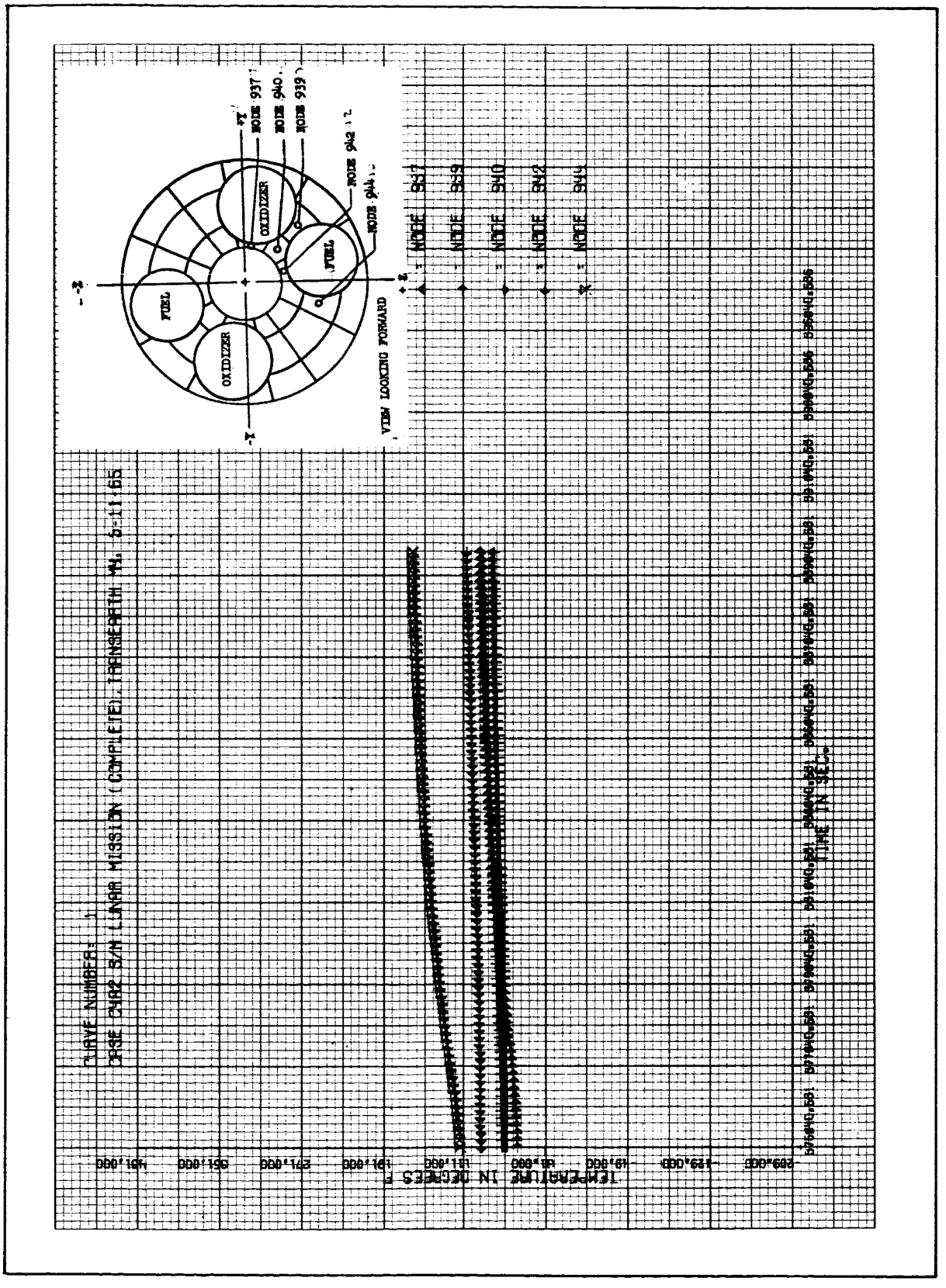

Figure 6-9c Aft Bulkhead Temperature Histories for Lunar Orbit Rendezvous Mission (Continued)

LOCKHEED
CALIFORNIA COMPANY

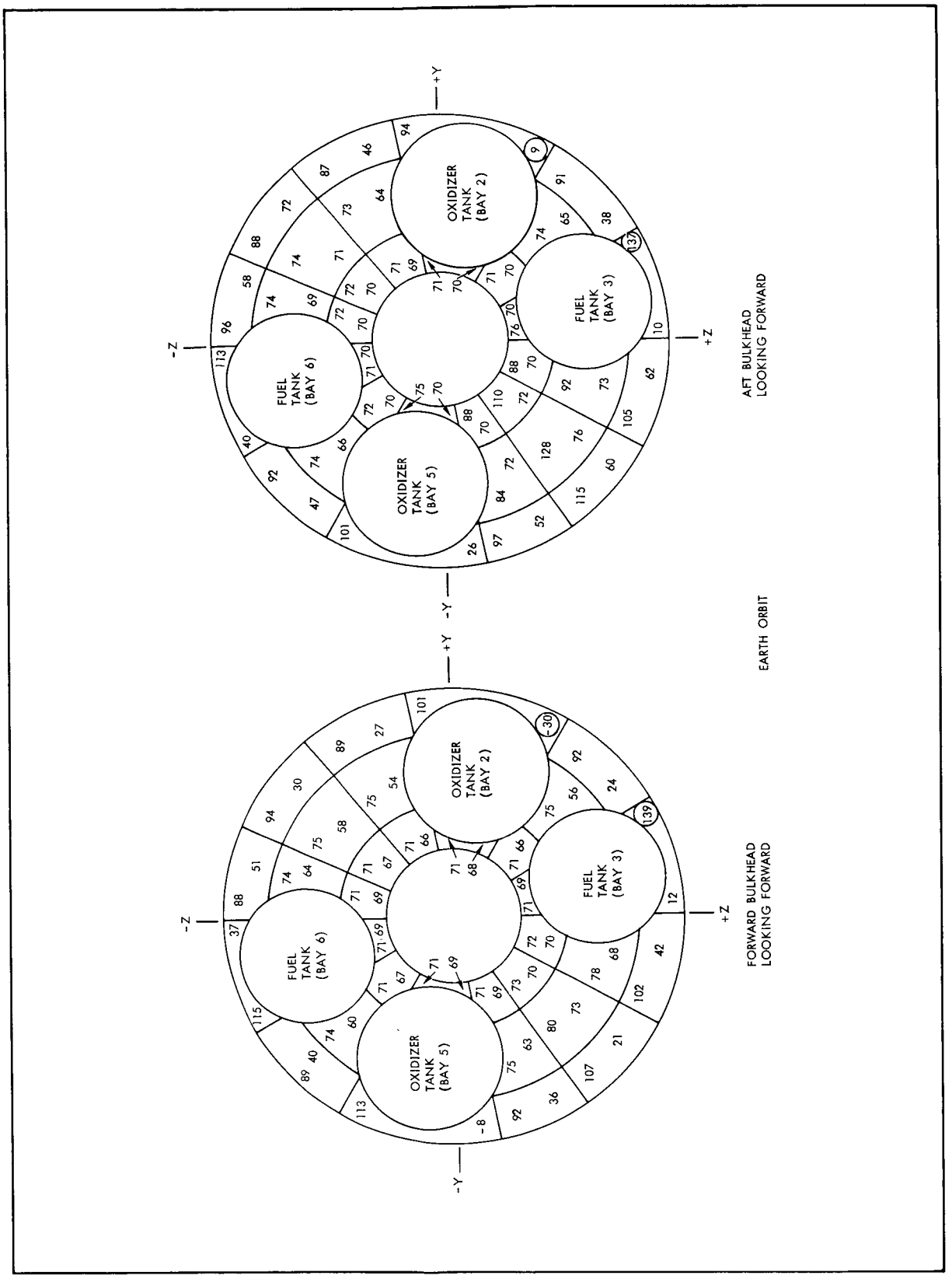

Figure 6-10a Maximum/Minimum Temperatures for Bulkhead Nodes, Lunar Orbit Rendezvous Mission

LOCKHEED
CALIFORNIA COMPANY

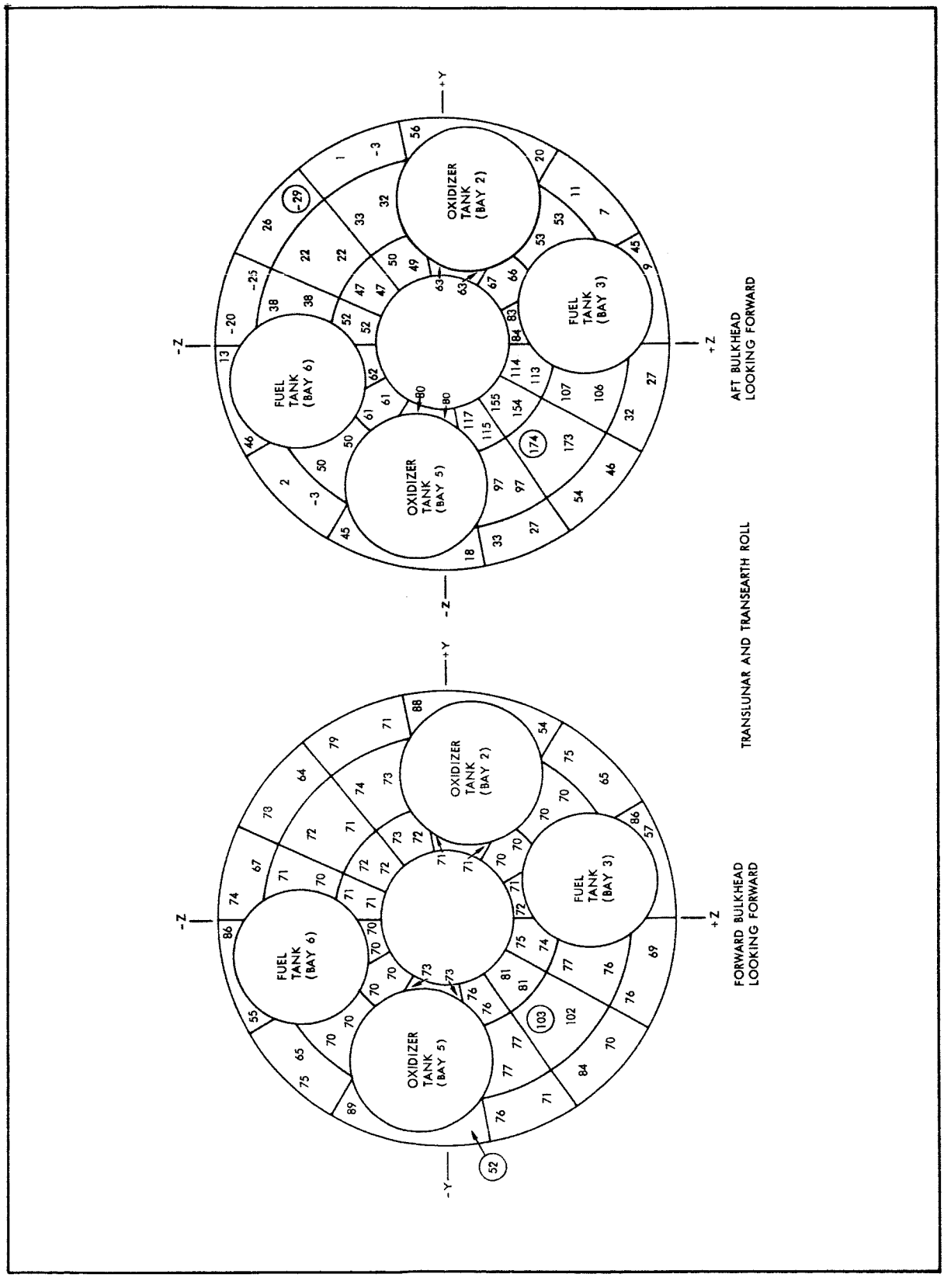

Figure 6-10b Maximum/Minimum Temperatures for Bulkhead Nodes, Lunar Orbit Rendezvous Mission (Continued)

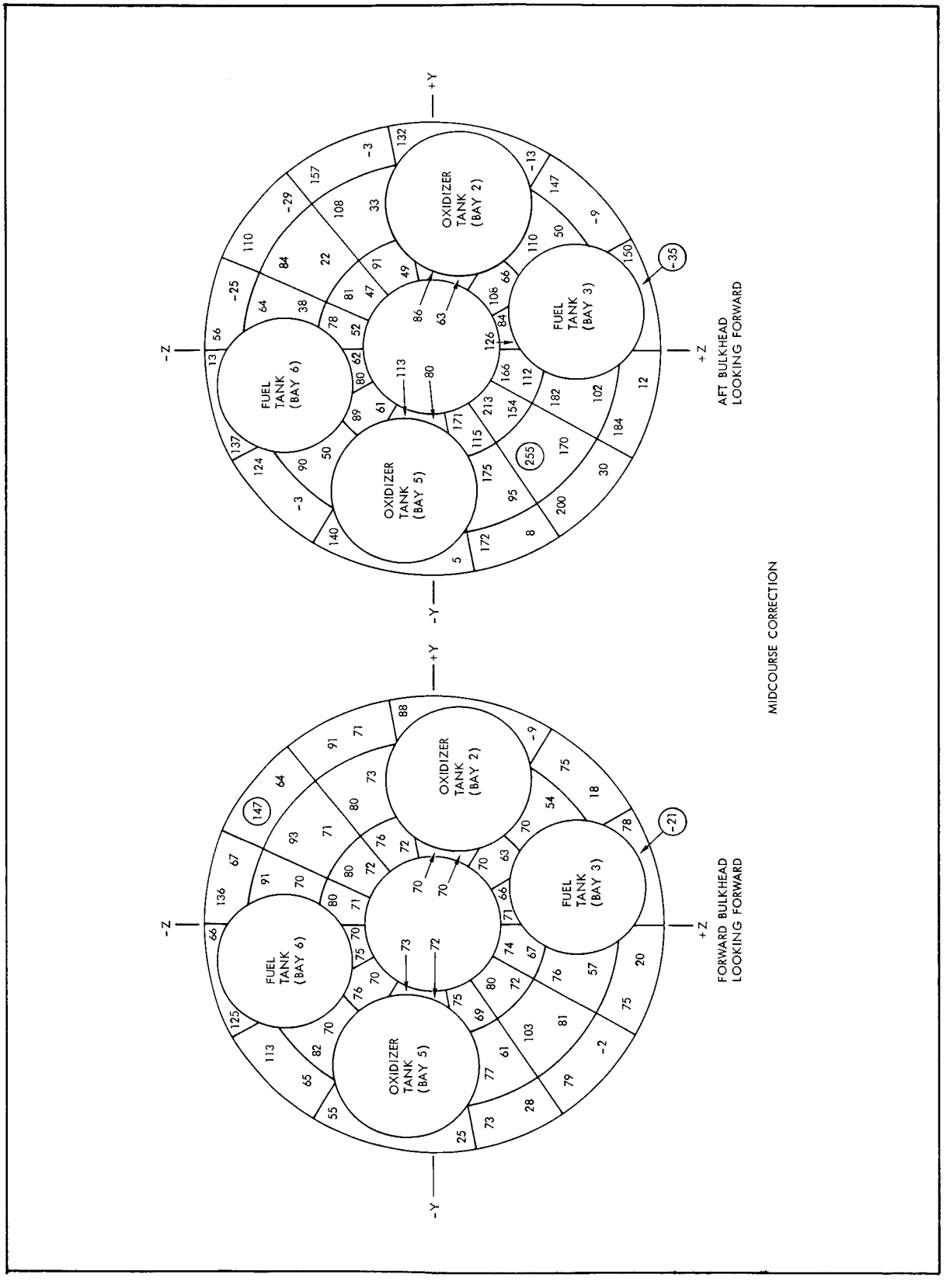

Figure 6-10c Maximum/Minimum Temperatures for Bulkhead Nodes, Lunar Orbit Rendezvous Mission (Continued)

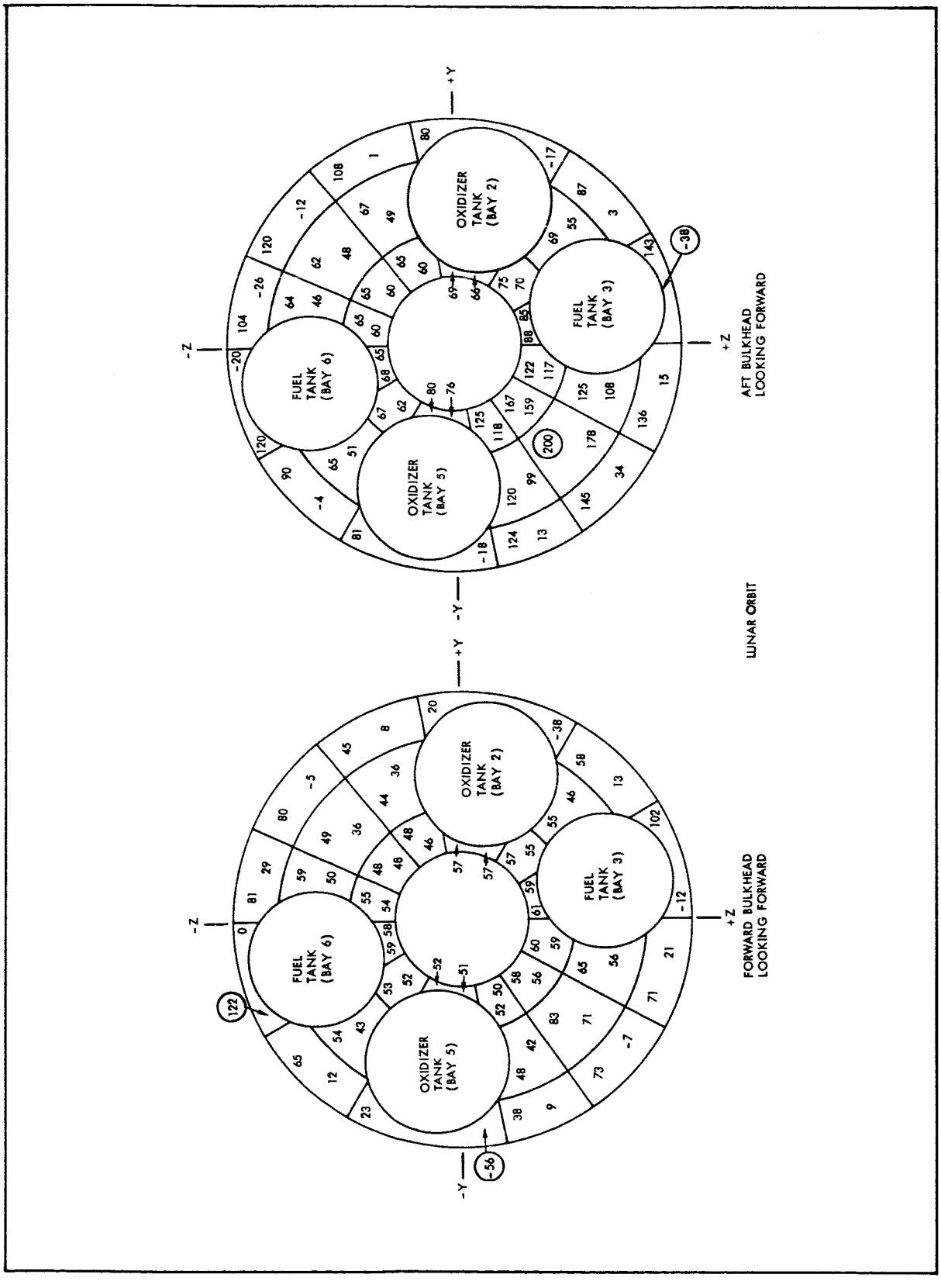

Figure 6-10d Maximum/Minimum Temperatures for Bulkhead Nodes, Lunar Orbit Rendezvous Mission (Continued)

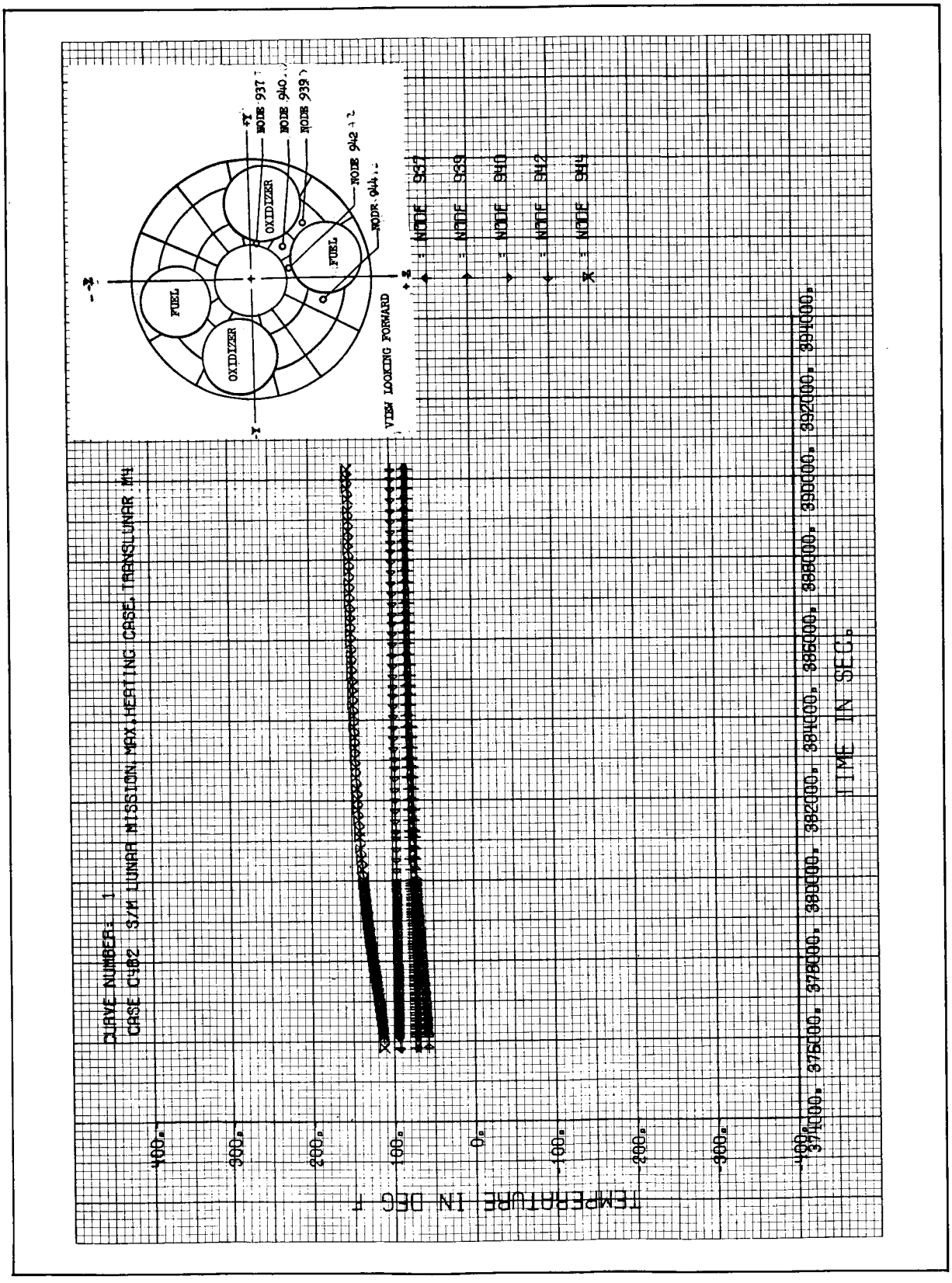

Figure 6-11a Aft Bulkhead Temperature Histories for Maximum Heating Orientation

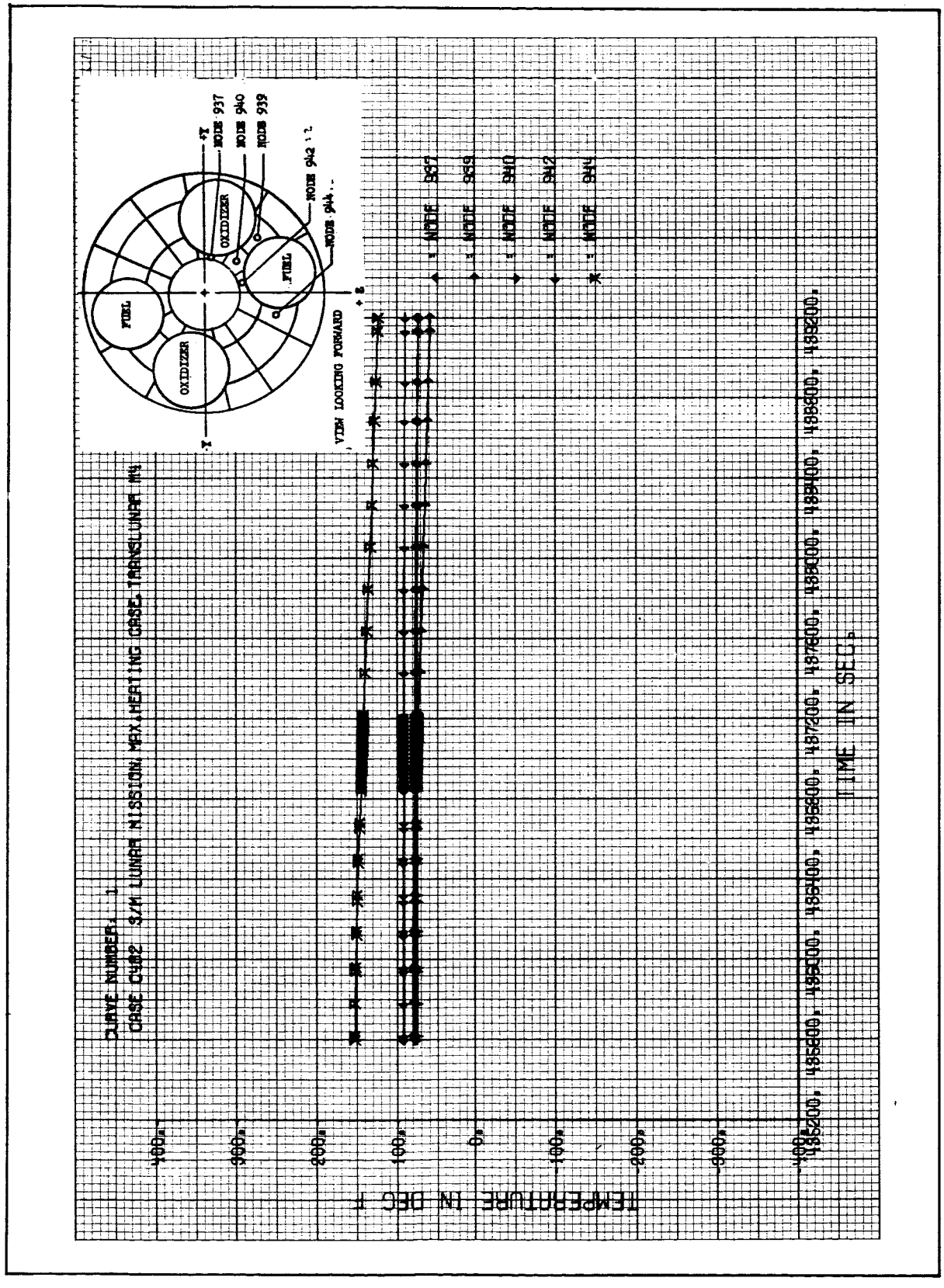

Figure 6-11b Aft Bulkhead Temperature Histories for Maximum Heating Orientation (Continued)

LOCKHEED CALIFORNIA COMPANY

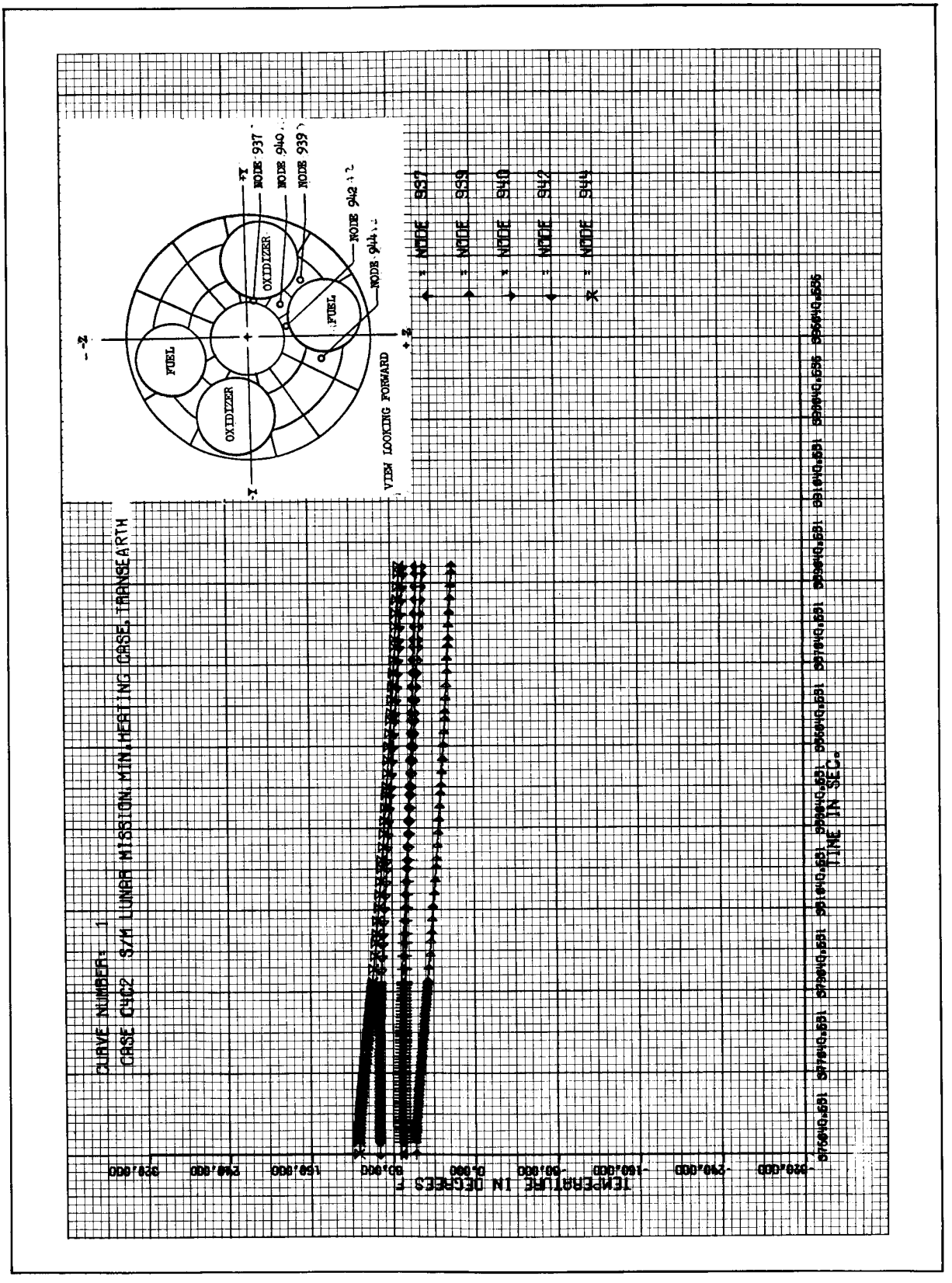

Figure 6-12a Aft Bulkhead Temperature Histories for Minimum Heating Orientation

LOCKHEED
CALIFORNIA COMPANY

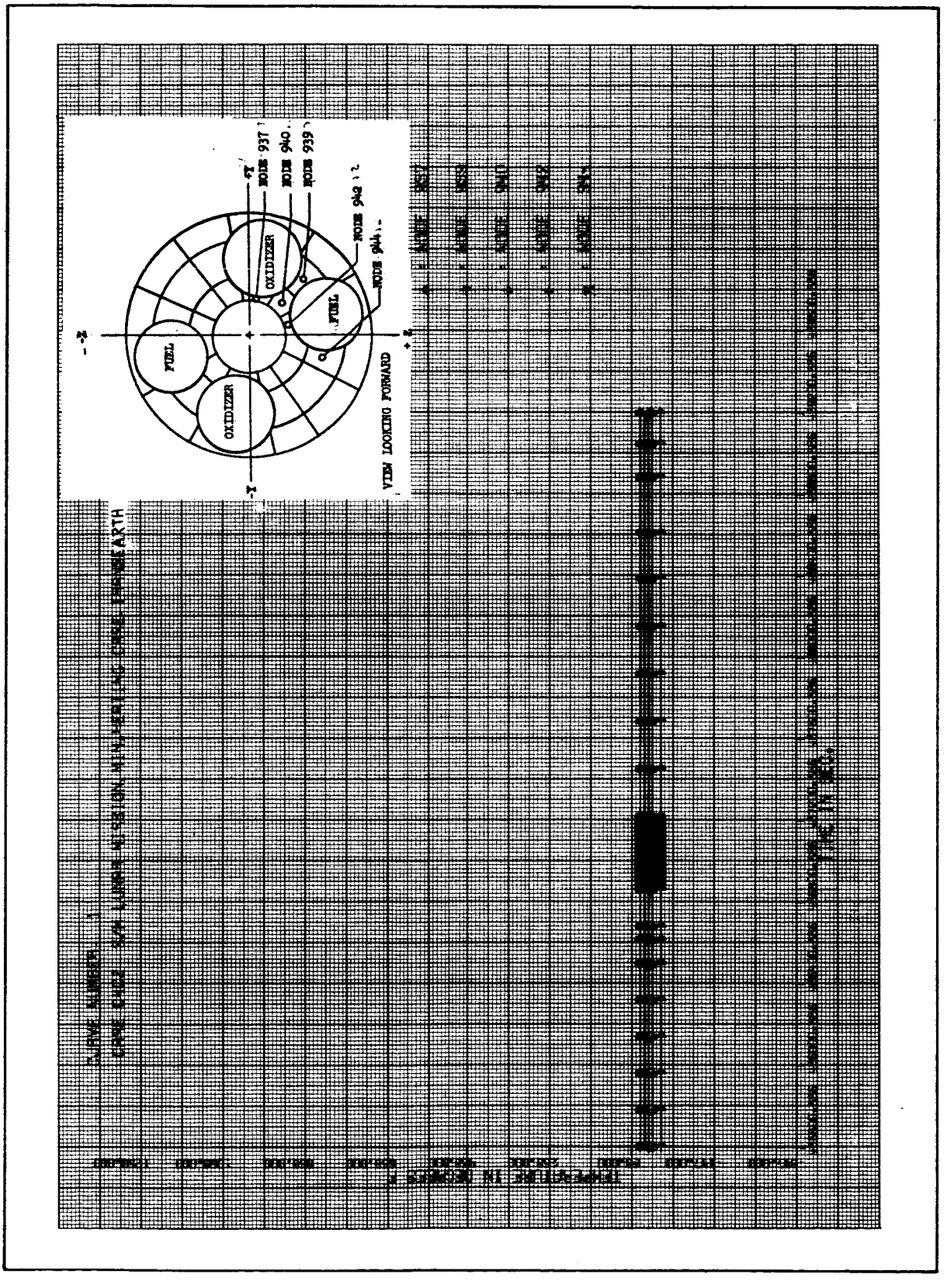

Figure 6-12b Aft Bulkhead Temperature Histories for Minimum Heating Orientation (Continued)

OTHER COMPONENTS

In addition to structure temperatures, other temperatures computed by the basic network are those of the nozzle extension, the aft head shield, and the fuel cells.

Except during periods of engine firing, when they are impressed using MSC supplied data, engine nozzle extension temperatures are computed by a heat balance. Nozzle temperatures are a strong function of spacecraft orientation with respect to the solar vector. Figure 6-13 shows representative nozzle extension temperatures immediately following a short midcourse correction firing and after the 320 second lunar orbit insertion firing.

Aft heat shield temperatures are always computed by a heat balance. Representative shield temperature histories are shown in Figure 6-14.

A history of the fuel cell temperature for the entire Lunar Mission is presented in Figure 6-15. For most of the mission the fuel cell environment causes a stabilization of this temperature at just over 300°F. However, following the transearth injection firing the fuel cell environment is modified due to the emptying of the bay 3 propellant tank. The decreased capacity of the then empty tank permits the tank temperature to increase, as it receives heat from the thrust chamber. The rise in the tank temperature is followed by a corresponding increase in the temperature of the bulkhead adjacent to the tank, which affects directly the temperature of the fuel cells. This results in the temperature rise shown in the figure at approximately 400,000 sec. A peak temperature of 335°F is obtained and maintained for about 40,000 sec., or until the fourth midcourse correction occurs. During the fourth midcourse correction, bay 3 is oriented away from the sun. The shell adjacent to this bay cools enough to also affect the temperature of the bay 3 tank, which drops to about 70°F. Its influence on the bulkhead and hence the fuel cell temperature is evident from the drop in fuel cell temperature which occurs. Since no additional heat pulses are received by the bay 3 tank for the remainder of the mission, its temperature never again rises significantly, and the fuel cells remain near their previous equilibrium temperature of 300°F.

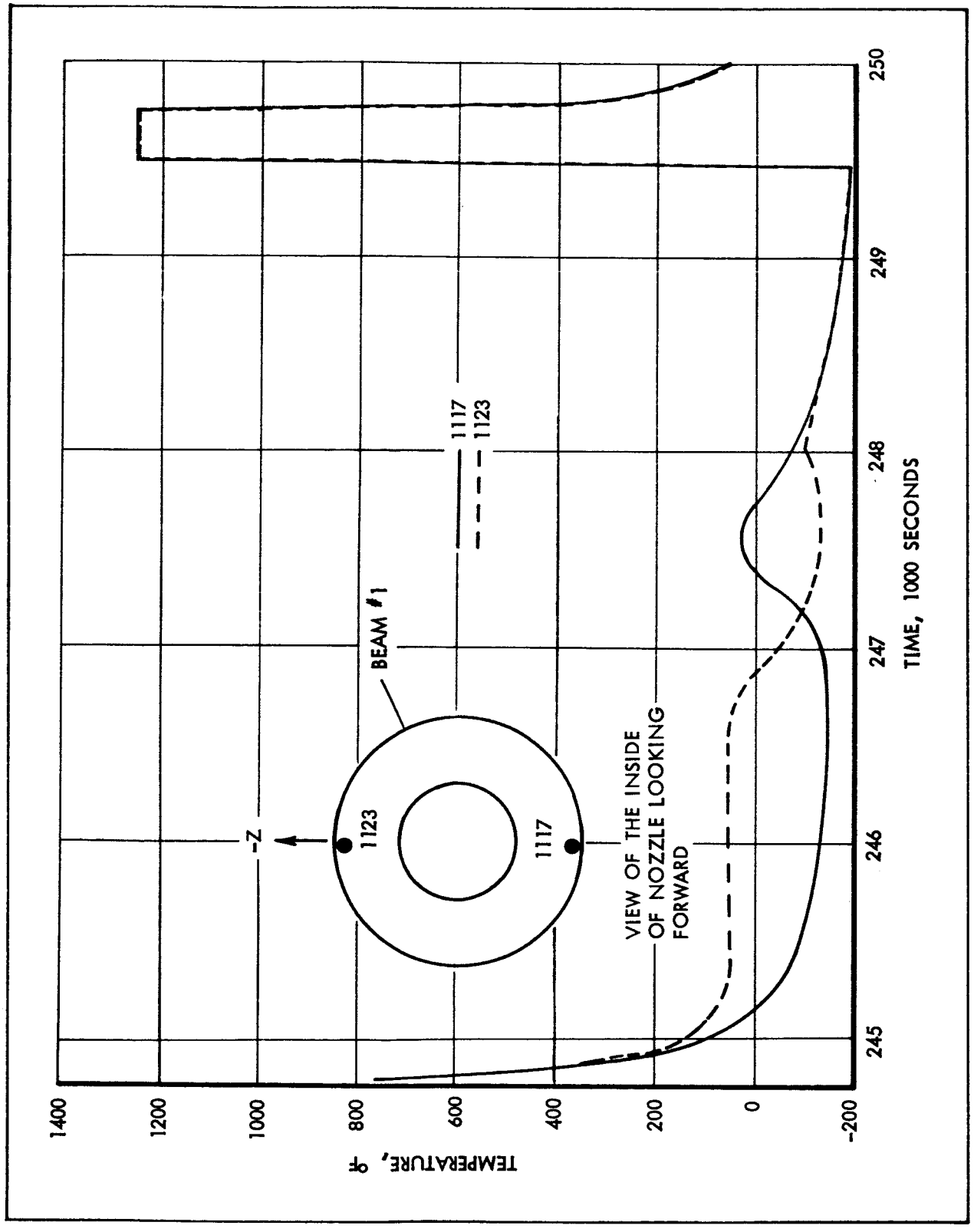

Figure 6-13 Nozzle Extension Temperature Histories for Engine Soak Periods

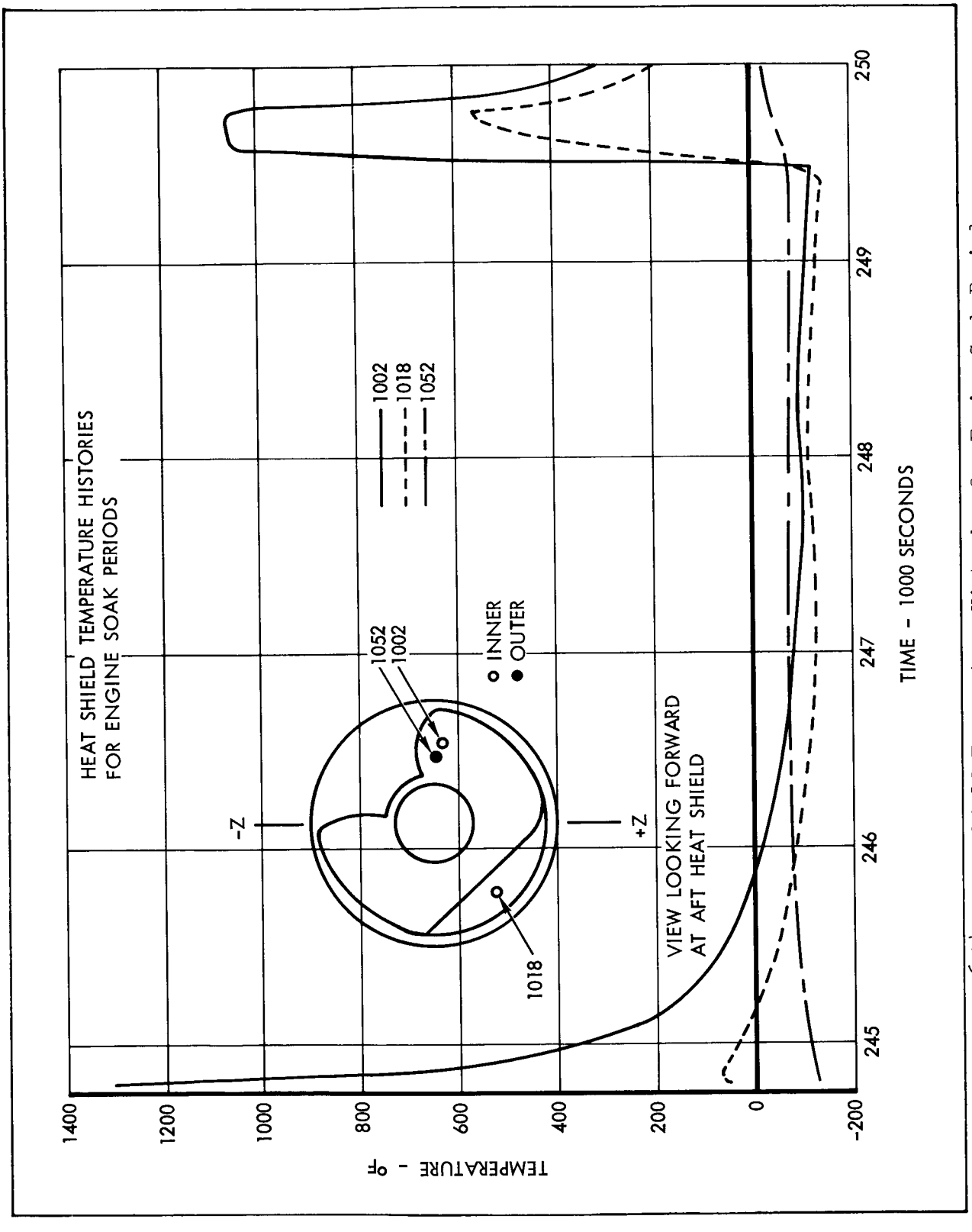

Figure 6-14 Heat Shield Temperature Histories for Engine Soak Periods

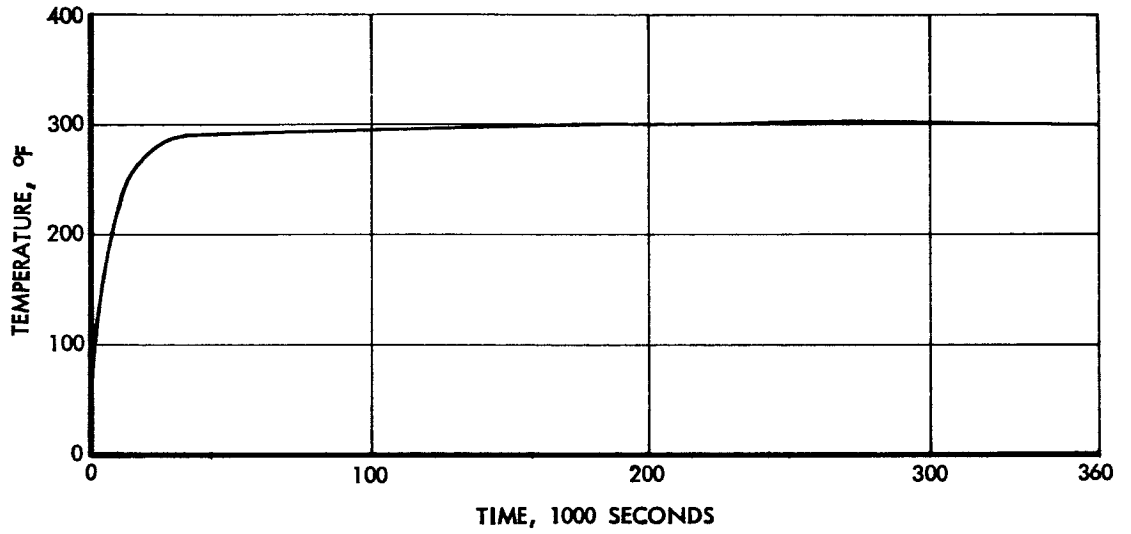

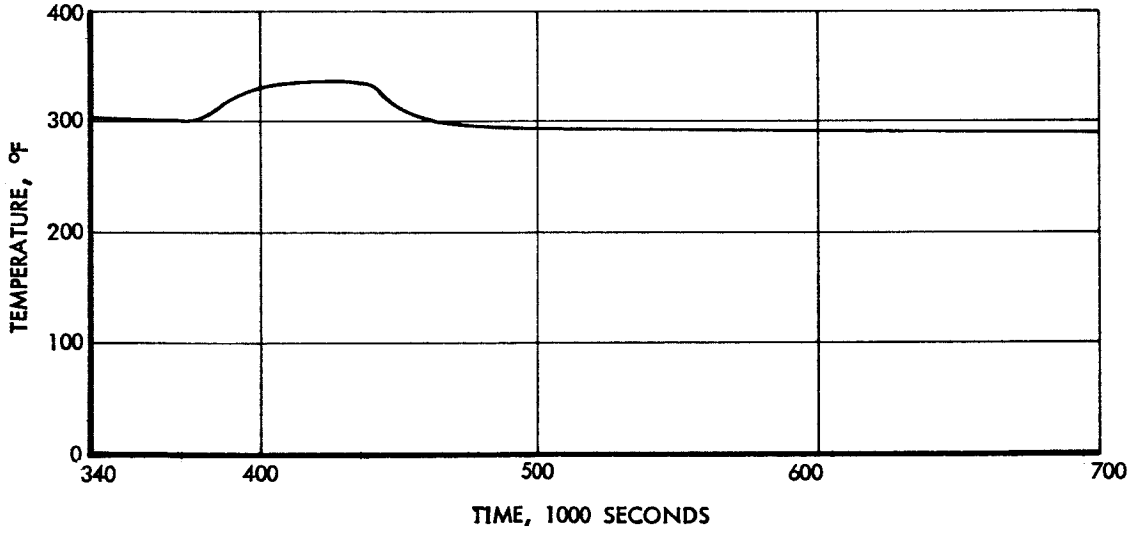

Figure 6-15 Fuel Cell Temperature History

As noted previously, the fuel cells are an extremely important internal heat source to the well insulated Service Module. Since this analysis was performed for the Block I configuration, significant errors could result in attempting to extrapolate the results of the study to the actual Block II configuration. Of primary concern is the effect that the fuel cell location has on the heating to the plumbing and the helium bottles. For example, during lunar orbit the temperature of aft bulkhead node 947, which is directly beneath the fuel cell, is maintained at around 190°F while aft bulkhead node 963, its diagonally opposite counterpart in bay I, averages 55°F. During the translunar phase, node 947 remains above 200°F. These values are unrealistic for the Block II configuration. Furthermore, relocation of the fuel cell to the upper portion of bay 4 will cause a sizeable increase in the temperature of the forward bulkhead and the inner web, causing a significant increase in the heating to the helium bottles.

VII - DETAILED ANALYSIS OF SERVICE PROPULSION SYSTEM, LUNAR ORBIT RENDEZVOUS MISSION

The detailed analysis of the Service Propulsion System (SPS) is comprised of analyses of the plumbing, engine, and fluid storage and pressurization system. Results of the analysis of the basic structure (Section VI) were used as boundary conditions for the SPS analyses.

SPS PLUMBING

A detailed plumbing analysis for the SPS was performed to determine temperature extremes of the various SPS components, and to compare these temperatures with the allowable limits set for the design as it exists. The analysis performed made maximum usage of the results of the basic SM analysis wherever the effect of the plumbing environment was important. All line and component temperatures were computed through heat balances, except during SPS engine firings. During these firings,the temperatures of lines which have fluid passing through them were set equal to the temperature of the fluid at its source. Thus helium line temperatures were set equal to the expanded helium temperatures, fuel line temperatures were set equal to the stored fuel temperature, and similarly for the oxidizer lines.

The results of the plumbing analysis are summarized in Table 7-1 and also in Figures 7-1 through 7-4. Table 7-1 lists all SPS plumbing components which have prescribed temperature limits, the values of these limits, and the calculated temperature extremes for each component. No calculated temperatures are tabulated for the two fill and drain couplings or the oxidizer vent coupling because the exact location of these components is not defined. Since the gradients in the lines connected to the disconnect panels are large near the panels, the exact location is necessary if temperature extremes are to be determined. However, temperatures are supplied for both the panels and many locations on the lines. Figures 7-1 through 7-4 show the actual system which was analyzed, and include maximum and minimum temperatures throughout the network.

Table 7-1 shows that the only plumbing components which exceed their temperature limits are the helium components near the fuel cells, the propellant feed lines parallel to the thrust chamber, and some components near the disconnect panels. Components of the helium pressurization system in Bay 4 are overheated because of the inability of the fuel cell heat output to escape from the bay. The bay is insulated on three of its interior walls - the shell and both beams. However, on Beam 4 where the helium pressure regulators and valves are located, a region of insulation is removed. This is one region of the helium pressurization system which is heated excessively

Table 7-1 SPS PLUMBING ALLOWABLE TEMPERATURE LIMITS AND CALCULATED TEMPERATURE EXTREMES LUNAR ORBIT RENDEZVOUS MISSION

COMPONENTS SPEC	ITEM	ALLOWABLE LIMITS (°F) MAX	MIN	CALCULATED TEMPERATURES VED (°F) MAX	MIN	PORTIONS OF MISSION FOR WHICH TEMPERATURE LIMITS ARE EXCEEDED
MC 273-0020	Fill & Drain Hyd/UDMH Tank Coupling	160	-65	*	*	
MC 273-0022	Fill Vent Disconnect N_2O_4 Tank Coupling	160	-65	*	*	
MC 273-0039	Propulsion System Flexible Connector (Fuel)	80	40	79	58	None
MC 273-0018	Fill & Drain N_2O_4 Tank Coupling	160	-65	*	*	
MC 273-0012B	SPS Propellant - Disconnect Coupling	80	40	70	35	L. O.
MC 273-0040	Propulsion System Flexible Connector (N_2O_4)	80	40	70	54	None
MC 901-0008A	Propulsion Quantity Indicator and Mixture Ratio Control	80	40	70	54	None
———	Heat Exchanger (Bay 2) (HE)	80	-150	70	-80	None
———	Heat Exchanger (Bay 6) (HE)	80	-150	72	-80	None
	Disconnect Panel (Bay 2)	140	40	79	-44	L.O., M.C.
	Disconnect Panel (Bay 6)	140	40	196	18	L.O., M.C.
MC 284-0027	Helium SPS Pressure Relief Value	120	40	238	*	All Portions

Table 7-1 (continued)

COMPONENTS		ALLOWABLE LIMITS (°F)		CALCULATED TEMPERATURES VED (°F)		PORTIONS OF MISSION FOR WHICH TEMPERATURE LIMITS ARE EXCEEDED
SPEC	ITEM	MAX	MIN	MAX	MIN	
MC 144-0023	System Test Point Dis connect Coupling	150	30	238	*	All Portions
MC 284-0020	Helium SPS Pressure Regulator Unit	150	30	240	*	All Portions
MC 273-0009	Helium Tank Fill Couplings	80	-150	241	*	All Portions
MC 284-0018	Helium 5/8 inch Solenoid Value	150	30	241	*	All Portions
———	Propellant Feed Lines (Adjacent to Engine)	135	40	379	69	LOI, TEI

*See Text for Explanation

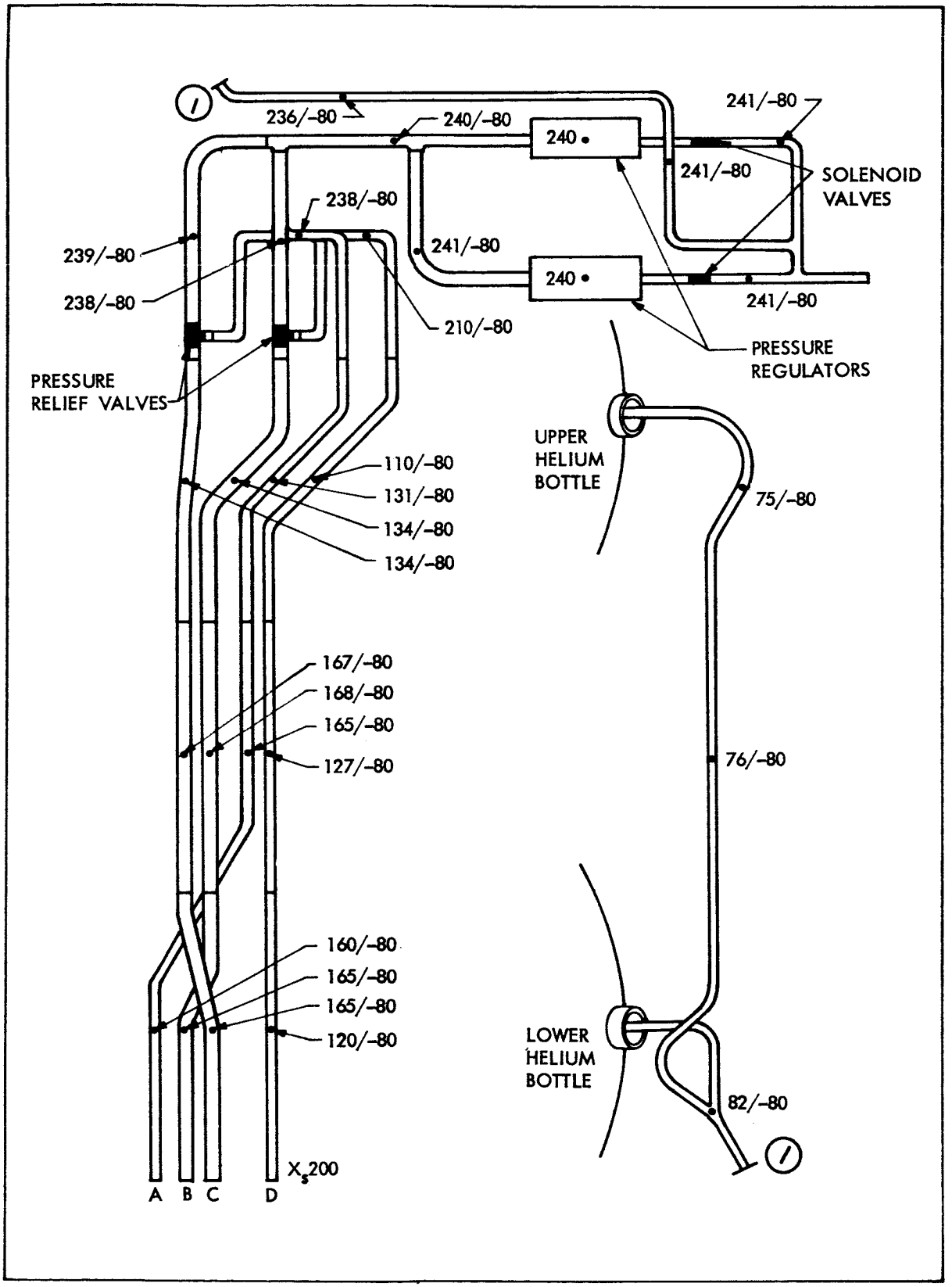

Figure 7-1 Maximum/Minimum Temperatures of Bay 4 Helium Lines and Components

LOCKHEED CALIFORNIA COMPANY

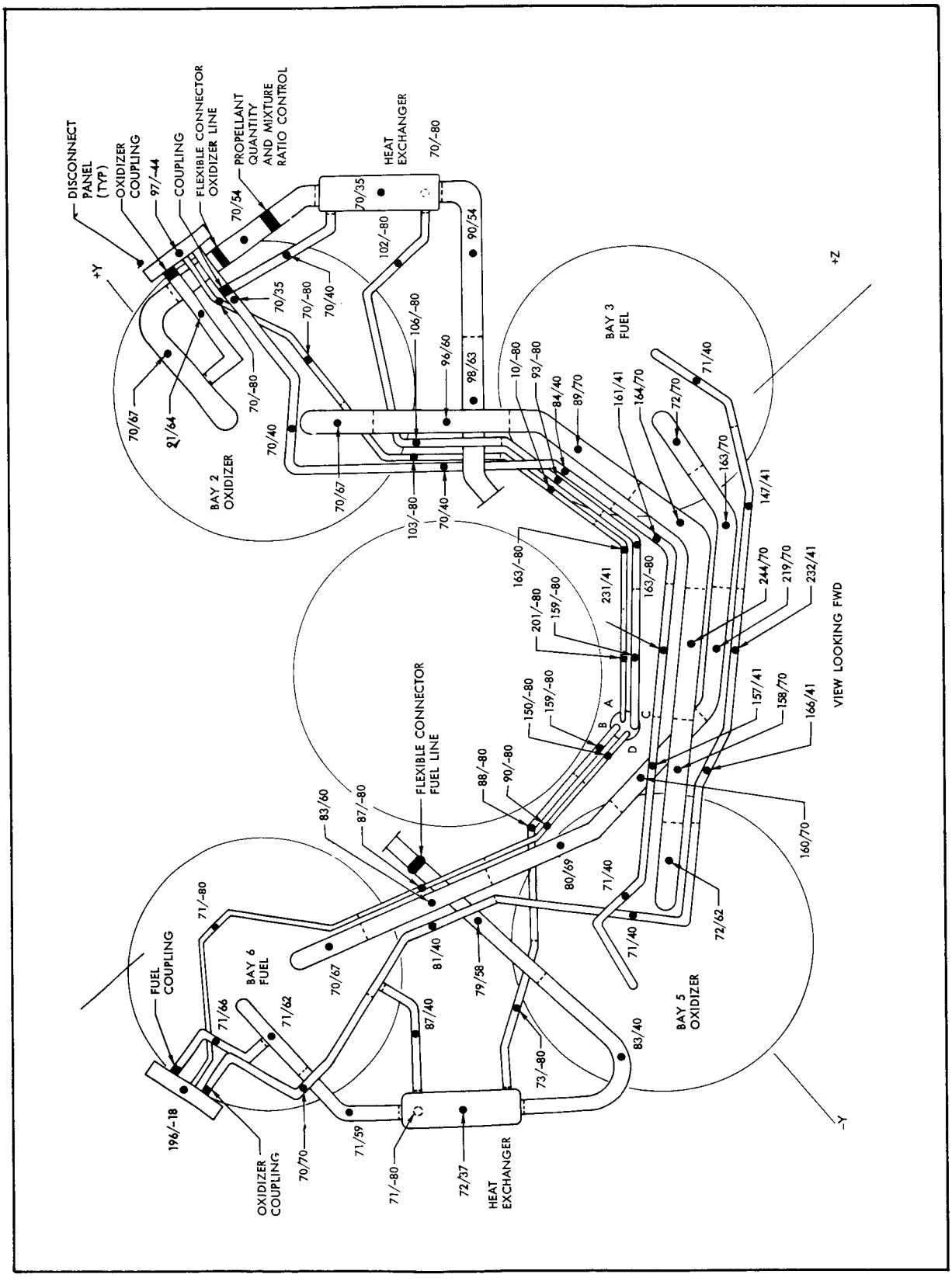

Figure 7-2 Maximum/Minimum Temperatures of Plumbing Lines Enclosed by Aft Bulkhead and Heat Shield

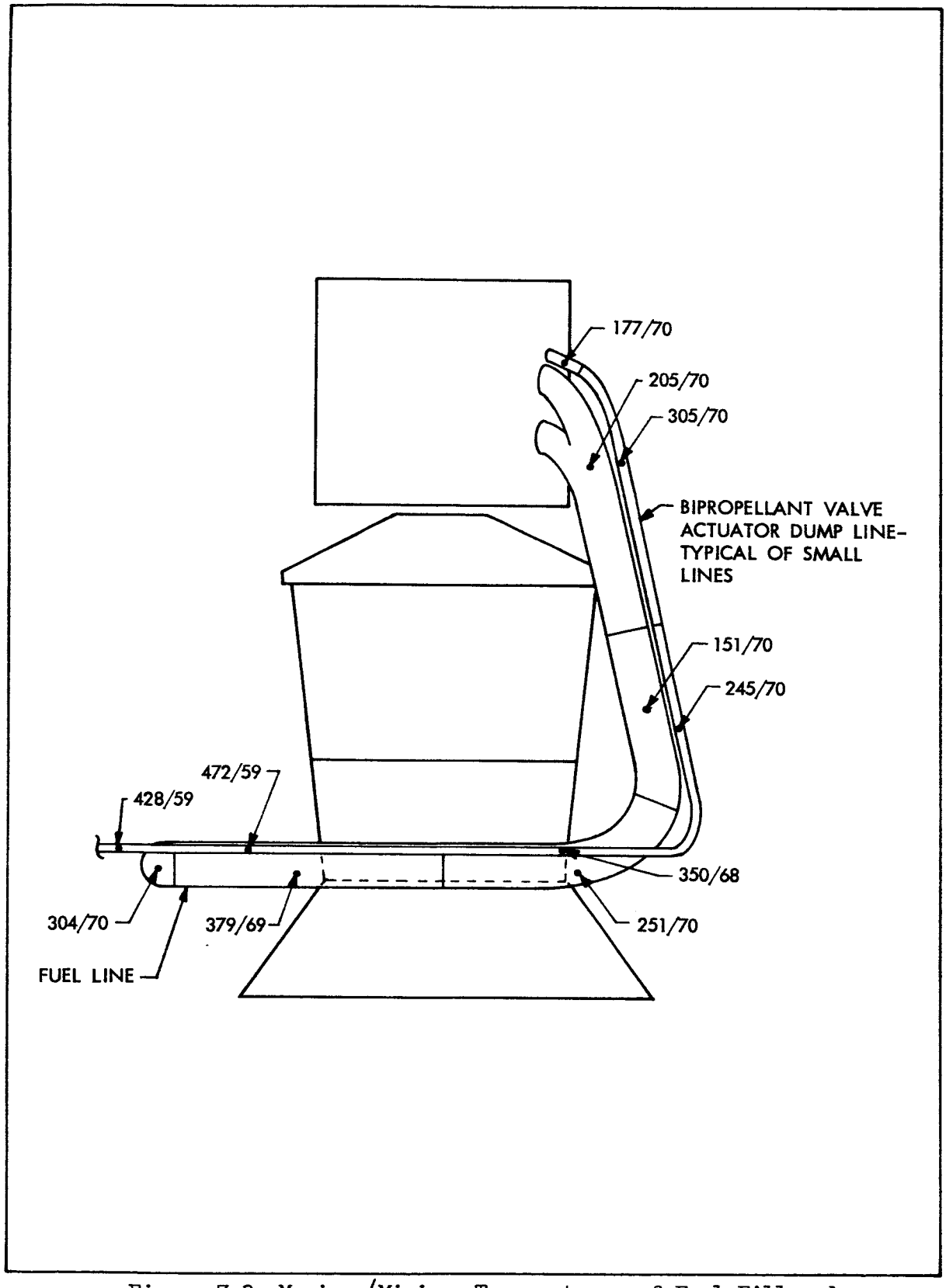

Figure 7-3 Maximum/Minimum Temperatures of Fuel Fill and Adjacent Lines - Forward of Aft Bulkhead

LOCKHEED CALIFORNIA COMPANY

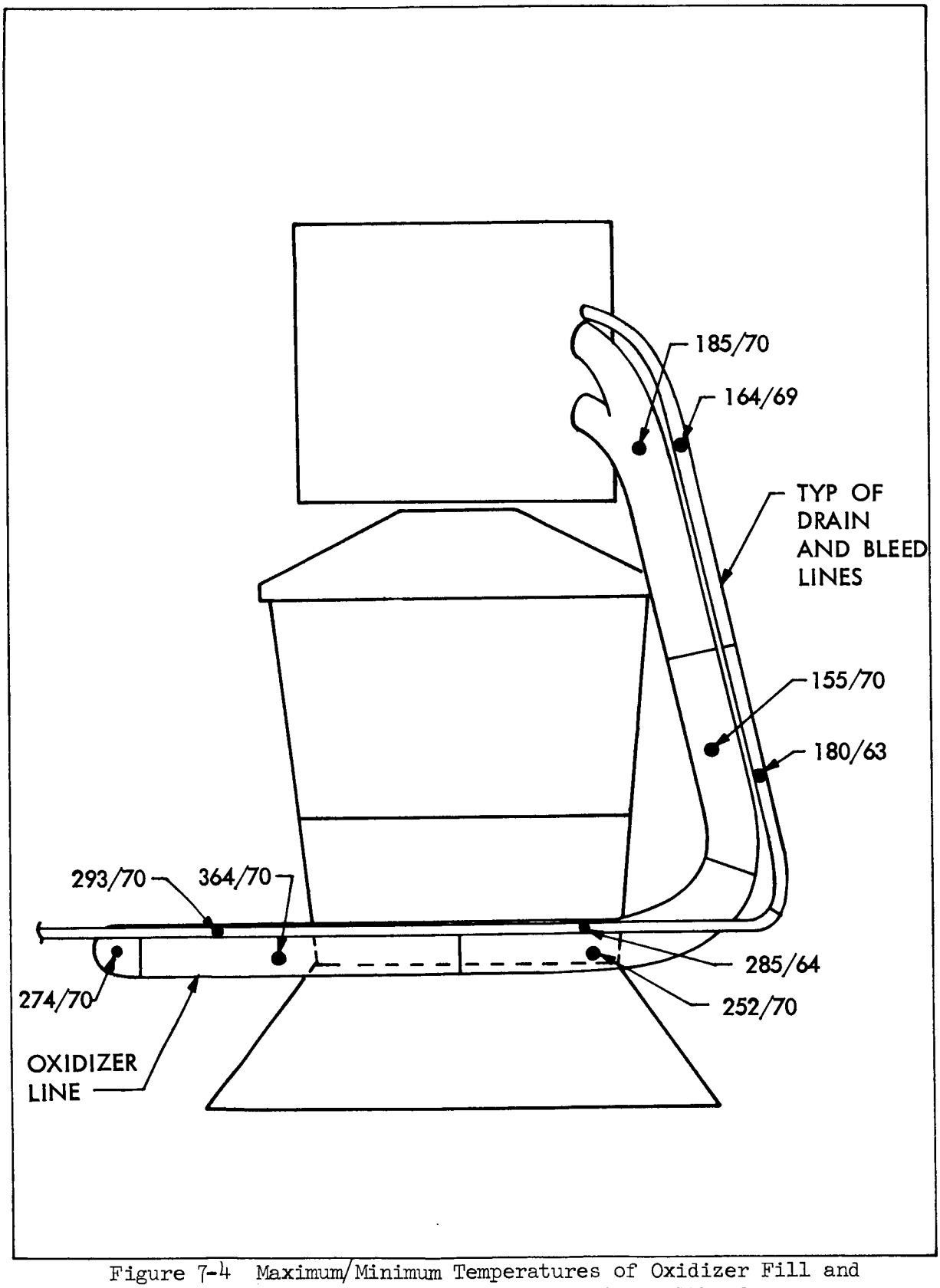

Figure 7-4 Maximum/Minimum Temperatures of Oxidizer Fill and Adjacent Lines - Forward of Aft Bulkhead

LOCKHEED
CALIFORNIA COMPANY

(240°F). Figure 7-5 gives the complete temperature-time history of one of the pressure regulators, which is located in this region.

The minimum temperatures calculated are those impressed on the line while the SPS engine fires. For components such as pressure regulators and valves this assumption that the component reaches equilibrium with the fluid passing through it is poor. Due to the lack of any details on these components, and the complexity of the highly transient convection problem occurring, the components minimum temperatures could not be computed. Therefore, their temperatures were arbitrarily set equal to that of their adjacent line. Their minimum temperatures do, however, occur at the times shown. Maximum temperatures on the components are quasi-steady state values, and should be reasonably accurate.

The fuel cells also affect the temperatures of plumbing beneath the aft bulkhead. The bulkhead is heated by the cells while radiating heat to the nearby plumbing lines. The maximum allowable line temperature is specified as 135°F, and is greatly exceeded in certain segments of the line. Figure 7-6 shows a typical temperature history for such a location.

All plumbing lines which extend from the aft bulkhead region to the SPS valve assembly are critically overheated. Upper temperature limits on the propellant lines are prescribed as 135°F for normal engine operation. Although these lines reach 370°F following the lunar insertion firing, the highest residual temperature of the lines which exists immediately preceding an engine firing is 200°F. This occurs at the fourth midcourse correction, and is a consequence of heat soak from the two previous long lunar firings. Following the midcourse correction firings these propellant lines are not excessively heated.

The reason why these lines overheat is that both the thrust chamber backwall and the engine web mounts reach high temperatures following the lunar firings. Little heat relief is available for these lines except during propellant flow periods. Figures 7-3 and 7-4 show the fuel and oxidizer lines in this region with the maximum and minimum temperatures achieved for segments of the lines. Also shown are typical fill, drain or bleed lines from actuators, seals etc. which closely parallel the propellant

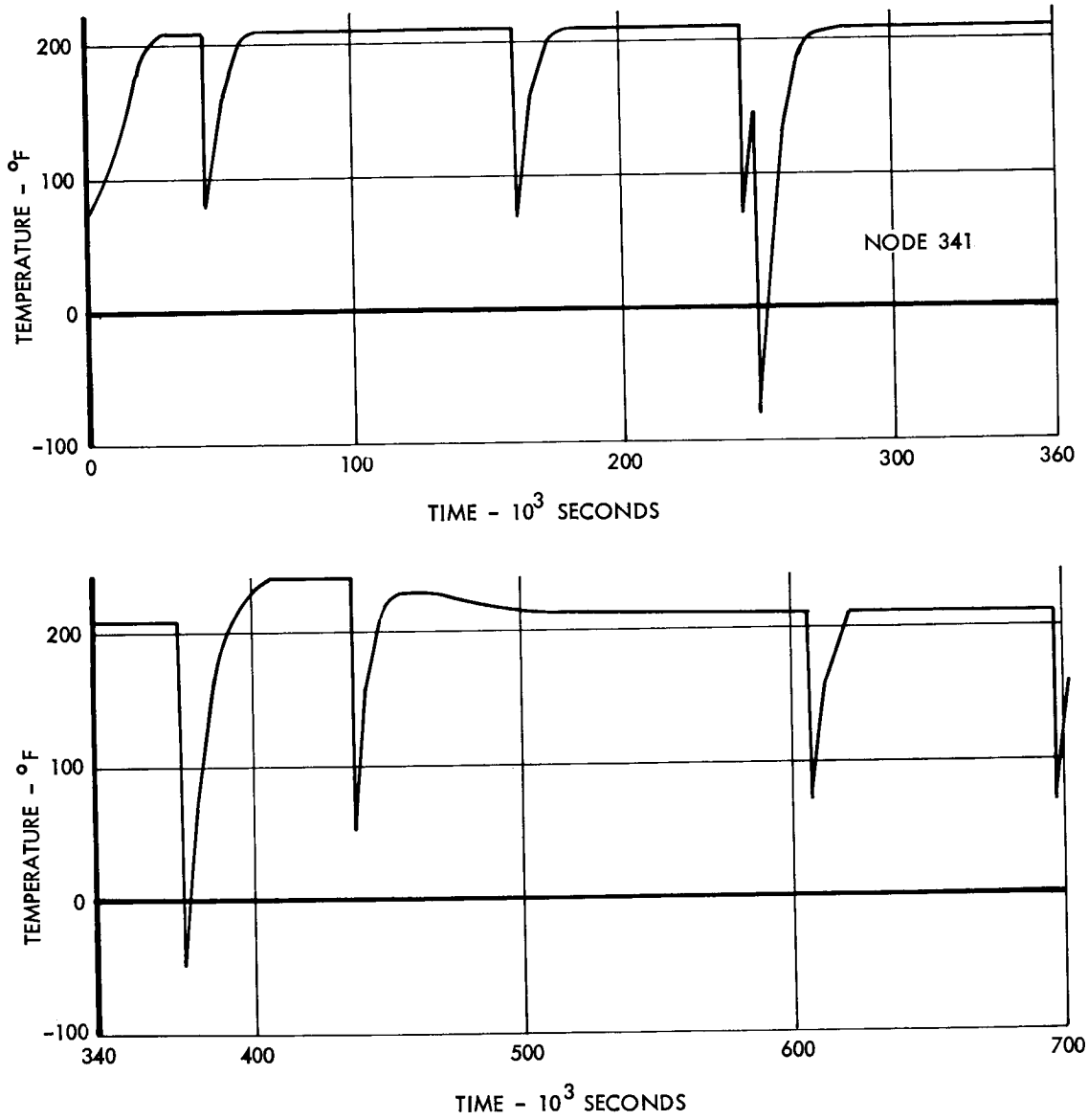

Figure 7-5 Helium Pressure Regulator Temperature History

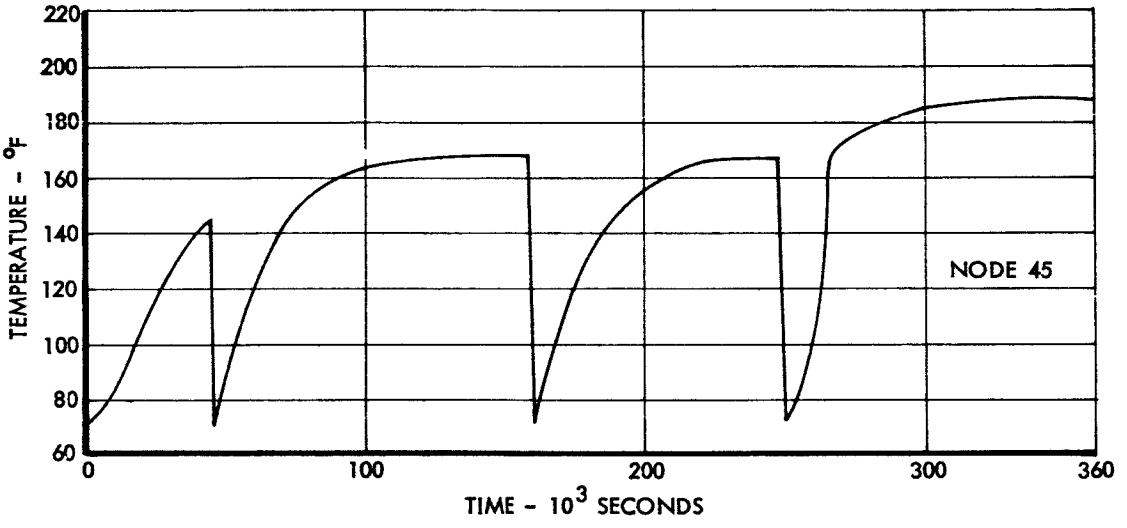

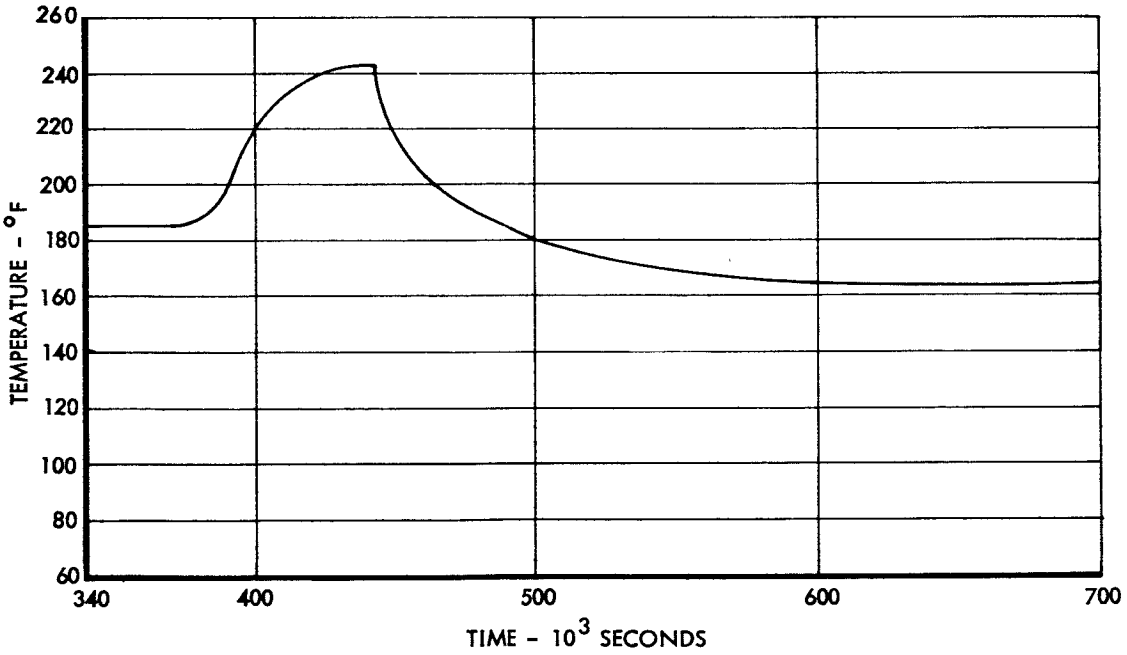

Figure 7-6 Propellant Line Temperature History - Aft Bulkhead Beneath Fuel Cells

LOCKHEED CALIFORNIA COMPANY

lines. The temperatures of these lines are considerably above those of the propellant lines for two reasons:

1) They have considerably less thermal capacitance

2) They are partially blocked from any cool surroundings by other lines

Figure 7-7 presents the temperature history of a bipropellant valve actuator dump line node which is situated opposite the thrust chamber. Its history is similar to that of all line temperatures for this region of the SPS. The significance of the high temperatures achieved ($>450^{o}F$) are not definite, since no limits were given.

The only regions on the SPS which are cooled beyond their temperature limits are on and near the disconnect panels. The temperature histories of both panels are shown in Figures 7-8 and 7-9, and the maximum and minimum temperatures allowable and achieved are given in Table 7-1. Both upper and lower temperature limits are exceeded on the Bay 6 panel, but only the lower is exceeded on the Bay 2 panel. Figure 7-10 shows a propellant-disconnect coupling which exceeds its allowable minimum. These temperature limits are achieved during lunar orbit when the panels experience their maximum cold and solar soak periods.

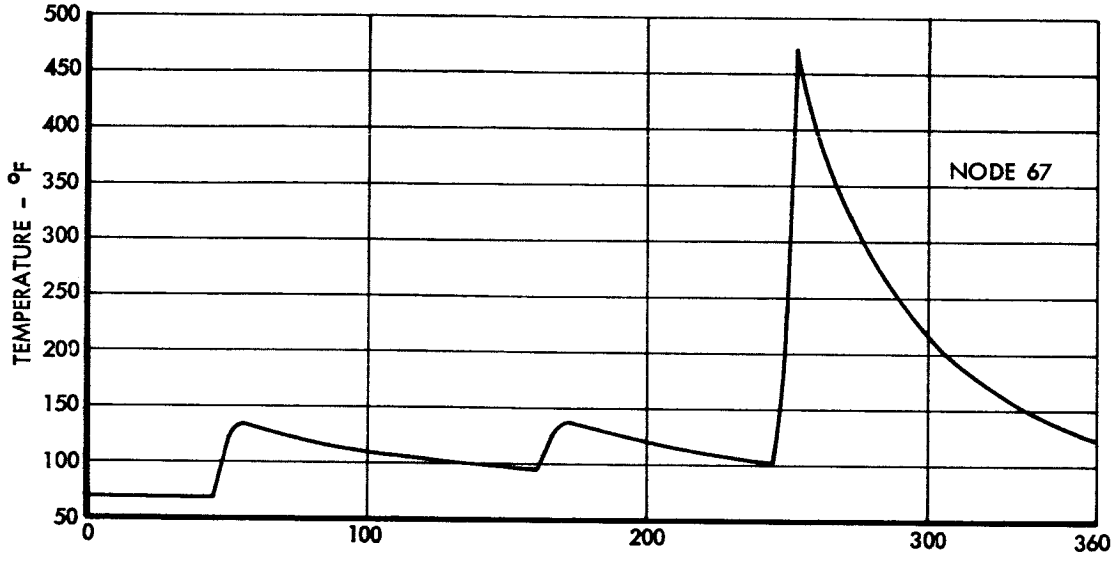

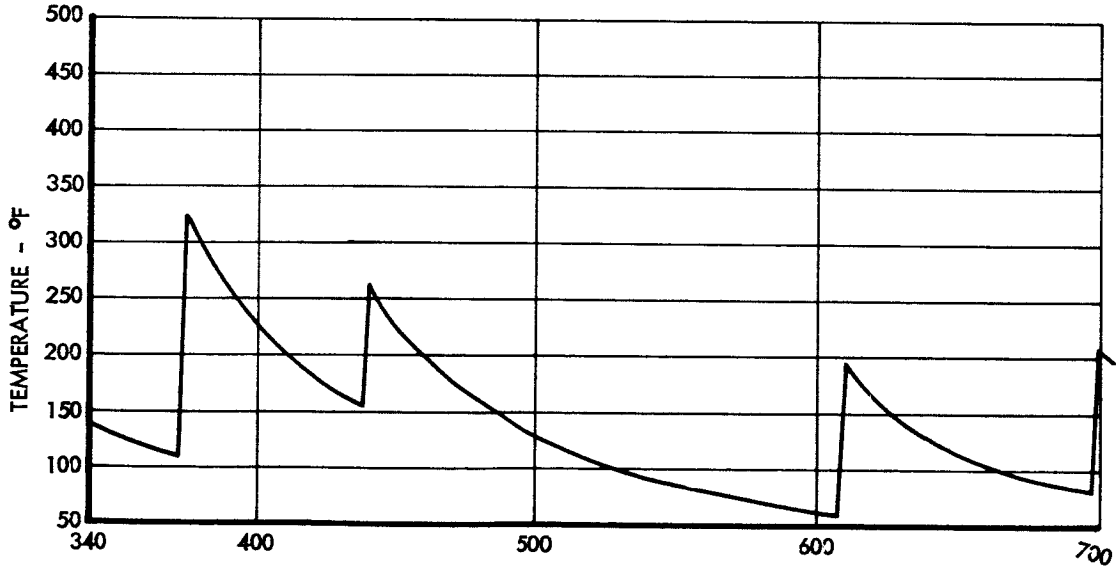

Figure 7-7 Bipropellant Valve Actuator Dump Line Temperature History - Adjacent to Thrust Chamber

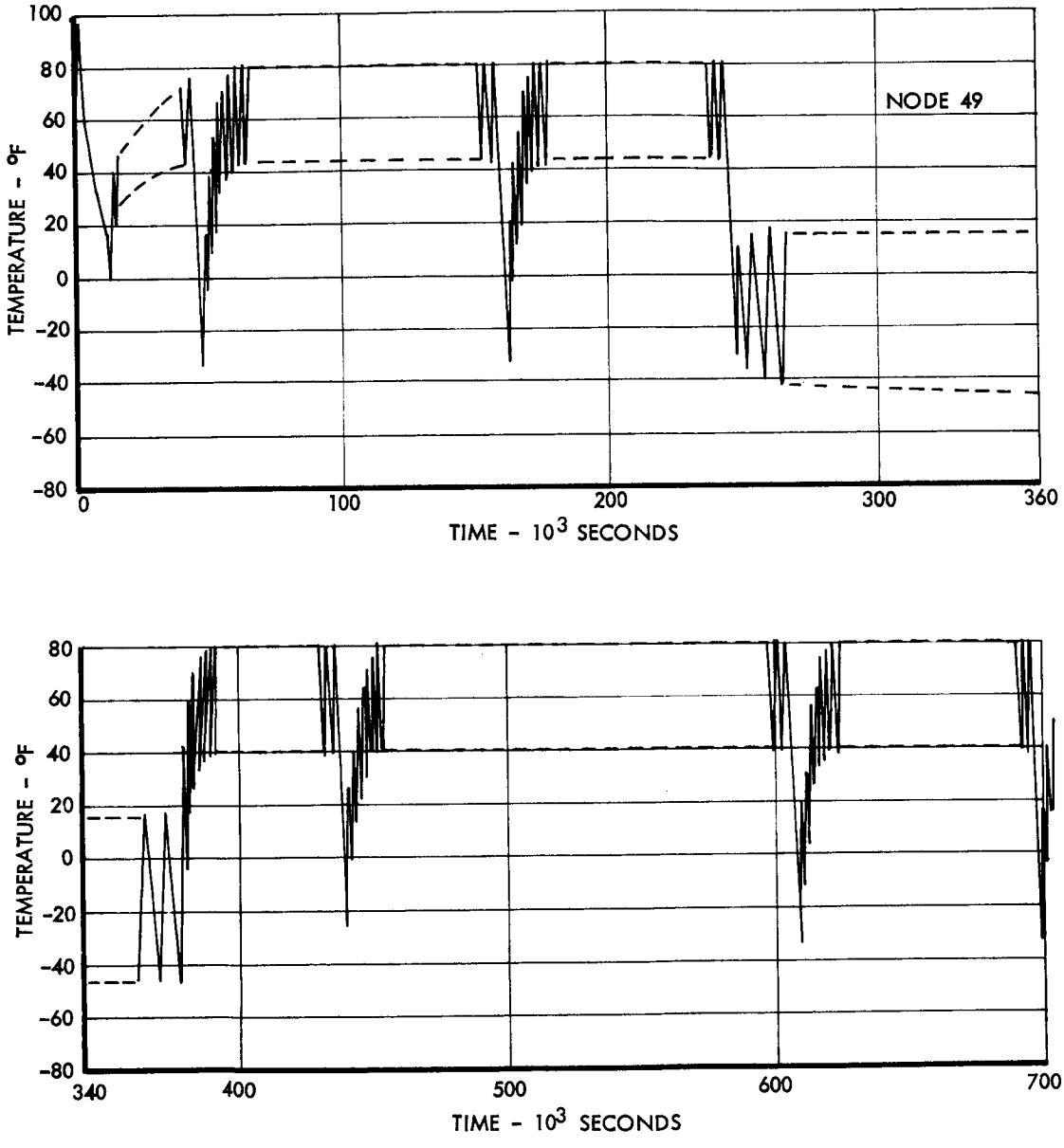

Figure 7-8 Bay 2 Disconnect Panel Temperature History

LOCKHEED
CALIFORNIA COMPANY

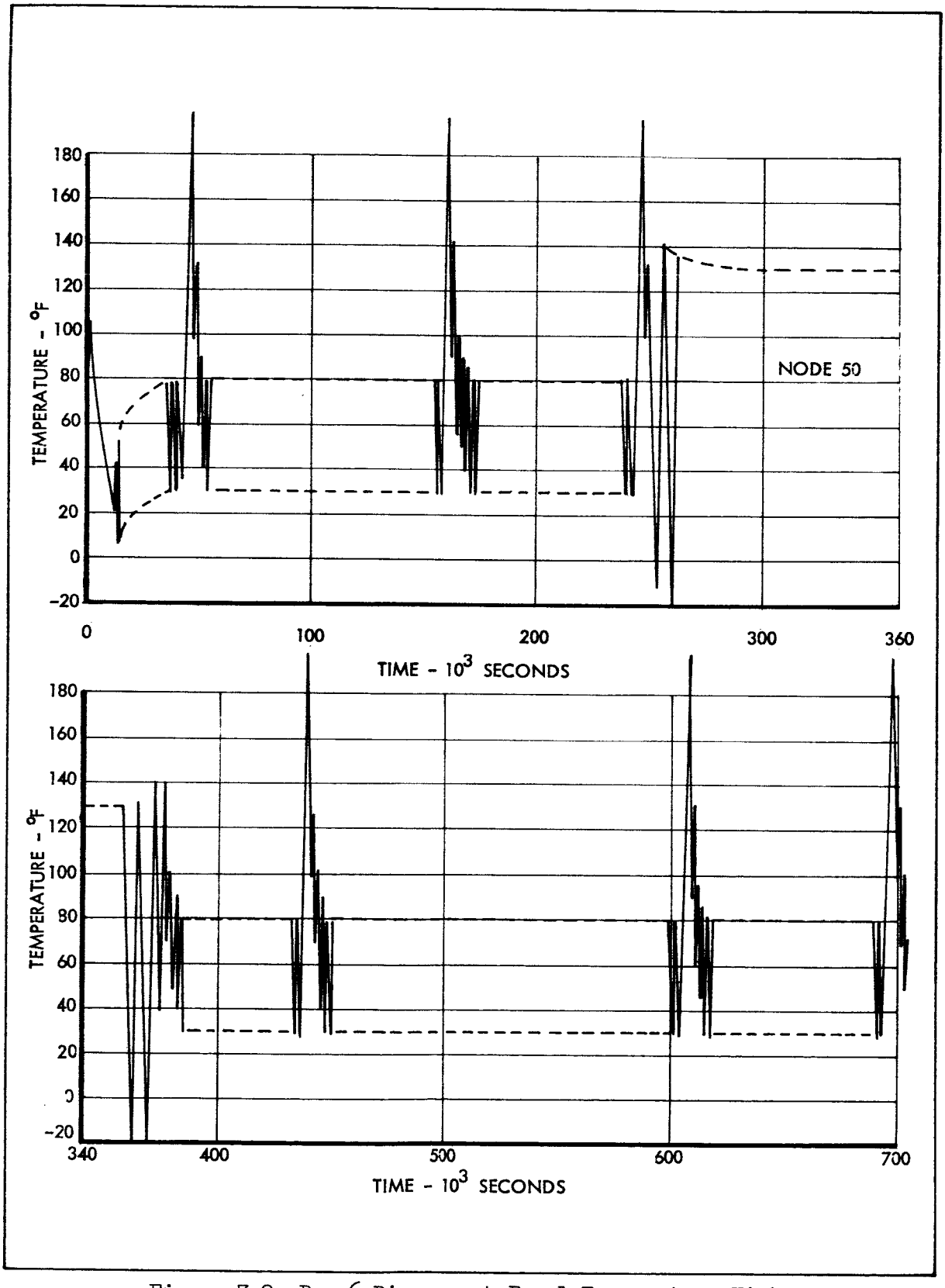

Figure 7-9 Bay 6 Disconnect Panel Temperature History

LOCKHEED CALIFORNIA COMPANY

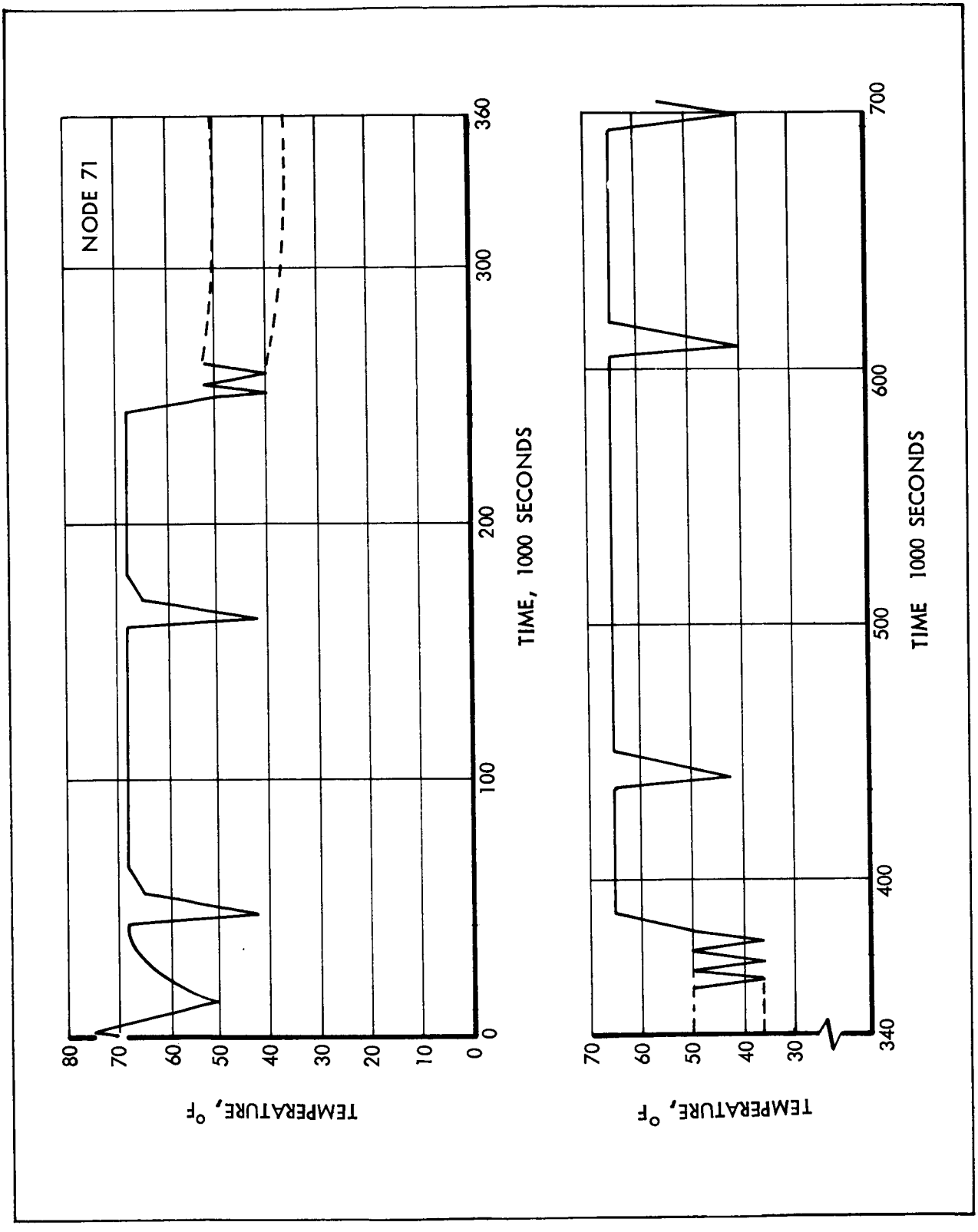

Figure 7-10 Propellant Line Disconnect Panel Coupling Temperature History

Maximum and Minimum Heating Orientations

Plumbing temperatures for the alternate maximum heating orientation demonstrate little change from those of the normal orientations. The similarity can be ascribed to the following:

1) For the roll orientation heat conducts from the heated shell to the aft bulkhead whereas for the maximum heating orientation conduction is reversed.
2) For both orientations the portion of the nozzle extension which radiates to the aft bulkhead is at nearly the same temperature.
3) In regions other than the aft bulkhead, either the fuel cells or the SPS engine controls the plumbing temperatures, and neither of these is influenced by the orientation.

The only appreciable difference in temperatures occurs at the disconnect panels, for no solar flux reaches the panels for the alternate orientations. Figure 7-11 presents both disconnect panel temperatures and an adjoining disconnect propellant coupling temperature for a portion of the mission's transearth phase. The coupling temperature is noted to drop to $-4^{o}F$, whereas the same coupling for the roll orientation dropped to only $35^{o}F$. This orientation would greatly increase the chance of propellant freezing near the disconnect.

The minimum heating orientation results in much lower plumbing temperatures for all lines and components in the aft bulkhead region. The only heat sources available to these lines are the fuel cells and propellant tanks. Figure 7-12 presents the minimum temperatures obtained on these lines for a minimum heating orientation mission. The maximums are not included, for they are identical to those of the normal orientation mission. It is clear from this figure that the effects of the propellant tanks and fuel cells on the plumbing are considerable. Plumbing temperatures on lines opposite Bay 4 and near the tanks are held much higher than those of adjacent line. Once these lines leave the bulkhead region, the fuel cells and thrust chamber control their temperatures, so almost no change from the normal orientation temperatures occurs.

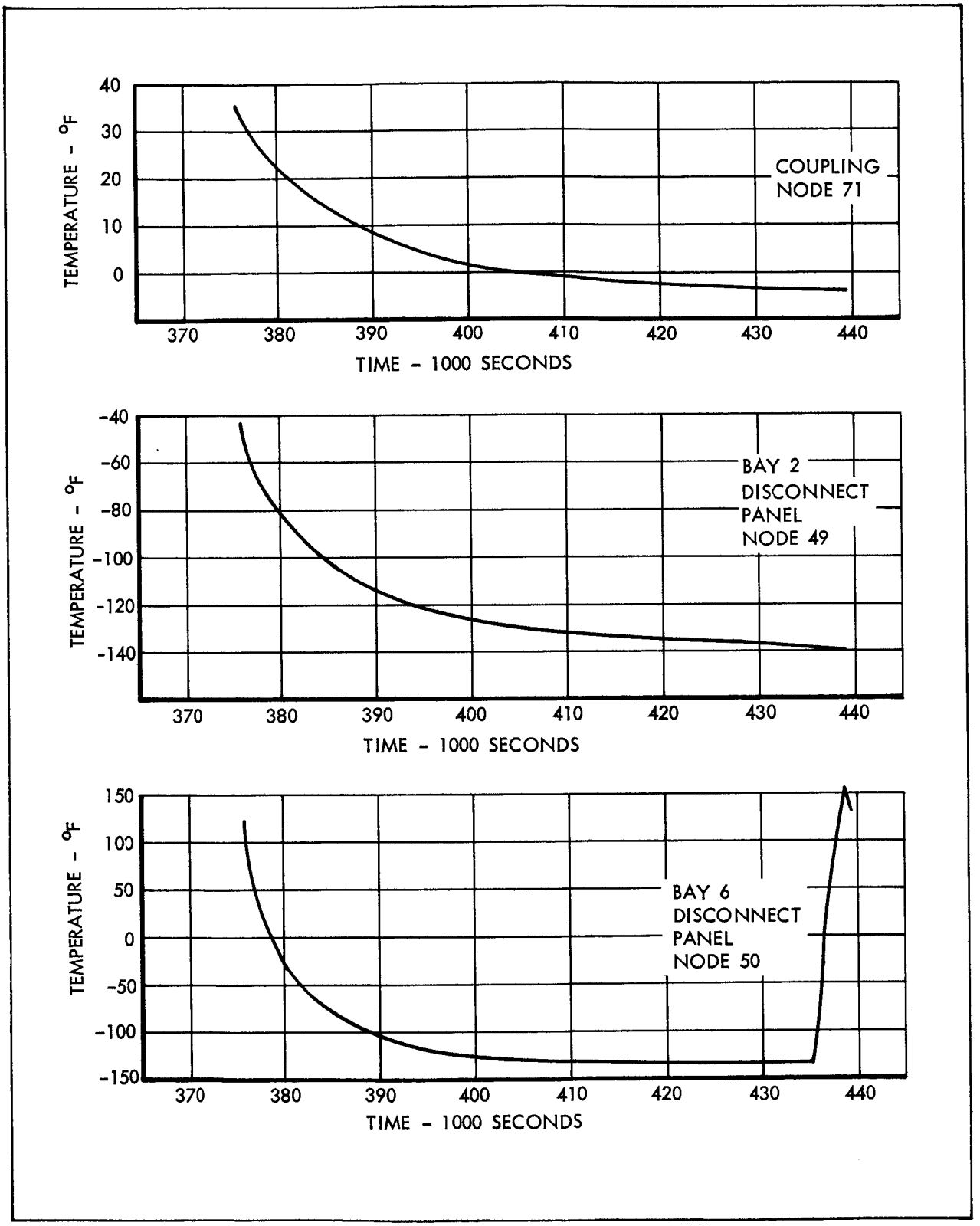

Figure 7-11 Disconnect Panels and Coupling Temperature Histories for Maximum Heating Orientation

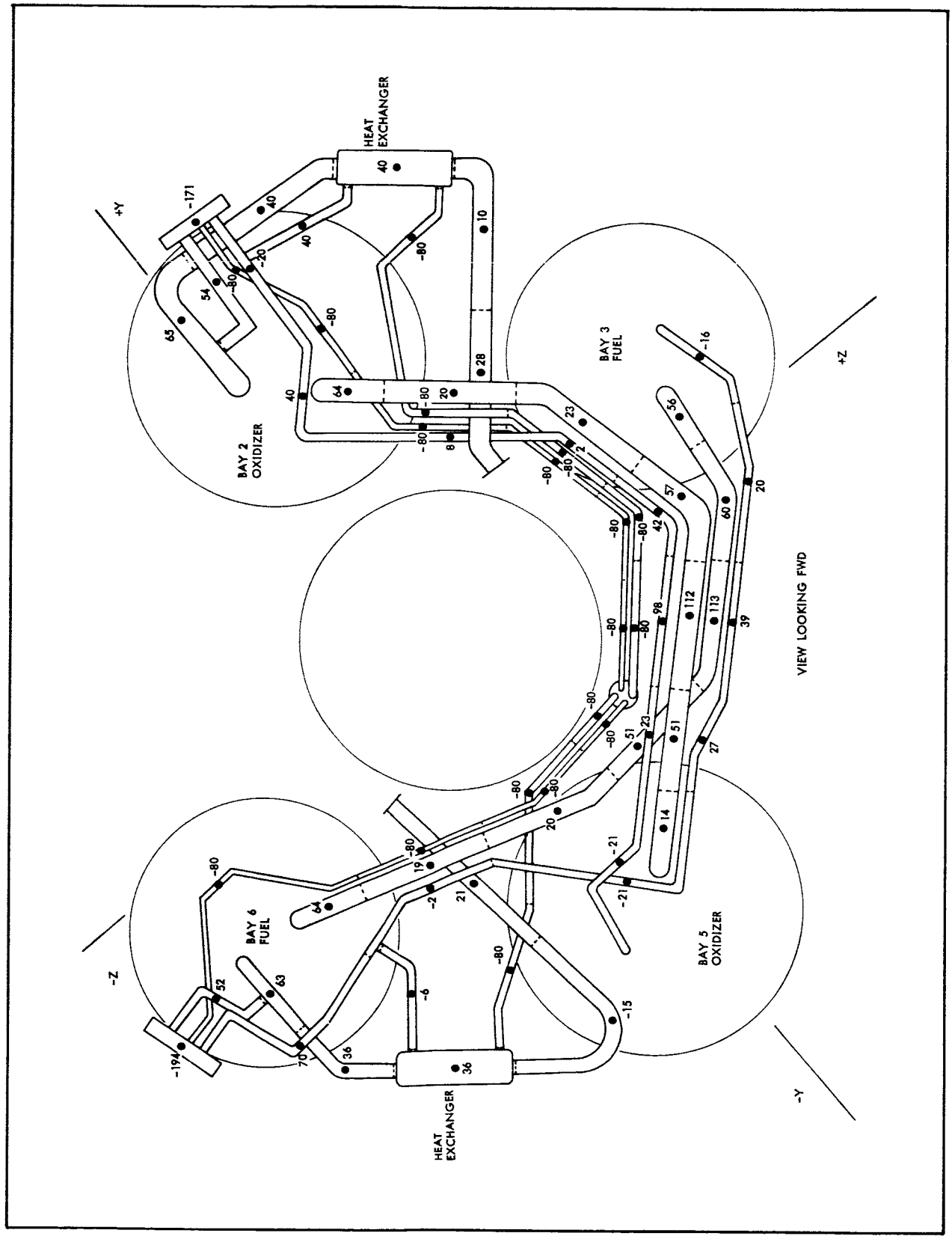

Figure 7-12 Minimum Temperatures for Plumbing Lines Enclosed by Aft Bulkhead and Heat Shield for Minimum Heating Orientation

For this orientation, just as for the maximum heating orientation, the disconnect panels do not receive any solar flux. Their temperature histories are given in Figure 7-13 for the cold soak portion of the mission. Also shown is the temperature history of the coupling discussed above. Table 7-2 contains a list of those SPS components whose temperatures are appreciably changed for a minimum heating orientation during translunar and transearth flight. The Bay 4 helium components' minimum temperatures remain undetermined, as before.

Except in a few isolated regions the SPS plumbing appears to be correctly designed and insulated. For the roll orientation the plumbing situated between the aft bulkhead and heat shield is thermally well protected. Possible propellant freezing near the disconnect panels, which may be a problem, could be eliminated by the proper selection of surface finishes or coatings on the panels and lines, or possibly by insulating the lines from the panels. Likewise the problem of excessive thermal expansion and contraction of the disconnect couplings could be solved by the same methods. These freezing problems near the panels are definitely magnified for either of the alternate orientation, but may possibly be solved in the same ways as were suggested for the normal orientation. In addition, however, the minimum heating orientation allows much of the line and components in the aft bulkhead region to cool enough to allow propellant freezing in this region. The alleviation of this problem could best be carried out by a modification of the exposed aft bulkhead's surface properties. Overheating problems in this aft region are confined to the area immediately beneath Bay 4 (fuel cells). Removal of the fuel cells from the aft end of this Bay would eliminate the excessive heating.

Bay 4 helium components are overheated as much as 90° F for portions of this mission. Several methods exist whereby these temperatures may be reduced. One would be to eliminate all insulation from the Bay. This would allow more fuel cell heat to escape from Bay 4 and less to be absorbed by the plumbing in that Bay. Another method would be to extend the insulation over the valves, pressure regulators, etc., which would reduce their maximum temperatures approximately 70° F. If the fuel cells are moved to the forward portion of Bay 4, and situated on a shelf, radiation

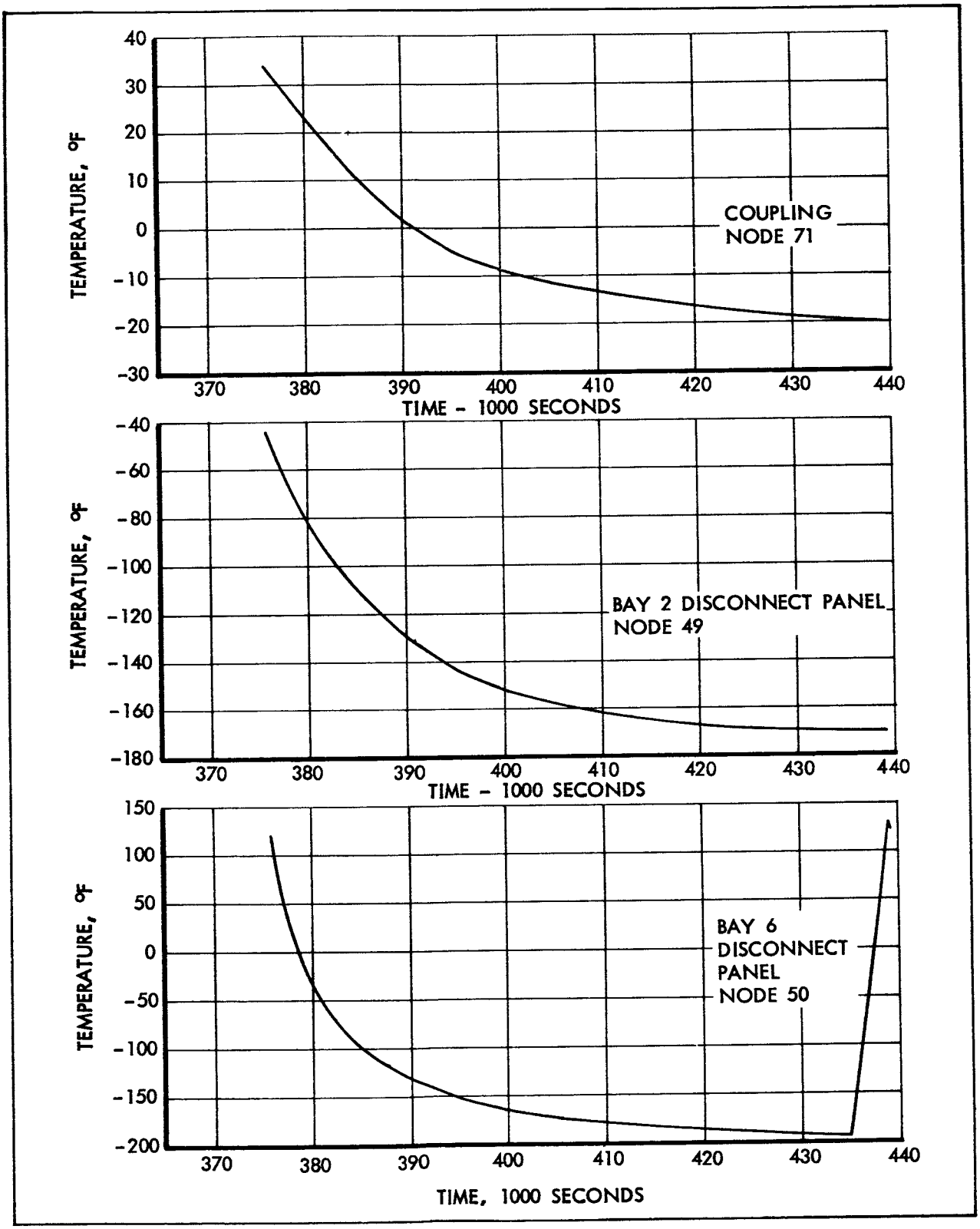

Figure 7-13 Disconnect Panels and Coupling Temperature Histories for Minimum Heating Orientation

TABLE 7-2
COMPARISON OF SPS COMPONENT MINIMUM TEMPERATURES FOR NORMAL AND MINIMUM HEATING ORIENTATIONS

COMPONENT		MINIMUM TEMPERATURE (^{o}F)		
Spec	Item	Allowable	Normal Orientation	Min. Orien.
MC 273-0012 B	SPS Propellant-Disconnect Coupling	40	35	-20
MC 273-0040	Propulsion System Flexible Connector N204)	40	54	40
MC901-0008 A	Propulsion Quantity Indicator and Mixture Ratio Control	40	54	40
MC 273-0039	Propulsion System Flexible Connector (fuel)	40	58	21
	Bay 2 Disconnect Panel	40	-44	-171
	Bay 6 Disconnect Panel	40	-18	-194

from the cells to the plumbing will be reduced enough to probably eliminate the overheating problem.

The high temperatures resulting in the propellant feed lines, actuator dump lines, etc., where these lines receive radiation from the thrust chamber and engine web mounts, would be greatly reduced if the thrust chamber temperatures could be reduced. The removal of the fuel cells from the lower part of Bay 4 would also help to eliminate this problem. If the engine web mount in this region was not required to absorb heat from the fuel cells, it would be able to absorb more of the heat rejected from the thrust chamber. A reduction of 100° F in local thrust chamber temperatures could be effected by this move. This reduction would consequently be felt by the lines adjacent to the chamber, and could possibly reduce their temperatures to the allowable limits preceedir engine firings.

SPS ENGINE

A study of the complete SPS engine was integrated into the SPS plumbing analysis. In order to best account for the actual engine environment, immediate engine surroundings were included in the heat balances. Thus the engine web mounts, the gimbal ring,and all other supporting structure appear in the analysis. Thrust chamber temperatures were impressed for various lengths of time following each of the engine ignitions, after which time the chamber was allowed to soak.

Before presenting the results, it is essential to discuss the methods used to adapt the supplied thrust chamber temperatures with the present analysis. (See Sect. IX, Temperature Response of the Thrust Chamber Exterior.) These temperatures were not directly applicable to the analysis because of several assumptions used in their determination. First, for each firing with the exception of the lunar orbit insertion, all thrust chamber temperatures were initially set at 80°F sink, which is incorrect for most of the mission. For each firing the following had to be determined:

1) What part of the thrust chamber structure should have impressed temperatures
2) How long these temperatures should be impressed.

For the first two midcourse correction firings both the sink temperature and initial temperature assumptions were acceptable. For this reason the thrust chamber temperatures were impressed for the entire time over which they were supplied (5000 sec), and for the entire thrust chamber structure. By the third midcourse correction it was concluded that residual temperatures in the thrust chamber wall were high enough that only the interior, i.e., ablative surface nodes should be impressed for subsequent firings. Also it was concluded that these temperatures should only be impressed as long as they were more accurate than those which could be recalculated through the heat balance. Temperatures computed by a heat balance had the advantage of being determined for a correct thermal environment. However, the temperatures supplied by MSC were determined for a much finer thrust chamber network than used in this analysis. Thus, during that part

of the engine soak where temperature gradients through the chamber wall are large, the finer network would supply the more accurate ablative surface temperatures. For the midcourse correction firings the surface temperatures were impressed for 200 sec, which was time enough for gradients between successive nodes to reduce to approximately 50°F. For both lunar firings, temperatures were impressed for 1000 sec, which reduced the gradients to nearly 200° F. This was assumed to be a small enough gradient so that the nodal lump size would not seriously affect the results.

Both injector and engine valve assembly temperatures were also impressed during each firing to account for propellant flow. The valves were held at 70° F, the actual propellant temperature, and the injector at 100°F, an arbitrarily modified value to account for the influence of radiation to the injector. The temperatures of both components were computed by heat balances immediately following engine shutdown.

The results of the SPS engine analysis are summarized in Figures 7-14 and 7-15, which contain maximum and minimum calculated temperatures for each component of the engine. All maximum temperatures occur during the soak periods following either the lunar insertion or transearth injection firings. The large amount of heat absorbed by the thrust chamber during these firings is rejected primarily in two ways. The first is by radiation to space through the nozzle throat. The second is by conduction through the chamber wall and subsequently by radiation to the surrounding structure. Radiation to space is extremely limited due to the low view factors from the thrust chamber to space (.05). The alternate mode of heat rejection is dependent on the temperature of the surrounding structure. Less heat is rejected from the chamber in an area facing the fuel cell bay than in an area facing a propellant tank. Figure 7-16 shows the effect of the location relative to Bay 4 on the exterior temperature of the thrust chamber. Figure 7-17 shows how the engine web mounts opposite these thrust chamber locations react. These web mounts are representative of the surroundings to which the thrust chamber surface radiates.

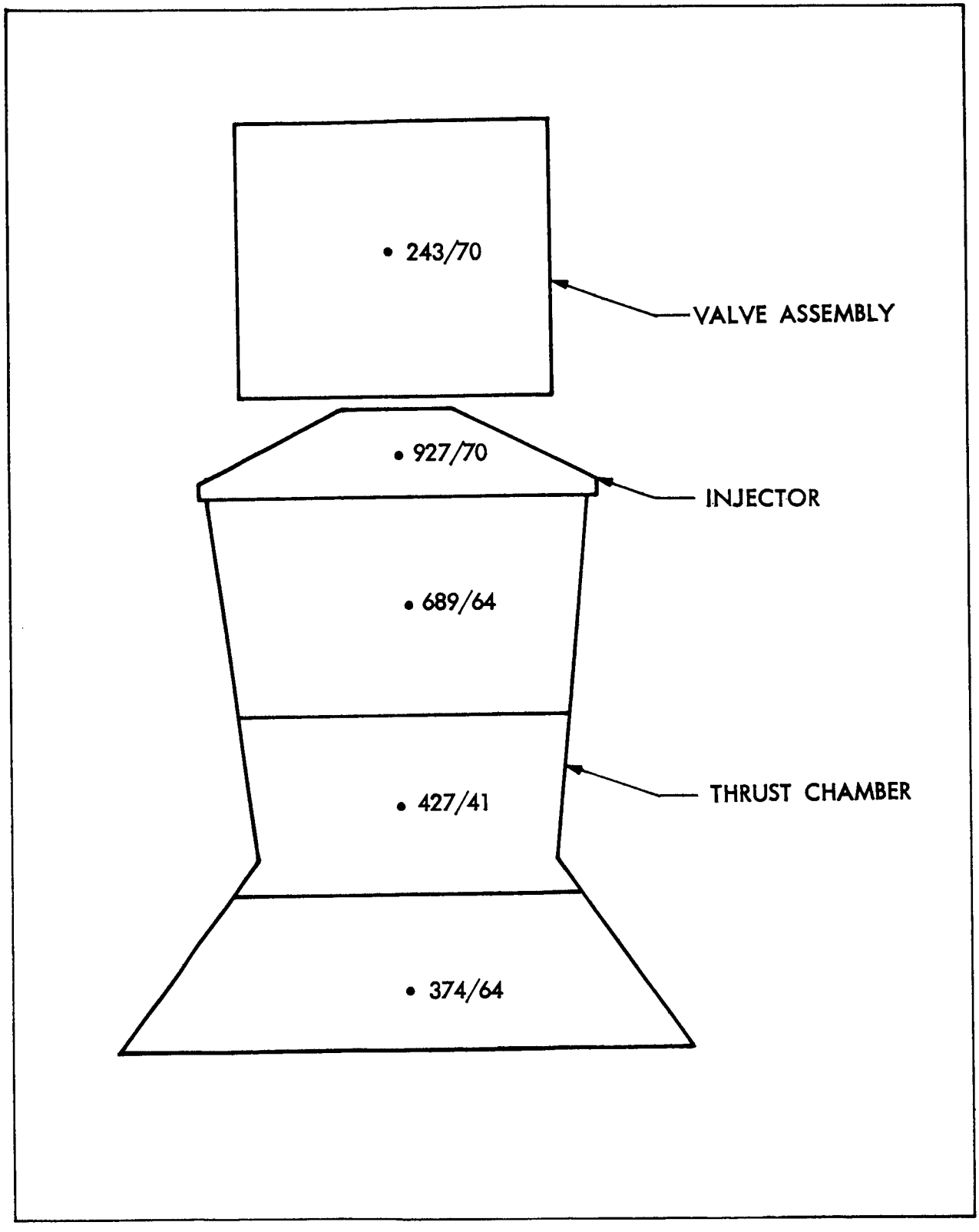

Figure 7-14 Maximum/Minimum SPS Engine Components Temperatures

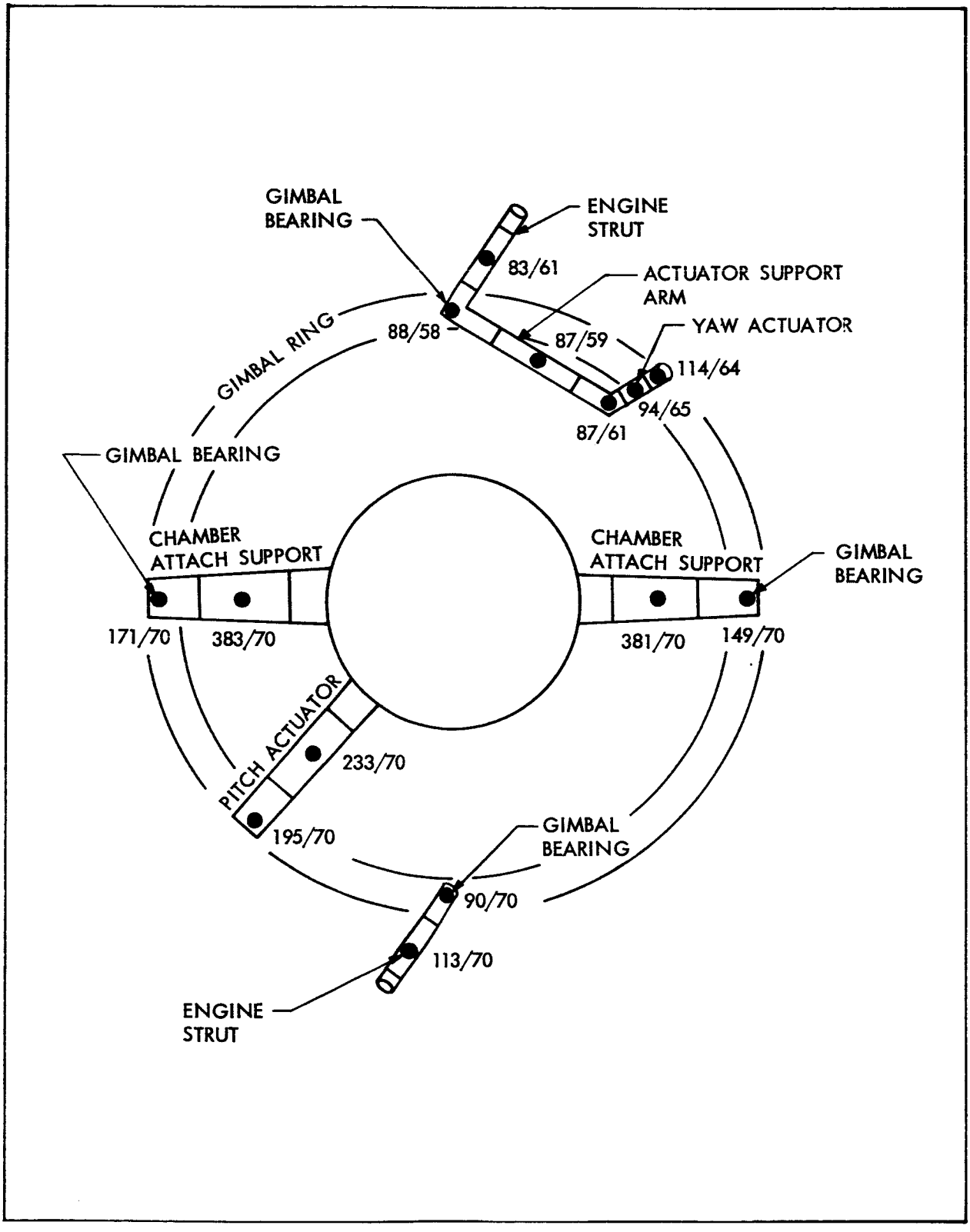

Figure 7-15 Maximum/Minimum SPS Engine Support Structure Temperatures

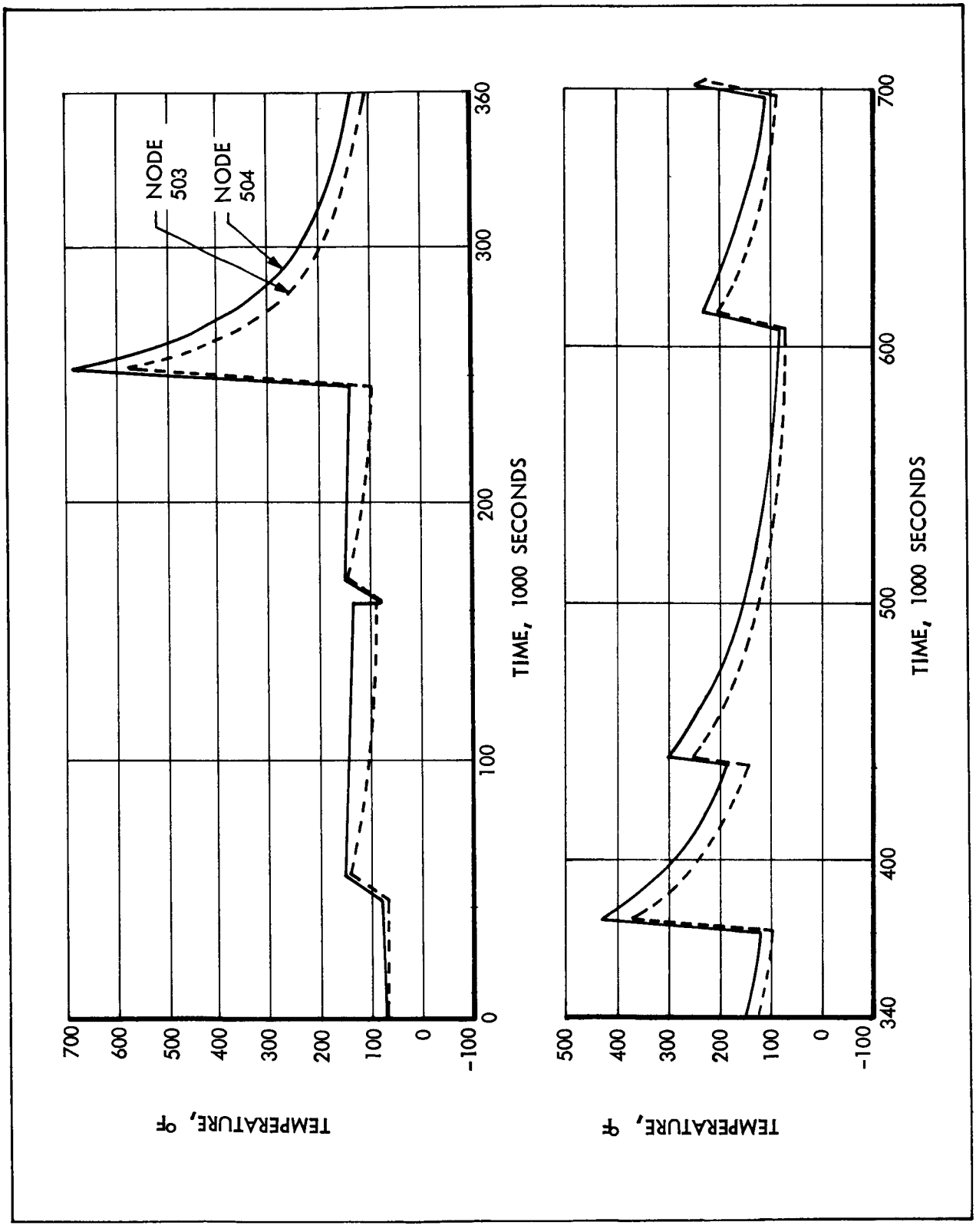

Figure 7-16 Thrust Chamber Temperature Histories for Two Positions on Exterior Surface

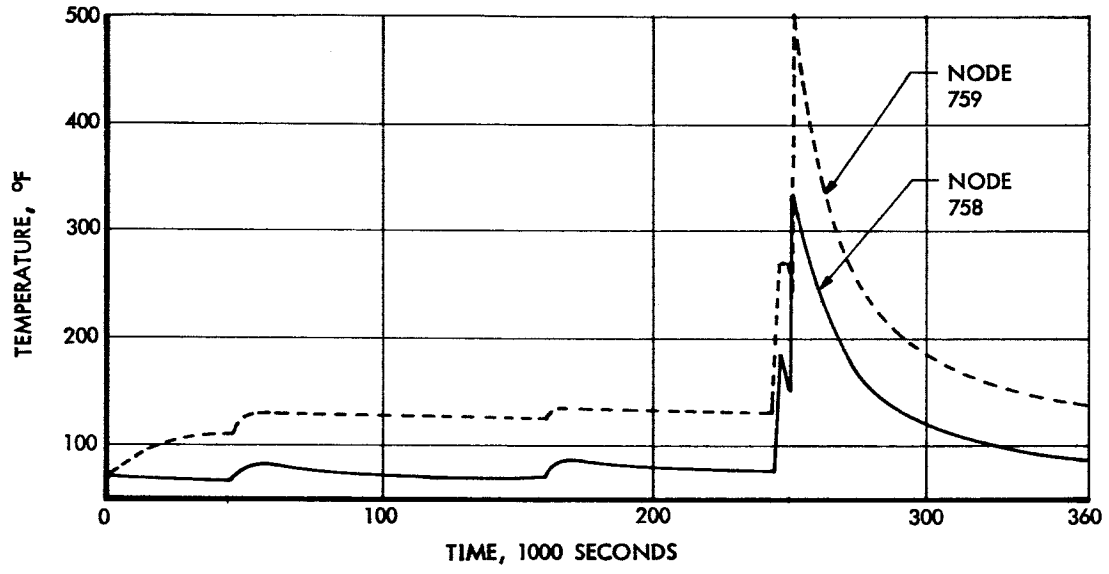

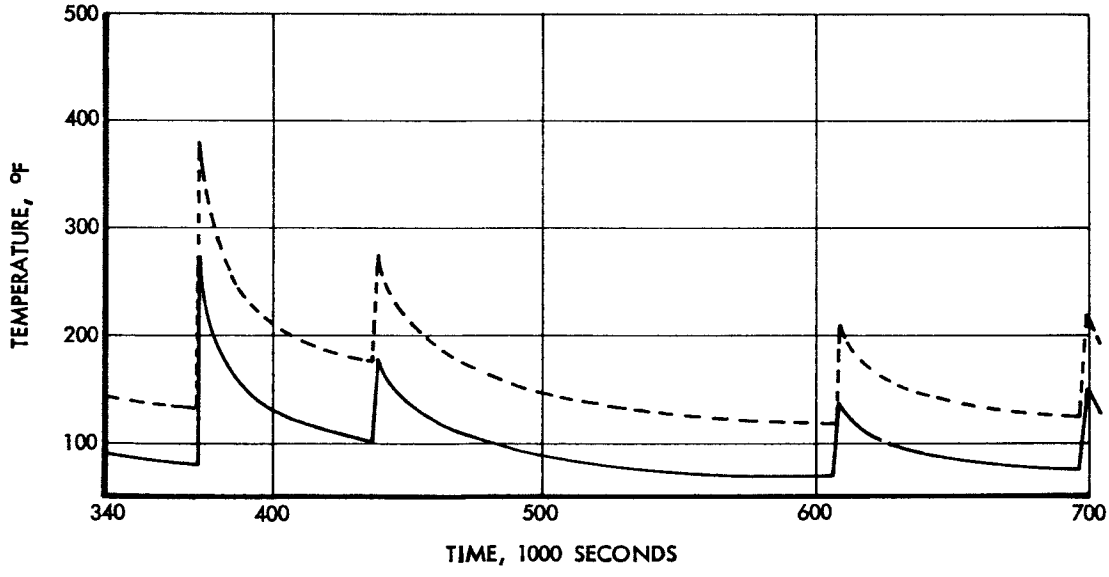

Figure 7-17 Engine Web Mount Temperature Histories

A typical temperature history for the chamber interior is shown in Figure 7-18 during the lunar insertion firing soak period. Figure 7-18 also shows the injector and valve assembly temperatures for this same soak period. The extremely high injector temperature is a consequence of the limited heat relief available to the injector (the only appreciable amount being radiation to deep space and the valve assembly), coupled with the high flux from the chamber walls. The only way in which the injector temperature could be lowered appreciably is if some additional means of heat rejection from the combustion chamber or injector is included. Similarly, valve assembly temperatures are primarily determined by conduction and radiation from the injector. Peak temperatures calculated for the various engine gimballing structure which appeared in Figure 7-15 and are summarized in Table 7-3. The limits which have been prescribed for some of the components are also included. These limits are only exceeded by the Gimbal Pitch Actuator - a history of this component's average temperature is presented in Figure 7-19. Its peak temperatures are a consequence of the high heat flux leaving the thrust chamber subsequent to the lunar firings.

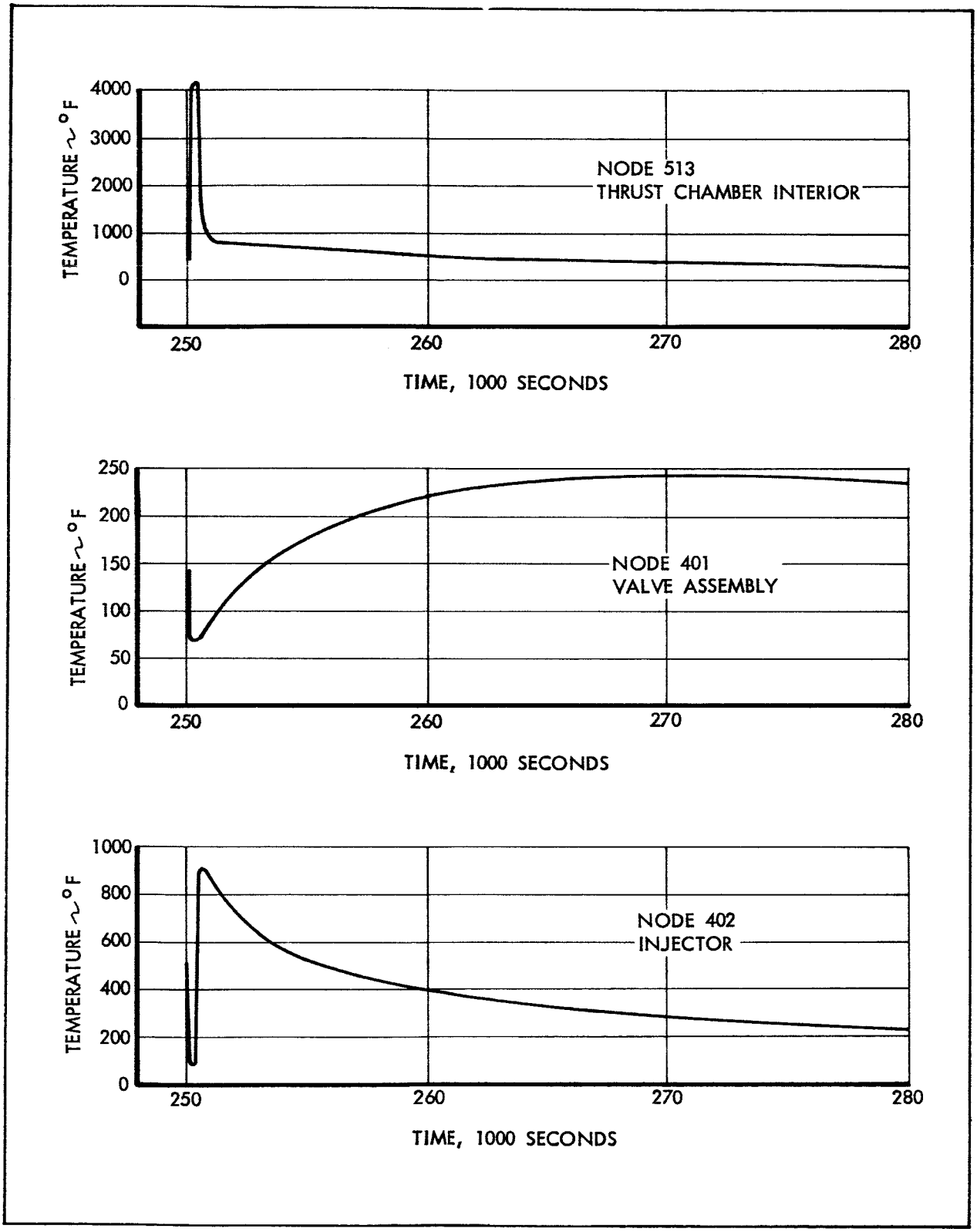

Figure 7-18 SPS Engine Component Temperature Histories During Lunar Orbit Insertion

Table 7-3 SPS Engine Gimbal Structure Allowable Temperature Limits and Calculated Temperature Extremes, Lunar Orbit Rendezvous Mission

Component	Allowable Limits (°F)		Calculated Temperatures (°F)	
	Max	Min	Max	Min
Pitch Actuator	140	-10	233	70
Yaw Actuator	140	-10	94	65
Gimbal Bearings	200	-10	170	58
Engine Struts	-	-	113	58
Chamber Attach Supports	-	-	383	70
Actuator Support Arm	-	-	87	58

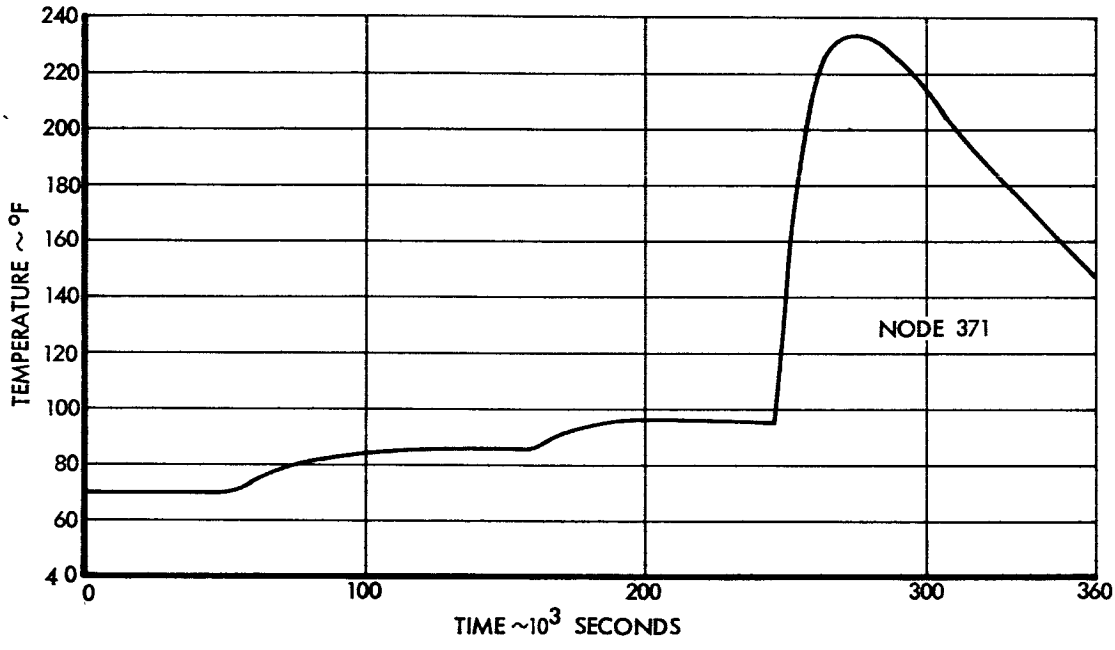

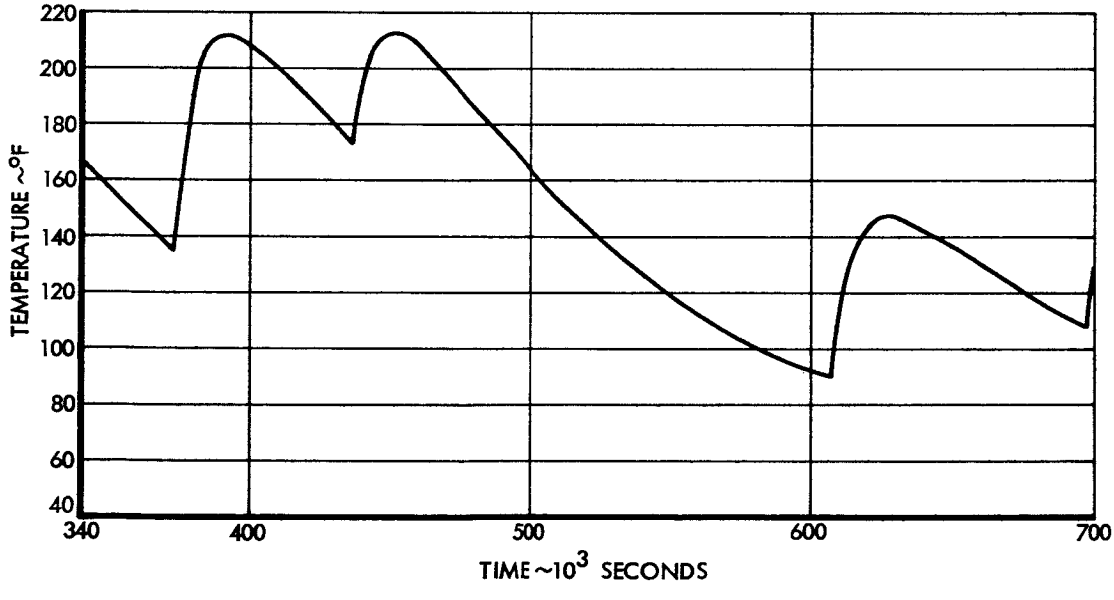

Figure 7-19 SPS Engine Gimbal Pitch Actuator Temperature History

Thrust chamber temperatures, and the temperatures of some of the attached SPS equipment, present definite design problems for the period following the long lunar insertion firing. The thrust chamber structural limit is specified as 500° F for over three and a half hours. The pitch actuator's limit (140° F) is exceeded for 32 hours continuously. Similarly the injector and valve assembly temperatures are predicted far above their allowable values. There is no clearly evident manner in which these temperatures can be lowered. If more heat is allowed to escape from the outer wall to the chamber's surroundings, in order to lower the injector's temperature, excessive heating of lines and gimbal structure will occur. If less heat is rejected through the chamber wall, the injector, valve assembly, and thrust chamber itself will overheat further. The only suggestion that can be made is that further analyses of the thrust chamber and its surroundings be made in which a more detailed network representation of the engine is combined with the network and boundary temperatures generated herein. This analysis should make full use of the existing network joining the engine and its surroundings, and should include immediate engine surrounding structure, i.e., web mounts, etc., in the calculated heat balances. Conclusions involving any change in the SPS engine design should only be made following such an analysis.

FLUID STORAGE AND PRESSURIZATION SYSTEM

Results of Program Analysis

The important results of the fluid storage and pressurization system analysis are summarized in Figures 7-20 to 7-25. These results are (plotted as functions of time): the temperatures of propellant and tanks, the fluid mass remaining in the propellant tanks, the temperature and pressure of the pressurant gas, and the mass remaining in the helium bottles.

As can be seen from Figures 7-20 and 7-21, the propellant temperature exhibits very minor changes except during the long flow periods - lunar orbit injection at about 250,000 sec. from launch and transearth injection at about 372,000 sec. The oxidizer temperature drops more than that of the fuel due to the oxidizer's greater vapor pressure and corresponding larger cooling effect from evaporation. The lower temperatures of the sump tanks, are due to lower environmental temperatures. Both bay 3 and bay 5 tanks show less of a temperature drop than bays 2 and 6 tanks due to the warming influence of the fuel cells in bay 4.

The mass of propellant remaining is shown in Figure 7-22. The small changes occur at midcourse corrections and the larger ones at the lunar orbit and transearth injections. During lunar orbit injection, the propellant in the primary tanks is consumed and henceforth the fuel and oxidizer are removed from the sump tanks. The tank pressures are not shown since they remain very close to the minimum pressure of 175 psia at nearly all times, except during the first 45,000 seconds when the initial pressure of 197 psia is impressed.

Figures 7-23 to 7-25 show the conditions of the pressurant. Again the small dips in the curves occur at the midcourse corrections and the larger ones at the lunar orbit and transearth injections. Figure 7-23 shows the temperature variations, and illustrates the sharp fluctuations during long flow periods. The temperature recovery is more pronounced than the pressure recovery since it is independent of the mass in the tank. The helium dips to a minimum temperature of -79° F during lunar orbit insertion. The rate of temperature recovery is a function of the bottle surroundings, the minimum temperature reached, and the thermal capacity of the gas.

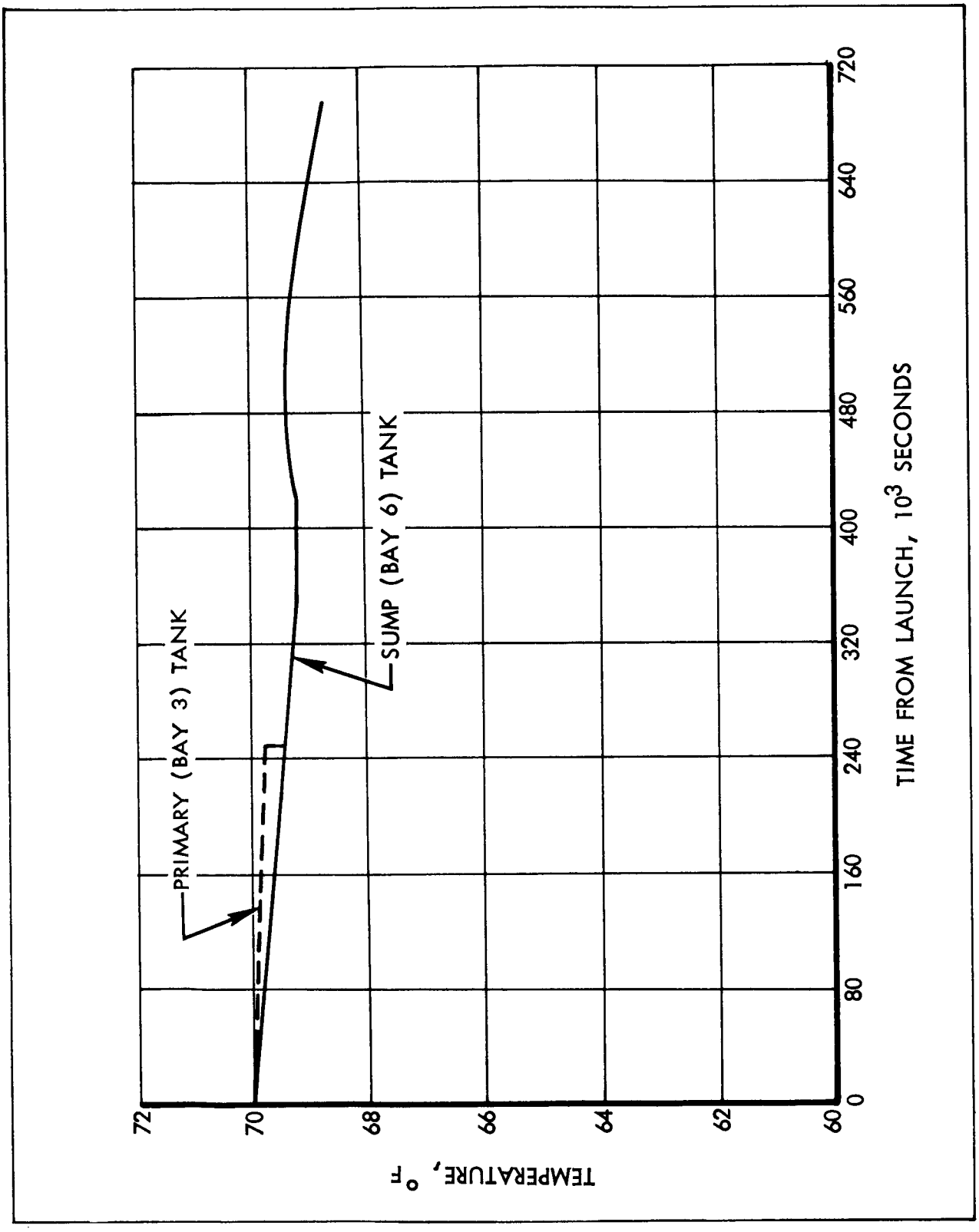

Figure 7-20 Bulk Temperature History of Fuel

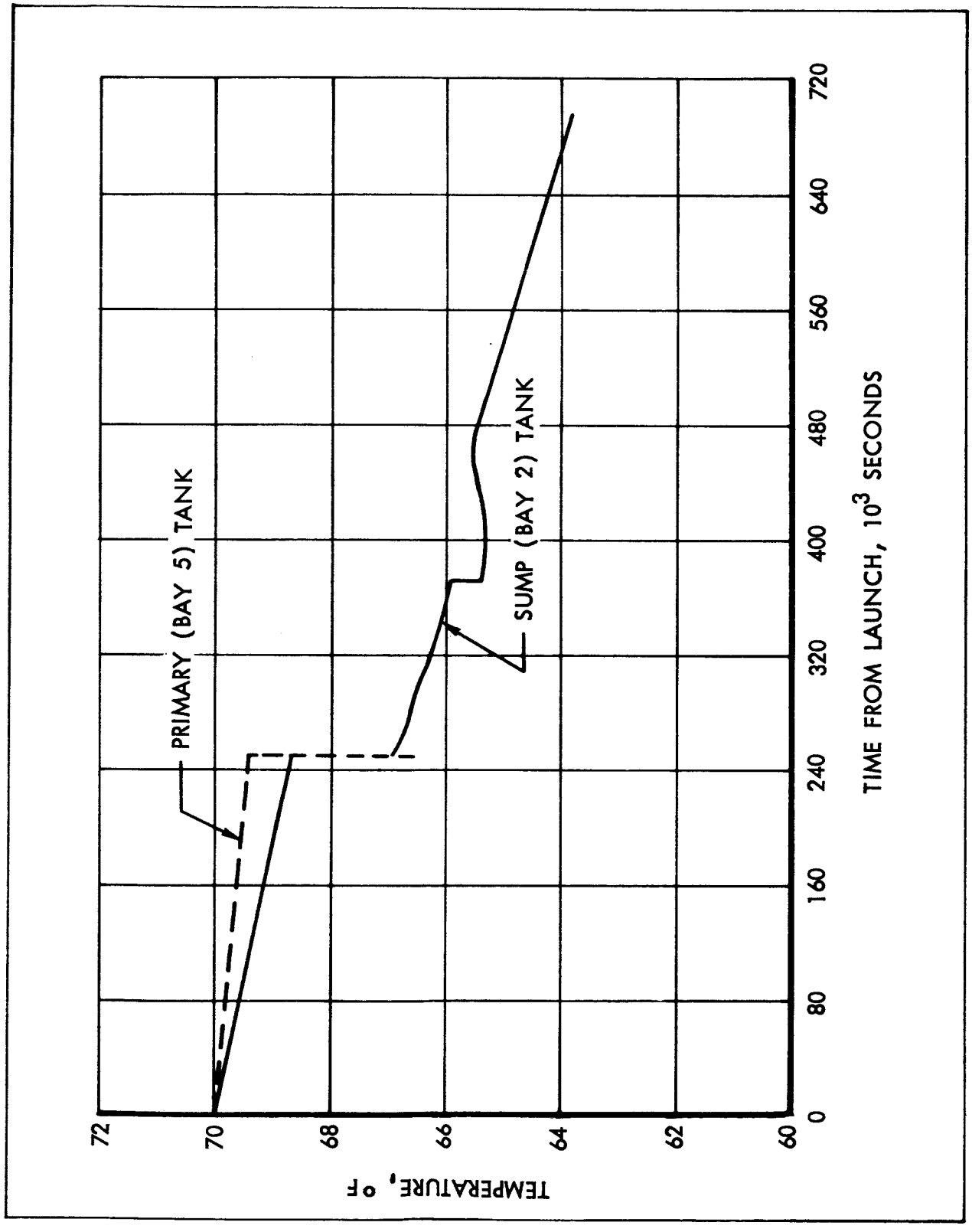

Figure 7-21 Bulk Temperature History of Oxidizer

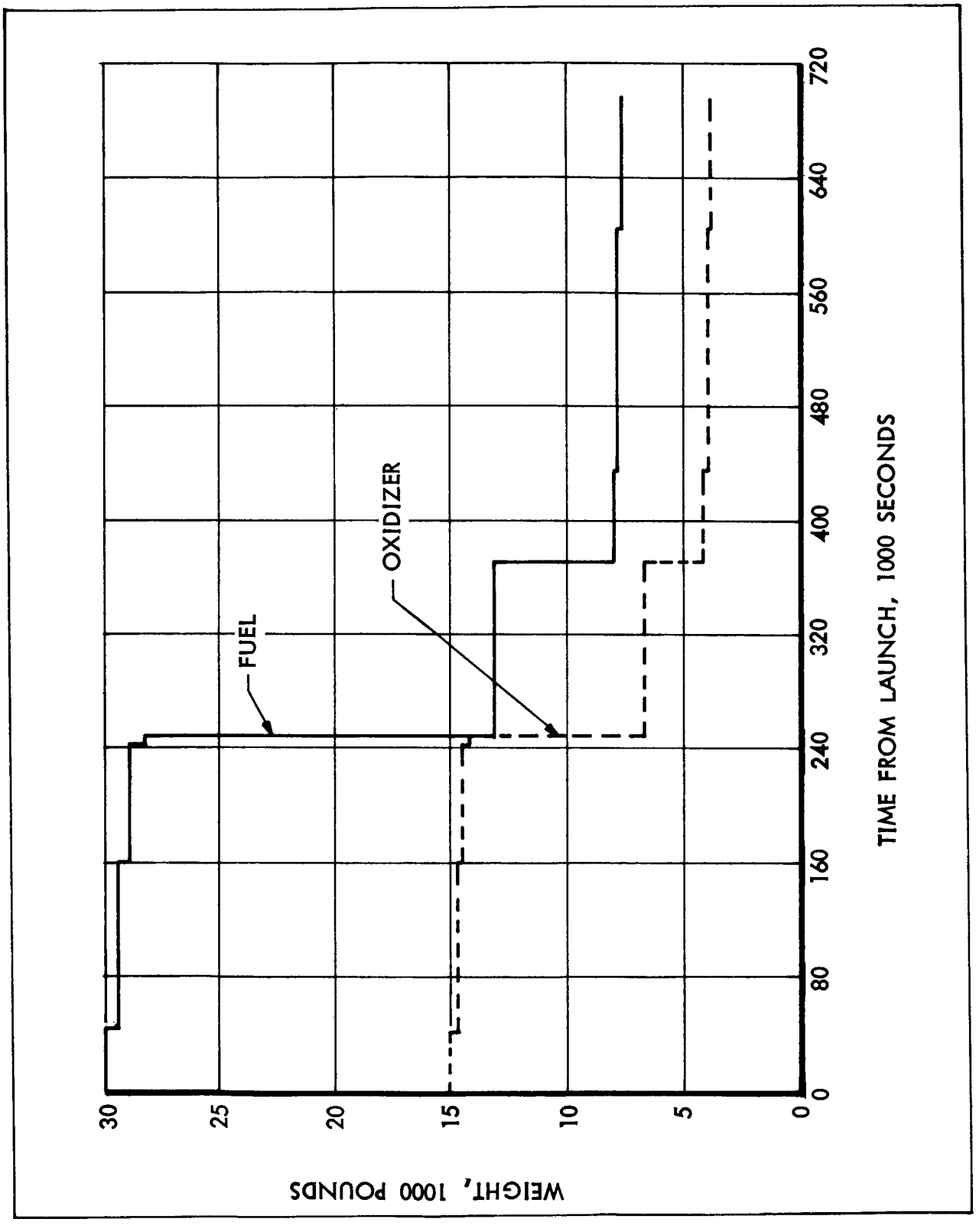

Figure 7-22 Mass of Propellant Remaining in Tanks

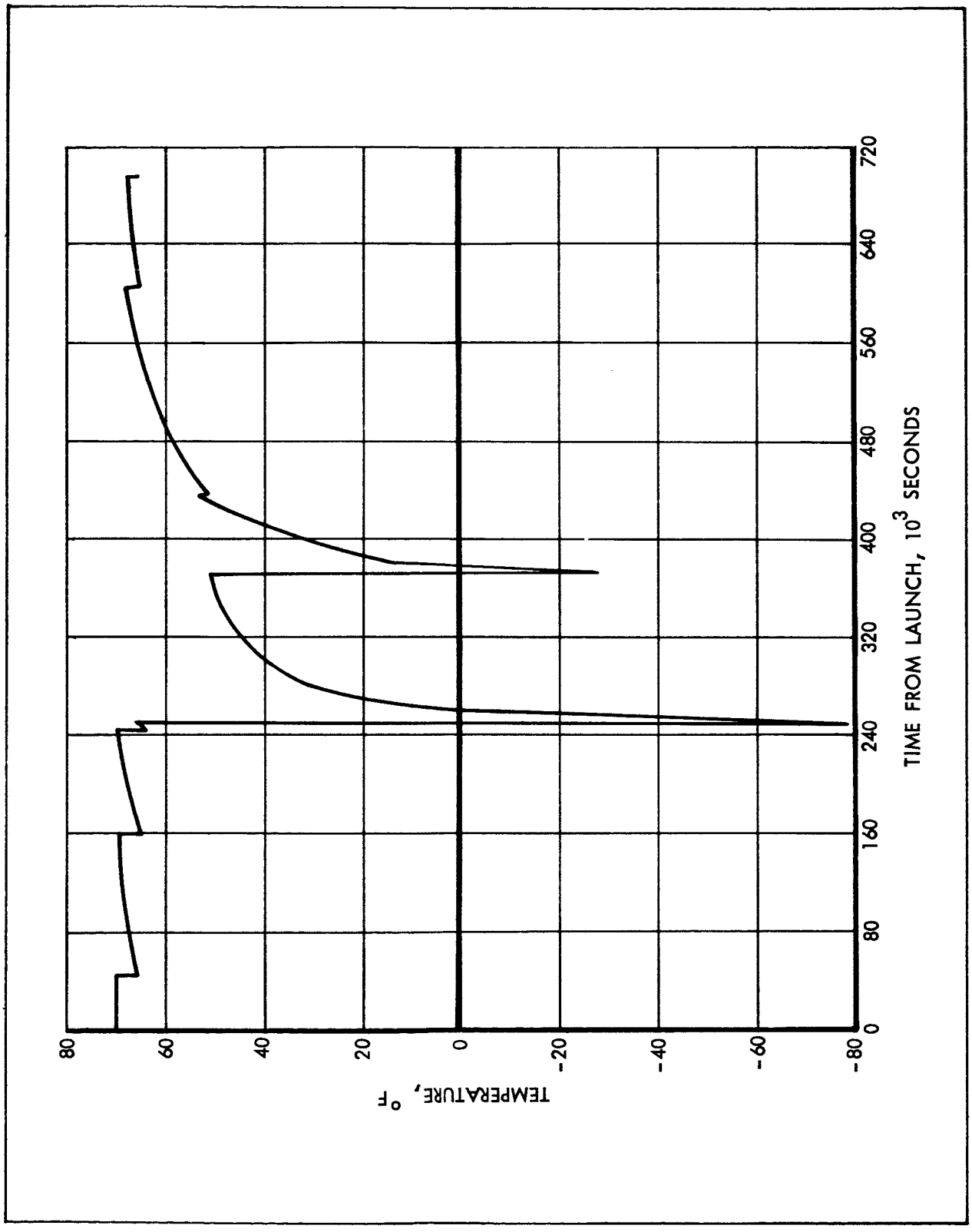

Figure 7-23 Temperature History of Helium Gas

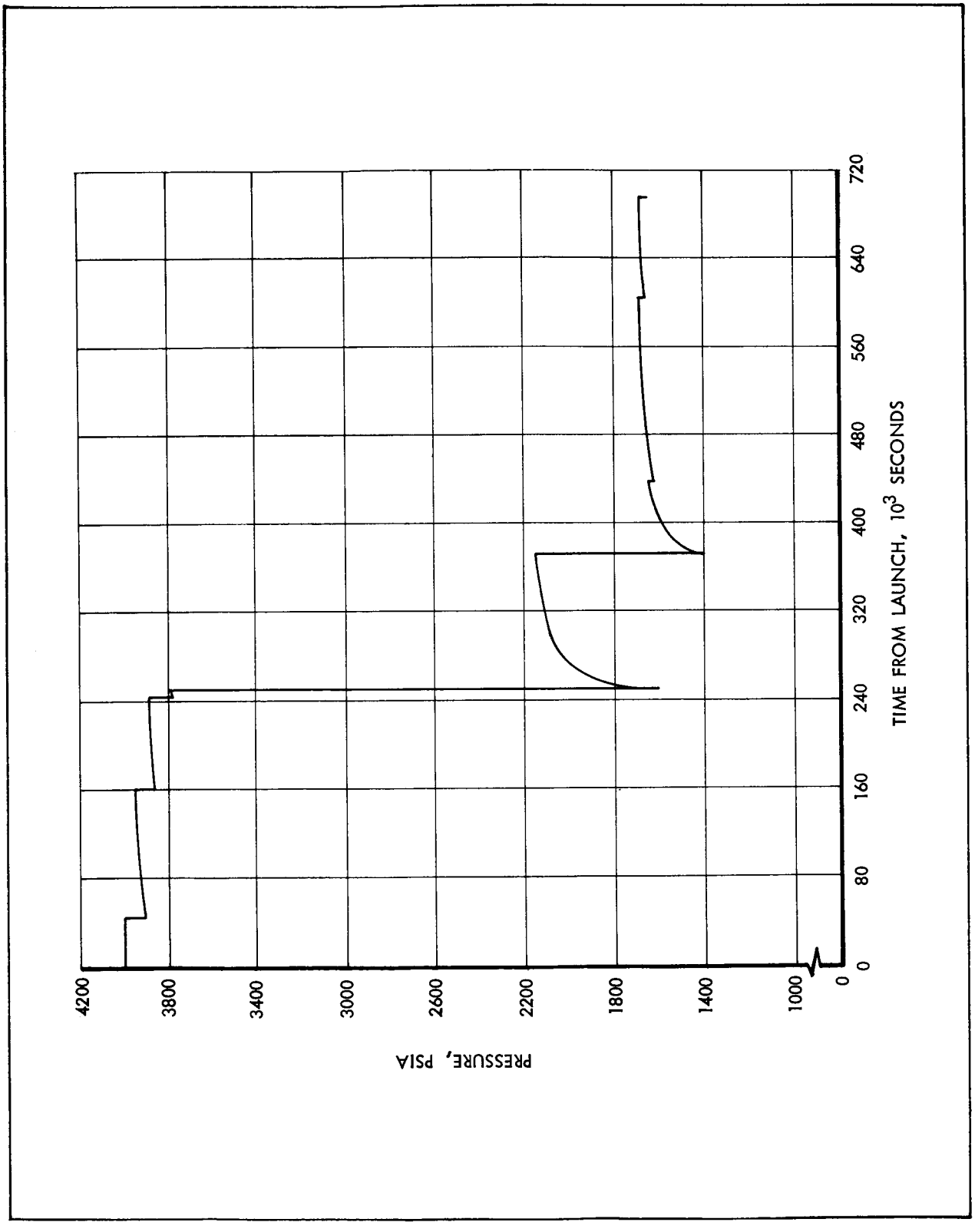

Figure 7-24 Pressure History of Helium Gas

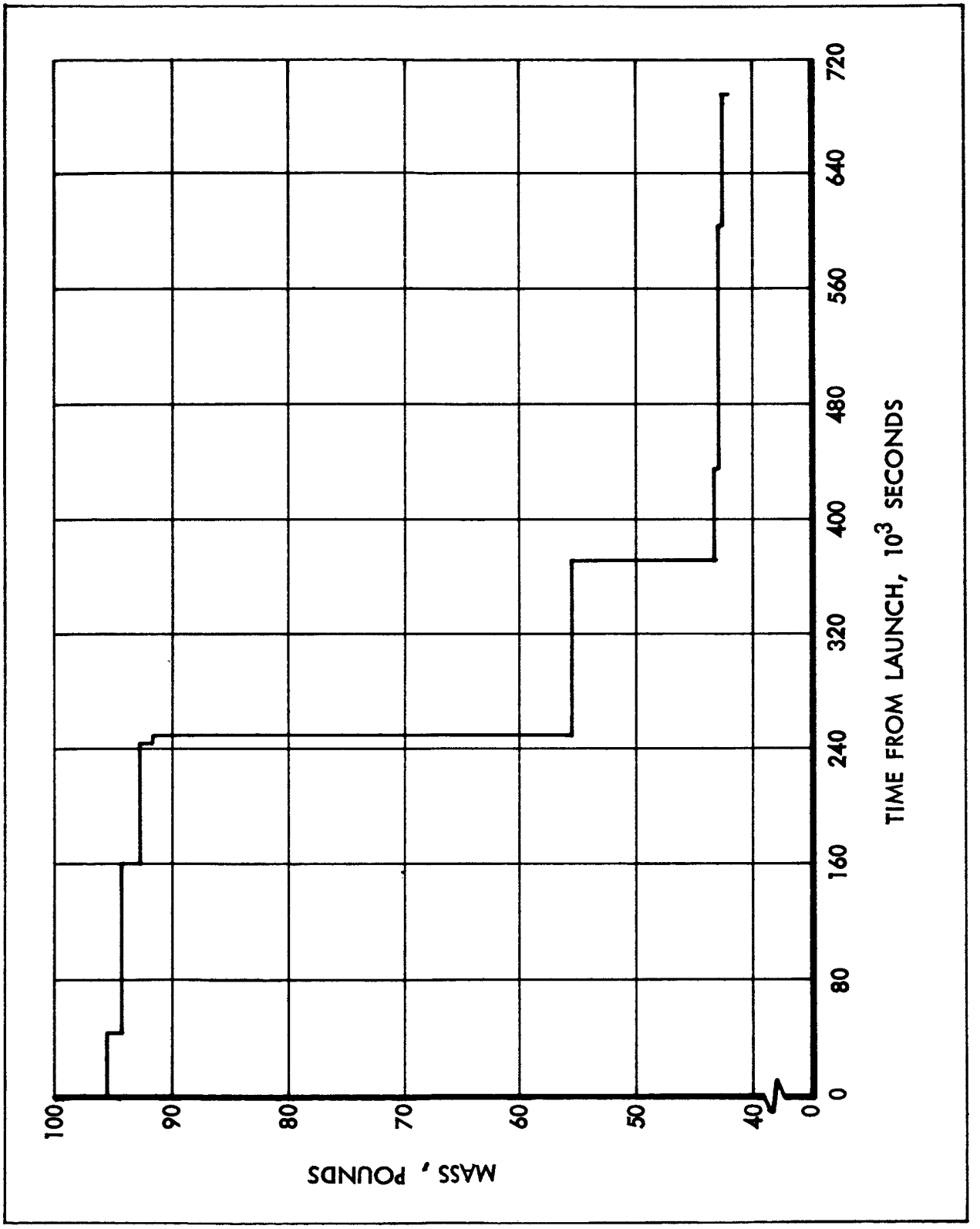

Figure 7-25 Mass of Helium Remaining

There are some temperature gradients within the liquid propellants as shown in Figures 7-26 and 7-27. The maximum gradients are about 8 and 10° F for the oxidizer and fuel tanks respectively. At engine firings the liquid is assumed to be mixed and temperature gradients destroyed.

Temperature change in the ullage gas during lunar orbit insertion is shown in Figure 7-28. As noted, it is small being about 1.5° F. The reason for such a small change is that the incoming helium is warm initially, and when it gets cooler, its thermal capacity is small compared to the ullage gas. The engine firing illustrated is that due to lunar orbit insertion, which is the longest firing and exhibits the greatest ullage temperature drop.

The temperatures of the propellant and pressurant tanks remain within the allowable limits. The propellant minimum temperatures are well above the freezing or high viscosity points, reaching a minimum of about 64° F. The helium temperature drops to -79° F during lunar orbit insertion. Even in the event of an abort where lunar orbit insertion and transearth injection might occur essentially back to back, the lowest temperature inside the helium bottle would be about -140° F, which is higher than the minimum allowable of -150° F.

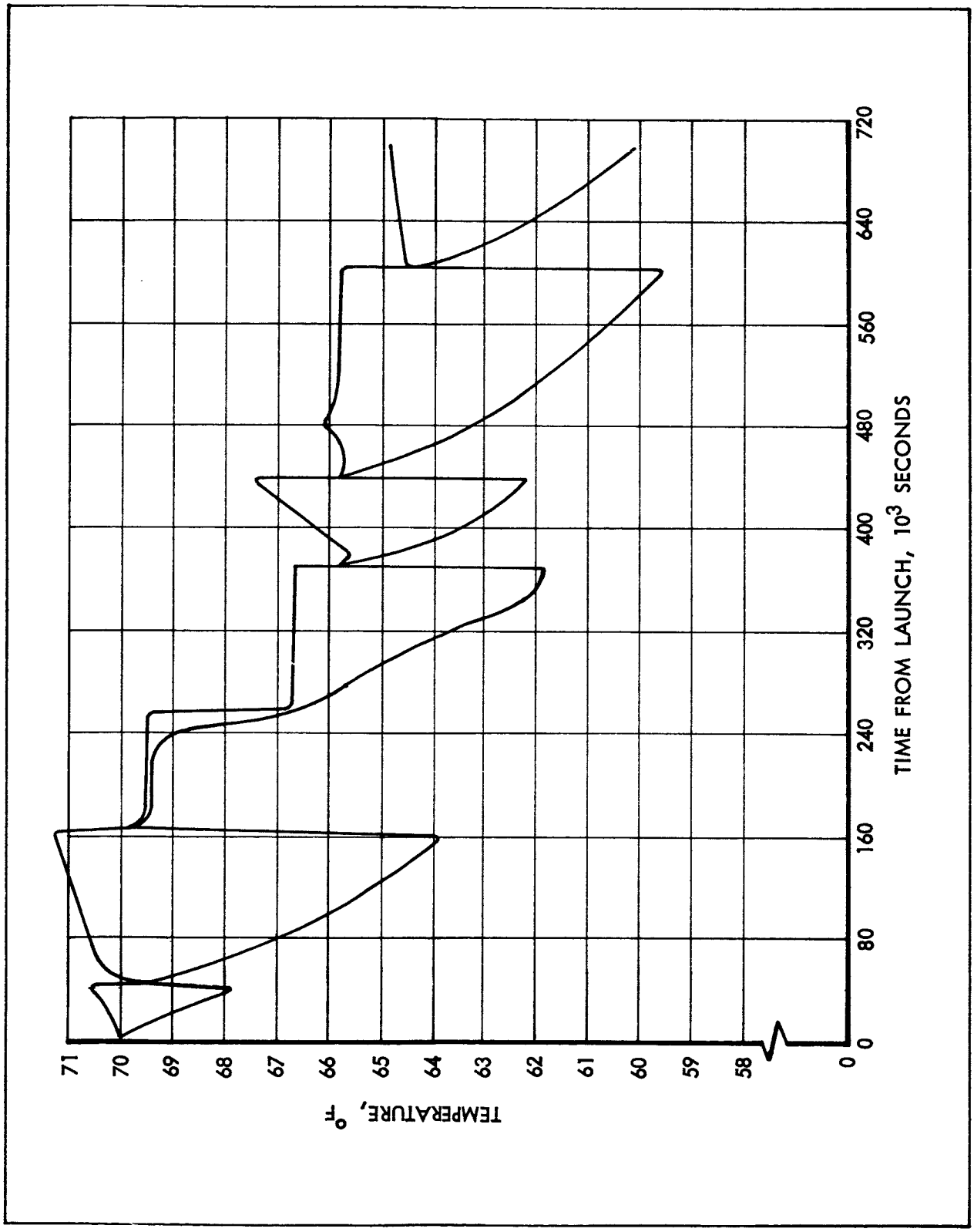

Figure 7-26 Maximum and Minimum Oxidizer Temperature vs Time

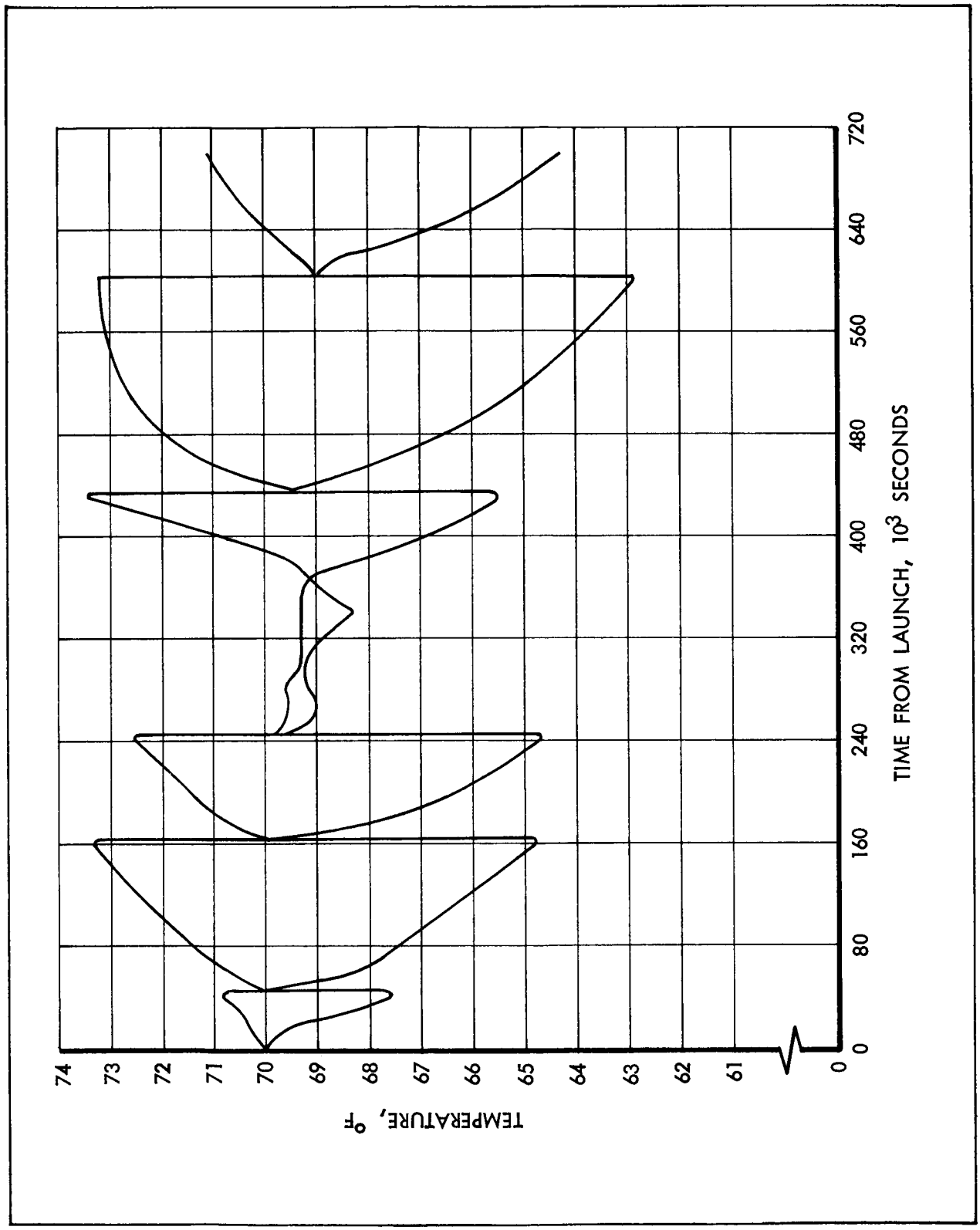

Figure 7-27 Maximum and Minimum Fuel Temperature vs Time

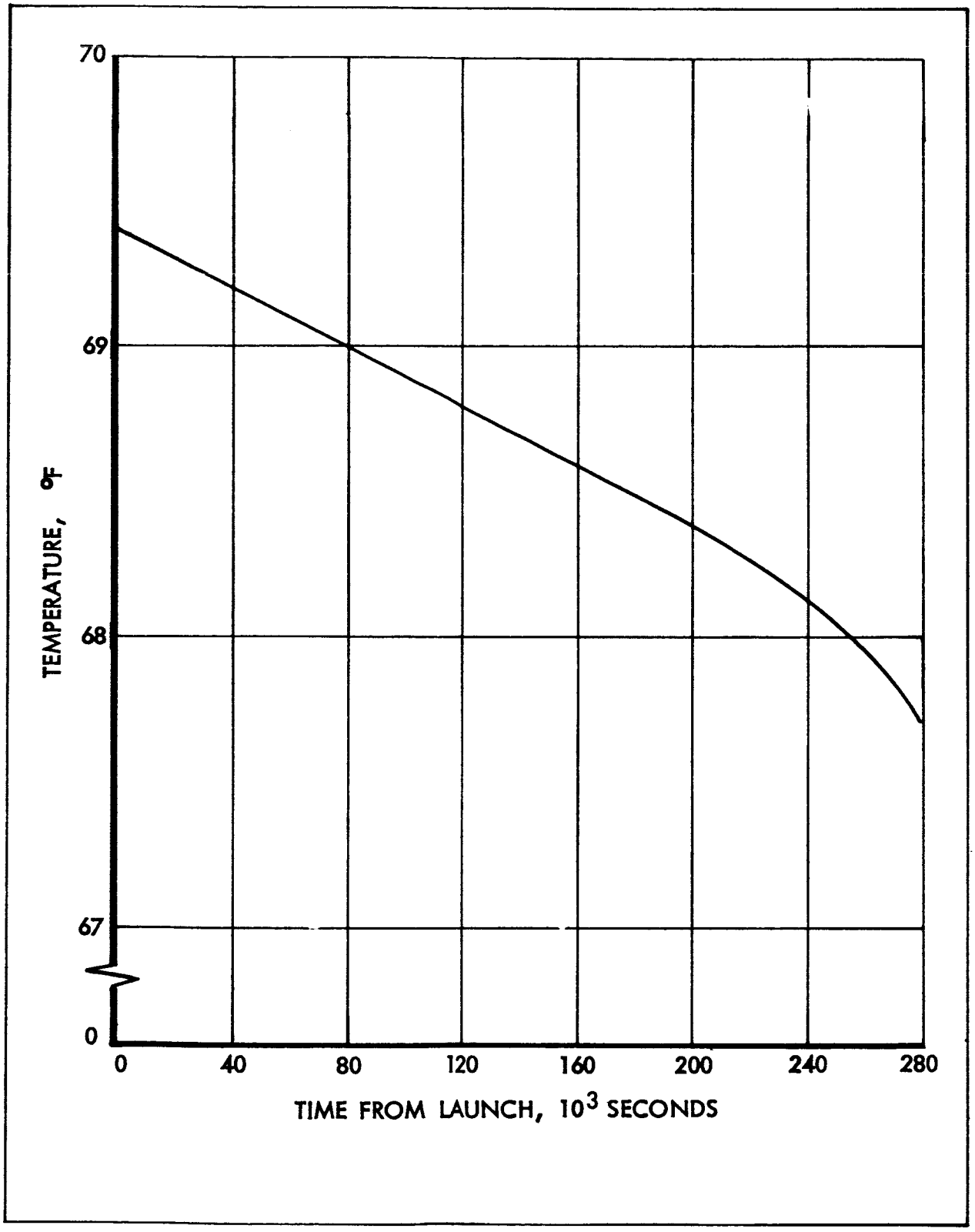

Figure 7-28 Average Gas Temperature vs Time After Engine Start

Assumptions and Simplifications

To analyze the Apollo SPS propellant and pressurant system, the following assumptions and simplifications were made:

1. The system can be analyzed one tank at a time, beginning with the primary tank (which empties first). The two helium bottles can be considered to have a similar thermal environment and, since they are connected in parallel, behave in the same manner so that only one of the bottles need be analyzed.
2. Thermodynamic properties (k, C_p) of Aerozine-50 vapor can be neglected due to the low vapor pressure of this material.
3. During the roll periods, a weak gravity field is established. This increases the rate of heat transfer between the tank wall and the liquid. This was similated by using a convection resistor in parallel with the internal conduction resistors, or by multiplying the value of the liquid thermal conductivity by a constant.
4. During non-flow periods the magnitude of the gravity vector is zero and the vapor phase is in the shape of a spherical bubble located at the center of the tank. During flow periods (engine firings), the magnitude of the gravity vector was unity and was aligned parallel to the principal axis of the S/M.
5. Heat capacity for the gas phases is that at constant volume. The constant pressure heat capacity as tabulated in the materials library is corrected by using the expression $C_v = C_p - Z\ R/M$. This was used because the process in the ullage space and helium bottle is a constant volume process, during non-flow periods.
6. The effects of internal tank plumbing and structure were neglected. This is due to the very minor thermal effect these have on the system. The thermal gradients within the fluid regions are small so that the amount of heat transferred through these internals can be neglected. The thermal capacity of these internals would be small when compared to the liquid nodes they pass through and are of the same order of magnitude as the gas nodes.
7. The primary tanks were analyzed only up to the time at which they have no more liquid (lunar orbit insertion). After this point they

have only a minor influence on the system. The sump tanks were analyzed from the time the primary tanks are empty until the last midcourse correction. Analysis of the primary tanks showed only a small change in average liquid temperature, less than 1° F. Results of the basic SM thermal analysis, Sect. VI, showed the sump tanks about 1° F cooler than the primary tanks at the time of lunar orbit insertion. Due to the above two reasons, and in order to reduce the amount of machine time, the partial analysis of the sump tanks was made.

8. The flow from the pressurant bottles was proportioned according to flowrate, density and vapor pressure, depending upon whether a fuel or oxidizer tank is being analyzed. The helium demand was computed and then the amount withdrawn from the pressurant bottle was found by using the correct ratios of relative fuel and oxidizer flowrate, liquid density and vapor pressure.
9. The pressurant-propellant heat exchanger was simulated by an energy balance across the exchanger. The balance considered that the helium must be delivered within 20°F of the propellant temperature. Also that the minimum helium inlet temperature will be -150° F, and a maximum propellant temperature of 80° F.
10. Pressurant enters the sump tank from the primary tank, and when the latter is empty, the inlet sump gas temperature was assumed to be the same as that on the exit of the heat exchanger. This is because the gas in passing through the empty primary tank should exhibit only a small temperature change.
11. The effects of the reaction control system firings on fluid mixing were neglected. This was done to reduce machine time. The effect of fluid mixing would be to maintain a lower vapor pressure, since the highest liquid nodal temperature determines the vapor pressure. However, upon engine firing, the liquid is mixed, minimizing the effects of the above assumption.

Low Gravity Fluid Mechanics and Heat Transfer Analysis

A low gravity fluid mechanics and heat transfer study was conducted to:

1. Provide judgment as to the location and shape of the liquids in propellant tanks.
2. Provide judgment regarding the effect of maneuvers on the location of liquids.
3. Determine the effect of the expected low gravity during the major portion of the mission on the heat transfer phenomena and its effect on liquid propellant temperatures.
4. Estimate the importance of mass diffusion as an energy transfer mechanism inside the tanks.

The results of this study and the conclusions drawn are as follows:

1. The effect of internal tank hardware is to change the shape of the capillary surface only slightly. The 2.5" diameter standpipe in the center of all tanks will change the shape of the liquid meniscus only locally in the center of the tank. The wetted area of the tank can be expected to remain virtually unchanged when the capillary surface intercepts only the standpipe. When the meniscus intercepts the liquid containment device (15" diameter) the shape of the capillary surface is materially changed. The wetted area of the tank wall is reduced by about 3.9" in the oxidizer tank. The fuel tank size is so similar that these results will apply there also.
2. The largest long term steady acceleration acting on the propellant tanks is that centripetal acceleration resulting from the two rev/hr rate. This acceleration is approximately $1.5 \times 10^{-6} g_o$.
3. This acceleration causes negligible change in the shape of the liquid meniscus in the tanks.
4. The above acceleration causes heat transfer from the tank walls to the liquid to increase by a maximum of 10 to 20 times over that due to conduction alone. This effect can be accounted for by using a coefficient of heat transfer of 0.6 and 0.47 for the fuel and oxidizer, respectively, to calculate a convective thermal resistance paralleling conduction resistance or by simply multiplying the thermal conductivity of the liquids by 10 for the fuel and 20 for the oxidizer.

5. The largest accelerations acting on the liquid (other than those due to propellant settling or main engine operations) are caused by impulsive operation of the RCS. These will cause standing waves to form in the tanks the amplitudes of which are of the order of 1 tank radius. Such liquid motion will serve to mix the liquid in the tanks; 64 maneuvers are of the intensity required to achieve wave amplitudes of the order indicated.
6. Service propulsion system engine operation will completely mix the liquids at the bottoms of their respective tanks. The liquids will repose to the zero g shape in 2 or 3 minutes after such maneuvers are completed.
7. The mass diffusion phenomena was found to have only a slight effect on the liquid oxidizer temperatures. A thermal model of the oxidizer tank was developed and the cases of including and not including the effect of mass diffusion were investigated. When the predicted oxidizer temperatures for the two cases were compared, it was found that during the periodic translunar roll the effect of mass diffusion was to change the oxidizer temperatures by less than 1.0° F.
8. The concentration of oxidizer vapor (ratio of oxidizer vapor density to sum of oxidizer and helium vapor density) was found to have only a small gradient throughout the gaseous phase. Throughout the time period investigated, the maximum difference between the maximum and minimum values of concentration was calculated to be only 0.03. This small gradient results in a small amount of oxidizer vapor diffusing through the gaseous phase and minimal energy transferred by mass diffusion.
9. The time constant for the diffusion process was of the order of two of the translunar roll periods. The case of not including the effect of mass diffusion was investigated first and the resulting temperatures averaged over the period, were used as start temperatures for the case including mass diffusion. The time constant was taken as the time it took the liquid oxidizer temperatures to reach a condition where the same temperature history was repeated from one period to the next.

This supporting analysis is presented in detail in Appendix C.

VIII - ANALYSIS OF EARTH SUBORBITAL AND ORBITAL MISSIONS

EARTH SUBORBITAL MISSION

For the suborbital mission spacecraft internal heat transfer is anayzed in the same manner as the main mission (Section III). External heat input is composed of two distinct types, ascent heating and orbital heating. With these impressed heat inputs, temperature histories for the vehicle structure and components are determined. Analysis of the results indicates no thermal problem areas, mainly because of the less severe thermal environment and the short duration of the mission. Although there is a 240 second engine firing, the thermal interaction between the structure and the SPS is negligible because the firing occurs just prior to CM/SM separation. It was decided that a detailed analysis of the SPS engine, plumbing, and pressurization system would not have provided useful and significant results. The following paragraphs present and briefly discuss the results in the various parts of the spacecraft. Data are presented in the form of maximum-minimum temperatures and representative temperature histories.

Maximum shell temperatures,which occur during ascent, are shown in Figure 8-1. The honeycomb shell nodes reach a maximum temperature of 432°F, while the RCS heat shield nodes reach a maximum temperature of 662°F. These higher RCS heat shield temperatures are caused by high protuberance heating and small thermal capacity. Shell node temperatures that do not exceed 175°F are protected from external heat input by the RCS heat shield. Temperature histories of representative shell nodes are shown in Figure 8-2. Shell node 710, typical for sectors 3 and 4, reaches a peak temperature of 340°F during ascent, then rapidly cools down to 160°F until it begins to receives solar heating, which driyes the temperature back up to 240°F. On the other side of the spacecraft, typically node 703, the shell node cools down continuously from its peak ascent temperature because there is no solar heating. The temperature history of node 810, which is in the same axial row as node 710, does not show a characteristic peak ascent temperature because its temperature is influenced by the bulkhead.

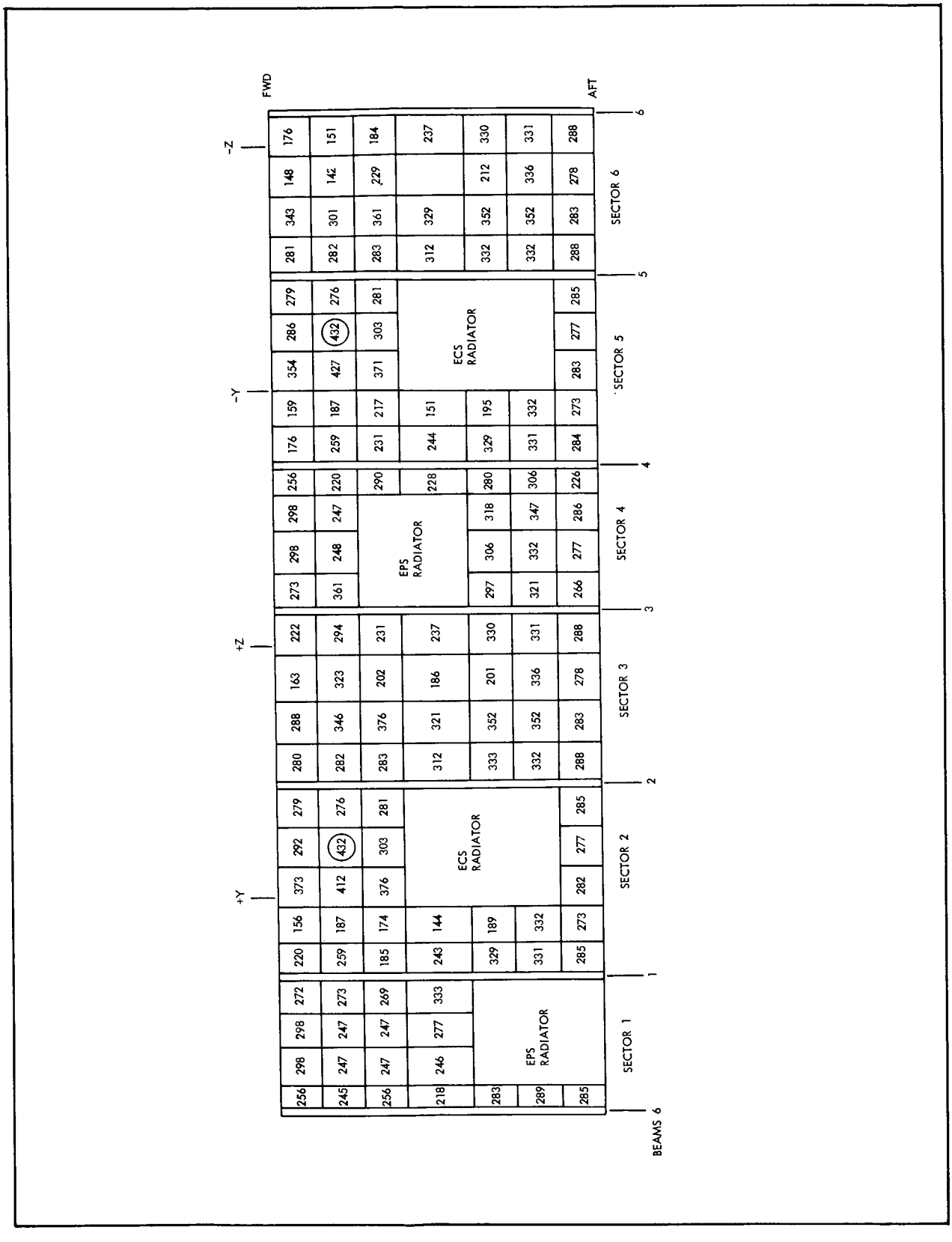

Figure 8-1 Maximum Temperatures for Shell Nodes, Earth Suborbital Mission

LOCKHEED CALIFORNIA COMPANY

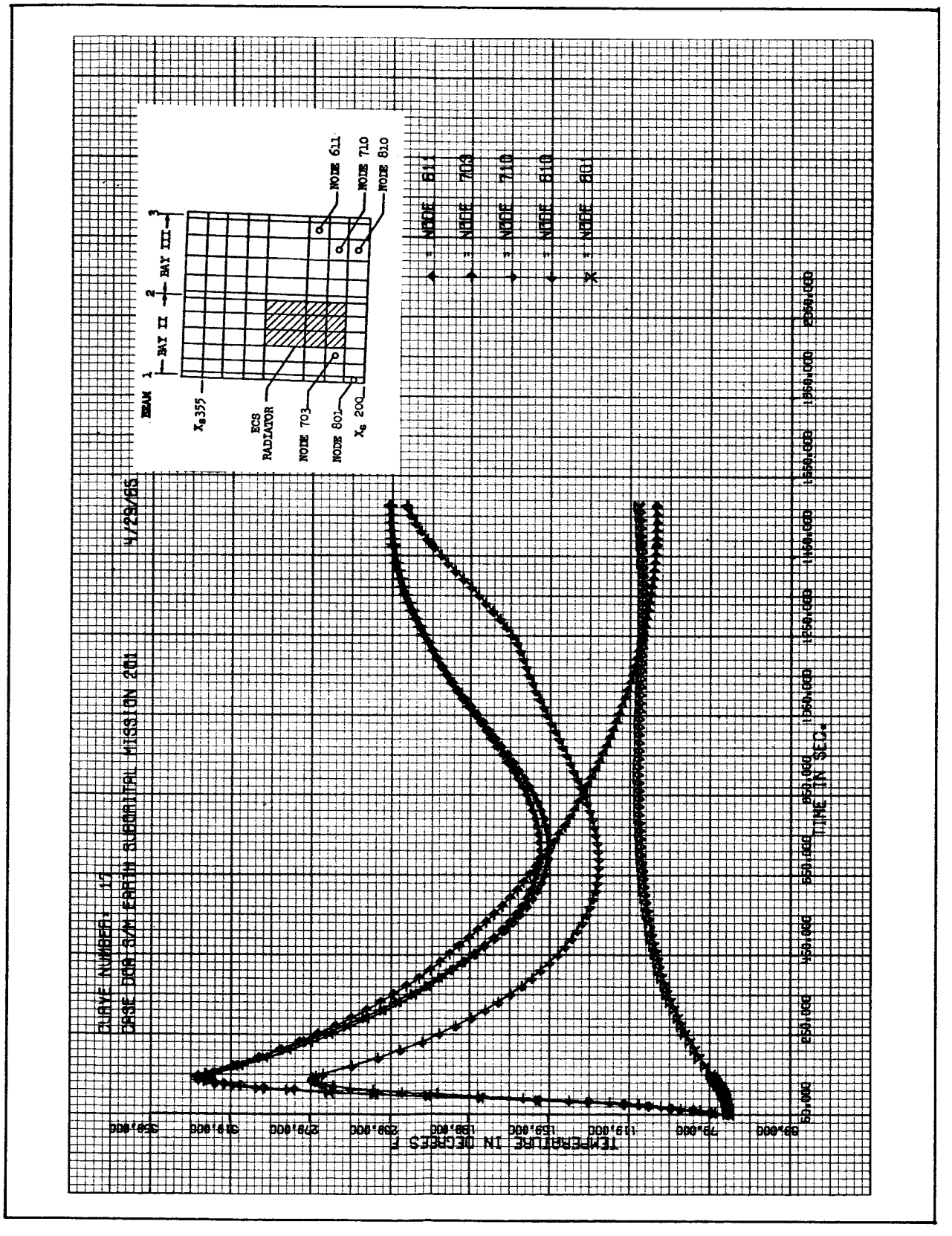

Figure 8-2 Shell Temperature Histories for Earth Suborbital Mission

Figure 8-3 shows maximum temperatures for the bulkhead nodes. Except for the outer ring of nodes, which are connected with the shell nodes, bulkhead temperatures do not exceed 80°F. Shown in Figure 8-4 are maximum temperatures for the beam nodes. Temperatures of the beam nodes adjacent to the shell are 20°F to 40°F warmer than the intermost beam nodes, which are 70°F for the entire mission. Five beam temperature histories are plotted in Figure 8-5. This figure shows nodes 548 and 645, which are adjacent to the shell, heating up to a temperature of 95°F while temperatures of the other 3 nodes, which are inboard from the shell, remain unchanged. Similar to the shell, the minimum temperature on the bulkheads and beams are 70°F.

After the S-IVB stage separates from the service module, the aft end of the vehicle is exposed to external heat transfer. The heat shield nodes that are shaded from external heating cool to a minimum temperature of -35°F, while nodes in direct view of the nozzle extension reach a maximum temperature of 1100°F. Just prior to engine firing, the nozzle extension temperatures are 150°F on the side of the nozzle that faces the sun and -16°F on the opposite side of the nozzle. During the 240 second engine firing, the nozzle extension temperatures of 1900°F are impressed as boundary conditions.

The temperature of the helium bottles are 70°F except after engine firing when they cool to 65°F due to the expansion of the helium gas. Assuming adiabatic expansion of the helium gas, its temperature drops from 70°F to 5°F during engine firing. External heating rate to the helium bottles as well as to the propellant tanks is negligibly small. The propellant tank temperatures are 70°F for the entire mission.

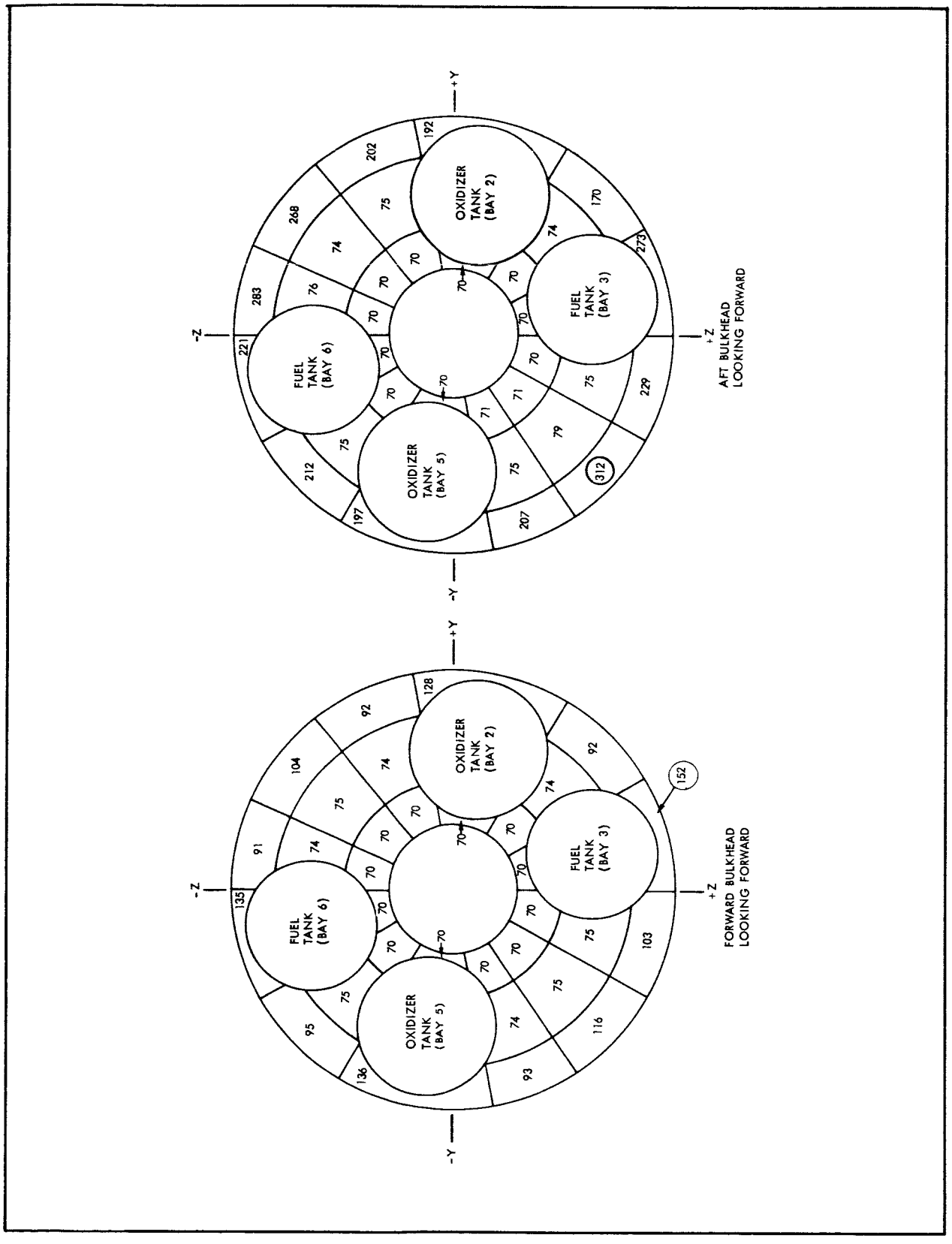

Figure 8-3 Maximum Temperatures for Bulkhead Nodes, Earth Suborbital Mission

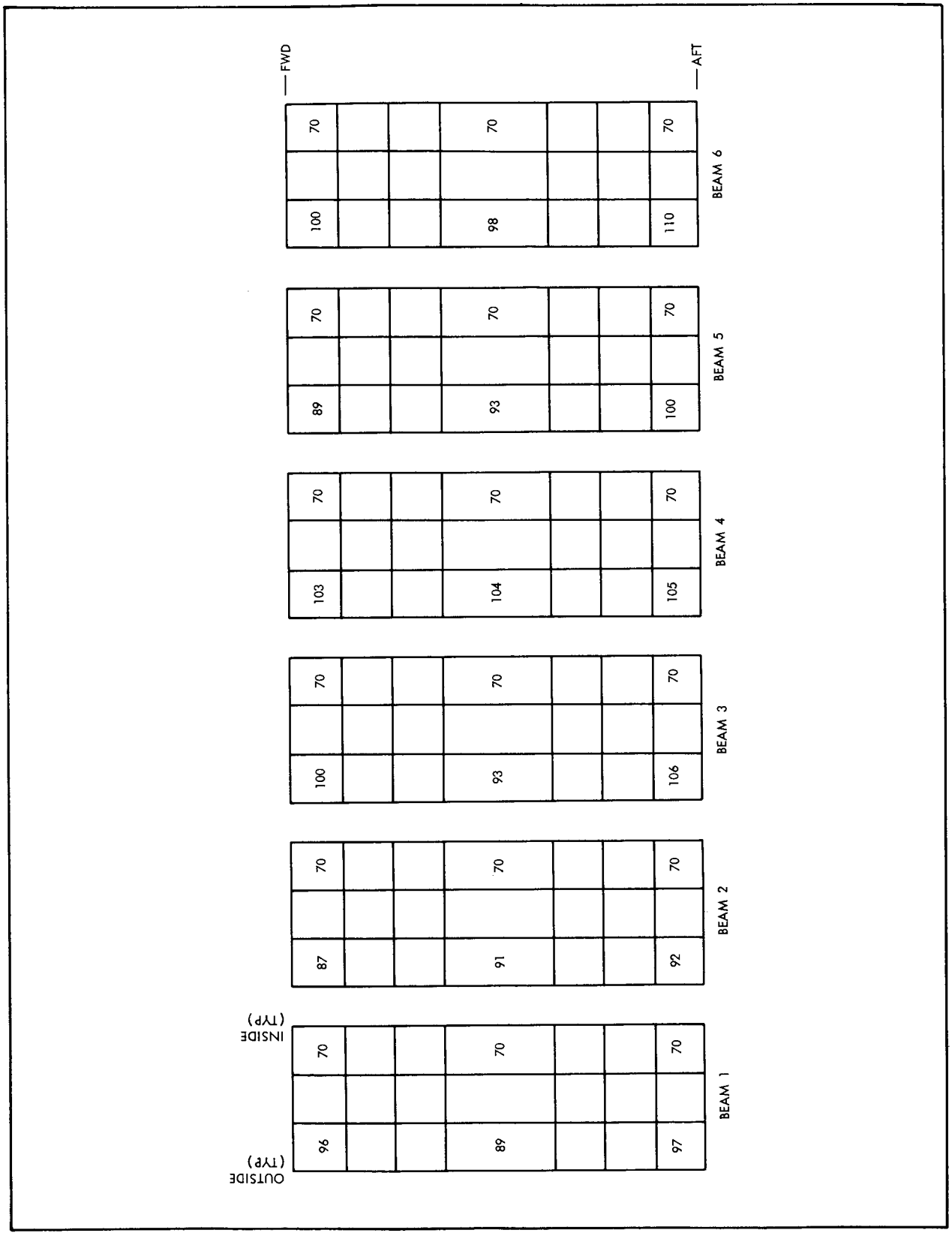

Figure 8-4 Maximum Temperatures for Beam Nodes, Earth Suborbital Mission

LOCKHEED CALIFORNIA COMPANY

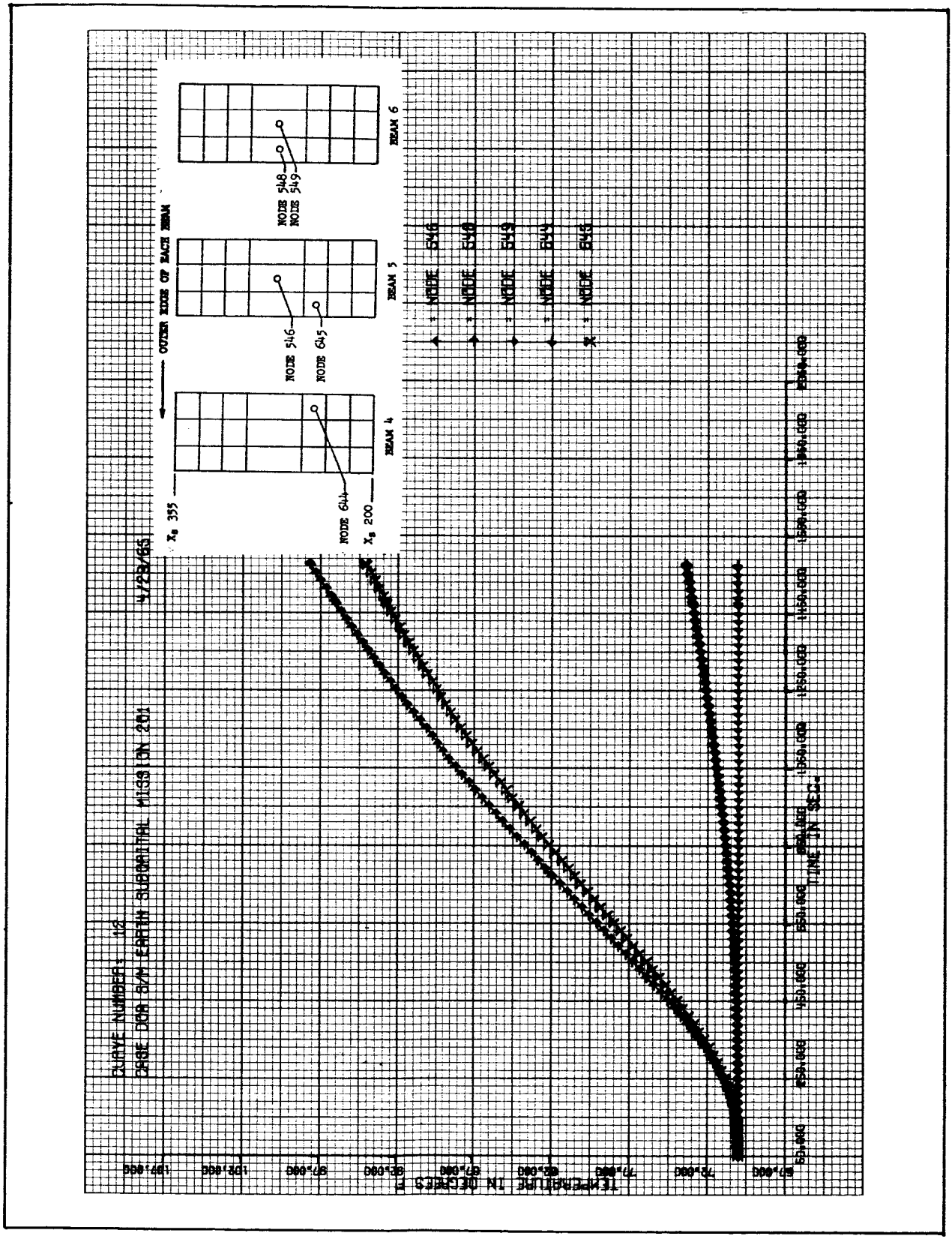

Figure 8-5 Beam Temperature Histories for Earth Suborbital Mission

EARTH ORBITAL MISSION

Analysis of the Service Module Basic Structure

The Earth Orbital Mission analysis employs the same structure thermal network as the main mission except for one change. In Bay 4, which contains the fuel cells, the aluminized Mylar insulation is not applied to the radial beams. Since the boosters used for the Earth Orbital Mission and the Lunar Orbit Rendezvous Mission give similar ascent temperatures (Sect. V) the spacecraft temperature distribution obtained in the main mission analysis at the end of 150 seconds of ascent is impressed as the initial conditions for the earth orbital mission. In addition, temperatures obtained from MSC are impressed as boundary conditions on the thrust chamber for the entire mission, while nozzle extension temperatures are impressed only during the SPS engine firing.

The Earth Orbital Mission is divided into five orbital segments (Sect. II), which are of different orbit parameters and orientations. During this phase of the analysis,it was found that orbital segments involving the same basic orientation yield similar results. Therefore, the results of the three planetary orientations are presented together, and the results of the two solar orientations are presented together. The first orbital segment, which has planetary orientation and has as initial conditions the peak ascent temperatures, does not achieve dynamic equilibrium temperatures because of the relatively short duration of that mission segment. The term "dynamic equilibrium" denotes the condition where temperature variations are repetetive from orbit to orbit. Temperature histories of representative shell and beam nodes are shown in Figures 8-6 and 8-7. From Figure 8-6 it is seen that the shell nodes rapidly cool down from their peak ascent temperatures to a mean cyclic temperature of approximately $40^{\circ}F$. The beam node temperatures, Figure 8-7, show a small initial increase due to the warm shell nodes, then a gradual cyclic decrease in temperature to $54^{\circ}F$ at the end of the orbital segment. Also shown in this figure is the linear increase in temperature of beam node 644, which is due to the heating from the fuel cell. In all the machine plotted graphs the change in plotting interval

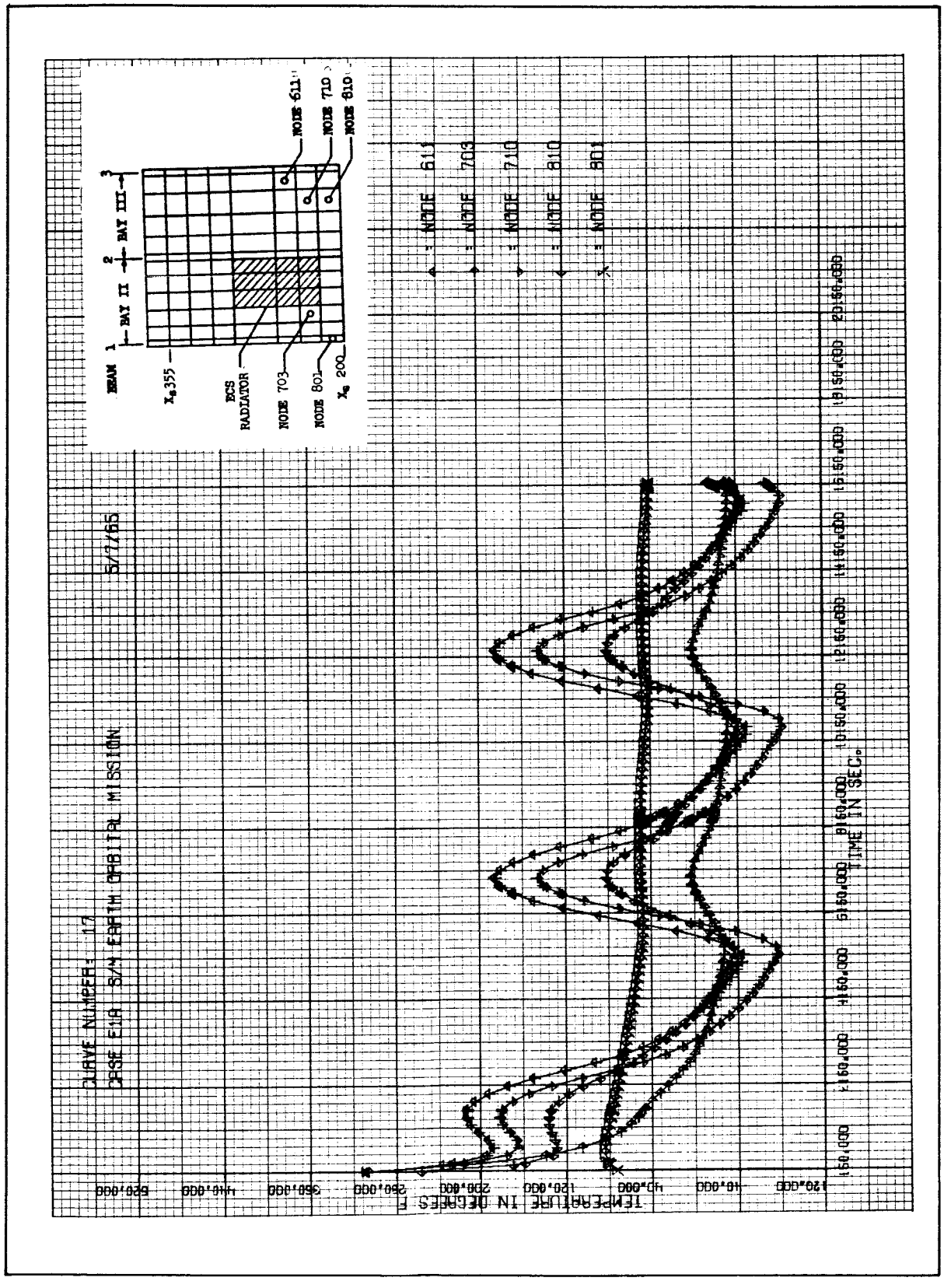

Figure 8-6 Shell Temperature Histories for Earth Orbital Mission, Planetary Orientation

LOCKHEED CALIFORNIA COMPANY

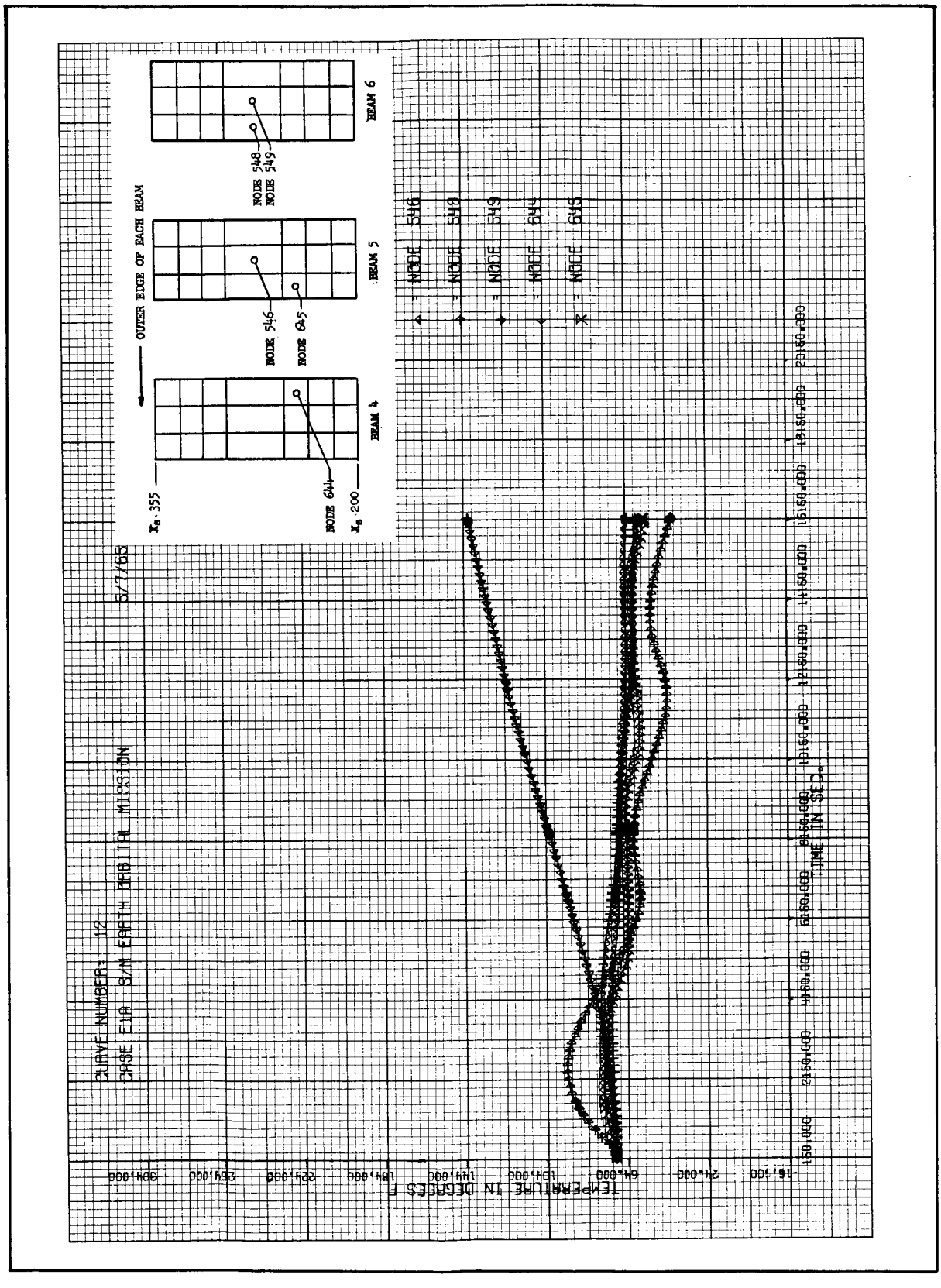

Figure 8-7 Beam Temperature Histories for Earth Orbital Mission, Planetary Orientation

LOCKHEED CALIFORNIA COMPANY

indicates the region of an engine firing.

The third and fifth orbital segments involve planetary orientation. For this orientation the maximum and minimum temperatures of the shell nodes, which occur after dynamic equilibrium conditions are attained, are presented in Figure 8-8. This figure shows that mean shell temperatures in Sector 6, which view the earth, are $50^{\circ}F$ with approximately $\pm 30^{\circ}F$ cyclic variation, while mean shell temperatures in Sector 4, which view the sun, are about $100^{\circ}F$, with $\pm 100^{\circ}F$ cyclic variation. This orbital temperature fluctuation is most graphically seen in Figure 8-9, which shows temperature histories of representative shell nodes.

Maximum and minimum temperatures of the beams and bulkhead are shown in Figures 8-10 and 8-11 respectively. The aft bulkhead runs considerably warmer than the forward bulkhead primarily because of heating from the fuel cells. Engine firing influence on the aft bulkhead cannot be readily detected as seen from the temperature history of aft bulkhead shown in Figure 8-12. Also observed from that figure is the lack of cyclic temperature variation because there is no direct external heat input, and the thermal capacity of the bulkhead is relatively large. Temperature histories of representative beam nodes are shown in Figure 8-13. This graph, which is plotted for only three orbital revolutions, shows a gradual cyclic temperature increase from the cooler preceding orientation. However, by the fifth orbital revolution, these temperatures level off at their equilibrium values. Beam node 644 runs considerably warmer than the other beam nodes shown in Figure 8-13 because of its immediate proximity to the fuel cells. Removal of the insulation of Bay 4 allows the beams forming that bay to run $30^{\circ}F$ to $40^{\circ}F$ warmer than the insulated case in an equivalent orbital environment. In addition, the fuel cells, which have a constant total heat leak of $750 \frac{Btu}{hr}$, operates at a temperature of $300^{\circ}F$ for the insulated bay and $235^{\circ}F$ for the uninsulated bay.

The second and fourth orbital segments are solar oriented; the second being a solar soak with the nozzle facing the sun; the fourth being a cold soak with the Command Module facing the sun. For these orientations the average shell temperature is approximately $-50^{\circ}F$ with a orbital temperature variation of $\pm 20^{\circ}F$. Figure 8-14 shows the maximum

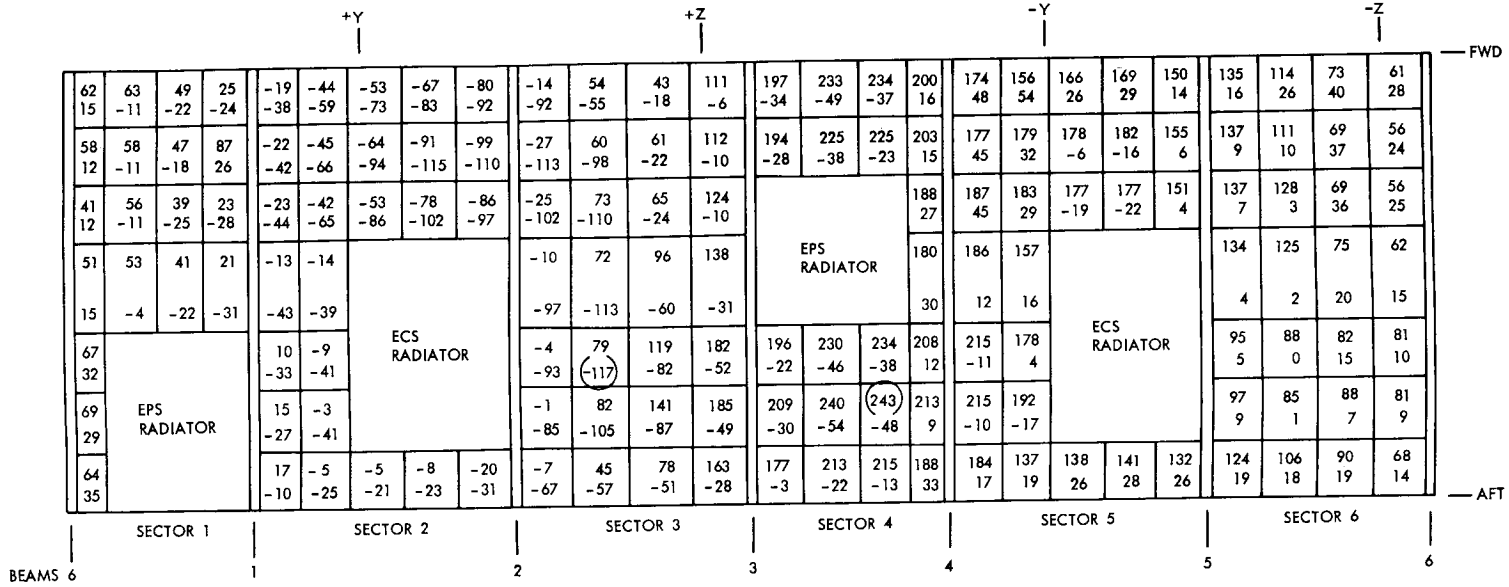

Figure 8-8 Earth Orbital Maximum/Minimum Temperatures for Shell Nodes, Planetary Orientation

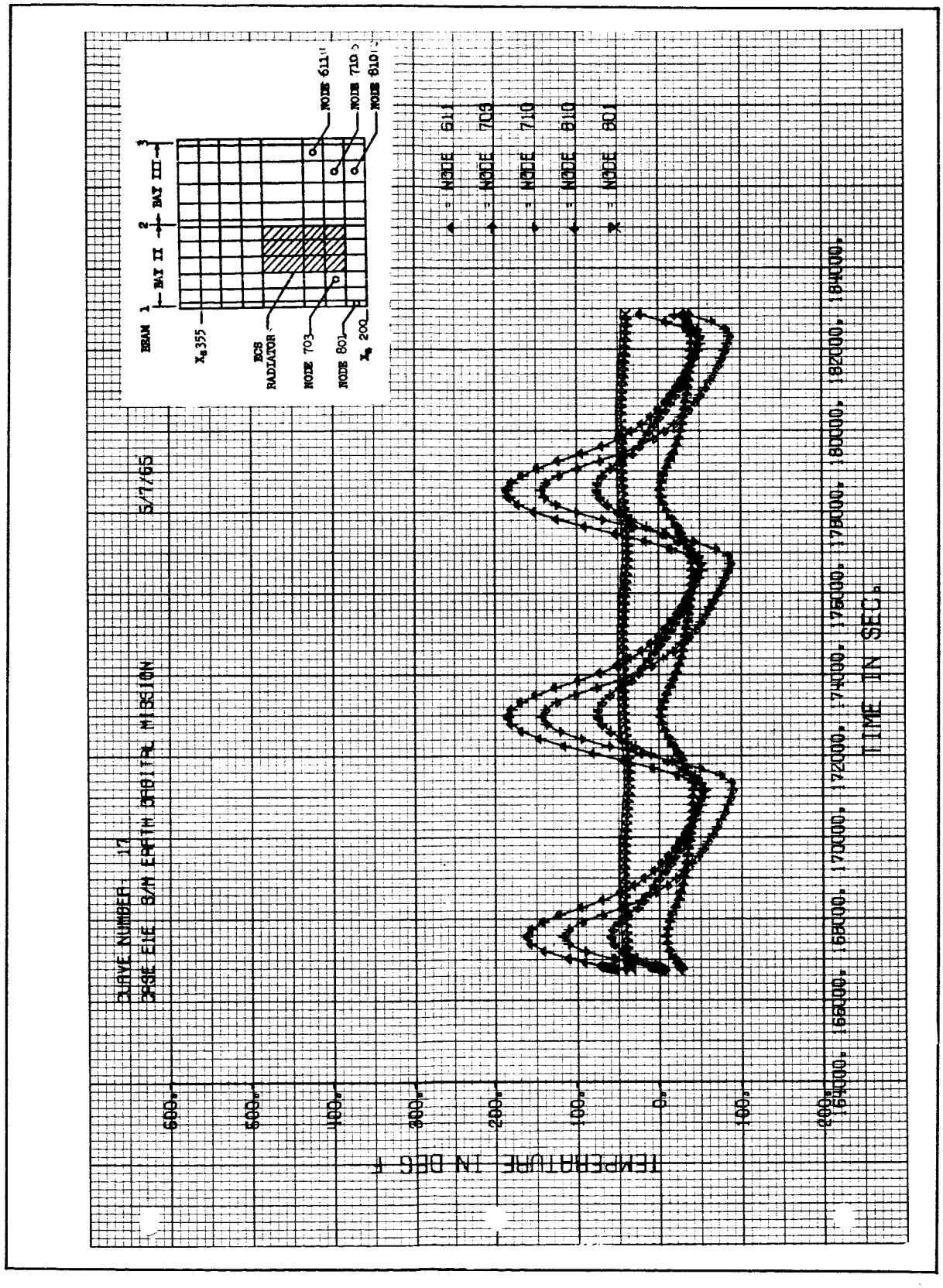

Figure 8-9 Shell Temperature Histories for Earth Orbital Mission, Planetary Orientation

LOCKHEED CALIFORNIA COMPANY

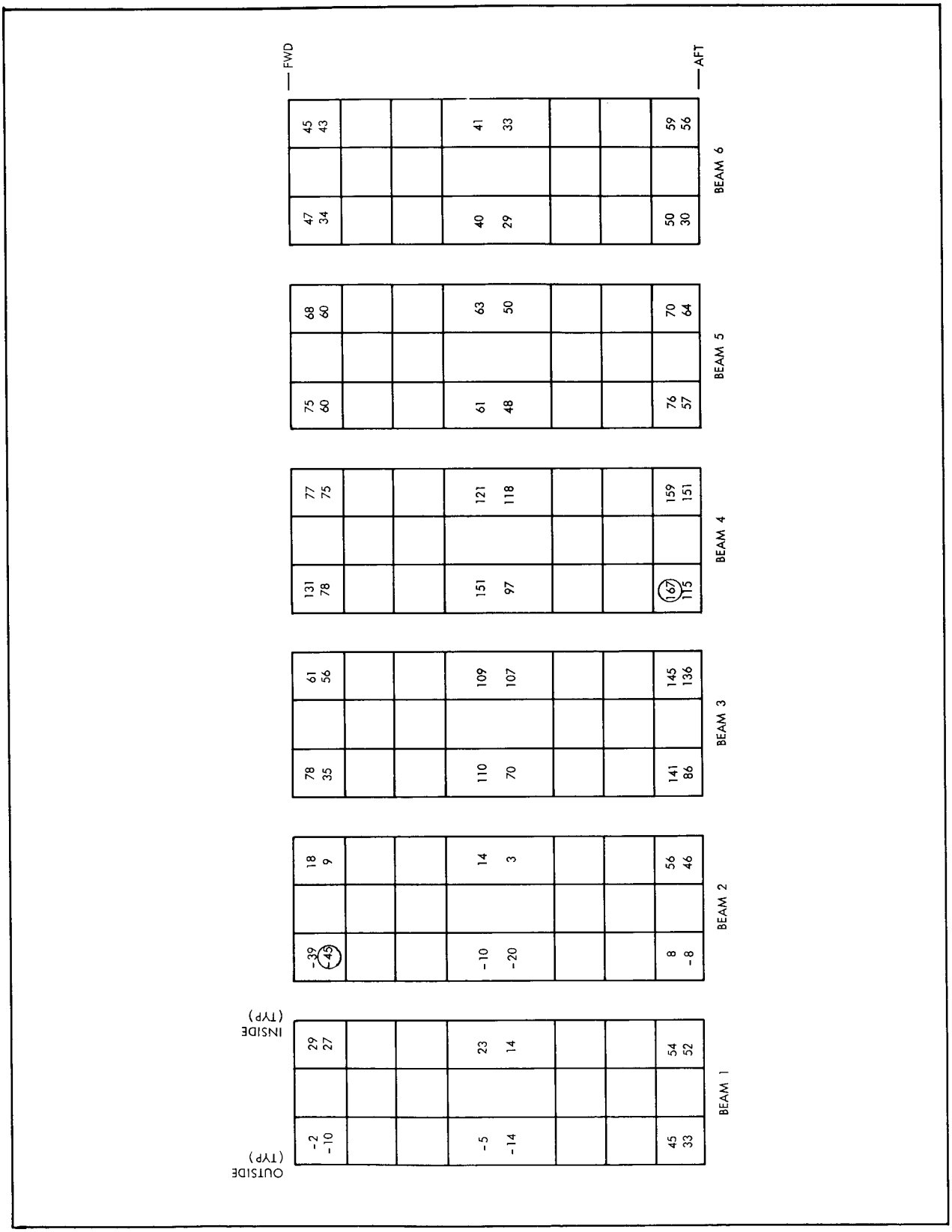

Figure 8-10 Earth Orbital Maximum/Minimum Temperatures for Beam Nodes, Planetary Orientation

LOCKHEED CALIFORNIA COMPANY

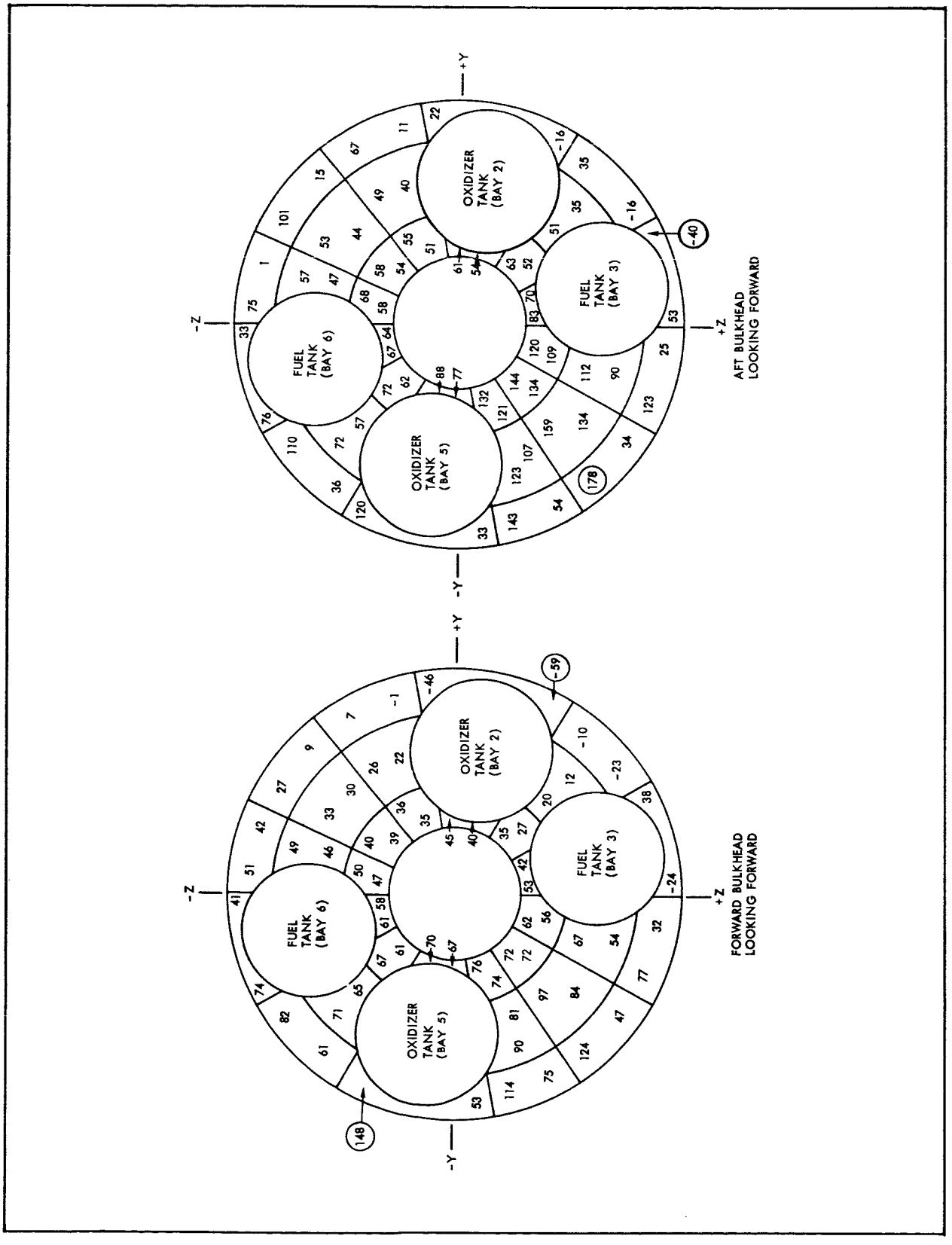

Figure 8-11 Earth Orbital Maximum/Minimum Temperatures for Bulkhead Nodes, Planetary Orientation

LOCKHEED
CALIFORNIA COMPANY

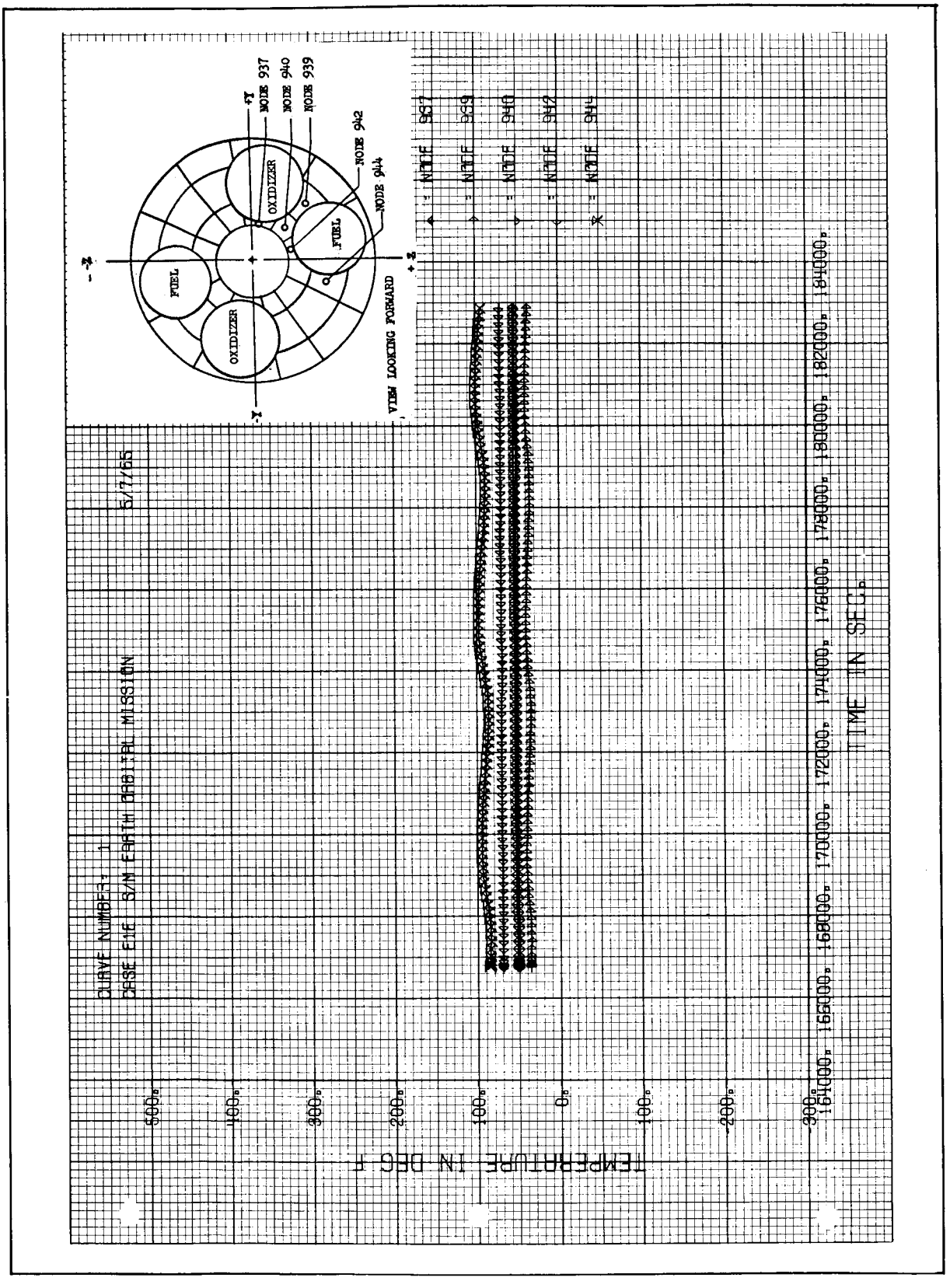

Figure 8-12 Aft Bulkhead Temperature Histories for Earth Orbital Mission, Planetary Orientation

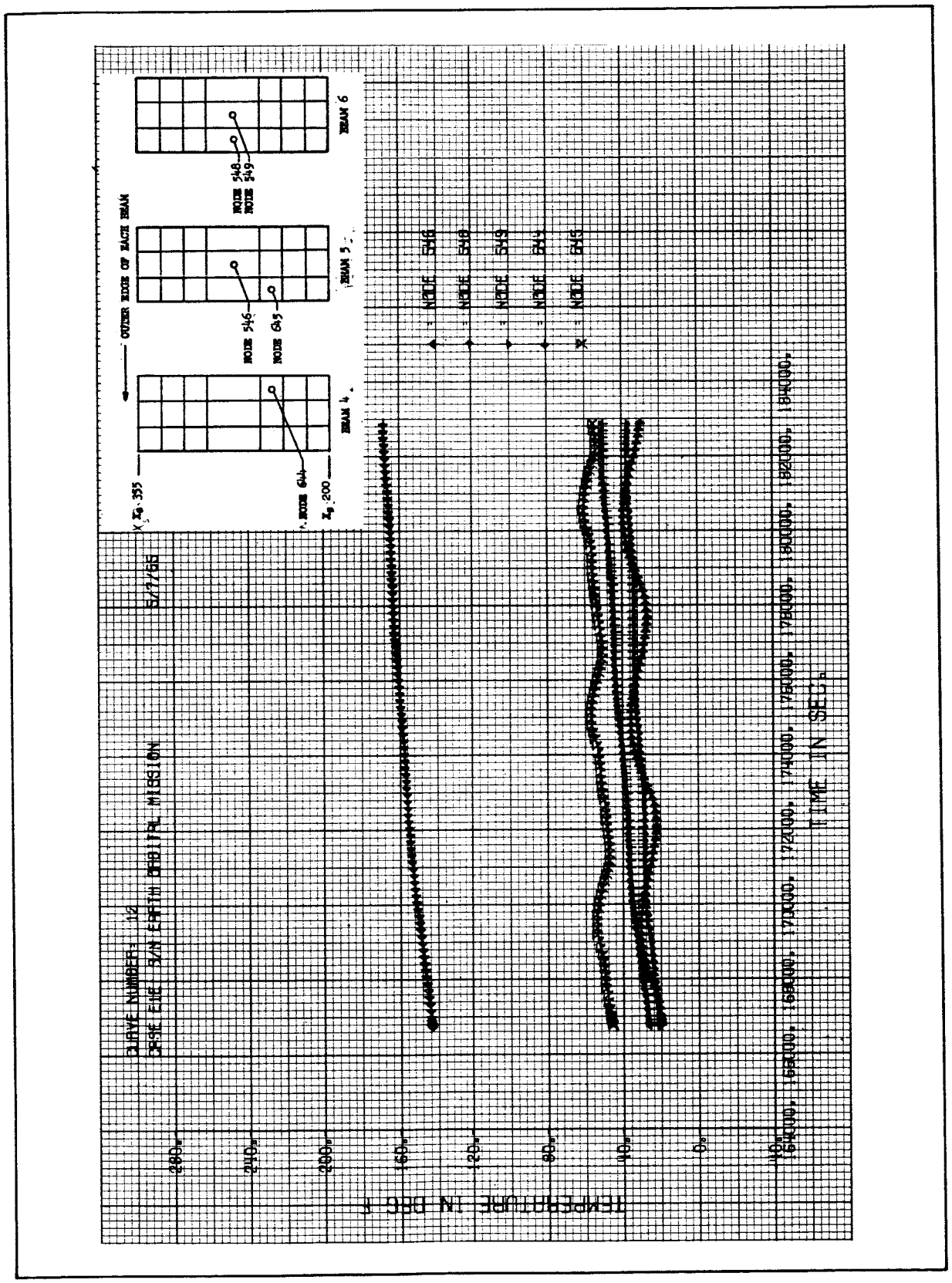

Figure 8-13 Beam Temperature Histories for Earth Orbital Mission, Planetary Orientation

LOCKHEED CALIFORNIA COMPANY

and minimum temperatures of the shell nodes after dynamic equilibrium is attained. The maximum shell temperature is 43 °F, while the minimum shell temperature is -110 °F. In contrast to the planetary orientation, the shell temperatures during solar orientation run approximately 125°F cooler with a much smaller cyclic variation because there is no direct solar heat input. Temperature histories of representative shell nodes for the solar soak, which are also similar to the cold soak, are shown in Figure 8-15. As expected, the shell nodes rapidly cool down from the warmer planetary orientation values and reach dynamic equilibrium after two orbital revolutions.

For the solar soak and cold soak orientations, the maximum and minimum temperatures of the beam nodes are as shown in Figures 8-16 and 8-17. Average beam temperatures for the solar soak are 20°F warmer than for the cold soak. During the solar soak, the axial temperature gradiant in the beams is 50°F to 70°F, while during the cold soak, the gradiant is only 10°F to 20°F. This is because there is no solar heating of the Service Module for the cold soak, whereas there is solar heating of the aft end for the solar soak. Beam temperatures for solar orientation are generally 40°F cooler than for planetary orientation. Figure 8-18 shows representative temperature histories of the beam nodes for the solar soak which are also representative of the cold soak. Noteworthy in this figure is the 60°F to 80°F cool down of the beam nodes except for node 644 which continues to be heated by the fuel cell to a temperature of 160°F.

Maximum and minimum temperatures of the bulkhead nodes for the solar soak and the cold soak orientations are shown in Figures 8-19 and 8-20. The average aft bulkhead temperature for the solar soak is about 85°F, which is 20°F warmer than for the cold soak, while the average forward bulkhead temperatures for both orientations are approximately equal, primarily due to the proximity of the CM heat shield which is assumed to be a 70°F sink.

Two representative nozzle extension temperature histories during a typical 12 second engine firing are plotted in Figure 8-21. The two nodes plotted, 1093 and 1117, are both aligned with the +Z axis of the spacecraft with node 1093 nearer to the engine. Peak temperature for

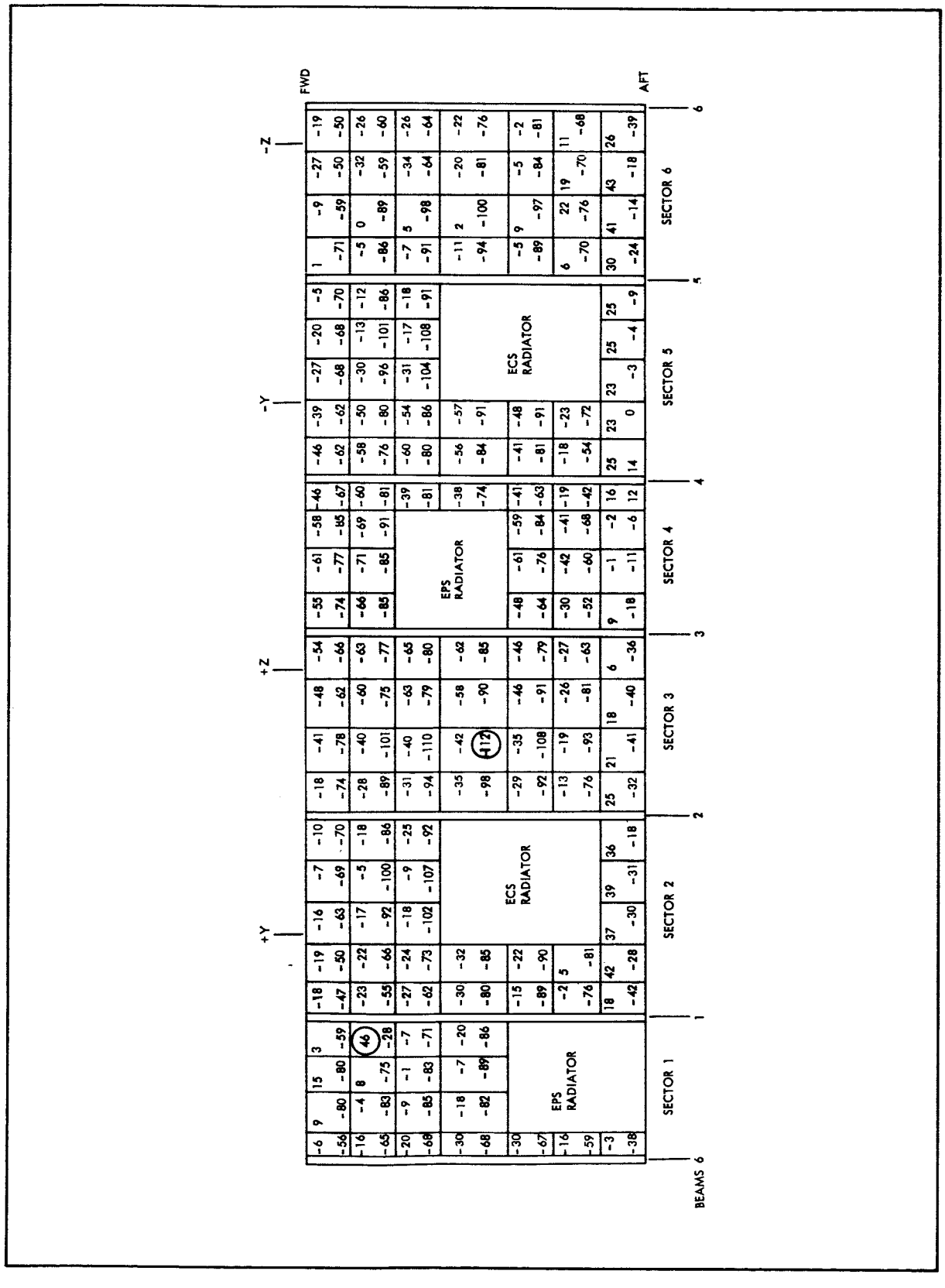

Figure 8-14 Earth Orbital Maximum/Minimum Temperatures for Shell Nodes, Solar Orientation

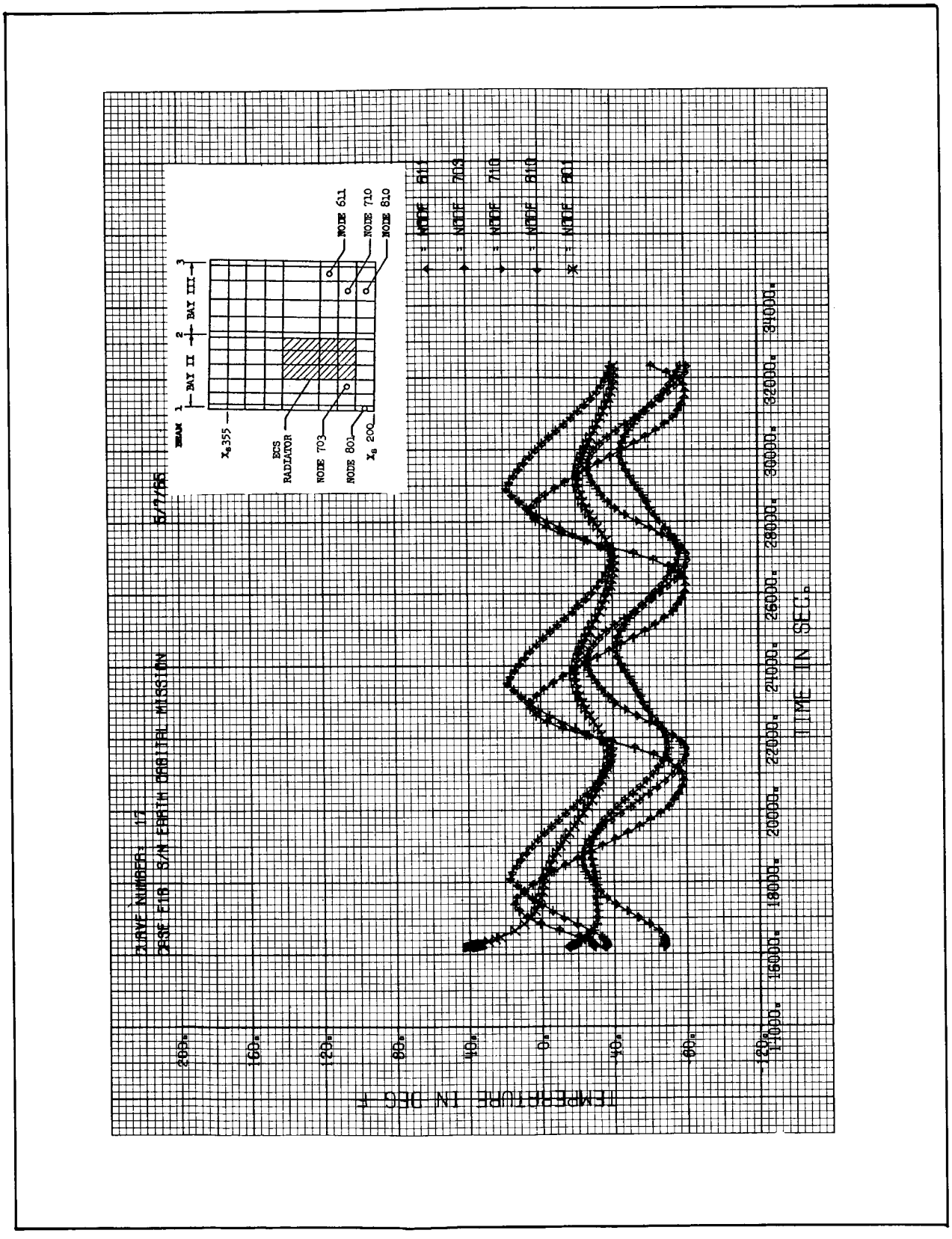

Figure 8-15 Shell Temperature Histories for Earth Orbital Mission, Solar Soak

LOCKHEED
CALIFORNIA COMPANY

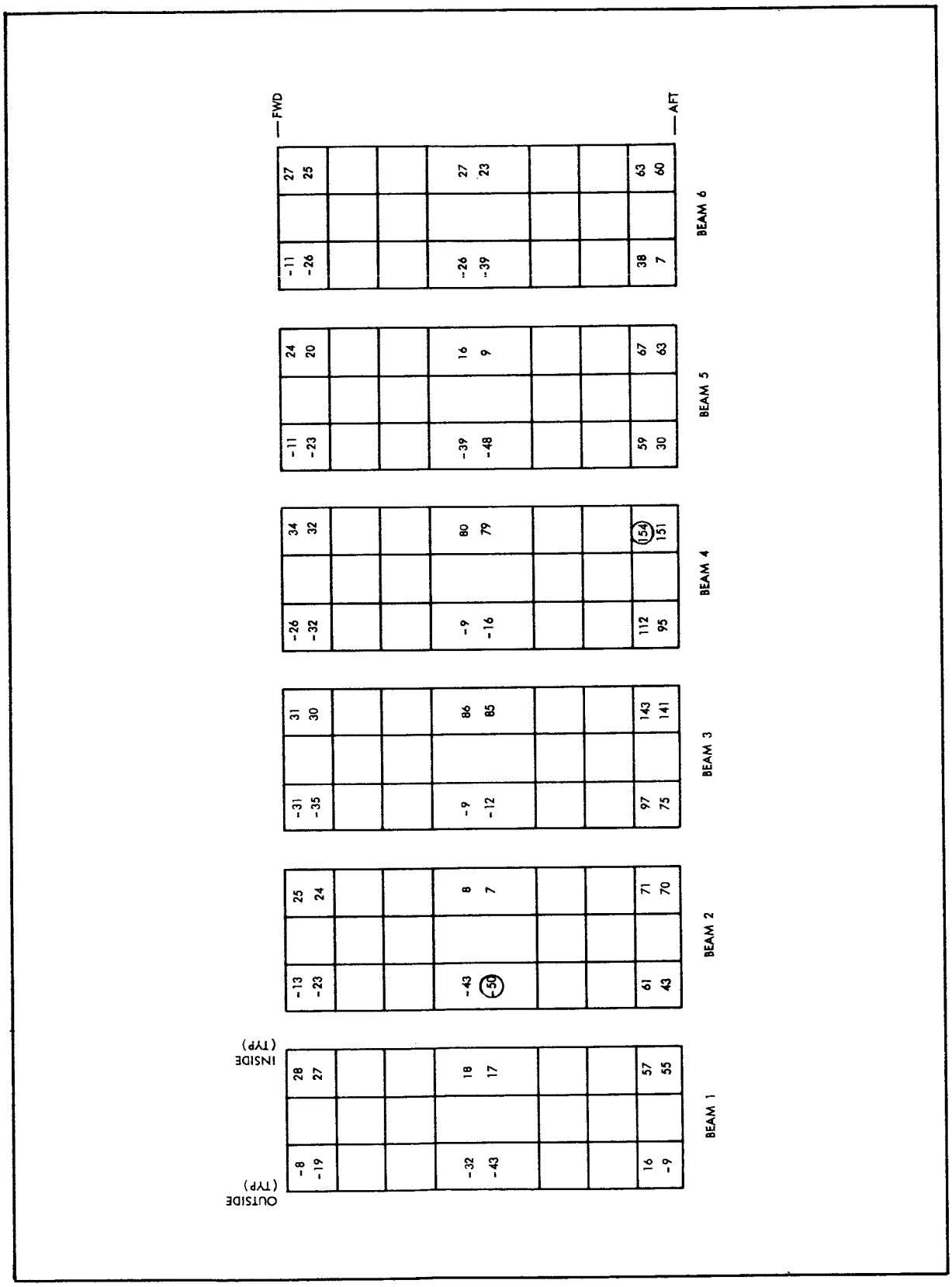

Figure 8-16 Earth Orbital Maximum/Minimum Temperatures for Beam Nodes, Solar Soak

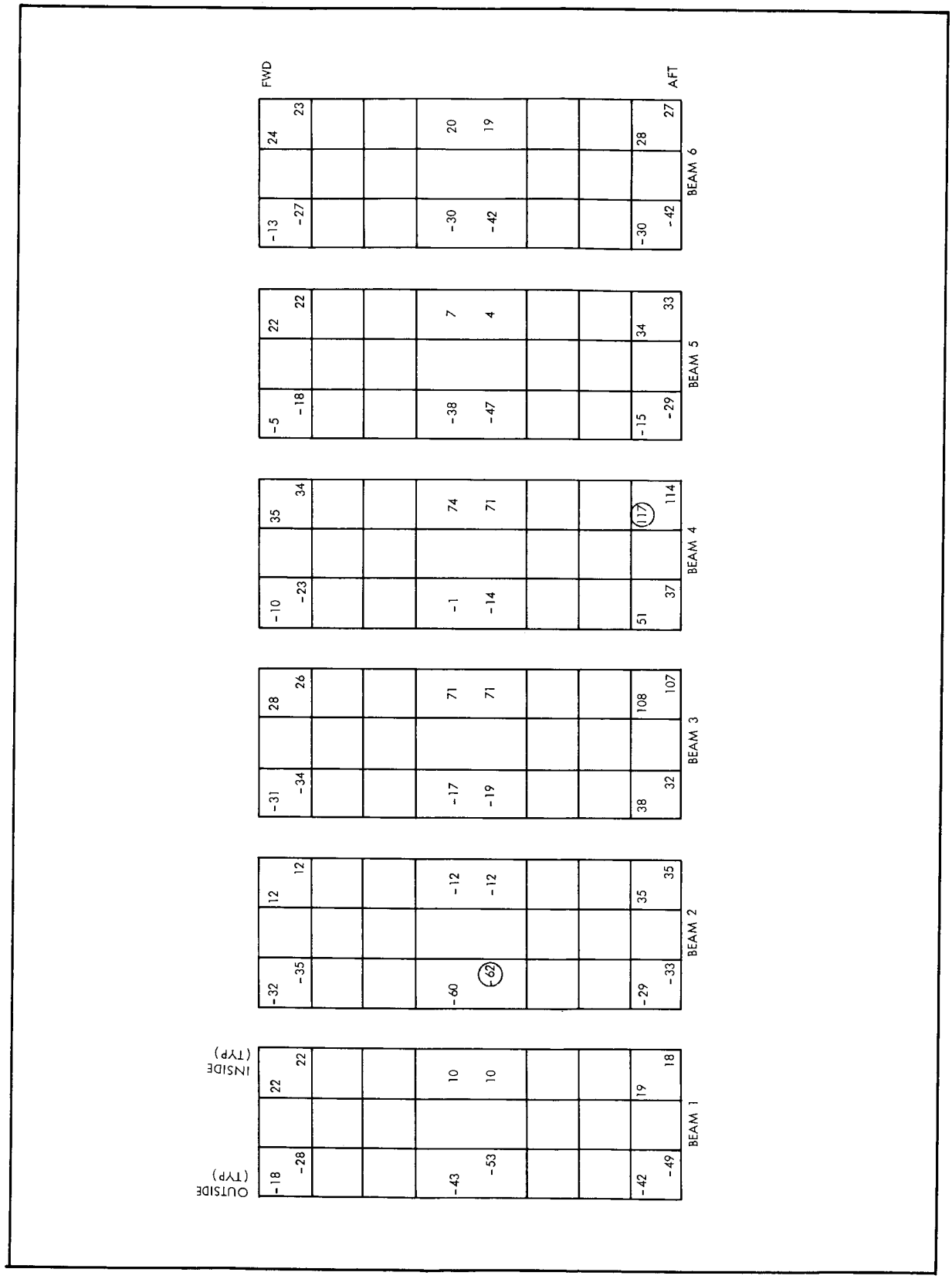

Figure 8-17 Earth Orbital Maximum/Minimum Temperatures for Beam Nodes, Cold Soak

LOCKHEED CALIFORNIA COMPANY

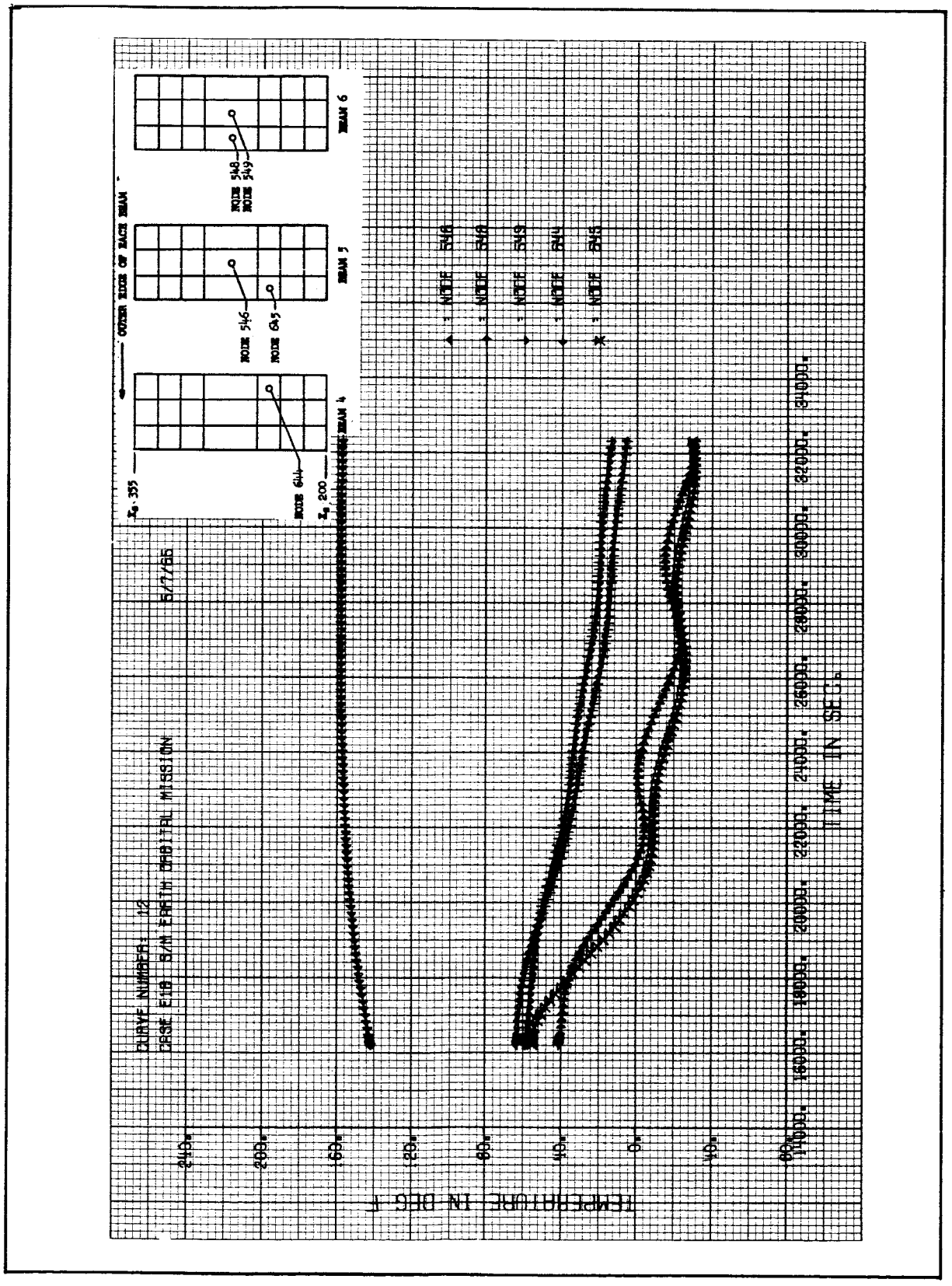

Figure 8-18 Beam Temperature Histories for Earth Orbital Mission, Solar Soak

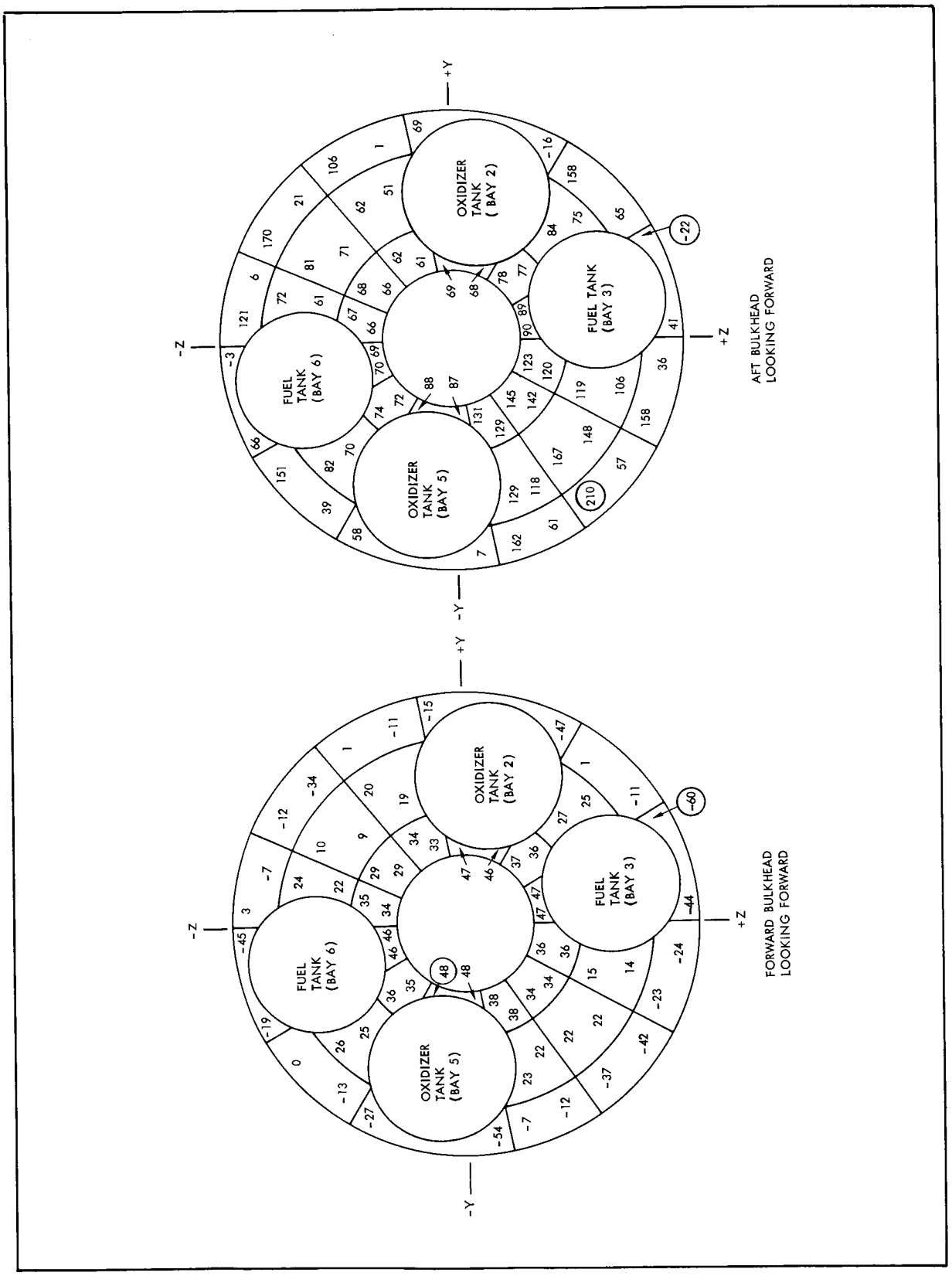

Figure 8-19 Earth Orbital Maximum/Minimum Temperatures for Bulkhead Nodes, Solar Soak

LOCKHEED CALIFORNIA COMPANY

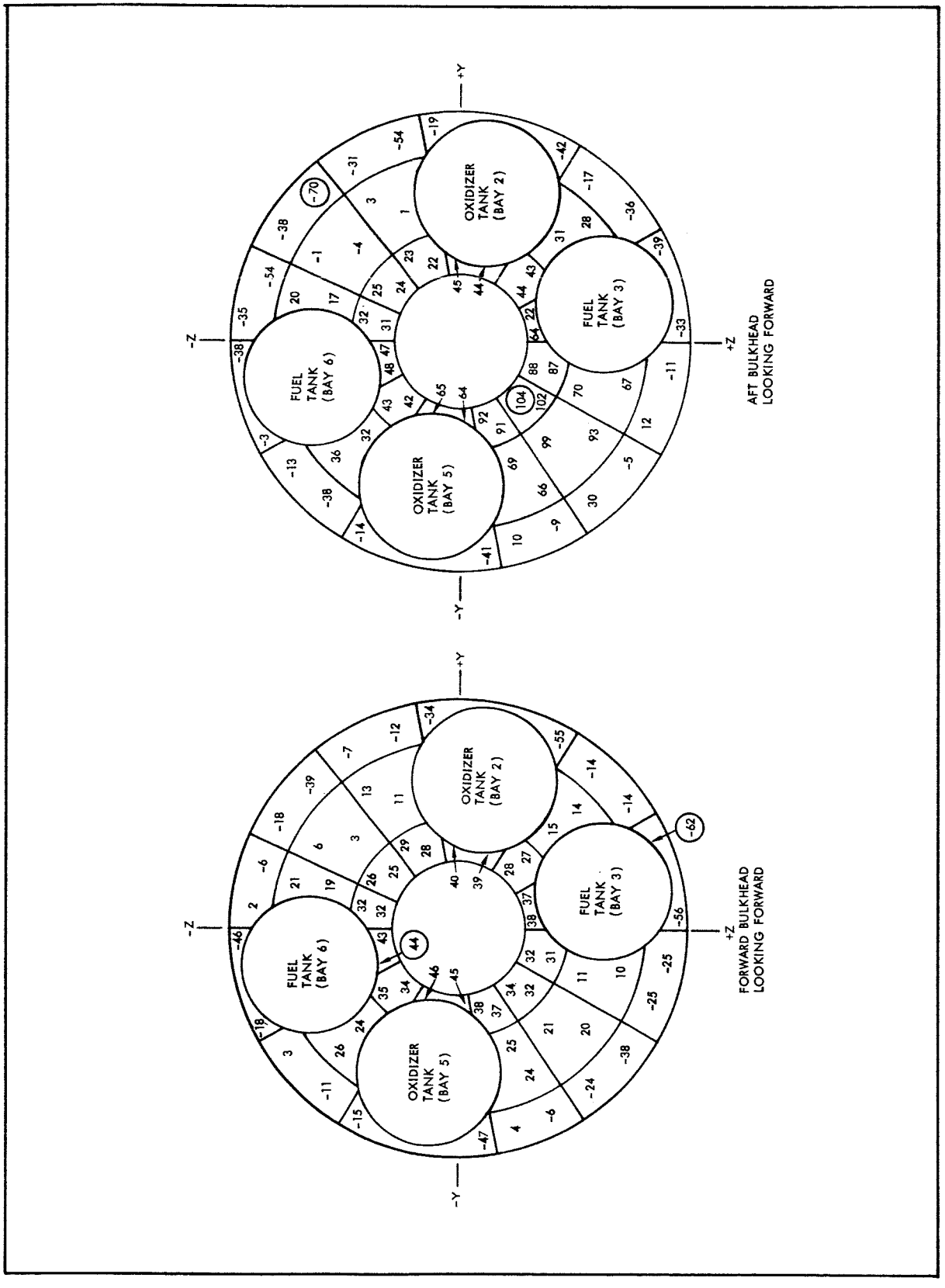

Figure 8-20 Earth Orbital Maximum/Minimum Temperatures for Bulkhead Nodes, Cold Soak

node 1093 is 1570°F, with cool down to 300°F taking 300 seconds. For node 1117 peak temperature is 770°F, and in the same cool down period (300 seconds) the temperature reaches 110°F. Figure 8-22 shows two representative temperature histories of the heat shield nodes. Nodes 1004 and 1027 are also both aligned with the +Z axis of the spacecraft and are both located on the stainless steel portion of the heat shield. Node 1004 has a good view of the nozzle extension, whereas node 1027 is on the side of the heat shield and is not in direct view of the nozzle extension. As shown in Figure 8-21, the sharp temperature rise from -20°F to 160°F for node 1004 is due to the hot nozzle extension. For node 1027 part of the temperature rise is due to orbital heating and part is due to conduction from adjacent nodes.

Propellant and Pressurization System

Although the pressurization program was not run for the Earth Orbital Mission, temperature histories and heating rates for the propellant tanks and helium bottles were obtained along with the analysis of the basic structure.

Based upon results of the detailed pressurization analysis performed for the Lunar Mission (Section VII), it was decided that such an analysis was not necessary for the Earth Orbital Mission. This conclusion results from the fact that propellant tank temperatures do not change appreciably during the course of the mission. Therefore, a detailed analysis would not yield propellant tank temperature estimates appreciably better than would the simplified analysis, in view of the excessive computer time that would be required.

In this analysis each propellant tank and its propellant are lumped together and represented by a single node that is connected to the surrouding structure by radiation and conduction resistors. For the lunar mission this method of analysis yielded temperatures which agreed with those of the detailed pressurization analysis within $\pm$ 5°F. The helium bottle and the helium gas are represented by two nodes, connected by a convection resistor. The expansion process during engine firings was assumed isentropic. For the lunar mission this method of analysis yielded a helium gas temperature history which generally agreed with that of the pressurization program analysis within $\pm$ 5°F. However, during lunar orbit insertion and transearth injection the temperature decrease of the gas was overpredicted by 40% in the simplified analysis due to an

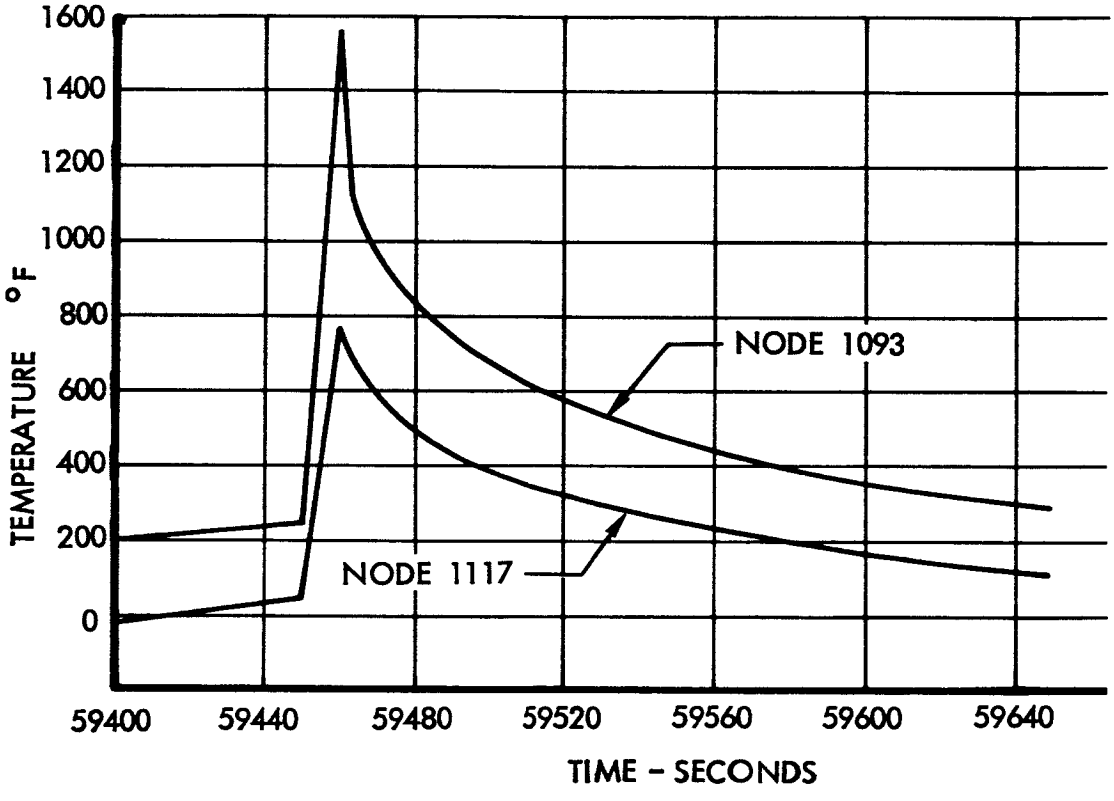

Figure 8-21 Temperature History of Nozzle Extension for 12-Second Engine Firing

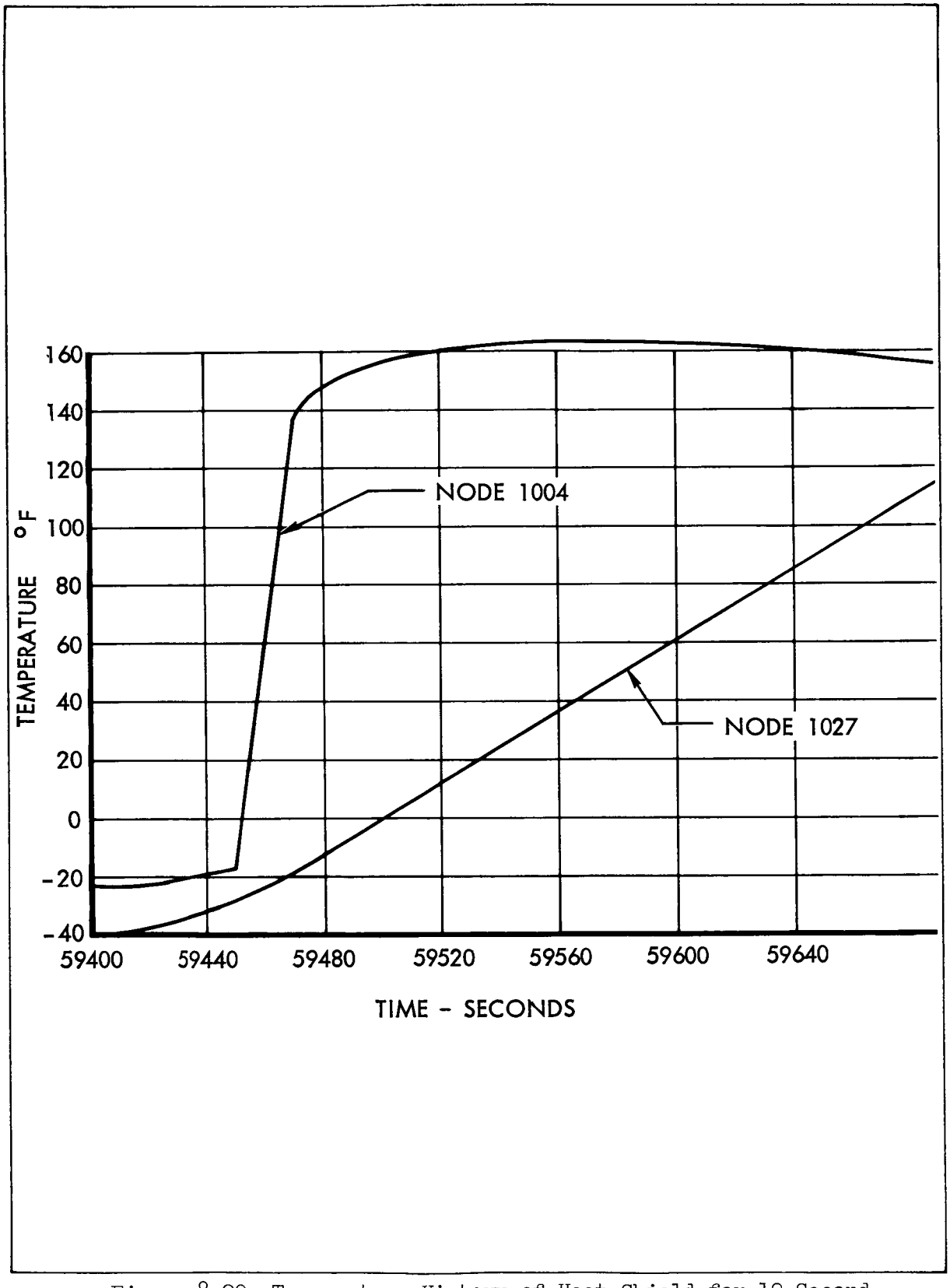

Figure 8-22 Temperature History of Heat Shield for 12-Second Engine Firing

erroneous assumption for the gas usage rate. The temperature histories for the bottle, however, agreed within $\pm$ 10°F so the overall results for the main analysis were unaffected. The pressurant gas usage rate for the Earth Orbital Mission was accurately known so the temperature predictions presented below should closely approximate those which would be computed by the Fluid Storage and Pressurization Program.

Helium bottle temperature histories along with helium gas temperature histories are plotted in Figure 8-23. The maximum helium bottle temperature is 70°F (assumed at launch), while the minimum helium bottle temperature is 47°F. Although this is above the minimum allowable tank temperature of 40°F, the helium gas temperature drops to 10°F due to the expansion process. The heating rate to the helium bottle is extremely small, and for most of the mission it is less than 0.002 $\frac{\text{Btu}}{\text{sec}}$.

Propellant tank temperature histories for the entire Earth Orbital Mission are shown in Figure 8-24. Nodes 200 and 600 are the Bay 2 oxidizer sump and Bay 6 fuel sump tanks respectively. Because they empty last, their temperatures do not vary much. Since their orbital environment is cooler than the launch environment, their temperatures decrease slowly from 70°F to 60°F. The temperature of node 500 (Bay 5 primary oxidizer tank) is approximately 70°F for planetary orientation, and when it empties, the temperature decreases to a minimum value of 58°F for solar orientation. Node 300 (Bay 3 primary fuel tank) is in a cooler bay than node 500 and has a steady temperature decrease that finally approaches an equilibrium value of 48°F during the last mission segment.

Heating rates for the propellant tanks are plotted in Figures 8-25 and 8-26. For most of the mission, the net heat flow is away from the tanks. The minimum heat rate is -0.1 $\frac{\text{Btu}}{\text{sec}}$ for oxidizer sump tank and occurs during the cold soak. The maximum heat rate is 0.035 $\frac{\text{Btu}}{\text{sec}}$ for the primary oxidizer tank and occurs during planetary orientation. Thus, Bay 2 provides the coolest tank environment, while Bay 5 provides the warmest tank environment. As seen from the tank temperature histories (Figure 8-24) the orbital variation in heating rates is dampened out by the relatively large thermal capacity of the propellant tanks.

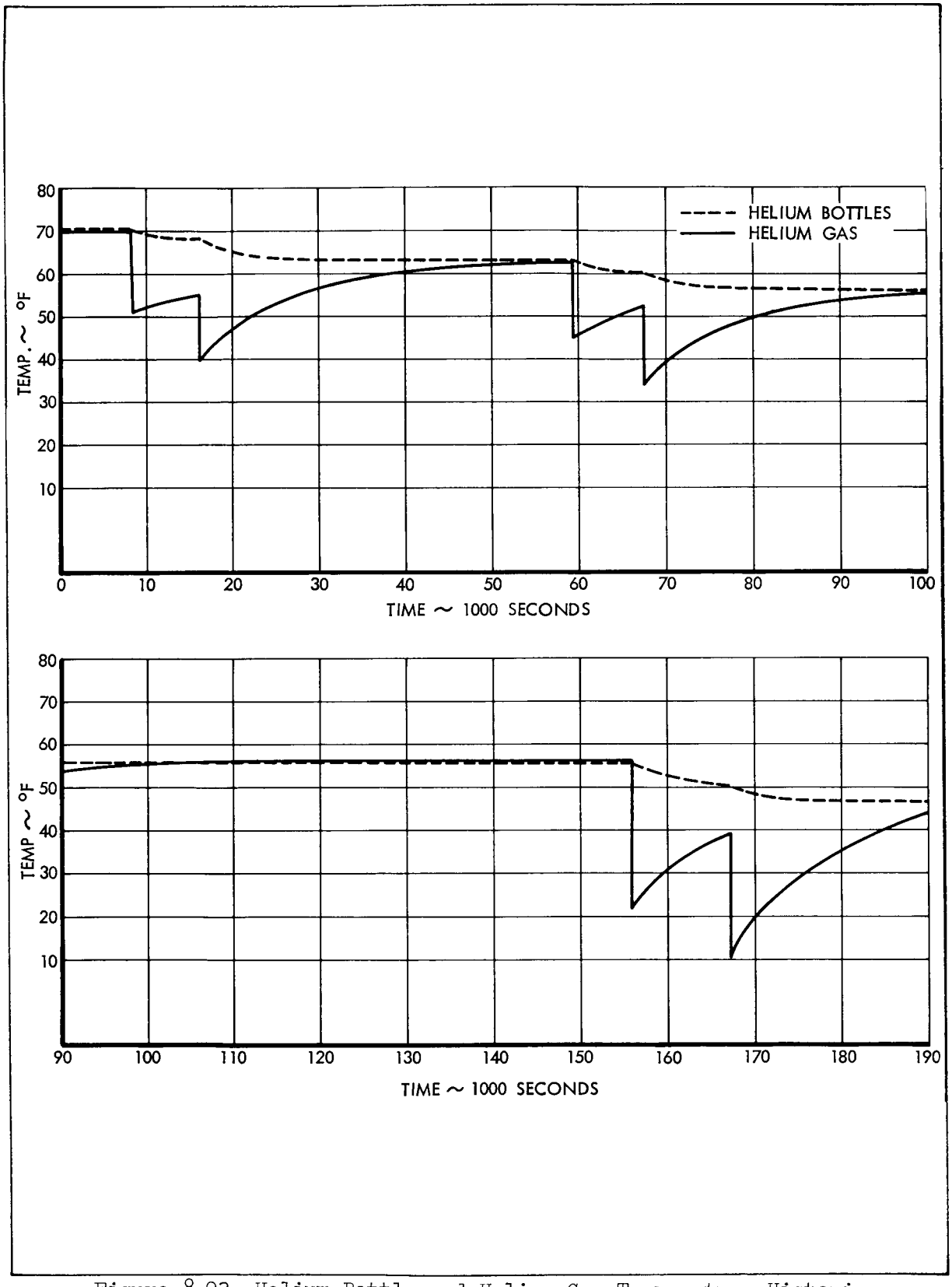

Figure 8-23 Helium Bottle and Helium Gas Temperature Histories

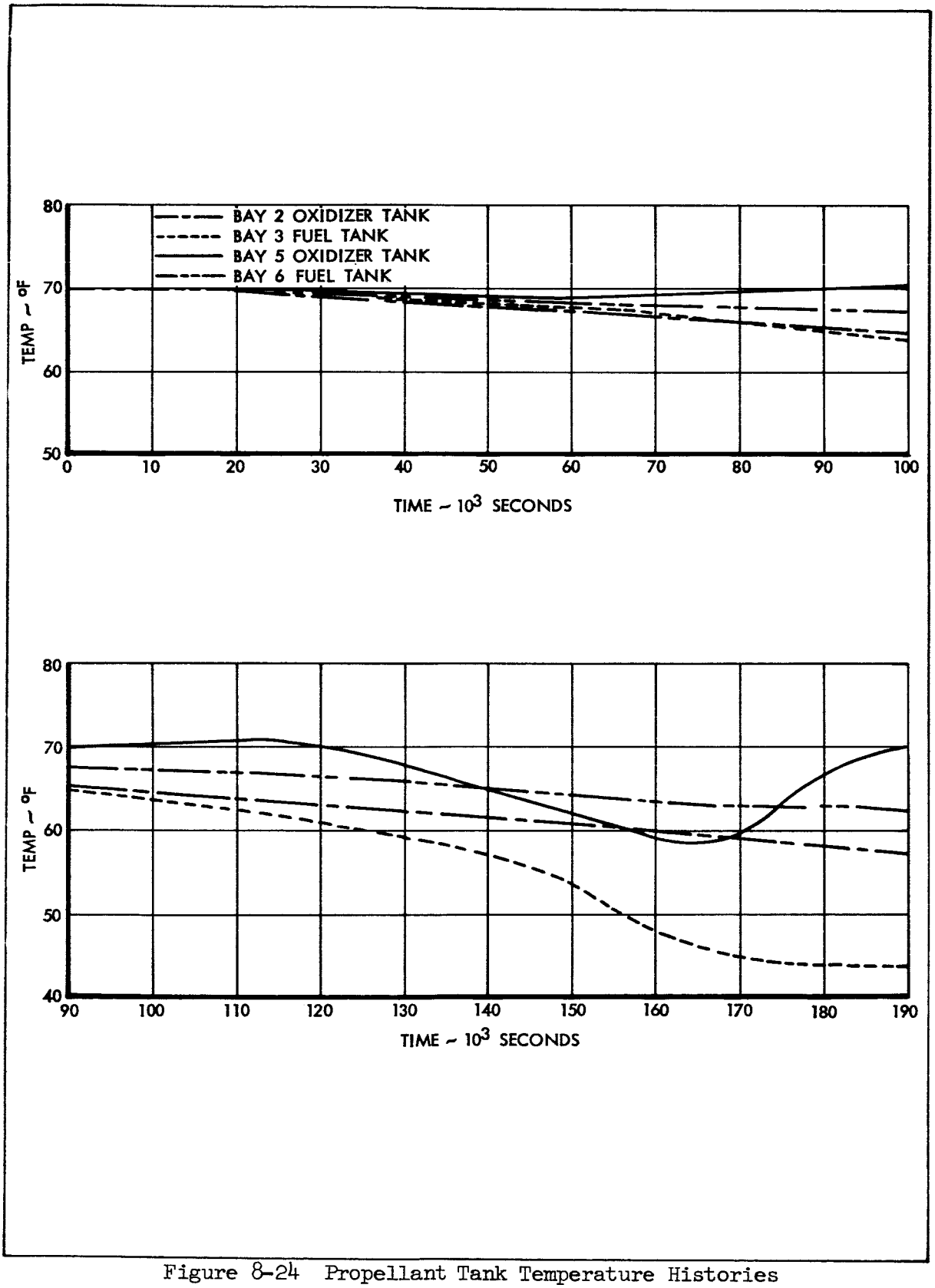

Figure 8-24 Propellant Tank Temperature Histories

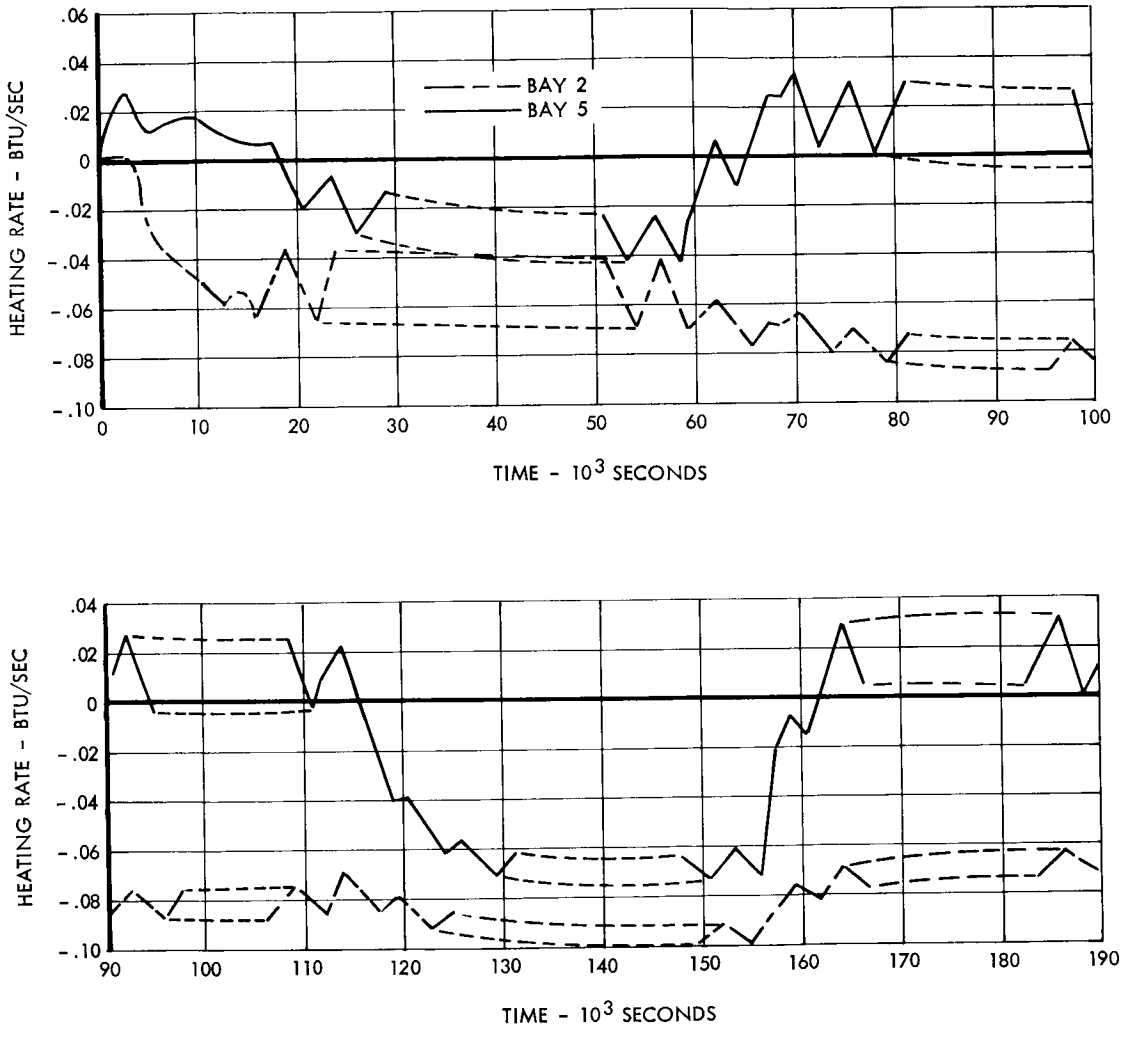

Figure 8-25 Oxidizer Tank Heating Rates

LOCKHEED
CALIFORNIA COMPANY

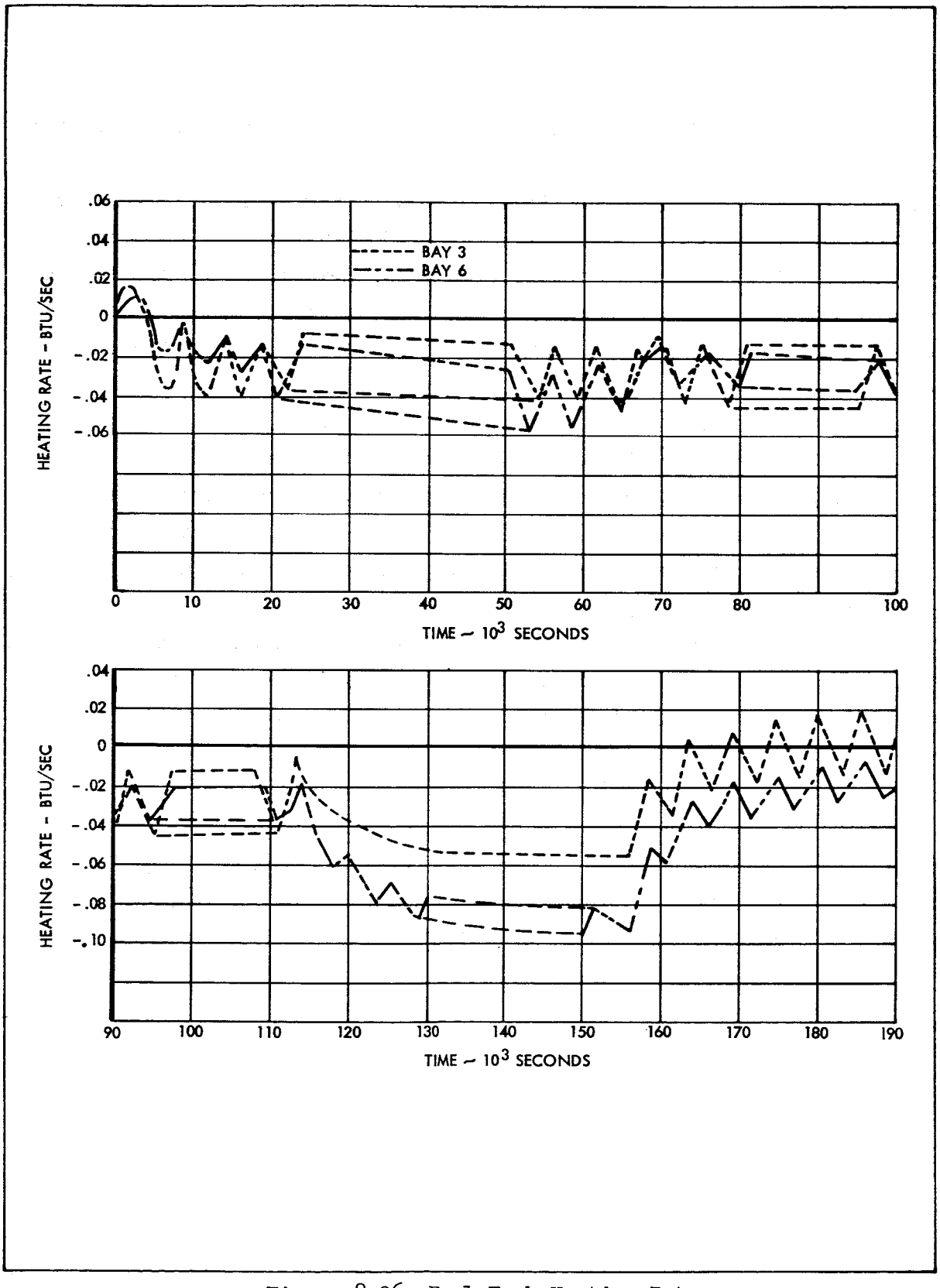

Figure 8-26 Fuel Tank Heating Rates

Detailed Analysis of SPS Plumbing

The Earth Orbital plumbing analysis was performed in the same manner as the Lunar Rendezvous Mission (Sect. VII) except for one important difference-insulation is not present on the beams in Bay 4. It is removed so that fuel cell heat may more easily escape from the bay. Changes in the network are the addition of radiation resistors from the plumbing to beam 3 and the modification of the resistors to the fuel cell. Removal of the insulation provides a cooler environment for the critical plumbing components mounted on beam 4, and consequently these components run from 60° F to 70° F cooler than they would if the bay were insulated.

Presented in Table 8-1 is a summary of the results of the plumbing analysis. In this table are listed the SPS components, their allowable temperature limits, their predicted temperature extremes, and the portion of the mission the limits are exceeded. As shown in Table 8-1, the components which exceed the allowable temperature limits are the helium valves and regulators, disconnect panels, and propellant feed lines beneath the bulkhead in Bay 4.

Helium pressurization components in Bay 4 reach a maximum temperature of 171° F, which exceeds the upper allowable limit by 20° F. As explained in Sect. VII, the minimum predicted temperatures could not be accurately determined because of insufficient details on these components. Their minimum temperatures were set equal to the helium gas temperature during engine firing. Shown in figure 8-27 are the maximum and minimum temperatures of the helium pressurization lines and components in Bay 4. Maximum temperature of the helium line is 196° F. This is due to heating from the fuel cell, which operates at a maximum temperature of 235° F.

Table 8-1 SPS PLUMBING ALLOWABLE TEMPERATURE LIMITS AND CALCULATED TEMPERATURE EXTREMES, EARTH ORBITAL MISSION

COMPONENTS		ALLOWABLE LIMITS (°F)		CALCULATED TEMPERATURES (°F)		PORTIONS OF MISSION FOR WHICH TEMPERATURE LIMITS ARE EXCEEDED
SPEC	ITEM	MAX	MIN	MAX	MIN	
MC 273-0020	Fill & Drain Hyd/UDMH	160	-65	*	*	
MC 273-0022	Fill Vent Disconnect N_2O_4 Tank Coupling	160	-65	*	*	
MC 273-0039	Propulsion System Flexible Connector (Fuel)	80	40	75	58	None
MC 273-0018	Fill & Drain N_2O_4 Tank Coupling	160	-65	*	*	
MC 273-0012B	Propellant-SPS-Disconnect Coupling	80	40	*	*	
MC 273-0040	Propulsion System Flexible Connector (N_2O_4)	80	40	70	59	None
MC 901-0008A	Propulsion Quanity Indicator and Mixture Ratio Control	80	40	70	59	None
——	Heat Exchanger (Bay 2) (HE)	80	-150	70	12	None
——	Heat Exchanger (Bay 6) (HE)	80	-150	70	12	None
	Disconnect Panel (Bay 2)	140	40	150	-73	All Portions
	Disconnect Panel (Bay 6)	140	40	226	122	All Portions
MC 284-0027	Helium SPS Pressure Relief Value	120	40	170	*	Planetary Orientation
MC 144-0023	System Test Point Disconnect Coupling	150	30	160	*	Planetary Orientation

Table 8-1 (continued)

COMPONENTS SPEC	ITEM	ALLOWABLE LIMITS (°F) MAX	MIN	CALCULATED TEMPERATURES (°F) MAX	MIN	PORTIONS OF MISSION FOR WHICH TEMPERATURE LIMITS ARE EXCEEDED
MC 284-0020	Helium SPS Pressure Regulator Unit	150	30	171	*	Planetary Orientation
MC 273-0009	Helium Tank Fill Coupling	80	-150	171	*	All Portions
MC 284-0018	Helium 5/8 inch Solenoid Value	150	30	171	*	Planetary Orientation
———	Propellant Feed Lines Beneath Bay IV	135	40			Planetary Orientation and Solar Soak

*See Text for Explanation

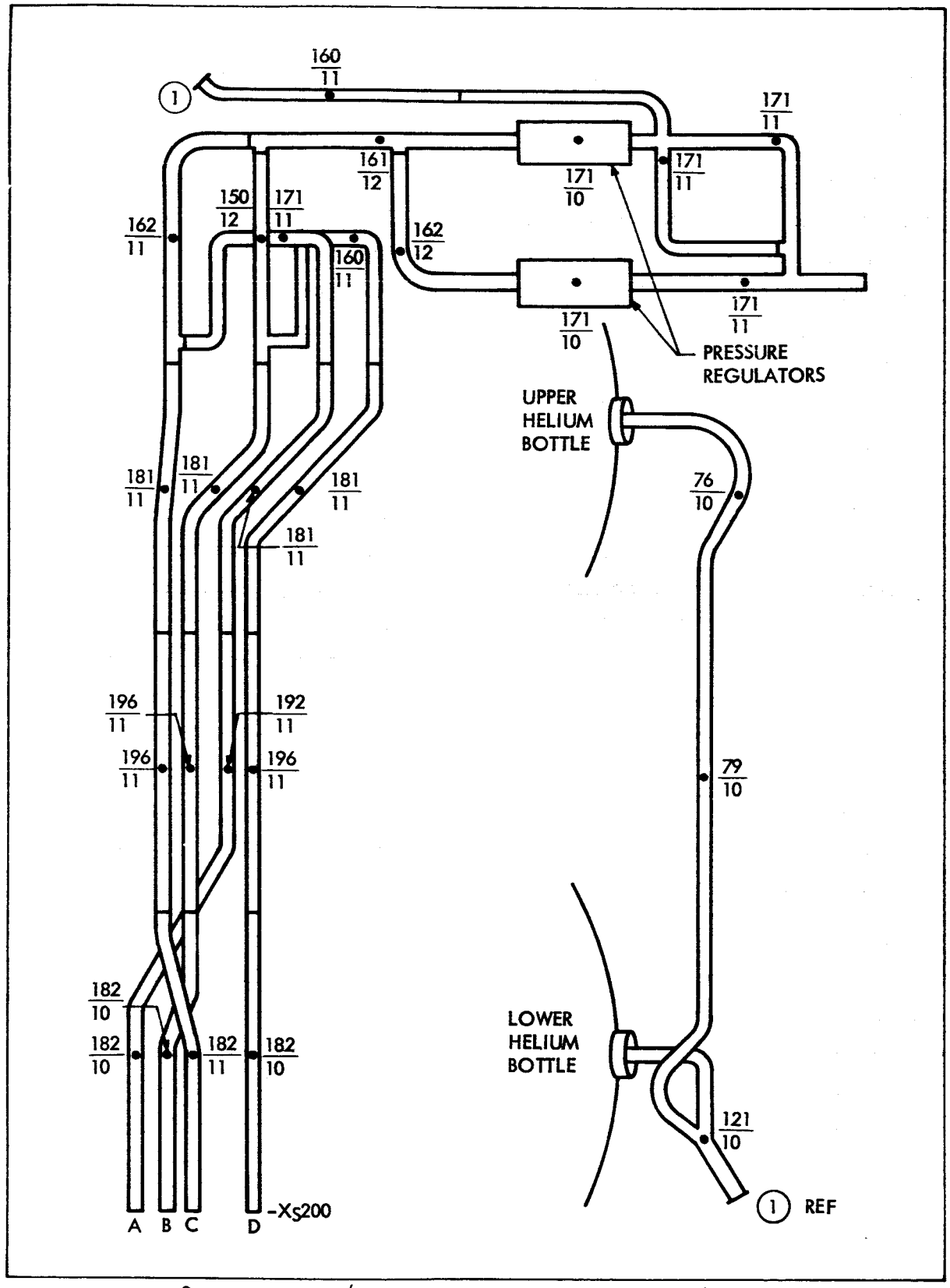

Figure 8-27 Maximum/Minimum Temperatures of Bay 4 Helium Lines and Components

LOCKHEED CALIFORNIA COMPANY

The disconnect panel located on Sector 2 of the aft bulkhead achieves a maximum temperature of 150° F, which exceeds the allowable limit by 10° F, and a minimum temperature of -73° F, which is below the allowable limit by 100° F. The disconnect panel located on Sector 6 achieves a maximum temperature of 226° F, which exceeds the allowable limit by 80° F, and a minimum temperature of 122° F, which does not exceed the minimum limit of 40° F. Shown in figures 8-28 and 8-29 are the temperature histories of the disconnect panels. As seen in figure 8-28 the temperature of the disconnect panel on Sector 2 runs about -50° F for the solar orientation orbits, and -70° F for the planetary orientation orbits. The disconnect panel temperature on Sector 6, however, runs about 130° F for solar orientation, and 210° F for planetary orientation. The maximum temperature occuring during planetary orientation is caused primarily by solar heating.

Maximum and minimum temperatures of the plumbing lines protected by the heat shield are shown in figure 8-30. Except for lines under the fuel cell bay, maximum temperatures do not exceed 85° F, however, below Bay 4 maximum temperatures are 130° F to 150° F because the aluminized mylar insulation on the inner surface of the heat shield causes these propellant lines to follow the temperature of the aft bulkhead which is heated by the fuel cell. The maximum allowable line temperature is 135° F and is exceeded in this region. Figure 8-31 shows a temperature history of a representative plumbing node beneath Bay 4. When fluid flows through the lines, the temperature of the lines are set equal to the fluid. Hence, there is a sharp drop in temperature during an engine firing.

The conclusions which can be drawn about the basic plumbing structure are identical to those presented in Section VII for the Lunar Orbit Rendezvous Mission. Temperatures are basically well behaved except where the fuel cells affect them. Removal of the fuel cells or thermally isolating them from the aft portion of Bay 4 and the proper selection of surface finishes on the disconnect panels will alleviate the basic problems which exist in these regions.

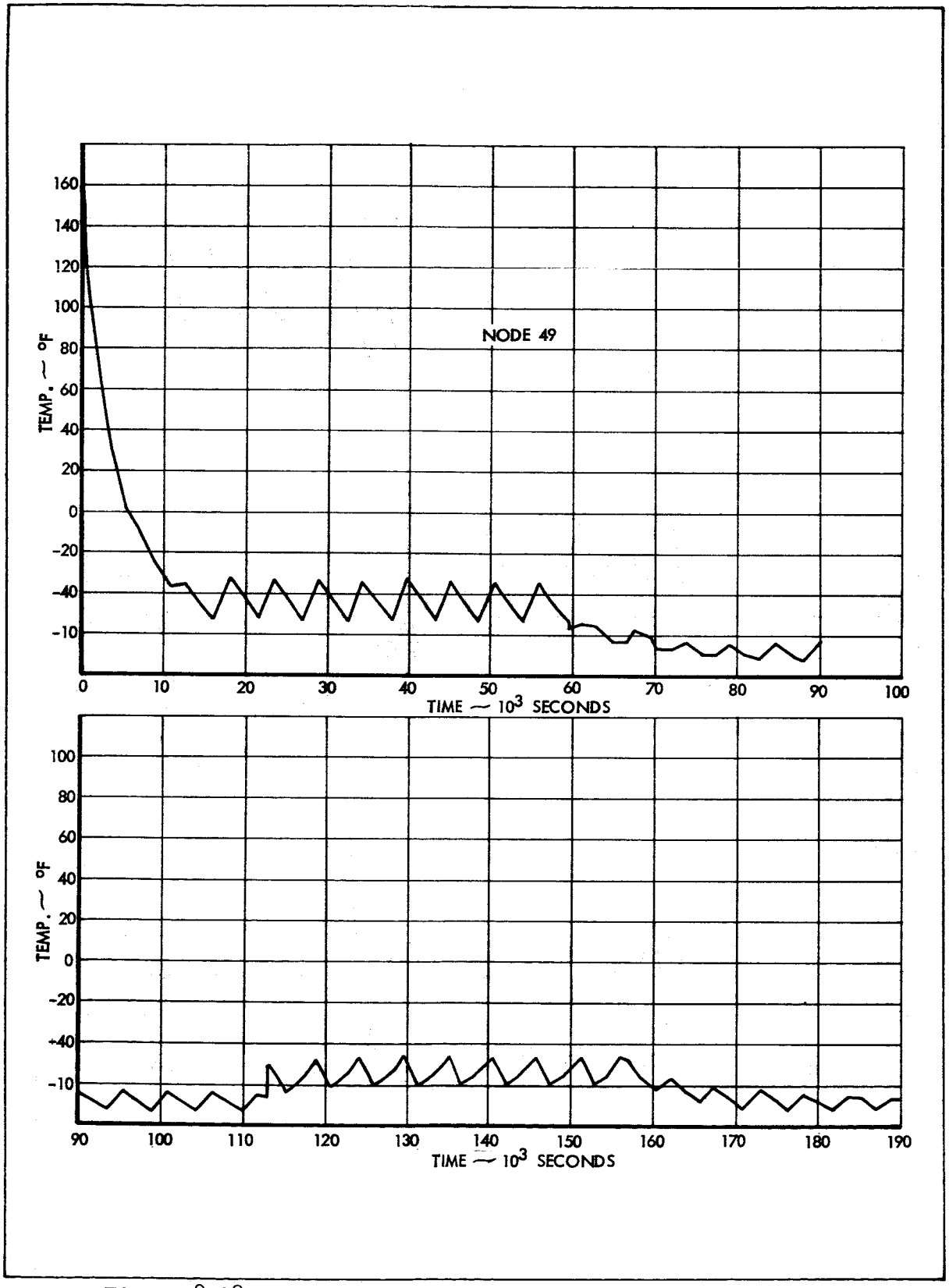

Figure 8-28 Temperature History of the Bay 2 Disconnect Panel

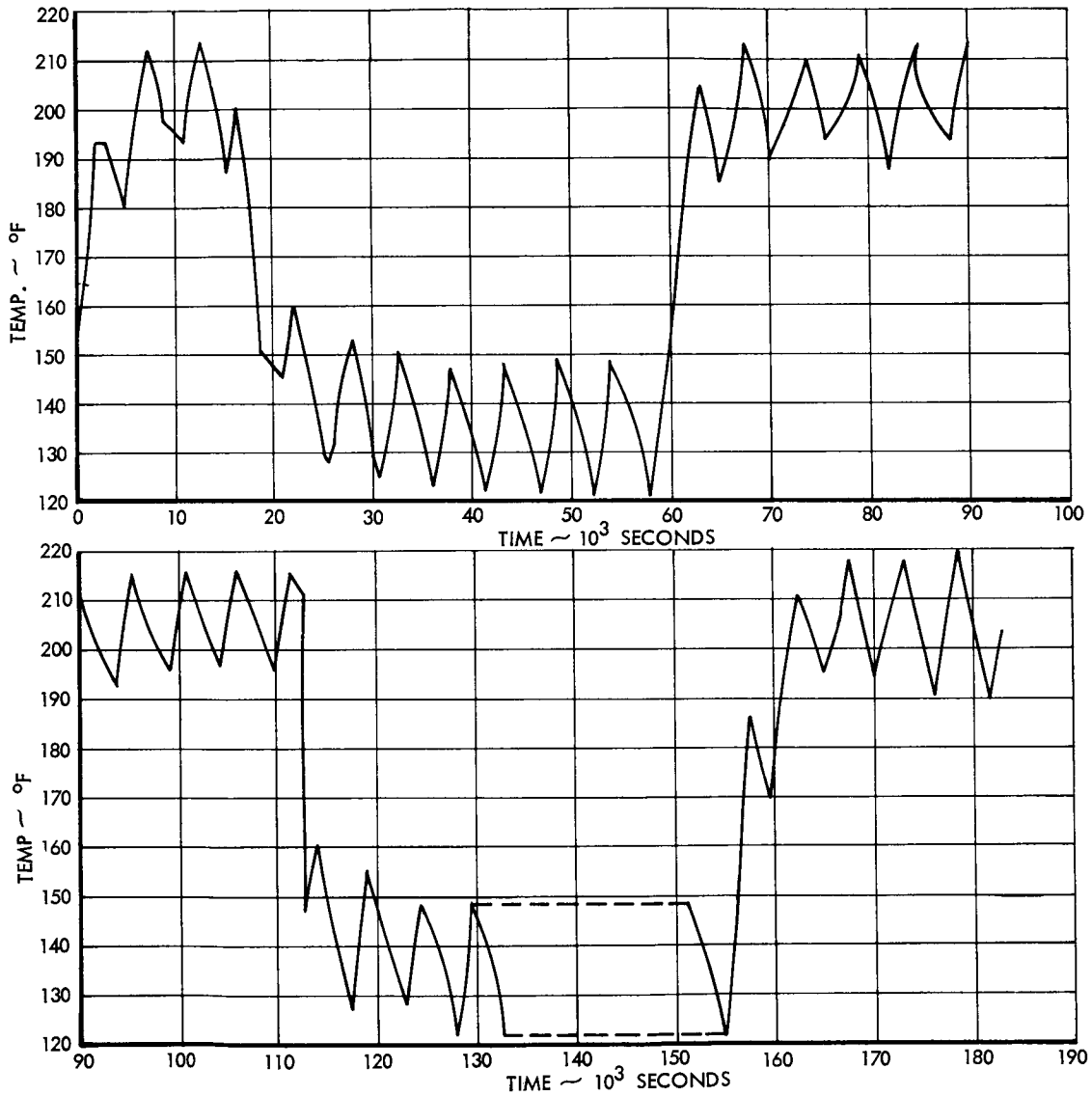

Figure 8-29 Temperature History of the Bay 6 Disconnect Panel

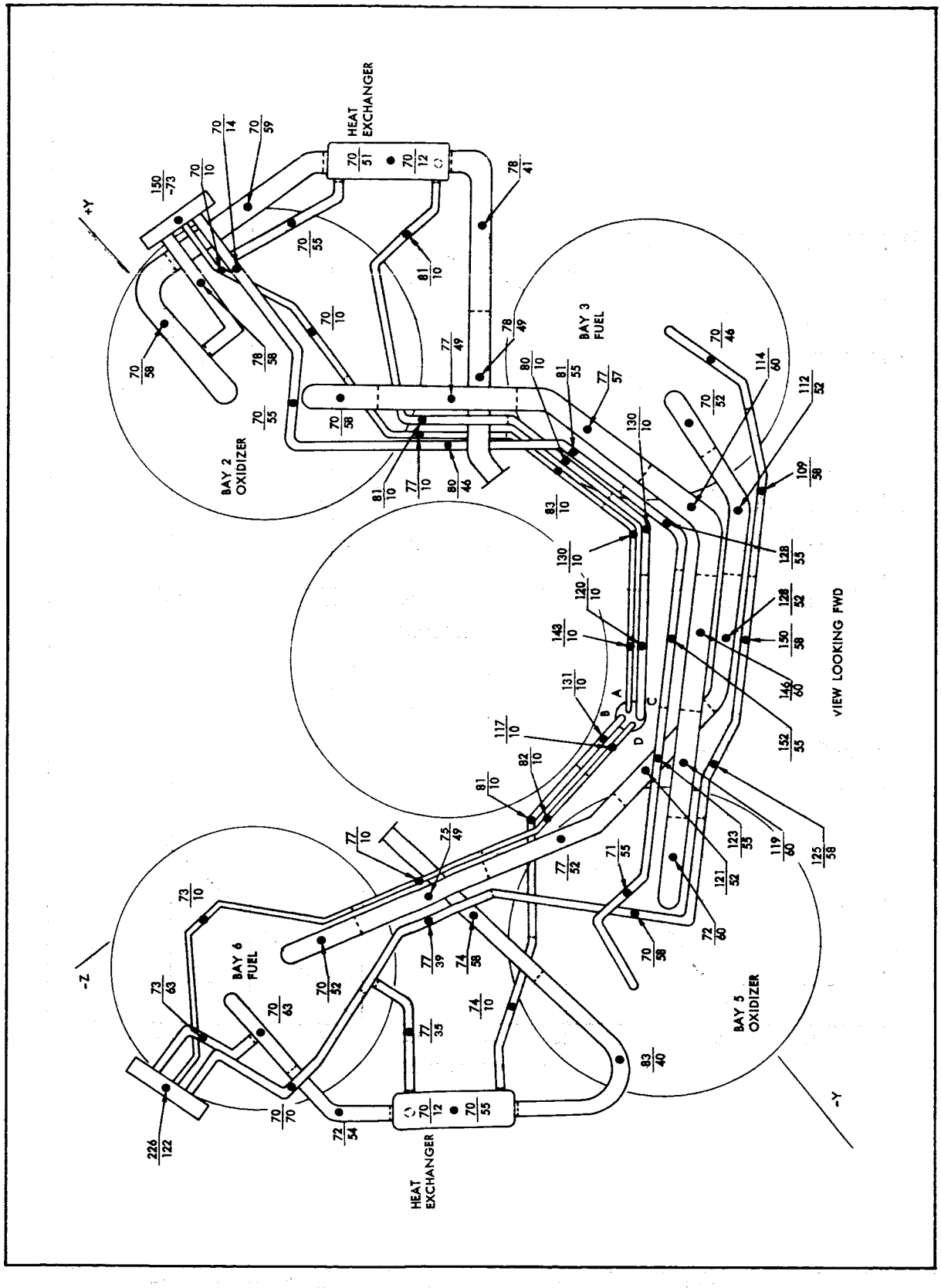

Figure 8-30 Maximum/Minimum Temperatures of Plumbing Lines Enclosed by Aft Bulkhead and Heat Shield

LOCKHEED CALIFORNIA COMPANY

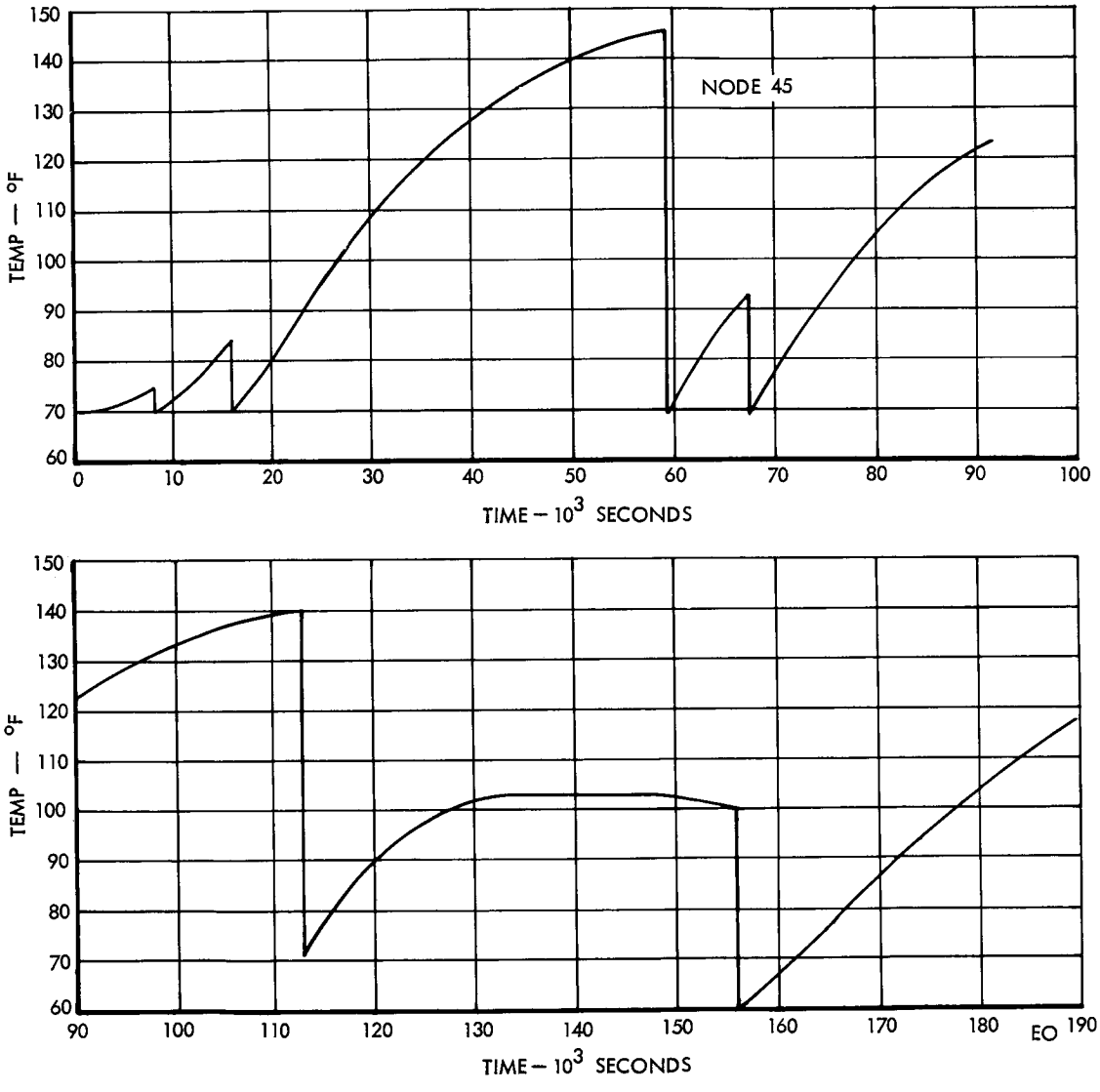

Figure 8-31 Temperature History of Oxidizer Line Beneath Bay 4

Detailed Analysis of SPS Engine

The Earth Orbital engine analysis, which is an integral part of the plumbing analysis, was also performed in a similiar manner as the Lunar Rendezvous Mission. For the Earth Orbital Mission, engine firing times ranged from 3 sec. to 21 sec. All engine firing times were assumbed to be 12 sec. because of the lack of thrust chamber data for the other firing times. As discussed in the Lunar Mission engine analysis (Sect. VII), temperatures on the interior of the thrust chamber were impressed for 200 sec. after the engine firing. In addition, during the engine firing, the valve assembly was set equal to 70° F, and the injector was set equal to 100° F. In this analysis temperatures were obtained for the thrust chamber, engine valves, engine web mounts, and gimbal ring.

Allowable temperature limits and predicted temperatures extremes of the engine components are summarized in Table 8-2.

TABLE 8-2

SPS Engine Components Allowable Temperature Limits and Calculated Temperature Extremes, Earth Orbital Mission.

Component	Allowable Limits (°F)		Calculated Temperatures (°F)	
	Max	Min	Max	Min
Injector Valve	135	40	119	70
Gimbal Actuator	140	-10	170	70
Propellant Feed Lines	135	40	211	70
Gimbal Bearing	200	-10	83	46
Ablative Chamber	140	---	200	68

The main reason some of the SPS engine components overheat is that the spacecraft provides a relatively warm thermal environment for the engine. The primary sink temperatures for the engine are the engine web mounts, which act as radiation barriers that prevent heat loss from the thrust chamber. Temperature histories of two representative engine web mounts are plotted in Figure 8-32. Node 757 runs approximately 40° F warmer than 759 because it sees the hot fuel cell. The maximum engine web mount temperature is 200° F

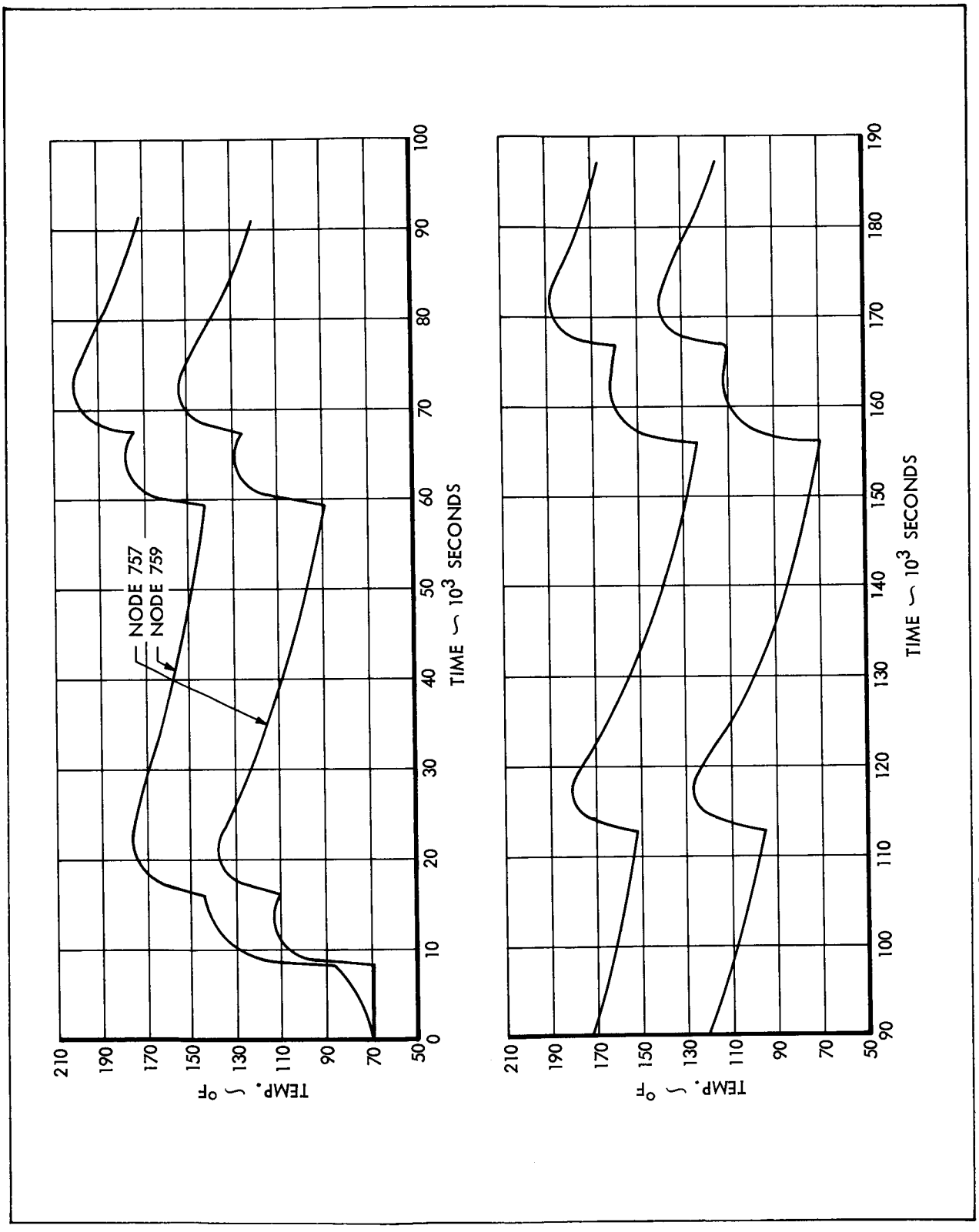

Figure 8-32 Temperature History of Engine Web Mounts

which occurs shortly after the 4th engine firing. Just prior to all but the first engine firing the average engine web mount temperature is 130° F, which is only 10° F cooler than the maximum allowable thrust chamber backwall temperature before an engine firing.

For the valve assembly the maximum temperature is 119° F and the minimum temperature is 70° F. As indicated in Table 8-2, these temperatures are within the allowable temperature limits. The engine injector, which is located between the valve assembly and thrust chamber, reaches a maximum temperature of 326° F as shown in Figure 8-33. The reason there is a large difference in temperature between the injector and the valve assembly is that 1) the injector views the inside of the thrust chamber and 2) there is a poor thermal connection, consisting primarily of radiation, between the injector and the valve assembly.

Also shown in Figure 8-33 are the maximum and minimum temperatures of the propellant and pressurization lines adjacent to the engine. These lines overheat slightly due to the high thrust chamber back wall temperature, which has an average peak temperature of 250° F. The maximum predicted temperature for these lines is 211° F, while the maximum allowable temperature is 135° F. Also overheating is the bipropellant actuator dump line that runs parallel to the propellant lines near the thrust chamber. This line reaches a maximum temperature of 238° F and has a maximum allowable limit of 135° F preceding firing. Figure 8-34 shows the temperature history of the hottest node on the bipropellant actuator dump line. The shape of this curve is representative of all plumbing nodes adjacent to the engine except that the propellant lines are set equal to their fluid temperatures during firing. Minimum allowable temperature limits are not exceeded by any of the SPS engine components.

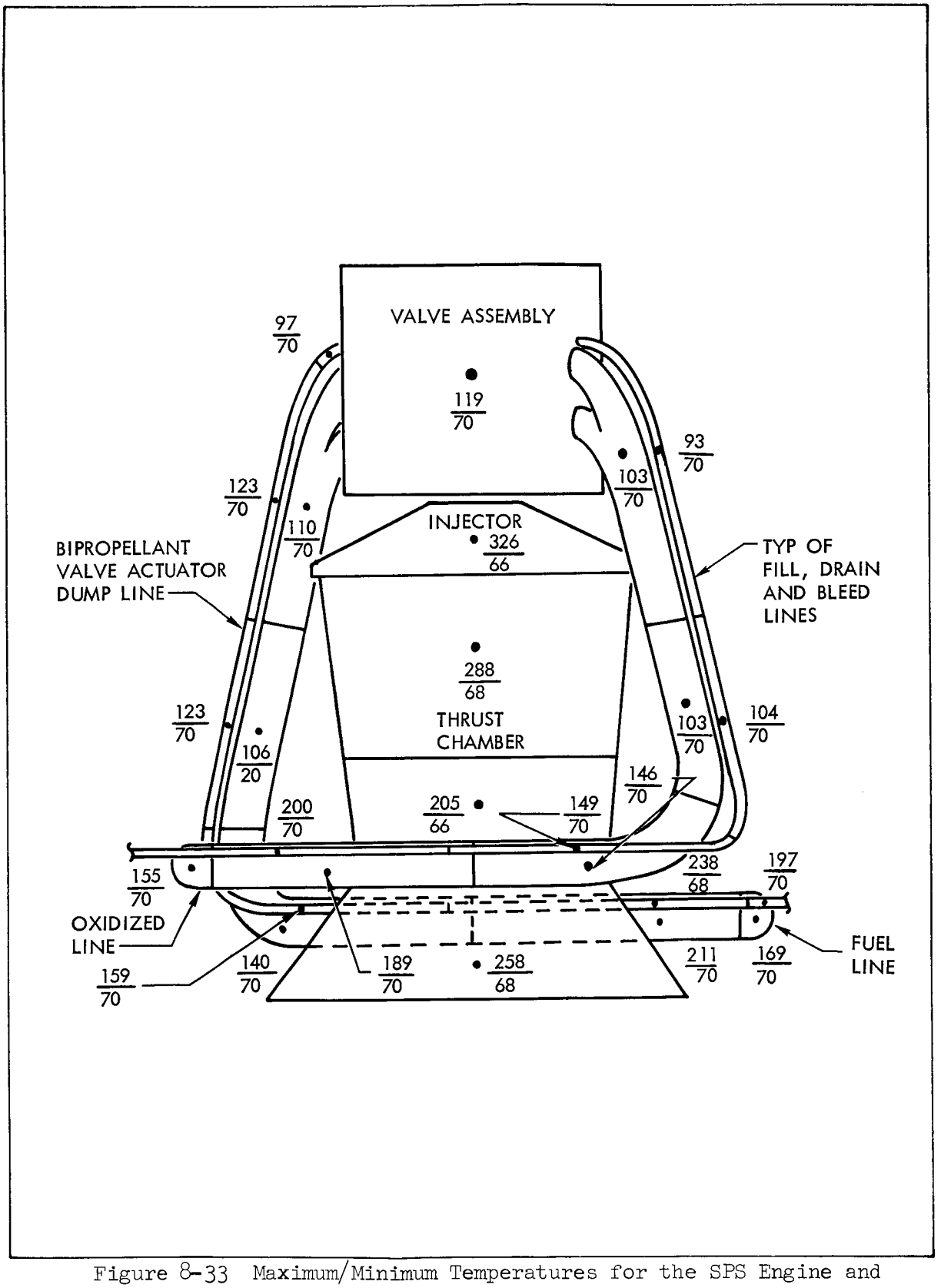

Figure 8-33 Maximum/Minimum Temperatures for the SPS Engine and Adjacent Lines

LOCKHEED CALIFORNIA COMPANY

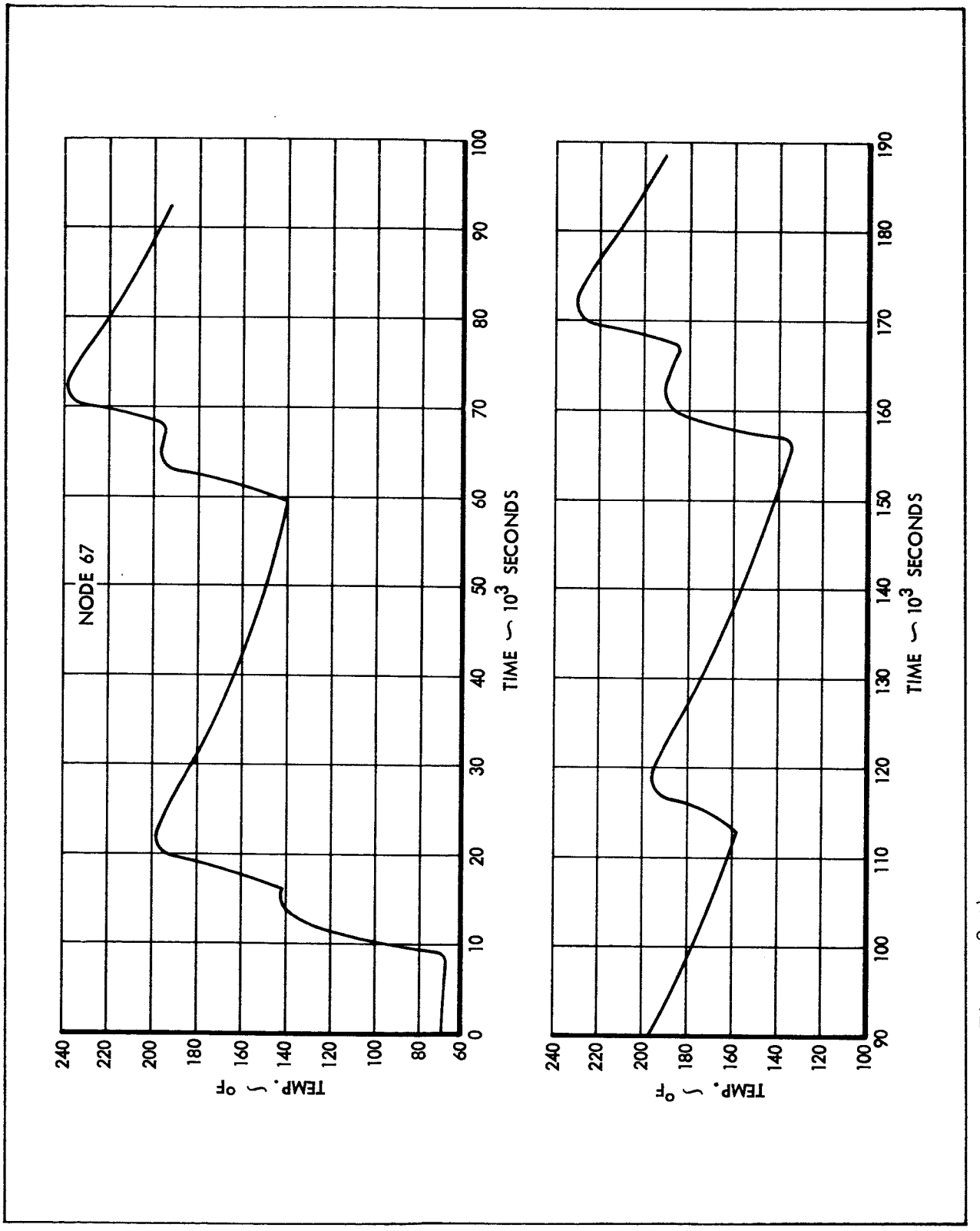

Figure 8-34 Temperature History of Bipropellant Valve Actuator Dump Line

Shown in Figure 8-35 are the temperature histories of the valve assembly, injector, and thrust chamber for a typical 12 sec. engine firing. The thermal response of the valve assembly is much slower than that of the injector because the valve assembly has a relatively large thermal capacitance, and it receives a very low heating pulse from the injector. Maximum thrust chamber inner wall temperature is 3750° F which was impressed as a boundary condition. Most noteworthy in the plot of the temperature history of the thrust chamber inner wall is the sharp decrease in cool down rate 200 sec. after engine firing. This is because at that time the temperature is no longer impressed as a boundary condition which suggests that the analysis predicts a much slower cool down than the available boundary conditions. This problem is discussed in Sect. VII. The thrust chamber backwall temperature history is shown in figure 8-36. As shown in Table 8-2, the maximum allowable temperature limit for the thrust chamber backwall is specified as 140° F just prior to an engine firing, and there is no minimum allowable limit. The maximum temperature limit is exceeded by 60° F, however, because of the relatively short burn times during the Earth Orbital Mission,there is little danger of overheat after an engine firing.

Maximum and minimum temperatures for the engine gimbal assembly are shown in Figure 8-37. As indicated in Table 8-2, temperature limits are not exceeded on the gimbal bearing, however, the upper temperature limit is exceeded on the gimbal actuator. This is due primarily to the warm thrust chamber temperatures. A maximum temperature of 191° F occurs on the chamber attach support,while a minimum temperature of 43° F occurs on the engine strut.

To summarize, the SPS engine components that exceed their maximum allowable limits are the plumbing adjacent to the engine, thrust chamber backwall, and the gimbal actuator. Although there is no specified temperature limit for the injector, its temperature runs excessively high. None of the minimum allowable temperature limits are exceeded. Since the thrust chamber temperature data which was impressed during engine firings were obtained from analyses which incorrectly account for the engine environment, it is again suggested that a detailed engine network be integrated with the network generated for the surrounding structure, and the analysis rerun before design modifications are suggested.

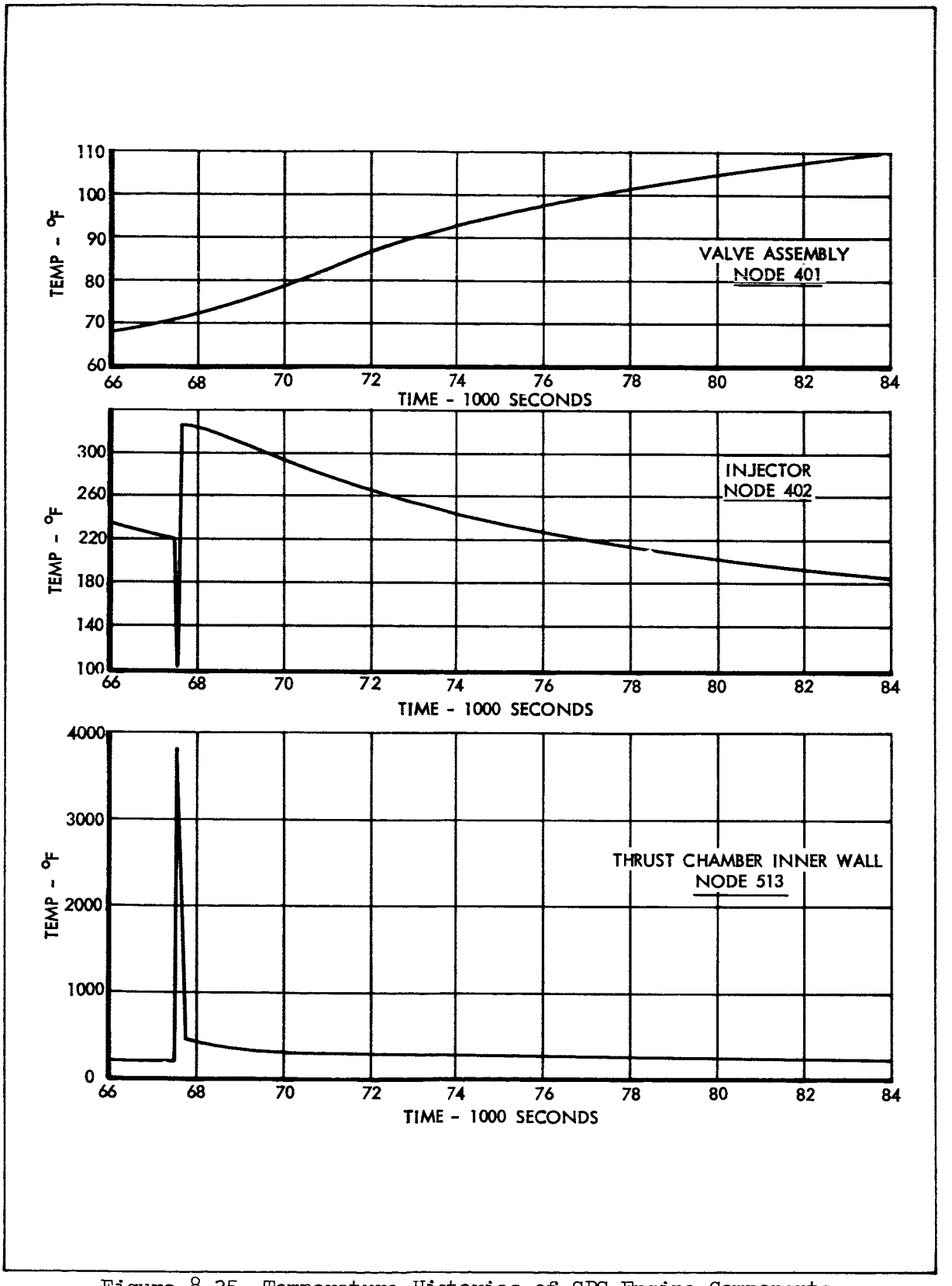

Figure 8-35 Temperature Histories of SPS Engine Components

LOCKHEED
CALIFORNIA COMPANY

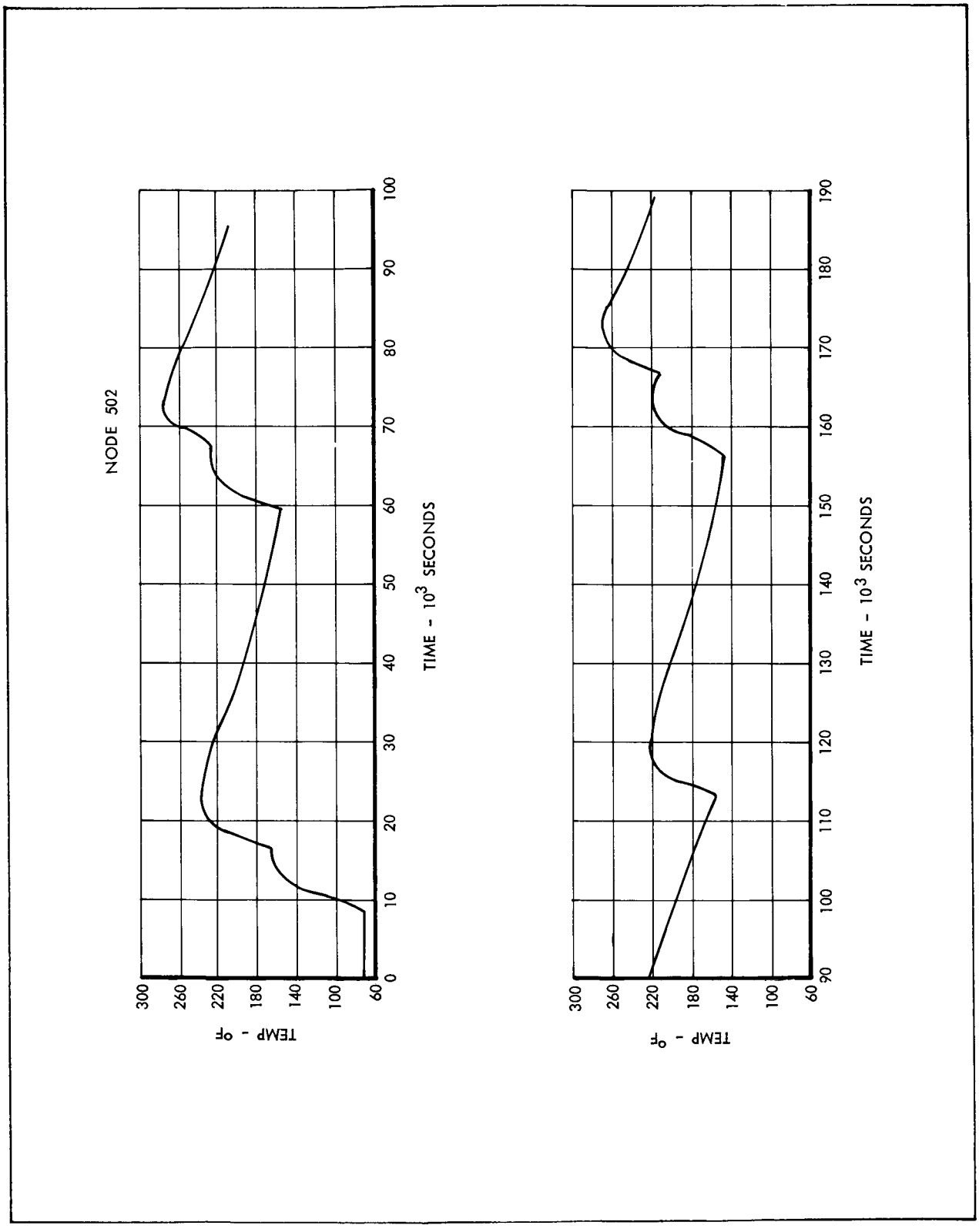

Figure 8-36 Temperature History of Thrust Chamber Backwall

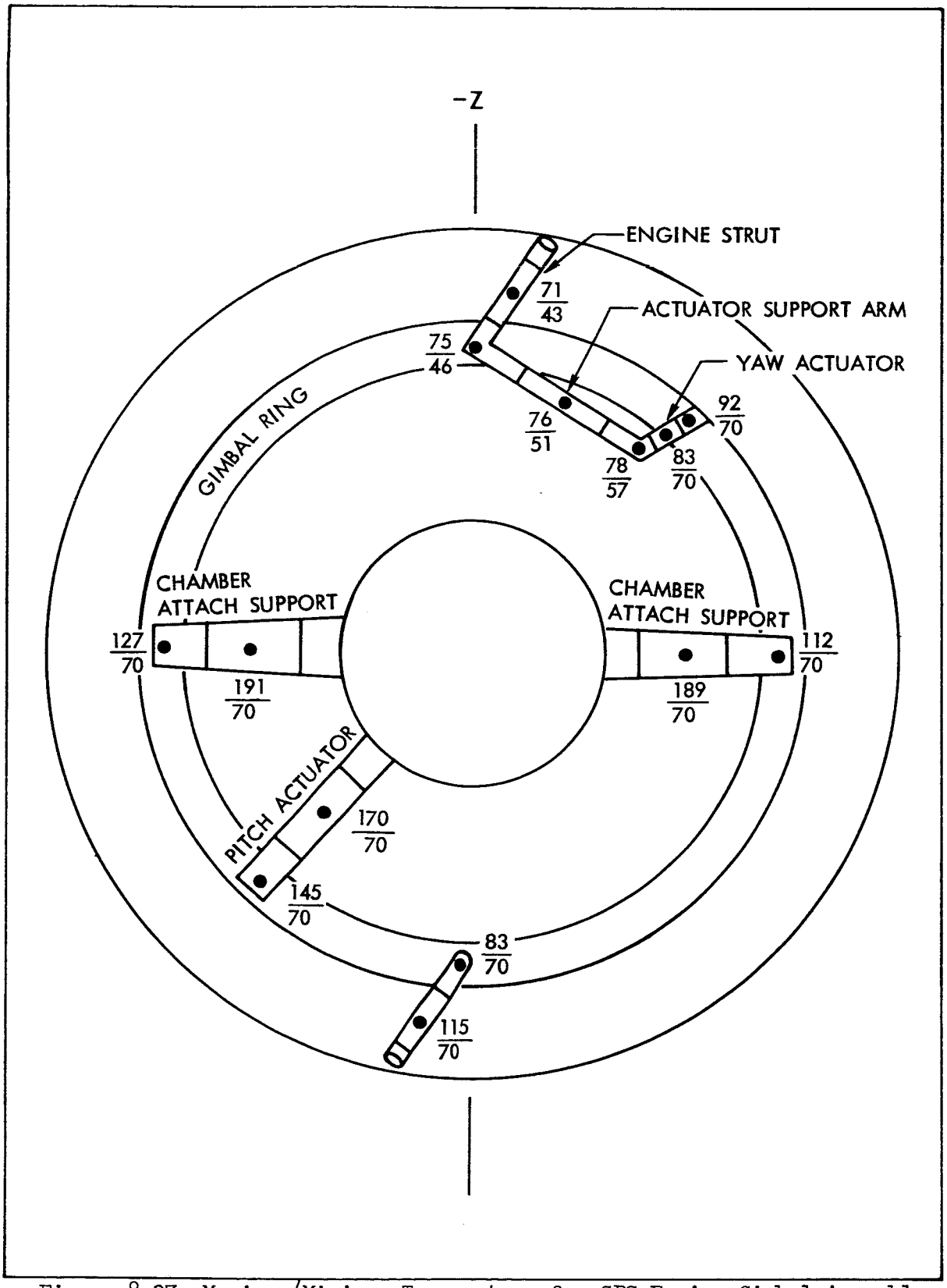

Figure 8-37 Maximum/Minimum Temperature for SPS Engine Gimbal Assembly

IX - ADDITIONAL ANALYSES

During the course of the study several side analyses were performed to justify the method of approach in specific areas. The results of one such analysis to determine the temperature gradient through the outer shell during ascent were discussed in Section V. Three additional analyses are described below.

TEMPERATURE RESPONSE OF HEAT SHIELD AND SHELL DURING RCS ENGINE OPERATION

An analysis was performed to determine the temperature response of RCS heat shields and adjacent skin nodes during RCS engine firings. The heat flux distribution over the heat shield was determined by test data provided by MSC. An initial temperature of 250° F was assumed for both the heat shield and skin nodes. The thermal model used was the actual SM network around the RCS package in Bay 2. Figure 9-1 shows the maximum temperatures as a function of engine firing duration. Although the temperatures of heat shield nodes increase by several hundred degrees, the maximum shell temperature rise is only 30° F for a 60 sec engine firing. Figure 9-2 shows the temperature response of heat shield and shell nodes for a 15 sec burn and subsequent soaking. The maximum heat shield temperature rise is 190° F. The shell temperatures increased by 5° F to 12°F, depending on their location with respect to the nozzle. Since the maximum projected RCS engine firing duration is only 15 sec, it was concluded that RCS engine operation has a negligible effect on the thermal performance of the SPS, and was therefore not considered in the study.

TEMPERATURE GRADIENTS THROUGH THE OUTER SHELL

A transient thermal analysis was conducted to determine the temperature gradient through the shell honeycomb panels during the translunar roll, to justify the lumping of the facing sheets and core into a single node for the basic analysis. The thermal model used in the investigation was a portion of the outer shell with the inner and outer skins connected by a conduction resistor. The effective conductivity of the core was 8 Btu in/hr ft^2 °F, based on MSC supplied test data. The inner skin was radiating to a 70°F sink through 40 layers of aluminized Mylar insulation. The outer skin was exposed to the

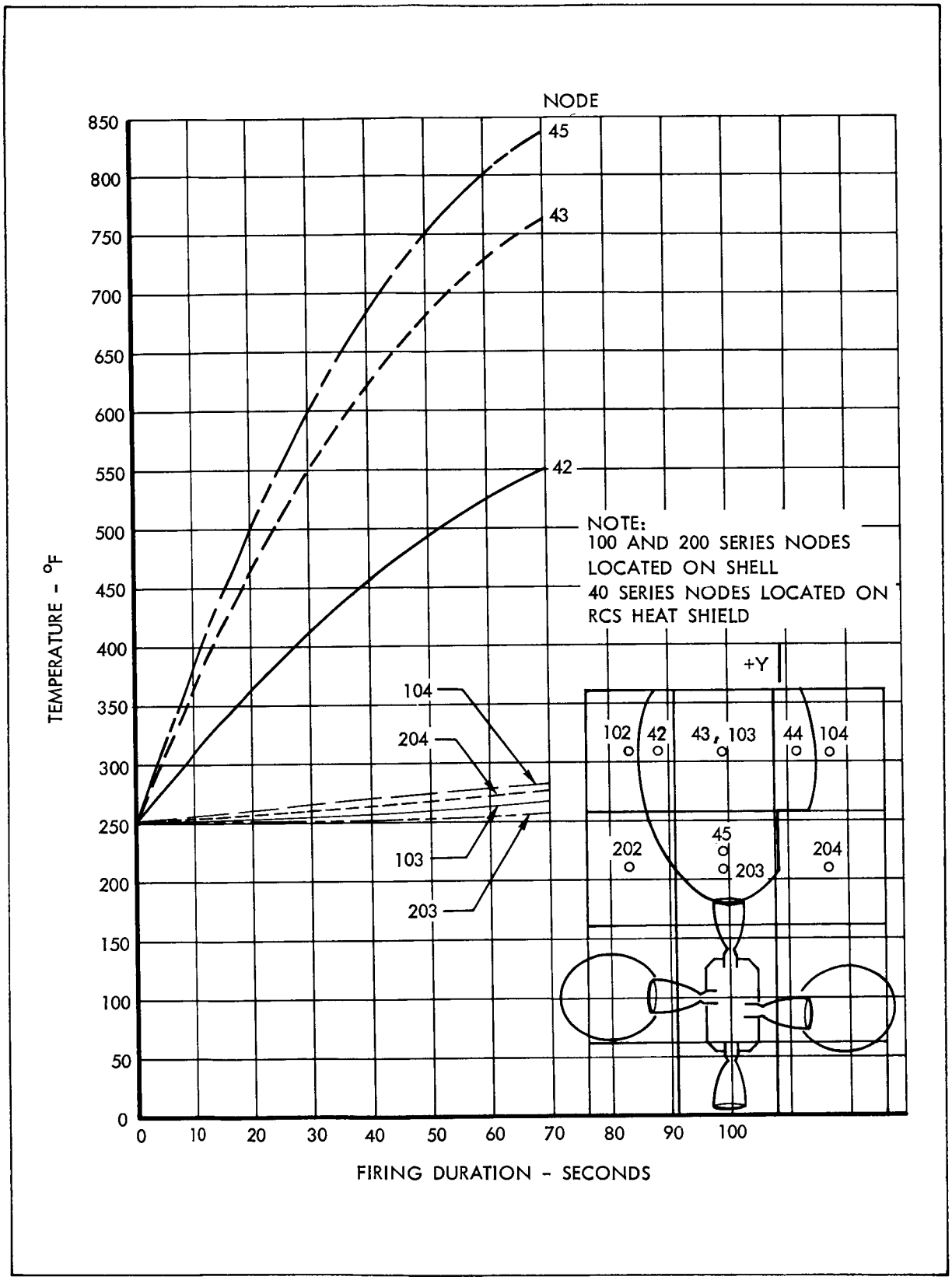

Figure 9-1 Maximum Skin Temperatures for RCS Heat Shield and Shell During RCS Firings

LOCKHEED CALIFORNIA COMPANY

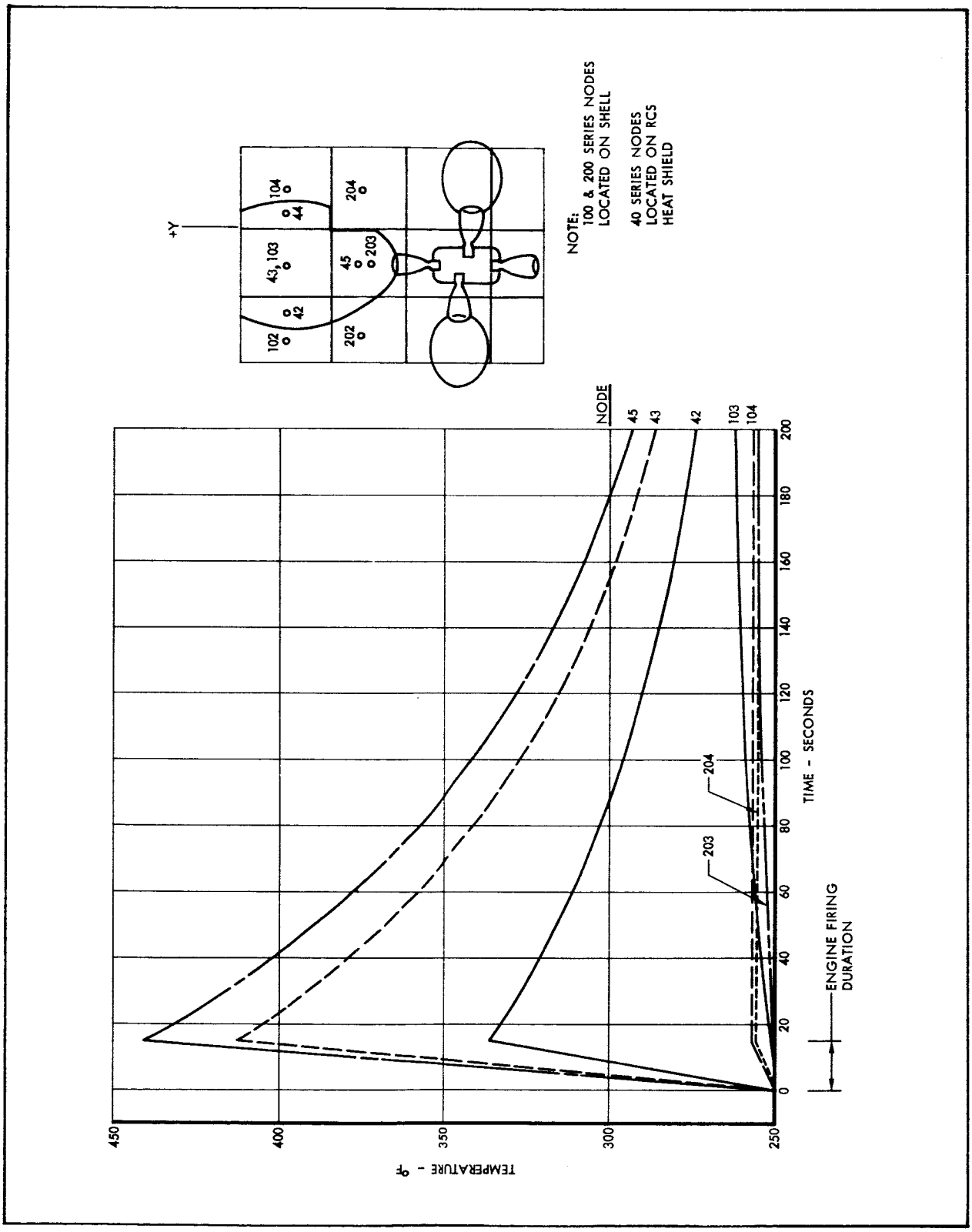

Figure 9-2 Maximum Skin Temperatures for RCS Heat Shield and Shell for 15-Second Engine Firing

sinusoidal translunar solar heat pulse, and was radiating to space. The roll rate was one revolution per hour (this was one of the study ground rules in effect at the time of this analysis). The transient temperature response of the inner and outer skins is shown in Figure 9-3. Although the skin temperature cycles over a 250° F range, the gradient through the skin never exceeds 6° F. The single node representation for the shell was therefore completely justified since this small discrepancy has no effect on the thermal performance of the SPS.

TEMPERATURE RESPONSE OF THE THRUST CHAMBER EXTERIOR

In the basic network, the thrust chamber was to be represented as a heat source, using external surface temperatures computed by MSC. The data provided, however, were terminated at the time of maximum external surface temperatures following each engine firing. Since the thrust chamber is a significant heat source, an additional transient thermal analysis was performed to extend these data to include the temperature decay. A relatively coarse one-dimensional thermal network was generated for each of three longitudinal stations. The initial temperature distributions through the chamber walls were based on the MSC data for the time of maximum external surface temperature. It was assumed that the outer surface nodes were radiating to a sink temperature of 80°F with an emissivity of 0.7, the same values used in the MSC analysis. The temperature decay at the three longitudinal stations was computed for the 12 sec., 120 sec., and 320 sec., engine firings. Each run was terminated after 10,000 sec. Figure 9-4 shows the resulting surface temperature-time history at the throat. This curve represents the MSC data for the time of engine firing to the time of maximum temperature, the Lockheed analysis for the next 10,000 sec., and an extrapolation back to 80° F. This and two similar curves were input to the Thermal Analyzer Program to represent the thrust chamber during the entire Lunar Orbit Rendezvous Mission. In lieu of precise data, the temperature response for the 3 sec. firings was assumed to be identical to that of the 12 sec. firing.

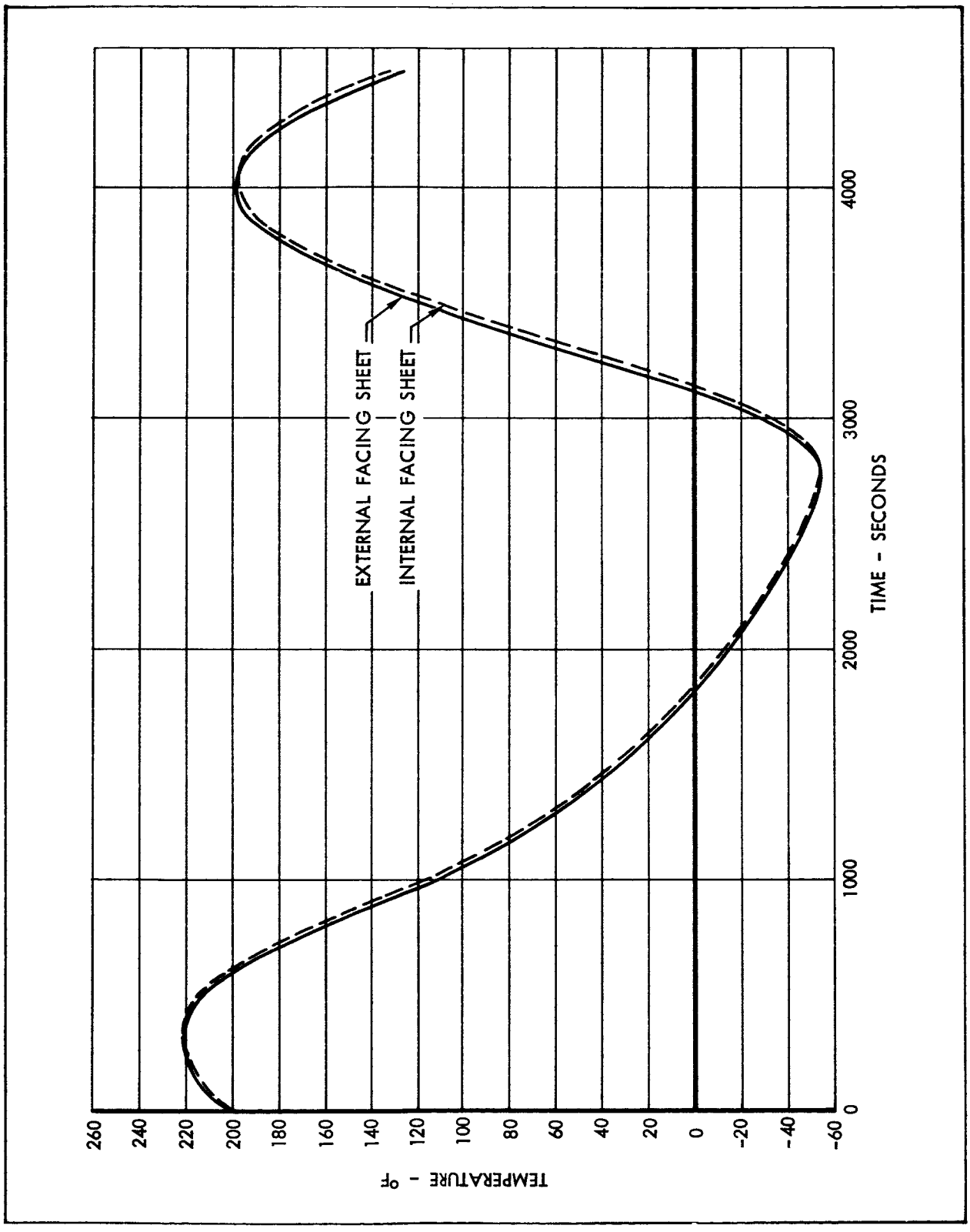

Figure 9-3 Predicted Temperature Response for SM External Shell Facing Sheets

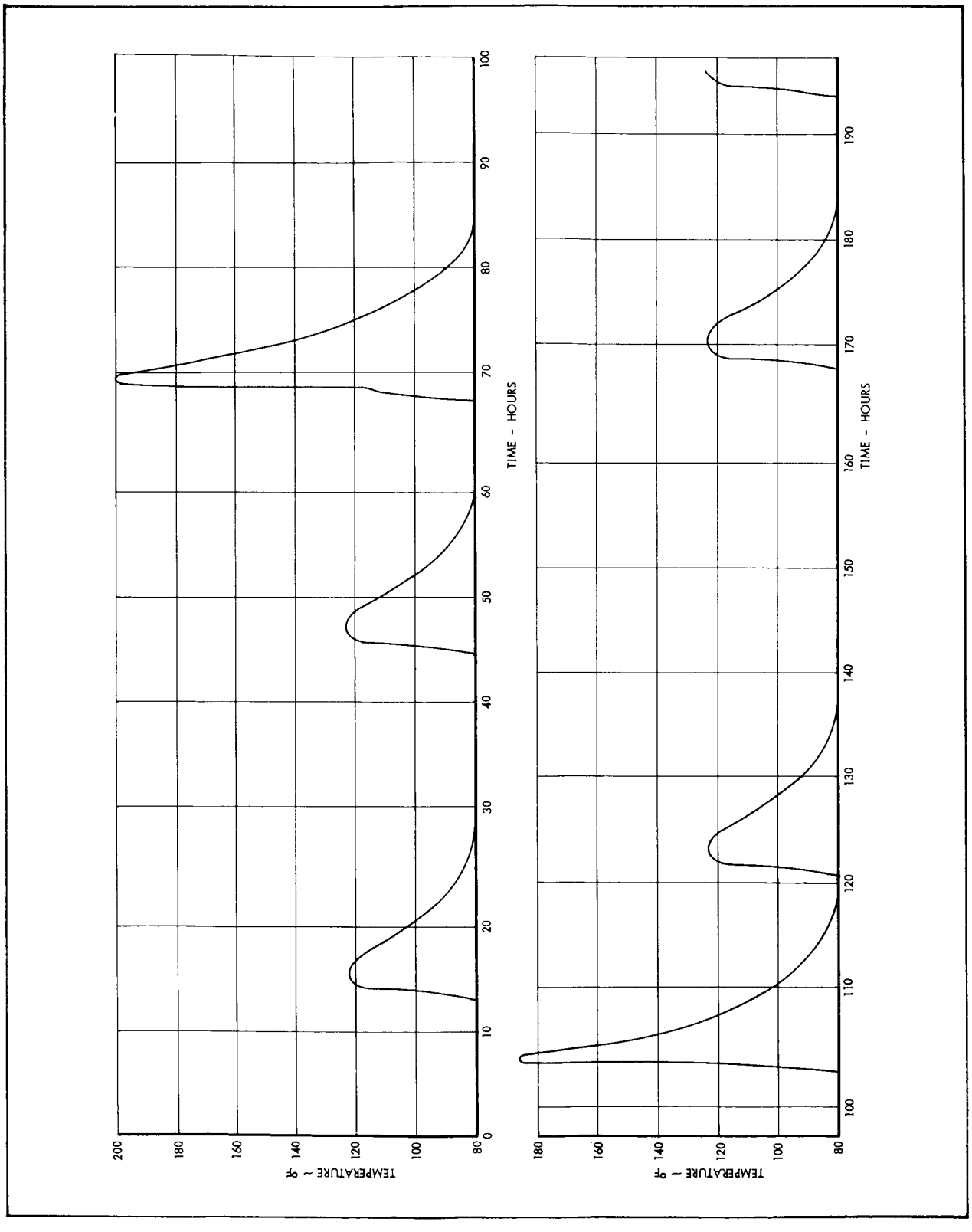

Figure 9-4 Temperature History for the Thrust Chamber External Surface at the Throat

X - CONCLUSIONS

The following conclusions are reached as a result of the transient heat transfer and the thermodynamic analysis of the Apollo Service Module Propulsion System performed for the Lunar Orbit Rendezvous, Earth Suborbital and Earth Orbital Missions:

1. The thermal design philosophy of the Apollo Service Module is basically sound. The liberal use of lightweight super-insulation, the heavy thermal mass of the propellant tanks, and the selected surface finishes effectively control the general SM temperature level.
2. The temperature of several SPS components exceed their prescribed limits during the Lunar Orbit Rendezvous and Earth Orbital Missions. These components are in the vicinity of the fuel cells and the SPS engine thrust chamber.
3. The fuel cells are a very significant heat source for the SM and are largely responsible for every over-temperature problem discovered. The moving of the fuel cells to their forward Block II location should eliminate or reduce the over-temperature problems.
4. The only SPS components which experience unacceptably low temperatures during the Lunar Orbit Rendezvous and Earth Orbital Missions are the propellant disconnect couplings adjacent to the disconnect panels.
5. No SPS thermal problems were found for the Earth Suborbital Mission because of the short mission duration and the absence of fuel cell operation.
6. No Thermal problems were found for the propellant storage and pressurization systems.
7. The Lunar Orbit Rendezvous Mission nominal and maximum heating orientations result in nearly identical thermal environments for the SPS engine and plumbing lines.
8. The minimum heating orientation results in unacceptably low temperatures on all plumbing lines and associated hardware in the aft bulkhead region.

9. A major problem in performing an accurate thermal analysis of the SM is the proper accounting of radiation interreflections between the highly reflective internal surfaces. In general, the more accurate techniques, such as the radiation networks of Hottel and Oppenheim, cannot be employed due to computer storage capacity restrictions. As a result, the radiation analysis must be considerably simplified.

XI - RECOMMENDATIONS

The objectives of this study were to perform a thermal analysis of the SPS, to identify possible problem areas, and to provide MSC with the thermal networks and the analytical tools necessary to perform future analyses. Providing a positive solution to all of the problems discovered is beyond the scope of the study and hence the following recommendations are qualitative, rather than quantitative, in nature. It should be emphasized that the fuel cell location and heat rejection both have a significant influence on the thermal performance of the SPS, and the current methods for representing the fuel cells are inadequate. No attempt should be made to extrapolate the results of the Block I analysis in an attempt to predict the thermal performance of the SPS on the Block II spacecraft. In future thermal analysis of both configurations it is recommended that the thermal networks for the fuel cells, EPS radiators, and thrust chamber be integrated with the thermal network representing the basic SM structure. This is necessary because of the thermal interrelationship among these items.

It appears that the SPS thermal problems will be more difficult to solve for the Block I configuration (Earth Orbital Mission) than for the Block II configuration (Lunar Orbit Rendezvous Mission). If the assumed fuel cell heat rejection (750 Btu/hr) is realistic, most of the plumbing lines will exceed their prescribed temperature limits. A possible solution is to insulate the aft bulkhead and engine web mount in Bay 4, and to remove part of the super-insulation covering the Bay 4 shell, thus affording a more direct method of dissipating the fuel cell heat and at the same time providing additional protection to the plumbing lines below the bulkhead. The propellant lines between the bulkhead and the bipropellant valves will apparently have to be insulated if their temperature is to remain below 135°F during the entire mission. An alternate approach would be to provide these lines with an extremely low surface emissivity and thereby reduce their net heat exchange with the thrust chamber and engine web mounts. Before the most efficient method of thermal control is determined, however, a more detailed analysis of the thrust chamber temperature history is required. The thermal network

constructed for the chamber in this analysis was relatively coarse. It should be noted however, that an analysis of the thrust chamber was was not a study requirement since the chamber surface temperature-time history was to be provided by NASA and used as a boundary condition for the analysis. an analysis was performed, however, when it became evident that the NASA results were inaccurate due to the assumption of an 80°F radiation sink temperature.

During the latter stages of the study, Lockheed was informed that the aluminized Mylar insulation was to be removed from the Bay 4 side of radial beams 3 and 4. The Earth Orbital Mission was analyzed on this assumption and it was discovered that the temperatures of the helium pressure regulators and val es on beam 4 were approximately 170°F, far in excess of the prescribed upper limits. This design change appears unreasonable, unless dictated by circumstances unknown to Lockheed. With the insulation there appeared to be no possibility of these components ever exceeding their temperature limits.

The unacceptably low temperatures on the propellant disconnect couplings during the Earth Orbital Mission are due to conduction exchange with the cold disconnect panels, which view deep space during most of the mission and receive little, if any, external heating. The problem can be reduced by providing a low emissivity finish, such as aluminum foil, to the exterior face of the disconnect panel. The temperatures presented here are based on a bare fiberglass exterior face with a surface emissivity of 0.8. A lower external emissivity will cause the disconnect panel temperature to be more dependent on the aft bulkhead temperature which is at an acceptable level.

As noted above, it is impossible to draw conclusions regarding the thermal performance of the Block II SPS from an analysis of the Block I spacecraft. However, it can be stated with certainty that the over-temperature problems found for the Lunar Orbit Rendevous Mission will be either reduced or eliminated by moving the fuel cells to their forward Block II location. The problem of overheating the plumbing lines in the aft bulkhead area will undoubtedly disappear since it is due almost entirely to the fuel cell. Because the periphery of the bulkhead is exposed to deep space and receives no direct

solar heating during the translunar/transearth roll, the fuel cell relocation may actually produce unacceptably low temperatures on these lines. A low emissivity coating to that portion of the bulkhead which is exposed to space will help alleviate this problem.

Appendix A

Material Properties Data

Table A-1 lists the material property values used to perform the SM thermal analyses. The data listed are density, specific heat, thermal conductivity, solar absorptivity, and emissivity. Where no value appears, the information was not required. Most of the data shown can be found in standard thermophysical properties handbooks. The data provided by NASA are listed both here and in Table 2-1. Temperature and pressure dependent properties were considered only in the detailed fluid storage and pressurization analysis. These data were obtained from a special Material Properties library prepared for NASA under this contract. The library contains tables of physical properties of a number of propellants, pressurants, structural materials, and insulations. Reference 8 contains a complete listing of these properties data.

Table A-1 Material Property Values Used For The SM Thermal Analysis

COMPONENT	MATERIAL	ρ lb/in^3	C Btu/lb$^\circ$F	k Btu/hr ft$^\circ$F	α_s	ϵ
Radial Beams	7075-T651 Al.	0.101	0.20	76.		0.25
Outer Shell Skins	7178-T6 Al.	0.101	0.21	70.	0.548	0.548
Outer Shell Core	5052-H39 Al.	0.097	0.21	80.		
Outer Shell Edge Members	7075 Al.	0.101	0.20	76.		
Bulkhead Skins	7178-T6 Al.	0.101	0.21	70.		0.25
Bulkhead Core	5052-H39 Al.	0.097	0.21	80.		
Bulkhead Stiffeners	7075 Al.	0.101	0.20	76.		
Engine Web Mount	7075-T6 Al.	0.101	0.20	76.		0.25
Center Webs	2024-T3 Al.	0.101	0.20	73.		0.25
Propellant Tanks	6AL4V Titanium	0.161	0.13			0.25
Propellant Tank Skirts	2024-T4 Al.	0.101	0.20	73.		
Helium Bottles	6AL4V Titanium	0.161	0.13			0.25
RCS Heat Shield Skins	321 Cres	0.283	0.11	8.2	0.55	0.55
RCS Heat Shield Insulation	Quartz Fiber	0.00174	0.18	0.023		
Aft Heat Shield Ext. Skins	347 Cres	0.283	0.11		0.36	0.40
Aft Heat Shield Int. Skins	Fiberglass	0.058	0.21		0.80	0.80
Aft Head Shield Insulation	Quartz Fiber	0.00348	0.18	0.023		
Nozzle Extension	Titanium Columbium	0.161 0.324	0.13 0.060		0.65 0.90	0.85 0.90
Thrust Chamber	Uncharred Charred	0.052 0.035	0.30 0.30	0.086 0.260		0.70 0.80
Fuel Cells Propellant Lines	304L S.S.	0.283	0.11	9.4		0.30 0.30

LOCKHEED
CALIFORNIA COMPANY

Appendix B

Resistor And Capacitor Values

The values of resistors and capacitors used during the analyses are tabulated in this appendix. In the tables that follow, the item on the left, "DECOI," "DECO2," and "DECO3," refer to the number of resistor or capacitor values listed on that line. Each resistor entry consists of the resistor number, the two node numbers connected by the resistor, and the value of the resistor in sec.^{o}F/Btu. A value of 0. is a "dummy" value, indicating a radiation resistor. Radiation resistors are listed again separately, giving the radiation "k" values (see Sect. IV). Capacitor entries consist of node number followed by the capacity of the node in Btu/^{o}F. The listings are given in the following tables :

Table Number	Listing
B-1	Resistors for Basic Structure Analysis
B-2	Capacitors for Basic Structure Analysis
B-3	Resistors for Detailed Engine and Plumbing Analysis
B-4	Capacitors for Detailed Engine and Plumbing Analysis
B-5	Resistors for Bay 2 Oxidizer Tank Analysis
B-6	Resistors for Bay 3 Fuel Tank Analysis
B-7	Resistors for Bay 5 Oxidizer Tank Analysis
B-8	Resistors for Bay 6 Fuel Tank Analysis
B-9	Capacitors for Propellant Tank Analyses

Table B-1 includes portions of the Thermal Analyzer Program FUNCT Subroutine and data block, which were used to store several radiation "k" factors. Table B-3 lists the resistor values for the detailed engine/plumbing analysis and also the changes which were required to account for the removal of the insulation from the bay 4 side of radial beams 3 and 4. These modifications were used for the Earth Orbital Analysis.

Only the external networks are shown for the detailed propellant storage and pressurization analyses. The propellant tank internal network is automatically generated by the computer program.

TABLE B-1

RESISTORS FOR BASIC STRUCTURE ANALYSIS

DEC02	1	102	133	23220.	2	103	11	9620.	FAIRING	200012266
DEC02	3	104	11	9350.	4	105	11	9350.		200032266
DEC02	5	106	136	22610.	6	108	136	21750.		200052266
DEC02	7	109	13	8850.	8	110	13	8850.		200072266
DEC02	9	111	139	21750.	10	113	139	23220.		200092266
DEC02	11	201	133	40600.	12	202	133	13600.	SHELL TO	20011
DEC02	13	203	11	1000.	14	204	11	2000.	BLKDS.	20013
DEC02	15	205	11	2500.	16	206	136	13300.		20015
DEC02	17	207	136	40600.	18	208	136	12900.		20017
DEC02	19	209	13	2000.	20	210	13	500.		20019
DEC02	21	201	301	6950.	22	202	302	4910.	SHELL	200212266
DEC02	23	203	303	4910.	24	204	304	15900.	AXIAL RS	200232266
DEC02	25	205	305	15900.	26	206	306	14400.		200252266
DEC02	27	207	307	6620.	28	208	308	13600.		200272266
DEC02	29	209	309	15000.	30	210	310	3780.		200292266
DEC02	31	301	401	6950.	32	302	402	4910.		200312266
DEC02	33	303	403	4910.	34	304	404	15900.		200332266
DEC02	35	305	405	15900.	36	306	406	14400.		200352266
DEC02	37	307	407	6650.	38	308	408	13600.		200372266
DEC02	39	309	409	15000.	40	310	410	3780.		200392266
DEC02	41	401	501	11200.	42	402	502	19600.		200412266
DEC02	43	403	503	19600.	44	404	504	25100.		200432266
DEC02	45	405	505	25100.	46	406	506	22800.		200452266
DEC02	47	407	507	10900.	48	408	508	21500.		200472266
DEC02	49	409	509	23700.	50	410	510	17080.		200492266
DEC02	51	501	601	11200.	52	502	602	22800.		200512266
DEC01	53	503	603	22800.						200532088
DEC02	57	507	607	10800.	58	508	608	21500.		200572266
DEC02	59	509	609	23700.	60	510	610	19400.		200592266
DEC02	61	601	701	7100.	62	602	702	22800.		200612266
DEC01	63	603	703	22800.						200632088
DEC02	67	607	707	6740.	68	608	708	13600.		200672266
DEC02	69	609	709	15000.	70	610	710	12300.		200692266
DEC02	71	701	801	7100.	72	702	802	9120.		200712266
DEC02	73	703	803	9120.	74	704	804	10000.		200732266
DEC02	75	705	805	8170.	76	706	806	9100.		200752266
DEC02	77	707	807	6620.	78	708	808	8600.		200772266
DEC02	79	709	809	9460.	80	710	810	7740.		200792266
DEC02	81	801	933	11100.	82	802	933	4900.	SHELL TO	20081
DEC02	83	803	936	1000.	84	804	936	1000.	BLKDS.	20083
DEC02	85	805	936	1000.	86	806	938	4900.		20085
DEC02	87	807	938	11100.	88	808	938	8600.		20087
DEC02	89	809	941	1000.	90	810	941	1000.		20089
DEC02	91	114	15	23220.	92	115	15	23220.	FAIRING	200912266
DEC02	93	116	142	36900.	94	118	142	23220.		200932266
DEC02	95	119	18	9620.	96	120	18	9350.		200952266
DEC02	97	121	18	9350.	98	122	145	22610.		200972266
DEC02	99	124	145	21750.	100	125	20	8850.		200992266
DEC02	101	126	20	8850.	107	127	148	21750.		201012266
DEC02	102	102	103	8640.	103	103	104	8756.	SHELL	201022266
DEC02	104	104	105	8873.	105	105	106	8873.	LATERAL RS	201042266
DEC02	106	106	108	9130.	108	108	109	9400.		201062266
DEC02	109	109	110	9400.	110	110	111	9400.		201092266
DEC02	111	111	113	9020.	113	113	114	8640.		201112266
DEC02	112	129	148	36900.	117	130	22	23220.		201122266
DEC02	114	114	115	8640.	115	115	116	6795.		201142266
DEC02	116	116	118	6795.	118	118	119	8640.		201162266
DEC02	119	119	120	8756.	120	120	121	8873.		201192266
DEC02	121	121	122	8873.	122	122	124	9130.		201212266
DEC02	123	131	22	23220.	128	132	133	23220.		201232266
DEC02	124	124	125	9400.	125	125	126	9400.		201242266

TABLE B-1 (Cont.)

DEC02	126	126	127	9400.	127	127	129	7407.		201262266
DEC02	129	129	130	6795.	130	130	131	8640.		201292266
DEC02	131	131	132	8640.	132	132	102	8640.		201312266
DEC02	134	133	134	5330.	135	134	135	10500.	FWD BLKD.	201342266
DEC02	136	22	23	11600.	137	136	137	4230.		201362266
DEC02	138	137	138	7050.	139	23	24	15600.		201382266
DEC02	140	139	140	5570.	141	140	141	10100.		201402266
DEC02	142	15	16	11600.	143	142	143	6450.		201422266
DEC02	144	143	144	10900.	145	16	17	15600.		201442266
DEC02	146	145	146	4230.	147	146	147	7050.		201462266
DEC02	149	148	149	6950.	150	149	150	10750.		201492266
DEC02	151	211	139	12900.	152	212	139	40600.	SHELL TO	20151
DEC02	153	213	139	13600.	154	214	15	13600.	BLKDS.	20153
DEC02	155	215	15	13600.	156	216	142	21600.		20155
DEC02	157	217	142	40600.	158	218	142	13600.		20157
DEC02	159	219	18	1500.	160	220	18	2000.		20159
DEC02	161	221	18	1500.	162	222	145	13300.		20161
DEC02	163	223	145	40600.	164	224	145	12900.		20163
DEC02	165	225	20	1500.	166	226	20	1500.		20165
DEC02	167	227	148	12900.	168	228	148	40600.		20167
DEC02	169	229	148	21600.	170	230	22	13600.		20169
DEC02	171	231	22	13600.	172	232	133	13600.		20171
DEC02	173	251	351	21800.	174	351	451	21800.	BEAMS	201732266
DEC02	175	451	551	24100.	176	551	651	44700.	AXIAL RS	201752266
DEC02	177	651	751	21800.	178	751	851	12900.		201772266
DEC02	179	252	352	20900.	180	352	452	20900.		201792266
DEC02	181	452	552	37300.	182	552	652	37300.		201812266
DEC02	183	652	752	20200.	184	752	852	9610.		201832266
DEC02	185	253	353	21800.	186	353	453	21800.		201852266
DEC02	187	453	553	24100.	188	553	653	44700.		201872266
DEC02	189	653	753	21800.	190	753	853	12900.		201892266
DEC02	191	133	11	15200.	192	135	12	10300.	FWD. BLKD.	201912266
DEC02	193	11	136	15500.	194	12	138	10300.		201932266
DEC02	195	254	354	20900.	196	354	454	20900.	BEAM	201952266
DEC02	197	454	554	37300.	198	554	654	37300.	AXIAL RS	201972266
DEC02	199	654	754	20200.	200	754	854	9610.		201992266
DEC02	201	201	202	1960.	202	202	203	4010.	SHELL	202012266
DEC02	203	203	204	9140.	204	204	205	15200.	LATERAL RS	202032266
DEC02	205	205	206	15200.	206	206	207	6400.		202052266
DEC02	207	207	208	7980.	208	208	209	15960.		202072266
DEC02	209	209	210	15960.	210	210	211	4360.		202092266
DEC02	211	211	212	2180.	212	212	213	6060.		202112266
DEC02	213	213	214	12500.	214	214	215	12500.		202132266
DEC02	215	215	216	10200.	216	216	217	3380.		202152266
DEC02	217	217	218	1960.	218	218	219	4010.		202172266
DEC02	219	219	220	9140.	220	220	221	15200.		202192266
DEC02	221	221	222	15200.	222	222	223	6400.		202212266
DEC02	223	223	224	7980.	224	224	225	15960.		202232266
DEC02	225	225	226	15960.	226	226	227	4360.		202252266
DEC02	227	227	228	2180.	228	228	229	3380.		202272266
DEC02	229	229	230	12500.	230	230	231	12500.		202292266
DEC02	231	231	232	12500.	232	232	201	6250.		202312266
DEC02	233	201	233	3600.	234	233	234	8760.	BEAMS	202332266
DEC02	235	234	235	8760.	236	207	236	3600.	RADIAL RS	202352266
DEC02	237	236	237	8040.	238	237	238	8550.		202372266
DEC02	239	212	239	3780.	240	239	240	9200.		202392266
DEC02	241	240	241	9200.	242	217	242	3000.		202412266
DEC02	243	242	243	9100.	244	243	244	9580.		202432266
DEC02	245	223	245	3050.	246	245	246	7420.		202452266
DEC02	247	246	247	2960.	248	228	248	2500.		202472266
DEC02	249	248	249	11900.	250	249	250	2790.		202492266

TABLE B-1 (Cont.)

DEC02	251	211	311	4530.	252	212	312	6960.	SHELL	202512266
DEC02	253	213	313	14300.	254	214	314	16300.	AXIAL RS	202532266
DEC02	255	215	315	16300.	256	216	316	22100.		202552266
DEC02	257	217	317	9300.	258	218	318	4910.		202572266
DEC02	259	219	319	4910.	260	220	320	15900.		202592266
DEC02	261	221	321	15900.	262	222	322	14400.		202612266
DEC02	263	223	323	6620.	264	224	324	13600.		202632266
DEC02	265	225	325	15000.	266	226	326	3780.		202652266
DEC02	267	227	327	4530.	268	228	328	6960.		202672266
DEC02	269	229	329	22100.	270	230	330	16300.		202692266
DEC02	271	231	331	16300.	272	232	332	14300.		202712266
DEC02	273	233	333	36700.	274	234	334	33900.	BEAMS	202732266
DEC02	275	235	335	36700.	276	236	336	36700.	AXIAL RS	202752266
DEC02	277	237	337	33900.	278	238	338	9600.		202772266
DEC02	279	239	339	36800.	280	240	340	33800.		202792266
DEC02	281	241	341	36800.	282	242	342	36800.		202812266
DEC02	283	243	343	33800.	284	244	344	36800.		202832266
DEC02	285	245	345	36700.	286	246	346	33900.		202852266
DEC02	287	247	347	9600.	288	248	348	36800.		202872266
DEC02	289	249	349	15300.	290	250	350	19500.		202892266
DEC02	291	136	13	12300.	292	138	14	6500.	FWD. BLKD.	202912266
DEC02	293	13	139	12300.	294	14	141	6500.		202932266
DEC02	295	235	251	3600.	296	241	252	3780.	BEAMS	202952266
DEC02	297	244	253	3950.	298	250	254	2500.	RADIAL RS	202972266
DEC01	300	357	700	555.		HELIUM TO CONTAINER				20300
DEC02	301	301	302	3020.	302	302	303	6160.	SHELL	203012266
DEC02	303	303	304	10200.	304	304	305	15200.	LATERAL RS	203032266
DEC02	305	305	306	15200.	306	306	307	6400.		203052266
DEC02	307	307	308	7980.	308	308	309	15960.		203072266
DEC02	309	309	310	15960.	310	310	311	6700.		203092266
DEC02	311	311	312	3350.	312	312	313	6250.		203112266
DEC02	313	313	314	12900.	314	314	315	12900.		203132266
DEC02	315	315	316	5700.	316	316	317	3490.		203152266
DEC02	317	317	318	3020.	318	318	319	6160.		203172266
DEC02	319	319	320	10200.	320	320	321	15200.		203192266
DEC02	321	321	322	15200.	322	322	323	6400.		203212266
DEC02	323	323	324	7980.	324	324	325	15960.		203232266
DEC02	325	325	326	15960.	326	326	327	6700.		203252266
DEC02	327	327	328	3350.	328	328	329	3490.		203272266
DEC02	329	329	330	12900.	330	330	331	12900.		203292266
DEC02	331	331	332	12900.	332	332	301	6450.		203312266
DEC02	333	301	333	8800.	334	333	334	21400.	BEAMS	203332266
DEC02	335	334	335	21400.	336	307	336	9150.	RADIAL RS	203352266
DEC02	337	336	337	22300.	338	337	338	22300.		203372266
DEC02	339	312	339	9500.	340	339	340	23100.		203392266
DEC02	341	340	341	23100.	342	317	342	17100.		203412266
DEC02	343	342	343	41700.	344	343	344	41700.		203432266
DEC02	345	323	345	9150.	346	345	346	22300.		203452266
DEC02	347	346	347	22300.	348	328	348	7800.		203472266
DEC02	349	348	349	19000.	350	349	350	19000.		203492266
DEC02	351	311	411	4530.	352	312	412	7100.	SHELL	203512266
DEC02	353	313	413	14000.	354	314	414	16300.	AXIAL RS	203532266
DEC02	355	315	415	16300.	356	316	416	21400.		203552266
DEC02	357	317	417	9360.	358	318	418	4910.		203572266
DEC02	359	319	419	4910.	360	320	420	15900.		203592266
DEC02	361	321	421	15900.	362	322	422	14400.		203612266
DEC02	363	323	423	6650.	364	324	424	13600.		203632266
DEC02	365	325	425	15000.	366	326	426	3780.		203652266
DEC02	367	327	427	4530.	368	328	428	7100.		203672266
DEC02	369	329	429	22100.	370	330	430	16300.		203692266
DEC02	371	331	431	16300.	372	332	432	14000.		203712266

LOCKHEED
CALIFORNIA COMPANY

TABLE B-1 (Cont.)

DEC02	373	333	433	36700.	374	334	434	33900. BEAMS	203732266
DEC02	375	335	435	36700.	376	336	436	36700. AXIAL RS	203752266
DEC02	377	337	437	33900.	378	338	438	10000.	203772266
DEC02	379	339	439	27000.	380	340	440	25880.	203792266
DEC02	381	341	441	36800.	382	342	442	36800.	203812266
DEC02	383	343	443	33800.	384	344	444	36800.	203832266
DEC02	385	345	445	36700.	386	346	446	33900.	203852266
DEC02	387	347	447	10000.	388	348	448	36800.	203872266
DEC02	389	349	449	15300.	390	350	450	24600.	203892266
DEC02	391	139	15	24300.	392	140	16	15500. FWD.BLKD.	203912266
DEC02	393	141	17	11500.	394	15	142	19600.	203932266
DEC02	395	16	143	14200.	396	17	144	10000.	203952266
DEC02	397	335	351	8800.	398	341	352	9500. BEAMS	203972266
DEC02	399	344	353	17100.	400	350	354	7800. RADIAL RS	203992266
DEC02	401	401	402	3020.	402	402	403	6160. SHELL	204012266
DEC02	403	403	404	10200.	404	404	405	15200. LATERAL RS	204032266
DEC02	405	405	406	15200.	406	406	407	6400.	204052266
DEC02	407	407	408	7980.	408	408	409	15960.	204072266
DEC02	409	409	410	15960.	410	410	411	6700.	204092766
DEC02	411	411	412	3350.	412	412	413	6320.	204112266
DEC02	415	415	416	10500.	416	416	417	3510.	204152266
DEC02	417	417	418	3020.	418	418	419	6160.	204172266
DEC02	419	419	420	10200.	420	420	421	15200.	204192266
DEC02	421	421	422	15200.	422	422	423	6400.	204212266
DEC02	423	423	424	7980.	424	424	425	15960.	204232266
DEC02	425	425	426	15960.	426	426	427	6700.	204252266
DEC02	427	427	428	3350.	428	428	429	3510.	204272266
DEC02	429	429	430	13000.	430	430	431	13000.	204292266
DEC02	431	431	432	13000.	432	432	401	6500.	204312266
DEC02	433	401	433	8800.	434	433	434	21400. BEAMS	204332266
DEC02	435	434	435	21400.	436	407	436	9150. RADIAL RS	204352266
DEC02	437	436	437	22300.	438	437	438	22300.	204372266
DEC02	439	412	439	9500.	440	439	440	23100.	204392266
DEC02	441	440	441	23100.	442	417	442	17100.	204412266
DEC02	443	442	443	41700.	444	443	444	41700.	204432266
DEC02	445	423	445	9150.	446	445	446	22300.	204452266
DEC02	447	446	447	22300.	448	428	448	9320.	204472266
DEC02	449	448	449	22600.	450	449	450	22600.	204492266
DEC02	451	411	511	19000.	452	412	512	11500. SHELL	204512266
DEC01	456	416	516	27000.				AXIAL RS	204562088
DEC02	457	417	517	15700.	458	418	518	19600.	204572266
DEC02	459	419	519	19600.	460	420	520	25100.	204592266
DEC02	461	421	521	25100.	462	422	522	22800.	204612266
DEC02	463	423	523	10900.	464	424	524	21500.	204632266
DEC02	465	425	525	23700.	466	426	526	17080.	204652266
DEC02	467	427	527	19000.	468	428	528	11500.	204672266
DEC02	469	429	529	13830.	470	430	530	13100.	204692266
DEC02	471	431	531	25800.	472	432	532	20200.	204712266
DEC02	473	433	533	58000.	474	434	534	53500. BEAMS	204732266
DEC02	475	435	535	58000.	476	436	536	58000. AXIAL RS	204752266
DEC02	477	437	537	53500.	478	438	538	16200.	204772266
DEC02	479	439	539	39100.	480	440	540	53400.	204792266
DEC02	481	441	541	44600.	482	442	542	45600.	204812266
DEC02	483	443	543	53500.	484	444	544	58300.	204832266
DEC02	485	445	545	58000.	486	446	546	53500.	204852266
DEC02	487	447	547	16200.	488	448	548	37100.	204872266
DEC02	489	449	549	31400.	490	450	550	58100.	204892266
DEC02	491	142	18	15200.	492	144	19	10300. FWD.BLKD.	204912766
DEC02	493	18	145	15500.	494	19	147	10300.	204932266
DEC02	495	435	451	8800.	496	441	452	9500. BEAMS	204952266
DEC02	497	444	453	17100.	498	450	454	9320. RADIAL RS	204972266

TABLE B-1 (Cont.)

DEC01	500	557	800	555.		HELIUM TO CONTAINER			20500
DEC02	501	501	502	1590.	502	502	503	3250. SHELL	205012266
DEC02	503	503	504	4830.	506	506	507	2880. LATERAL RS	205032088
DEC02	507	507	508	3600.	508	508	509	7200.	205072266
DEC02	509	509	510	7200.	510	510	511	3530.	205092266
DEC02	511	511	512	1770.	512	512	513	2950.	205112266
DEC02	515	515	516	4340.	516	516	517	1200.	205152266
DEC02	517	517	518	1590.	518	518	519	3250.	205172266
DEC02	519	519	520	4830.	522	522	523	2880.	205192088
DEC02	523	523	524	3600.	524	524	525	7200.	205232266
DEC02	525	525	526	7200.	526	526	527	3530.	205252266
DEC02	527	527	528	1770.	528	528	529	1030.	205272266
DEC02	529	529	530	3800.	530	530	531	6060.	205292266
DEC02	531	531	532	6060.	532	532	501	3030.	205312266
DEC02	533	501	533	4020.	534	533	534	9800. BEAMS	205332266
DEC02	535	534	535	9800.	536	507	536	3780. RADIAL RS	205352266
DEC02	537	536	537	9200.	538	537	538	9200.	205372266
DEC02	539	512	539	4400.	540	539	540	10700.	205392266
DEC02	541	540	541	10700.	542	517	542	3600.	205412266
DEC02	543	542	543	8650.	544	543	544	8650.	205432266
DEC02	545	523	545	3780.	546	545	546	9200.	205452266
DEC02	547	546	547	9200.	548	528	548	3960.	205472266
DEC02	549	548	549	9630.	550	549	550	9630.	205492266
DEC02	551	511	611	21000.	552	512	612	11400. SHELL	205512266
DEC02	553	513	613	21600.	554	514	614	25800. AXIAL RS	205532266
DEC02	555	515	615	25800.	556	516	616	20280.	205552266
DEC02	557	517	617	16300.	558	518	618	22800.	205572266
DEC01	559	519	619	22800.					205592088
DEC02	563	523	623	10800.	564	524	624	21500.	205632266
DEC02	565	525	625	23700.	566	526	626	19400.	205652266
DEC02	567	527	627	21000.	568	528	628	11400.	205672266
DEC02	569	529	629	35000.	570	530	630	25800.	205692266
DEC02	571	531	631	25800.	572	532	632	20200.	205712266
DEC02	573	533	633	58000.	574	534	634	53500. BEAMS	205732266
DEC02	575	535	635	58000.	576	536	636	58000. AXIAL RS	205752266
DEC02	577	537	637	53500.	578	538	638	14600.	205772266
DEC02	579	539	639	38400.	580	540	640	36400.	205792266
DEC02	581	541	641	29300.	582	542	642	58300.	205812266
DEC02	583	543	643	53500.	584	544	644	58300.	205832266
DEC02	585	545	645	58000.	586	546	646	53500.	205852266
DEC02	587	547	647	14600.	588	548	648	58100.	205872266
DEC02	589	549	649	33500.	590	550	650	31400.	205892266
DEC02	591	145	20	12300.	592	147	21	6500. FWD.BLKD.	205912266
DEC02	593	20	148	12300.	594	21	150	6500.	205932266
DEC02	595	535	551	5620.	596	541	552	4400. BEAMS	205952266
DEC02	597	544	553	3600.	598	550	554	3960. RADIAL RS	205972266
DEC02	601	601	602	7180.	602	602	603	14700. SHELL	206012266
DEC02	603	603	604	15200.	606	606	607	6400. LATERAL RS	206032088
DEC02	607	607	608	7980.	608	608	609	15960.	206072266
DEC02	609	609	610	15960.	610	610	611	15960.	206092266
DEC02	611	611	612	7980.	612	612	613	4200.	206112266
DEC02	613	613	614	8640.	614	614	615	8640.	206132266
DEC02	615	615	616	7640.	616	616	617	2330.	206152266
DEC02	617	617	618	7180.	618	618	619	14700.	206172266
DEC02	619	619	620	15200.	622	622	623	6400.	206192088
DEC02	623	623	624	7980.	624	624	625	15960.	206232266
DEC02	625	625	626	15960.	626	626	627	15960.	206252266
DEC02	627	627	628	7980.	628	628	629	2330.	206272266
DEC02	629	629	630	8640.	632	632	601	4320.	206292088
DEC02	633	601	633	8800.	634	633	634	21400. BEAMS	206332266
DEC02	635	634	635	21400.	636	607	636	9150. RADIAL RS	206352266

LOCKHEED
CALIFORNIA COMPANY

TABLE B-1 (Cont.)

DEC02	637	636	637	22300.	638	637	638	22300.	206372266
DEC02	639	612	639	7090.	640	639	640	8280.	206392266
DEC02	641	640	641	23100.	642	617	642	17100.	206412266
DEC02	643	642	643	11300.	644	643	644	26500.	206432266
DEC02	645	623	645	9150.	646	645	646	22300.	206452266
DEC02	647	646	647	22300.	648	628	648	9320.	206472266
DEC02	649	648	649	22600.	650	649	650	22600.	206492266
DEC02	651	611	711	21000.	652	612	712	7320. SHELL	206512266
DEC02	653	613	713	14300.	654	614	714	14700. AXIAL RS	206532266
DEC02	655	615	715	16300.	656	616	716	22100.	206552266
DEC02	657	617	717	10400.	658	618	718	22800.	206572266
DEC01	659	619	719	22800.					206592088
DEC02	663	623	723	6740.	664	624	724	13600.	206632266
DEC02	665	625	725	15000.	666	626	726	12300.	206652266
DEC02	667	627	727	21000.	668	628	728	7320.	206672266
DEC01	669	629	729	22100.					206692088
DEC02	673	633	733	36000.	674	634	734	33900. BEAMS	206732266
DEC02	675	635	735	36700.	676	636	736	36700. AXIAL RS	206752266
DEC02	677	637	737	33900.	678	638	738	8280.	206772266
DEC02	679	639	739	36800.	680	640	740	33800.	206792266
DEC02	681	641	741	36800.	682	642	742	36800.	206812266
DEC02	683	643	743	33800.	684	644	744	36800.	206832266
DEC02	685	645	745	36700.	686	646	746	33900.	206852266
DEC02	687	647	747	8580.	688	648	748	36800.	206872266
DEC02	689	649	749	17000.	690	650	750	28600.	206892266
DEC02	691	148	22	19600.	692	149	23	14200. FWD.BLKD.	206912266
DEC02	693	150	24	10000.	694	22	133	24300.	206932266
DEC02	695	23	134	15500.	696	24	135	11500.	206952266
DEC02	697	635	651	8800.	698	641	652	9500. BEAMS	206972266
DEC02	699	644	653	17100.	700	650	654	9320. RADIAL RS	206992266
DEC02	701	701	702	7180.	702	702	703	14700. SHELL	207012266
DEC02	703	703	704	15200.	706	706	707	6400. LATERAL RS	207032088
DEC02	707	707	708	7980.	708	708	709	15960.	207072266
DEC02	709	709	710	15960.	710	710	711	15960.	207092266
DEC02	711	711	712	7980.	712	712	713	7080.	207112266
DEC02	713	713	714	14600.	714	714	715	14600.	207132266
DEC02	715	715	716	13300.	716	716	717	3940.	207152266
DEC02	717	717	718	7180.	718	718	719	14700.	207172266
DEC02	719	719	720	15200.	722	722	723	6400.	207192088
DEC02	723	723	724	7980.	724	724	725	15960.	207232266
DEC02	725	725	726	15960.	726	726	727	15960.	207252266
DEC02	727	727	728	7980.	728	728	729	3940.	207272266
DEC02	729	729	730	14600.	732	732	701	7300.	207292088
DEC02	733	701	733	8800.	734	733	734	21400. BEAMS	207332266
DEC02	735	734	735	21400.	736	707	736	9150. RADIAL RS	207352266
DEC02	737	736	737	22300.	738	737	738	22300.	207372266
DEC02	739	712	739	9500.	740	739	740	23100.	207392266
DEC02	741	740	741	23100.	742	717	742	17100.	207412266
DEC02	743	742	743	41700.	744	743	744	41700.	207432266
DEC02	745	723	745	9150.	746	745	746	22300.	207452266
DEC02	747	746	747	22300.	748	728	748	6250.	207472266
DEC02	749	748	749	15200.	750	749	750	15200.	207492266
DEC02	751	711	811	8400.	752	712	812	7320. SHELL	207512266
DEC02	753	713	813	10900.	754	714	814	11200. AXIAL RS	207532266
DEC02	755	715	815	12400.	756	716	816	16900.	207552266
DEC02	757	717	817	10100.	758	718	818	9120.	207572266
DEC02	759	719	819	9120.	760	720	820	10000.	207592266
DEC02	761	721	821	8170.	762	722	822	9100.	207612266
DEC02	763	723	823	6620.	764	724	824	8600.	207632266
DEC02	765	725	825	9460.	766	726	826	7740.	207652266
DEC02	767	727	827	8400.	768	728	828	7320.	207672266

LOCKHEED CALIFORNIA COMPANY

TABLE B-1 (Cont.)

DEC01	769	729	829	16200.						207692088
DEC02	773	733	833	31400.	774	734	834	35800.	BEAMS	207732266
DEC02	775	735	835	31400.	776	736	836	31400.	AXIAL RS	207752266
DEC02	777	737	837	35800.	778	738	838	7450.		207772266
DEC02	779	739	839	36800.	780	740	840	23300.		207792266
DEC02	781	741	841	17800.	782	742	842	18400.		207812266
DEC02	783	743	843	20300.	784	744	844	19200.		207832266
DEC02	785	745	845	31400.	786	746	846	35800.		207852266
DEC02	787	747	847	7450.	788	748	848	36800.		207872266
DEC02	789	749	849	17000.	790	750	850	36800.		207892266
DEC02	795	735	751	8800.	796	741	752	9500.	BEAMS	207952266
DEC02	797	744	753	17100.	798	750	754	6250.	RADIAL RS	207972266
DEC02	799	738	755	9000.	899	838	855	4700.		207992266
DEC02	800	747	756	9000.	900	847	856	4700.		208002266
DEC02	801	801	802	6100.	802	802	803	12500.	SHELL	208012266
DEC02	803	803	804	12900.	804	804	805	12900.	LATERAL RS	208032266
DEC02	805	805	806	12900.	806	806	807	5420.		208052266
DEC02	807	807	808	6780.	808	808	809	13560.		208072266
DEC02	809	809	810	13560.	810	810	811	13560.		208092266
DEC02	811	811	812	6780.	812	812	813	2700.		208112266
DEC02	813	813	814	6600.	814	814	815	6600.		208132266
DEC02	815	815	816	5350.	816	816	817	1780.		208152266
DEC02	817	817	818	6100.	818	818	819	12500.		208172266
DEC02	819	819	820	12900.	820	820	821	12900.		208192266
DEC02	821	821	822	12900.	822	822	823	5420.		208212266
DEC02	823	823	824	6780.	824	824	825	13960.		208232266
DEC02	825	825	826	13960.	826	826	827	13560.		208252266
DEC02	827	827	828	6780.	828	828	829	1780.		208272266
DEC02	829	829	830	6600.	832	832	801	3300.		208292088
DEC02	833	801	833	4780.	834	833	834	11700.	BEAMS	208332266
DEC02	835	834	835	11700.	836	807	836	4540.	RADIAL RS	208352266
DEC02	837	836	837	10900.	838	837	838	11100.		208372266
DEC02	839	812	839	4600.	840	839	840	11200.		208392266
DEC02	841	840	841	11200.	842	817	842	4820.		208412266
DEC02	843	842	843	11700.	844	843	844	11700.		208432266
DEC02	845	823	845	4260.	846	845	846	10350.		208452266
DEC02	847	846	847	4260.	848	828	848	4320.		208472266
DEC02	849	848	849	10500.	850	849	850	10500.		208492266
DEC02	851	811	943	8600.	852	812	943	11100.	SHELL TO	20851
DEC02	853	813	943	9100.	854	814	946	9100.	BLKDS.	20853
DEC02	855	815	946	9100.	856	816	949	16000.		20855
DEC02	857	817	949	11100.	858	818	949	4500.		20857
DEC02	859	819	952	1000.	860	820	952	1000.		20859
DEC02	861	821	952	1000.	862	822	954	4900.		20861
DEC02	863	823	954	11100.	864	824	954	8600.		20863
DEC02	865	825	957	1000.	866	826	957	1000.		20865
DEC02	867	827	959	8600.	868	828	959	11100.		20867
DEC02	869	829	959	16000.	870	830	962	9800.		20869
DEC02	871	831	962	9800.	872	832	933	9800.		20871
DEC02	875	25	11	4250.	876	26	12	4574.	SKIRTS TO	208752266
DEC02	877	27	137	6448.	878	137	28	6784.	AFT. BLKD.	208772266
DEC02	879	29	13	10040.	880	30	14	3629.		208792266
DEC02	881	31	140	6784.	882	32	143	5761.		208812266
DEC02	883	33	8	4250.	884	34	9	4574.		208832266
DEC02	885	35	146	6448.	886	36	146	6784.		208852266
DEC02	887	37	20	10040.	888	38	21	3629.		208872266
DEC02	889	39	149	6784.	890	40	134	5761.		208892266
DEC02	895	835	851	4780.	896	841	852	4600.	BEAMS	208952266
DEC02	897	844	853	4820.	898	850	854	4320.	RADIAL RS	208972266
DEC02	933	933	934	3100.	934	934	935	5550.	AFT BLKD	209332266
DEC02	935	935	937	5350.	936	933	936	10000.		209352266

TABLE B-1 (Cont.)

DEC02	937	936	938	10000.	938	938	939	3770.		209372266
DEC02	939	939	940	3570.	940	940	937	5350.		209392266
DEC02	941	941	938	17900.	942	942	940	3670.		209412266
DEC02	943	943	941	17900.	944	944	943	4950.		209432266
DEC02	945	945	944	6450.	946	945	942	3330.		209452266
DEC02	947	943	946	10400.	948	944	947	6500.		209472266
DEC02	950	948	945	6800.	951	946	947	6170.		209502266
DEC02	952	947	948	7500.	953	946	949	10400.		209522266
DEC02	954	947	950	6500.	955	948	951	6800.		209542266
DEC02	956	949	950	4200.	957	950	951	5150.		209562266
DEC02	958	952	949	10000.	959	953	951	5350.		209582266
DEC02	960	952	954	10000.	961	953	956	5350.		209602266
DEC02	962	954	955	3770.	963	955	956	3570.		209622266
DEC02	964	954	957	17900.	965	956	958	3670.		209642266
DEC02	966	957	959	17900.	967	958	961	3330.		209662266
DEC02	968	959	960	5650.	969	960	961	6450.		209682266
DEC02	970	959	962	9200.	971	960	963	6800.		209702266
DEC02	972	961	964	3270.	973	963	962	7300.		209722266
DEC02	974	964	963	7000.	975	962	933	11000.		209742266
DEC02	976	963	934	11800.	977	964	935	5600.		209762266
DEC02	983	983	936	1266.	984	984	937	1620.	SKIRTS TO	209832266
DEC02	985	985	939	2360.	986	986	939	1500.	AFT BLKD.	209852266
DEC02	987	987	941	1320.	988	988	942	1440.		209872266
DEC02	989	989	944	1500.	990	990	950	2360.		209892266
DEC02	991	991	952	1266.	992	992	953	1620.		209912266
DEC02	993	993	955	2360.	994	994	955	1500.		209932266
DEC02	995	995	957	1320.	996	996	958	1440.		209952266
DEC02	997	997	960	1500.	998	998	934	2360.		209972266
DEC01	1000	300	236	0.		RAD RES FROM RADIAL BEAMS				210002266
INC	3	0	100	0.	6	TO PROPELLANT TANKS				210002266
DEC01	1001	300	237	0.						210012266
INC	3	0	100	0.	6					210012266
DEC01	1002	300	238	0.						210022266
INC	3	0	100	0.	6					210022266
DEC01	1021	600	245	0.						210212266
INC	3	0	100	0.	6					210212266
DEC01	1022	600	246	0.						210222266
INC	3	0	100	0.	6					210222266
DEC01	1023	600	247	0.						210232266
INC	3	0	100	0.	6					210232266
DEC02	1042	251	255	14400.	1043	255	254	14400.	IN. PANEL	210422266
DEC02	1044	351	355	22800.	1045	355	354	22800.		210442266
DEC02	1046	451	455	10500.	1047	455	454	10500.		210462266
DEC02	1048	551	555	13700.	1049	555	554	13700.		210482266
DEC02	1050	651	655	12400.	1051	655	654	12400.		210502266
DEC02	1052	24	255	23540.	1053	255	355	22200.		210522266
DEC02	1054	355	455	27200.	1055	455	555	33000.		210542266
DEC02	1056	555	655	30000.	1057	253	256	14400.		210562266
DEC02	1058	256	252	14400.	1059	353	356	22800.		210582266
DEC02	1060	356	352	22800.	1061	453	456	10500.		210602266
DEC02	1062	456	452	10500.	1063	553	556	19500.		210622266
DEC02	1064	556	552	19500.	1065	17	256	23540.		210642266
DEC02	1066	256	356	22200.	1067	356	456	27200.		210662266
DEC02	1068	456	556	28600.	1069	355	357	575.		210682266
DEC02	1070	555	557	575.	1071	356	357	575.		210702266
DEC01	1072	556	557	575.						210722266
DEC01	1101	101	1	0.		SHELL RAD.RES.TO SPACE				211012266
INC	1	1	0	0.	31					211022266
DEC02	1142	42	102	10000.	1143	43	103	2240.	COND.RES.	211422266
DEC02	1144	44	104	16000.	1145	45	203	4000.	THRU RCS	211442266
DEC02	1146	46	302	6420.	1147	47	304	6420.	HEATSHIELD	211462266

TABLE B-1 (Cont.)

DEC02	1148	48	403	20000.	1149	49	502	4940.		211482266
DEC02	1150	50	503	1215.	1151	51	603	3470.		211502266
DEC02	1152	52	110	2060.	1153	53	111	16000.		211522266
DEC02	1154	54	210	4000.	1155	55	309	6420.		211542266
DEC02	1156	56	311	6420.	1157	57	510	1120.		211562266
DEC02	1158	58	511	3830.	1159	59	610	3470.		211582266
DEC02	1160	60	118	10000.	1161	61	119	2240.		211602266
DEC02	1162	62	120	16000.	1163	63	219	4000.		211622266
DEC02	1164	64	318	6420.	1165	65	320	6420.		211642266
DEC02	1166	66	419	20000.	1167	67	518	4940.		211662266
DEC02	1168	68	519	1215.	1169	69	619	3470.		211682266
DEC02	1170	70	126	2060.	1171	71	127	16000.		211702266
DEC02	1172	72	226	4000.	1173	73	325	6420.		211722266
DEC02	1174	74	327	6420.	1175	75	526	1120.		211742266
DEC02	1176	76	527	3830.	1177	77	626	3470.		211762266
DEC02	1180	357	255	0.	1181	357	355	0.	RAD RES TO	211802266
DEC02	1182	357	455	0.	1183	357	555	0.	HELIUM	211822266
DEC02	1187	557	455	0.	1188	557	555	0.	BOTTLES	211872266
DEC02	1189	557	655	0.	1190	357	256	0.		211892266
DEC02	1191	357	356	0.	1192	357	456	0.		211912266
DEC02	1193	357	556	0.	1196	557	456	0.		211932266
DEC01	1197	557	556	0.						211972266
DEC02	1198	357	557	0.	1199	7	357	0.		211982266
DEC01	1201	201	1	0.		SHELL RAD.RES.TO SPACE				212012266
INC	1	1	0	0.	31					212022266
DEC01	1233	233	200	0.		RAD RES FROM RADIAL BEAMS				212332266
INC	100	100	0	0.	6	TO PROPELLANT TANKS				212332266
DEC01	1234	234	200	0.						212342266
INC	100	100	0	0.	6					212342266
DEC01	1235	235	200	0.						212352266
INC	100	100	0	0.	6					212352266
DEC01	1236	236	200	0.						212362266
INC	100	100	0	0.	6					212362266
DEC01	1237	237	200	0.						212372266
INC	100	100	0	0.	6					212372266
DEC01	1238	238	200	0.						212382266
INC	100	100	0	0.	6					212382266
DEC01	1239	239	300	0.						212392266
INC	100	100	0	0.	6					212392266
DEC01	1240	240	300	0.						212402266
INC	100	100	0	0.	6					212402266
DEC01	1241	241	300	0.						212412266
INC	100	100	0	0.	6					212412266
DEC01	1242	242	500	0.						212422266
INC	100	100	0	0.	6					212422266
DEC01	1243	243	500	0.						212432266
INC	100	100	0	0.	6					212432266
DEC01	1244	244	500	0.						212442266
INC	100	100	0	0.	6					212442266
DEC01	1245	245	500	0.		RAD RES FROM RADIAL BEAMS				212452266
INC	100	100	0	0.	6	TO PROPELLANT TANKS				212452266
DEC01	1246	246	500	0.						212462266
INC	100	100	0	0.	6					212462266
DEC01	1247	247	500	0.						212472266
INC	100	100	0	0.	6					212472266
DEC01	1248	248	600	0.						212482266
INC	100	100	0	0.	6					212482266
DEC01	1249	249	600	0.						212492266
INC	100	100	0	0.	6					212492266
DEC01	1250	250	600	0.						212502266
INC	100	100	0	0.	6					212502266

TABLE B-1 (Cont.)

DEC01	1252	202	200	0.			RAD RES FROM EXTERNAL SHELL			212522266
INC	100	100	0	0.	6		TO PROPELLANT TANKS			212522266
DEC01	1253	203	200	0.						212532266
INC	100	100	0	0.	6					212532266
DEC01	1254	204	200	0.						212542266
INC	100	100	0	0.	6					212542266
DEC01	1255	205	200	0.						212552266
INC	100	100	0	0.	6					212552266
DEC01	1256	206	200	0.						212562266
INC	100	100	0	0.	6					212562266
DEC01	1257	935	851	7660.					WEB MOUNT	212572266
DEC01	1258	208	300	0.						212582266
INC	100	100	0	0.	6					212582266
DEC01	1259	209	300	0.						212592266
INC	100	100	0	0.	6					212592266
DEC01	1260	210	300	0.						212602266
INC	100	100	0	0.	6					212602266
DEC01	1261	211	300	0.						212612266
INC	100	100	0	0.	6					212612266
DEC02	1262	751	757	12680.	1263	757	754	26200.	ENGINE WEB	212622266
DEC02	1264	754	758	18530.	1265	758	756	21600.	MOUNT RS	212642266
DEC02	1266	757	857	11250.	1267	758	858	7890.		212662266
DEC01	1268	218	500	0.						212682266
INC	100	100	0	0.	6					212682266
DEC01	1269	219	500	0.						212692266
INC	100	100	0	0.	6					212692266
DEC01	1270	220	500	0.						212702266
INC	100	100	0	0.	6					212702266
DEC01	1271	221	500	0.						212712266
INC	100	100	0	0.	6					212712266
DEC01	1272	222	500	0.						212722266
INC	100	100	0	0.	6					212722266
DEC01	1273	961	854	5430.					WEB MOUNT	212732266
DEC01	1274	224	600	0.						212742266
INC	100	100	0	0.	6					212742266
DEC01	1275	225	600	0.						212752266
INC	100	100	0	0.	6					212752266
DEC01	1276	226	600	0.						212762266
INC	100	100	0	0.	6					212762266
DEC01	1277	227	600	0.						212772266
INC	100	100	0	0.	6					212772266
DEC02	1278	851	857	12680.	1279	857	854	26200.	ADDITIONAL	212782266
DEC02	1280	854	858	18530.	1281	858	856	21600.	ENGINE WEB	212802266
DEC02	1282	964	857	8030.	1283	958	858	4560.	MOUNT RS	212822266
DEC02	1284	753	759	12680.	1285	759	752	26200.		212842266
DEC02	1286	752	760	18530.	1287	760	755	21600.		212862266
DEC02	1288	759	859	11250.	1289	760	860	7890.		212882266
DEC02	1290	853	859	12680.	1291	859	852	26200.		212902266
DEC02	1292	852	860	18530.	1293	860	855	21600.		212922266
DEC02	1294	948	859	8300.	1295	942	860	4560.		212942266
DEC02	1296	956	856	4640.	1297	951	853	7710.		212962266
DEC02	1298	945	852	5910.	1299	940	855	4640.		212982266
DEC02	1300	855	755	10500.	1400	856	756	10500.		21300
DEC01	1301	301	1	0.			SHELL RAD.RES.TO SPACE			21302
INC	1	1	0	0.	30					213032266
DEC02	1380	357	200	0.	1381	357	300	0.	HE. BOT.	213802266
DEC02	1382	357	500	0.	1383	357	600	0.	RADIATION	213822266
DEC02	1384	557	200	0.	1385	557	300	0.		213842266
DEC02	1386	557	500	0.	1387	557	600	0.		213862266
DEC02	1388	933	1	0.	1389	936	1	0.	AFT BLKD	213882266
DEC02	1390	938	1	0.	1391	941	1	0.	TO SPACE	213902266

TABLE B-1 (Cont.)

DEC02	1392	943	1	0.	1393	946	1	0.		213922266
DEC02	1394	949	1	0.	1395	952	1	0.		213942266
DEC02	1396	954	1	0.	1397	957	1	0.		213962266
DEC02	1398	959	1	0.	1399	962	1	0.		213982266
DEC01	1401	401	1	0.		SHELL RAD.RES.TO SPACE				214012266
INC	1	1	0	0.	31					214022266
DEC02	1478	983	985	25400.	1479	984	985	22200.	AFT SKIRT	214782266
DEC02	1480	986	987	25000.	1481	987	989	25000.		214802266
DEC02	1482	986	988	28100.	1483	988	989	28100.		214822266
DEC02	1484	990	992	22200.	1485	990	991	25400.		214842266
DEC02	1486	992	993	22200.	1487	991	993	25400.		214862266
DEC02	1488	994	996	28100.	1489	994	995	25000.		214882266
DEC02	1490	996	997	28100.	1491	995	997	25000.		214902266
DEC02	1492	984	998	22200.	1493	998	983	25400.		214922266
DEC02	1494	280	200	0.	1495	280	500	0.	PROP-CHAM.	214942266
DEC02	1496	282	857	0.	1497	282	858	0.	CHAMBER	214962266
DEC02	1498	282	859	0.	1499	282	860	0.	TO WEB MT.	214982266
DEC01	1500	278	279	0.					VALVE-INJ.	215002266
DEC01	1501	501	1	0.		SHELL RAD.RES.TO SPACE				215012266
INC	1	1	0	0.	31					215022266
DEC02	1578	278	757	0.	1579	278	758	0.	PROP.VALVE	215782266
DEC02	1580	278	759	0.	1581	278	760	0.	TO WEB MT.	215802266
DEC02	1582	933	1113	0.	1583	936	1114	0.	AFT BLKD.	215822266
DEC02	1584	938	1115	0.	1585	941	1116	0.	TO NOZZLE	215842266
DEC02	1586	943	1117	0.	1587	946	1118	0.		215862266
DEC02	1588	949	1119	0.	1589	952	1120	0.		215882266
DEC02	1590	954	1121	0.	1591	957	1122	0.		215902266
DEC02	1592	959	1123	0.	1593	962	1124	0.		215922266
DEC01	1601	601	1	0.		SHELL RAD.RES.TO SPACE				216012266
INC	1	1	0	0.	31					216022266
DEC02	1678	279	757	0.	1679	279	758	0.	INJECTOR	216782266
DEC02	1680	279	759	0.	1681	279	760	0.	TO WEB MT.	216802266
DEC02	1682	135	151	6000.	1683	151	152	10200.	C/M SUPPORT	21682
DEC02	1684	152	7	5100.	1685	7	153	5130.	ARMS	21684
DEC02	1686	153	133	5130.	1687	138	154	6000.		21686
DEC02	1688	154	155	10200.	1689	155	7	5100.		21688
DEC02	1690	7	156	3620.	1691	156	136	3340.		21690
DEC02	1692	141	157	6000.	1693	157	158	10200.		21692
DEC02	1694	158	7	5100.	1695	7	159	5130.		21694
DEC02	1696	159	139	5130.	1697	144	160	6000.		21696
DEC02	1698	160	161	10200.	1699	161	7	5100.		21698
DEC01	1700	7	162	3620.						21700
DEC01	1701	701	1	0.		SHELL RAD.RES.TO SPACE				217012266
INC	1	1	0	0.	31					217022266
DEC02	1778	280	757	0.	1779	280	758	0.	CHAMBER	217782266
DEC02	1780	280	759	0.	1781	280	760	0.	TO WEB MT.	217802266
DEC01	1782	1041	282	0.		RAD. FROM H.S. TO THRUST CH.				217822266
DEC01	1783	1042	282	0.						217832266
DEC01	1784	1043	282	0.						217842266
DEC01	1785	1044	282	0.						217852266
DEC01	1786	1045	282	0.						217862266
DEC01	1787	1046	282	0.						217872266
DEC01	1788	1047	282	0.						217882266
DEC01	1789	1048	282	0.						217892266
DEC01	1790	1049	282	0.						217902266
DEC01	1791	1084	282	0.						217912266
DEC01	1792	1085	282	0.						217922266
DEC01	1793	1083	282	0.						217932266
DEC01	1801	801	1	0.		SHELL RAD.RES.TO SPACE				218012266
INC	1	1	0	0.	31					218022266
DEC02	1878	28	300	4170.	1879	29	300	7020.		218782266

TABLE B-1 (Cont.)

DEC02	1880	30	300	2560.	1881	31	300	4170.		218802266
DEC02	1882	32	500	4600.	1883	33	500	2460.		218822266
DEC02	1884	34	500	3960.	1885	35	500	4600.		218842266
DEC02	1886	36	600	4170.	1887	37	600	7020.		218862266
DEC02	1888	38	600	2560.	1889	39	600	4170.		218882266
DEC01	1890	40	200	4600.						218902266
DEC02	1891	25	200	2460.	1892	26	200	3960.	TANK TO	218912266
DEC01	1893	27	200	4600.					FWD SKIRT	218932266
DEC02	1894	162	142	3340.	1895	147	163	6000.	C/M SUPPORT	21894
DEC02	1896	163	164	10200.	1897	164	7	5100.	ARMS	21896
DEC02	1898	7	165	5130.	1899	165	145	5130.		21898
DEC02	1933	150	166	6000.	1934	166	167	10200.	C/M SUPPORT	21933
DEC02	1935	167	7	5100.	1936	7	168	3620.	ARMS	21935
DEC01	1937	168	148	3340.						21937
DEC01	1942	42	1	0.			RCS HEAT SHIELD RAD. RES.			219422266
INC	1	1	0	0.	35		TO SPACE			219432266
DEC02	1978	281	857	0.	1979	281	858	0.	CHAMBER	219782266
DEC02	1980	281	859	0.	1981	281	860	0.	TO WEB MT.	219802266
DEC02	1983	983	200	1266.	1984	984	200	1620.	TANK TO	219832266
DEC02	1985	985	200	2360.	1986	986	300	1500.	AFT SKIRT	219852266
DEC02	1987	987	300	1320.	1988	988	300	1440.		219872266
DEC02	1989	989	300	1500.	1990	990	500	2360.		219892266
DEC02	1991	991	500	1266.	1992	992	500	1620.		219912266
DEC02	1993	993	500	2360.	1994	994	600	1500.		219932266
DEC02	1995	995	600	1320.	1996	996	600	1440.		219952266
DEC02	1997	997	600	1500.	1998	998	200	2360.		219972266
DEC01	2000	100	943	0.			FUEL CELL RAD TO AFT BHD			220002266
INC	1	0	1	0.	8					220012266
DEC01	2009	100	16	0.			FUEL CELL RAD TO FWD BHD			220092266
DEC01	2010	100	739	0.			FUEL CELL RAD TO BEAMS 3,4			220102266
INC	1	0	1	0.	5					220112266
DEC01	2016	100	713	0.			FUEL CELL RAD TO SHELL			220162266
INC	1	0	1	0.	3					220172266
DEC01	2020	100	752	0.			FUEL CELL RAD TO ENGINE WEB			220202266
DEC01	2021	100	753	0.			MOUNT IN BAY 4			220212266
DEC01	2022	100	759	0.						220222266
DEC01	2023	100	852	0.						220232266
DEC01	2024	100	853	0.						220242266
DEC01	2025	100	859	0.						220252266
DEC01	2026	100	556	0.			FUEL CELL RAD TO CENTER			220262266
DEC01	2027	100	655	0.			CYLINDER			220272266
DEC01	2028	100	557	0.			FUEL CELL RAD TO HE BOTTLE			220282266
DEC02	2030	133	233	9350.	2031	134	234	9350.	BEAMS TO	220302266
DEC02	2032	135	235	5030.	2033	136	236	9350.	BLKD.	220322266
DEC02	2034	137	237	9350.	2035	138	238	5030.		220342266
DEC02	2036	139	239	9350.	2037	140	240	9350.		220362266
DEC02	2038	141	241	5030.	2039	142	242	9530.		220382266
DEC02	2040	143	243	9530.	2041	144	244	5070.		220402266
DEC02	2042	145	245	9350.	2043	146	246	9350.		220422266
DEC02	2044	147	247	5030.	2045	148	248	9350.		220442266
DEC02	2046	149	249	9350.	2047	150	250	5030.		220462266
DEC02	2048	833	933	8700.	2049	834	934	8700.		220482266
DEC02	2050	835	935	4720.	2051	836	938	8200.		220502266
DEC02	2052	837	939	8200.	2053	838	940	4570.		220522266
DEC02	2054	839	943	9130.	2055	840	944	9130.		220542266
DEC02	2056	841	945	4850.	2057	842	949	9570.		220562266
DEC02	2058	843	950	9570.	2059	844	951	4980.		220582266
DEC02	2060	845	954	8200.	2061	846	955	8200.		220602266
DEC02	2062	847	956	4570.	2063	848	959	9350.		220622266
DEC02	2064	849	960	9350.	2065	850	961	5030.		220642266
DEC02	2093	933	1063	0.	2094	934	1051	0.	AFT H.S.	220932266

TABLE B-1 (Cont.)

DEC02	2095	935	1075	0.	2096	936	1034	0.	TO BLKD.	220952266
DEC02	2097	937	1041	0.	2098	938	1035	0.		220972266
DEC02	2099	939	1065	0.	2100	940	1042	0.		220992266
DEC02	2101	941	1036	0.	2102	942	1043	0.		221012266
DEC02	2103	943	1067	0.	2104	944	1055	0.		221032266
DEC02	2105	945	1044	0.	2106	946	1068	0.		221052266
DEC02	2107	947	1078	0.	2108	948	1045	0.		221072266
DEC02	2109	949	1069	0.	2110	950	1057	0.		221092266
DEC02	2111	951	1046	0.	2112	952	1037	0.		221112266
DEC02	2113	953	1047	0.	2114	954	1038	0.		221132266
DEC02	2115	955	1071	0.	2116	956	1048	0.		221152266
DEC02	2117	957	1039	0.	2118	958	1049	0.		221172266
DEC02	2119	959	1073	0.	2120	960	1061	0.		221192266
DEC02	2121	961	1081	0.	2122	962	1074	0.		221212266
DEC02	2123	963	1062	0.	2124	964	1082	0.		221232266
DEC02	2125	-25	27	29300.	2126	26	40	25100.		221252266
DEC02	2127	26	27	25100.	2128	28	30	35200.		221272266
DEC02	2129	28	29	37000.	2130	29	31	37000.		221292266
DEC02	2131	30	31	35200.	2132	32	34	25100.		221312266
DEC02	2133	32	33	29300.	2134	34	35	25100.		221332266
DEC02	2135	33	35	29300.	2136	36	37	37000.		221352266
DEC02	2137	37	39	37000.	2138	36	38	35200.		221372266
DEC02	2139	38	39	35200.	2140	25	40	29300.		221392266
DEC02	2175	1025	1001	0.	2176	1026	1001	0.	H.S.TO H.S	221752266
DEC02	2177	1027	1017	0.	2178	1028	1018	0.		221772266
DEC02	2179	1029	1019	0.	2180	1030	1011	0.		221792266
DEC02	2181	1031	1011	0.	2182	1032	1012	0.		221812266
DEC01	2183	1089	1095	0.						221832265
INC	1	1	1	0.	5					221842266
DEC01	2189	1101	1107	0.						221892266
INC	1	1	1	0.	5					221902266
DEC01	2195	1113	1119	0.						221952266
INC	1	1	1	0.	5					221962266
DEC01	2201	1001	1101	0.					AFT H.S. RAD.	222012266
INC	1	1	1	0.	23					2266
DEC01	2225	1025	1	0.						222252266
INC	1	1	0	0.	15				AFT H.S. RAD.	2266
DEC01	2241	1001	1	0.						222412266
INC	1	1	0	0.	23					2266
DEC01	2265	1089	1	0.						222652266
INC	1	1	0	0.	35					222662266
DEC01	2301	1001	1051	39200.			CONDUCTION ON AFT H.S.			223012266
DEC01	2302	1002	1052	33400.			THRU QUARTZ FIBER			223022266
DEC01	2303	1003	1053	51600.						223032266
DEC01	2304	1004	1054	51600.						223042266
DEC01	2305	1005	1055	40000.						223052266
DEC01	2306	1006	1056	40000.						223062266
DEC01	2307	1007	1057	40000.						223072266
DEC01	2308	1008	1058	51600.						223082266
DEC01	2309	1009	1059	51600.						223092266
DEC01	2310	1010	1060	33400.						223102266
DEC01	2311	1011	1061	39200.						223112266
DEC01	2312	1012	1062	39200.						223122266
DEC01	2313	1013	1063	39200.						223132266
DEC01	2314	1014	1064	33400.						223142266
DEC01	2315	1015	1065	51600.						223152266
DEC01	2316	1016	1066	51600.						223162266
DEC01	2317	1017	1067	53300.						223172266
DEC01	2318	1018	1068	35600.						223182266
DEC01	2319	1019	1069	53300.						223192266
DEC01	2320	1020	1070	51600.						223202266

LOCKHEED
CALIFORNIA COMPANY

TABLE B-1 (Cont.)

DEC01	2321	1021	1071	51600.	223212266
DEC01	2322	1022	1072	33400.	223222266
DEC01	2323	1023	1073	39200.	223232266
DEC01	2324	1024	1074	39200.	223242266
DEC01	2325	1025	1075	146000.	223252266
DEC01	2326	1026	1076	48800.	223262266
DEC01	2327	1027	1077	45700.	223272266
DEC01	2328	1028	1078	45700.	223282266
DEC01	2329	1029	1079	45700.	223292266
DEC01	2330	1030	1080	48500.	223302266
DEC01	2331	1031	1081	146000.	223312266
DEC01	2332	1032	1082	146000.	223322266
NBK					299992266

TABLE B-1 (Cont.)

```
      DATA (KFACT(I),I=1,68) / .706E-4,3.99E-4,4.38E-4,4.47E-4,4.47E-4,  22662010
     1 4.12E-4,.706E-4,4.39E-4,4.75E-4,4.75E-4,4.39E-4,.706E-4,3.99E-4,  22662011
     2 4.38E-4,4.38E-4,2.38E-4,.706E-4,3.99E-4,4.38E-4,4.47E-4,4.47E-4,  22662012
     3 4.12E-4,.706E-4,4.39E-4,4.75E-4,4.75E-4,4.39E-4,.706E-4,2.38E-4,  22662013
     4 4.38E-4,4.38E-4,3.99E-4,.975E-4,4.36E-4,.609E-4,2.45E-4,1.52E-4,  22662014
     5 1.52E-4,.488E-4,1.98E-4,8.03E-4,2.81E-4,4.75E-4,.609E-4,2.45E-4,  22662015
     6 1.52E-4,1.52E-4,8.73E-4,2.54E-4,2.81E-4,.975E-4,4.36E-4,.609E-4,  22662016
     7 2.45E-4,1.52E-4,1.52E-4,.488E-4,1.98E-4,8.03E-4,2.81E-4,4.75E-4,  22662017
     8 .609E-4,2.45E-4,1.52E-4,1.52E-4,8.73E-4,2.54E-4,2.81E-4/          22662018
      DATA (FKR1(I),I=1,9) /2.32E-4,0.50E-4,1.E-4,1.93E-4,1.93E-4,          202
     1  1.93E-4,1.00E-4,0.50E-4,2.32E-4/                                   2021
      DATA (FKR(I),I=1,3)/8.7E-5,3.17E-4,6.23E-4/                         203
      DATA ((FKR2(I,J),I=1,3),J=1,7)/ 7.81E-7,1.73E-6,1.41E-6,9.50E-7,    204
     1 1.77E-6,1.50E-6,9.67E-7,1.77E-6,1.505E-6,4.03E-6,7.34E-6,6.25E-6,  2041
     2 9.67E-7,1.77E-6,1.505E-6,9.50E-7,1.77E-6,1.50E-6,7.81E-7,1.73E-6,  2042
     3 1.41E-6/                                                           2043
C        NOZZLE TO NOZZLE RADIATION RESISTORS                             300
      DO 28 I=1,6                                                        2266301
      R(I+2182)=RAD((I+1088),(I+1094),1.95E-4)                           2266302
   28 CONTINUE                                                           2266303
      DO 29 I=1,6                                                        2266304
      R(I+2188)=RAD((I+1100),(I+1106),4.16E-4)                             305
   29 CONTINUE                                                           2266306
      DO 30 I=1,6                                                        2266308
      R(I+2194)=RAD((I+1112),(I+1118),3.36E-4)                           2266309
   30 CONTINUE                                                           2266310
C        NOZZLE TO SPACE RADIATION RESISTORS                              311
      DO 31 I=1,12                                                       2266311
      R(I+2264)=RAD((I+1088),1,3.24E-4)                                  2266312
   31 CONTINUE                                                           2266323
      DO 32 I=1,12                                                       2266324
      R(I+2276)=RAD((I+1100),1,1.07E-3)                                  2266325
   32 CONTINUE                                                           2266334
      DO 33 I=1,12                                                       2266335
      R(I+2288)=RAD((I+1112),1,2.32E-3)                                  2266336
   33 CONTINUE                                                           2266347
C        NOZZLE TO HEAT SHIELD RADIATION RESISTORS                        A347
      R(2201)=RAD(1001,1101,5.28E-5)                                     2266348
      R(2202)=RAD(1002,1102,13.5E-5)                                     2266349
      R(2203)=RAD(1003,1103,8.65E-5)                                     2266350
      R(2204)=RAD(1004,1104,8.65E-5)                                     2266351
      R(2205)=RAD(1005,1105,8.85E-5)                                     2266352
      R(2206)=RAD(1006,1106,12.1E-5)                                     2266353
      R(2207)=RAD(1007,1107,7.38E-5)                                     2266354
      R(2208)=RAD(1008,1108,8.65E-5)                                     2266355
      R(2209)=RAD(1009,1109,8.65E-5)                                     2266356
      R(2210)=RAD(1010,1110,13.5E-5)                                     2266357
      R(2211)=RAD(1011,1111,5.28E-5)                                     2266358
      R(2212)=RAD(1012,1112,5.70E-5)                                     2266359
      R(2213)=RAD(1013,1113,4.22E-5)                                     2266360
      R(2214)=RAD(1014,1114,7.80E-5)                                     2266361
      R(2215)=RAD(1015,1115,5.02E-5)                                     2266362
      R(2216)=RAD(1016,1116,5.02E-5)                                     2266363
      R(2217)=RAD(1017,1117,2.64E-5)                                     2266364
      R(2218)=RAD(1018,1118,4.96E-5)                                     2266365
      R(2219)=RAD(1019,1119,2.64E-5)                                     2266366
      R(2220)=RAD(1020,1120,4.43E-5)                                     2266367
      R(2221)=RAD(1021,1121,4.20E-5)                                     2266368
      R(2222)=RAD(1022,1122,6.38E-5)                                     2266369
      R(2223)=RAD(1023,1123,4.22E-5)                                     2266370
      R(2224)=RAD(1024,1124,4.22E-5)                                     2266371
```


LOCKHEED CALIFORNIA COMPANY

TABLE B-1 (Cont.)

HEAT SHIELD TO SPACE RADIATION RESISTORS	372
R(2225)=RAD(1025,1,.42E-4)	2266373
R(2226)=RAD(1026,1,2.70E-4)	2266374
R(2227)=RAD(1027,1,1.62E-4)	2266375
R(2228)=RAD(1028,1,1.62E-4)	2266376
R(2229)=RAD(1029,1,1.62E-4)	2266377
R(2230)=RAD(1030,1,1.78E-4)	2266378
R(2231)=RAD(1031,1,0.42E-4)	2266379
R(2232)=RAD(1032,1,0.42E-4)	2266380
R(2233)=RAD(1033,1,3.02E-4)	2266381
R(2234)=RAD(1034,1,5.82E-4)	2266382
R(2235)=RAD(1035,1,3.20E-4)	2266383
R(2236)=RAD(1036,1,3.20E-4)	2266384
R(2237)=RAD(1037,1,3.20E-4)	2266385
R(2238)=RAD(1038,1,3.20E-4)	2266386
R(2239)=RAD(1039,1,5.82E-4)	2266387
R(2240)=RAD(1040,1,3.02E-4)	2266388
R(2241)=RAD(1001,1,1.32E-4)	2266389
R(2242)=RAD(1002,1,2.37E-4)	2266390
R(2243)=RAD(1003,1,1.48E-4)	2266391
R(2244)=RAD(1004,1,1.48E-4)	2266392
R(2245)=RAD(1005,1,2.16E-4)	2266393
R(2246)=RAD(1006,1,1.82E-4)	2266394
R(2247)=RAD(1007,1,2.32E-4)	2266395
R(2248)=RAD(1008,1,1.48E-4)	2266396
R(2249)=RAD(1009,1,1.48E-4)	2266397
R(2250)=RAD(1010,1,2.30E-4)	2266398
R(2251)=RAD(1011,1,1.32E-4)	2266399
R(2252)=RAD(1012,1,1.39E-4)	2266400
R(2253)=RAD(1013,1,1.77E-4)	2266401
R(2254)=RAD(1014,1,2.89E-4)	2266402
R(2255)=RAD(1015,1,1.86E-4)	2266403
R(2256)=RAD(1016,1,1.86E-4)	2266404
R(2257)=RAD(1017,1,1.85E-4)	2266405
R(2258)=RAD(1018,1,2.77E-4)	2266406
R(2259)=RAD(1019,1,1.85E-4)	2266407
R(2260)=RAD(1020,1,1.94E-4)	2266408
R(2261)=RAD(1021,1,1.95E-4)	2266409
R(2262)=RAD(1022,1,3.04E-4)	2266410
R(2263)=RAD(1023,1,1.77E-4)	2266411
R(2264)=RAD(1024,1,1.77E-4)	2266412
HEAT SHIELD TO HEAT SHIELD AND BULKHEAD RADIATION RESISTORS	A412
R(2175)=RAD(1025,1001,2.64E-5)	2266413
R(2176)=RAD(1026,1001,10.4E-5)	2266414
R(2177)=RAD(1027,1017,3.38E-5)	2266415
R(2178)=RAD(1028,1018,3.38E-5)	2266416
R(2179)=RAD(1029,1019,3.38E-5)	2266417
R(2180)=RAD(1030,1011,4.78E-5)	2266418
R(2181)=RAD(1031,1011,2.64E-5)	2266419
R(2182)=RAD(1032,1012,2.64E-5)	2266420
R(2093)=RAD(933,1063,2.93E-6)	2266421
R(2094)=RAD(934,1051,2.50E-6)	2266422
R(2095)=RAD(935,1075,0.99E-6)	2266422
R(2096)=RAD(936,1034,1.97E-6)	2266423
R(2097)=RAD(937,1041,0.19E-6)	2266424
R(2098)=RAD(938,1035,3.08E-6)	2266425
R(2099)=RAD(939,1065,1.30E-6)	2266426
R(2100)=RAD(940,1042,0.96E-6)	2266427
R(2101)=RAD(941,1036,1.32E-6)	2266428
R(2102)=RAD(942,1043,0.38E-6)	2266429
R(2103)=RAD(943,1067,2.96E-6)	2266430

TABLE B-1 (Cont.)

R(2104)=RAD(944,1055,2.28E-6)	2266431
R(2105)=RAD(945,1044,1.15E-6)	2266432
R(2106)=RAD(946,1068,3.00E-6)	2266433
R(2107)=RAD(947,1078,3.60E-6)	2266434
R(2108)=RAD(948,1045,1.32E-6)	2266435
R(2109)=RAD(949,1069,2.38E-6)	2266436
R(2110)=RAD(950,1057,1.75E-6)	2266437
R(2111)=RAD(951,1046,0.80E-6)	2266438
R(2112)=RAD(952,1037,1.97E-6)	2266439
R(2113)=RAD(953,1047,0.19E-6)	2266440
R(2114)=RAD(954,1038,3.08E-6)	2266441
R(2115)=RAD(955,1071,1.30E-6)	2266442
R(2116)=RAD(956,1048,0.96E-6)	2266443
R(2117)=RAD(957,1039,1.32E-6)	2266444
R(2118)=RAD(958,1049,0.38E-6)	2266445
R(2119)=RAD(959,1073,2.16E-6)	2266446
R(2120)=RAD(960,1061,1.63E-6)	2266447
R(2121)=RAD(961,1081,0.84E-6)	2266448
R(2122)=RAD(962,1074,3.00E-6)	2266449
R(2123)=RAD(963,1062,3.60E-6)	2266450
R(2124)=RAD(964,1082,1.32E-6)	2266451
BULKHEAD TO SPACE RADIATION RESISTORS	A451
R(1388)=RAD(933,1,5.1E-4)	2266451
R(1389)=RAD(936,1,3.3E-4)	2266452
R(1390)=RAD(938,1,4.0E-4)	2266453
R(1391)=RAD(941,1,4.6E-4)	2266454
R(1392)=RAD(943,1,4.6E-4)	2266455
R(1393)=RAD(946,1,4.8E-4)	2266456
R(1394)=RAD(949,1,4.0E-4)	2266457
R(1395)=RAD(952,1,4.8E-4)	2266458
R(1396)=RAD(954,1,5.1E-4)	2266459
R(1397)=RAD(957,1,3.7E-4)	2266460
R(1398)=RAD(959,1,5.7E-4)	2266461
R(1399)=RAD(962,1,5.3E-4)	2266462
BULKHEAD TO NOZZLE RADIATION RESISTORS	A462
R(1582)=RAD(933,1113,8.1E-5)	2266463
R(1583)=RAD(936,1114,5.5E-5)	2266464
R(1584)=RAD(938,1115,6.4E-5)	2266465
R(1585)=RAD(941,1116,7.5E-5)	2266466
R(1586)=RAD(943,1117,7.5E-5)	2266467
R(1587)=RAD(946,1118,7.7E-5)	2266468
R(1588)=RAD(949,1119,6.4E-5)	2266469
R(1589)=RAD(952,1120,7.9E-5)	2266470
R(1590)=RAD(954,1121,8.1E-5)	2266471
R(1591)=RAD(957,1122,5.9E-5)	2266472
R(1592)=RAD(959,1123,9.7E-5)	2266473
R(1593)=RAD(962,1124,8.4E-5)	2266474
SPS ENGINE TO SURROUNDINGS	A474
R(1578)=RAD(278,757,2.13E-5)	2266475
R(1579)=RAD(278,758,2.40E-5)	2266476
R(1580)=RAD(278,759,2.13E-5)	2266477
R(1581)=RAD(278,760,2.40E-5)	2266478
R(1678)=RAD(279,757,2.13E-5)	2266479
R(1679)=RAD(279,758,2.40E-5)	2266480
R(1680)=RAD(279,759,2.13E-5)	2266481
R(1681)=RAD(279,760,2.40E-5)	2266482
R(1778)=RAD(280,757,4.00E-5)	2266483
R(1779)=RAD(280,758,4.48E-5)	2266484
R(1780)=RAD(280,759,4.00E-5)	2266485
R(1781)=RAD(280,760,4.48E-5)	2266486
R(1978)=RAD(281,857,3.37E-5)	2266487

TABLE B-1 (Cont.)

```
      R(1979)=RAD(281,858,3.78E-5)                                    2266488
      R(1980)=RAD(281,859,3.37E-5)                                    2266489
      R(1981)=RAD(281,860,3.78E-5)                                    2266490
      R(1494)=RAD(280,200,1.60E-5)                                    2266491
      R(1495)=RAD(280,500,1.60E-5)                                    2266492
      R(1496)=RAD(282,857,2.62E-5)                                    2266493
      R(1497)=RAD(282,858,2.88E-5)                                    2266494
      R(1498)=RAD(282,859,2.62E-5)                                    2266495
      R(1499)=RAD(282,860,2.88E-5)                                    2266496
      R(1500)=RAD(278,279,7.80E-5)                                    2266497
C        SHELL TO SPACE                                                  6600
  27  DO 271 I=1,32                                                   22666601
      R(I+1100)=RAD(I+100,1,KFACT(I))                                 22666602
      R(I+1200)=RAD(I+200,1,KFACT(I)*0.855)                           22666603
      R(I+1300)=RAD(I+300,1,KFACT(I)*0.855)                           22666604
      R(I+1400)=RAD(I+400,1,KFACT(I)*0.855)                           22666605
      R(I+1500)=RAD(I+500,1,KFACT(I)*1.845)                           22666606
      R(I+1600)=RAD(I+600,1,KFACT(I)*0.855)                           22666607
      R(I+1700)=RAD(I+700,1,KFACT(I)*0.855)                           22666608
      R(I+1800)=RAD(I+800,1,KFACT(I)*0.855)                           22666609
 271  CONTINUE                                                        22666610
C        RCS HEAT SHIELD TO SPACE                                        A6610
      DO 272 J=42,77                                                  22666611
      R(J+1900)=RAD(J,1,KFACT(J-9))                                   22666612
 272  CONTINUE                                                        22666613
C        OVERRIDE ON SHELL-SPACE RAD.RES. FOR NODES COVERED BY RCS H/S   6619
      R(1102)=RAD(102,1,3.38E-4)                                      22666620
      R(1103)=RAD(103,1,1.0E-20)                                      22666621
      R(1104)=RAD(104,1,3.87E-4)                                      22666622
      R(1110)=RAD(110,1,1.0E-20)                                      22666623
      R(1111)=RAD(111,1,4.14E-4)                                      22666624
      R(1118)=RAD(118,1,3.38E-4)                                      22666625
      R(1119)=RAD(119,1,1.0E-20)                                      22666626
      R(1120)=RAD(120,1,3.87E-4)                                      22666627
      R(1126)=RAD(126,1,1.0E-20)                                      22666628
      R(1127)=RAD(127,1,4.14E-4)                                      22666629
      R(1203)=RAD(203,1,1.27E-4)                                      22666630
      R(1210)=RAD(210,1,1.60E-4)                                      22666631
      R(1219)=RAD(219,1,1.27E-4)                                      22666632
      R(1226)=RAD(226,1,1.60E-4)                                      22666633
      R(1302)=RAD(302,1,2.19E-4)                                      22666634
      R(1304)=RAD(304,1,2.30E-4)                                      22666635
      R(1309)=RAD(309,1,2.52E-4)                                      22666636
      R(1311)=RAD(311,1,2.52E-4)                                      22666637
      R(1318)=RAD(318,1,2.19E-4)                                      22666638
      R(1320)=RAD(320,1,2.30E-4)                                      22666639
      R(1325)=RAD(325,1,2.52E-4)                                      22666640
      R(1327)=RAD(327,1,2.52E-4)                                      22666641
      R(1403)=RAD(403,1,3.22E-4)                                      22666642
      R(1419)=RAD(419,1,3.22E-4)                                      22666643
      R(1502)=RAD(502,1,6.06E-4)                                      22666644
      R(1503)=RAD(503,1,1.0E-20)                                      22666645
      R(1510)=RAD(510,1,1.0E-20)                                      22666646
      R(1511)=RAD(511,1,6.19E-4)                                      22666647
      R(1518)=RAD(518,1,6.06E-4)                                      22666648
      R(1519)=RAD(519,1,1.0E-20)                                      22666649
      R(1526)=RAD(526,1,1.0E-20)                                      22666650
      R(1527)=RAD(527,1,6.19E-4)                                      22666651
      R(1603)=RAD(603,1,.900E-4)                                      22666652
      R(1610)=RAD(610,1,1.23E-4)                                      22666653
      R(1619)=RAD(619,1,.900E-4)                                      22666654
```

TABLE B-1 (Cont.)

```
R(1626)=RAD(626,1,1.23E-4)                                    22666655
   PROPELLANT TANKS TO RADIAL BEAMS                              6699
J2=135                                                           6700
J3=1000                                                          6700
DO 276 I1=1,2                                                    6701
J1=300*I1                                                        6702
DO 275 I2=1,7                                                    6703
DO 274 I3=1,3                                                    6704
J4=J2 +I2*100+I3                                                 6705
R(J3)=RAD(J1,J4,FKR2(I3,I2))                                     6706
J3=J3+1                                                          6707
CONTINUE                                                         6708
CONTINUE                                                         6709
J2=144                                                           6710
CONTINUE                                                         6711
   HELIUM BOTTLES TO SURROUNDINGS RADIATION RESISTORS            6749
R(1180)=RAD(357,255,4.5E-5)                                   22666750
R(1181)=RAD(357,355,3.9E-5)                                   22666751
R(1182)=RAD(357,455,5.7E-5)                                   22666752
R(1183)=RAD(357,555,5.7E-6)                                   22666753
R(1187)=RAD(557,455,1.74E-5)                                  22666757
R(1188)=RAD(557,555,5.55E-5)                                  22666758
R(1189)=RAD(557,655,2.78E-5)                                  22666759
R(1190)=RAD(357,256,4.5E-5)                                   22666760
R(1191)=RAD(357,356,3.9E-5)                                   22666761
R(1192)=RAD(357,456,5.7E-5)                                   22666762
R(1193)=RAD(357,556,6.6E-6)                                   22666763
R(1196)=RAD(557,456,1.74E-5)                                  22666766
R(1197)=RAD(557,556,3.8E-5)                                   22666767
R(1198)=RAD(357,557,9.74E-5)                                  22666768
R(1199)=RAD(357,7,17.4E-5)                                    22666769
R(1380)=RAD(357,200,1.8E-4)                                   22666770
R(1381)=RAD(357,300,1.6E-4)                                   22666771
R(1382)=RAD(357,500,1.8E-4)                                   22666772
R(1383)=RAD(357,600,1.6E-4)                                   22666773
R(1384)=RAD(557,200,1.67E-4)                                  22666774
R(1385)=RAD(557,300,1.46E-4)                                  22666775
R(1386)=RAD(557,500,1.67E-4)                                  22666776
R(1387)=RAD(557,600,1.46E-4)                                  22666777
   FUEL CELLS TO SURROUNDINGS                                    6779
R(2000)=RAD(100,943,.423E-4)                                  20886780
R(2001)=RAD(100,944,.505E-4)                                  20886781
R(2002)=RAD(100,945,.092E-4)                                  20886782
R(2003)=RAD(100,946,.975E-4)                                  20886783
R(2004)=RAD(100,947,1.62E-4)                                  20886784
R(2005)=RAD(100,948,.350E-4)                                  20886785
R(2006)=RAD(100,949,.197E-4)                                  20886786
R(2007)=RAD(100,950,.252E-4)                                  20886787
R(2008)=RAD(100,951,.054E-4)                                  20886788
R(2009)=RAD(100,16,.1880E-4)                                  20886789
R(2010)=RAD(100,739,.0258E-4)                                 20886790
R(2011)=RAD(100,740,.0400E-4)                                 20886791
R(2012)=RAD(100,741,.0235E-4)                                 20886792
R(2013)=RAD(100,742,.0258E-4)                                 20886793
R(2014)=RAD(100,743,.0400E-4)                                 20886794
R(2015)=RAD(100,744,.0235E-4)                                 20886795
R(2016)=RAD(100,713,.0327E-4)                                 20886796
R(2017)=RAD(100,714,.0477E-4)                                 20886797
R(2018)=RAD(100,715,.0411E-4)                                 20886798
R(2019)=RAD(100,716,.0162E-4)                                 20886799
R(2020)=RAD(100,752,.079E-4)                                  20886800
```


LOCKHEED
CALIFORNIA COMPANY

TABLE B-1 (Cont.)

```
      R(2021)=RAD(100,753,.100E-4)                                    20886801
      R(2022)=RAD(100,759,.185E-4)                                    20886802
      R(2023)=RAD(100,852,.064E-4)                                    20886803
      R(2024)=RAD(100,853,.082E-4)                                    20886804
      R(2025)=RAD(100,859,.155E-4)                                    20886805
      R(2026)=RAD(100,556,.0164E-4)                                   20886806
      R(2027)=RAD(100,655,.0382E-4)                                   20886807
      R(2028)=RAD(100,557,.0940E-4)                                   20886808
      DO 300 J= 1,28                                                  2266681
      L(J)=LOC(J+431)                                                 22666811
  300 CONTINUE                                                        22666819
C         PROPELLANT TANKS TO SURROUNDINGS                            A6819
      DO 301 I=1,7                                                    2266682
      J2=L(1)+I                                                       C0A 6821
      J1=P(J2)                                                        C0A 6822
      J33=L(2)+I                                                      22666833
      J34=L(3)+I                                                      22666834
      J35=L(4)+I                                                      22666835
      J36=L(5)+I                                                      22666836
      J37=L(6)+I                                                      22666837
      J38=L(7)+I                                                      22666838
      J39=L(8)+I                                                      22666839
      J40=L(9)+I                                                      22666840
      J41=L(10)+I                                                     22666841
      J42=L(11)+I                                                     22666842
      J43=L(12)+I                                                     22666843
      J44=L(13)+I                                                     22666844
      J45=L(14)+I                                                     22666845
      J46=L(15)+I                                                     22666846
      J47=L(16)+I                                                     22666847
      J48=L(17)+I                                                     22666848
      J49=L(18)+I                                                     22666849
      J50=L(19)+I                                                     22666850
      J51=L(20)+I                                                     22666851
      J52=L(21)+I                                                     22666852
      J53=L(22)+I                                                     22666853
      J54=L(23)+I                                                     22666854
      J55=L(24)+I                                                     22666855
      J56=L(25)+I                                                     22666856
      J57=L(26)+I                                                     22666857
      J58=L(27)+I                                                     22666858
      J59=L(28)+I                                                     22666859
      R(J1+1133)=RAD((J1+133),200,P(J33)*1.E-6)                       22666863
      R(J1+1134)=RAD((J1+134),200,P(J34)*1.E-6)                       22666864
      R(J1+1135)=RAD((J1+135),200,P(J35)*1.E-6)                       22666865
      R(J1+1136)=RAD((J1+136),200,P(J36)*1.E-6)                       22666866
      R(J1+1137)=RAD((J1+137),200,P(J37)*1.E-6)                       22666867
      R(J1+1138)=RAD((J1+138),200,P(J38)*1.E-6)                       22666868
      R(J1+1139)=RAD((J1+139),300,P(J39)*1.E-6)                       22666869
      R(J1+1140)=RAD((J1+140),300,P(J40)*1.E-6)                       22666870
      R(J1+1141)=RAD((J1+141),300,P(J41)*1.E-6)                       22666871
      R(J1+1142)=RAD((J1+142),500,P(J42)*1.E-6)                       22666872
      R(J1+1143)=RAD((J1+143),500,P(J43)*1.E-6)                       22666873
      R(J1+1144)=RAD((J1+144),500,P(J44)*1.E-6)                       22666874
      R(J1+1145)=RAD((J1+145),500,P(J45)*1.E-6)                       22666875
      R(J1+1146)=RAD((J1+146),500,P(J46)*1.E-6)                       22666876
      R(J1+1147)=RAD((J1+147),500,P(J47)*1.E-6)                       22666877
      R(J1+1148)=RAD((J1+148),600,P(J48)*1.E-6)                       22666878
      R(J1+1149)=RAD((J1+149),600,P(J49)*1.E-6)                       22666879
      R(J1+1150)=RAD((J1+150),600,P(J50)*1.E-6)                       22666880
      R(J1+1152)=RAD((J1+102),200,P(J51)*1.E-6)                       22666882
```

TABLE B-1 (Cont.)

```
R(J1+1153)=RAD((J1+103),200,P(J52)*1.E-6)                    22666883
R(J1+1154)=RAD((J1+104),200,P(J53)*1.E-6)                    22666884
R(J1+1155)=RAD((J1+105),200,P(J54)*1.E-6)                    22666885
R(J1+1156)=RAD((J1+106),200,P(J55)*1.E-6)                    22666886
R(J1+1158)=RAD((J1+108),300,P(J56)*1.E-6)                    22666888
R(J1+1159)=RAD((J1+109),300,P(J57)*1.E-6)                    22666889
R(J1+1160)=RAD((J1+110),300,P(J58)*1.E-6)                    22666890
R(J1+1161)=RAD((J1+111),300,P(J59)*1.E-6)                    22666891
R(J1+1168)=RAD((J1+118),500,P(J51)*1.E-6)                    22666898
R(J1+1169)=RAD((J1+119),500,P(J52)*1.E-6)                    22666899
R(J1+1170)=RAD((J1+120),500,P(J53)*1.E-6)                    22666900
R(J1+1171)=RAD((J1+121),500,P(J54)*1.E-6)                    22666901
R(J1+1172)=RAD((J1+122),500,P(J55)*1.E-6)                    22666902
R(J1+1174)=RAD((J1+124),600,P(J56)*1.E-6)                    22666904
R(J1+1175)=RAD((J1+125),600,P(J57)*1.E-6)                    22666905
R(J1+1176)=RAD((J1+126),600,P(J58)*1.E-6)                    22666906
R(J1+1177)=RAD((J1+127),600,P(J59)*1.E-6)                    22666907
CONTINUE                                                     22666909
    THRUST CHAMBER TO AFT HEAT SHIELD                          A6909
DO 302 I=1,9                                                    6910
R(I+1781)=RAD(I+1040,282,FKR1(I))                               6911
CONTINUE                                                        6912
R(1791)=RAD(1084,282,1.12E-4)                                22666919
R(1792)=RAD(1085,282,1.12E-4)                                22666920
R(1793)=RAD(1083,282,1.12E-4)                                22666921
                                                                0391
                                                              000391
```


LOCKHEED
CALIFORNIA COMPANY

TABLE B-1 (Cont.)

DEC 432	STORAGE FOR DO LOOP 301						432012266
DEC06	100.	200.	300.	400.	500.	600.	432022266
DEC01	700.						432032266
DEC -432							432042266
DEC 433	RADIATION K-FACTORS RADIAL BEAMS TO PROPELLANT TANKS						433012266
DEC06	.738	.920	.945	2.04	.945	.920	433022266
DEC01	.738						433032266
DEC -433							433042266
DEC 434							434012266
DEC06	1.63	1.69	1.70	3.66	1.70	1.69	434022266
DEC01	1.63						434032266
DEC -434							434042266
DEC 435							435012266
DEC06	1.66	1.72	1.72	3.71	1.72	1.72	435022266
DEC01	1.66						435032266
DEC -435							435042266
DEC 436							436012266
DEC06	.738	.920	.945	2.05	.945	.920	436022266
DEC01	.738						436032266
DEC -436							436042266
DEC 437							437012266
DEC06	1.63	1.69	1.70	3.66	1.70	1.69	437022266
DEC01	1.63						437032266
DEC -437							437042266
DEC 438							438012266
DEC06	1.66	1.72	1.72	3.71	1.72	1.72	438022266
DEC01	1.66						438032266
DEC -438							438042266
DEC 439							439012266
DEC06	.760	.932	.950	3.96	.950	.932	439022266
DEC01	.760						439032266
DEC -439							439042266
DEC 440							440012266
DEC06	1.72	1.765	1.77	7.32	1.77	1.765	440022266
DEC01	1.72						440032266
DEC -440							440042266
DEC 441							441012266
DEC06	1.41	1.51	1.51	6.28	1.51	1.51	441022266
DEC01	1.41						441032266
DEC -441							441042266
DEC 442							442012266
DEC06	.738	.920	.945	2.04	.945	.920	442022266
DEC01	.738						442032266
DEC -442							442042266
DEC 443							443012266
DEC06	1.63	1.69	1.70	3.66	1.70	1.69	443022266
DEC01	1.63						443032266
DEC -443							443042266
DEC 444							444012266
DEC06	1.66	1.72	1.72	3.71	1.72	1.72	444022266
DEC01	1.66						444032266
DEC -444							444042266
DEC 445							445012266
DEC06	.738	.920	.945	2.04	.945	.920	445022266
DEC01	.738						445032266
DEC -445							445042266
DEC 446							446012266
DEC06	1.63	1.69	1.70	3.66	1.70	1.69	446022266
DEC01	1.63						446032266
DEC -446							446042266
DEC 447							447012266

LOCKHEED CALIFORNIA COMPANY

TABLE B-1 (Cont.)

DEC06	1.66	1.72	1.72	3.71	1.72	1.72	447022266
DEC01	1.66						447032266
DEC -447							447042266
DEC 448							448012266
DEC06	.760	.932	.950	3.96	.950	.932	448022266
DEC01	.760						448032266
DEC -448							448042266
DEC 449							449012266
DEC06	1.72	1.765	1.77	7.32	1.77	1.765	449022266
DEC01	1.72						449032266
DEC -449							449042266
DEC 450							450012266
DEC06	1.41	1.51	1.51	6.28	1.51	1.51	450022266
DEC01	1.41						450032266
DEC -450							450042266
DEC 451	RADIATION K-FACTORS SHELL TO PROPELLANT TANKS						451012266
DEC06	.815	1.04	1.07	2.33	1.07	1.04	451022266
DEC01	.815						451032266
DEC -451							451042266
DEC 452							452012266
DEC06	1.40	1.54	1.55	3.36	1.55	1.54	452022266
DEC01	1.40						452032266
DEC -452							452042266
DEC 453							453012266
DEC06	1.73	1.84	1.90	4.21	1.90	1.84	453022266
DEC01	1.73						453032266
DEC -453							453042266
DEC 454							454012266
DEC06	1.47	1.61	1.62	3.5	1.62	1.61	454022266
DEC01	1.47						454032266
DEC -454							454042266
DEC 455							455012266
DEC06	.83	1.07	1.10	2.39	1.10	1.07	455022266
DEC01	.83						455032266
DEC -455							455042266
DEC 456							456012266
DEC06	.94	1.18	1.21	2.61	1.21	1.18	456022266
DEC01	.94						456032266
DEC -456							456042266
DEC 457							457012266
DEC06	1.65	1.77	1.78	3.84	1.78	1.77	457022266
DEC01	1.65						457032266
DEC -457							457042266
DEC 458							458012266
DEC06	1.66	1.78	1.79	3.84	1.79	1.78	458022266
DEC01	1.66						458032266
DEC -458							458042266
DEC 459							459012266
DEC06	.94	1.17	1.18	2.61	1.18	1.17	459022266
DEC01	.94						459032266
DEC -459							459042266

LOCKHEED
CALIFORNIA COMPANY

TABLE B-2

DEC03	11	1.355	12	.351	13	.99	FWD. BULKHEAD	300112266
DEC03	14	.268	15	.692	16	.546		300142266
DEC03	17	.236	18	1.355	19	.351		300172266
DEC03	20	.99	21	.268	22	.692		300202266
DEC02	23	.546	24	.236				300232266
DEC03	25	1.14	26	.895	27	.61	TANK SKIRT	300252266
DEC03	28	.453	29	.515	30	.47		300282266
DEC03	31	.453	32	.61	33	1.14		300312266
DEC03	34	.895	35	.61	36	.453		300342266
DEC03	37	.515	38	.47	39	.453		300372266
DEC01	40	.61						300402266
DEC03	42	.0600	43	.250	44	.0400	RCS HEAT SHIELD	300422266
DEC03	45	.147	46	.0690	47	.0690		300452266
DEC03	48	.0305	49	.1020	50	.385		300482266
DEC03	51	.144	52	.280	53	.0430		300512266
DEC03	54	.147	55	.0750	56	.0810		300542266
DEC03	57	.433	58	.131	59	.144		300572266
DEC03	60	.0600	61	.250	62	.0395		300602266
DEC03	63	.148	64	.0750	65	.0690		300632266
DEC03	66	.0307	67	.1010	68	.385		300662266
DEC03	69	.144	70	.280	71	.0433		300692266
DEC03	72	.148	73	.0700	74	.0750		300722266
DEC03	75	.433	76	.131	77	.144		300752266
DEC01	100	10.					FUEL CELL	301002266
DEC03	101	1.E20	107	1.E20	112	1.E20	DUMMY VALUES	301002266
DEC03	117	1.E20	123	1.E20	128	1.E20	CSM FAIRING	301012266
DEC03	102	.525	103	.525	104	.540	SHELL	301022266
DEC03	105	.540	106	.540	108	.572		301052266
DEC03	109	.572	110	.572	111	.572		301092266
DEC03	113	.525	114	.525	115	.525		301132266
DEC03	116	.329	118	.525	119	.525		301162266
DEC03	120	.54	121	.54	122	.54		301202266
DEC03	124	.572	125	.572	126	.572		301242266
DEC03	127	.572	129	.329	130	.525		301272266
DEC02	131	.525	132	.525				301312266
DEC03	133	.786	134	.79	135	.373	FWD. BLKD.	301332266
DEC03	136	.91	137	.976	138	.536		301362266
DEC03	139	.835	140	.75	141	.388		301392266
DEC03	142	.628	143	.682	144	.342		301422266
DEC03	145	.91	146	.976	147	.536		301452266
DEC03	148	.673	149	.66	150	.334		301482266
DEC03	151	.321	152	.373	153	.373	C/M SUPPORT ARMS	30151
DEC03	154	.321	155	.373	156	.673		30154
DEC03	157	.321	158	.373	159	.373		30157
DEC03	160	.321	161	.373	162	.673		30160
DEC03	163	.321	164	.373	165	.373		30163
DEC03	166	.321	167	.373	168	.673		30166
DEC01	200	0.					PROP. TANK	302002266
DEC03	201	.613	202	.825	203	.825	SHELL	302012266
DEC03	204	.316	205	.316	206	.357		302042266
DEC03	207	.645	208	.378	209	.336		302072266
DEC03	210	1.54	211	.896	212	.613		302102266
DEC03	213	.365	214	.308	215	.308		302132266
DEC03	216	.248	217	.462	218	.825		302162266
DEC03	219	.825	220	.316	221	.316		302192266
DEC03	222	.357	223	.645	224	.378		302222266
DEC03	225	.336	226	1.54	227	.896		302252266
DEC03	228	.613	229	.248	230	.308		302282266
DEC02	231	.308	232	.365				302312266
DEC03	233	.412	234	.448	235	.412	BEAMS	302332266
DEC03	236	.412	237	.486	238	.68		302362266

LOCKHEED CALIFORNIA COMPANY

TABLE B-2 (Cont.)

DEC03	239	.468	240	.51	241	.468		302392266
DEC03	242	.457	243	.44	244	.355		302422266
DEC03	245	.518	246	.556	247	.83		302452266
DEC03	248	.453	249	.642	250	.511		302482266
DEC03	251	.211	252	.221	253	.224		302512266
DEC01	254	.265						302542266
DEC02	255	.207	256	.207			IN. PANELS	302552266
DEC02	278	14.2	279	6.80			VALVES/INJECTOR	302782266
DEC01	300	0.					PROP. TANK	303002266
DEC03	301	.613	302	.775	303	.775	SHELL	303012266
DEC03	304	.331	305	.331	306	.372		303042266
DEC03	307	.640	308	.378	309	.336		303072266
DEC03	310	1.48	311	.842	312	.606		303102266
DEC03	313	.409	314	.452	315	.452		303132266
DEC03	316	.340	317	.458	318	.775		303162266
DEC03	319	.775	320	.331	321	.331		303192266
DEC03	322	.372	323	.640	324	.378		303222266
DEC03	325	.336	326	1.48	327	.842		303252266
DEC03	328	.606	329	.274	330	.452		303282266
DEC02	331	.452	332	.409				303312266
DEC03	333	.167	334	.182	335	.167	BEAMS	303332266
DEC03	336	.16	337	.174	338	.395		303362266
DEC03	339	.259	340	.262	341	.15		303392266
DEC03	342	.149	343	.16	344	.149		303422266
DEC03	345	.16	346	.174	347	.395		303452266
DEC03	348	.185	349	.376	350	.185		303482266
DEC03	351	.203	352	.186	353	.171		303512266
DEC01	354	.253						303542266
DEC01	355	.630					IN. PANELS	303552266
DEC02	356	.630	357	49.0			IN. PANELS,HE	303562266
DEC03	401	.682	402	.775	403	.775	SHELL	304012266
DEC03	404	.316	405	.316	406	.357		304042266
DEC03	407	.640	408	.378	409	.336		304072266
DEC03	410	1.48	411	.842	412	.594		304102266
DEC03	416	.276	417	.446	418	.775		304162266
DEC03	419	.775	420	.316	421	.316		304192266
DEC03	422	.357	423	.640	424	.378		304222266
DEC03	425	.336	426	1.48	427	.842		304252266
DEC03	428	.594	429	.248	430	.452		304282266
DEC02	431	.452	432	.378				304312266
DEC03	433	.203	434	.182	435	.167	BEAMS	304332266
DEC03	436	.16	437	.174	438	.395		304362266
DEC03	439	.15	440	.164	441	.15		304392266
DEC03	442	.149	443	.16	444	.149		304422266
DEC03	445	.16	446	.174	447	.395		304452266
DEC03	448	.267	449	.477	450	.153		304482266
DEC03	451	.203	452	.186	453	.165		304512266
DEC01	454	.224						304542266
DEC01	455	.202					IN. PANELS	304552266
DEC01	456	.202					IN. PANELS	304562266
DEC01	500	0.					PROP. TANK	305002266
DEC03	501	1.3	502	.869	503	.869	SHELL	305012266
DEC03	507	1.33	508	.812	509	.766		305072266
DEC03	510	.918	511	.944	512	1.25		305102266
DEC03	516	.823	517	.900	518	.869		305162266
DEC03	519	.869	523	1.33	524	.812		305192088
DEC03	525	.766	526	.918	527	.944		305252266
DEC03	528	1.25	529	.883	530	1.19		305282266
DEC02	531	.95	532	.789				305312266
DEC03	533	.481	534	.428	535	.422	BEAMS	305332266
DEC03	536	.386	537	.42	538	.86		305362266

TABLE B-2 (Cont.)

DEC03	539	.489	540	.436	541	.522		305392266
DEC03	542	.488	543	.426	544	.403		305422266
DEC03	545	.386	546	.42	547	.86		305452266
DEC03	548	.477	549	.487	550	.478		305482266
DEC03	551	.43	552	.407	553	.375		305512266
DEC01	554	.444						305542266
DEC02	555	.650	556	.630			IN. PANELS	305552266
DEC01	557	49.0					HE. BOT.	305572266
DEC01	600	0.					PROP. TANK	306002266
DEC03	601	.601	602	.348	603	.348	SHELL	306012266
DEC03	607	.620	608	.376	609	.336		306072266
DEC03	610	.367	611	.378	612	.587		306102266
DEC03	613	.425	614	.410	615	.379		306132266
DEC03	616	.283	617	.411	618	.348		306162266
DEC03	619	.348	623	.620	624	.376		306192088
DEC03	625	.336	626	.367	627	.378		306252266
DEC02	628	.587	629	.276				306282088
DEC03	633	.167	634	.182	635	.167	BEAMS	306332266
DEC03	636	.16	637	.174	638	.395		306362266
DEC03	639	.445	640	.459	641	.237		306392266
DEC03	642	.390	643	.351	644	.390		306422266
DEC03	645	.16	646	.174	647	.395		306452266
DEC03	648	.153	649	.295	650	.253		306482266
DEC03	651	.168	652	.21	653	.182		306512266
DEC01	654	.253						306542266
DEC01	655	.171					IN. PANELS	306552266
DEC01	700	62.			HELIUM			30700
DEC03	701	.601	702	.348	703	.348	SHELL	307012266
DEC03	707	.635	708	.376	709	.336		307072266
DEC03	710	.367	711	.378	712	.594		307102266
DEC03	713	.369	714	.349	715	.318		307132266
DEC03	716	.245	717	.411	718	.348		307162266
DEC03	719	.348	723	.635	724	.376		307192088
DEC03	725	.336	726	.367	727	.378		307252266
DEC02	728	.587	729	.276				307282088
DEC03	733	.233	734	.182	735	.167	BEAMS	307332266
DEC03	736	.16	737	.174	738	.4		307362266
DEC03	739	.15	740	.164	741	.15		307392266
DEC03	742	.201	743	.20	744	.175		307422266
DEC03	745	.16	746	.174	747	.40		307452266
DEC03	748	.232	749	.379	750	.232		307482266
DEC03	751	.271	752	.514	753	.253	BEAMS PLUS	307512266
DEC03	754	.541	755	.315	756	.315	ENGINE WEB	307542266
DEC03	757	.147	758	.210	759	.147	MOUNT	307572266
DEC01	760	.210						307602266
DEC01	800	62.			HELIUM			30800
DEC03	801	.598	802	.450	803	.450	SHELL	308012266
DEC03	804	.434	805	.452	806	.460		308042266
DEC03	807	.645	808	.487	809	.459		308072266
DEC03	810	.478	811	.489	812	.590		308102266
DEC03	813	.506	814	.486	815	.455		308132266
DEC03	816	.421	817	.425	818	.450		308162266
DEC03	819	.450	820	.434	821	.452		308192266
DEC03	822	.460	823	.645	824	.487		308222266
DEC03	825	.459	826	.478	827	.489		308252266
DEC02	828	.587	829	.310				308282088
DEC03	833	.372	834	.407	835	.372	BEAMS	308332266
DEC03	836	.432	837	.583	838	.68		308362266
DEC03	839	.372	840	.458	841	.401		308392266
DEC03	842	.396	843	.434	844	.389		308422266
DEC03	845	.372	846	.40	847	.757		308452266

TABLE B-2 (Cont.)

DEC03	848	.345	849	.539	850	.345		308482266
DEC03	851	.303	852	.364	853	.253	BEAMS PLUS	308512266
DEC03	854	.391	855	.340	856	.340	ENGINE WEB	308542266
DEC03	857	.147	858	.210	859	.147	MOUNT	308572266
DEC01	860	.210						308602266
DEC03	933	2.48	934	2.03	935	.644	AFT BLKD	309332266
DEC03	936	1.98	937	.366	938	2.88		309362266
DEC03	939	1.49	940	.834	941	1.48		309392266
DEC03	942	.500	943	1.94	944	1.25		309422266
DEC03	945	.768	946	1.20	947	.852		309452266
DEC03	948	.393	949	2.0	950	1.41		309482266
DEC03	951	.62	952	2.95	953	.336		309512266
DEC03	954	2.38	955	1.50	956	0.97		309542266
DEC03	957	1.69	958	.500	959	1.59		309572266
DEC03	960	1.12	961	.668	962	1.63		309602266
DEC02	963	1.61	964	.715				309632266
DEC03	983	1.03	984	.815	985	.555	AFT TANK SKIRTS	309832266
DEC03	986	.493	987	.56	988	.515		309862266
DEC03	989	.493	990	.555	991	1.03		309892266
DEC03	992	.815	993	.555	994	.493		309922266
DEC03	995	.56	996	.515	997	.493		309952266
DEC01	998	.555						309982266
DEC03	1001	.11	1002	.23	1003	.15	AFT HEAT SHIELD	310012266
DEC03	1004	.15	1005	.19	1006	.19		310042266
DEC03	1007	.19	1008	.15	1009	.15		310072266
DEC03	1010	.23	1011	.11	1012	.11		310102266
DEC03	1013	.11	1014	.23	1015	.15		310132266
DEC03	1016	.15	1017	.115	1018	.17		310162266
DEC03	1019	.115	1020	.15	1021	.15		310192266
DEC03	1022	.23	1023	.11	1024	.11		310222266
DEC03	1025	.053	1026	.175	1027	.165		310252266
DEC03	1028	.165	1029	.165	1030	.175		310282266
DEC03	1031	.053	1032	.053	1033	.052		31031
DEC03	1034	.10	1035	.054	1036	.054		31034
DEC03	1037	.054	1038	.054	1039	.10		31037
DEC03	1040	.052	1051	.258	1052	.213		31040
DEC03	1053	.138	1054	.138	1055	.178		310532266
DEC03	1056	.178	1057	.178	1058	.138		310562266
DEC03	1059	.138	1060	.213	1061	.258		310592266
DEC03	1062	.258	1063	.258	1064	.213		310622266
DEC03	1065	.138	1066	.138	1067	.115		310652266
DEC03	1068	.17	1069	.115	1070	.138		310682266
DEC03	1071	.138	1072	.213	1073	.258		310712266
DEC03	1074	.258	1075	.053	1076	.145		310742266
DEC03	1077	.156	1078	.156	1079	.156		310772266
DEC03	1080	.145	1081	.053	1082	.053		310802266
DEC03	1083	.00	1084	.00	1085	.00		31083
DEC01	1089	.155				EXTEND. NOZZLE CAPACITORS		310892266
INC	1	0.	11					310902266
DEC01	1101	.252						31101
INC	1	0.	11					311022266
DEC01	1113	.488						31113
INC	1	0.	11					311142266
NBK								399992266

LOCKHEED CALIFORNIA COMPANY

TABLE B-3

RESISTORS FOR DETAILED ENGINE AND PLUMBING ANALYSIS

DEC01	2	401	402	20000.					
DEC01	6	31	48	1.66E5					200062266
DEC02	8	200	41	1.18E5	49	500	47	6.0E5	200082266
DEC02	9	600	11	2.1E5	7	600	21	.9E5	200092266
DEC02	10	10	11	4.29E5	11	11	12	2.91E5	200102266
DEC02	12	12	13	1.40E5	13	13	14	1.40E5	200122266
DEC01	14	14	15	7.20E5					200142266
DEC02	15	15	16	3.8E5	16	16	17	2.5E5	200152266
DEC02	17	17	18	3.9E5	18	18	19	4.55E5	200172266
DEC02	19	19	20	5.2E5	20	20	401	2.6E5	200192266
DEC02	21	21	22	2.91E5	22	22	23	3.79E5	200212266
DEC02	23	23	24	3.26E5	24	24	25	2.73E5	200232266
DEC02	25	25	26	3.00E5	26	26	27	2.64E5	200252266
DEC02	27	300	27	.9E5	30	200	31	2.06E5	200272266
DEC02	28	28	29	6.6E5	29	29	30	5.8E5	200282266
DEC02	31	31	32	4.12E5	32	32	33	2.06E5	200312266
DEC02	33	33	34	2.06E5	34	34	35	3.33E5	200332266
DEC02	35	35	36	2.0E5	36	36	37	1.36E5	200352266
DEC02	37	37	38	2.2E5	38	38	39	2.68E5	200372266
DEC02	39	39	40	3.14E5	40	40	278	1.57E5	200392266
DEC02	41	41	42	2.70E5	42	42	43	2.70E5	200412266
DEC02	43	43	44	2.46E5	44	44	45	3.02E5	200432266
DEC02	45	45	46	2.93E5	46	46	47	2.46E5	200452266
DEC02	47	13	124	1000.	48	33	116	1000.	200472266
DEC02	51	51	52	4.99E5	52	52	53	5.57E5	200512266
DEC02	53	53	54	6.12E5	54	54	55	6.28E5	200532266
DEC01	55	55	56	6.28E5					200552266
DEC01	56	48	49	1.59E5					200562266
DEC01	57	56	49	3.22E5					200572266
DEC01	58	71	49	1.88E5					200582266
DEC01	59	61	50	7.10E5					200592266
DEC01	60	10	50	4.29E5					200602266
DEC02	61	61	62	10.3E5	62	62	63	6.45E5	200612266
DEC02	63	63	64	5.15E5	64	70	65	5.8E5	200632266
DEC02	65	30	66	4.1E5	66	66	67	5.E5	200652266
DEC02	67	67	68	5.8E5	68	68	69	6.8E5	200672266
DEC02	69	69	70	7.8E5	70	65	401	3.9E5	200692266
DEC02	71	71	91	9.81E5	72	155	156	5.3E6	200712266
DEC02	73	156	157	5.2E6	75	127	129	2.5E6	200732266
DEC02	76	129	130	3.0E6	77	130	131	3.5E6	200762266
DEC02	78	131	132	4.1E6	79	132	133	4.7E6	200782266
DEC02	80	163	401	2.3E6	81	81	101	13.58E5	200802266
DEC02	82	165	166	5.3E6	83	166	167	5.2E6	200822266
DEC02	85	167	169	2.5E6	86	169	170	3.0E6	200852266
DEC02	87	170	171	3.5E6	88	171	172	4.1E6	200872266
DEC02	89	172	173	4.7E6	90	173	401	2.3E6	200892266
DEC02	91	91	92	15.10E5	92	92	93	11.09E5	200912266
DEC02	93	93	94	7.55E5	94	94	95	7.55E5	200932266
DEC02	95	95	96	8.06E5	96	96	97	8.30E5	200952266
DEC01	97	97	98	10.83E5					200972266
DEC01	98	98	500	5.50E5					200982266
DEC01	99	81	50	9.00E5					200992266
DEC02	101	101	102	9.81E5	102	102	103	13.33E5	201012266
DEC02	103	103	104	13.58E5	104	104	105	9.56E5	201032266
DEC02	105	105	106	11.07E5	106	106	107	10.83E5	201052266
DEC01	107	107	300	5.50E5					201072266
DEC02	109	1	49	0.	110	2	50	0.	20109
DEC02	111	111	112	8.06E5	112	112	113	8.82E5	201112266
DEC02	113	113	114	10.57E5	114	114	115	9.81E5	201132266
DEC02	115	115	116	4.90E5	116	116	91	4.90E5	201152266
DEC02	117	1	72	0.	118	1	73	0.	20117

TABLE B-3 (Cont.)

DEC01	119	1	75	0.					20119
DEC02	121	121	122	9.32E5	122	122	123	16.6E5	201212266
DEC02	123	123	124	8.30E5	124	124	101	8.3E5	201232266
DEC02	125	1	74	0.	126	1	76	0.	20125
DEC02	127	10	600	0.	132	11	600	0.	201272266
DEC02	134	12	600	0.	137	12	272	0.	201342266
DEC02	139	14	271	0.	142	14	500	0.	201392266
DEC02	143	15	273	0.	144	15	500	0.	201432266
DEC02	149	21	600	0.	150	22	272	0.	201492266
DEC02	151	22	273	0.	156	23	261	0.	201512266
DEC02	157	23	500	0.	160	24	252	0.	201572266
DEC02	161	24	253	0.	165	25	45	0.	201612266
DEC02	166	25	242	0.	167	25	243	0.	201662266
DEC02	174	26	233	0.	175	26	232	0.	201742266
DEC02	176	26	44	0.	177	27	200	0.	201762266
DEC02	180	48	200	0.	183	31	200	0.	201802266
DEC02	186	32	200	0.	187	32	201	0.	201862266
DEC02	188	34	212	0.	191	35	213	0.	201882266
DEC02	192	35	212	0.	195	41	200	0.	201922266
DEC02	199	42	213	0.	200	42	212	0.	201992266
DEC02	205	43	221	0.	206	43	300	0.	202052266
DEC02	210	44	232	0.	211	44	233	0.	202102266
DEC02	215	45	242	0.	219	46	253	0.	202152266
DEC02	220	46	252	0.	221	47	500	0.	202202266
DEC02	226	51	243	0.	227	51	111	0.	202262266
DEC02	230	52	233	0.	231	52	112	0.	202302266
DEC02	232	52	26	0.	233	52	44	0.	202322266
DEC02	237	53	221	0.	238	53	300	0.	202372266
DEC02	239	53	113	0.	240	53	43	0.	202392266
DEC02	244	54	213	0.	245	54	114	0.	202442266
DEC02	246	54	42	0.	247	55	200	0.	202462266
DEC01	249	56	200	0.					202492266
DEC02	252	61	600	0.	259	62	273	0.	202522266
DEC02	260	62	272	0.	261	63	122	0.	202602266
DEC02	265	63	500	0.	266	63	261	0.	202652266
DEC02	270	64	252	0.	271	64	121	0.	202702266
DEC02	272	71	200	0.	275	81	600	0.	202722266
DEC02	278	91	200	0.	280	92	200	0.	202782266
DEC02	284	93	213	0.	285	93	42	0.	202842266
DEC02	288	94	221	0.	289	94	300	0.	202882266
DEC02	290	94	43	0.	291	95	233	0.	202902266
DEC02	294	95	44	0.	295	95	26	0.	202942266
DEC02	299	96	242	0.	300	96	45	0.	202992266
DEC02	301	96	25	0.	304	97	252	0.	203012266
DEC02	305	97	24	0.	306	97	46	0.	203052266
DEC02	307	98	500	0.	310	101	272	0.	203072266
DEC02	311	102	22	0.	316	102	273	0.	203112266
DEC02	317	102	272	0.	322	103	500	0.	203172266
DEC02	325	104	253	0.	326	104	252	0.	203252266
DEC02	327	104	46	0.	329	105	45	0.	203272266
DEC02	330	105	25	0.	331	105	243	0.	203302266
DEC02	332	105	242	0.	333	106	300	0.	203322266
DEC02	335	106	44	0.	336	106	232	0.	203352266
DEC02	337	106	233	0.	340	107	300	0.	203372266
DEC02	346	111	25	0.	347	112	233	0.	203462266
DEC02	350	112	26	0.	351	112	44	0.	203502266
DEC02	356	113	221	0.	357	113	300	0.	203562266
DEC02	358	113	43	0.	363	114	213	0.	203582266
DEC02	364	114	212	0.	365	115	212	0.	203642266
DEC02	368	121	253	0.	374	122	500	0.	203682266
DEC02	375	122	261	0.	376	123	500	0.	203752266

TABLE B-3 (Cont.)

DEC02	377	123	272	0.	399	341	340	0.	203772266
DEC02	380	49	155	2.65E6	381	49	165	2.65E6	20380
DEC02	382	50	125	2.00E6	383	50	135	2.00E6	20382
DEC02	384	50	145	2.00E6	385	49	72	1000.	20384
DEC02	386	49	73	1000.	387	49	74	3000.	20386
DEC02	388	50	75	1000.	389	50	76	3000.	20388
DEC02	390	125	126	4.E6	391	126	127	3.5E6	203902266
DEC02	392	133	128	3.5E6	393	127	129	2.5E6	203922266
DEC02	394	129	130	3.E6	395	130	131	3.5E6	203942266
DEC02	396	131	132	4.1E6	397	132	133	4.7E6	203962266
DEC01	398	128	401	2.3E6					203982266
DEC02	400	303	310	0.	401	302	310	0.	204002266
DEC02	402	301	310	0.	403	304	310	0.	204022266
DEC02	404	311	310	0.	405	312	310	0.	204042266
DEC02	406	313	310	0.	407	314	310	0.	204062266
DEC02	408	321	320	0.	409	322	320	0.	204082266
DEC02	410	323	320	0.	411	324	320	0.	204102266
DEC02	412	331	330	0.	413	334	330	0.	204122266
DEC02	414	332	330	0.	415	333	330	0.	204142266
DEC02	416	335	330	0.	417	336	330	0.	204162266
DEC02	418	337	330	0.	419	342	340	0.	204182266
DEC02	420	343	340	0.	421	344	340	0.	204202266
DEC02	422	345	340	0.	423	351	330	0.	204222266
DEC02	424	352	305	0.	425	353	306	0.	204242266
DEC02	426	51	303	5.15E5	427	121	302	8.9E5	204262266
DEC02	428	111	301	7.89E5	429	64	304	5.47E5	204282266
DEC02	430	303	313	6.44E5	431	301	311	9.65E5	204302266
DEC02	432	302	312	9.65E5	433	304	314	6.12E5	204322266
DEC02	434	311	321	9.57E5	435	312	322	9.94E5	204342266
DEC02	436	313	323	6.6E5	437	314	324	6.5E5	204362266
DEC02	438	321	331	9.15E5	439	322	334	8.65E5	204382266
DEC02	440	323	332	6.92E5	441	324	333	6.92E5	204402266
DEC02	442	332	331	4.86E5	443	333	334	3.45E5	204422266
DEC02	445	331	336	9.94E5	446	334	336	3.52E5	204452266
DEC02	447	336	335	4.13E5	448	336	341	4.53E5	204472266
DEC02	449	335	342	4.13E5	450	342	345	3.35E5	204492266
DEC02	451	345	344	2.95E5	452	345	343	4.90E5	204512266
DEC02	453	344	341	2.95E5	454	343	337	7.63E5	204532266
DEC02	455	337	351	4.21E5	456	351	355	3.66E5	204552266
DEC02	457	351	352	8.52E5	458	352	353	6.58E5	204572266
DEC01	459	353	354	3.53E5					204592266
DEC02	460	36	860	0.	461	36	533	0.	204602266
DEC02	462	36	517	0.	464	37	859	0.	204622266
DEC02	466	37	536	0.	467	37	520	0.	204662266
DEC02	468	38	519	0.	469	38	535	0.	204682266
DEC01	470	38	500	0.					204702266
DEC02	472	39	500	0.	473	39	519	0.	204722266
DEC02	474	39	503	0.	475	39	858	0.	204742266
DEC02	476	39	600	0.	477	40	758	0.	204762266
DEC02	478	40	402	0.	479	40	503	0.	204782266
DEC02	480	40	600	0.	481	40	401	0.	204802266
DEC01	482	40	500	0.					204822266
DEC02	490	135	136	4.E6	491	136	137	3.5E6	204902266
DEC02	493	127	129	2.5E6	494	129	130	3.0E6	204932266
DEC02	495	130	131	3.5E6	496	131	132	4.1E6	204952266
DEC02	497	132	133	4.7E6	498	143	401	2.3E6	204972266
DEC01	501	501	505	1240.					205012266
INC	1	1	1	0.	3				205022266
DEC01	505	505	509	1320.					205052266
INC	1	1	1	0.	3				205062266
DEC01	509	509	513	935.					205092266

TABLE B-3 (Cont.)

INC	1	1	1	0.	3				205102266
DEC01	517	517	521	2540.					205172266
INC	1	1	1	0.	3				205182266
DEC01	521	521	525	2750.					205212266
INC	1	1	1	0.	3				205222266
DEC01	525	525	529	1790.					205252266
INC	1	1	1	0.	3				205262266
DEC01	533	533	537	888.					205332266
INC	1	1	1	0.	3				205342266
DEC01	537	537	541	916.					205372266
INC	1	1	1	0.	3				205382266
DEC01	541	541	545	690.					205412266
INC	1	1	1	0.	3				205422266
DEC01	545	402	401	0.					
DEC02	560	16	858	0.	561	16	535	0.	205602266
DEC02	562	16	519	0.	564	17	857	0.	205622266
DEC02	566	17	534	0.	567	17	518	0.	205662266
DEC02	568	18	517	0.	569	18	533	0.	205682266
DEC01	570	18	200	0.					205702266
DEC02	572	19	200	0.	573	19	517	0.	205722266
DEC02	574	19	501	0.	575	19	860	0.	205742266
DEC02	576	19	300	0.	577	20	760	0.	205762266
DEC02	578	20	402	0.	579	20	501	0.	205782266
DEC02	580	20	300	0.	581	20	401	0.	205802266
DEC01	582	20	200	0.					205822266
DEC02	583	401	355	0.	584	200	401	0.	205832266
DEC02	585	401	500	0.	586	757	401	0.	205852266
DEC02	587	401	758	0.	588	759	401	0.	205872266
DEC01	589	401	760	0.					205892266
DEC02	590	145	146	4.E6	591	146	147	3.5E6	205902266
DEC02	593	127	129	2.5E6	594	129	130	3.0E6	205932266
DEC02	595	130	131	3.5E6	596	131	132	4.1E6	205952266
DEC02	597	132	133	4.7E6	598	153	401	2.3E6	205972266
DEC02	600	66	858	0.	601	66	535	0.	206002266
DEC02	602	66	519	0.	604	67	857	0.	206022266
DEC02	606	67	534	0.	607	67	518	0.	206062266
DEC02	608	68	517	0.	609	68	533	0.	206082266
DEC01	610	68	200	0.					206102266
DEC02	612	69	200	0.	613	69	517	0.	206122266
DEC02	614	69	501	0.	615	69	860	0.	206142266
DEC02	616	69	300	0.	617	70	760	0.	206162266
DEC02	618	70	402	0.	619	70	501	0.	206182266
DEC02	620	70	300	0.	621	70	401	0.	206202266
DEC02	622	70	200	0.	623	65	401	0.	206222266
DEC02	624	65	500	0.	625	65	600	0.	206242266
DEC02	626	28	600	0.	627	29	600	0.	206262266
DEC02	628	30	600	0.	629	30	282	0.	206282266
DEC02	630	155	200	0.	631	156	200	0.	206302266
DEC02	632	157	200	0.	633	157	202	0.	206322266
DEC02	634	159	536	0.	635	159	520	0.	206342266
DEC02	636	160	859	0.	637	160	520	0.	206362266
DEC02	638	160	37	0.	639	160	536	0.	206382266
DEC02	640	161	519	0.	641	161	38	0.	206402266
DEC02	642	161	500	0.	643	161	535	0.	206422266
DEC02	644	162	39	0.	645	162	535	0.	206442266
DEC02	646	162	858	0.	647	162	600	0.	206462266
DEC02	648	163	40	0.	649	163	758	0.	206482266
DEC01	650	163	600	0.					206502266
DEC02	660	165	200	0.	661	166	200	0.	206602266
DEC02	662	167	200	0.	663	167	202	0.	206622266
DEC02	664	169	536	0.	665	169	520	0.	206642266

LOCKHEED
CALIFORNIA COMPANY

TABLE B-3 (Cont.)

DEC02	666	170	859	0.	667	170	520	0.	206662266
DEC02	668	170	37	0.	669	170	536	0.	206682266
DEC02	670	171	519	0.	671	171	38	0.	206702266
DEC02	672	171	500	0.	673	171	535	0.	206722266
DEC02	674	172	39	0.	675	172	535	0.	206742266
DEC02	676	172	858	0.	677	172	600	0.	206762266
DEC02	678	173	40	0.	679	173	758	0.	206782266
DEC01	680	173	600	0.					206802266
DEC01	690	358	518	0.	RAD. FROM GIMBAL RING				206902266
DEC02	691	359	517	0.	692	360	520	0.	206912266
DEC02	693	361	520	0.	694	362	519	0.	206932266
DEC02	695	363	518	0.	696	364	501	0.	206952266
DEC01	697	365	503	0.					206972266
DEC02	700	129	858	0.	701	129	66	0.	207002266
DEC02	702	129	519	0.	703	129	535	0.	207022266
DEC02	704	130	857	0.	705	130	534	0.	207042266
DEC02	706	130	67	0.	707	130	518	0.	207062266
DEC02	708	131	517	0.	709	131	68	0.	207082266
DEC02	710	131	200	0.	711	131	533	0.	207102266
DEC02	712	132	200	0.	713	132	517	0.	207122266
DEC02	714	132	501	0.	715	132	860	0.	207142266
DEC02	716	132	69	0.	717	133	760	0.	207162266
DEC02	718	133	402	0.	719	133	501	0.	207182266
DEC02	720	133	401	0.	721	133	200	0.	207202266
DEC02	722	133	70	0.	723	128	401	0.	207222266
DEC02	724	128	500	0.	725	128	600	0.	207242266
DEC02	726	125	600	0.	727	126	600	0.	207262266
DEC02	728	127	600	0.	729	127	282	0.	207282266
DEC02	730	501	200	0.	731	503	500	0.	20730
DEC02	732	534	857	0.	733	535	858	0.	20732
DEC02	734	536	859	0.	735	533	860	0.	20734
DEC02	736	402	401	0.	737	401	757	0.	20736
DEC02	738	401	758	0.	739	401	759	0.	20738
DEC02	740	401	760	0.	741	402	757	0.	20740
DEC02	742	402	758	0.	743	402	759	0.	20742
DEC02	744	402	760	0.	745	502	757	0.	20744
DEC02	746	503	758	0.	747	504	759	0.	20746
DEC02	748	501	760	0.	749	518	857	0.	20748
DEC02	750	519	858	0.	751	520	859	0.	20750
DEC01	752	517	860	0.					20752
DEC02	755	49	201	0.	756	50	281	0.	20755
DEC02	760	751	851	12900.	761	752	852	9610.	207602266
DEC02	762	753	853	12900.	763	754	854	9610.	207622266
DEC02	764	935	851	7660.	765	751	757	12680.	207642266
DEC02	766	757	754	26200.	767	754	758	18530.	207662266
DEC02	768	758	756	21600.	769	757	857	11250.	207682266
DEC02	770	758	858	7890.	771	961	854	5430.	207702266
DEC02	772	851	857	12680.	773	857	854	26200.	207722266
DEC02	774	854	858	18530.	775	858	856	21600.	207742266
DEC02	776	964	857	8030.	777	282	858	4560.	207762266
DEC02	778	753	759	12680.	779	759	752	26200.	207782266
DEC02	780	752	760	18530.	781	760	755	21600.	207802266
DEC02	782	759	859	11250.	783	760	860	7890.	207822266
DEC02	784	853	859	12680.	785	859	852	26200.	207842266
DEC02	786	852	860	18530.	787	860	855	21600.	207862266
DEC02	788	243	859	8300.	789	221	860	4560.	207882266
DEC02	790	273	856	4640.	791	253	853	7710.	207902266
DEC02	792	233	852	5910.	793	213	855	4640.	207922266
DEC02	794	855	755	10500.	795	856	756	10500.	207942266
DEC02	800	139	858	0.	801	139	535	0.	208002266
DEC02	802	139	66	0.	803	139	535	0.	208022265

TABLE B-3 (Cont.)

DEC02	804	140	857	0.	805	140	534	0.	208042266
DEC02	806	140	534	0.	807	140	67	0.	208062266
DEC02	808	141	68	0.	809	141	533	0.	208082266
DEC02	810	141	200	0.	811	141	533	0.	208102266
DEC02	812	142	200	0.	813	142	517	0.	208122266
DEC02	814	142	501	0.	815	142	860	0.	208142266
DEC02	816	142	69	0.	818	143	402	0.	208162266
DEC02	819	143	501	0.	820	143	401	0.	208192266
DEC02	821	143	200	0.	822	143	70	0.	208212266
DEC02	826	135	600	0.	827	136	600	0.	208262266
DEC02	828	137	600	0.	829	137	282	0.	208282266
DEC02	841	358	359	35200.	842	359	360	68800.	208412266
DEC02	843	360	361	33700.	844	361	362	35200.	208432266
DEC02	845	362	363	68800.	846	363	358	33700.	208452266
DEC02	847	363	961	3170.	848	360	945	3170.	208472266
DEC02	849	359	364	62000.	850	364	402	62000.	208492266
DEC02	851	362	365	62000.	852	365	402	62000.	208512266
DEC02	853	363	366	71000.	854	366	754	71000.	208532266
DEC02	855	360	367	71000.	856	367	752	71000.	208552266
DEC02	857	363	368	3700.	858	368	369	5000.	208572266
DEC02	859	369	370	12000.	860	370	358	12000.	208592266
DEC02	861	361	371	12000.	862	371	402	12000.	208612266
DEC02	865	758	600	0.	866	858	600	0.	208652266
DEC02	867	760	300	0.	868	860	300	0.	208672266
DEC02	900	149	858	0.	901	149	66	0.	209002266
DEC02	903	149	535	0.	904	150	857	0.	209032266
DEC02	905	150	534	0.	906	150	67	0.	209052266
DEC02	908	151	68	0.	910	151	200	0.	209082266
DEC02	911	151	533	0.	912	152	200	0.	209112266
DEC02	913	152	517	0.	914	152	501	0.	209132266
DEC02	915	152	69	0.	917	153	760	0.	209152266
DEC02	918	153	402	0.	919	153	501	0.	209182266
DEC02	920	153	401	0.	921	153	200	0.	209202266
DEC02	922	153	70	0.	926	145	600	0.	209222266
DEC02	927	146	600	0.	928	147	600	0.	209272266
DEC01	929	147	282	0.					209292266
DEC02	1100	400	1	0.	1101	400	3	0.	
DEC02	1102	402	400	0.	1103	513	413	0.	
DEC02	1104	514	414	0.	1105	515	415	0.	
DEC02	1106	516	416	0.	1107	525	429	0.	
DEC02	1108	526	430	0.	1109	527	431	0.	
DEC02	1110	528	432	0.	1113	413	1	0.	
DEC02	1114	414	1	0.	1115	415	1	0.	
DEC02	1116	416	1	0.	1129	429	1	0.	
DEC02	1130	430	1	0.	1131	431	1	0.	
DEC02	1132	432	1	0.	1133	429	3	0.	
DEC02	1134	430	3	0.	1135	431	3	0.	
DEC02	1136	432	3	0.	1137	413	416	0.	
DEC02	1138	413	414	0.	1145	414	415	0.	
DEC02	1156	415	416	0.	1146	414	416	0.	
DEC02	1139	413	415	0.	1141	400	413	0.	
DEC02	1140	400	414	0.	1150	400	415	0.	
DEC02	1160	400	416	0.	1231	413	431	0.	
DEC02	1242	414	432	0.	1259	415	429	0.	
DEC02	1260	416	430	0.	1162	429	430	0.	
DEC02	1161	430	431	0.	1163	431	432	0.	
DEC02	1164	432	429	0.	1165	429	431	0.	
DEC02	1166	430	432	0.	1167	400	429	0.	
DEC02	1168	400	430	0.	1169	400	431	0.	
DEC01	1170	400	432	0.					
DEC02	1190	545	1	0.	1191	546	1	0.	

LOCKHEED
CALIFORNIA COMPANY

TABLE B-3 (Cont.)

DEC02	1192	547	1	0.	1193	548	1	0.	214122266
DEC02	1412	100	331	0.	1413	100	334	0.	
DEC02	1414	100	332	0.	1415	100	333	0.	214142266
DEC02	1416	100	335	0.	1417	100	336	0.	214162266
DEC02	1418	100	337	0.	1419	100	342	0.	214182266
DEC02	1420	100	343	0.	1421	100	344	0.	214202266
DEC02	1422	100	345	0.	1399	100	341	0.	214222266
NBK									29999 2266

TABLE B-3 (Cont.)

R(109)=RAD(1,49,3.34E-4)	2990
R(110)=RAD(1,50,3.34E-4)	
R(117)=RAD(1,72,6.7E-6)	2992
R(118)=RAD(1,73,6.7E-6)	2993
R(119)=RAD(1,75,6.7E-6)	2994
R(125)=RAD(1,74,1.85E-6)	2995
R(126)=RAD(1,76,1.85E-6)	2996
R(127)=RAD(10,600,41.6E-6)	22663001
R(132)=RAD(11,600,51.6E-6)	22663002
R(134)=RAD(12,600,23.7E-6)	22663003
R(137)=RAD(12,272,25.6E-6)	22663004
R(139)=RAD(14,271,52.9E-6)	22663005
R(142)=RAD(14,500,77.6E-6)	22663006
R(143)=RAD(15,273,66.9E-6)	22663007
R(144)=RAD(15,500,36.4E-6)	22663008
R(149)=RAD(21,600,55.5E-6)	22663009
R(150)=RAD(22,272,42.2E-6)	22663010
R(151)=RAD(22,273,49.8E-6)	22663011
R(156)=RAD(23,261,39.2E-6)	22663012
R(157)=RAD(23,500,59.2E-6)	22663013
R(160)=RAD(24,252,28.4E-6)	22663014
R(161)=RAD(24,253,40.7E-6)	22663015
R(165)=RAD(25,45,2.04E-6)	22663016
R(166)=RAD(25,242,14.5E-6)	22663017
R(167)=RAD(25,243,20.2E-6)	22663018
R(174)=RAD(26,233,32.1E-6)	22663019
R(175)=RAD(26,232,31.3E-6)	22663020
R(176)=RAD(26,44,6.0E-6)	22663021
R(177)=RAD(27,200,55.3E-6)	22663022
R(180)=RAD(48,200,47.6E-6)	22663023
R(183)=RAD(31,200,144.2E-6)	22663024
R(186)=RAD(32,200,26.9E-6)	22663025
R(187)=RAD(32,201,26.9E-6)	22663026
R(188)=RAD(34,212,111.1E-6)	22663027
R(191)=RAD(35,213,64.7E-6)	22663028
R(192)=RAD(35,212,57.5E-6)	22663029
R(195)=RAD(41,200,77.6E-6)	22663030
R(199)=RAD(42,213,51.9E-6)	22663031
R(200)=RAD(42,212,51.9E-6)	22663032
R(205)=RAD(43,221,28.7E-6)	22663033
R(206)=RAD(43,300,53.2E-6)	22663034
R(210)=RAD(44,232,40.5E-6)	22663035
R(211)=RAD(44,233,39.6E-6)	22663036
R(215)=RAD(45,242,83.0E-6)	22663037
R(219)=RAD(46,253,41.3E-6)	22663038
R(220)=RAD(46,252,43.3E-6)	22663039
R(221)=RAD(47,500,72.2E-6)	22663040
R(226)=RAD(51,243,14.6E-6)	22663041
R(227)=RAD(51,111,.567E-6)	22663042
R(230)=RAD(52,233,14.6E-6)	22663043
R(231)=RAD(52,112,.727E-6)	22663044
R(232)=RAD(52,26,.363E-6)	22663045
R(233)=RAD(52,44,.363E-6)	22663046
R(237)=RAD(53,221,8.7E-6)	22663047
R(238)=RAD(53,300,8.5E-6)	22663048
R(239)=RAD(53,113,.817E-6)	22663049
R(240)=RAD(53,43,.408E-6)	22663050
R(244)=RAD(54,213,19.4E-6)	22663051
R(245)=RAD(54,114,1.132E-6)	22663052
R(246)=RAD(54,42,.453E-6)	22663053
R(247)=RAD(55,200,22.0E-6)	22663054

TABLE B-3 (Cont.)

R(249)=RAD(56,200,19.8E-6)	22663055
R(252)=RAD(61,600,51.0E-6)	22663056
R(259)=RAD(62,273,14.5E-6)	22663057
R(260)=RAD(62,272,9.1E-6)	22663058
R(261)=RAD(63,122,1.365E-6)	22663059
R(265)=RAD(63,500,10.3E-6)	22663060
R(266)=RAD(63,261,10.3E-6)	22663061
R(270)=RAD(64,252,8.2E-6)	22663062
R(271)=RAD(64,121,.89E-6)	22663063
R(272)=RAD(71,200,11.2E-6)	22663064
R(275)=RAD(81,600,66.7E-6)	22663065
R(278)=RAD(91,200,59.3E-6)	22663066
R(280)=RAD(92,200,51.9E-6)	22663067
R(284)=RAD(93,213,22.4E-6)	22663068
R(285)=RAD(93,42,3.20E-6)	22663069
R(288)=RAD(94,221,8.3E-6)	22663070
R(289)=RAD(94,300,12.3E-6)	22663071
R(290)=RAD(94,43,2.55E-6)	22663072
R(291)=RAD(95,233,19.3E-6)	22663073
R(294)=RAD(95,44,2.04E-6)	22663074
R(295)=RAD(95,26,1.358E-6)	22663075
R(299)=RAD(96,242,17.7E-6)	22663076
R(300)=RAD(96,45,4.27E-6)	22663077
R(301)=RAD(96,25,3.10E-6)	22663078
R(304)=RAD(97,252,20.2E-6)	22663079
R(305)=RAD(97,24,1.61E-6)	22663080
R(306)=RAD(97,46,5.67E-6)	22663081
R(307)=RAD(98,500,48.3E-6)	22663082
R(310)=RAD(101,272,33.3E-6)	22663083
R(311)=RAD(102,22,4.33E-6)	22663084
R(316)=RAD(102,273,15.3E-6)	22663085
R(317)=RAD(102,272,17.2E-6)	22663086
R(322)=RAD(103,500,65.8E-6)	22663087
R(325)=RAD(104,253,11.5E-6)	22663088
R(326)=RAD(104,252,15.3E-6)	22663089
R(327)=RAD(104,46,3.92E-6)	22663090
R(329)=RAD(105,45,3.92E-6)	22663091
R(330)=RAD(105,25,.922E-6)	22663092
R(331)=RAD(105,243,11.3E-6)	22663093
R(332)=RAD(105,242,12.0E-6)	22663094
R(333)=RAD(106,300,12.0E-6)	22663095
R(335)=RAD(106,44,2.28E-6)	22663096
R(336)=RAD(106,232,13.8E-6)	22663097
R(337)=RAD(106,233,14.8E-6)	22663098
R(340)=RAD(107,300,33.4E-6)	22663099
R(346)=RAD(111,25,.698E-6)	22663100
R(347)=RAD(112,233,21.2E-6)	22663101
R(350)=RAD(112,26,.775E-6)	22663102
R(351)=RAD(112,44,.582E-6)	22663103
R(356)=RAD(113,221,10.6E-6)	22663104
R(357)=RAD(113,300,18.2E-6)	22663105
R(358)=RAD(113,43,.692E-6)	22663106
R(363)=RAD(114,213,24.2E-6)	22663107
R(364)=RAD(114,212,11.7E-6)	22663108
R(365)=RAD(115,212,29.7E-6)	22663109
R(368)=RAD(121,253,18.5E-6)	22663110
R(374)=RAD(122,500,34.2E-6)	22663111
R(375)=RAD(122,261,34.2E-6)	22663112
R(376)=RAD(123,500,20.4E-6)	22663113
R(377)=RAD(123,272,20.4E-6)	22663114
R(399)=RAD(341,340,50.0E-6)	22663115

TABLE B-3 (Cont.)

R(400)=RAD(303,310,36.4E-6)	22663116
R(401)=RAD(302,310,22.2E-6)	22663117
R(402)=RAD(301,310,22.2E-6)	22663118
R(403)=RAD(304,310,34.6E-6)	22663119
R(404)=RAD(311,310,21.6E-6)	22663120
R(405)=RAD(312,310,21.6E-6)	22663121
R(406)=RAD(313,310,36.4E-6)	22663122
R(407)=RAD(314,310,34.6E-6)	22663123
R(408)=RAD(321,320,21.6E-6)	22663124
R(409)=RAD(322,320,23.2E-6)	22663125
R(410)=RAD(323,320,38.2E-6)	22663126
R(411)=RAD(324,320,39.1E-6)	22663127
R(412)=RAD(331,330,11.1E-6)	22663128
R(413)=RAD(334,330,8.0E-6)	22663129
R(414)=RAD(332,330,21.8E-6)	22663130
R(415)=RAD(333,330,19.6E-6)	22663131
R(416)=RAD(335,330,9.4E-6)	22663132
R(417)=RAD(336,330,10.2E-6)	22663133
R(418)=RAD(337,330,15.5E-6)	22663134
R(419)=RAD(342,340,50.0E-6)	22663135
R(420)=RAD(343,340,27.7E-6)	22663136
R(421)=RAD(344,340,15.8E-6)	22663137
R(422)=RAD(345,340,13.7E-6)	22663138
R(423)=RAD(351,330,60.1E-6)	22663139
R(424)=RAD(352,305,34.6E-6)	22663140
R(425)=RAD(353,306,40.0E-6)	22663141
R(460)=RAD(36,860,5.75E-6)	22663142
R(461)=RAD(36,533,80.5E-6)	22663143
R(462)=RAD(36,517,23.0E-6)	22663144
R(464)=RAD(37,859,3.83E-6)	22663145
R(466)=RAD(37,536,53.6E-6)	22663146
R(467)=RAD(37,520,15.3E-6)	22663147
R(468)=RAD(38,519,15.3E-6)	22663148
R(469)=RAD(38,535,38.3E-6)	22663149
R(470)=RAD(38,500,23.0E-6)	22663150
R(472)=RAD(39,500,22.0E-6)	22663151
R(473)=RAD(39,519,16.4E-6)	22663152
R(474)=RAD(39,503,5.50E-6)	22663153
R(475)=RAD(39,858,55.E-6)	22663154
R(476)=RAD(39,600,11.E-6)	22663155
R(477)=RAD(40,758,38.E-6)	22663156
R(478)=RAD(40,402,5.5E-6)	22663157
R(479)=RAD(40,503,5.5E-6)	22663158
R(480)=RAD(40,600,27.E-6)	22663159
R(481)=RAD(40,401,11.E-6)	22663160
R(482)=RAD(40,500,22.E-6)	22663161
R(545)=RAD(401,402,7.8E-5)	
R(546)=RAD(402,1,7.7E-6)	22663342
R(553)=RAD(402,513,1.02E-5)	22663347
R(554)=RAD(402,514,1.02E-5)	22663348
R(555)=RAD(402,515,1.02E-5)	22663349
R(556)=RAD(402,516,1.02E-6)	22663350
R(560)=RAD(16,858,2.50E-6)	22663162
R(561)=RAD(16,535,35.0E-6)	22663163
R(562)=RAD(16,519,10.0E-6)	22663164
R(564)=RAD(17,857,2.8E-6)	22663165
R(566)=RAD(17,534,38.5E-6)	22663166
R(567)=RAD(17,518,11.E-6)	22663167
R(568)=RAD(18,517,11.E-6)	22663168
R(569)=RAD(18,533,27.5E-6)	22663169
R(570)=RAD(18,200,16.5E-6)	22663170

TABLE B-3 (Cont.)

R(572)=RAD(19,200,14.5E-6)	22663171
R(573)=RAD(19,517,10.8E-6)	22663172
R(574)=RAD(19,501,1.1E-6)	22663173
R(575)=RAD(19,860,36.E-6)	22663174
R(576)=RAD(19,300,7.2E-6)	22663175
R(577)=RAD(20,760,25.E-6)	22663176
R(578)=RAD(20,402,3.6E-6)	22663177
R(579)=RAD(20,501,3.6E-6)	22663178
R(580)=RAD(20,300,18.E-6)	22663179
R(581)=RAD(20,401,7.2E-6)	22663180
R(582)=RAD(20,200,14.5E-6)	22663181
R(583)=RAD(401,355,4.2E-6)	22663351
R(584)=RAD(401,200,2.8E-6)	22663352
R(585)=RAD(401,500,2.8E-6)	22663353
R(586)=RAD(401,757,2.13E-6)	22663354
R(587)=RAD(401,758,2.4E-6)	22663355
R(588)=RAD(401,759,2.13E-6)	22663356
R(589)=RAD(401,760,2.4E-6)	22663357
R(600)=RAD(66,858,1.54E-6)	22663182
R(601)=RAD(66,535,21.6E-6)	22663183
R(602)=RAD(66,519,6.2E-6)	22663184
R(604)=RAD(67,857,2.1E-6)	22663185
R(606)=RAD(67,534,29.3E-6)	22663186
R(607)=RAD(67,518,8.3E-6)	22663187
R(608)=RAD(68,517,8.3E-6)	22663188
R(609)=RAD(68,533,20.8E-6)	22663189
R(610)=RAD(68,200,12.5E-6)	22663190
R(612)=RAD(69,200,11.2E-6)	22663191
R(613)=RAD(69,517,8.4E-6)	22663192
R(614)=RAD(69,501,2.8E-6)	22663193
R(615)=RAD(69,860,28.E-6)	22663194
R(616)=RAD(69,300,5.6E-6)	22663195
R(617)=RAD(70,760,19.5E-6)	22663196
R(618)=RAD(70,402,2.8E-6)	22663197
R(619)=RAD(70,501,2.8E-6)	22663198
R(620)=RAD(70,300,14.E-6)	22663199
R(621)=RAD(70,401,5.6E-6)	22663200
R(622)=RAD(70,200,11.2E-6)	22663201
R(623)=RAD(65,401,13.7E-6)	22663202
R(624)=RAD(65,500,8.3E-6)	22663203
R(625)=RAD(65,600,5.5E-6)	22663204
R(626)=RAD(28,600,50.E-6)	22663205
R(627)=RAD(29,600,44.E-6)	22663206
R(628)=RAD(30,600,15.7E-6)	22663207
R(629)=RAD(30,282,23.7E-6)	22663208
R(630)=RAD(155,200,10.E-6)	22663209
R(631)=RAD(156,200,11.7E-6)	22663210
R(632)=RAD(157,200,2.8E-6)	22663211
R(633)=RAD(157,202,6.5E-6)	22663212
R(634)=RAD(159,536,2.5E-6)	22663213
R(635)=RAD(159,520,2.5E-6)	22663214
R(636)=RAD(160,859,1.3E-6)	22663215
R(637)=RAD(160,520,.65E-6)	22663216
R(638)=RAD(160,37,2.0E-6)	22663217
R(639)=RAD(160,536,2.6E-6)	22663218
R(640)=RAD(161,519,.65E-6)	22663219
R(641)=RAD(161,38,2.0E-6)	22663220
R(642)=RAD(161,500,2.0E-6)	22663221
R(643)=RAD(161,535,2.0E-6)	22663222
R(644)=RAD(162,39,3.7E-6)	22663223
R(645)=RAD(162,535,.9E-6)	22663224

TABLE B-3 (Cont.)

```
R(646)=RAD(162,858,1.8E-6)                                    22663225
R(647)=RAD(162,600,2.8E-6)                                    22663226
R(648)=RAD(163,40,3.7E-6)                                     22663227
R(649)=RAD(163,758,1.8E-6)                                    22663228
R(650)=RAD(163,600,3.7E-6)                                    22663229
R(660)=RAD(165,200,10.0E-6)                                   22663230
R(661)=RAD(166,200,11.7E-6)                                   22663231
R(662)=RAD(167,200,2.8E-6)                                    22663232
R(663)=RAD(167,202,6.5E-6)                                    22663233
R(664)=RAD(169,536,2.5E-6)                                    22663234
R(665)=RAD(169,520,2.5E-6)                                    22663235
R(666)=RAD(170,859,1.3E-6)                                    22663236
R(667)=RAD(170,520,.65E-6)                                    22663237
R(668)=RAD(170,37,2.0E-6)                                     22663238
R(669)=RAD(170,536,2.6E-6)                                    22663239
R(670)=RAD(171,519,.65E-6)                                    22663240
R(671)=RAD(171,38,2.0E-6)                                     22663241
R(672)=RAD(171,500,2.0E-6)                                    22663242
R(673)=RAD(171,535,2.0E-6)                                    22663243
R(674)=RAD(172,39,3.7E-6)                                     22663244
R(675)=RAD(172,535,.9E-6)                                     22663245
R(676)=RAD(172,858,1.8E-6)                                    22663246
R(677)=RAD(172,600,2.8E-6)                                    22663247
R(678)=RAD(173,40,2.8E-6)                                     22663248
R(679)=RAD(173,758,1.8E-6)                                    22663249
R(680)=RAD(173,600,4.6E-6)                                    22663250
R(690)=RAD(358,518,1.14E-5)                                   22663358
R(691)=RAD(359,517,1.14E-5)                                   22663359
R(692)=RAD(360,520,1.14E-5)                                   22663360
R(693)=RAD(361,520,1.14E-5)                                   22663361
R(694)=RAD(362,519,1.14E-5)                                   22663362
R(695)=RAD(363,518,1.14E-5)                                   22663363
R(696)=RAD(364,501,1.14E-5)                                   22663364
R(697)=RAD(365,503,1.14E-5)                                   22663365
R(700)=RAD(129,858,2.5E-7)                                    22663251
R(701)=RAD(129,66,12.5E-7)                                    22663252
R(702)=RAD(129,519,10.E-7)                                    22663253
R(703)=RAD(129,535,25.E-7)                                    22663254
R(704)=RAD(130,857,3.3E-7)                                    22663255
R(705)=RAD(130,534,33.3E-7)                                   22663256
R(706)=RAD(130,67,16.7E-7)                                    22663257
R(707)=RAD(130,518,13.3E-7)                                   22663258
R(708)=RAD(131,517,13.3E-7)                                   22663259
R(709)=RAD(131,68,13.3E-7)                                    22663260
R(710)=RAD(131,200,20.E-7)                                    22663261
R(711)=RAD(131,533,20.E-7)                                    22663262
R(712)=RAD(132,200,18.3E-7)                                   22663263
R(713)=RAD(132,517,18.3E-7)                                   22663264
R(714)=RAD(132,501,9.2E-7)                                    22663265
R(715)=RAD(132,860,22.9E-7)                                   22663266
R(716)=RAD(132,69,22.9E-7)                                    22663267
R(717)=RAD(133,760,22.9E-7)                                   22663268
R(718)=RAD(133,402,4.6E-7)                                    22663269
R(719)=RAD(133,501,4.6E-7)                                    22663270
R(720)=RAD(133,401,9.2E-7)                                    22663271
R(721)=RAD(133,200,18.3E-7)                                   22663272
R(722)=RAD(133,70,32.E-7)                                     22663273
R(723)=RAD(128,401,22.9E-7)                                   22663274
R(724)=RAD(128,500,13.8E-7)                                   22663275
R(725)=RAD(128,600,9.1E-7)                                    22663276
R(726)=RAD(125,600,83.3E-7)                                   22663277
```

TABLE B-3 (Cont.)

R(727)=RAD(126,600,75.E-7)	22663278
R(728)=RAD(127,600,26.7E-7)	22663279
R(729)=RAD(127,282,40.0E-7)	22663280
R(730)=RAD(501,200,1.60E-5)	
R(731)=RAD(503,500,1.60E-5)	
R(732)=RAD(534,857,2.62E-5)	
R(733)=RAD(535,858,2.88E-5)	
R(734)=RAD(536,859,2.62E-5)	
R(735)=RAD(533,860,2.88E-5)	
R(736)=RAD(402,401,7.80E-5)	
R(737)=RAD(401,757,2.13E-5)	
R(738)=RAD(401,758,2.40E-5)	
R(739)=RAD(401,759,2.13E-5)	
R(740)=RAD(401,760,2.40E-5)	
R(741)=RAD(402,757,2.13E-5)	
R(742)=RAD(402,758,2.40E-5)	
R(743)=RAD(402,759,2.13E-5)	
R(744)=RAD(402,760,2.40E-5)	
R(745)=RAD(502,757,4.00E-5)	
R(746)=RAD(503,758,4.48E-5)	
R(747)=RAD(504,759,4.00E-5)	
R(748)=RAD(501,760,4.48E-5)	
R(749)=RAD(518,857,3.37E-5)	
R(750)=RAD(519,858,3.78E-5)	
R(751)=RAD(520,859,3.37E-5)	
R(752)=RAD(517,860,3.78E-5)	
R(755)=RAD(49,201,4.2E-5)	2997
R(756)=RAD(50,281,4.25E-5)	2998
R(800)=RAD(139,858,2.5E-7)	22663281
R(801)=RAD(139,535,10.E-7)	22663282
R(802)=RAD(139,66,12.5E-7)	22663283
R(803)=RAD(139,535,25.E-7)	22663284
R(804)=RAD(140,857,3.3E-7)	22663285
R(805)=RAD(140,534,33.3E-7)	22663286
R(806)=RAD(140,534,13.3E-7)	22663287
R(807)=RAD(140,67,16.7E-7)	22663288
R(809)=RAD(141,533,13.3E-7)	22663289
R(810)=RAD(141,200,20.E-7)	22663290
R(811)=RAD(141,533,20.E-7)	22663291
R(812)=RAD(142,200,18.3E-7)	22663292
R(813)=RAD(142,517,18.3E-7)	22663293
R(814)=RAD(142,501,9.2E-7)	22663294
R(815)=RAD(142,860,22.9E-7)	22663295
R(816)=RAD(142,69,22.9E-7)	22663296
R(818)=RAD(143,402,4.6E-7)	22663297
R(819)=RAD(143,501,4.6E-7)	22663298
R(820)=RAD(143,401,9.2E-7)	22663299
R(821)=RAD(143,200,18.3E-7)	22663300
R(822)=RAD(143,70,50.3E-7)	22663301
R(826)=RAD(135,600,83.3E-7)	22663302
R(827)=RAD(136,600,75.E-7)	22663303
R(828)=RAD(137,600,26.7E-7)	22663304
R(829)=RAD(137,282,40.E-7)	22663305
R(865)=RAD(758,600,7.35E-5)	22663366
R(866)=RAD(858,600,7.35E-5)	22663367
R(867)=RAD(760,300,7.35E-5)	22663368
R(868)=RAD(860,300,7.35E-5)	22663369
R(900)=RAD(149,858,2.5E-7)	22663306
R(901)=RAD(149,66,22.5E-7)	22663307
R(903)=RAD(149,535,25.E-7)	22663308
R(904)=RAD(150,857,3.3E-7)	22663309

TABLE B-3 (Cont.)

```
      R(905)=RAD(150,534,33.3E-7)                                    22663310
      R(906)=RAD(150,67,30.E-7)                                      22663311
      R(908)=RAD(151,68,26.6E-7)                                     22663312
      R(910)=RAD(151,200,20.E-7)                                     22663313
      R(911)=RAD(151,533,20.E-7)                                     22663314
      R(912)=RAD(152,200,18.3E-7)                                    22663315
      R(913)=RAD(152,517,18.3E-7)                                    22663316
      R(914)=RAD(152,501,9.2E-7)                                     22663317
      R(915)=RAD(152,69,45.8E-7)                                     22663318
      R(917)=RAD(153,760,22.9E-7)                                    22663319
      R(918)=RAD(153,402,4.6E-7)                                     22663320
      R(919)=RAD(153,501,4.6E-7)                                     22663321
      R(920)=RAD(153,401,9.2E-7)                                     22663322
      R(921)=RAD(153,200,18.3E-7)                                    22663323
      R(922)=RAD(153,70,32.E-7)                                      22663324
      R(926)=RAD(145,600,83.3E-7)                                    22663325
      R(927)=RAD(146,600,75.E-7)                                     22663326
      R(928)=RAD(147,600,26.7E-7)                                    22663327
      R(929)=RAD(147,282,40.E-7)                                     22663328
      R(1100)=RAD(400,1,2.6E-5)
      R(1101)=RAD(400,3,.70E-5)
      R(1102)=RAD(402,400,1.57E-4)
      DO 10 I=1,4
      R(I+1102)=RAD((I+512),(I+412),1.5E-4)
      R(I+1106)=RAD((I+524),(I+428),.83E-4)
      R(I+1112)=RAD((I+412),1,.20E-5)
10    CONTINUE
      R(1129)=RAD(429,1,1.1E-5)
      R(1130)=RAD(430,1,1.1E-5)
      R(1131)=RAD(431,1,1.1E-5)
      R(1132)=RAD(432,1,1.1E-5)
      R(1133)=RAD(429,3,12.6E-5)
      R(1134)=RAD(430,3,12.6E-5)
      R(1135)=RAD(431,3,12.6E-5)
      R(1136)=RAD(432,3,12.6E-5)
      R(1137)=RAD(413,416,7.5E-5)
      R(1138)=RAD(413,414,7.5E-5)
      R(1139)=RAD(415,413,15.E-5)
      R(1140)=RAD(400,414,7.1E-5)
      R(1141)=RAD(400,413,7.1E-5)
      R(1145)=RAD(414,415,7.5E-5)
      R(1146)=RAD(414,416,15.E-5)
      R(1150)=RAD(400,415,7.1E-5)
      R(1156)=RAD(415,416,7.5E-5)
      R(1160)=RAD(400,416,7.1E-5)
      R(1161)=RAD(430,431,2.1E-5)
      R(1162)=RAD(429,430,2.1E-5)
      R(1163)=RAD(431,432,2.1E-5)
      R(1164)=RAD(432,429,2.1E-5)
      R(1165)=RAD(429,431,4.2E-5)
      R(1166)=RAD(430,432,4.2E-5)
      R(1167)=RAD(400,429,3.7E-5)
      R(1168)=RAD(400,430,3.7E-5)
      R(1169)=RAD(400,431,3.7E-5)
      R(1170)=RAD(400,432,3.7E-5)
      R(1190)=RAD(545,1,1.0E-5)
      R(1191)=RAD(546,1,1.0E-5)
      R(1192)=RAD(547,1,1.0E-5)
      R(1193)=RAD(548,1,1.0E-5)
      R(1231)=RAD(413,431,1.9E-5)
      R(1242)=RAD(414,432,1.9E-5)
```

TABLE B-3 (Cont.)

```
R(1259)=RAD(415,429,1.9E-5)
R(1260)=RAD(416,430,1.9E-5)
R(1399)=RAD(100,341,50.0E-6)                                    22663340
R(1412)=RAD(100,331,11.1E-6)                                    22663329
R(1413)=RAD(100,334,8.00E-6)                                    22663330
R(1414)=RAD(100,332,21.8E-6)                                    22663331
R(1415)=RAD(100,333,19.6E-6)                                    22663332
R(1416)=RAD(100,335,9.40E-6)                                    22663333
R(1417)=RAD(100,336,10.2E-6)                                    22663334
R(1418)=RAD(100,337,15.5E-6)                                    22663335
R(1419)=RAD(100,342,50.0E-6)                                    22663336
R(1420)=RAD(100,343,27.7E-6)                                    22663337
R(1421)=RAD(100,344,15.8E-6)                                    22663338
R(1422)=RAD(100,345,13.7E-6)                                    22663339
                                                                      0441

                                                                 000441
```


LOCKHEED CALIFORNIA COMPANY

TABLE B-3 (Cont.)

The following data are either additions or modifications to the engine/plumbing analysis to account for the removal of insulation from the Bay 4 side of beams 3 and 4. These network changes were used in the Earth Orbital Analysis.

DEC01	1	5	6	150.					
DEC02	400	303	300	0.	401	302	300	0.	204002266
DEC02	402	301	300	0.	403	304	300	0.	204022266
DEC01	1025	321	319	1.					310252266
DEC01	1028	322	319	1.					310282266
DEC01	1031	323	319	1.					310312266
DEC01	1034	324	319	1.					310342266
DEC01	1037	331	329	1.					310372266
DEC01	1040	332	329	1.					310402266
DEC01	1043	333	329	1.					310432266
DEC01	1046	334	329	1.					310462266
DEC01	1049	335	329	1.					310492266
DEC01	1052	336	329	1.					310522266
DEC01	1055	341	339	1.					310552266
DEC01	1058	342	339	1.					310582266
DEC01	1061	343	339	1.					310612266
DEC01	1064	344	339	1.					310642266
DEC01	1067	345	339	1.					310672266
DEC01	1070	351	329	1.					310702266
DEC01	1073	352	290	1.					310732266
DEC01	1076	353	291	1.					310762266
DEC01	1079	337	329	1.					310792266
DEC02	1108	530	430	0.	1109	531	431	0.	
DEC02	1110	532	432	0.	1113	413	1	0.	
DEC01	1301	301	100	1.					213012266
DEC01	1302	302	100	1.					213022266
DEC01	1303	303	100	1.					213032266
DEC01	1304	304	100	1.					213042266
DEC01	1311	311	100	1.					213052266
DEC01	1312	312	100	1.					213062266
DEC01	1313	313	100	1.					213072266
DEC01	1314	314	100	1.					213082266
DEC01	1321	321	100	1.					213092266
DEC01	1322	322	100	1.					213102266
DEC01	1323	323	100	1.					213112266
DEC01	1324	324	100	1.					213122266
DEC01	1331	331	100	1.					213132266
DEC01	1332	332	100	1.					213142266
DEC01	1333	333	100	1.					213152266
DEC01	1334	334	100	1.					213162266
DEC01	1335	335	100	1.					213172266
DEC01	1336	336	100	1.					213182266
DEC01	1337	337	100	1.					213192266
DEC01	1341	341	100	1.					213202266
DEC01	1342	342	100	1.					213212266
DEC01	1343	343	100	1.					213222266
DEC01	1344	344	100	1.					213232266
DEC01	1345	345	100	1.					213242266
DEC01	1351	351	100	1.					213252266

TABLE B-3 (Cont.)

R(400)=RAD(303,300,18.2E-6)	3116
R(401)=RAD(302,300,11.1E-6)	3117
R(402)=RAD(301,300,11.1E-6)	3118
R(403)=RAD(304,300,17.3E-6)	3119
R(404)=RAD(311,310,10.8E-6)	3120
R(405)=RAD(312,310,10.8E-6)	3121
R(406)=RAD(313,310,18.2E-6)	3122
R(407)=RAD(314,310,17.3E-6)	3123
R(408)=RAD(321,320,10.3E-6)	3124
R(409)=RAD(322,320,11.6E-6)	3125
R(410)=RAD(323,320,19.1E-6)	3126
R(411)=RAD(324,320,19.6E-6)	3127
R(423)=RAD(351,330,30.05E-6)	3128
R(424)=RAD(352,305,17.3E-6)	3129
R(425)=RAD(353,306,20.0E-6)	3130
R(1025)=RAD(321,319,10.3E-6)	22664025
R(1028)=RAD(322,319,11.6E-6)	22664026
R(1031)=RAD(323,319,19.1E-6)	22664027
R(1034)=RAD(324,319,19.6E-6)	22664028
R(1037)=RAD(331,329,11.1E-6)	22664029
R(1040)=RAD(332,329,8.00E-6)	22664030
R(1043)=RAD(333,329,21.8E-6)	22664031
R(1046)=RAD(334,329,19.6E-6)	22664032
R(1049)=RAD(335,329,9.40E-6)	22664033
R(1052)=RAD(336,329,10.2E-6)	22664034
R(1055)=RAD(341,339,50.0E-6)	22664036
R(1058)=RAD(342,339,50.0E-6)	22664037
R(1061)=RAD(343,339,27.7E-6)	22664038
R(1064)=RAD(344,339,15.8E-6)	22664039
R(1067)=RAD(345,339,13.7E-6)	22664040
R(1070)=RAD(351,329,60.1E-6)	22664041
R(1073)=RAD(352,290,34.6E-6)	22664042
R(1076)=RAD(353,291,40.0E-6)	22664043
R(1079)=RAD(337,329,15.5E-6)	22664035
R(1301)=RAD(301,100,5.2E-6)	22664000
R(1302)=RAD(302,100,5.2E-6)	22664001
R(1303)=RAD(303,100,8.6E-6)	22664002
R(1304)=RAD(304,100,7.7E-6)	22664003
R(1311)=RAD(311,100,5.1E-6)	22664004
R(1312)=RAD(312,100,5.1E-6)	22664005
R(1313)=RAD(313,100,5.0E-6)	22664006
R(1314)=RAD(314,100,8.6E-6)	22664007
R(1321)=RAD(321,100,2.7E-6)	22664008
R(1322)=RAD(322,100,2.8E-6)	22664009
R(1323)=RAD(323,100,4.6E-6)	22664010
R(1324)=RAD(324,100,4.7E-6)	22664011
R(1331)=RAD(331,100,1.0E-6)	22664012
R(1332)=RAD(332,100,1.8E-6)	22664013
R(1333)=RAD(333,100,1.7E-6)	22664014
R(1334)=RAD(334,100,0.7E-6)	22664015
R(1335)=RAD(335,100,0.8E-6)	22664016
R(1336)=RAD(336,100,0.9E-6)	22664017
R(1337)=RAD(337,100,1.4E-6)	22664018
R(1341)=RAD(341,100,6.0E-6)	22664019
R(1342)=RAD(342,100,6.0E-6)	22664020
R(1343)=RAD(343,100,3.3E-6)	22664021
R(1344)=RAD(344,100,1.9E-6)	22664022
R(1345)=RAD(345,100,1.7E-6)	22664023
R(1351)=RAD(351,100,2.8E-6)	22664024

0059

LOCKHEED CALIFORNIA COMPANY

TABLE B-4

CAPACITORS FOR DETAILED ENGINE AND PLUMBING ANALYSIS

DEC03	10	.599	11	1.014	12	.796	300102266
DEC03	13	1.42	14	2.46	15	2.03	300132266
DEC03	16	1.25	17	1.08	18	1.08	300162266
DEC02	19	1.44	20	1.44			300192266
DEC03	21	1.351	22	2.367	23	2.473	300212266
DEC03	24	1.688	25	1.799	26	2.025	300242266
DEC03	27	1.351	28	.067	29	.059	300272266
DEC03	30	.052	31	3.620	32	3.620	300302266
DEC03	33	1.29	34	2.786	35	3.061	300332266
DEC03	36	3.46	37	1.95	38	1.95	300362266
DEC02	39	2.78	40	2.78			300392266
DEC03	41	1.951	42	2.786	43	1.951	300412266
DEC03	44	2.364	45	2.649	46	2.511	300442266
DEC02	47	1.812	48	.710			300472266
DEC02	49	.54	50	.55			30049
DEC03	51	.0705	52	.0752	53	.0847	300512266
DEC03	54	.0941	55	.0893	56	.0941	300542266
DEC03	61	.2069	62	.0941	63	.0941	300612266
DEC03	64	.0564	65	.037	66	.041	300642266
DEC03	67	.055	68	.055	69	.074	300672266
DEC02	70	.074	71	.0192	81	.0986	300702266
DEC03	72	.3	73	.3	74	.1	30072
DEC02	75	.3	76	.1			30075
DEC03	91	.0877	92	.0767	93	.0438	300912266
DEC03	94	.0384	95	.0438	96	.0438	300942266
DEC02	97	.0466	98	.0712			300972266
DEC03	101	.0493	102	.0575	103	.0959	301012266
DEC03	104	.0520	105	.0520	106	.0685	301042266
DEC01	107	.0493					301072266
DEC03	111	.0438	112	.0438	113	.0520	301112266
DEC03	114	.0630	115	.0438	116	.27	301142266
DEC03	121	.0329	122	.0685	123	.0602	301212266
DEC03	124	.270	125	.011	126	.010	301242266
DEC03	127	.009	128	.006	129	.007	301272266
DEC03	130	.009	131	.009	132	.012	301302266
DEC03	133	.012	135	.011	136	.010	301332266
DEC02	137	.009	139	.007			301372266
DEC03	140	.009	141	.009	142	.012	301402266
DEC03	143	.012	145	.011	146	.010	301432266
DEC02	147	.009	149	.007			301472266
DEC03	150	.009	151	.009	152	.012	301502266
DEC03	153	.012	155	.013	156	.014	301532266
DEC02	157	.012	159	.007			301572266
DEC03	160	.009	161	.009	162	.012	301602266
DEC03	163	.012	165	.013	166	.014	301632266
DEC02	167	.012	169	.007			301672266
DEC03	170	.009	171	.009	172	.012	301702266
DEC01	173	.012					301732266
DEC03	301	.05338	302	.05338	303	.09406	303012266
DEC01	304	.08937					303042266
DEC03	311	.05205	312	.05205	313	.09406	303112266
DEC01	314	.08937					303142266
DEC03	321	.05205	322	.05615	323	.09875	303212266
DEC01	324	.10100					303242266
DEC03	331	.05338	332	.11283	333	.10100	303312266
DEC03	334	.03839	335	.04517	336	.04928	303342266
DEC03	341	1.0	342	1.0	343	.14334	303412266
DEC02	344	.08702	345	.07059			303442266
DEC03	351	.15517	352	.08937	353	.10345	303512266
DEC01	337	.07998					303372266
DEC03	358	.733	359	2.15	360	3.42 GIMBAL RING	303582266

TABLE B-4 (Cont.)

DEC03	361	.733	362	2.15	363	3.42	ENGINE INSTL.	303612266
DEC03	364	.503	365	.503	366	.277	ATTACHMENTS	303642266
DEC03	367	.277	368	.529	369	.200		303672266
DEC02	370	3.60	371	3.90			YAW/PITCH ACT.	303702266
DEC02	401	14.2	402	6.8				304012266
DEC03	400	0.	413	0.	414	0.		
DEC03	415	0.	416	0.	429	0.		
DEC03	430	0.	431	0.	432	0.		
DEC01	501	.980						305012266
INC	1	0.	3					305022266
DEC01	505	1.84						305052266
INC	1	0.	3					305062266
DEC01	509	1.73						305092266
INC	1	0.	3					305102266
DEC01	513	.565						305132266
INC	1	0.	3					305142266
DEC01	517	.672						305172266
INC	1	0.	3					305182266
DEC01	521	1.24						305212266
INC	1	0.	3					305222266
DEC01	525	1.14						305252266
INC	1	0.	3					305262266
DEC01	529	.362						305292266
INC	1	0.	3					305302266
DEC01	533	.858						305332266
INC	1	0.	3					305342266
DEC01	537	1.67						305372266
INC	1	0.	3					305382266
DEC01	541	1.62						305412266
INC	1	0.	3					305422266
DEC01	545	.552						305452266
INC	1	0.	3					305462266
DEC03	757	.147	758	.210	759	.147	MOUNT	307572266
DEC01	760	.210						307602266
DEC03	857	.147	858	.210	859	.147	MOUNT	308572266
DEC01	860	.210						308602266
NBK								39999 2266

LOCKHEED CALIFORNIA COMPANY

TABLE B-5

RESISTORS FOR BAY 2 OXIDIZER TANK ANALYSIS

DEC02	551	201	250	0.	552	202	250	0.	20012266
DEC02	553	201	20	0.	554	203	20	0.	20022266
DEC02	555	204	20	0.	556	201	36	0.	20032266
DEC02	557	203	36	0.	558	205	36	0.	20042266
DEC02	559	206	36	0.	560	205	52	0.	20052266
DEC02	561	206	52	0.	562	205	52	0.	20062266
DEC02	563	207	52	0.	564	205	68	0.	20072266
DEC02	565	207	68	0.	566	204	68	0.	20082266
DEC02	567	208	68	0.	568	209	254	0.	20092266
DEC02	569	210	254	0.	570	211	253	0.	20102266
DEC02	571	211	24	0.	572	211	40	0.	20112266
DEC02	573	212	40	0.	574	212	56	0.	20122266
DEC02	575	213	56	0.	576	213	72	0.	20132266
DEC02	577	214	257	0.	578	215	253	0.	20142266
DEC02	579	216	253	0.	580	217	24	0.	20152266
DEC02	581	216	24	0.	582	215	24	0.	20162266
DEC02	583	215	40	0.	584	216	40	0.	20172266
DEC02	585	218	40	0.	586	218	56	0.	20182266
DEC02	587	218	72	0.	588	219	72	0.	20192266
DEC02	589	220	257	0.	590	221	252	0.	20202266
DEC02	591	221	28	0.	592	221	44	0.	20212266
DEC02	593	218	44	0.	594	218	60	0.	20222266
DEC02	595	218	76	0.	596	219	76	0.	20232266
DEC02	597	220	256	0.	598	222	44	0.	20242266
DEC02	599	222	60	0.	600	223	76	0.	20252266
DEC02	601	223	256	0.	602	224	252	0.	20262266
DEC02	603	224	28	0.	604	225	28	0.	20272266
DEC02	605	225	44	0.	606	226	44	0.	20282266
DEC02	607	226	60	0.	608	225	60	0.	20292266
DEC02	609	225	76	0.	610	225	256	0.	20302266
DEC02	611	224	251	0.	612	224	32	0.	20312266
DEC02	613	225	32	0.	614	225	48	0.	20322266
DEC02	615	227	48	0.	616	226	48	0.	20332266
DEC02	617	227	64	0.	618	226	64	0.	20342266
DEC02	619	226	80	0.	620	228	255	0.	20352266
DEC02	621	226	255	0.	622	229	251	0.	20362266
DEC02	623	229	32	0.	624	229	48	0.	20372266
DEC02	625	206	48	0.	626	206	64	0.	20382266
DEC02	627	207	64	0.	628	207	80	0.	20392266
DEC02	629	208	80	0.	630	210	255	0.	20402266
DEC02	631	230	98	0.	632	231	98	0.	20412266
DEC02	633	232	98	0.	634	233	98	0.	20422266
DEC02	635	234	98	0.	636	235	98	0.	20432266
DEC02	637	236	98	0.	638	237	258	22200.	20442266
DEC02	639	238	258	22800.	640	239	258	22800.	20452266
DEC02	641	240	259	22800.	642	241	259	22800.	20462266
DEC02	643	235	259	22200.	644	234	259	27200.	20472266
DEC02	645	236	258	27200.	646	242	250	4250.	20482266
DEC02	647	243	251	6450.	648	244	252	4570.	20492266
DEC02	649	245	253	5760.	650	246	254	1270.	20502266
DEC02	651	247	255	2360.	652	248	256	1620.	20512266
DEC02	653	249	257	2360.	654	250	20	2460.	20522266
DEC02	655	251	32	4600.	656	252	28	3960.	20532266
DEC02	657	253	24	4600.	658	254	68	1270.	20542266
DEC02	659	255	80	2360.	660	256	76	1620.	20552266
DEC02	661	257	72	2360.	662	258	98	575.	20562266
DEC02	663	259	98	575.	664	28	98	0.	20572266

TABLE B-5 (Cont.)

```
R(551)=RAD(201,230,1.45E-6)                                    22662101
R(552)=RAD(202,250,3.55E-6)                                    22662102
R(553)=RAD(201,20,1.98E-6)                                     22662103
R(554)=RAD(203,20,3.68E-6)                                     22662104
R(555)=RAD(204,20,1.17E-6)                                     22662105
R(556)=RAD(201,36,0.47E-6)                                     22662106
R(557)=RAD(203,36,1.17E-6)                                     22662107
R(558)=RAD(205,36,1.50E-6)                                     22662108
R(559)=RAD(206,36,3.68E-6)                                     22662109
R(560)=RAD(205,52,1.30E-6)                                     22662110
R(561)=RAD(206,52,3.22E-6)                                     22662111
R(562)=RAD(205,52,0.68E-6)                                     22662112
R(563)=RAD(207,52,1.64E-6)                                     22662113
R(564)=RAD(205,68,0.68E-6)                                     22662114
R(565)=RAD(207,68,1.55E-6)                                     22662115
R(566)=RAD(204,68,1.30E-6)                                     22662116
R(567)=RAD(208,68,3.22E-6)                                     22662117
R(568)=RAD(209,254,1.15E-6)                                    22662118
R(569)=RAD(210,254,2.81E-6)                                    22662119
R(570)=RAD(211,253,1.50E-6)                                    22662120
R(571)=RAD(211,24,2.05E-6)                                     22662121
R(572)=RAD(211,40,0.47E-6)                                     22662122
R(573)=RAD(212,40,1.57E-6)                                     22662123
R(574)=RAD(212,56,1.36E-6)                                     22662124
R(575)=RAD(213,56,0.68E-6)                                     22662125
R(576)=RAD(213,72,2.04E-6)                                     22662126
R(577)=RAD(214,257,1.19E-6)                                    22662127
R(578)=RAD(215,253,1.05E-6)                                    22662128
R(579)=RAD(216,253,2.44E-6)                                    22662129
R(580)=RAD(217,24,0.82E-6)                                     22662130
R(581)=RAD(216,24,3.35E-6)                                     22662131
R(582)=RAD(215,24,0.62E-6)                                     22662132
R(583)=RAD(215,40,0.34E-6)                                     22662133
R(584)=RAD(216,40,0.75E-6)                                     22662134
R(585)=RAD(218,40,3.68E-6)                                     22662135
R(586)=RAD(218,56,4.79E-6)                                     22662136
R(587)=RAD(218,72,1.57E-6)                                     22662137
R(588)=RAD(219,72,3.22E-6)                                     22662138
R(589)=RAD(220,257,2.77E-6)                                    22662139
R(590)=RAD(221,252,1.29E-6)                                    22662140
R(591)=RAD(221,28,1.78E-6)                                     22662141
R(592)=RAD(221,44,0.41E-6)                                     22662142
R(593)=RAD(218,44,1.36E-6)                                     22662143
R(594)=RAD(218,60,1.78E-6)                                     22662144
R(595)=RAD(218,76,0.62E-6)                                     22662145
R(596)=RAD(219,76,1.16E-6)                                     22662146
R(597)=RAD(220,256,1.03E-6)                                    22662147
R(598)=RAD(222,44,1.20E-4)                                     22662148
R(599)=RAD(222,60,0.50E-4)                                     22662149
R(600)=RAD(223,76,0.60E-5)                                     22662150
R(601)=RAD(223,256,1.0E-5)                                     22662151
R(602)=RAD(224,252,1.29E-6)                                    22662152
R(603)=RAD(224,28,1.03E-6)                                     22662153
R(604)=RAD(225,28,0.75E-6)                                     22662154
R(605)=RAD(225,44,0.41E-6)                                     22662155
R(606)=RAD(226,44,1.36E-6)                                     22662156
R(607)=RAD(226,60,1.16E-6)                                     22662157
R(608)=RAD(225,60,0.62E-6)                                     22662158
R(609)=RAD(225,76,1.78E-6)                                     22662159
R(610)=RAD(225,256,1.03E-6)                                    22662160
R(611)=RAD(224,251,3.50E-6)                                    22662161
```

TABLE B-5 (Cont.)

R(612)=RAD(224,32,2.74E-6)	22662162
R(613)=RAD(225,32,2.05E-6)	22662163
R(614)=RAD(225,48,1.10E-6)	22662164
R(615)=RAD(227,48,0.75E-6)	22662165
R(616)=RAD(226,48,2.58E-6)	22662166
R(617)=RAD(227,64,0.95E-6)	22662167
R(618)=RAD(226,64,3.83E-6)	22662168
R(619)=RAD(226,80,4.78E-6)	22662169
R(620)=RAD(228,255,0.84E-6)	22662170
R(621)=RAD(226,255,1.93E-6)	22662171
R(622)=RAD(229,251,1.50E-6)	22662172
R(623)=RAD(229,32,2.05E-6)	22662173
R(624)=RAD(229,48,0.48E-6)	22662174
R(625)=RAD(206,48,1.57E-6)	22662175
R(626)=RAD(206,64,1.36E-6)	22662176
R(627)=RAD(207,64,0.68E-6)	22662177
R(628)=RAD(207,80,0.68E-6)	22662178
R(629)=RAD(208,80,1.36E-6)	22662179
R(630)=RAD(210,255,1.19E-6)	22662180
R(631)=RAD(230,98,1.74E-4)	22662181
R(632)=RAD(231,98,1.60E-4)	22662182
R(633)=RAD(232,98,1.80E-4)	22662183
R(634)=RAD(233,98,1.60E-4)	22662184
R(635)=RAD(234,98,0.65E-4)	22662185
R(636)=RAD(235,98,0.77E-4)	22662186
R(637)=RAD(236,98,1.47E-4)	22662187
R(664)=RAD(28,98,1.8E-4)	22662188

TABLE B-6

RESISTORS FOR BAY 3 FUEL TANK ANALYSIS

DEC02	551	201	250	0.	552	202	250	0.	30012266
DEC02	553	203	20	0.	554	202	20	0.	30022266
DEC02	555	203	36	0.	556	202	36	0.	30032266
DEC02	557	204	36	0.	558	203	52	0.	30042266
DEC02	559	204	52	0.	560	205	52	0.	30052266
DEC02	561	203	68	0.	562	205	68	0.	30062266
DEC02	563	206	254	0.	564	207	253	0.	30072266
DEC02	565	208	24	0.	566	208	40	0.	30082266
DEC02	567	208	56	0.	568	208	72	0.	30092266
DEC02	569	209	257	0.	570	210	253	0.	30102266
DEC02	571	210	24	0.	572	211	24	0.	30112266
DEC02	573	211	40	0.	574	212	40	0.	30122266
DEC02	575	213	40	0.	576	212	56	0.	30132266
DEC02	577	213	56	0.	578	213	72	0.	30142266
DEC02	579	214	257	0.	580	213	257	0.	30152266
DEC02	581	210	252	0.	582	210	28	0.	30162266
DEC02	583	211	28	0.	584	211	44	0.	30172266
DEC02	585	213	44	0.	586	213	60	0.	30182266
DEC02	587	211	60	0.	588	211	76	0.	30192266
DEC02	589	211	256	0.	590	215	44	0.	30202266
DEC02	591	215	60	0.	592	216	76	0.	30212266
DEC02	593	216	256	0.	594	217	252	0.	30222266
DEC02	595	217	28	0.	596	217	44	0.	30232266
DEC02	597	218	44	0.	598	218	60	0.	30242266
DEC02	599	219	60	0.	600	219	76	0.	30252266
DEC02	601	220	76	0.	602	220	256	0.	30262266
DEC02	603	217	251	0.	604	217	32	0.	30272266
DEC02	605	217	48	0.	606	217	64	0.	30282266
DEC02	607	218	64	0.	608	218	80	0.	30292266
DEC02	609	221	80	0.	610	219	255	0.	30302266
DEC02	611	220	255	0.	612	202	251	0.	30312266
DEC02	613	221	32	0.	614	221	48	0.	30322266
DEC02	615	209	48	0.	616	209	64	0.	30332266
DEC02	617	203	64	0.	618	203	80	0.	30342266
DEC02	619	205	255	0.	631	230	98	0.	30352266
DEC02	632	231	98	0.	633	232	98	0.	30362266
DEC02	634	233	98	0.	635	234	98	0.	30372266
DEC02	636	235	98	0.	637	236	98	0.	30382266
DEC02	664	98	28	0.	638	237	258	22200.	30392266
DEC02	639	238	258	22800.	640	239	258	22800.	30402266
DEC02	641	240	259	22800.	642	241	259	22800.	30412266
DEC02	643	235	259	22200.	644	234	259	27200.	30422266
DEC02	645	236	258	27200.	646	242	250	10040.	30432266
DEC02	647	243	251	6780.	648	244	252	3630.	30442266
DEC02	649	245	253	6780.	650	246	254	1320.	30452266
DEC02	651	247	255	1500.	652	248	256	1440.	30462266
DEC02	653	249	257	1500.	654	250	20	7020.	30472266
DEC02	655	251	32	4170.	656	252	28	2560.	30482266
DEC02	657	253	24	4170.	658	254	68	1320.	30492266
DEC02	659	255	80	1500.	660	256	76	1440.	30502266
DEC02	661	257	72	1500.	662	258	98	575.	30512266
DEC02	663	259	98	575.	664	98	28	0.	30522266

TABLE B-6 (Cont.)

R(551)=RAD(201,250,1.74E-6)	22663301
R(552)=RAD(202,250,1.74E-6)	22663302
R(553)=RAD(203,20,3.24E-6)	22663303
R(554)=RAD(202,20,3.24E-6)	22663304
R(555)=RAD(203,36,3.24E-6)	22663305
R(556)=RAD(202,36,1.00E-6)	22663306
R(557)=RAD(204,36,2.25E-6)	22663307
R(558)=RAD(203,52,3.24E-6)	22663308
R(559)=RAD(204,52,2.25E-6)	22663309
R(560)=RAD(205,52,1.00E-6)	22663310
R(561)=RAD(203,68,5.48E-6)	22663311
R(562)=RAD(205,68,1.00E-6)	22663312
R(563)=RAD(206,254,2.87E-6)	22663313
R(564)=RAD(207,253,.80E-6)	22663314
R(565)=RAD(208,24,1.48E-6)	22663315
R(566)=RAD(208,40,1.48E-6)	22663316
R(567)=RAD(208,56,1.48E-6)	22663317
R(568)=RAD(208,72,1.48E-6)	22663318
R(569)=RAD(209,257,.66E-6)	22663319
R(570)=RAD(210,253,2.68E-6)	22663320
R(571)=RAD(210,24,3.50E-6)	22663321
R(572)=RAD(211,24,1.49E-6)	22663322
R(573)=RAD(211,40,1.49E-6)	22663323
R(574)=RAD(212,40,1.08E-6)	22663324
R(575)=RAD(213,40,2.42E-6)	22663325
R(576)=RAD(212,56,1.08E-6)	22663326
R(577)=RAD(213,56,3.91E-6)	22663327
R(578)=RAD(213,72,5.00E-6)	22663328
R(579)=RAD(214,257,.69E-6)	22663329
R(580)=RAD(213,257,1.52E-6)	22663330
R(581)=RAD(210,252,.97E-6)	22663331
R(582)=RAD(210,28,1.30E-6)	22663332
R(583)=RAD(211,28,.52E-6)	22663333
R(584)=RAD(211,44,.52E-6)	22663334
R(585)=RAD(213,44,1.30E-6)	22663335
R(586)=RAD(213,60,1.30E-6)	22663336
R(587)=RAD(211,60,.52E-6)	22663337
R(588)=RAD(211,76,1.81E-6)	22663338
R(589)=RAD(211,256,.80E-6)	22663339
R(590)=RAD(215,44,1.0E-4)	22663340
R(591)=RAD(215,60,.5E-4)	22663341
R(592)=RAD(216,76,.4E-4)	22663342
R(593)=RAD(216,256,1.1E-4)	22663343
R(594)=RAD(217,252,.97E-6)	22663344
R(595)=RAD(217,28,1.81E-6)	22663345
R(596)=RAD(217,44,.520E-6)	22663346
R(597)=RAD(218,44,1.30E-6)	22663347
R(598)=RAD(218,60,1.30E-6)	22663348
R(599)=RAD(219,60,.520E-6)	22663349
R(600)=RAD(219,76,.520E-6)	22663350
R(601)=RAD(220,76,1.3E-6)	22663351
R(602)=RAD(220,256,.8E-6)	22663352
R(603)=RAD(217,251,2.68E-6)	22663353
R(604)=RAD(217,32,5.00E-6)	22663354
R(605)=RAD(217,48,5.00E-6)	22663355
R(606)=RAD(217,64,3.50E-6)	22663356
R(607)=RAD(218,64,1.50E-6)	22663357
R(608)=RAD(218,80,2.57E-6)	22663358
R(609)=RAD(221,80,2.42E-6)	22663359
R(610)=RAD(219,255,.69E-6)	22663360
R(611)=RAD(220,255,1.52E-6)	22663361

LOCKHEED CALIFORNIA COMPANY

TABLE B-6 (Cont.)

R(612)=RAD(202,251,.81E-6)	22663362
R(613)=RAD(221,32,1.48E-6)	22663363
R(614)=RAD(221,48,.45E-6)	22663364
R(615)=RAD(209,48,1.03E-6)	22663365
R(616)=RAD(209,64,1.03E-6)	22663366
R(617)=RAD(203,64,.45E-6)	22663367
R(618)=RAD(203,80,1.48E-6)	22663368
R(619)=RAD(205,255,.66E-6)	22663369
R(631)=RAD(230,98,1.74E-4)	22663370
R(632)=RAD(231,98,1.8E-4)	22663371
R(633)=RAD(232,98,1.8E-4)	22663372
R(634)=RAD(233,98,1.6E-4)	22663373
R(635)=RAD(234,98,.65E-4)	22663374
R(636)=RAD(235,98,.77E-4)	22663375
R(637)=RAD(236,98,1.47E-4)	22663376
R(664)=RAD(28,98,1.6E-4)	22663377

LOCKHEED CALIFORNIA COMPANY

TABLE B-7

RESISTORS FOR BAY 5 OXIDIZER TANK ANALYSIS

DEC02	551	201	250	0.	552	202	250	0.	520012266
DEC02	553	203	250	0.	554	201	20	0.	520022266
DEC02	555	204	20	0.	556	205	20	0.	520032266
DEC02	557	201	36	0.	558	204	36	0.	520042266
DEC02	559	205	36	0.	560	206	6	0.	520052266
DEC02	561	207	36	0.	562	206	5	0.	520062266
DEC02	563	207	52	0.	564	208	52	0.	520072266
DEC02	565	206	68	0.	566	208	68	0.	520082266
DEC02	567	209	68	0.	568	210	68	0.	520092266
DEC02	569	211	254	0.	570	212	254	0.	520102266
DEC02	571	201	253	0.	572	201	24	0.	520112266
DEC02	573	201	40	0.	574	213	40	0.	520122266
DEC02	575	213	56	0.	576	214	56	0.	520132266
DEC02	577	214	72	0.	578	211	257	0.	520142266
DEC02	579	215	253	0.	580	215	24	0.	520152266
DEC02	581	215	40	0.	582	215	56	0.	520162266
DEC02	583	216	56	0.	584	217	56	0.	520172266
DEC02	585	216	72	0.	586	217	72	0.	520182266
DEC02	587	218	72	0.	588	219	257	0.	520192266
DEC02	589	218	257	0.	590	215	252	0.	520202266
DEC02	591	215	28	0.	592	215	44	0.	520212266
DEC02	593	216	44	0.	594	216	60	0.	520222266
DEC02	595	218	60	0.	596	218	76	0.	520232266
DEC02	597	220	76	0.	598	221	257	0.	520242266
DEC02	599	222	44	0.	600	222	60	0.	520252266
DEC02	601	223	76	0.	602	223	257	0.	520262266
DEC02	603	224	252	0.	604	224	28	0.	520272266
DEC02	605	225	28	0.	606	225	44	0.	520282266
DEC02	607	225	60	0.	608	225	76	0.	520292266
DEC02	609	225	257	0.	610	224	251	0.	520302266
DEC02	611	224	32	0.	612	225	32	0.	520312266
DEC02	613	224	48	0.	614	225	48	0.	520322266
DEC02	615	226	48	0.	616	227	48	0.	520332266
DEC02	617	226	64	0.	618	227	64	0.	520342266
DEC02	619	227	80	0.	620	228	255	0.	520352266
DEC02	621	227	255	0.	622	229	251	0.	520362266
DEC02	623	229	32	0.	624	229	48	0.	520372266
DEC02	625	207	48	0.	626	207	64	0.	520382266
DEC02	627	208	64	0.	628	208	80	0.	520392266
DEC02	629	210	80	0.	630	212	255	0.	520402266
DEC02	631	230	98	0.	632	231	98	0.	520412266
DEC02	633	232	98	0.	634	233	98	0.	520422266
DEC02	635	234	98	0.	636	235	98	0.	520432266
DEC02	637	236	98	0.	638	237	258	22200.	520442266
DEC02	639	238	258	22800.	640	239	258	22800.	520452266
DEC02	641	240	259	22800.	642	241	259	22800.	520462266
DEC02	643	235	259	22200.	644	234	259	27200.	520472266
DEC02	645	236	258	27200.	646	242	250	4250.	520482266
DEC02	647	243	251	6450.	648	244	252	4570.	520492266
DEC02	649	245	253	5760.	650	246	254	1270.	520502266
DEC02	651	247	255	2360.	652	248	256	1620.	520512266
DEC02	653	249	257	2360.	654	250	20	2460.	520522266
DEC02	655	251	32	4600.	656	252	28	3960.	520532266
DEC02	657	253	24	4600.	658	254	68	1270.	520542266
DEC02	659	255	80	2360.	660	256	76	1620.	520552266
DEC02	661	257	72	2360.	662	258	98	575.	520562266
DEC02	663	259	98	575.	664	28	98	0.	520572266

LOCKHEED
CALIFORNIA COMPANY

TABLE B-7 (Cont.)

R(551)=RAD(201,250,1.44E-6)	22669001
R(552)=RAD(202,250,2.10E-6)	22669002
R(553)=RAD(203,250,1.45E-6)	22669003
R(554)=RAD(201,20,1.98E-6)	22669004
R(555)=RAD(204,20,2.87E-6)	22669005
R(556)=RAD(205,20,1.98E-6)	22669006
R(557)=RAD(201,36,.48E-6)	22669007
R(558)=RAD(204,36,.68E-6)	22669008
R(559)=RAD(205,36,.48E-6)	22669009
R(560)=RAD(206,36,1.50E-6)	22669010
R(561)=RAD(207,36,3.68E-6)	22669011
R(562)=RAD(206,52,1.98E-6)	22669012
R(563)=RAD(207,52,3.22E-6)	22669013
R(564)=RAD(208,52,1.64E-6)	22669014
R(565)=RAD(206,68,.68E-6)	22669015
R(566)=RAD(208,68,1.64E-6)	22669016
R(567)=RAD(209,68,1.30E-6)	22669017
R(568)=RAD(210,68,3.22E-6)	22669018
R(569)=RAD(211,254,2.78E-6)	22669019
R(570)=RAD(212,254,1.18E-6)	22669020
R(571)=RAD(201,253,1.50E-6)	22669021
R(572)=RAD(201,24,2.05E-6)	22669022
R(573)=RAD(201,40,.48E-6)	22669023
R(574)=RAD(213,40,1.57E-6)	22669024
R(575)=RAD(213,56,1.36E-6)	22669025
R(576)=RAD(214,56,.68E-6)	22669026
R(577)=RAD(214,72,2.05E-6)	22669027
R(578)=RAD(211,257,1.19E-6)	22669028
R(579)=RAD(215,253,3.50E-6)	22669029
R(580)=RAD(215,24,4.78E-6)	22669030
R(581)=RAD(215,40,4.78E-6)	22669031
R(582)=RAD(215,56,3.22E-6)	22669032
R(583)=RAD(216,56,.48E-6)	22669033
R(584)=RAD(217,56,1.10E-6)	22669034
R(585)=RAD(216,72,1.35E-6)	22669035
R(586)=RAD(217,72,1.10E-6)	22669036
R(587)=RAD(218,72,2.26E-6)	22669037
R(588)=RAD(219,257,.83E-6)	22669038
R(589)=RAD(218,257,1.95E-6)	22669039
R(590)=RAD(215,252,1.30E-6)	22669040
R(591)=RAD(215,28,1.78E-6)	22669041
R(592)=RAD(215,44,.41E-6)	22669042
R(593)=RAD(216,44,1.36E-6)	22669043
R(594)=RAD(216,60,1.17E-6)	22669044
R(595)=RAD(218,60,.62E-6)	22669045
R(596)=RAD(218,76,.62E-6)	22669046
R(597)=RAD(220,76,1.17E-6)	22669047
R(598)=RAD(221,257,1.03E-6)	22669048
R(599)=RAD(222,44,1.2E-4)	22669049
R(600)=RAD(222,60,.5E-4)	22669050
R(601)=RAD(223,76,.60E-5)	22669051
R(602)=RAD(223,257,1.0E-5)	22669052
R(603)=RAD(224,252,1.30E-6)	22669053
R(604)=RAD(224,28,1.03E-6)	22669054
R(605)=RAD(225,28,.75E-6)	22669055
R(606)=RAD(225,44,1.78E-6)	22669056
R(607)=RAD(225,60,1.78E-6)	22669057
R(608)=RAD(225,76,1.78E-6)	22669058
R(609)=RAD(225,257,1.03E-6)	22669059
R(610)=RAD(224,251,3.50E-6)	22669060
R(611)=RAD(224,32,3.35E-6)	22669061

TABLE B-7 (Cont.)

R(612)=RAD(225,32,1.43E-6)	22669062
R(613)=RAD(224,48,.34E-6)	22669063
R(614)=RAD(225,48,.75E-6)	22669064
R(615)=RAD(226,48,1.10E-6)	22669065
R(616)=RAD(227,48,2.59E-6)	22669066
R(617)=RAD(226,64,.97E-6)	22669067
R(618)=RAD(227,64,3.84E-6)	22669068
R(619)=RAD(227,80,4.78E-6)	22669069
R(620)=RAD(228,255,.84E-6)	22669070
R(621)=RAD(227,255,1.93E-6)	22669071
R(622)=RAD(229,251,1.50E-6)	22669072
R(623)=RAD(229,32,2.06E-6)	22669073
R(624)=RAD(229,48,.48E-6)	22669074
R(625)=RAD(207,48,1.57E-6)	22669075
R(626)=RAD(207,64,1.36E-6)	22669076
R(627)=RAD(208,64,.68E-6)	22669077
R(628)=RAD(208,80,.68E-6)	22669078
R(629)=RAD(210,80,1.36E-6)	22669079
R(630)=RAD(212,255,1.19E-6)	22669080
R(631)=RAD(230,98,1.74E-4)	22669081
R(632)=RAD(231,98,1.6E-4)	22669082
R(633)=RAD(232,98,1.8E-4)	22669083
R(634)=RAD(233,98,1.6E-4)	22669084
R(635)=RAD(234,98,.65E-4)	22669085
R(636)=RAD(235,98,.77E-4)	22669086
R(637)=RAD(236,98,1.47E-4)	22669087
R(664)=RAD(98,28,1.8E-4)	22669088

TABLE B-8

RESISTORS FOR BAY 6 FUEL TANK ANALYSIS

DEC02	551	201	250	0.	552	202	250	0.	60012266
DEC02	553	203	20	0.	554	202	20	0.	60022266
DEC02	555	203	36	0.	556	202	36	0.	60032266
DEC02	557	204	36	0.	558	203	52	0.	60042266
DEC02	559	204	52	0.	560	205	52	0.	60052266
DEC02	561	203	68	0.	562	205	68	0.	60062266
DEC02	563	206	254	0.	564	202	251	0.	60072266
DEC02	565	202	32	0.	566	202	48	0.	60082266
DEC02	567	207	48	0.	568	207	64	0.	60092266
DEC02	569	203	64	0.	570	203	80	0.	60102266
DEC02	571	205	255	0.	572	208	251	0.	60112266
DEC02	573	208	32	0.	574	208	48	0.	60122266
DEC02	575	208	64	0.	576	208	80	0.	60132266
DEC02	577	209	80	0.	578	210	255	0.	60142266
DEC02	579	208	253	0.	580	208	28	0.	60152266
DEC02	581	208	44	0.	582	208	60	0.	60162266
DEC02	583	208	76	0.	584	209	76	0.	60172266
DEC02	585	210	256	0.	586	211	44	0.	60182266
DEC02	587	211	60	0.	588	212	76	0.	60192266
DEC02	589	212	256	0.	590	213	253	0.	60202266
DEC02	591	213	28	0.	592	214	28	0.	60212266
DEC02	593	214	44	0.	594	214	60	0.	60222266
DEC02	595	214	76	0.	596	214	256	0.	60232266
DEC02	597	213	253	0.	598	213	24	0.	60242266
DEC02	599	214	24	0.	600	213	40	0.	60252266
DEC02	601	214	40	0.	602	215	40	0.	60262266
DEC02	603	216	40	0.	604	215	56	0.	60272266
DEC02	605	216	56	0.	606	216	72	0.	60282266
DEC02	607	217	257	0.	608	216	257	0.	60292266
DEC02	609	218	253	0.	610	218	24	0.	60302266
DEC02	611	218	40	0.	612	218	56	0.	60312266
DEC02	613	218	72	0.	614	207	257	0.	60322266
DEC02	631	230	98	0.	632	231	98	0.	60332266
DEC02	633	232	98	0.	634	233	98	0.	60342266
DEC02	635	234	98	0.	636	235	98	0.	60352266
DEC02	637	236	98	0.	638	237	258	22200.	60362266
DEC02	639	238	258	22800.	640	239	258	22800.	60372266
DEC02	641	240	259	22800.	642	241	259	22800.	60382266
DEC02	643	235	259	22200.	644	234	259	27200.	60392266
DEC02	645	236	258	27200.	646	242	250	10040.	60402266
DEC02	647	243	251	6780.	648	244	252	3630.	60412266
DEC02	649	245	253	6780.	650	246	254	1320.	60422266
DEC02	651	247	255	1500.	652	248	256	1440.	60432266
DEC02	653	249	257	1500.	654	250	20	7020.	60442266
DEC02	655	251	32	4170.	656	252	28	2560.	60452266
DEC02	657	253	24	4170.	658	254	68	1320.	60462266
DEC02	659	255	80	1500.	660	256	76	1440.	60472266
DEC02	661	257	72	1500.	662	258	98	575.	60482266
DEC02	663	259	98	575.	664	98	28	0.	60492266

TABLE B-8 (Cont.)

```
R(551)=RAD(201,250,1.75E-6)                                    22666601
R(552)=RAD(202,250,1.75E-6)                                    22666602
R(553)=RAD(203,20,3.25E-6)                                     22666603
R(554)=RAD(202,20,3.25E-6)                                     22666604
R(555)=RAD(203,36,3.25E-6)                                     22666605
R(556)=RAD(202,36,1.0E-6)                                      22666606
R(557)=RAD(204,36,2.25E-6)                                     22666607
R(558)=RAD(203,52,3.25E-6)                                     22666608
R(559)=RAD(204,52,2.25E-6)                                     22666609
R(560)=RAD(205,52,1.0E-6)                                      22666610
R(561)=RAD(203,68,5.5E-6)                                      22666611
R(562)=RAD(205,68,1.0E-6)                                      22666612
R(563)=RAD(206,254,2.87E-6)                                    22666613
R(564)=RAD(202,251,.80E-6)                                     22666614
R(565)=RAD(202,32,1.48E-6)                                     22666615
R(566)=RAD(202,48,.45E-6)                                      22666616
R(567)=RAD(207,48,1.04E-6)                                     22666617
R(568)=RAD(207,64,1.04E-6)                                     22666618
R(569)=RAD(203,64,.45E-6)                                      22666619
R(570)=RAD(203,80,1.48E-6)                                     22666620
R(571)=RAD(205,255,.66E-6)                                     22666621
R(572)=RAD(208,251,2.69E-6)                                    22666622
R(573)=RAD(208,32,4.98E-6)                                     22666623
R(574)=RAD(208,48,4.98E-6)                                     22666624
R(575)=RAD(208,64,4.98E-6)                                     22666625
R(576)=RAD(208,80,1.49E-6)                                     22666626
R(577)=RAD(209,80,3.48E-6)                                     22666627
R(578)=RAD(210,255,2.22E-6)                                    22666628
R(579)=RAD(208,253,.98E-6)                                     22666629
R(580)=RAD(208,28,1.82E-6)                                     22666630
R(581)=RAD(208,44,1.82E-6)                                     22666631
R(582)=RAD(208,60,1.82E-6)                                     22666632
R(583)=RAD(208,76,.52E-6)                                      22666633
R(584)=RAD(209,76,1.30E-6)                                     22666634
R(585)=RAD(210,256,.80E-6)                                     22666635
R(586)=RAD(211,44,1.0E-4)                                      22666636
R(587)=RAD(211,60,.50E-4)                                      22666637
R(588)=RAD(212,76,.40E-4)                                      22666638
R(589)=RAD(212,256,1.1E-4)                                     22666639
R(590)=RAD(213,253,.98E-6)                                     22666640
R(591)=RAD(213,28,1.30E-6)                                     22666641
R(592)=RAD(214,28,.520E-6)                                     22666642
R(593)=RAD(214,44,1.82E-6)                                     22666643
R(594)=RAD(214,60,1.82E-6)                                     22666644
R(595)=RAD(214,76,1.82E-6)                                     22666645
R(596)=RAD(214,256,.80E-6)                                     22666646
R(597)=RAD(213,253,2.52E-6)                                    22666647
R(598)=RAD(213,24,4.53E-6)                                     22666648
R(599)=RAD(214,24,.48E-6)                                      22666649
R(600)=RAD(213,40,.48E-6)                                      22666650
R(601)=RAD(214,40,1.02E-6)                                     22666651
R(602)=RAD(215,40,1.08E-6)                                     22666652
R(603)=RAD(216,40,2.42E-6)                                     22666653
R(604)=RAD(215,56,1.08E-6)                                     22666654
R(605)=RAD(216,56,3.93E-6)                                     22666655
R(606)=RAD(216,72,5.00E-6)                                     22666656
R(607)=RAD(217,257,.69E-6)                                     22666657
R(608)=RAD(216,257,1.52E-6)                                    22666658
R(609)=RAD(218,253,.98E-6)                                     22666659
R(610)=RAD(218,24,1.48E-6)                                     22666660
R(611)=RAD(218,40,1.48E-6)                                     22666661
```


LOCKHEED
CALIFORNIA COMPANY

TABLE B-8 (Cont.)

R(612)=RAD(218,56,1.48E-6)	22666662
R(613)=RAD(218,72,1.48E-6)	22666663
R(614)=RAD(207,257,.66E-6)	22666664
R(631)=RAD(230,98,1.74E-4)	22666665
R(632)=RAD(231,98,1.8E-4)	22666666
R(633)=RAD(232,98,1.8E-4)	22666667
R(634)=RAD(233,98,1.6E-4)	22666668
R(635)=RAD(234,98,.65E-4)	22666669
R(636)=RAD(235,98,.77E-4)	22666670
R(637)=RAD(236,98,1.47E-4)	22666671
R(664)=RAD(28,98,1.6E-4)	22666672

TABLE B-9

CAPACITORS FOR PROPELLANT TANK ANALYSES

BAY 2	**OXIDIZER TANK**								
DEC04	250	1.14	251	.610	252	.895	253	.610	20602266
DEC04	254	1.03	255	.555	256	.815	257	.555	20612266
DEC02	258	.600	259	.600					20622266
BAY 3	**FUEL TANK**								
DEC04	250	.515	251	.453	252	.470	253	.453	31012266
DEC04	254	.560	255	.493	256	.515	257	.493	31022266
DEC02	258	.600	259	.600					31032266
BAY 5	**OXIDIZER TANK**								
DEC04	250	1.14	251	.610	252	.895	253	.610	530012266
DEC04	254	1.03	255	.555	256	.815	257	.555	530022266
DEC02	258	.600	259	.600					530032266
BAY 6	**FUEL TANK**								
DEC04	250	.515	251	.453	252	.470	253	.453	61012266
DEC04	254	.560	255	.493	256	.515	257	.493	61022266
DEC02	258	.600	259	.600					61032266

Appendix C

Analysis of Low-Gravity Fluid Mechanics and Heat Transfer

This appendix presents the work performed by the Lockheed Missiles and Space Company (LMSC) in support of this contract.

I - ANALYSIS

ACCELERATIONS ACTING ON THE SERVICE MODULE

The Apollo spacecraft,in the projected mission, will orbit the earth for a short period, then be injected into a translunar trajectory. At the end of the translunar flight, the vehicle will be injected into a lunar orbit. After the lunar mission is completed, the vehicle will enter a transearth trajectory. During the translunar and transearth phases the vehicle will undergo a number of reorientation maneuvers which will be effected by small thrusts from the reaction control system. It will also undergo two velocity correction maneuvers during which the service propulsion system engines will be operated.

The major portion of the vehicle's mission is outside the earth's atmosphere thus the acceleration caused by atmospheric drag is negligible. During the translunar and transearth mission phases, the vehicle will undergo a roll rotation rate of two rev/hr. It has been assumed in this study that the vehicle is broadside to the direct rays of the sun. The vehicle thus oriented with respect to the sun will be acted upon by solar pressure which will produce a small acceleration. Because the vehicle is oriented relative to the sun, tiny accelerations will result from its slow rotation about the sun. Liquid particles not located at the center of mass of the vehicle and liquid system will be acted upon by centripetal accelerations caused by the small heliocentric rate. Further, liquid particles not located at the center of mass of the system but which are closer to or farther away from the sun will experience tiny accelerations due to the gradient in the sun's gravitational field. Similarly, during the earth orbit and lunar orbit phases, liquid particles not at the center of mass will experience centripetal and gravity gradient accelerations.

The order of magnitude of the solar pressure acceleration has been estimated from Equation C-1 using values obtained from Reference C-1

$$\frac{a_{\text{solar pressure}}}{g_o} = \frac{P_s \quad A}{m \; g_o} \qquad \text{(C-1)}$$

where

P_s = solar pressure = 2×10^{-7} lbf/ft^2

A = vehicle projected area = 260 ft^2

m = vehicle mass = 621 slugs

The centripetal accelerations and gravity gradient accelerations have been calculated using Equations C-2 and C-3 together with information in Reference C-2

$$\frac{a_{\text{centripetal}}}{g_o} = \frac{L\omega^2}{g_o} \qquad \text{(C-2)}$$

$$\frac{a_{\text{gravity gradient}}}{g_o} = \frac{2L \; g_{\text{local}}}{R_o} \left(\frac{R_o}{R_o + h}\right)^3 \qquad \text{(C-3)}$$

where

ω = angular rate of the vehicle

L = distance from vehicle center of mass to liquid particle

R_o = radius of sun, earth, or moon

h = distance to vehicle from surface of sun, earth or moon

A value of L of 15 ft. was used to calculate the centripetal acceleration caused by the heliocentric, geocentric, and lunar orbit rates, a value of 4 ft. was used to calculate the acceleration caused by the vehicle roll rate, and L = 10 ft. was used to calculate the gravity gradient accelerations. All of the steady accelerations acting on the vehicle are listed in Table C-1.

TABLE C-1

Steady Accelerations Acting on the Service Module

	a/g_o*		
	Sun	Earth	Moon
Radiation pressure	2.6×10^{-9}		
Centripetal due to orbital rate (L = 15 ft)	4.0×10^{-14}	1.4×10^{-6}	7.2×10^{-7}
Gravity gradient (L = 10 ft)	7.9×10^{-15}	2.7×10^{-7}	1.3×10^{-7}
Centripetal due to roll rate (L = 4 ft)	1.5×10^{-6}		
*g_o = 32.2 ft/sec^2 = 980 cm/sec^2			

LIQUID LOCATION

The effect of the small acceleration induced body forces acting on the liquids can be determined by calculating the Bond number. This is defined in terms of the tank radius by Equation C-4

$$B = \frac{\rho g r_o^2}{\sigma} \qquad (C\text{-}4)$$

where

r_o = the radius of the tank = 24.5 in. for the oxidizer tank and 22.5 in. for the fuel tank

g = the local acceleration

ρ = the liquid density

σ = the surface tension of the liquid

This has been calculated using liquid properties given in Table C-2 and is plotted in Figure C-1.

TABLE C-2

Liquid Properties
(at 60°F)

	Oxidizer	Fuel
Density, gm/cm^3	1.455	0.908
Surface tension, dyne/cm.	26.4	30.3
Dynamic viscosity, lbm/ft-sec	2.97×10^{-4}	6.3×10^{-4}
Bulk coefficient of thermal expansion, $1/^{\circ}F$	9.02×10^{-4}	5.54×10^{-4}
Specific heat, Btu/lbm-°F	0.365	0.69
Conductivity, Btu/hr-ft-°F	0.0778	0.151

This dimensionless quantity can be considered the ratio of gravitational body forces to surface tension forces acting on the liquid. The effect of internal tank hardware is to reduce the level of acceleration which will cause the liquid to run from one end of the tank to the other. The critical Bond number is estimated from the material in Reference C-4 to be about 0.25 when the meniscus intercepts the liquid containment can and about 0.75 when the meniscus intercepts only the central standpipe.* The highest accelerations indicated in Table C-1 are about $1.5 \times 10^{-6} g_o$ and are caused by centripetal acceleration experienced in the earth orbit and during the 2 rev/min roll rate. The first of these has an axial component and will produce a Bond number of about 0.29 in the oxidizer tank. From this it might be concluded that the stability of liquid location is marginal when the lowest value of the critical Bond number previously indicated is used. However, this value is appropriate only when little liquid is left in the tanks closest to the

* The ordinate in Figure 4.7 of Reference C-4 should be the Bond number based upon tank radius only, i.e., $\frac{\rho g R_o^2}{\sigma}$ rather than $\frac{\rho g (R_o - R_i)^2}{\sigma}$ as is shown. The reference is in error.

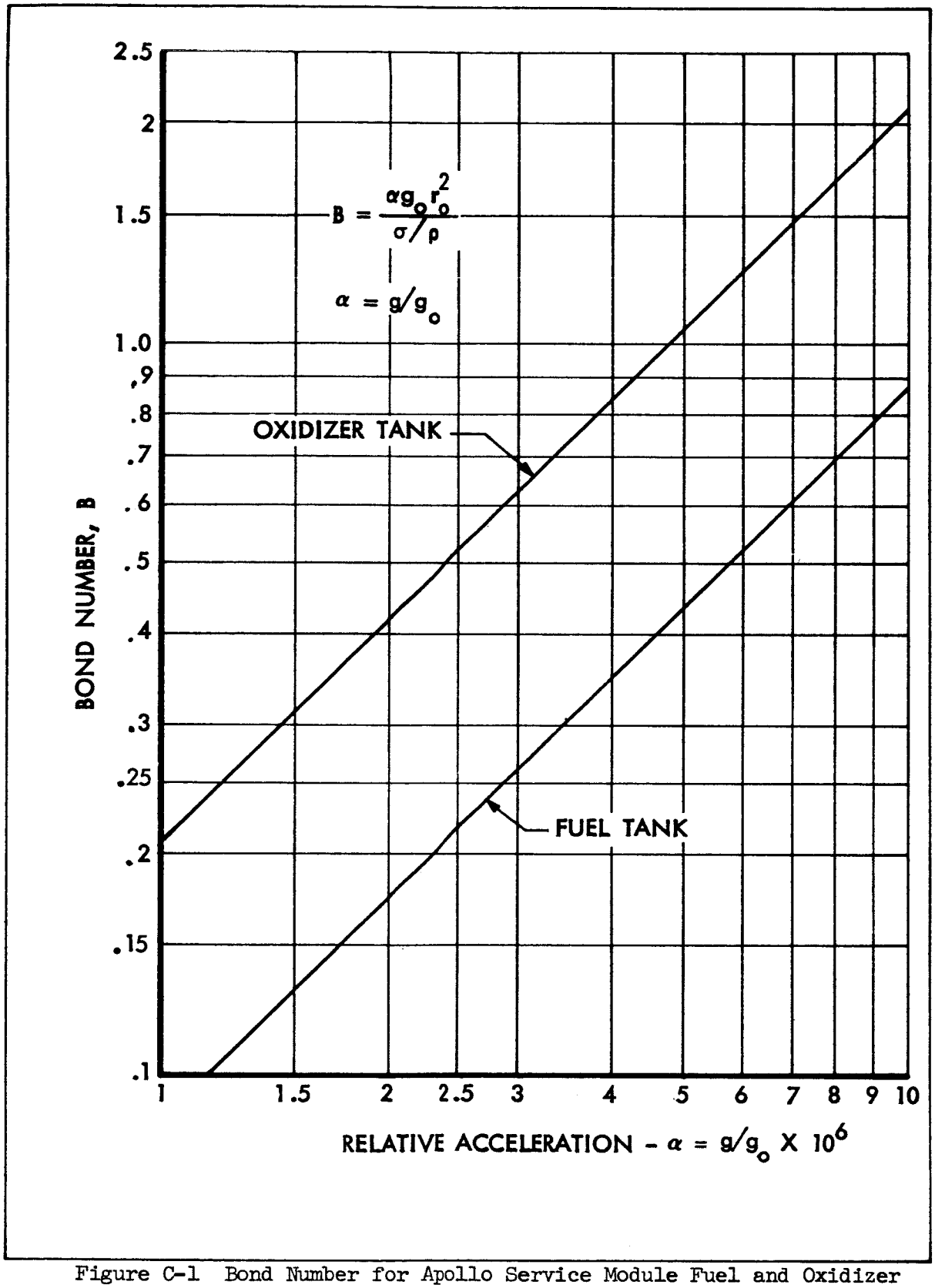

Figure C-1 Bond Number for Apollo Service Module Fuel and Oxidizer Tanks

LOCKHEED CALIFORNIA COMPANY

engine and the meniscus intercepts the liquid containment can. (This condition would exist only when the SPS is almost spent. This liquid level only occurs during the last firing of the SPS.) The liquid can be considered to be stably located and not subject to reorientation by even the largest steady acceleration acting on the vehicle.

The most important long term acceleration is that centripetal acceleration caused by the vehicle roll rate during its lunar and its earth mission phases. Here the Bond number is about 0.31. The Bond numbers are the highest for the oxidizer.

Liquid Shape

The effect of the small Bond numbers resulting from the accelerations previously calculated will be quite small. This is illustrated by referring to Figure 43 B of Reference C-4 where it is seen that the height of the meniscus at the wall is changed by less than 10% for the greatest Bond number previously indicated.

Zero g Shape in an Annular Tank

The wetting area required for heat transfer calculations depends upon the meniscus shape. The presence of internal hardware in the SPS propellant tanks will effect to some degree the meniscus shape and therefore the wetted area. Two cases were studied in the course of this investigation. They are the 2-1/2" diameter standpipe inside the fuel tank and the 15" diameter liquid containment can also in the fuel tank.

The differential equation of the free liquid surface in an annular tank is given in Section II of this appendix. The method of solution is also shown. The differential equation is a second order non-linear ordinary differential equation. This equation can be integrated once to obtain the slope of the meniscus at any radial distance from the axis of the tank. The slope then can be integrated numerically to obtain the meniscus shape. Simpson's rule was used for the integration process in this study. The resultant shape was then redefined such that the volume contained under the surface is the same as if the surface were a plane. This

was done to faciliate location of the curve with the known volume of liquid under the surface. The two shapes calculated are plotted in Figure C-2 and the parameters important to the location of the curves are given in Table C-3.

TABLE C-3

Wetted Area Parameters in a 49-in. Diameter Annular Tank

Case	Inner Radius	Inner Wetted* Length	Outer Wetted* Length
	in.	in.	in.
I	1.25	-3.02	+16.4
II	7.50	-0.51	+12.5

*Relative to liquid height for a flat meniscus

In the absence of internal hardware, the meniscus shape in a cylindrical tank would be essentially a hemisphere. The meniscus rises along the wall a distance equal to 2/3 of the radius of the tank beyond the height if the free surface were a plane. The introduction of internal hardware converting the cylindrical tank into an annular tank reduces this meniscus rise height. In the case of the narrow standpipe, the wetted area is reduced a negligible amount. When the meniscus intercepts the liquid containment can, the additional wetted length is reduced by 3.9" (16%).

EFFECT OF STEADY ACCELERATIONS ON HEAT TRANSFER TO THE LIQUID

The steady state transverse accelerations which will be experienced by the propellant tanks during the translunar and transearth mission phases will cause some liquid circulation. This will be attended by increased heat transfer at the wall over that expected for motionless liquid. Consider the geometry shown in Figure C-3. The temperature distribution on the surface of this tank is as shown. Here liquid is assumed to fill a cylindrical container the axis of which is perpendicular to the local acceleration vector. This model is appropriate for the propellant tanks in the service module since the steady state acceleration experienced by

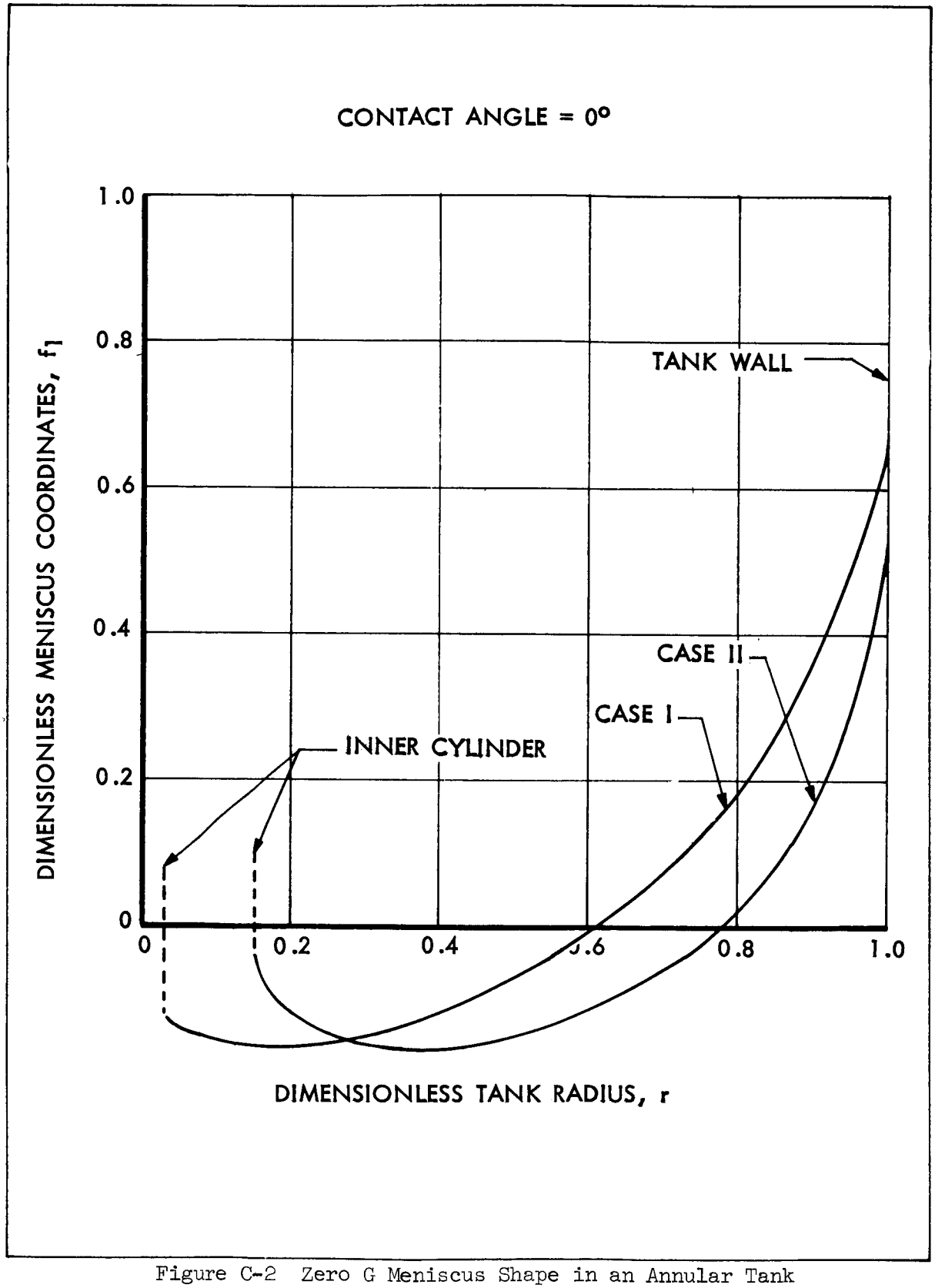

Figure C-2 Zero G Meniscus Shape in an Annular Tank

LOCKHEED
CALIFORNIA COMPANY

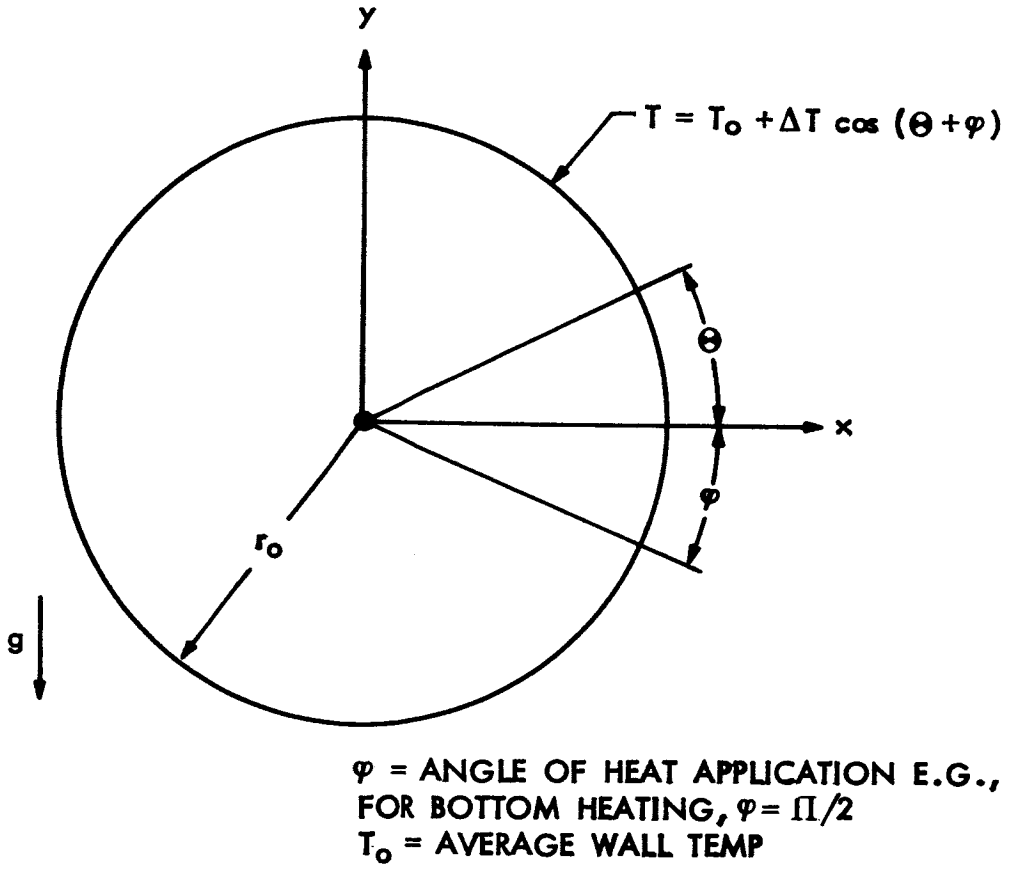

φ = ANGLE OF HEAT APPLICATION E.G.,
FOR BOTTOM HEATING, φ = Π/2
T$_o$ = AVERAGE WALL TEMP

Figure C-3 Geometry for Natural Convection in a Horizontal Cylinder

these tanks will be directed radially outward. The work of Weinbaum (Reference C-5) can be used to obtain a quantitative idea of the heat transfer increase due to natural convection. The heat transfer is a function of the Rayleigh number ($Ra = g \rho^2 B \Delta T r_o^3 C_p / \mu K$). If $Q = -\pi/2$, (see Figure C-3) no circulation of liquid will result. For higher Rayleigh numbers and $Q = \pi/2$, liquid circulation results. Rayleigh numbers appropriate for the fuel and oxidizer tanks have been calculated using the fluid properties shown in Table C-3. These are plotted in Figure C-4.

The thermal analysis to follow indicates that ΔT ranges from 1 to $3^{\circ}F$. It is also indicated that the value of Q considered in terms of a geometry of Figure C-3 varies with time. The location of the point of maximum temperature thus varies throughout each revolution of the vehicle. The worst case occurs when $Q = 0$. For $Q = 0$ and $\Delta T = 3^{\circ}F$, $Ra = 3.38 \times 10^5$ and 4.7×10^4 for oxidizer and fuel, respectively. Since no closed form solution exists for the Nusselt number in this Rayleigh number range, formula 7-4b in Reference C-6 was used to obtain an approximation to the heat transfer coefficient. Using $2 r_o$ as the characteristic length, heat transfer coefficients of 0.59 and 0.47 for the fuel and oxidizer were obtained. These can be compared to pseudo-heat transfer coefficients of about 0.051 and 0.023 for purely conduction heat transfer from

$$Nu_{conduction} = 2/\pi$$

as indicated in Reference C-5.

Thus, convection increases heat transfer by an average of 15 times. The effect of natural convection can be included in calculations by paralleling conduction resistances from the skin to adjacent liquid nodes with convective thermal resistances.

Alternatively, the value of the thermal conductivity of the liquid used to calculate the conduction resistances adjacent to the wall can be increased by a factor of 15.

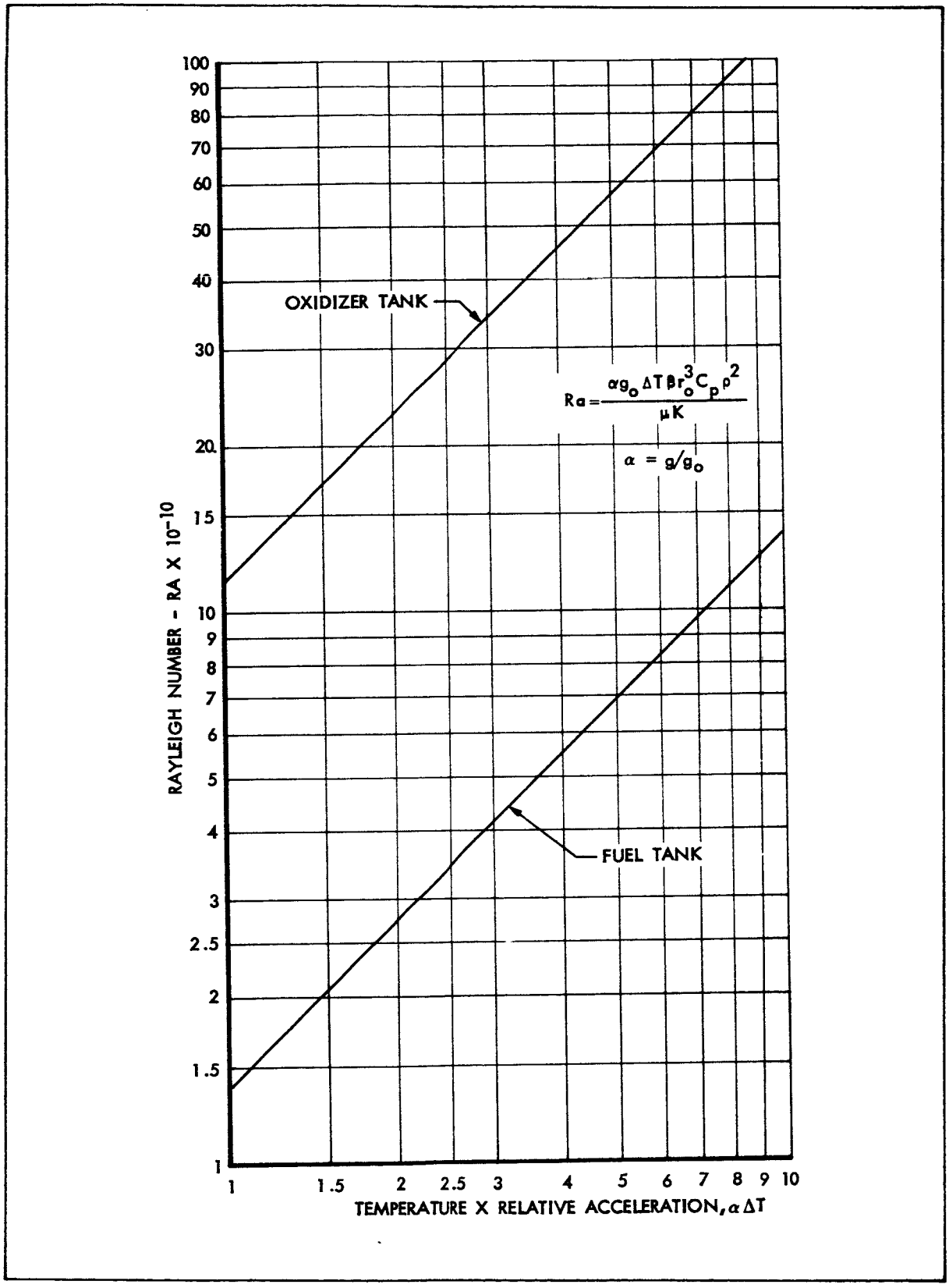

Figure C-4 Rayleigh Number for Apollo Service Module Fuel and Oxidizer Tanks

LOCKHEED CALIFORNIA COMPANY

Realistically, however, the point of maximum temperature on the propellant tanks varies. It can be expected that the natural convection flow inside the tanks will accelerate and then decelerate and even reverse. The mean heat transfer coefficient then would be much less than the worst case indicated above. The true heat transfer coefficient is bracketed between the worst case calculated and zero. One effect of the cyclic reversal of the convective flow will be the propagation of a temperature wave into the liquid from the wall. Because of this, heat transfer between locations inside the tank will be generally increased over that for conduction alone. It is therefore recommended that the effective conductivity of the liquid be increased by a factor of 7 (as an average value). This will include both the effect of increased heat transfer at the wall of the tank and the effect of energy propagation due to the viscous flow in the body of liquid.

THE EFFECT OF THE REACTION CONTROL SYSTEM ON LIQUID LOCATION

During the translunar and transearth phases a number of maneuvers will be carried out. These will be effected by the operation of one or more of the jets of the RCS. The purpose of these impulses is to produce rotation about one or more of the principal axes of the vehicle. The important effect as far as liquid behavior is concerned, however, results from the fact that the vehicle experiences high angular accelerations during the operation of the RCS. Assuming an arm of 10 feet from the vehicle center of mass to the liquid surface in any tank, the transverse acceleration experienced by the liquid will be of the order of 0.3 ft/sec^2 acting for a period of the order 0.1 sec. This is calculated on the basis of the 0.5 deg/sec angular rates required in all pitch and yaw maneuvers.

The small amplitude sloshing of liquids in cylindrical tanks under low gravitational conditions has been studied in Reference C-7. However, this study treated the free vibrations of the liquid surface and not the forced vibrations which will result from periodic or impulsive forces acting on the vehicle. Considering that the liquids in the Service Module tanks will behave as if no internal hardware were present, this theory can be extended for some special cases for which closed form solutions exist to obtain an

indication of the low g forced motion behavior of the tank liquids. The motivation for using this much simplified theory (small amplitude theory restricted to the flat equilibrium interface shape case) is that some judgment can be obtained in this way. There is no present way of obtaining answers from the more realistic and less restrictive problem. The analysis used herein is based upon the assumptions that the contact angle of the liquid is 90°, that the liquid in the tank is deep (greater than $r_o/2$) and that the contact angle does not vary dynamically. The small amplitude theory of forced motion sloshing under low g conditions are given in Section III of this Appendix. Statement of the specialized problem and the calculations are given in Section IV. The simplified boundary value problem in dimensionless form is specified in terms of equations C-5 through C-9 with reference to Figure C-5.

$$\nabla^2 \Phi = 0 \text{ in } D \qquad \text{(C-5)}$$

$$h_{rr} + \frac{1}{r} h_r + \frac{1}{r^2} h_{\theta\theta} - B_\alpha h + B_t \cos\theta - (1 + B_\alpha) \Phi_t = 0 \qquad \text{(C-6)}$$

$$\text{on } Z = 0$$

$$h_t = \Phi_Z \qquad \text{on } Z = 0 \qquad \text{(C-7)}$$

$$\Phi_n = 0 \qquad \text{on W} \qquad \text{(C-8)}$$

$$h_r = 0 \qquad \text{on } Z = 0,\ r = 1 \qquad \text{(C-9)}$$

where the velocity in the liquid is defined by $\vec{u} = \nabla\Phi$

The demensionless nomenclature for this problem is given in Section III of this Appendix. The solution to equation C-5 subject to equations C-7, C-8 and C-9 can be written down in closed form. This is then substituted into equation C-6 with $B_t = 0$ to obtain the natural frequency of the free surface.

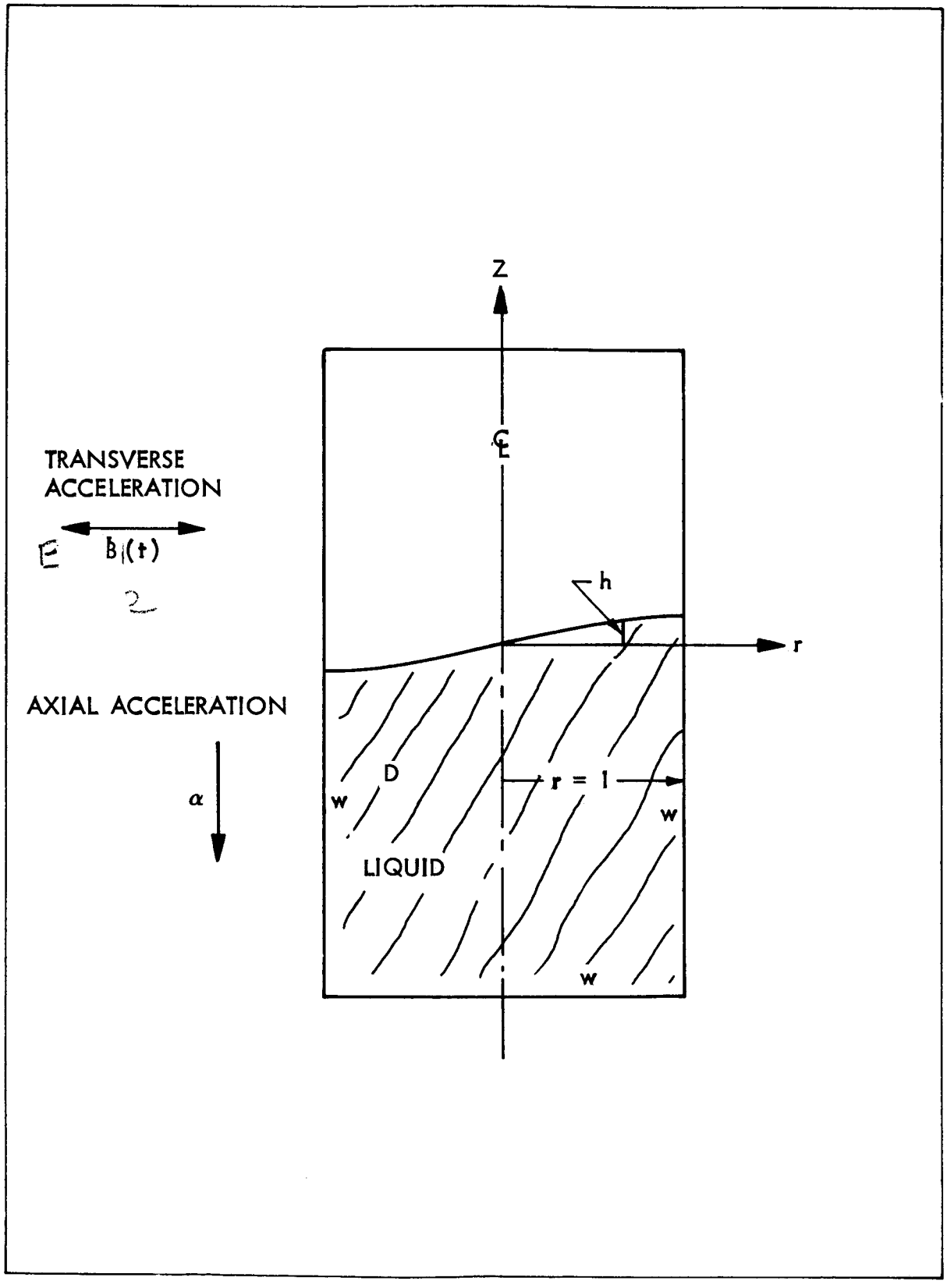

Figure C-5 Geometry of Liquid Sloshing in a Deep Cylinder

The solution to the forced motion can then be obtained as indicated in Section III and carried out in Section IV of this Appendix. The result is

$$\left| h_{wall,\,max} \right| \approx 0.67\,\alpha\, g_o\, \bar{t}\, \sqrt{\frac{r_o}{\sigma/\rho}}$$

where

$h_{wall,max}$ = maximum wave height at the tank wall, cm

g_o = local acceleration, cm/sec^2

$\bar{t}$ = time length of impulse, sec

r_o = tank radius, cm

σ = liquid surface tension, dyne/cm

ρ = liquid density, gm/cm^e

Using values appropriate to the longest operation of the RCS the amplitude of the wave at the wall is calculated to be 0.8 r_o for the fuel tank and 1.1 for the oxidizer tank. These are large amplitudes. The liquid will very likely be mixed by such maneuvers. In order to consider liquid essentially unmixed, the amplitude at the wall should remain less than 0.2 r_o. The time length for the RCS pitch and yaw impulses must therefore be less than 0.018 sec. Examination of Reference C-3 indicates that there are 64 orientation maneuvers with impulses greater than this value during the translunar and transearth mission phases. During lunar and transearth mission phases, the liquid can thus be assumed to be mixed during the entire mission 64 times not including propellant settling and other long thrust duration operations.

APPROACH TO THE MASS DIFFUSION STUDY

To assess the importance of mass diffusion as an energy transfer mechanism, a model of the service module oxidizer tank was developed for use with a thermal analyzer program together with a subroutine for the thermal analyzer, as described in Section VI of this Appendix. to calculate the heat transferred by mass diffusion. The results obtained when heat and mass transfer were considered were compared to results obtained considering only heat transfer.

Propellant Loading and Time of Analysis

The study was performed for the oxidizer tank which would be drained first. This tank was regarded as the most temperature critical since it would have its minimum propellant loading prior to the critical lunar insertion maneuver. With the tank only partially filled, the primary means of energy transfer across the tank is by radiation. When the tanks are nearly full, conduction through the propellant is dominant and enables more energy to be transferred than is transferred by radiation in a partially filled tank. Thus, at small propellant loadings, the gradient around the tank is largest and the propellant experiences its largest variations in temperature. An analysis of a typical lunar mission duty cycle for the service module oxidizer tanks showed that the first tank to be emptied would be approximately 85% filled prior to lunar insertion and would be emptied during the insertion maneuver. However, it was decided to investigate a condition where the tank was only about 15% filled which would result in somewhat wider extremes of propellant temperatures than if the tank was 85% filled.

Structural temperature histories at points around the oxidizer tank were furnished for the first 54000 seconds of the lunar mission. Since the objective of this study was not to predict propellant temperatures for the entire mission but to provide judgment as to the effect of mass diffusion, only a portion of the total mission was studied. The translunar roll period was chosen because of its periodic nature which enabled the Thermal Analyzer to run repeatedly through the period until a stabilized condition was reached, i.e., the computed temperature histories were the same from

one period to the next. The structural temperature histories used in the analysis are presented in Figure C-6 together with their locations.

Calculation of Mass Diffusivity and Thermal Conductivity

The methods presented in Reference C-8 were used to calculate the mass diffusivity and thermal conductivity for both the hydrazine-helium and the nitrogen tetroxide-helium gaseous mixture. These calculations are discussed in Section V of this Appendix and the details of N_2O_4-He calculations are presented since the oxidizer tank was a primary interest in the diffusion study. Assuming that the hydrazine vaporizes to all UDMH, the results of the mass diffusivity calculation were:

$$D_{He\text{-}H_2O_4} = 0.0373 \text{ sq. cm/sec}$$

$$D_{He\text{-}50:50} = 0.0366 \text{ sq. cm/sec}$$

The thermal conductivity results are a function of the ratio of mole fractions. For a ratio of unity, the results were

$$k_{He\text{-}N_2O_4} = 0.092 \text{ BTU/hr-ft-}^{o}\text{F}$$

$$k_{He\text{-}50:50} = 0.045 \text{ BTU/hr-ft-}^{o}\text{F}$$

Based on the thermal model developed for the oxidizer tank, the ratio of helium to nitrogen tetroxide mole fraction was calculated to be 5.45 and the resultant conductivity was

$$k_{He\text{-}N_2O_4} = 0.097 \text{ BTU/hr-ft-}^{o}\text{F}$$

This value was then used in the thermal model to calculate the gaseous conduction resistors.

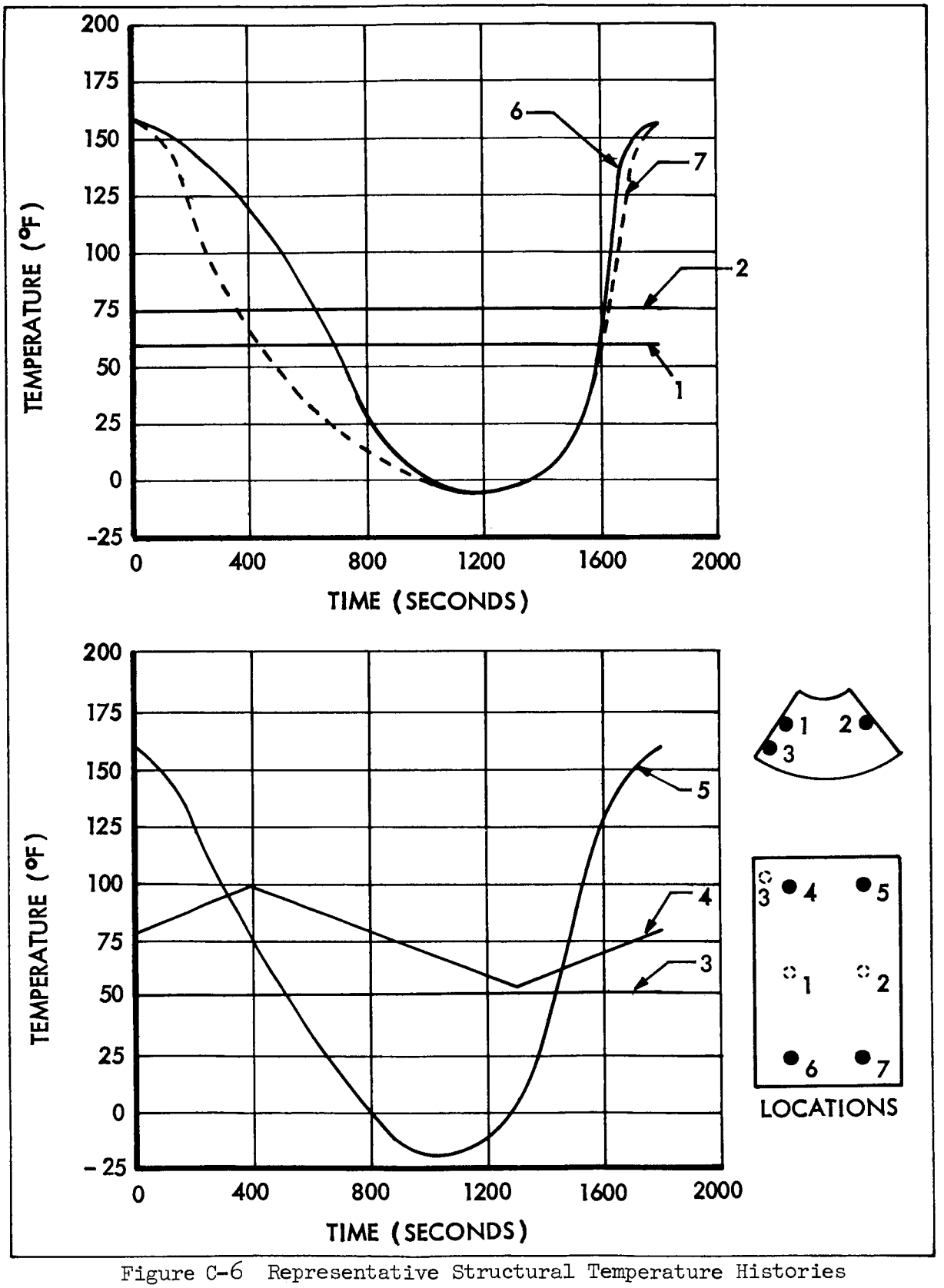

Figure C-6 Representative Structural Temperature Histories

LOCKHEED
CALIFORNIA COMPANY

Thermal Model

The detailed thermal model of the oxidizer tank was developed as an electrical analog for solution on a digital computer by a standard thermal analyzer program. A subroutine was then used with the thermal analyzer to solve for the energy exchange due to mass transfer.

A sketch of the model is presented in Figure C-7. The liquid-gas interface shape was assumed circular in cross-section as shown. This does not represent the true surface shape which is flatter and has less surface area. Use of this shape has a small effect on propellant temperatures.

The model divided the oxidizer tank into 45 gaseous nodes, 18 liquid nodes and 33 solid nodes. In addition, 16 nodes for the skirt at each end, 16 nodes for the support structure and 8 nodes for the surrounding structure were added to complete the model. Conduction through the gaseous phase was included using a thermal conductivity of the gaseous mixture at 70°F as presented in Section V of this Appendix. The studies made with the model showed the 70° gas temperature to be a good assumption. Radiation within the tank was neglected because of the expected small temperature around the tank and the low emittance of the internal tank wall surface. This assumption was not verified by comparison of cases with and without radiation. The gradient around the tank was found to have only a 6°F between the maximum and minimum temperatures at any time during the roll period.

Results of Diffusion Study

The results for the studies with and without the effect of mass diffusion are presented in Figure C-8 as the maximum, minimum and average liquid oxidizer temperatures. The same model was used for both cases and each time the program was run until the temperature histories were the same from one period to the next. Variation in the liquid temperatures over the 1800 second periodic roll was negligible and only the average temperature over the orbit is shown in Figure C-8. The maximum and minimum temperatures shown are for the liquid nodes having the highest and lowest temperatures. The average of all 18 liquid node temperatures is also presented. Figure C-8 shows that the mass diffusion evens out the propellant extreme temperatures by reducing the maximum 0.7°F and raising the minimum 0.3°F. The large

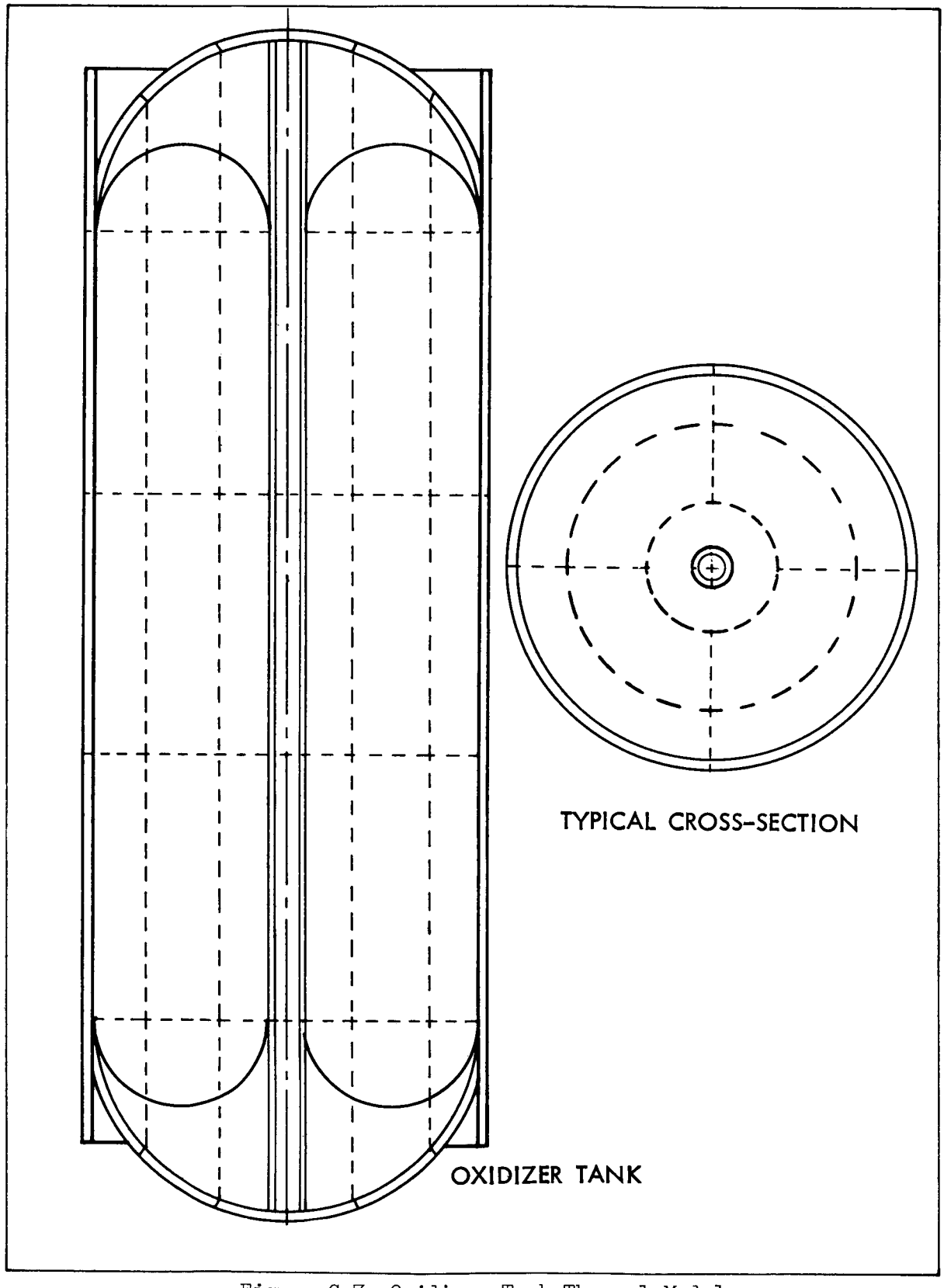

Figure C-7 Oxidizer Tank Thermal Model

LOCKHEED
CALIFORNIA COMPANY

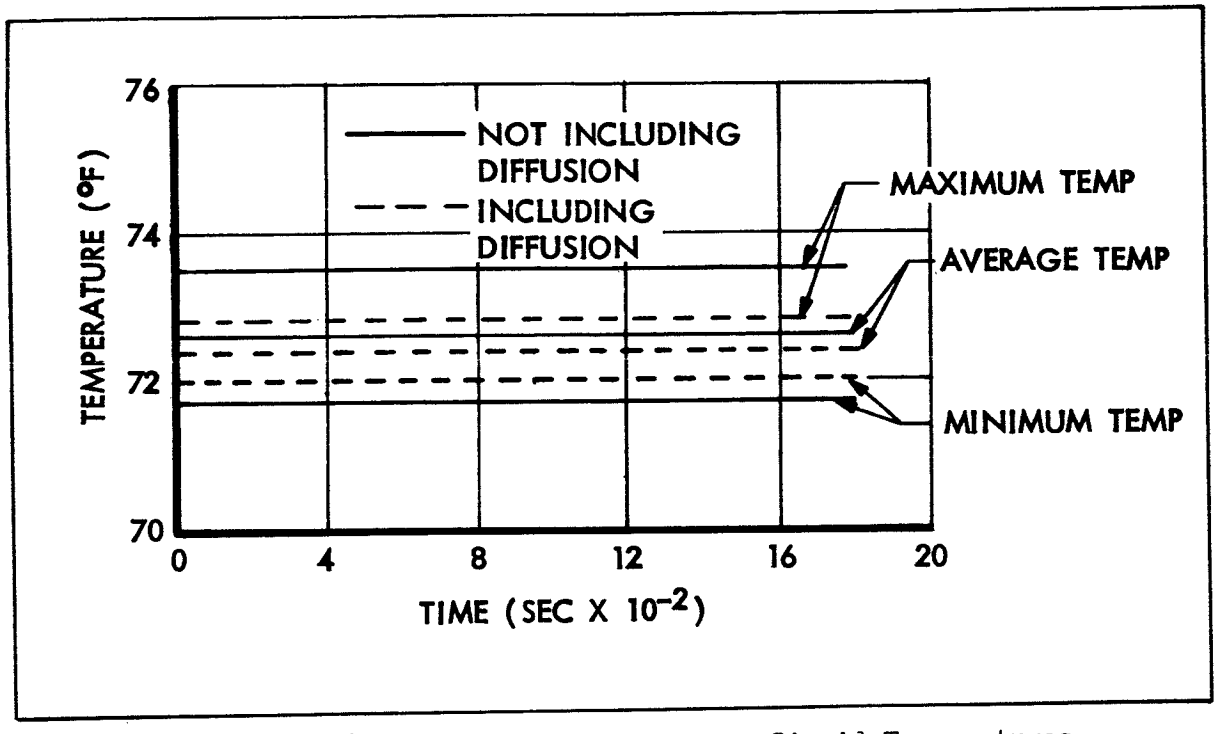

Figure C-8 Effect of Diffusion on Liquid Temperatures

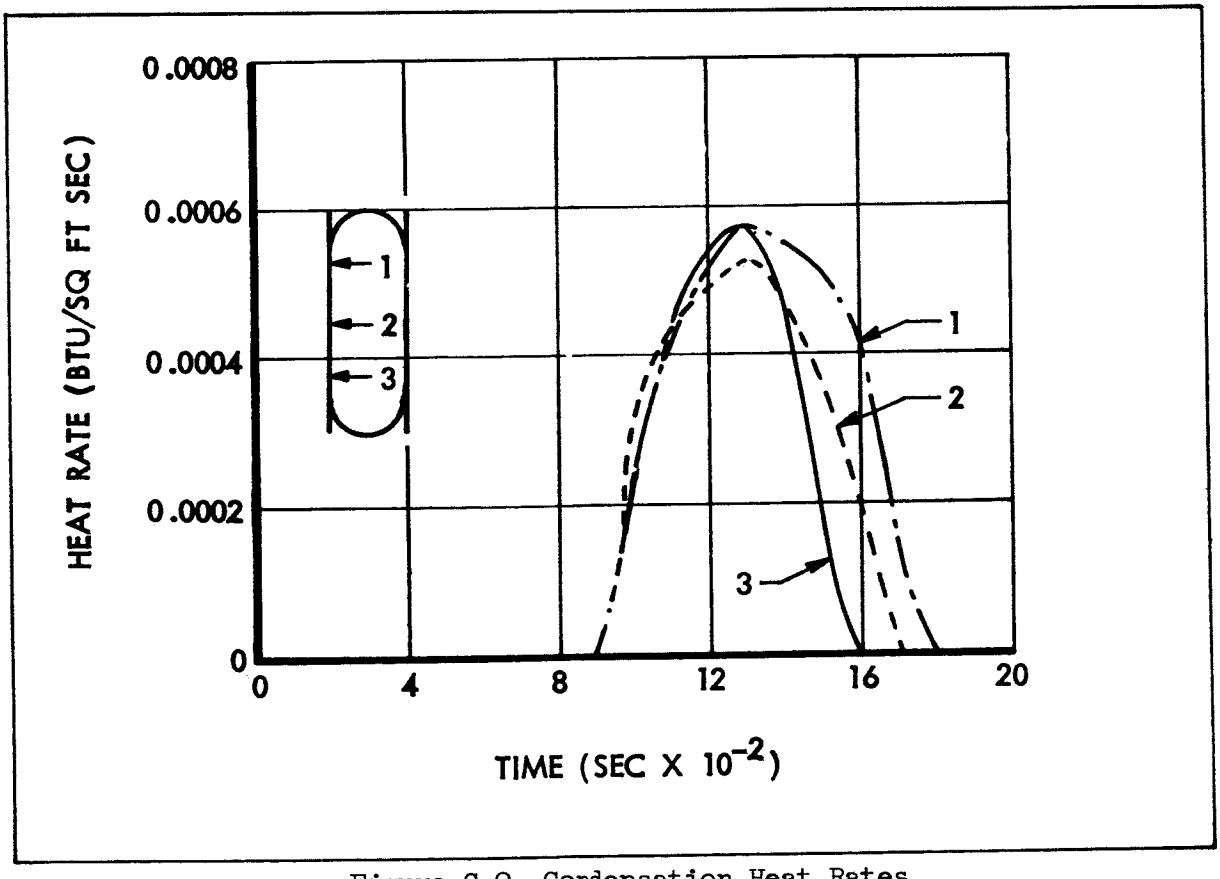

Figure C-9 Condensation Heat Rates

total pressure within the tank yields a small diffusion coefficient and minimizes the effect of diffusion.

The oxidizer diffuses through the gaseous mixture toward the cold side and condenses on the cold wall. These condensation heat rates, at three points along the cylindrical section of the tank wall, are presented in Figure C-9. It can be seen that these heat rates are quite small and occur during less than one-half of the roll period thus causing only a small change in temperature.

II - THE ZERO GRAVITY MENISCUS SHAPE IN AN ANNULAR TANK

Referring to the geometry of Figure C-10, the shape of the capillary surface of an annular tank, when gravitationally induced body forces are negligible, is given by the solution to the following ordinary differential equation and boundary conditions.

$$\frac{1}{r}\frac{d}{dr}\frac{r f'}{\sqrt{1 + f'^2}} = K \qquad \text{(C-10)}$$

$$f' = \cot \Theta, \quad r = r_o$$

$$f' = -\cot \Theta, \quad r = r_i$$

This differential equation can be found in Reference C-7. This equation can be non-dimensionalized by using the following quantities: $R = r/r_o$, $F = f/r_o$, $R_i = r_i/r_o$. The result is

$$\frac{1}{R}\frac{d}{dR}\frac{RF'}{\sqrt{1 + F'^2}} = K \qquad \text{(C-11)}$$

$$F'(1) = \cot \Theta$$

$$F'(R_i) = -\cot \Theta$$

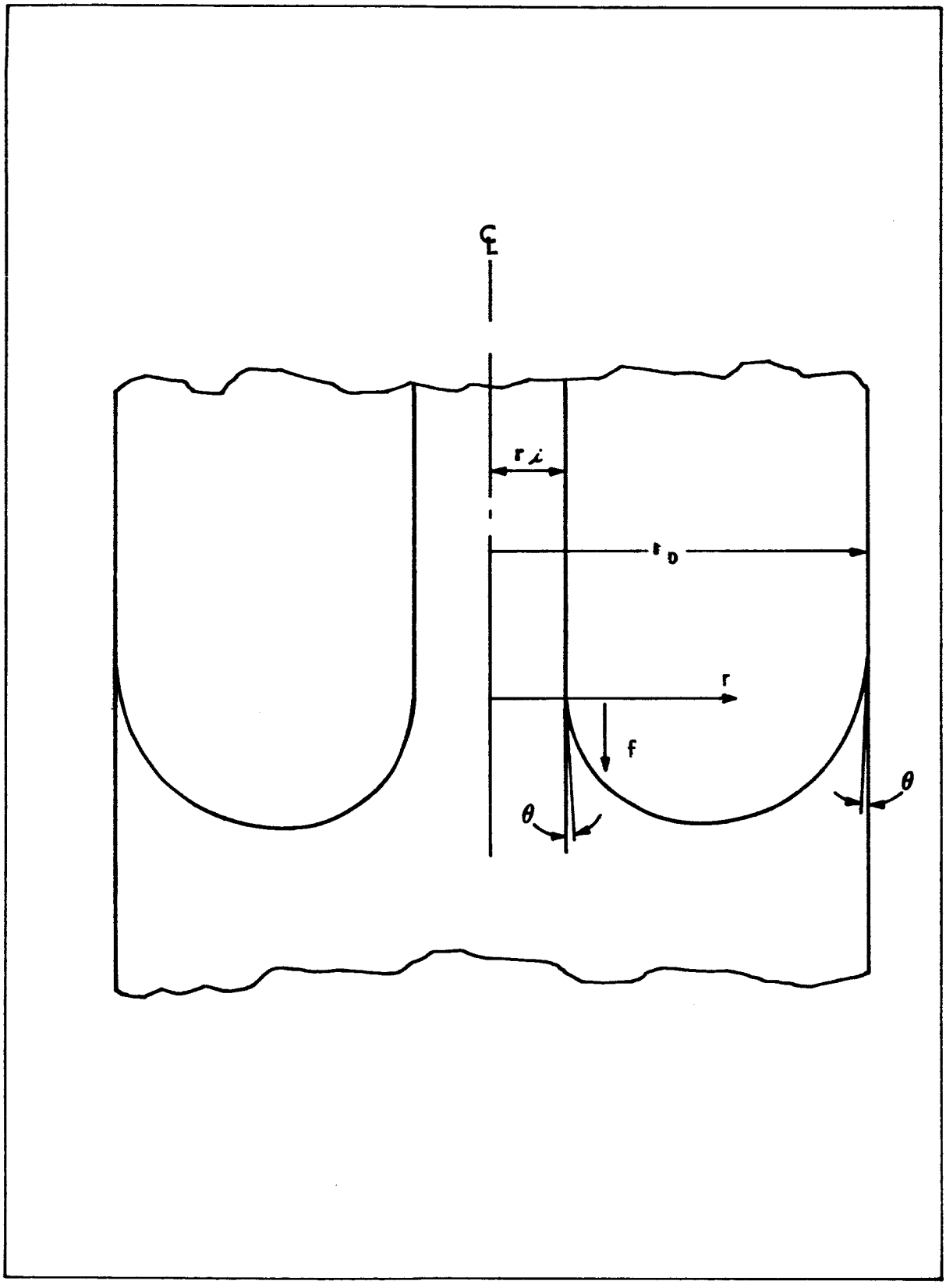

Figure C-10 Liquid and Container Geometry

Determining the solution involves evaluating the parameter K. Equation C-11 can be investigated once to obtain K

$$K = \frac{2 \cos \Theta}{1 - R_i} \qquad \text{(C-12)}$$

The integral of Equation C-11 over (R,1) can be solved for F

$$\int_R^1 d \frac{R F'}{\sqrt{1 + F'^2}} = K \int_R^1 R d R$$

$$\frac{R F'}{\sqrt{1 + F'^2}} \Bigg|_R^1 = \frac{K}{2} \left(1 - R^2\right)$$

$$\cos \Theta - \frac{R F'}{\sqrt{1 + F'^2}} \Bigg|_{R'} = - \frac{K}{2} \left(R^2 - 1\right)$$

Rearranging

$$F' = \frac{\left[\cos \Theta - \frac{K}{2} (1 - R^2)\right]^2}{R^2 - \left[\cos \Theta - \frac{K}{2} (1 - R^2)\right]^2} \qquad \text{(C-13)}$$

This can now be integrated numerically to obtain the solution, F.

Interpretation of the results will be facilitated by shifting the R axis so that the volume between the R axis and F below the R axis equals that between the R axis and F above the R axis. This will allow easier location of the capillary shape in the tank when only the volume of the liquid is known. A new solution may thus be defined by

$$F_I = F + \bar{F} \qquad \text{(C-14)}$$

with

$$\bar{F} = \frac{2}{1 - R_i} \int_{R_i}^1 F R d R \qquad \text{(C-15)}$$

The value of $F_1(1)$ can be compared with the same value if there were no inner cylinder. The liquid shape in this case is a hemisphere (for $\Theta = 0$) and $F_1(1)$ would be 2/3.

Numerical integration of Equation C-13 can be carried out by using any of the standard quadrature formulas. In this calculation, Simpson's rule was used with the interval $(R_i, 1)$ being divided into 20 equal spaces. Mesh points defined are numbered from 0 to 20. The curve, F, in the vicinity $R = R_i$ and $R = 1$ may be approximated by a parabola to facilitate starting and stopping the integration. The parabola at $(R_i, 0)$ will be

$$F = 2F_I' \left(R_I - R_i\right) \qquad \text{(C-16)}$$

where F_1 is the slope at point 1. The value of F at this point is given by

$$F_1 = 2F_1 \left(R_I - R_i\right) \qquad \text{(C-17)}$$

Similarly

$$F(1) = F_{20} = F_{19} + 2F_{19} \left(1 - R_{19}\right) \qquad \text{(C-18)}$$

Using these, the integration can be started by the trapezoidal rule and continued to $R = R_{19}$ using Simpson's rule. These are:

$$F_{n+1} = F_n + \frac{\Delta R}{2} \left(F_n' + F_{n+1}'\right) \qquad \text{(C-19)}$$

$$F_n = F_{n-2} + \frac{\Delta R}{3} \left(F_{n-2}' + 4F_{n-1}' + F_n'\right) \qquad \text{(C-20)}$$

For the two cases being considered, the tank radius, $r_o = 49"$, and $r_i = 1.25"$ and $r_i = 7.50"$. Necessary quantities for the numerical integration in both cases are tabulated in Table C-4, and the results are given in Table C-5.

TABLE C-4

Quantities for Numerical Integration

	Case I	Case II
r_i	1.25	7.50
R_i	0.025510	0.153060
$\Delta R = \frac{1 - R_i}{20}$	0.048725	0.042347
$\Delta R/2$	0.024363	0.021174
$\Delta R/3$	0.016242	0.014116
$K = 2/(1 - R_i)$	2.052356	2.361142
$K/2$	1.026178	1.180721

TABLE C-5

Zero-G Wetted Wall Parameters

CASE	R_i	$F(R_i)$	$F(R_o)$
I	0.0255	-0.123	0.763
II	0.153	-0.026	0.509

The numerical integration was carried out in Tables C-6 and C-7 and is illustrated in Figure C-11. The values of $F_I(R_i)$ and $F_I(1)$ for Case I are attributed to the error introduced by the large mesh size.

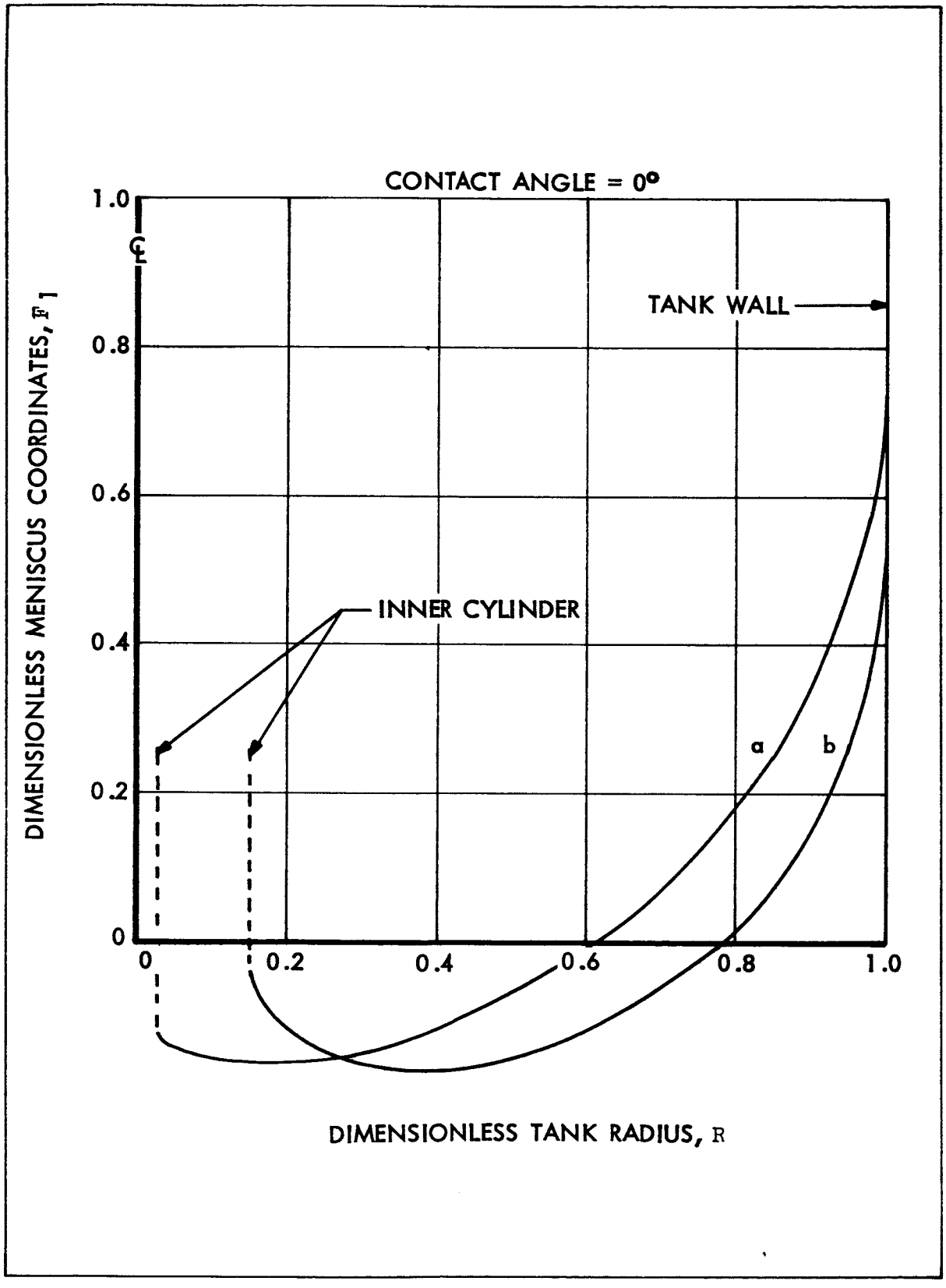

Figure C-11 Zero G Capillary Shape in an Annular Tank

TABLE C-6

NUMERICAL INTEGRATION FOR CASE I

n	① R	② R^2	③ $1-R^2$	④ $\frac{K}{2}(1-R^2)$	⑤ $[\cos\theta-\frac{K}{2}(\ )]$	⑥ $[\ ]^2$	⑦ $R^2-[\ ]^2$	⑧ F'^2	⑨ F'	⑩ F	⑪ $FR\,\Delta r$	⑫ Simpson	⑬ $\bar{F}$	⑭ $F_I\ F_E$
		①^2	1 - ②	$\frac{K}{2}$ ③	1 - ④	⑤^2	② - ⑥	⑥ / ⑦	$\sqrt{⑧}$		⑩ ①	Sum	= 0.122832	⑩ - ⑬
0	.025510	.000650	.999350	1.025511	-.02551	.000651	.000000	∞	∞	0.000000				-.122832
1	.074235	.005511	.994489	1.0205523	-.020552	.000422	.005089	.082923	-.287964	-.028062	-.002083			-.150394
2	.12296	.015119	.984881	1.010663	-.010663	.000114	.015005	.007597	-.087161	-.037201	-.004574			-.160033
3	.171685	.029476	.970524	.995930	.004070	.000017	.029459	.000577	-.024021	-.038792	-.006660	$+\ 7.661638$		-.161624
4	.220410	.048581	.951419	.976325	.023675	.000561	.048020	.011682	+.108033	-.040014	-.008819	$-\ .111344$		-.162846
5	.269135	.072434	.927566	.951848	.048152	.002319	.070115	.033074	.181863	-.029210	-.007861	$+\ 7.546292$		-.152042
6	.317860	.101035	.898965	.922498	.077502	.006007	.095028	.063213	.251422	-.022360	-.007107			-.145192
7	.366585	.134385	.865615	.888275	.111725	.012482	.121898	.102413	.320020	-.004725	-.001732			-.127557
8	.415310	.172482	.827518	.849181	.150819	.022746	.149736	.151907	.389752	+.008845	+.003673			-.113987
9	.464350	.215621	.784479	.805015	.194985	.038019	.177602	.214018	.462621	-.033308	.015467			-.089524
10	.512760	.262923	.737077	.756372	.243628	.059355	.203568	.291573	.539974	.054001	.027690			-.068831
11	.561486	.315265	.684735	.702660	.297340	.088411	.226854	.389726	.624280	.086042	.048311			-.036790
12	.610210	.372356	.627644	.644074	.355926	.126683	.245673	.515657	.718093	.114943	.070170			-.007839
13	.658935	.434195	.565805	.580617	.419383	.175882	.258313	.680887	.825159	.156237	.102950			.033405
14	.707660	.500783	.499217	.512286	.487714	.237865	.262918	.904712	.951163	.195714	.138499			.072882
15	.756385	.572118	.427882	.439083	.560917	.314628	.257490	1.221904	1.105397	.249388	.188633			.126556
16	.805110	.648202	.351798	.361007	.638993	.408312	.239890	1.702080	1.304638	.304168	.244889			.181336
17	.853835	.729034	.270966	.278059	.721941	.521199	.207835	2.507754	1.583589	.377822	.322598			.254990
18	.902560	.814615	.185385	.190238	.819762	.672010	.142605	4.712387	2.170803	.463498	.418335			.340666
19	.951285	.904943	.095057	.097545	.902455	.814425	.090478	9.001369	3.000226	.593336	.564403			.470474
20	1.000010	1.000000	.000000	.000000	1.000000	1.000000	.000000	∞	∞	.885678	.885678			.762846

TABLE C-7

NUMERICAL INTEGRATION FOR CASE II

n	① R	② R^2	③ $1-R^2$	④ $\frac{K}{2}(1-R^2)$	⑤ $[\cos\theta-\frac{K}{2}(\ )]$	⑥ $[\ ]^2$	⑦ ②-⑥	⑧ ⑥/⑦	⑨ $\sqrt{⑧}$	⑩ F	⑪ ⑩①	⑫ Simpson	⑬ $\bar{F}$	⑭ F_I
		$①^2$	1 - ②	$\frac{K}{2}$ ③	1 - ④	$⑤^2$	$R^2-[\ ]^2$	F'^2	F'		FR	Sum	= .025577	⑩ - ⑬
0	.153060	.023427	.976573	1.153060	-.153060	.023427	0	∞	∞	0	0			-.023517
1	.195407	.038183	.961817	1.135637	-.135637	.018397	.019786	.929798	-.964259	-.081667	-.015958			-.107844
2	.237754	.056526	.943474	1.113979	-.113979	.012991	.043535	.298403	-.546862	-.113650	-.027021			-.139227
3	.280101	.078456	.921544	1.088086	-.088086	.007759	.070697	.109750	-.331285	-.130799	-.036637			-.156376
4	.322448	.103972	.896028	1.057959	-.057959	.003359	.100613	.033385	-.182715	-.142646	-.045996			-.168223
5	.364795	.133075	.866925	1.023596	-.023596	.000556	.132519	.004195	-.064768	-.146707	-.053518			-.172284
6	.407142	.165764	.834236	.984999	.015001	.000225	.165539	.001359	.036864	-.148362	-.060404			-.173939
7	.449489	.202040	.797960	.942168	.057832	.003344	.198696	.016829	.129726	-.143709	-.064596			-.169286
8	.491836	.241902	.758098	.895102	.104898	.011003	.230899	.047652	.218293	-.137435	-.067592			-.163012
9	.534183	.285351	.714694	.843801	.156199	.024393	.260953	.093495	.305769	-.125236	-.066899			-.150813
10	.576530	.332386	.667614	.788265	.211735	.044831	.287555	.155904	.394846	-.11515	-.064292			-.137092
11	.618877	.383008	.616992	.728495	.271505	.073714	.309294	.238329	.488189	-.091734	-.056772			-.117311
12	.661824	.437217	.562783	.664489	.335511	.112567	.324650	.346733	.588840	-.070064	-.046328			-.095641
13	.703571	.495012	.504988	.596249	.403751	.163014	.331998	.491008	.700719	-.041703	-.029341			-.067280
14	.745918	.556393	.443607	.523776	.476224	.226789	.329604	.688065	.829496	-.010477	-.007815			-.036054
15	.788265	.621361	.378639	.447067	.552933	.305734	.315627	.968656	.984203	+.028918	+.022795			+.003341
16	.830612	.689916	.310084	.366122	.633878	.401801	.288115	1.394585	1.180925	+.073474	+.061028			+.047897
17	.872959	.762057	.237943	.280944	.719056	.517041	.245016	2.110233	1.452664	+.12997	+.113482			+.104420
18	.915306	.837785	.162215	.191530	.808470	.653623	.184162	3.549174	1.883925	+.198761	+.181927			+.173184
19	.957653	.917099	.082901	.097882	.902118	.813816	.103283	7.879476	2.807040	+.296501	+.283945			+.270924
20	1.000000	1.000000	0	0	1.000000	1.000000	0	∞	∞	+.534240	+.534240			+.508663

+ 2.701038
- 1.933786
+ .767292

III - PROPOSED ANALYSIS AND METHOD OF SOLUTION

GENERAL FORMULATION OF THE PROBLEM

The mathematical problem of the forced vibration of liquid in a container can be most generally posed in terms of the equations of viscous motion of a fluid. These equations apply to the internal motion of the liquid and are subject to the boundary conditions appropriate to the problem. Consider liquid in the container in Fig. C-12. The boundary condition applying at the solid container wall for viscous motion is one of zero liquid velocity, i.e., no slip. A pressure boundary condition connecting the pressure difference across the surface to viscous and hydrostatic forces applies to the free surface. In addition, a condition must be applied to the behavior of the edge of the free surface to indicate whether or not the contact angle changes during oscillation of the free surface.

THE IMPORTANCE OF VISCOSITY

Sufficient experimental evidence (Ref. C-4) is now available to indicate that viscous forces are not greatly important in determining the natural frequency of oscillatory motion of a liquid in a container even under very low gravity conditions. Viscous forces are important near the wall, but in the bulk of the liquid, it can be considered that the liquid behavior is irrotational. Additionally, the edge condition for the free surface indicating the nature of contact angle changes might be considered inconsistent with the no-slip velocity condition used as a boundary condition for the viscous problem. Sloshing experiments have been carried out under very low gravity conditions in which very little, if any, dynamic contact angle variation was observed. The steady-state dynamic behavior of the free surface of a body of liquid in a container can thus be treated as being irrotational. The effects of viscosity can be assessed by other means.

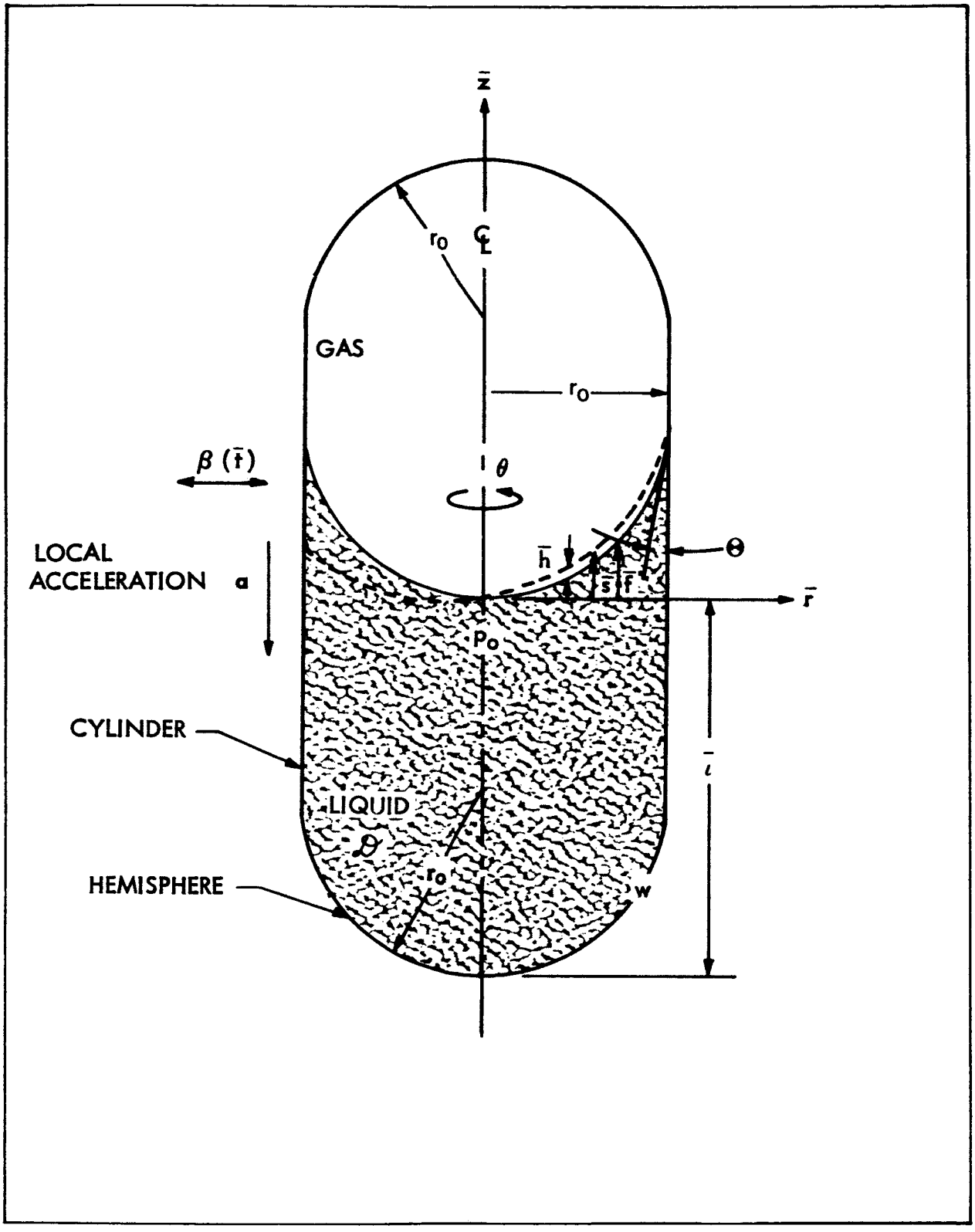

Figure C-12 Container Geometry and Coordinate System

THE INVISCID PROBLEM

General Formulation

The equation governing irrotational, incompressible liquid motion is the equation of continuity (Laplace's equation). In polar cylindrical coordinates, this is

$$\phi_{rr} + \frac{1}{r}\phi_r + \frac{1}{r^2}\phi_{\theta\theta} + \phi_{zz} = 0 \qquad \text{(C-21)}$$

where ϕ is the velocity potential defined by

$$\vec{u} = \nabla\varphi \qquad \text{(C-22)}$$

and $\vec{u}$ is the velocity vector. The choice of coordinates is motivated by the geometry of the tank. We shall restrict attention to cylindrical containers with hemispherical ends. The location of the free surface is further restricted in that under zero gravity conditions, the ullage space cannot be swallowed into the interior of the liquid. Thus, the interface will always intersect the cylinder or the bottom hemisphere. A convenient coordinate system is the polar cylindrical system shown in Figure C-12.

The solution of Eq. C-21 is subject to a no-normal-flow boundary condition at the solid wall. This is written

$$\varphi_n = 0 \quad , \quad \text{on } w \qquad \text{(C-23)}$$

where $\bar{n}$ is the outward-directed normal. The boundary condition applying at the free surface is a pressure boundary condition derived from Bernoulli's equation.

$$\frac{p}{\rho} + \frac{\vec{u}^2}{2} + \alpha\bar{s} - \beta(\bar{t})\,\bar{r}\cos\theta + \varphi_{\bar{t}} = C(t) \qquad \text{(C-24)}$$

where $\beta(t)$ is a time-dependent acceleration field and C (t) is the arbitrary function of time in the general Bernoulli equation. In addition, p and ρ are liquid pressure and density, respectively. The pressure difference across a capillary surface is, in polar cylindrical coordinates,

$$p_g - p = \sigma\left\{\frac{1}{\bar{r}}\frac{\partial}{\partial\bar{r}}\frac{\bar{r}\,\bar{s}_{\bar{r}}}{\left(1 + \bar{s}_{\bar{r}}^2 + \frac{1}{\bar{r}^2}\bar{s}_\theta^2\right)^{1/2}} + \frac{1}{\bar{r}^2}\frac{\partial}{\partial\theta}\frac{\bar{s}_\theta}{\left(1 + \bar{s}_{\bar{r}}^2 + \frac{1}{\bar{r}^2}\bar{s}_\theta^2\right)^{1/2}}\right\} \qquad \text{(C-25)}$$

where σ is the surface tension. By setting C (t) = p_o/ρ where p_o is the equilibrium pressure in the liquid at the origin, Eq. C-24 can be written as follows:

$$\frac{\sigma}{\rho}\left\{\frac{1}{\bar{r}}\frac{\partial}{\partial\bar{r}}\frac{\bar{r}\,\dot{\bar{s}}_{\bar{r}}}{\left(1 + \bar{s}_{\bar{r}}^2 + \frac{1}{\bar{r}^2}\bar{s}_\theta^2\right)^{1/2}} + \frac{1}{\bar{r}^2}\frac{\partial}{\partial\theta}\frac{\bar{s}}{\left(1 + \bar{s}_{\bar{r}}^2 + \frac{1}{\bar{r}^2}\bar{s}_\theta^2\right)^{1/2}}\right\}$$

$$- \frac{\vec{u}^2}{2} - \alpha\bar{s} + \beta(t)\,\bar{r}\cos\theta - \varphi_{\bar{t}} = \frac{p_g - p_o}{\rho} \qquad \text{(C-26)}$$

where the motion of the free surface is related to the velocity potential by the kinematic condition.

$$-\bar{s}_{\bar{t}} = -\varphi_{\bar{z}} + \varphi_{\bar{r}}\,\bar{s}_{\bar{r}} + \frac{1}{\bar{r}^2}\varphi_{\theta}\,\bar{s}_{\theta} \qquad \text{(C-27)}$$

which is derived from the equation of the free surface

$$\bar{s} = \bar{s}\,(\bar{r}\,,\ \theta\,,\ \bar{t})$$

Equation C-21 is the equation governing the liquid behavior subject to boundary conditions given by Eqs. C-23 and C-26 and further subject to Eq. C-27 and an additional condition imposed on the contact angle at the wall which will be described later.

The Linearized Dimensionless Problem

The free surface boundary conditions are nonlinear. Solution of this problem is thus not possible with use of classical techniques of applied mathematics. If attention is limited to small amplitude vibrations of the free surface, however, then the problem can be rendered more tractable mathematically by linearizing about the equilibrium surface. This process is accomplished by defining $\bar{s}$ as

$$\bar{s}\,(\bar{r}\,,\ \theta\,,\ \bar{t}) = \bar{f}\,(\bar{r}) + \bar{h}\,(\bar{r}\,,\ \theta\,,\ \bar{t}) \qquad \text{(C-28)}$$

where $\bar{h}$ and its derivatives are small compared to $\bar{f}$ and its derivatives, $\bar{f}$ being the equilibrium shape of the free surface. It is also convenient to nondimensionalize the equations by assuming that $r = \bar{r}/r_o$, $z = \bar{z}/r_o$ $f = \bar{f}/r_o$, $h = \bar{h}/r_o$, $\ell = \bar{\ell}/r_o$, $n = \bar{n}/r_o$, $t = \bar{t}\sqrt{(1 + B_\alpha)\sigma/\rho r_o^3}$,

$\Phi = \varphi/\sqrt{(1 + B\,\alpha)\sigma r_o/\rho}$, $B_\alpha = \rho\alpha r_o^2/\sigma$, and $B_t = \rho\beta\,(t) r_o^2/\sigma$, where r_o is the cylinder radius. Using Eq. C-28, the linearized nondimensionalized equations become as follows

$$\Phi_{rr} + \frac{1}{r}\Phi_r + \frac{1}{r^2}\Phi_{\theta\theta} + \Phi_{zz} = 0 \quad \text{in } \mathcal{D} \tag{C-29}$$

$$\Phi_n = 0 \text{ , on } w \tag{C-30}$$

$$\frac{1}{r}\frac{\partial}{\partial r}\frac{r\,h_r}{\left(\sqrt{1 + f_r^2}\right)^3} + \frac{1}{r^2}\frac{\partial}{\partial\theta}\frac{h_\theta}{\sqrt{1 + f_r^2}} - B_\alpha h + B_t\, r\cos\theta - (1 + B_\alpha)\Phi_t = 0, \text{on } f \tag{C-31}$$

$$-h_t = -\Phi_z + f_r\Phi_r = -\sqrt{1 + f_r^2}\,\frac{\partial\Phi}{\partial n} \tag{C-32}$$

and, using $\Gamma = r_o\gamma$,

$$h_r = \Gamma h \tag{C-33}$$

Here, $\Gamma = 0$ corresponds to the condition of zero contact angle hysteresis. This relation is obtained by the assumption that h_r is related to h according to the expansion

$$h_r = \gamma h + o\,(h^2)$$

The linearization of the problem reduces this to Eq. C-33. It is demonstrated in Ref. C-7 that the constraint imposed by Eq. C-33 is consistent with the linearized, irrotational problem under study.

The function h must satisfy the boundary conditions that

$$h(0\ ,\ t) = h_r\ (1\ ,\ t) = 0$$

for $\Gamma = 0$

The equilibrium surface shape is found as the solution to the differential equation

$$B_\alpha f = \frac{1}{r}\frac{\partial}{\partial r}\left(\frac{r\, f_r}{\sqrt{1 + f_r^2}}\right)\Bigg]_0^r$$

see Eq. (6) with the boundary conditions that

$$f(0) = 0\ ,\ f_r\ (1) = \infty$$

METHOD OF SOLUTION

Introduction

The steady-state oscillation of a linear system induced by a forcing function can be determined if the motion of the system in a free vibration can be described. The behavior of a linear system undergoing a free vibration is described in terms of a linear homogeneous differential equation.

The solution to this is expressed in terms of sine or cosine functions of time. The behavior of the same linear system being acted upon by an arbitrary forcing function is described by an inhomogeneous linear differential equation. If the solution of the homogeneous problem can be expressed in terms of orthogonal functions, the complete solution to the inhomogeneous problem can be represented by a series of the functions satisfying homogeneous problem. In the boundary value problem just described, the transverse acceleration is the arbitrary forcing function.

With these remarks, the problem of determining the dynamic response to the transverse acceleration fields may be solved in four separated steps: solution to the homogeneous equation; response to sinusoidal excitation; response to square-pulse excitation; and response to an impulse. These steps are considered in order.

Solution to the Homogeneous Equation

If the periodic time dependence and the angular dependence of Φ and h are assumed in the form

$$\Phi = \Phi_n (r , z) \cos \theta \cos \omega_n t$$

$$h = h_n (r) \cos \theta \sin \omega_n t$$

When these expressions are applied to Eq. C-31 with $B_t = 0$ and to Eq. C-32 they become

$$(1 + B_\alpha)\omega\Phi_n - B_\alpha h_n + \frac{1}{r}\frac{\partial}{\partial r}\frac{r\, h_{n_r}}{\left(\sqrt{1 + f_r^2}\right)^3}\cdot\frac{1}{r^2}\frac{h_n}{\sqrt{1 + f_r^2}} = 0 \qquad \text{(C-34)}$$

$$- \omega_n h_n = -\Phi_{n_z} + f_r \Phi_{n_r} \qquad \text{(C-35)}$$

$\Big\}\ z = f(r)$

The boundary conditions on h_n are, for $\Gamma = 0$

$$h_n(0) = 0\ ,\ h_{n_r}(1) = 0$$

and

$$\Phi(0\ ,\ z) = 0$$

The success in obtaining solutions Φ_n and h_n (and subsequent dynamic response solutions) depends crucially on the method of solving for these functions. At present, two methods have much to offer by way of simplicity of application and ease in computation, and both will be described briefly. In the first, Φ_n is expressed as a linear combination of known solutions to Laplace's equation which satisfies the rigid and free-surface boundary conditions exactly when both tank bottom and free surface are flat

$$\Phi_n = \sum_{m=1}^{\infty} a_{nm}\, \psi_m \qquad \text{(C-16)}$$

where

$$\psi_m = c_m J_1 (k_m r) \cosh k_m (\ell + z) \qquad \text{(C-37)}$$

and c_m is the normalization coefficient for the ψ_m's:

$$\frac{1}{c_m^2} = \pi \int_0^{\ell} \int_0^1 [\psi_m]^2 \, r dr dz$$

A set of surface functions ζ can be obtained through Eq. C-33

$$- \zeta_m = - \frac{1}{\omega_n} \left(\psi_{m_z} - f_r \psi_{m_r} \right) \qquad \text{(C-38)}$$

and thus,

$$h_n = \Sigma a_{nm} \zeta_m \qquad \text{(C-39)}$$

The k_m's are determined by use of boundary condition (3) along the vertical walls of the container at r = 1:

$$\frac{d}{dr} J_1 \left(k_m \right) = 0 \qquad \text{(C-40)}$$

Boundary conditions along the free surface and the hemispherical bottom of the container [Eqs. (C-31) and C-23)] are satisfied at a finite number of points (collocation technique), giving rise to a sufficient number of equations for the determination of the eigenfrequencies ω_n and the eigenfunctions Φ_n.

For example, defining temporarily $\Lambda^2 = (1 + B_\alpha)\omega^2$, Eq. C-34 can be evaluated at N/2 points on free surface. This results in N/2 equations in N unknowns of the form

$$\left|A_{ij} + \Lambda^2 B_{ij}\right| \cdot \left|a_i\right| = 0$$

Equation C-30 can be evaluated at (N/2)-1 points on the bottom giving (N/2)-1 equations in N unknown of the form

$$\left|A_{ij} + 0\ B_{ij}\right| \cdot \left|a_i\right| = 0$$

Equation C-33 can be used to obtain the Nth equation in N unknowns of the same form.

All of these are a set of N equations in N unknowns. A necessary condition for a nontrivial solution is

$$\left|A_{ij} + \Lambda^2 B_{ij}\right| = 0$$

The zeros of the determinant are the N eigenvalues Λ_n^2 which are related to the fundamental frequency of the free surface and the first N-1 harmonics.

The eigenvalues can then be used to calculate all the a_n's except a single arbitrary value, say a, which establishes a set of functions

$$\Phi_1, \Phi_2, \cdots \quad \cdots \Phi_n$$

describing the first N normal vibrations of the free curved surface.

In the second method, the eigenfrequencies and eigenfunctions are calculated by a finite difference scheme using a method of successive iterations corresponding to the Wielandt method. First, assume that the j-th approximations to ω_n^2 and Φ_n are $\omega_n^{(j)2}$ and $\Phi_n^{(j)}$. Then $\omega_n^{(j+1)2}$ and $\Phi_n^{(j+1)}$ are calculated as follows:

Solve

$$\left(\frac{\partial^2}{\partial r^2} + \frac{1}{r}\frac{\partial}{\partial r} - \frac{1}{r^2} + \frac{\partial^2}{\partial z^2}\right)\Phi_n^{(j+1)} = 0$$

in the interior subject to $\partial\Phi_n^{(j+1)}/\partial n = 0$ on the container wall

and $\Phi_n^{(J+1)}(0, z) = 0$

In addition, the free-surface boundary conditions are

$$\left.\begin{aligned} (1 + B_\alpha)\omega_n^{(j)}\,\Phi_n^{(j+1)} - B_\alpha\, h_n^{(j)} + \frac{1}{r}\frac{\partial}{\partial r}\frac{rh_{n,r}^{(j)}}{\left(\sqrt{1+f_r^2}\right)^3} - \frac{1}{r^2}\frac{h_n^{(j)}}{\sqrt{1+f_r^2}} &= 0 \\ -\omega_n^{(j)}\,h_n^{(j)} = -\Phi_{n,z}^{(j+1)} + f_r\,\Phi_{n,r}^{(j+1)} & \end{aligned}\right\} z = f(r)$$

where $h_n^{(j)}$ is the j-th approximation to h_n. The solution is effected by a finite difference iteration technique for $\Phi_n^{(j+1)}$.

Normalize $\Phi_n^{(j+1)}$ and then compute $\omega_n^{(j+1)^2}$ from

$$\omega_n^{(j+1)^2} = \frac{\int_0^1 \left\{ B_\alpha \sqrt{1+f_r^2}\, h_n \left(\frac{\partial \Phi_n}{\partial n}\right) - h_n \frac{1}{r}\frac{\partial}{\partial r}\left[\frac{r\frac{\partial}{\partial r}\left(\frac{\partial \Phi_n}{\partial n}\sqrt{1+f_r^2}\right)}{\left(\sqrt{1+f_r^2}\right)^3}\right] + \frac{h_n}{r^2}\frac{\partial \Phi_n}{\partial n} \right\} r\,dr}{(1+B_\alpha)\int_0^1 h_n \Phi_n\, r\,dr} \qquad \text{(C-41)}$$

on $z = f(r)$ which is obtained by combining, multiplying by h_n, and integrating the free-surface boundary conditions. In the preceding equation, $\Phi_n^{(j+1)}$ is used for Φ_n and $h_n^{(j+1)}$ for h_n. The $h_n^{(j+1)}$ corresponding to $\omega_n^{(j+1)^2}$ and $\Phi_n^{(j+1)}$ is found by Eq. C-32:

$$h_n^{(j+1)} = \frac{1}{\omega_n^{(j+1)}} \sqrt{1+f_r^2}\, \frac{\partial \Phi_n^{(j+1)}}{\partial n}$$

The initial approximation for $\omega_n^{(0)^2}$ and $\Phi_n^{(0)}$ on the surface may be taken from the known values for the cylindrical tank with flat bottom and free surface.

Response to Sinusoidal Excitation

Once the eigenfunctions and eigenfrequencies are obtained, the motion of the fluid excited by a uniform periodic horizontal acceleration field may be represented by a series of the eigenfunctions:

$$\Phi(r,z) = \sum_n A_n \Phi_n \quad (r,z) \qquad \text{(C-42)}$$

When B_τ is expressed as A sin ωt, combination of Eqs. C-31 and C-32 gives

$$(1 + B_\alpha) \sum_n \left(\omega_n^2 - \omega^2\right) A_n \Phi_n \ (r,z) - \omega A r = 0 \quad \text{on } z = f(r)$$

Since the Φ_n's and the corresponding h_n's form an orthogonal set, r may be expressed as an expansion in Φ_n evaluated on z = f(r):

$$r = \sum_n D_n \Phi_n \ [r, f(r)]$$

where

$$D_n = \frac{\int_0^1 h_n \, r^2 \, dr}{\int_0^1 \Phi_n \, h_n \, r dr}$$

Thus, the solution for A_n is

$$A_n = \frac{\omega A B_n}{\omega_n^2 - \omega^2} \frac{1}{1 + B_\alpha}$$

so that the velocity potential becomes

$$\Phi = \sum_n \frac{\omega A D_n}{\omega_n^2 - \omega^2} \frac{\Phi_n(r,z)}{1 + B_\alpha}$$

The free surface shape is found from Eq. C-32.

$$h = \frac{1}{\omega} \sqrt{1 + f_r^2} \frac{\partial \Phi}{\partial n}$$

Of course, this linearized solution requires that $\omega \neq \omega_n$. If $\omega = \omega_n$, resonance is obtained.

Response to Square-Wave Excitation

The procedure for obtaining the solution for any periodic horizontal acceleration field that possesses a Fourier series expansion of the form $r \cos\theta \sum_m C_m \sin m\omega_o t$ is similar. The solution is

$$(1 + B_\alpha)A_n = -D_n \sum_m \frac{mC_m \omega_o}{m^2\omega_o^2 - \omega_n^2}$$

In particular, if the field is

$$B_t \; r \cos\theta \quad , \; 0 \leqq t < \pi/\omega_o$$

$$-B_t \; r \cos\theta \quad , \; \pi/\omega_o \leqq t < 2\pi/\omega_o$$

and periodic with period $2\pi/\omega_o$, then

$$C_m = \begin{cases} \frac{4}{\pi m} B_t \; , & m \text{ odd} \\ 0 \; , & m \text{ even} \end{cases}$$

and

$$-(1 + B_\alpha)A_n = D_n B_t \sum_{m \text{ odd}} \frac{4\omega_o/\pi}{m^2\omega_o^2 - \omega_n^2}$$

Response to Unit Impulse Excitation

The solution for an initial value problem in which the liquid is initially at rest and a horizontal acceleration with arbitrary time variation acts for $t \geqq 0$, can also be obtained directly. If the field is $B_t \; r \cos\theta \; h(t)$, $t \geqq 0$ and $\Phi(r,z,s) \cos\theta$ is the Laplace transform of the velocity potential $\Phi(r,z,t) \cos\theta$, and

$$\Phi = \sum_n A_n(t) \Phi_n(r,z)$$

then

$$(1 + B_\alpha)\bar{A}_n(s) = \frac{s B_t D_n \bar{h}(s)}{s^2 + \omega_n^2}$$

is the Laplace transform of $A_n(t)$ where $\bar{h}(s)$ is the Laplace transform of $h(t)$. In particular, if $h(t) = \delta(t)$, the unit impulse, then $\bar{h}(s) = 1$, and

$$(1 + B_\alpha)\bar{A}_n(s) = \frac{s B_t D_n}{s^2 + \omega_n^2}$$

so that by use of the inversion integral, A_n may be written directly as

$$(1 + B_\alpha) A_n(t) = B_t D_n \cos \omega_n t$$

Thence,

$$(1 + B_\alpha)\Phi = \sum_n B_t D_n \Phi_n(r,z) \cos \omega_n t$$

It must be emphasized that the response to the three forcing functions can be obtained starting with the velocity potentials for the normal mode oscillations. The method used to obtain these is immaterial.

terms of a series of the velocity potentials for normal mode vibrations.

$$\Phi = \sum_{n=1}^{\infty} a_n \Phi_n \tag{C-50}$$

This may be substituted into C-44 and C-45 to obtain

$$(1 + B_\alpha) \sum_{n=1}^{\infty} (\omega_n^2 - \omega^2)\, a_n \Phi_n = \omega A r \tag{C-51}$$

r can be expanded in a series of the eigen-functions.

$$r = \sum_{n=1}^{\infty} D_n \Phi_n \left[r,\ z = 0\right] \tag{C-52}$$

where

$$D_n = \frac{\int_o^1 r^2 h_n\, dr}{\int_o^1 r \Phi_n h_n\, dr} \tag{C-53}$$

In the case of the flat interface the D_n's are readily computed from

$$D_n = \frac{\int_o^1 r^2 J_1 (K_n r) dr}{\int_o^1 r J_1^2 (K_n r) dr}$$

These are tabulated in Table C-8. These can be used to calculate the amplitude of the forced motion caused by a sinusoidal transverse acceleration of amplitude A.

However, investigation of the motion imparted to the liquids in propellant tanks by impulsive acceleration is more important than that which would be caused by a sinusoidal acceleration. Here again, the velocity potential can be expressed in terms or Equation C-50 where the a_n's are defined by

$$(1 + B_\alpha) a_n(t) = B_t\, D_n \cos \omega_n t \tag{C-54}$$

thus

$$\Phi = \frac{B_t}{(1 + B_\alpha)} \sum_{n=1}^{\infty} D_n J_1 (K_n r) e^{-K_n z} \cos \omega_n t \tag{C-55}$$

*Here, B_t must be considered the product of the dimensionless transverse Bond number and a unit dimensionless time.

TABLE C-8

NORMALIZING COEFFICIENTS FOR SLOSHING CALCULATIONS

n	D_n
1	1.436
2	-0.185
3	0.108
4	-0.077
5	+0.042

IV - CALCULATION OF ZERO G IMPULSIVE FORCED MOTION SLOSH WAVE HEIGHTS

The small amplitude theory derived in Section III of this appendix allows a closed form solution in only one specialized case: when the contact angle is 90 degrees and does not vary dynamically. In the interest of further simplicity, calculations given in this appendix have been made for deep liquid, i. e. depth greater than half the tank radius. This simplification is appropriate since in no period of the Apollo SPS mission does the depth of liquid in any of the tanks remain small. The depth can either be considered great or zero.

The boundary value problem derived in Section III specialized according to the foregoing assumptions is as follows.

$$\nabla^2 \Phi = 0 \qquad \text{in D} \qquad \text{(C-43)}$$

$$h_{rr} + \frac{1}{r} h_r + \frac{1}{r^2} h_{\theta\theta} - B_\alpha h + B_t \cos\theta - (1 + B_\alpha)\Phi_t = 0 \qquad \text{on } z = 0 \qquad \text{(C-44)}$$

$$h_t = \Phi_z \qquad \text{on } z = 0 \qquad \text{(C-45)}$$

$$\Phi_n = 0 \qquad \text{on W} \qquad \text{(C-46)}$$

$$h_r = 0 \qquad \text{on } z = 0,\ r = 1 \qquad \text{(C-47)}$$

(See Section III of this appendix and Figure C-13 for definition of nomenclature). The solution to Equation C-43 subject to Equations C-46 and C-47 for normal modes (i.e. $B_t = 0$) can be written down as

$$\Phi_n = J_1 (K_n r) e^{-K_n z} \cos\theta \cos \omega_n t \qquad \text{(C-48)}$$

Substitution of this into C-44 and C-45 gives for the normal mode frequencies

$$\omega_n^2 = K_n^3 + B_\alpha K_n \qquad \text{(C-49)}$$

When the liquid in the tank is subjected to a transverse periodic acceleration such as when $B_t = A \sin \omega t$, the velocity potential can be expressed in

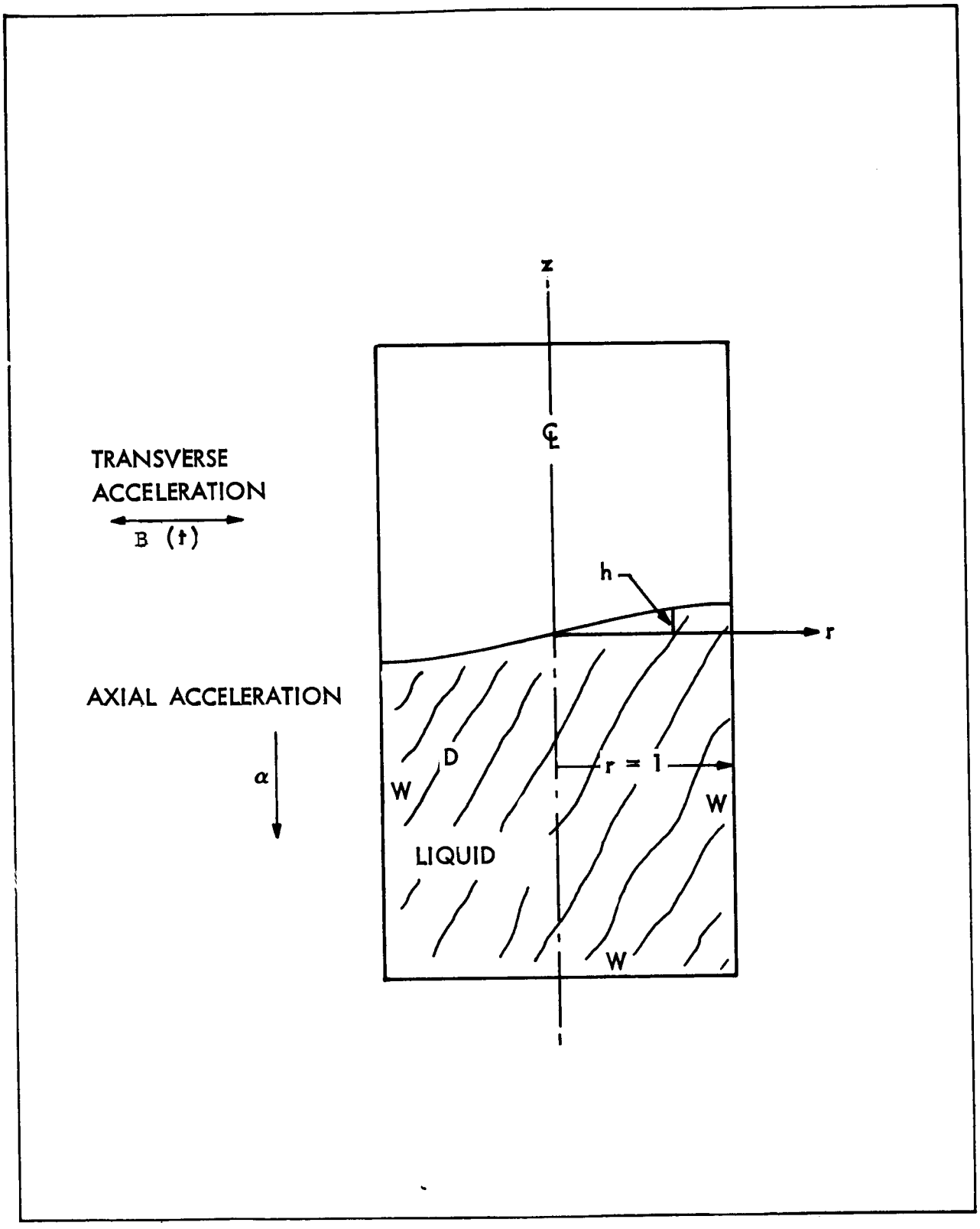

Figure C-13 Geometry of Liquid Sloshing in a Deep Cylinder

and

$$\left|h_t\right| = \left|\Phi_z\right| = \frac{B_t}{(1 + B_\alpha)} \sum_{n=1}^{\infty} D_n K_n J_1 (K_n r) \cos \omega_n t \qquad \text{(C-56)}$$

Assuming that h (r,0) = 0, the amplitude at the wall of the wave a quarter cycle (of the fundamental frequency) later is

$$\left|h_{wall}\right| = \frac{B_t}{(1 + B_\alpha)} \sum_{n=1}^{\infty} \frac{D_n K_n}{\omega_n} J_1 (K_n) \int_o^{\pi/2} \cos \omega_n t \, d(\omega_n t)$$

This can be integrated with respect to time. When Equation C-49 is substituted an expression for the maximum possible (for $B_\alpha = 0$) amplitude of the wave resulting from an impulsive acceleration can be obtained.

$$\left|h_{wall,\ max}\right| = B_t \sum_{n=1}^{\infty} \frac{D_n J_1 (K_n)}{\sqrt{Kn}} \qquad \text{(C-57)}$$

Substituting values from Table C-8 the amplitude of the wave at the wall is given by

$$\left|h_{wall,\ max}\right| \cong 0.67\ B_t \qquad \text{(C-58)}$$

The transverse Bond number, B_t, for the impulsive acceleration can be obtained from Equation C-59.

$$B_t = \alpha g_o \bar{t} \sqrt{\frac{r_o}{(\sigma/\rho)}} \qquad \text{(C-59)}$$

where $\bar{t}$ is the dimensional time length of the impulse.

V - DETAILS OF MASS DIFFUSIVITY AND CONDUCTIVITY CALCULATIONS

For the calculation of the mass diffisivity, the method of Reference C-8 was used. The Chapman-Euskog kinetic theory for the gaseous state at low density was used to obtain:

$$D_{AB} = 0.0018583 \frac{\sqrt{T^3\left(\frac{1}{M_A} + \frac{1}{M_B}\right)}}{P\sigma_{AB}^2 \Omega_{D,AB}} \qquad \text{(C-60)}$$

Where D_{AB} = mass diffusivity for gases A & B, sq. cm/sec.

T = gas temperature, $^{\circ}K$

M_A = molecular weight of gas A

M_B = molecular weight of gas B

P = pressure, atm.

σ_{AB} = characteristic diameter, angstronic units

$\Omega_{D,AB}$ = dimensionless function of temperature and intermolecular potential field.

The data used for the oxidizer tank utilizing the subscript A for the helium gas and B for the N_2O_4 vapor was:

$M_A = 4.0$

$M_B = 92.0$

$\sigma_A = 2.576$ Å

$P = 196.7$ psia - 31.4 atm.

The characteristic diameter for helium was obtained from Reference C-8, Table B-1. The following was used to calculate the diameter for nitrogen tetroxide:

$$\sigma_B = 2.44 \left(\frac{T_o}{P_c}\right)^{1/3} \qquad \text{(C-61)}$$

$$T_C = 316^{\circ}F = 436^{\circ}K$$

$$P_C = 1469 \text{ psia} = 100 \text{ atm.}$$

$$\sigma_B = 2.44\ (436/100)^{1/3}$$

$$\sigma_B = 3.99\ \text{Å}$$

Fairly satisfactory estimates of the characteristic diameter for molecule pairs can be made by combing the individual molecule diameters empirically:

$$\sigma_{AB} = \frac{1}{2}\ (\sigma_A + \sigma_B)$$

$$= \frac{1}{2}\ (2.576 + 3.99)$$

$$= 3.283\ \text{Å}$$

The dimensionless function of temperature and intermolecular field can be expressed as

$$\Omega_{D,AB} = f\left(\frac{KT}{\epsilon_{AB}}\right) \qquad \text{(C-62)}$$

This function is given in Table B-2 of Reference 8 as values of $\Omega_{D,AB}$ for values of KT/ϵ_{AB}

where K = Boltzmann's Constant

T = Temperature, $^{\circ}K$

ϵ = Characteristic energy of interaction between the molecules.

For helium, the value

$$\frac{\epsilon_A}{K} = 10.2^{\circ}K$$

was obtained from Table B-1, Reference C-8. The value for nitrogen tetroxide was computed from

$$\frac{\epsilon_B}{K} = 1.15\ T_b \qquad \text{(C-63)}$$

$$T_b = 70^{\circ}F = 294^{\circ}K$$

$$\frac{\epsilon_B}{K} = 1.15 \times 294 = 338^{\circ}K$$

The characteristic energies can be combined as

$$\epsilon_{AB} = \sqrt{\epsilon_A \times \epsilon_B}$$

$$\frac{\epsilon_{AB}}{K} = \frac{1}{K}\sqrt{\epsilon_A \times \epsilon_B}$$

$$= 10.2 \times 338$$

$$= 58.7^{\circ}K$$

At a gaseous temperature of $294^{\circ}K$

$$\frac{\epsilon_{AB}}{K} = 5.01$$

From Table B-2, Reference C-8,

$$\Omega_{D,AB} = 0.8966$$

Utilizing these calculated values in the equation for mass diffusivity yields

$$D_{AB} = 0.0018583 \frac{\left((294)^3 \left(\frac{1}{4} + \frac{1}{92}\right)\right)^{\frac{1}{2}}}{13.4\ (3.283)^2\ 0.8966}$$

$$= 0.0373 \text{ sq. cm/sec}$$

The methods presented in Reference C-8 were also utilized in calculating the gaseous thermal conductivity. The Chapman-Enskog theory is again the basis for the Mason-Saxena equation predicting the thermal conductivity of a gaseous mixture as

$$k_{12} = k_1\left(1 + G_{12}\frac{X_2}{X_1}\right)^{-1} + k_2\left(1 + G_{21}\frac{X_1}{X_2}\right)^{-1} \qquad \text{(C-65)}$$

where k = thermal conductivity

X = mole fraction

for subscripts 1 and 2 equal to helium and nitrogen tetroxide, respectively. The coefficient G_{12} and G_{21} are expressed as

$$G_{ij} = \frac{1.065}{\sqrt{8}}\left(1 + \frac{M_i}{M_j}\right)^{-\frac{1}{2}}\left[1 + \left(\frac{\mu_i}{\mu_j}\right)^{\frac{1}{2}}\left(\frac{M_j}{M_i}\right)^{\frac{1}{4}}\right]^2 \qquad \text{(C-66)}$$

The viscosity in gm/cm-sec was calculated for a pure monatomic gas of molecular weight M at temperature T (^{o}K) as

$$\mu = 2.6693 \times 10^{-5} \sqrt{\frac{MT}{\sigma^2 \Omega_\mu}}$$

For the helium gas as calculated above

$$\frac{KT}{\epsilon} = 28.8$$

and from Table B-2 for viscosity calculations

$$\Omega_\mu = 0.7056$$

Using these values,

$$\mu_1 = 1.955 \times 10^{-4} \text{ gm/cm-sec}$$

From the calculation shown above for nitrogen tetroxide:

$$\frac{\epsilon_2}{K} = 338$$

At $T = 70^{o}F$,

$$\frac{KT}{\epsilon_2} = 0.87$$

and $$\Omega_2 = 1.705$$

This yields,

$$\mu_2 = 2.6693 \times 10^{-5} \frac{\sqrt{92 \times 294}}{(3.94)^2 \times 1.705}$$

$$= 1.625 \times 10^{-4} \text{ gm/cm-sec}$$

The coefficients G_{ij} can now be calculated

$$G_{12} = \frac{1.065}{\sqrt{8}} \left(1 + \frac{4}{92}\right)^{-\frac{1}{2}} \left[1 + \left(\frac{1.955}{1.625}\right)^{\frac{1}{2}} \left(\frac{4}{92}\right)^{\frac{1}{4}}\right]^2$$

$$= 0.832$$

$$G_{21} = \frac{1.065}{\sqrt{8}} \left(1 + \frac{92}{4}\right)^{-\frac{1}{2}} \left[1 + \left(\frac{1.625}{1.955}\right)^{-\frac{1}{2}} \left(\frac{92}{4}\right)^{\frac{1}{4}}\right]^2$$

$$= 0.461$$

The ratio of the mole fractions was calculated from the perfect gas law uitlizing the partial pressures of He and N_2O_4 at 70°F as follows:

$$PV = nZRT$$

$$n_{N_2O_4} = \frac{P_{N_2O_4} V}{Z_{N_2O_4} RT}$$

$$n_{He} = \frac{P_{He} V}{Z_{He} RT}$$

$$\frac{X_{He}}{X_{N_2O_4}} = \frac{P_{He}}{P_{N_2O_4}} \cdot \frac{Z_{N_2O_4}}{Z_{He}}$$

From N_2O_4 vapor pressure curve

$$P_{N_2O_4} \text{ @ } 70^\circ F = 17 \text{ psia}$$

$$P_{total} = 196.4 \text{ psia}$$

$$P_{He} = 179.4 \text{ psia}$$

$$\frac{X_{He}}{X_{N_2O_4}} = \frac{179.4 \times 0.516}{1 \times 17} = 5.45$$

Using this ratio together with

$$k_{He} = 0.091 \text{ btu/hr-ft-}^\circ R$$

$$k_{N_2O_4} = 0.062 \text{ btu/hr/ft-}^\circ R$$

and the calculated values of the coefficients yields

$$k_{12} = 0.091 \left(1 + \frac{0.832}{5.45}\right)^{-1} + 0.062 \left[1 + 0.461\ (5.45)\right]^{-1}$$

$$= 0.0966 \text{ Btu/hr-ft-}^{\circ}\text{F}$$

as the thermal conductivity of the gaseous He - N_2O_4 mixture.

VI - DESCRIPTION OF SUBROUTINE TO CALCULATE THE HEAT TRANSFERRED BY MASS DIFFUSION

A subroutine for use with a Thermal Analyzer was developed at LMSC to calculate the heat transferred by mass diffusion within the propellant tanks of an orbiting vehicle. The analysis of the diffusion phenomena and the derivation of the equations is presented in Reference C-9.

Since the vapor flow in the gaseous phase is quite small, the heat exchange between gaseous nodes due to the diffusion phenomena is neglected. The heat exchanged at the solid-gas and liquid-gas interface is calculated by the subroutine. The problem was solved using the bumped parameter concept because of the impossibility of utilizing a closed form solution. Thus, when the heat balance in the Thermal Analyzer was performed for the solid and liquid nodes and adjacent gaseous nodes, a term was included which was calculated in the subroutine as the heat transferred due to phase change at that interface.

To each of the vapor nodes an unknown concentration, C_i, equal to the ratio of the propellant density to the total vapor density, was assigned. At the liquid-vapor interface, a saturated condition was assumed, and based on the temperature of each liquid node, the following equation was solved for the interface concentration:

$$P_v(T_i) = \frac{P_o \, \delta \, C_i}{1 - C_i + \delta \, C_i} \qquad \text{(C-68)}$$

where P_o = total pressure, atm.

$P_v(T_i)$ = vapor pressure of propellant

δ = ratio of pressurant gas molecular weight to that of the propellant.

At the solid-gas interface where condensation occurs, saturated conditions were assumed and Equation C-68 was used to calculate the unknown concentration. For those where no condensation occurs, the interface concentration was set equal to the adjacent gas node concentration.

The total pressure within the tank was related to the amount of helium mass, m_{He}, contained in the tank by

$$P_o = \frac{m_{He}}{\sum_{\substack{\text{gas} \\ \text{nodes}}} \frac{M\,(1-C_i)\,V_i}{RT_i\,(1-C_i+\delta C_i)}} \qquad \text{(C-69)}$$

where M = helium molecular weight

V_i = volume of node i

R = gas constant

T_i = temperature of node i

With these boundary conditions, the concentrations for each of the gaseous nodes were computed from

$$\sum_j \frac{A_{ij}}{d_{ij}} \frac{(C_j - C_i)}{\left[1 - \left(\frac{C_i + C_j}{2}\right)\right]\left[1 - (\delta - 1)\left(\frac{C_i + C_j}{2}\right)\right]} \qquad \text{(C-70)}$$

for: j in contact with node i

A_{ij} = contact area between nodes i and j

d_{ij} = centroid distance between nodes i and j

The subroutine then iterated Equation C-70 together with the boundary conditions until the change in concentrations from one iteration to the next was quite small.

Using these computed values of concentrations the heat transferred by phase change at the interfaces was computed from

$$Q = \lambda D \frac{A_{ij}}{d_{ij}} \frac{(C_j - C_i)}{(1 - C_j)(1 - C_j + \delta C_j)}$$

where i = solid or liquid node

j = gas node in contact with node i

λ = latent heat

D = mass diffusivity

This result was then used in the heat balance performed by the Thermal Analyzer.

VII - REFERENCES FOR APPENDIX C

C-1. Space Technology, ed. by H. S. Seifert, Johns Wiley and Sons, pp. 8-24.

C-2. Space Technology, op. cit. pp. 8-07 to 8-15.

C-3. Encl. (1) to LAC 597227.

C-4. W. C. Reynolds, M. A. Saad, and H. M. Satterlee: Capillary Hydrostatics and Hydrodynamics at Low-g. Tech. Rpt. No. LG-3, Stanford University Department of Mechanical Engineering, September 1964, pp. 55-6.

C-5. S. Weinbaum: Natural Convection in a Horizontal Circular Cylinder, Journal of Fluid Mechanics., Vol. 18, No. 3, March 1964, p. 409.

C-6. W. H. McAdams: Heat Transmission. McGraw-Hill Book Co., New York, 1954, p. 173.

C-7. H. M. Satterlee and W. C. Reynolds: The Dynamics of the Free Liquid Surface in Cylindrical Containers Under Strong Capillary and Weak Gravity Conditions. Department of Mechanical Engineering Rpt. No. LG-2, Stanford University, Stanford California.

C-8. R. B. Bird, W. E. Steward, E. N. Lightfoot: Transport Phenomena. John Wiley and Sons, Inc., New York, 1960.

C-9. Study of Forces on Propellants due to Heat Transfer Influencing Propellant Temperature in a Recovery-Type Vehicle. Dynamic Science Corporation, South Pasadena, California.

REFERENCES

1. North American Aviation Drawing V17-000002, "General Assembly Complete-Service Module"

2. Apollo Mission Planning Task Force, Phase I Progress Report (U), Grumman Aircraft Engineering Corporation, LED-540-7, 4 May 1964, Confidential

3. Project Apollo Preliminary Mission 201 Trajectory Profile, NASA Manned Spacecraft Center Internal Note No. 64-FM-20, 2 July, 1964.

4. Apollo Earth Orbital Mission Profile (U), NASA Manned Spacecraft Center, Undated, Confidential

5. Schultz, H.D. Thermal Analyzer Computer Program for the Solution of General Heat Transfer Problems, Lockheed-California Company, LR 18902, 16 July, 1965.

6. Hirasawa, P.S., Josephine Laue and I.Shuldiner Thermal Analyzer Computer Program for the Solution of Fluid Storage and Pressurization Problems, Lockeed-California Company, LR 18903, 10 August, 1965.

7. Nevelli, B.A. Computer Program for the Calculation of Incident Orbital Radiant Heat Flux, Lockheed-California Company, LR 18904, 18 June, 1965.

8. An Introduction to Spacecraft Thermal Control, Lockheed-California Company, LR 18901, 10 August, 1965.

9. Linneman, E.R. Computer Program for the Calculation of Three-Dimensional Configuration Factors, Lockheed-California Company, LR 18905, 30 June, 1965.